JOURNAL OF ATMOSPHERIC AND TERRESTRIAL PHYSICS

EDITORIAL ADVISORY BOARD

H. O. G. ALFVÉN–STOCKHOLM · J. BARTELS–GÖTTINGEN · P. M. S. BLACKETT–LONDON · E. G. BOWEN–SYDNEY · SIR DAVID BRUNT–LONDON · R. BUREAU–BAGNEUX · S. CHAPMAN–ALASKA · J. EGEDAL–COPENHAGEN · H. FICKER–VIENNA V. F. HESS–NEW YORK · E. O. HULBURT–WASHINGTON, D.C. · H. ISRAEL–AACHEN D. K. MENZEL–CAMBRIDGE, MASS. · S. K. MITRA–CALCUTTA · M. NICOLET–UCCLE E. H. NORINDER–UPSALA · B. van der POL–GENEVA · N. V. PUSHKOV–MOSCOW J. A. RATCLIFFE–CAMBRIDGE · O. E. H. RYDBECK–GOTHENBURG · SIR GEORGE SIMPSON–LONDON · H. SOLBERG–OSLO · C. STØRMER–OSLO · J. VELDKAMP–DE BILT · M. WALDMEIER–ZÜRICH · J. ZENNECK–ALTHEGNENBERG

EDITOR IN CHIEF

SIR EDWARD APPLETON, F.R.S.

EDINBURGH

VOL. 10 1957

VOLUME 10

1957

PERGAMON PRESS LONDON · NEW YORK · PARIS

J. Atmosph. Terr. Phys.

VO
1
19

CONTENTS

No. 1.

SIR EDWARD APPLETON and A. J. LYON: Studies of the *E* layer of the ionosphere—I. Some relevant theoretical relationships 1
J. D. WHITEHEAD: The absorption of short radio waves in the ionosphere 12
SYDNEY CHAPMAN and C. GORDON LITTLE: The nondeviative absorption of high-frequency radio waves in auroral latitudes 20
S. N. MITRA and S. C. MAZUMDAR: Some measurements of ionospheric absorption at Delhi . 32
Research Notes:
L. HARANG, and K. PEDERSEN: Drift measurement of the *E* layer during the solar eclipse 30 June 1954 44
JOHN E. MAXFIELD and R. G. SELFRIDGE: On the intersection of two slender cones . . 46
F. LIED: Ionospheric absorption observed on the 23rd February 1956 at Kjeller and Tromsö 48
V. I. KRASSOVSKY: On the remarks of D. R. Bates and B. L. Moiseiwitsch regarding the O_3 and O_1 hypotheses of the excitation of the OH airglow 49
D. R. BATES, M. R. C. MCDOWELL, and A. OMHOLT: On the energy distribution of secondary auroral electrons 51
K-indices of geomagnetic activity of the observatories Abinger, Eskdalemuir, and Lerwick, July 1956 54

No. 2.

VON R. ESHLEMAN: The theoretical length distribution of ionized meteor trails 57
G. V. GROVES: Velocity of a body falling through the atmosphere and the propagation of its shock wave to earth 73
J. J. GILVARRY: Temperatures in the earth's interior 84
D. R. BATES and M. R. C. MCDOWELL: Recombination in the ionosphere during an eclipse . . 96
JOHN M. KELSO: The calculation of ionospheric electron density distributions 103
A. H. ALLAN, D. D. CROMBIE, and W. A. PENTON: Long-path V.L.F.-frequency variations associated with the solar flare of 23 February 1956 110
Research Notes:
B. LANDMARK and F. LIED: Note on a "QL-QT" transition level in the ionosphere . . 114
P. L. MARSDEN, J. G. WILSON, and D. C. ROSE: Geomagnetic variations in the cosmic-ray disturbance of 23 February 1956 117
Erratum 120
Books received 120

VOL. 10 1957

No. 3.

F. HEPBURN: Wave-guide interpretation of atmospheric waveforms 121
R. E. HOUSTON JR., W. J. ROSS, and E. R. SCHMERLING: Some effects of intense solar activity on radio propagation 136
A. P. MITRA: Night-time ionization in the lower ionosphere—I. Recombination processes . . 140
A. P. MITRA: Night-time ionization in the lower ionosphere—II. Distribution of electrons and positive and negative ions 153
Research Notes:
S. MATSUSHITA: Lunar effects on the equatorial *Es* 163
J. W. KING: Ionospheric self-demodulation of radio waves 166
J. N. BHAR: Relation between noon *F2*-layer ionization and magnetic dip 168
D. R. BARBER: Photoelectric observations of anomalously polarized twilight emission at 5893 Å 172
M. GADSEN: The colour of the zenith twilight sky: absorption due to ozone 176
Announcement 181
Book Review:
L. H. ALLER: Gaseous Nebulae (reviewed by T. G. COWLING) 184

No. 4.

ARMIN W. MANNING: Measurement of the soft component of cosmic radiation by an absorption "well method" 189
M. DAGG: The correlation of radio-star-scintillation phenomena with geomagnetic disturbances and the mechanism of motion of the ionospheric irregularities in the *F* region 194
M. DAGG: Diurnal variations of radio-star-scintillations, spread *F* and geomagnetic activity . 204
P. A. FORSYTH and E. L. VOGAN: The frequency dependence of radio reflections from aurora 215
C. M. MINNIS: Ionospheric changes at Singapore during the solar eclipse of 20 June 1955 . . 229
Research Notes:
S. C. CORONITI and N. C. GERSON: Scatter-field strengths and large ion concentration . . 237
F. MARIANI: The electron density in the *F*2 layer and its correlation with the solar activity 239
Letter to the Editor:
D. LEPECHINSKY: The Q.L.-Q.T. transition level 243

M. I. Large: The radio interference produced by corona discharge 245
M. I. Large and E. T. Pierce: The dependence of point-discharge currents on wind as examined by a new experimental approach 251
J. R. Kirkman and J. Alan Chalmers: Point discharge from an isolated point 258
F. Hepburn: Atmospheric waveforms with very low-frequency components below 1 kc/s known as slow tails 266
B. Landmark: The fading of radio waves reflected from the *E* layer 288
I. L. Jones, B. Landmark, and C. S. G. K. Setty: Movements of ionospheric irregularities observed simultaneously by different methods 296
G. R. Ellis: Low-frequency radio emission from aurorae 302
M. Sribama Rao and B. Ramachandra Rao: Analysis of fading records from four spaced receivers for ionospheric wind measurements 307
D. T. Stewart: A spectrophotometric investigation of the air afterglow 318
A. Omholt: The red and near-infra-red auroral spectrum 320
G. L. Rogers: Diffraction microscopy and the ionosphere 332
Research Note:
S. A. Bowhill: The effect of the recorder time constant on the apparent speed of fading of a radio signal 338
K-indices of geomagnetic activity from the observatories at Abinger, Eskdale, and Lerwick, from October 1956 to March 1957 340
Book Reviews:
M. Schuler and H. Gebelein: Eight and Nine Place Tables of Elliptical Functions (reviewed by I. N. Sneddon) 345
G. C. McVittie: General Relativity and Cosmology (reviewed by V. C. Reddish) 346
H. E. Landsberg: Advances in Geophysics (reviewed by S. K. Runcorn) 347
Books received 348

AUTHOR INDEX TO VOLUME 10

(B) denotes a book review

Allan, A. H. p. 110
Appleton, Sir Edward p. 1
Barber, D. R. p. 172
Bates, D. R. pp. 51, 96
Bhar, J. N. p. 168
Bowhill, S. A. p. 338
Chalmers, J. Alan p. 258
Chapman, Sydney p. 20
Coroniti, S. C. p. 237
Cowling, T. G. p. 184 (B)
Crombie, D. D. p. 110
Dagg, M. pp. 194, 204
Ellis, G. R. pp. 185, 302
Eshleman, von R. p. 57
Forsyth, P. A. p. 215
Gadsen, M. p. 176
Gerson, N. C. p. 237
Gilvarry, J. J. p. 84
Groves, G. V. p. 73
Harang, L. p. 44
Hepburn, F. pp. 121, 266
Houston, R. E. jr. p. 136
Jones, I. L. p. 296
Kelso, John M. p. 103
King, J. W. p. 166
Kirkman, J. R. p. 258
Krassovsky, V. I. p. 49
Landmark, B. pp. 114, 288, 296
Large, M. I. pp. 245, 251
Lepechinsky, D. p. 243
Lied, F. pp. 48, 114
Little, C. Gordon p. 20
Lyon, A. J. p. 1
Manning, Armin W. p. 189
Mariani, F. p. 239
Marsden, P. L. p. 117
Matsushita, S. p. 163
Maxfield, John E. p. 46
Mazumdar, S. C. p. 32
McDowell, M. R. C. pp. 51, 96
Minnis, C. M. p. 229
Mitra, A. P. pp. 140, 153
Mitra, S. N. p. 32
Newstead, G. p. 185
Omholt, A. p. 51, 320
Pedersen, K. p. 44
Penton, W. A. p. 110
Pierce, E. T. p. 251
Rao, B. Ramachandra p. 307
Rao, M. Sbirama p. 307
Reddish, V. C. p. 346 (B)
Rogers, G. L. p. 332
Rose, D. C. p. 117
Ross, W. J. p. 136
Runcorn, S. K. p. 347 (B)
Schmerling, E. R. p. 136
Selfridge, R. G. p. 46
Setty, C. S. G. K. p. 296
Sneddon, I. N. p. 345 (B)
Stewart, D. T. p. 318
Vogan, E. L. p. 215
Whitehead, J. D. p. 12
Wilson, J. G. p. 117

Journal of Atmospheric and Terrestrial Physics, 1957, Vol. 10, pp. 1 to 11. Pergamon Press Ltd., London

Studies of the *E* layer of the ionosphere

I. Some relevant theoretical relationships

Sir Edward Appleton and A. J. Lyon
University of Edinburgh

(*Received* 3 *October* 1956)

Abstract—In the course of an extended investigation of the *E* layer of the ionosphere, using vertical-sounding data from many stations in different parts of the world, we have identified a number of ways in which *E* layer behaviour is not adequately explained in terms of current theories of ionized layer formation and variation. As the first part of that investigation, it was necessary to develop, in their most convenient form, certain quantitative expressions of the accepted theory, by which the experimental data could most readily be checked. A notable simplification in this connection is effected by the assumption that the maximum ionization density in the *E* layer assumes quasi-stationary values over the hours of daylight, for which alone experimental measurements are generally available. At the same time we have developed formulae expressing variations from the simple theory, based on what we consider to be possible alterations in the basic physical assumptions on which that theory was founded. Notable among these is the assumption that the *E* layer is influenced by vertical drift, behaving as a motor as well as a dynamo.

In this Part I of the paper an account is given of such theoretical relationships. Part II will be devoted to our examination of the experimental data in the light of them, leading to the identification of certain extraneous influences, such as that of the S_q overhead current system, which account in part for the anomalous *E*-layer behaviour.

VOL.
10
1957

1. Introductory

We have recently made a detailed study of the *E* layer of the ionosphere. The general object of our enquiry has been to discover how far the world morphology of the *E* layer, as disclosed by the results of vertical incidence radio-sounding, is explicable in terms of current theories of ionized layer formation and variation; and to identify and measure any departures from the predicted "normal" behaviour. A more specific aim was also to see whether we could detect, and if possible measure, any influence of the solar atmospheric tide in the *E* layer: indeed, this aspect of the matter, originally a secondary one, came to play a major part in our investigation.

At the start of our investigation we felt the need to develop, in their most convenient form, certain quantitative expressions of current *E* layer theory by which the experimental data could be checked, for conformity or otherwise. At the same time we have developed formulae expressing variations from the simple theory, involving what we consider to be likely possible alterations in the basic physical assumptions on which that theory has been based. This first paper is devoted wholly to theoretical matters. In Part II, which will follow, we take up the discussion of the experimental data and the identification of the extraneous influences which we believe are responsible for some of the anomalies in *E*-layer behaviour.

It has been accepted now for many years that the classical theory of ionized layer production developed by Chapman (1931a,b) can be considered as providing a fairly satisfactory explanation of *E*-layer phenomena. Such approximate agreement between theory and experiment was, however, reached at a time

when the accuracy of ionospheric measurements was not as high as it is today. Moreover, with the passage of time and with the general extension of ionospheric radio-sounding all over the world, a greater wealth of ionospheric data is now available for detailed analysis. Such considerations, then, prompted us to re-examine the whole matter afresh.

The classical Chapman theory of ionized layer production is based on two simple assumptions: the earth's atmosphere is considered to be of uniform temperature and composition, and the process by way of which electrons disappear is taken to be that of recombination. The basic continuity equation for electrons, according to Chapman's theory, may therefore be written

$$\frac{\partial}{\partial t} N(h,t) = q(h,\chi) - \alpha[N(h,t)]^2 \tag{1}$$

where $N(h, t)$ is the electron density at height h and at time t; $q(h, \chi)$ is the rate of electron production per unit volume and so is a function of both height and solar zenith distance χ, while α is the recombination coefficient, assumed independent of h and t. In an isothermal atmosphere it is found that the maximum value of q is given by

$$q_m = \left(\frac{S_\infty}{H \exp 1}\right) \cos \chi = q_0 \cos \chi \tag{2}$$

where S_∞ is the photon flux of the ionizing radiation outside the earth's atmosphere and H is the scale height of the atmospheric absorbing constituent.

Now, in the experimental radio-sounding of the ionosphere at vertical incidence the direct measurements of ionization density relate to the maximum value, N_m, for any particular layer. In the full development of the theory of Chapman this quantity is not given directly and has to be found by way of numerical solutions of (1) for a series of heights. Such a procedure is laborious and was not considered sufficiently flexible for our purpose of making an exact comparison of theory and experiment. In a recent paper (APPLETON and LYON, 1955) we have therefore considered the theory of ionized layer formation afresh, with the object of obtaining explicit expressions for the value of N_m. As a result we have been able to show that, under quasi-stationary conditions, such as are believed to obtain in the E layer, the quantity N_m itself obeys an equation of the form (1); while, further, we can take $q(h,\chi)$ as being approximately equal to the value of q_m given in (2). More exactly we find that we can write, instead of (1),

$$\frac{dN_m}{dt} = q_0 \cos \chi \left(1 - \frac{\varepsilon^2}{2}\right) - \alpha N_m{}^2 \tag{3}$$

where both q_0 and α are taken as constant and where ε is a quantity small compared with unity. The magnitude of ε is an index of the difference between quasi-stationary conditions and truly stationary conditions, in that it is given by

$$\varepsilon \simeq \frac{\left|\frac{dN_m}{dt}\right|}{\alpha N_m{}^2} \simeq \frac{\left|\frac{dN_m}{dt}\right|}{q_0 \cos \chi} \tag{4}$$

We have given reasons for the assumption that, in the case of the *E* layer, $\varepsilon^2/2 \ll 1$ over the greater part of the day, in which case we can write, simply,

$$\frac{dN_m}{dt} = q_0 \cos \chi - \alpha N_m^2 \tag{5}$$

a relation which has formed the theoretical basis of much of our work.

Since the investigations to be described in Part II of this paper have shown that the *E* layer exhibits a number of anomalies not to be expected in the case of a simple ionized region obeying (5), and certainly not accountable to the approximations made in deriving that relation, it is clear that we must question, instead, the physical assumptions on which this equation is based. It is therefore of value to consider, in a quite general way, what modifications of the original theory are possible.

Let us therefore examine the most general form of the basic continuity equation. This may be written

$$\frac{dN}{dt} = q(t) - d(N) - \text{div}\,(Nv) \tag{6}$$

VOL. 10 1957

Here $q(t)$ is the term relating to the rate of electron production, $d(N)$ indicates the electron disappearance rate, while div (Nv) is the electron transport rate per unit volume, outwards from the point in question. We shall discuss these three terms in order.

In an isothermal atmosphere, $q(t)$ may, as we have mentioned, be written as $q_0 \cos \chi$ for the level of maximum production in which we are interested. As CHAPMAN (1939) has shown, this is the case when the electrons are produced as the result of band absorption as well as in the case of ionization by monochromatic radiation. As (2) shows, however, the value of q_0 is dependent on H, which involves both the temperature and mean molecular mass of the atmospheric constituents ionized. Since rocket observations indicate the existence of a gradient of temperature at the level of the *E* layer, and since recent theoretical studies have suggested that the transition from mainly molecular to mainly atomic oxygen occurs at or near this same level, it is clear that some variation of q_0 with height is to be expected.

In simple Chapman theory, the term $d(N)$, expressing the magnitude of the electron disappearance rate, is written as αN^2, with α constant. We must, however, also envisage the possibility of an electron disappearance rate varying less rapidly with N. For example, BATES and MASSEY (1946, 1947) have shown that under certain conditions the process of dissociative recombination gives rise to a recombination coefficient which is itself inversely proportional to N. In such a case $d(N)$ becomes βN, where β is independent of N, but nevertheless may vary with the concentration of some particular atmospheric constituent and so be dependent on $\cos \chi$.

The introduction of a transport term into the continuity equation is an extension of simple ionized layer theory which has arisen in studies of the profoundly anomalous behaviour of the *F2* layer. MARTYN (1947a,b; 1948a,b), for example, has shown that one possible type of such transport is the vertical

drift of neutral ionization, due to the influence of a horizontal electric field operating athwart the horizontal component of the earth's magnetic field. It may, however, be pointed out that the transport term div (Nv) is a quite general one, covering the effects of diffusion, ionospheric winds, and change of atmospheric temperature, as well as of electrodynamic drift, vertical or horizontal. As regards the vertical drift effect discussed by Martyn, we may note that, if the E layer were the locus of the S_q (or the L, or the S_D) system of currents, we should expect the ionization distribution to be affected wherever the current has a component normal to the geomagnetic meridian. It may not be superfluous to add that one might expect, additionally, a species of vertical drift arising from the electrodynamic attraction of the neighbouring elements of the extended ionospheric current system. Such an effect would depend, not on the permanent geomagnetic field, but on the magnetic field arising from the current components themselves. Presumably such attraction would give rise to a concentration of ionization, because of the layer shrinkage in both horizontal and vertical extent. Its influence would, however, be expected to be small.

In concluding this introductory section we may anticipate briefly the main results of the work to be described in Part II. In the first place, it may be stated that the E layer exhibits a number of anomalies, or departures from simple region behaviour, which, although not, in the main, very large effects—and certainly not comparable with the flagrant departures from simple region behaviour found in the $F2$ layer—are nevertheless sufficiently marked, and consistent enough to warrant serious attention. Moreover, some of the most striking of these anomalies can be shown to be related in a very simple way to the S_q currents produced by the dynamo action of solar tidal movements in the upper atmosphere. Indeed, it has proved possible to estimate, at any rate tentatively, both the magnitudes and the height-gradients of the vertical drifts which these currents induce and by means of which they make their influence felt. These results bring new confirmation both to the theory of vertical drift in general, and also to the view, already widely favoured, that a major portion of the S_q current system does in fact flow within the E layer.

2. Some Relevant Theoretical Relationships

As a preliminary to our discussion of the experimental data in Part II of this paper, it is convenient to summarize certain theoretical relationships. These are of two types. In the first place there are the relationships which are based on the fundamental equation (3) and which therefore apply to a simple region; in the second place there are the relationships expressing the effect of changes in the basic assumptions of Chapman theory.

(a) *Formulae based on Chapman assumptions*

Appleton and Lyon (1955) have shown that an approximate solution of equation (3), for quasi-stationary conditions, is

$$N_m = \sqrt{\frac{q_0 \cos \chi}{\alpha}} \left(1 + \frac{\varepsilon}{2} - \frac{7}{8}\varepsilon^2 - A\right) \qquad (7)$$

where A is generally negligible, and where

$$\varepsilon = \frac{\tan \chi \dfrac{d\chi}{dt}}{2(q_0 \alpha \cos \chi)^{1/2}} \tag{8}$$

$$= \frac{\omega}{2(\alpha q_0)^{1/2}} \frac{\cos \phi \cos \delta \sin \omega t}{(\cos \chi)^{3/2}} \tag{8a}$$

ω being the angular velocity of the earth's rotation, t the solar-hour angle, ϕ the latitude, and δ the solar declination. It is easily shown that

$$\varepsilon \approx \frac{dN_m/dt}{\alpha N_m^2}$$

so that, as we have already mentioned, ε may be used as an index of the degree of approach to truly stationary conditions.

It has also been shown in the above-mentioned paper that ε is, to a first approximation, a measure of the "height-lag" between the level of maximum q and the level of maximum N. This follows, since $\tan \chi (d\chi/dt)$ is the rate of descent (or ascent) of the layer, and $\dfrac{1}{2(q_0 \alpha \cos \chi)^{1/2}}$ is its "relaxation-time" (Appleton, 1953).

We can calculate an approximate value for ε, using (4) and experimental values of dN_m/dt and N_m, provided we assume a value for the recombination coefficient α. Now, the value of α for the E layer is not yet well determined though the general evidence available suggests that it is not less than 10^{-8} cm^3/sec. If this is so, such calculations show that, in the E layer, ε is less than 1/10 for the greater part of the sunlit day (generally for all but, possibly, the first and last hours for which E-layer ionospheric measurements are available). Under such circumstances the last two terms on the right-hand side of equation (7) are negligible and the theoretical solution for N_m takes the very simple form

$$N_m = \left(\frac{q_0 \cos \chi}{\alpha}\right)^{1/2} + \frac{1}{4\alpha} \tan \chi \frac{d\chi}{dt} \tag{9}$$

Now, equation (9) is instructive in three ways. It shows us that N_m values are, generally, less in the forenoon (when $d\chi/dt$ is negative) than in the afternoon (when $d\chi/dt$ is positive). If, for example, we consider two hours (of true solar time) symmetrical relative to noon, when χ is the same, we have for the difference in ionization density values, ΔN_m,

$$\Delta N_m = \frac{1}{2\alpha} \tan \chi \frac{d\chi}{dt} \tag{10}$$

a quantity which steadily increases away from noon. The second point to be noticed is that ΔN_m depends only on α and on the position and movement of the sun; its value should not therefore vary with q_0 (e.g. during the sunspot cycle). The third result which may be obtained from (9) is that the average

VOL. 10 1957

value of N_m for two times (a.m. and p.m.) equally spaced relative to noon is given by

$$\overline{N_m} = \left(\frac{q_0 \cos \chi}{\alpha}\right)^{1/2} \tag{11}$$

a quantity which we may appropriately call the "stationary value" of N_m.

An alternative form of (10) which is useful in the comparison of theory and observation may be derived directly from (5), without quasi-stationary approximations namely

$$\Delta N_m = \frac{|dN_m/dt|}{\alpha \overline{N_m}} \tag{12}$$

where $|dN_m/dt|$ is the numerical magnitude of the mean rate of change of the ionization density at two corresponding times, a.m. and p.m., at which χ is the same. It will be readily seen that this result is essentially that used by APPLETON (1937) in his method of determining α from the diurnal variation of N_m, for which we have

$$\alpha = \frac{|dN_m/dt|}{\Delta N_m \, \overline{N_m}} \tag{13}$$

It is convenient at this point to include mention of the alternative method of determining α from the asymmetry of the diurnal curve of N_m. APPLETON (1953) has shown that, if Δt is the delay between noon and the time of maximum N_m, we can determine α from the relation

$$\Delta t = \frac{1}{2\alpha N_0} \tag{14}$$

where N_0 is the noon value of N_m.

(In the work to be described in Part II it will be seen that we have used both (13) and (14) in testing experimental data for the constancy, or otherwise, of α. In employing the second method it is found that visual determinations of Δt from diurnal curves of N_m are not very reliable, and we are indebted to Professor A. C. AITKEN for furnishing us with a set of formulae—quoted in the Appendix—by means of which Δt can be computed from the individual values of N_m at the five (or seven) hours centred on noon. These formulae are based on the determination of the best fitting parabola through the points in question. When Δt is determined in this way, the two methods of determining α, by way of equations (13) and (14), are not strictly independent. Indeed, the Aitken formulae use, in fact, weighted means of dN_m/dt and ΔN_m around noon, whereas, in the use of (13), individual values of these quantities are employed.)

Returning now to our basic equation (5), we note that the observational evidence shows that dN_m/dt has closely equal numerical magnitudes, albeit of opposite signs, at times symmetrical with respect to noon. This, again, indicates that

$$\overline{N_m} = \sqrt{\frac{q_0 \cos \chi}{\alpha}}$$

Thus, if we wish to check the relation between maximum ionization density and cos χ, the average, $\overline{N}_m$, should be used rather than N_m itself, thus eliminating any extraneous effects due to the dN_m/dt term. It is also worth noting that the same averaging procedure will simultaneously eliminate, for example, the anti-symmetrical harmonics of a tidal variation and also the effect of any influence which increases linearly in magnitude throughout the day.

(b) *Formulae based on variations from Chapman assumptions*

We now consider some theoretical relationships derived for non-Chapman-like conditions. We consider first, in this connection, the possibility that q_0 is not constant, and assume, as our first example of a departure from simple-region conditions, the existence of a finite gradient of scale height H with height h. Since the height of the level of maximum rate of electron production, q_m, varies with χ, any variation of H with height h will make q_0 effectively a function of χ. If, for example, there is a linear gradient of scale height given by

$$H = H_0 + \lambda h$$

VOL. 10 1957

then it can be shown that H varies as $(\sec \chi)^{\lambda}$ and (2) becomes

$$q_m = q_1(\cos \chi)^{1+\lambda} \tag{15}$$

where

$$q_1 = \frac{S_\infty(1+\lambda)}{H_0 \exp{(1+\lambda)}}. \tag{16}$$

In such a case the dependence of $\overline{N}_m$ on cos χ is expressed by

$$\overline{N}_m = \sqrt{\frac{\overline{q_1(\cos \chi)^{1+\lambda}}}{\alpha}} \tag{17}$$

which shows that the main effect, say, of an atmospheric temperature increasing with height is that the average ionization density varies more rapidly with cos χ than it does when the atmosphere is isothermal.

We now consider the possibility that α is not constant but varies with height. Let us suppose that the height gradient of α, expressed as a fractional increase per scale height, is, say,

$$\frac{H}{\alpha}\frac{\partial \alpha}{\partial h} = \mu, \tag{18}$$

where μ is small compared to unity, and will be assumed to be constant.

The condition for a spatial maximum of N, obtained from (1), is then that

$$\frac{\partial^2 N}{\partial h \partial t} = \frac{\partial q}{\partial h} - N^2\frac{\partial \alpha}{\partial h} \tag{19}$$

From the expressions derived by Appleton and Lyon (1955) it then readily follows that a, the departure of the N_m level from the q_m level, is given simply by

$$a = \varepsilon + \mu \tag{20}$$

and the fractional effect of this departure on N_m can be shown to be of the order $a^2/4$. If μ is, as postulated, a small quantity, this effect will be negligible and

(11) will still be valid. For the recombination coefficient α, however, (18) now yields

$$\ln \alpha = \frac{\mu h}{H} + \text{const.}$$

and since h/H varies as ln sec χ

$$\alpha = \alpha_0(\sec \chi)^{\mu}$$

where α_0 is a constant, and so

$$\bar{N}_m = \sqrt{\frac{q_0(\cos \chi)^{1+\mu}}{\alpha_0}} \tag{21}$$

showing that, under the conditions stated, the effects of λ and μ are identical.

So far then as studies of the variation of $\bar{N}_m$ with cos χ are concerned, it is not possible to distinguish experimentally between a variation of α and a variation of H with height. Thus any departure from simple Chapman behaviour in this connection may be interpreted as a variation of the ratio q_0/α or, more usefully perhaps, as a variation of the product αH (since q_0 varies inversely with H).

We now turn to consider the case where the process of electron disappearance also includes attachments of electrons to positive ions. Clearly our basic continuity equation must then be written

$$\frac{dN_m}{dt} = q_0 \cos \chi - \alpha N_m{}^2 - \beta N_m \tag{22}$$

where β is the attachment rate coefficient. If, again, we consider the case of two corresponding hours, a.m. and p.m., when χ is the same, we can show that, approximately

$$\Delta N_m = \frac{|dN_m/dt|}{\alpha \overline{N_m} + \frac{1}{2}\beta} \tag{23}$$

corresponding to (12) for the case of simple recombination. Similarly, we can write instead of (13)

$$\alpha' = \frac{|dN_m/dt|}{\Delta N_m \overline{N_m}} = \alpha + \frac{\beta}{2\overline{N_m}} \tag{24}$$

where α' is now the "effective" recombination coefficient.

Under the same conditions it can be shown that the time delay of the N_m maximum after noon is given by

$$\Delta t = \frac{1}{2\alpha N_0 + \beta} \tag{25}$$

where N_0 is the noon value of N_m, which leads to an expression for the "effective" recombination coefficient

$$\alpha' = \frac{1}{2N_0\, \Delta t} = \alpha + \frac{\beta}{2N_0} \tag{26}$$

Finally, we consider the modification of our basic continuity equation by

the inclusion of an electron transport term. If we limit ourselves to the case of *vertical* transport, our basic equation (6) becomes

$$\frac{dN_m}{dt} = q - \alpha N_m^2 - \frac{\partial v}{\partial h} N_m \tag{27}$$

which is formally equivalent to (22), except that the vertical drift gradient $\partial v/\partial h$ has replaced the β-term. Thus a *constant* vertical drift gradient, when positive, has the effect of simulating electron attachment; when such drift gradient is negative, it correspondingly simulates the process of electron detachment.

When, however, we come to the possible effects of circulating currents due, for example, to solar tides, we must consider the case where the vertical drift varies with time. For the quasi-stationary conditions which obtain in the E layer this matter has already been examined by APPLETON and LYON (1955), on the assumption that the third term on the right side of (27) is small compared with the other two, and we shall quote our earlier results here without proof.

From a practical point of view we are concerned with two effects of vertical drift, namely the *alterations* it provokes both in the atmospheric level of maximum electron density and in the magnitude of the maximum ionization density itself. We shall refer to these two departures from normality as $\delta h(N_m)$ and δN_m respectively. The appropriate expressions for these quantities given by APPLETON and LYON (1955) are as follows:—

VOL. 10 1957

$$\delta h(N_m) = \frac{v}{2\alpha N_m} \tag{28}$$

and

$$\frac{\delta N_m}{N_m} = -\frac{\dfrac{\partial v}{\partial h}}{2\alpha N_m} - \frac{1}{4H^2}\left(\frac{v}{2\alpha N_m}\right)^2 \tag{29}$$

where v is the velocity of vertical drift, $\partial v/\partial h$ is its vertical gradient (both measured positive upwards), and H is the scale height of the atmospheric ionized component responsible for the E layer. As will be readily seen, the alterations in both $h(N_m)$ and N_m depend only on the vertical drift characteristics and on $1/2\alpha N_m$, a quantity which APPLETON (1953) has identified as the "time of relaxation" of an ionized layer.

It may not be superfluous to add a word or two here concerning the physical interpretation of the expressions for $\delta h(N_m)$ and δN_m, in view of the importance we shall later attach to them. We may note, first, the contending nature of the two processes of vertical drift and electron production, in that vertical drift is constantly moving ionization away from the level at which it originates, while electron production is constantly tending to replenish it at that particular level. Equation (28) tells us that the operation of a vertical-drift velocity in altering $h(N_m)$ is cumulative in time over a period equal to the "time of relaxation" of the ionized medium, since the value of $\delta h(H_m)$ is, in fact, simply the product of the drift velocity and the relaxation time.

In the expression for the fractional change in N_m, given in equation (29),

there are two points to be noticed. The term involving the drift gradient, $\partial v/\partial h$, expresses the alteration in N_m due to layer distortion, the same ionization being, for example, spread over a greater vertical depth if $\partial v/\partial h$ is positive, with a consequent reduction of N_m. However, here again we note that, at any given moment, the layer exhibits the distortion accumulated over a period equal to the layer relaxation time. The second term on the right-hand side of (29) is intimately connected with the expression for $\delta h(N_m)$, since it expresses the diminution of N_m due to the movement of the level $h(N_m)$ above or below the level of maximum electron production. The amount of such a diminution naturally depends on the quantity $\delta h(N_m)$ expressed as a fraction of the layer semi-thickness, a quantity which is itself proportional to the scale height H. Now, the semi-thickness of an ionized layer is approximately $2H$, which gives point to the fact that the second term in (29) can be written $-[\delta h(N_m)/2H]^2$. A further matter of interest is that the same term expresses the nonlinear property of an ionized layer subject to a vertical drift velocity. It should, however, be added that this property of ionospheric nonlinearity is of a different type from that to which MARTYN (1947b) has drawn attention, which depends on the height gradient of drift velocity and not, as here, on the drift velocity itself.

To complete the discussion of the examples of vertical drift phenomena with which we may be concerned in E-layer studies, we add the relevant equations for conditions in which both a recombination process and an attachment process are simultaneously operative. If our continuity equation is, in such a case,

$$\frac{dN_m}{dt} = q_0 \cos\chi - \alpha N_m^2 - \beta N_m - \frac{\partial v}{\partial z} N_m \tag{30}$$

under quasi-stationary conditions, we find (corresponding to (28) and (29))

$$\delta h(N_m) = \frac{v}{2\alpha N_m + \beta} \tag{31}$$

and

$$\frac{\delta N_m}{N_m} = -\frac{\dfrac{\partial v}{\partial h}}{2\alpha N_m + \beta} - \frac{b}{H^2}\left(\frac{v}{2\alpha N_m + \beta}\right)^2 \tag{32}$$

where

$$b = \frac{1}{2}\frac{\alpha N_m + \beta}{2\alpha N_m + \beta} \tag{32a}$$

It is seen that, when β is equal to zero, equations (31) and (32) reduce, as they should, to (28) and (29), the equations for a pure recombination process. If, on the other hand, attachment only is operative, the same equations reduce,

$$\delta h(N_m) = \frac{v}{\beta} \tag{33}$$

and

$$\frac{\delta N_m}{N_m} = -\frac{\dfrac{\partial v}{\partial h}}{\beta} - \frac{1}{2H^2}\left(\frac{v}{\beta}\right)^2 \tag{34}$$

APPENDIX

Formulae for Noon Delay and Maximum of N_m

If any variable u has the experimental values u_{-2}, u_{-1}, u_0, u_1, u_2 for the values -2, -1, 0, 1, 2 of the independent variable t, the best-fitting parabola is

$$u = (a_0 + 2a_2) + a_1 t - a_2 t^2$$

where
$$a_0 = \tfrac{1}{5}(u_{-2} + u_{-1} + u_0 + u_1 + u_2)$$
$$a_1 = \tfrac{1}{10}\{(u_1 - u_{-1}) + 2(u_2 - u_{-2})\}$$
$$a_2 = \tfrac{1}{14}\{(u_{-1} - u_{-2}) + (u_0 - u_2) + (u_0 - u_2) + (u_1 - u_2)\}$$

Hence the maximum occurs for $t = \Delta t$ where

$$\Delta t = a_1/2a_2$$

and the difference Δu between the values of u at $t = 0$ and $t = \Delta t$ is

$$\Delta u = a_1^2/4a_2$$

For seven points, the above equations for a_0, a_1 and a_2 become

$$a_0 = \tfrac{1}{7}(u_{-3} + u_{-2} + u_{-1} + u_0 + u_1 + u_2 + u_3)$$
$$a_1 = \tfrac{1}{28}\{(u_1 - u_{-1}) + 2(u_2 - u_{-2}) + 3(u_3 - u_{-3})\}$$
$$a_2 = \tfrac{1}{84}\{3(u_{-1} - u_{-3}) + 2(u_0 - u_{-3}) + 2(u_0 - u_3) + 3(u_1 - u_3)\}$$

We are indebted to Professor A. C. Aitken for the above results.

References

Appleton E. V.	1953	*J. Atmosph. Terr. Phys.* **3,** 282.
Appleton E. V. and Lyon A. J.	1955	*Physics of the Ionosphere* Phys Soc., p. 20.
Bates D. R. and Massey H. S. W.	1946	*Proc. Roy. Soc.* **A187,** 261.
	1947	*Proc. Roy. Soc.* **A192,** 1.
Chapman S.	1931a,b	*Proc. Phys. Soc.* **43,** 26, 483.
	1939	*Proc. Phys. Soc.* **51,** 93.
Martyn D. F.	1947a,b	*Proc. Roy. Soc.* **A189,** 241; **A190,** 273.
	1948a,b	*Proc. Roy. Soc.* **A194,** 429, 445.

Journal of Atmospheric and Terrestrial Physics, 1957, Vol. 10, pp. 12 to 19. Pergamon Press Ltd., London

The absorption of short radio waves in the ionosphere

J. D. WHITEHEAD*
Cavendish Laboratory, Cambridge

(*Received* 28 *May* 1956)

Abstract—It is shown that the reflection coefficients (ρ) measured for radio waves on 2 and 4 Mc sec^{-1} reflected vertically from the ionosphere do not fit the expression

$$-\log \rho = A(f + f_L)^{-2} \tag{1}$$

appropriate to "nondeviative" absorption. Since the two frequencies mentioned did not approach near to critical frequencies at the time of the measurements, this failure cannot be ascribed to excessive "deviative" absorption.

If the measured values are inserted into the expression

$$-\log \rho = C + B(f + f_L)^{-2} \tag{2}$$

it is found that

(a) C varies with the sun's zenith angle but not with solar epoch.

(b) B is a very variable quantity, it depends on the solar epoch and is greatest in winter.

With values of B and C deduced from measurements on 2 and 4 Mc sec^{-1}, equation (2) gives a reasonable approximation to the measured values of ρ on 2·4, 3·2, and 4·8 Mc sec^{-1}.

It is suggested that waves in the frequency range 2 to 4·8 Mc sec^{-1} are appreciably absorbed outside the nondeviating region, where equation (1) is appropriate.

1. INTRODUCTION

OVER a period of several years, the reflection coefficient (ρ) of radio waves incident vertically on the ionosphere has been measured on a series of frequencies at Slough, and in a recent publication (APPLETON and PIGGOTT, 1954) it has been suggested that for frequencies (f) not too near those critical for one or other of the layers, the results can be represented by the expression

$$-\log \rho = A(f + f_L)^{-2} \tag{1}$$

where f_L is the longitudinal gyrofrequency and A is constant at any one time.

The conclusion has been drawn that the absorption occurs predominantly in a nondeviative region where the refractive index μ is nearly unity, so that theory (BOOKER, 1935) would lead us to expect the relation (1) to hold.

In this paper the published results of the Slough measurements are examined in detail, and it is concluded that they are not in fact well represented by an expression of the type (1). If, however, two particular frequencies are selected because they are least affected by the penetration of the layers, the results can be formally represented by the equation

$$-\log \rho = C + B(f + f_L)^{-2} \tag{2}$$

The magnitude of C gives a measure of the departure of the results for the selected frequencies from equation (1).

* Now at the Royal Aircraft Establishment, Farnborough

In this paper it is shown that the magnitudes of B and C vary in quite different ways with time, and it is suggested that this implies that equation (2) has some real physical meaning.

2. The Experimental Measurements

The Slough measurements at noon

It was decided to test relation (1) by concentrating attention on measurements made at noon on two frequencies chosen so that, over the greater part of the period under review, neither came near to the critical frequency of a layer. For this purpose the frequencies chosen were 2 and 4 Mc sec^{-1}. The waves of frequency 4 Mc sec^{-1} were usually reflected from the F region and the frequency was not too near either f_0F1 or f_0F2. On certain disturbed days, however, there was considerable group retardation on 4 Mc sec^{-1} and the absorption was exceptionally great: these occasions were excluded from the analysis by omitting the results for which the absorption on 4 Mc sec^{-1} exceeded that on 4·8 Mc sec^{-1} by more than 0·5 neper. Results for echoes which were reflected from sporadic E or were spread were also omitted.

VOL. 10 1957

The waves of frequency 2 Mc sec^{-1} were always reflected from the E layer at noon.

The tables published in the Slough bulletins for the years 1949–52 yielded 430 pairs of results spread over the four years after selection as described above. There were more results from winter than from summer, when sporadic E was more frequent.

When pairs of noon results were inserted into equation (1), they failed to satisfy it by an appreciable amount. They were then inserted into equation (2) and the magnitudes of B and C were determined. These results are discussed in Section 3.

The Cambridge measurements

The absorption was measured at Cambridge, using the pulse technique, at vertical incidence, in the usual way. The measurements extended through the whole of several separate days during the period January to December 1953. The frequencies used were 2 and 4·2 Mc sec^{-1}, and the measurements at noon agreed with those made at Slough. Half-hour averages of the reflection coefficient were used in the analysis described in Section 3.

3. Analysis of the Measurements

The magnitude of C

From all the Slough measurements the mean values of C and B in equation (2) were found to be 1·2 nepers and 28 nepers (Mc sec^{-1})^2, respectively. On the frequency of 2 Mc sec^{-1} the corresponding contributions to $-\log \rho$ were 1·2 and 2·8, and on 4 Mc sec^{-1} were 1·2 and 1·0. It is at once noticeable that the two contributions are of the same order. This fact alone shows that for these specially selected frequencies, equation (1) does not represent the facts well. The magnitude

of C varies as shown in Fig. 1, where each point represents the mean of one month's results.

It appears

(a) that C varies through the seasons with solar zenith angle χ, and

(b) that C does not alter appreciably with the epoch of the solar cycle.

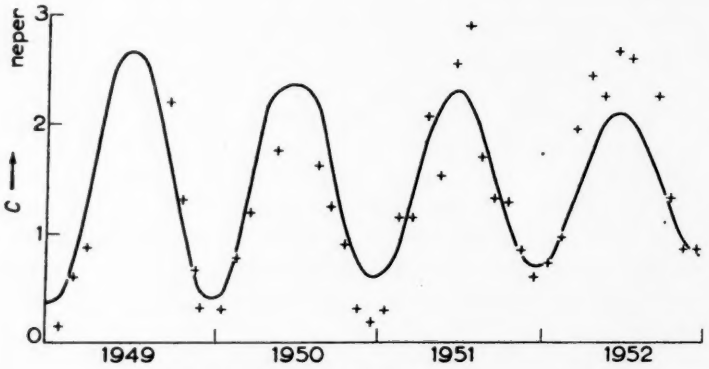

Fig. 1. The magnitudes of C and $C_{\min}$ through the years.

In Fig. 2 values of C determined from measurements made throughout the day at Cambridge are plotted against cos χ. Each point represents the average of ten separate half-hour's results at a fixed value of cos χ. χ varied both throughout

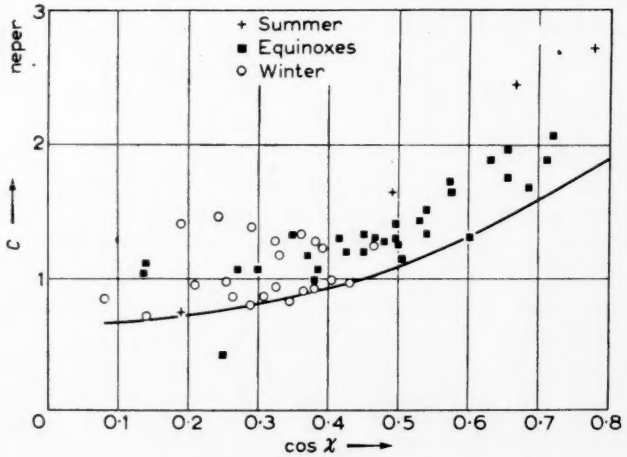

Fig. 2. The variation of C and $C_{\min}$ with cos χ changing through the day (1953).

the day and with season and the points are divided into three groups: summer (May to August), winter (November to February), and the equinoxes (the remaining four months). It is seen that the magnitude of C is determined by cos χ whether χ varies through the day or season.

The magnitude of B

Monthly mean values of B calculated from the Slough results are shown in Fig. 3. The most striking feature is the change with the epoch of the solar cycle.

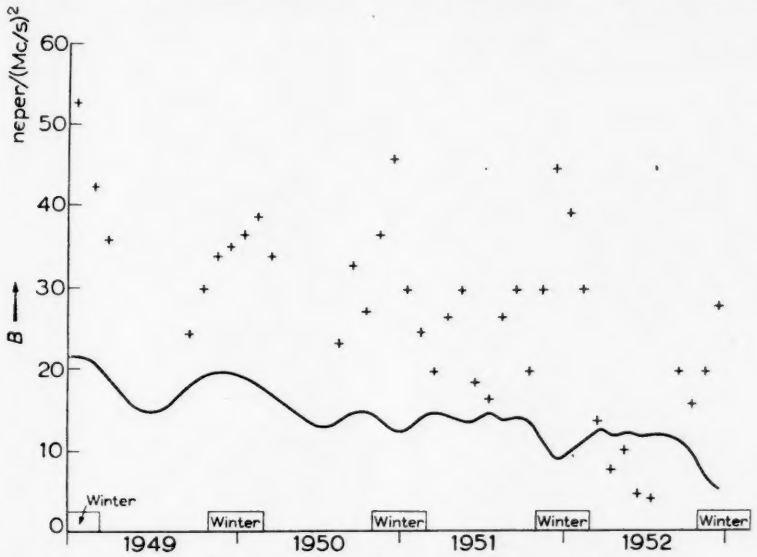

Fig. 3. The magnitudes of B and $B_{\min}$ through the years.

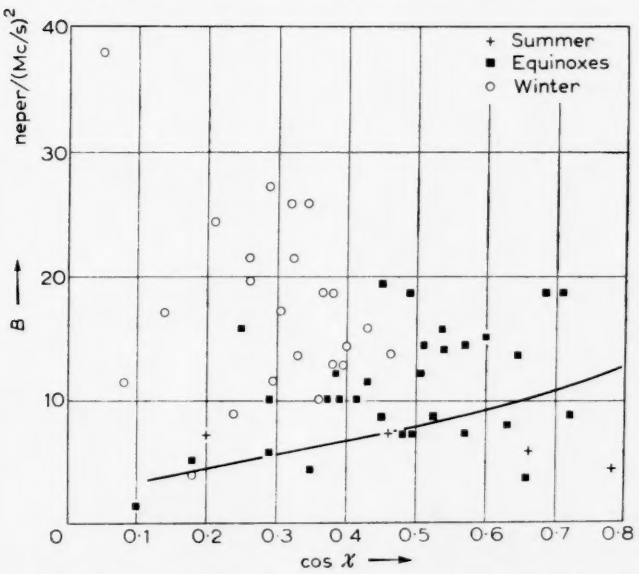

Fig. 4. The variation of B and $B_{\min}$ with cos χ changing through the day (1953).

The way in which B, calculated from the Cambridge results, depends on cos χ is shown in Fig. 4. In this figure, variations of χ are caused both by changes in the time of day and by changes of season. As before, the results appropriate to

VOL. 10 1957

the different seasons are shown separately. B is seen to depend mainly on the season, but not in any obvious way on χ.

The behaviour of B is seen to be quite different from that of C.

The minimum absorption

If all the acceptable values of $-\log \rho$ measured at noon for one of the frequencies

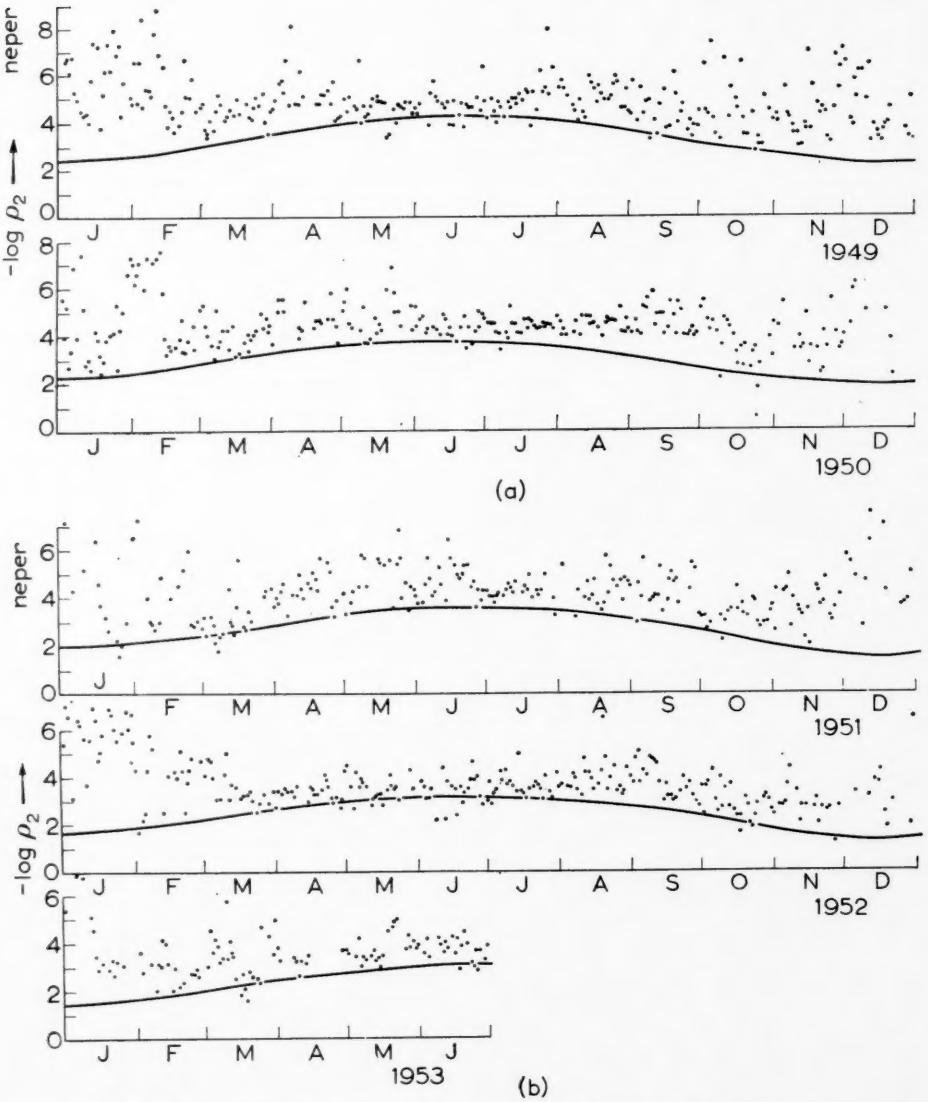

Fig. 5. The noon values of $-\log \rho$ for 2 Mc sec^{-1} plotted through the years, and the "minimum" absorption.

are plotted in the order of the days through the years, diagrams like Figs. 5 and 6 are obtained and it is clear that there is a wide spread of values. It is interesting to follow up the suggestion that the wide spread might be produced by the addition of some "sporadic" absorption superimposed on a certain irreducible minimum.

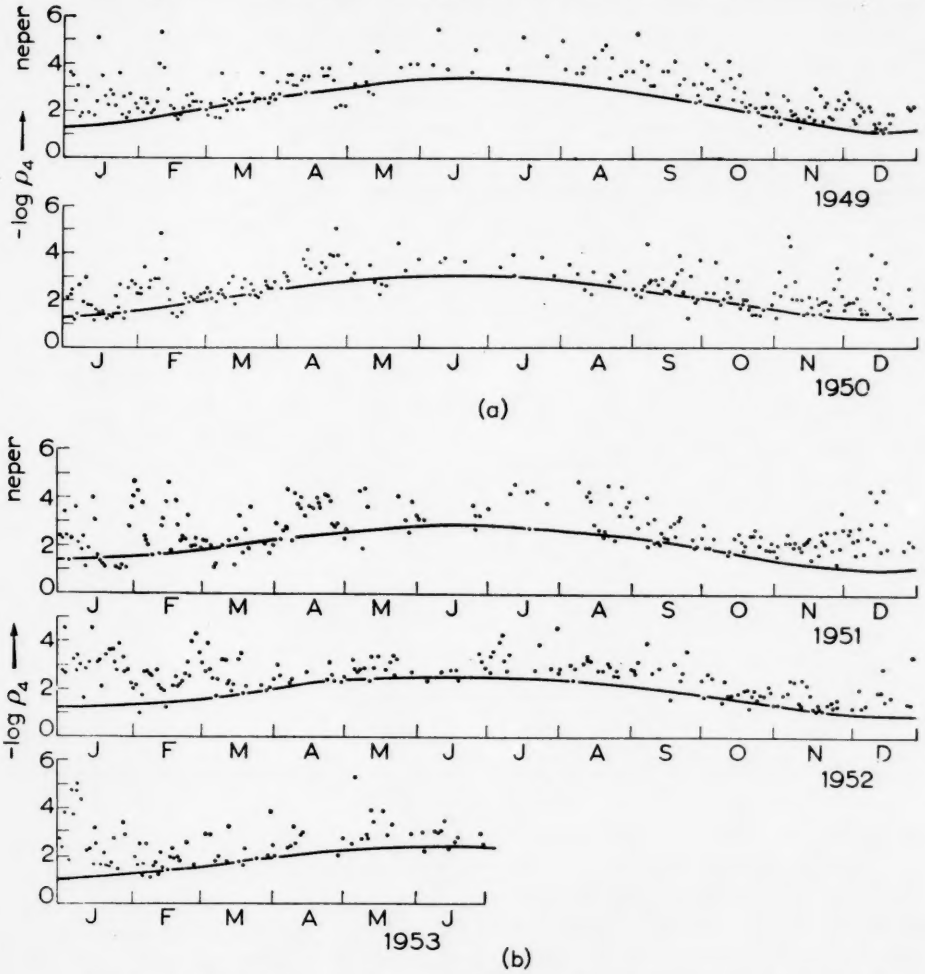

Fig. 6. The noon values of $-\log \rho$ for 4 Mc sec^{-1} plotted through the years, and the "minimum" absorption.

This minimum will be estimated by drawing smooth curves through the points of least absorption. These curves are shown in Figs. 5 and 6.

From these curves, the magnitude of $C_{\min}$ and $B_{\min}$ were deduced, using equation (2), and plotted as the continuous curves in Figs. 1, 2, 3, and 4. It is at once clear

(a) that C and $C_{\min}$ are nearly equal, and

(b) that B is often greater than $B_{\min}$, particularly in the winter months.

VOL. 10 1957

It thus appears that day-to-day variations in absorption can be ascribed to variations of B rather than C, and in particular that the large variations known to occur in winter correspond almost entirely to variations of B.

4. Results on Other Frequencies

There seems to be some real justification for dividing the absorption into two parts, one of which is independent of frequency, because then it is found, as shown in Section 3, that B and C vary differently with χ, with the seasons, and with the solar epoch. This appears to provide circumstantial evidence that they are associated with different parts of the ionosphere.

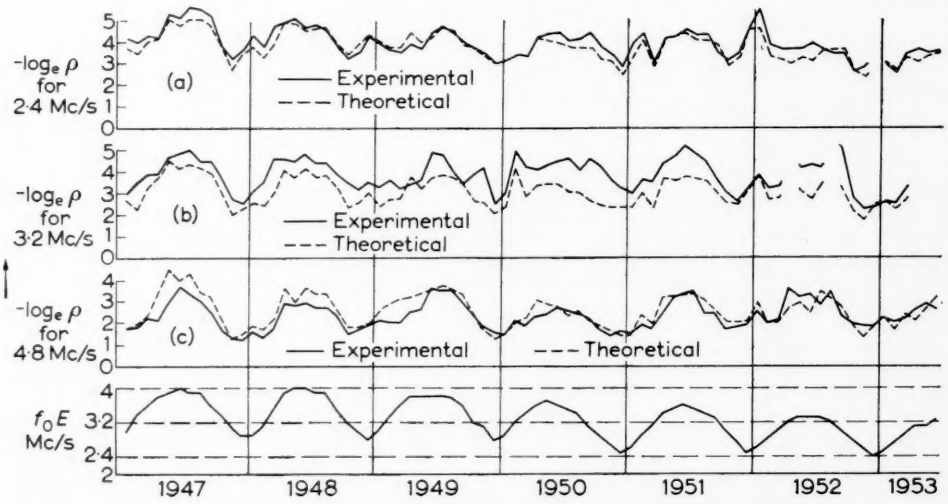

Fig. 7. Theoretical and experimental monthly means of $-\log \rho$ for 2·4, 3·2, and 4·8 Mc sec^{-1}.

On the expectation that the division into two parts as indicated by equation (2) might have some real meaning and that C would then be independent of frequency, it is interesting to use the monthly mean values of B and C derived from the experimental results on frequencies of 2 and 4 Mc sec^{-1} to deduce the mean values of $-\log \rho$ on other frequencies and to compare them with the results of the measurements. The results are shown in Fig. 7, where the broken curves show the values of $-\log \rho$ on 2·4, 3·0, and 4·8 Mc sec^{-1} calculated from the mean values of B and C, and the continuous curves represent the monthly means of the measured values. In finding these monthly means, spread echoes and those reflected from sporadic E were omitted. Only those days on which there were also acceptable measurements on 2 and 4 Mc sec^{-1} were used.

The corresponding values of f_0E are plotted in Fig. 7, and it is seen that there is quite good agreement between the calculated and observed values of $-\log \rho$ except when the working frequency was close to f_0E.

5. The Conclusions

The difference in behaviour of C and B suggests that the separation of the absorption into two parts has some real physical meaning. The significance of this result is being investigated.

The abnormally great and sporadic absorption in winter arose from an increase in the term B rather than from any change in C. The winter anomalous absorption must therefore have arisen in a region where the absorption is proportional to $(f + f_L)^{-2}$, i.e. in the D region. This is in agreement with the conclusions of Dieminger (1952) and Gnanalingham and Weekes (1954) from more direct evidence.

Acknowledgements—The work described in this paper was carried out at the Cavendish Laboratory, Cambridge. The author gratefully acknowledges the receipt of a Maintenance Award from the Department of Scientific and Industrial Research and of a Studentship from Gonville and Caius College. The author also wishes to thank Dr. J. W. Findlay for his help and encouragement.

VOL.
10
1957

References

Appleton E. V. and Piggott W. R.	1954	*J. Atmosph. Terr. Phys.* **5**, 141.
Booker H. G.	1935	*Proc. Roy. Soc.* **A150**, 267.
Dieminger W.	1952	*J. Atmosph. Terr. Phys.* **2**, 340.
Gnanalingham S. and Weekes K.	1954	*The Physics of the Ionosphere* (Phys. Soc.), p. 63.

Journal of Atmospheric and Terrestrial Physics, 1957, Vol. 10, pp. 20 to 31. Pergamon Press Ltd., London

The nondeviative absorption of high-frequency radio waves in auroral latitudes

SYDNEY CHAPMAN* and C. GORDON LITTLE†

(*Received* 4 *September* 1956)

Abstract—In auroral latitudes the nondeviative absorption of high-frequency radio waves is much more irregular, and often much stronger, than in subauroral latitudes. It is greater and more frequent by day than by night; this is the converse of the daily variation of magnetic activity. The electrons that produce the absorption in subauroral latitudes are mainly caused by solar ultra-violet light; in auroral latitudes, often the major source is bombardment of the atmosphere by solar gas.

According to J. A. VAN ALLEN's new interpretation of the soft radiation observed by himself and his colleagues in auroral latitudes, down to 50 km, a small minority of the primary bombarding particles generate X rays, which penetrate further than the particles themselves. It is here suggested that the layer ionized by these X rays is an important factor in the daytime radio absorption. Also, as D. R. BATES has pointed out, Lyman-alpha radiation will be generated by the auroral protons; ionization of nitric oxide molecules by this radiation may also contribute appreciably to the absorption. The same processes of ionization will occur likewise at night, and often still more strongly; however, loss of the electrons to form negative ions by attachment is countered by photodetachment during the day, but not at night. Very tentative tables are given, based on these ideas, indicating ionospheric conditions consistent with greater daytime absorption than at night, even when the nighttime bombardment is twenty times more intense than that by day. The corresponding absorption relaxation times, and daily variation of magnetic disturbance, will be examined in a later note.

1. NONDEVIATIVE ABSORPTION

THE magnetoionic theory of radio propagation (APPLETON, 1932, 1937; BOOKER, 1935; FARMER and RATCLIFFE, 1935) gives the following formula for the nondeviative absorption of the ordinary component of radio waves of high frequency (HF)‡: the absorption is expressed as D decibels:

$$D = -10 \log_{10} (p/p_0) = A/F_e^2, \tag{1}$$

where p_0 and p are the power fluxes at the initial and end points P_0, P of the path considered, and

$$F_e = F + F_L; \tag{2}$$

F and F_L are the radio and gyromagnetic frequencies expressed in Mc/s;

$$F_L = 10^{-6} eH_L/2\pi mc = 2{\cdot}80 H_L, \tag{3}$$

where c, m, e denote the speed of light, and the mass and charge (e.s.u.) of the electron; H_L denotes the geomagnetic field component (gauss) along the direction of radio propagation. Also

$$A = (20 \log_{10} 2{\cdot}718) \times 10^{-12} e^2 I/2\pi mc = 1{\cdot}17 \times 10^{-14} I, \tag{4}$$

where

$$I = \int \frac{N\nu \, ds}{1 + 10^{-12}\nu^2/4\pi^2 F_e^2}, \tag{5}$$

the integration being taken along the path P_0P traversed by the radio waves; N

* Geophysical Institute, College, Alaska; and High Altitude Observatory, Boulder, Colorado.

† Geophysical Institute, College, Alaska.

‡ Namely 3 to 30 Mc/s, in the nomenclature given (p. 45–11) in *The Radio and Television Engineer's Handbook*, Newnes, London, 1954.

and ν denote the number density and collision frequency of the electrons at each point along the path. Thus the frequency F_e is involved in (1) implicitly in A as well as explicitly.

For HF waves $F_e > F > 3$; hence if ν is small compared with $6\pi \times 10^6$ or 2×10^7, (5) reduces approximately to

$$I = \int N\nu \, ds, \tag{6}$$

and A is independent of F_e and F. Also, (4) gives

$$I = 8{\cdot}56 \times 10^{13} A = 8{\cdot}56 \times 10^{13} \, DF_e^{-2}. \tag{7}$$

2. The Collision Frequency

The laws of interaction between slow electrons and the neutral particles of the atmosphere (N_2, O_2, O, etc.) are not properly known; hence the values of ν in the ionosphere are uncertain on this account, as well as because the atmospheric temperature T and the number densities n of the atmospheric constituents are imperfectly known. Nicolet (1953) gives the formula

$$\nu = 5{\cdot}4 \times 10^{-10} n T^{\frac{1}{2}} \tag{8}$$

for levels below about 100 km, where the air is not much dissociated, and where electronic collisions with ions are relatively few; here n signifies the total particle number density. Using the Rocket Panel (1952) data for T and n, (8) gives the following valies of ν, which will be used in the subsequent discussion.

Table 1. The electron collision frequency

Numbers here expressed as a^b signify $a \times 10^b$.

Ht., km	40	45	50	55	60	65	70	75	80	85	90	95	100	105
ν	$7{\cdot}6^8$	$4{\cdot}0^8$	$2{\cdot}1^8$	$1{\cdot}2^8$	$6{\cdot}2^7$	$3{\cdot}3^7$	$1{\cdot}6^7$	$7{\cdot}6^6$	$3{\cdot}4^6$	$1{\cdot}5^6$	$6{\cdot}7^5$	$3{\cdot}1^5$	$1{\cdot}5^5$	$7{\cdot}1^4$

Some radio observers have given higher values of ν than those in Table 1; e.g., Shaw (1951) gave $1{\cdot}8 \times 10^6$ as the value at 90 km, nearly three times as great as the value given above. Nicolet regarded these values as excessive. The difficulties in inferring ν from radio measurements concern the accuracy of the formulae used and the attribution of the heights to which the results correspond. The formula (8) is also uncertain, perhaps by more than 25%.

In Section 3 values of ν are quoted (Table 2) for greater heights; these are taken from Chapman (1956), and are also uncertain. But materially greater values of ν in Tables 1 and 2 would seem inconsistent with the observed amount of nondeviative absorption in the ionosphere.

3. Nondeviative HF Radio Absorption in Subauroral Latitudes

Geomagnetic (gm) latitudes above 60°, and those between 60° and 45°, will be called respectively auroral and subauroral. The nondeviative absorption of HF radio waves in subauroral latitudes is illustrated by the valuable study made in southern England (latitude 52°, gm lat. 54°) since 1935, recently summarized and discussed by Appleton and Piggott (1954); the letters AP will be used to indicate reference to this paper.

In this case F_L is 1·16 (AP, p. 151). Their values of F range from 2 to about 5; hence their F_e is at least 3·16. Their measurements of D as a function of F_e fit the relation (1) with a value of A which is independent of F over the stated range of F. Hence (cf. Table 1 above) they conclude (p. 167) that the absorbing region lies mainly above 80 km. They show also that it lies below the E layer.

The factor A varies with the time of day, the season, and the sunspot cycle. The relation between the daytime values of A and the hour and season is illustrated (AP, Fig. 12) for the average over the period 1945–1948; A has a daily maximum at about 20 min after noon; its maximum value ranges from about 400 in mid-winter to rather more than 500 in midsummer. The corresponding absorption for 4-Mc/s waves is from 15 to about 20 dB. Near sunrise and sunset A falls below about 50.

The daily and seasonal variation of A is given approximately in terms of the solar zenith angle χ by C^n, where C densities $\cos\chi$ or $1/Ch(R, \chi)$—(CHAPMAN 1931; WILKES 1954)—according as the solar elevation is large or small (AP, p. 153, and Fig. 7); the exponent n has a mean value 0·75, with few values outside the range 0·6 to 0·95; it appears not to vary with the sunspot cycle (AP, p. 155).

In any one calendar month, over a series of years, the noon value of A varies nearly linearly with the annual mean sunspot number R: that is,

$$A_{\text{noon}} = \alpha + \beta R. \tag{9}$$

Both α and β are least in winter and greatest in summer: α increases from 230 in December to about 350 in July, and β from about 2 in midwinter to 3 in midsummer. These sunspot-cycle variations differ significantly from those of the peak electron densities in the E layer (AP, pp. 149, 150).

However, in the winter months (in every year from 1935 onwards) A has values anomalously great, by a factor of 2 to 3, on certain groups of days (AP, Fig. 9). APPLETON and PIGGOTT state (p. 164) that DIEMINGER (1952) finds these anomalies to be associated with weak reflections from low heights, of the order 75–90 km; such reflections occur on about one day in sixty in summer, but are much more frequent in winter. The above exponent n is also higher on such anomalous days (AP, p. 169). The winter variability of A is one indication (AP, p. 167) that the absorption does not occur mainly in the E layer, whose ionization does not show such winter irregularities. They conclude (p. 158) that there is a real physical change in the absorbing layer during such winter anomalies of A. "To account for this additional absorption in winter there would appear to be only two possibilities —either an additional ionizing source is present," or some agency is operating that redistributes the ionization so as to increase the integral I of Nv (AP, p. 169). They comment (p. 169): "we consider it unlikely that the excess absorption is caused by particle radiation, though we do not yet feel that this possibility can be entirely ruled out"; they noted also (p. 169) that the winter anomaly of A occurs in the Falkland Islands (gm lat. 40°), but not at Singapore. They note also (p. 165) that the winter anomaly seems to be slightly correlated with magnetic *calm*.

The July noon value of A, about 520, corresponds to

$$I = \int Nv\, ds = 4{\cdot}45 \times 10^{16}, \tag{10}$$

and to a solar zenith angle χ of 28°; hence $ds = (\sec 28°)\, dh = 1{\cdot}13dh$. As the waves whose absorption is observed have been reflected back to the ground in either the E or the F layer, the main absorbing layer, below both E and F, has been twice traversed; hence $\int N\nu\, ds$ integrated once through this absorbing region will have half the above value, namely $2{\cdot}2 \times 10^{16}$, and $\int N\nu\, dh$ will be $2{\cdot}0 \times 10^{16}$. The following table gives a tentative distribution of N and ν by which such a value of I might be provided. Up to 120 km the height sections are 10 km thick, above that level greater thicknesses are taken.

Table 2. Tentative electron distribution at latitude 52°, consistent with summer noon radio absorption data. Numbers here expressed as a^b signify $a \times 10^b$

Ht.	60	70	80	90	100	110	120	150	200	250	300	Combined integrals		
												Up to 105 km	105–325 km	Above 325 km
dh	55–65	65–75	75–85	85–95	95–105	105–115	115–125	125–175	175–225	225–275	275–325			
N	10	50	600	$6{\cdot}5^3$	$1{\cdot}5^4$	$3{\cdot}2^4$	1^5	$1{\cdot}5^5$	$2{\cdot}5^5$	4^5	6^5			
ν	$6{\cdot}2^7$	$1{\cdot}6^7$	$3{\cdot}4^6$	$6{\cdot}7^5$	$1{\cdot}5^5$	$3{\cdot}5^4$	$1{\cdot}0^4$	2^3	8^2	6^2	5^2			
$10^{-15}N\nu\, dh$	0·6	0·8	2·0	4·4	2·2	1·1	1·0	1·5	1·0	1·2	1·5	10·0	7·3	2·7

These numbers are uncertain, especially as regards ν, not only for the reasons given in Section 2, but also because the height distribution of density and temperature over southern England may differ significantly from that over New Mexico, to which the Rocket Panel results refer. However, English meteor evidence (EVANS, 1954) indicates nearly the same scale heights over the range 85–105 km.

According to the above tentative table, half the absorption occurs below 105 km, and the rate of absorption is greatest around 90 km.

4. NONDEVIATIVE ABSORPTION IN AURORAL LATITUDES

Radio absorption has been studied since March 1954 at College, Alaska (64·9° N, 167·8° W; gm lat. 64·5°), in the auroral region, about 275 km south of the maximum isochasm. At College, H_L for vertical incidence is 0·55 gauss, and F_L is 1·54.

The first such observations at College, continued for two months only (LITTLE, 1954), were made on 65-Mc/s natural radiation from celestial sources. Ionospheric sounding equipment (C-3) was also operated. LITTLE showed (l.c., Fig. 2) that there is great similarity, as regards daily variation of *frequency*, between polar blackouts observed with the C-3 equipment, and strong absorption (at least 10%, or 0·9 dB) of the 65-Mc/s radiation; such strong absorption was experienced for about a tenth of the time.

The 65-Mc/s radiation traversed the whole ionosphere once only; the C-3 man-made reflected radiation, if not absorbed, would pass twice through the part of the absorbing region that lies below the level of reflection. For waves that, if not absorbed, would be reflected by the E layer, the absorption must occur below the

VOL. 10 1957

E peak. For waves of a few Mc/s, such as are there reflected, the absorption corresponding to 1 dB for 65-Mc/s waves must amount to a blackout.

The daily frequency curves in LITTLE'S Fig. 2 have a main maximum shortly after noon, from which there is a steep descent towards the evening; after midnight there is another, rather smaller, maximum of frequency.

Since summer 1954 the studies of absorption of natural radiation at College have been continued on 30 instead of 65 Mc/s. The receiving antenna is directed towards the zenith; its cone of reception, to half power, is about 60° wide.

The absorption over southern England, discussed by APPLETON and PIGGOTT (1954), may be ascribed mainly to ionization produced by ultra-violet solar radiation. Over College the corresponding ionization must be smaller, because the sun's zenith angle is on the average greater than over southern England. The subauroral average noon value (450) of A for southern England must correspond to a value at College reduced in the ratio $(\cos 64{\cdot}9°/\cos 52°)^{0{\cdot}7}$, namely 345; for 30-Mc/s waves that traverse the (whole) ionosphere *once* only, as at College, this would correspond to an auroral average noon absorption of about 0·2 dB.

Actually the observed absorption (D dB) of 30-Mc/s waves at College often has much higher values. The greatest absorption is observed for brief intervals during the equinoctial months, when the peak values of D may reach or even exceed 10 dB by day, or 5 dB by night. The *variations* of absorption, as well as the peak values, are greatest at the equinoxes; in winter the variability of the absorption exceeds that observed in summer, but is below the equinoctial level.

For $D = 10$ dB at 30 Mc/s, the integral I through the absorbing region must equal 8×10^{17}—about forty times the maximum noon value for southern England.

At College D varies very irregularly, and intervals of strong absorption may occur at any hour of the day and night. As in the case of the 65-Mc/s absorption, the occurrence of strong attenuation of 30-Mc/s waves is highly correlated with the occurrence of large values of $f_{\min}$ and of polar blackouts recorded by the C-3 equipment. Both are most frequent during the equinoctial months, as are strong auroral and magnetic activity. These and other features of the absorption imply that the associated ionization of the upper atmosphere is produced by the entry of solar particles into the atmosphere.

At College the US Coast and Geodetic Survey maintains a magnetic observatory, which gives 3-hour K indices of magnetic activity based on its records. These indices (K_c) have been compared with the *maximum* values of D during the corresponding 3-hour periods; they show a high correlation (the coefficient r is 0·7 to 0·8). A similar good correlation is found between the College values of D and the 3-hour magnetic indices (K_s) given by the magnetic observatory at Sodankyla (67·4° N; 26·6° E; gm lat. 63·8°); Sodankyla is at almost the same gm latitude as College, but differs from it in longitude by 174° geographic or 135° gm. This latter observation suggests that the atmosphere is bombarded simultaneously above College and above Sodankyla, i.e. on the nighttime and the daytime sides of the auroral zone.

However, the daily variation of the mean value of K_c has a maximum near local midnight, whereas on the average D is greatest near local noon.

Daygraphs showing the average daily variation of the *frequency* of absorption

on 30 Mc/s at College have been drawn for each calendar month. They clearly indicate a solar control of the absorption, which is most frequent and intense during the daylight hours. But this control is not the simple regular control described for southern England in Section 3.

The auroral luminosity when brightest is usually distributed irregularly over the sky, and is often confined to areas extended along relatively thin arcs or bands. This suggests that the extraterrestrial particles enter the atmosphere in these restricted regions; the associated primary ionization is likely to be produced in the same regions. If the ionization lasts longer than the luminosity, it may be more widespread, when the luminous bombarded area moves across the sky, as commonly happens.

Radio absorption measurements have been made at College also with a rotating antenna whose main lobe of reception has a low elevation; they have shown that the absorption is often not uniform around the sky—in particular, round a circle whose radius at 100-km height is about 400 km; this result agrees with expectation based on the auroral appearances.

VOL. 10 1957

Thus it is likely that over the considerable area of the absorbing region included within the 60° cone of reception of the 30-Mc/s waves at College, there will be marked differences in the absorption, or in the value of the integral I. There may be strongly ionized patches where the absorption is effectively complete, surrounded by less-absorbing areas. However, the observation that at times the intensity of 30-Mc/s waves received in auroral latitudes is cut down by a half (corresponding to $D = 3{\cdot}0$ dB) indicates that on such occasions at least half the "viewed" area is affected by the absorption. This suggests a distribution of ionization more widespread than the auroral luminosity. Additional equipment recently brought into use, with a narrower cone of reception, will throw further light on this question of the uniformity of distribution of the absorbing region.

Some cases of simultaneous strong radio absorption and notable magnetic and earth-current fluctuations have been observed; but in the daytime there may be considerable radio absorption unaccompanied by much magnetic disturbance.

During sudden ionospheric disturbances (SID's) associated with solar flares, the natural radio waves observed at College show absorption to a degree corresponding with the associated solar zenith angle; but it by no means attains the high intensities above mentioned.

5. Interpretation of the Absorbing Region

The results quoted in Section 4 suggest that auroral agents from time to time enhance the electron density distribution so as to increase the value of the integral I up to forty times its undisturbed (solar ultra-violet) noon value.

Visual observation of the aurora, at nighttime, indicates that the luminosity is usually greatest between heights of 100 and 110 km, although it extends downwards with diminishing intensity to 90 km or so. The ionization directly produced by the incoming particles seems likely to be distributed in a somewhat similar way.

When the auroral and magnetic activity, for example around midnight, is not too intense, radio waves of frequencies up to 3 Mc/s are reflected by an abnormal nocturnal "E" layer at about 100 km. But during intense auroral and magnetic

disturbance, the C-3 radio waves are absorbed below this level, and are not received with measurable intensity. Until more powerful beams are used to explore the peak electron density N in this region, the peak levels and peak values must remain uncertain, or await determination by rocket-borne instruments. The presence, at such times, of intense electric currents along the auroral zone, as inferred from surface magnetic data, suggests that N may attain very large values, possibly as much as a hundred times the normal daytime peak value observed at College. Owing to the value of the collision frequency at this level, however, a hundredfold increase in N would not increase I in that proportion (see Table 2); if N were increased in the same proportion at all levels, a factor of 50 would suffice to increase I fiftyfold; if N were increased preferentially at heights below 90 km, its factor of increase could be still smaller.

The luminosity and accompanying ionization indicated by visible auroras are decidedly patchy; the width of auroral arcs and bands, in angular elevation in the gm north-south direction, is often confined to a few degrees.

Three main questions may be posed:

(a) Can the absorbing ionization be created at a level below the visible aurora?

(b) Why does the absorbing ionization appear to be more widespread over the sky than is the visible aurora?

(c) Why is the auroral absorption more prominent by day than by night, whereas magnetic activity has its maximum around midnight?

6. The Layer Ionized by Auroral X Rays

It seems likely that the answers to these questions are connected with the remarkable discovery that in auroral latitudes an ionizing radiation, much softer than cosmic rays, penetrates to levels as low as 50 km, or even 40 km (VAN ALLEN, private communication). This discovery was made by VAN ALLEN and his colleagues of the Physics Department of the State University of Iowa (MEREDITH, GOTTLIEB, and VAN ALLEN, 1955; VAN ALLEN, 1955, and other papers there cited). They used Geiger counters carried on a rockoon (or rocket launched from a balloon) up to about 100 km; ascents were made in gm latitudes ranging from 54° to 84°. In the auroral region, between gm latitudes 65° to 77°, in ten out of twelve flights the soft "auroral" radiation was detected; at the higher levels the radiation showed spatial nonuniformities of intensity on a scale of a few kilometres. At first this radiation was interpreted as being the high-energy "tail" of the energy distribution of the auroral particles; for penetration down to 50 km, the energy required by this interpretation was 1 MeV for electrons, and about 20 MeV for protrons.

Recently VAN ALLEN (1955) has revised this interpretation, in a way that much reduces the demands on the inferred energies. With the support of laboratory experiments, he now ascribes the rockoon Geiger counts to the action of X rays (Bremsstrahlung) generated by auroral (extraterrestrial) electrons with energies ranging from 10 to 100 keV—but probably lying mainly in the lower half of this range. At levels below about 80 km these counter-detected X rays come from impacts of the auroral electrons with atmospheric atoms higher up; above about 80 km some of the observed X rays may be generated in the rockoon nose by direct

impact of the primary auroral electrons; the spatial irregularity of the X rays at these higher levels gives further evidence that the injection of the electrons into the atmosphere is patchy.

Electrons of energies 10, 50, and 100 keV have ranges in air (NTP) of 0·2, 3·5, and 11·5 cm. These correspond to penetrations down to about 107, 87, and 79 km. Most of the auroral electrons whose occurrence is inferred from the rockoon measures will thus be stopped at or above the usual lower border of auroral luminosity. There they contribute by direct impact ionization to the electron density of the upper D and the lower E layer.

About 1 electron in 1000 will give rise to an X-ray photon; the energy of the photon may equal the whole, or any fraction, of the energy possessed by the generating electron at the level of its impact with the atmospheric atom in which the generation occurs. The upper limit of the photon energies is inferred by VAN ALLEN to be about 100 keV, with perhaps 30 keV as an average value. The X rays are emitted in all directions, but mainly in the forward direction, within a rather wide-angled cone around the direction of impact of the electron. Their ranges in air considerably exceed those of the electrons that generate them, whose influence is thereby extended to much lower levels than they themselves reach.

VOL. 10 1957

The X rays ionize and excite the air particles along their path. The average energy expended per electron-ion pair produced is about 40 eV, much the same as for the pairs directly produced by the auroral electrons. Hence about 1000 electrons are produced per X-ray photon. But for each X-ray photon produced, the number of ion-electron pairs directly produced by electrons that do not generate X rays will be of order 10^6. VAN ALLEN estimates the X-ray photon flux to be of order 10^5 photons/cm^2 sec. This corresponds to X-ray production of electron-ion pairs at the rate 10^8/cm^2 sec.

The region directly (and patchily) ionized by the auroral particles probably has a lower border between 80 and 90 km. The particles will be mainly protons and electrons—the electrons seem to be the more penetrating. The X rays produce a lower and more weakly ionized layer extending down to about 40 km.

As Table 1 indicates, ν increases by a factor of about 100 between 85 and 55 km. This factor is less than the ratio (about 1000) of the number of electrons that ionize directly, to the number of those that produce X rays. Hence the contribution to $\int N\nu\, ds$ made by the directly ionized layer will probably be decidedly greater than that made by the X-ray ionized layer; in the lower reaches of the latter layer the extra factor in the integrand of I will reduce the contribution to I. But whereas the directly ionized region will be patchy, with practically complete absorption (for 30 Mc/s waves) in some regions, surrounded by nonabsorbing (or transparent) areas at the same level, the underlying X-ray ionized region will have a more uniform horizontal distribution. Hence this X-ray ionized region may be a main cause of the absorption observed with a wide-angle receiving antenna, such as that so far used at College. It may therefore help to provide the answers to the first two questions, (a) and (b), posed at the end of Section 5.

D. R. BATES (1956) has pointed out an additional source of ionization by auroral particles, beyond that produced by their direct impacts. This source is the Lyman-alpha radiation emitted by the auroral protons during the intervals in their

descent in which they have become neutralized to hydrogen atoms. They are observed to emit H-alpha radiation, and hence their emission of L-alpha radiation can be inferred. The usual level of penetration of these heavy auroral particles probably lies above 95 km. Their L-alpha radiation will be emitted in all directions, and may be appreciable down to levels of 75 or even 70 km. It may be that the rate of ion-electron pair production, Q/c.c. sec, may have two levels of maximum, one determined by the heavy auroral particles, the other by the electrons. The ratio of the contributions made by the electrons and by the heavy particles cannot yet be stated.

7. The Daytime Maximum of Radio Absorption in Auroral Latitudes

The third question posed at the end of Section 5 concerned the contrast between the *daytime* maximum of radio *absorption*, in frequency and intensity, and the *nighttime* maximum of *magnetic* and auroral activity.

The answer here suggested is that below about 100 km the electrons become increasingly attached to form negative ions; but that in the daytime the ratio of electrons to negative ions is raised, as compared with nighttime, by photodetachment. Hence the same primary bombardment produces a weaker absorbing layer by night than by day. This effect is supposed sufficient to outweigh that of a greater flux of primary particles at night.

The rate coefficients of the various processes involved in the D layer are not known, hence the hypothesis here stated cannot yet be properly checked. All that will be attempted here is an *ad hoc* numerical solution showing how the observed effects might be produced. In view of the many uncertainties, various minor factors will be ignored: such as the ionization due to ultra-violet light: possible changes in the atmospheric temperature and the rate coefficients as between day and night: also collisional detachment, as this is likely to be about the same throughout the 24 hours.

Thus the equations of change of the electron density N and the positive and negative ion-densities N_+, N_- are taken to be:

$$\frac{dN_+}{dt} = Q - \alpha_e N N_+ - \alpha_- N_- N_+ \tag{11}$$

$$\frac{dN}{dt} = Q - \alpha_e N N_+ - \eta n N + \rho S N_- \tag{12}$$

$$\frac{dN_-}{dt} = \eta n N - \rho S N_- - \alpha_- N_- N_+ \tag{13}$$

The suffix n or m added to symbols in these equations will indicate reference to noon and midnight respectively. These equations are to be solved in conjunction with the equation of electrical neutrality, $N_+ = N + N_-$.

The symbols used in (11-13) have the following meanings: α_e and α_- are respectively the recombinances (or recombination coefficients) for collisions between electrons and positive ions, and between negative and positive ions. The attachment coefficient is denoted by ηn, where n denotes the number density of the

particles to which the electrons attach themselves; ρS denotes the photodetachment coefficient, S being the intensity of the solar radiation involved in the process; Q denotes the rate of production of electron-ion pairs. The notations agree with those used by BATES and MASSEY (1946) and MASSEY and BURHOP (1952), except that they use ρ for what is here denoted by ρS. The factor S, here introduced, will vary with latitude, season, and time of day; it is likely to refer to red or infra-red solar radiation, which will only be slightly absorbed, so that S may not vary much with height in the atmosphere.

Sets of values of Q and the N's are presented in Table 3, for the epochs of noon and midnight, that are consistent with (11–13), assuming a quasisteady state in each case, so that the d/dt terms are set equal to zero.

It is supposed that the noon absorption is about 10 dB, and the midnight absorption about 2·5 dB, although the midnight flux of particles is taken (rather arbitrarily) to be twenty times as great as the noon flux.

The values of the coefficients in (11–13) are not known; the following are the values adopted here:

$$\alpha_e = 10^{-8}; \qquad \alpha_- = 10^{-9}; \qquad \rho S = 0{\cdot}1 \tag{14}$$

VOL. 10 1957

The adopted values of ηn are shown in Table 3: they are proportional to the collision frequencies at the corresponding levels.

The solutions given in Table 3 have been obtained taking account of the

Table 3. 30 Mc/s radio wave absorption at College, Alaska, at noon and at midnight. Values of the electron and ion densities and other atmospheric characteristics. Numbers here expressed as a^b signify $a \times 10^b$

Layer (km)	40–50	50–60	60–70	70–80	80–90	90–100	100–110
ν (Table 1)	$4{\cdot}0^8$	$1{\cdot}2^8$	$3{\cdot}3^7$	$7{\cdot}6^6$	$1{\cdot}5^6$	$3{\cdot}1^5$	$7{\cdot}1^4$
ηn	89·4	26·9	7·4	1·7	0·33	0·069	0·0159
f	1	1	1	0·85	0·7	0·5	0·2
N_n	100	880	$6{\cdot}9^3$	$4{\cdot}3^4$	$1{\cdot}45^5$	$2{\cdot}46^5$	3^5
N_{+n}	$8{\cdot}9^4$	$2{\cdot}45^5$	$5{\cdot}2^5$	$7{\cdot}7^5$	$6{\cdot}2^5$	$4{\cdot}18^5$	$3{\cdot}5^5$
Q_n	8	62	300	900	1200	1100	1060
N_{m-}	1·8	44·6	810	$1{\cdot}04^4$	$6{\cdot}4^4$	$2{\cdot}06^5$	$4{\cdot}9^5$
N_{+m}	$4{\cdot}0^5$	$1{\cdot}12^6$	$2{\cdot}45^6$	$4{\cdot}2^6$	$4{\cdot}6^6$	$3{\cdot}75^6$	$2{\cdot}8^6$
$10^{-17}N_n\nu\,dh$	0·40	1·06	2·28	3·26	2·18	0·76	0·21
$10^{-17}N_m\nu\,dh$	0·007	0·05	0·27	0·79	0·96	0·64	0·35
$10^{-17}f\,dI_n$	0·008	0·80	2·28	2·78	1·52	0·38	0·04
$10^{-17}f\,dI_m$	0·002	0·04	0·27	0·67	0·67	0·32	0·07

limitation, indicated by the C-3 equipment at College, that N in the E layer does not exceed 5×10^5/c.c., even when the auroral flux has the high midnight values here adopted. The daytime integral of Q up to 80 km, during the intense absorption here considered, is taken to be not much more than ten times the value, 10^8/cm^2 sec, corresponding to VAN ALLEN'S estimate of the flux of X-ray protons as 10^5/cm^2 sec; the integral up to 80 km is here actually $1{\cdot}27 \times 10^9$cm^2 sec. Most of this ionization, mainly due to X rays, is indicated as being in the layer 70–80 km, which may also be slightly ionized by the fastest electrons and by Lyman-alpha photons.

Table 3 gives the values of Q, N and N_+ at the middle level of seven 10-km layers, and also the values of the collision frequency and the attachment coefficient. It gives also the product $10^{-17}N\nu\, dh$ (where $dh = 10$ km $= 10^6$ cm) and of $10^{-17}\, dI$, where dI denotes the contribution of the layer to I; the denominator in (5) is significantly different from unity, for 30 Mc/s waves, in the first two layers. The table also gives a tentative reduction factor f to allow for the patchiness of the upper layers; between patches of ionization the radio waves can pass unimpeded to the lower absorbing layers. The effective absorption depends on the sum of $f\, dI$ for the several layers.

No great accuracy has been attempted in the calculations leading to Table 3, because of the uncertainty of the assumed factors (14).

The total values of $10^{-17}\Sigma f\, dI$ at noon and midnight (the sums of the last two rows in Table 3) are 7·81 and 2·04; they correspond to absorption of 9·25 dB at noon and 2·4 dB at midnight. Higher rates of noctural primary bombardment would of course further increase the night-time radio absorption.

The level of greatest absorption per km of air traversed as shown by Table 3, is between 70 and 75 km at noon, and at about 80 km at midnight. At noon the region 50–90 km accounts for over 90% of the absorption, at midnight over 80% occurs in the region 70–100 km. At either epoch the region above 110 km contributes insignificantly to the absorption, and this would also be affected only slightly by moderate changes of N in the layers 40–50 km and 100–110 km.

Table 3 indicates a considerable density of ions even in the lowest region, 40–50 km, during auroral bombardment. It should be relatively easy to test whether this actually exists, by suitable equipment on rockets of moderate range. If it is not observed, it will probably imply that α_- is greater than 10^{-9}; the assumption of a materially greater value of α_- than that of (14) would involve adjustments of other constants used in the calculations for Table 3, in order to give the adopted noon and midnight values of I.

It must be emphasized again that Table 3 is speculative and uncertain; doubtless further observed radio and rocket data will require changes in it.

Prima facie, however, it presents a possible "model" of ionospheric conditions that can account for the data described earlier in this paper.

Other considerations that may require revision of these tables are (a) the time of relaxation of the absorption, and (b) the corresponding daily variation of magnetic activity. These topics will be discussed in a later note.

This work was supported in part by a grant from the National Science Foundation, and by the Geophysical Research Directorate, Air Force Cambridge Research Center, and the Boulder Laboratories of the National Bureau of Standards.

References

Appleton E. V.	1932	*J. Inst. Elec. Eng.* **71,** 642
Appleton E. V.	1937	*Proc. Roy. Soc.* **A162,** 451
Appleton E. V. and Piggott W. R.	1954	*J. Atmosph. Terr. Phys.* **5,** 141
Bates D. R.	1956	*Ann. Géophys.* (in publication)
Bates D. R. and Massey H. S. W.	1946	*Proc. Roy. Soc.* **A187,** 261
Bates D. R. and Massey H. S. W.	1947	*Proc. Roy. Soc.* **A192,** 1
Booker H. G.	1935	*Proc. Roy. Soc.* **A150,** 267
Chapman S.	1931	*Proc. Phys. Soc.* **43,** 483
Chapman S.	1956	*Nuovo Cimento* (in publication)
Dieminger W.	1952	*J. Atmosph. Terr. Phys.* **2,** 340
Evans S.	1954	*Monthly Not. Roy. Astron. Soc.* **114,** 63
Evans S.	1955	*J. Atmosph. Terr. Phys. Sp. Supp.* **2,** 90
Farmer F. T. and Ratcliffe J. A.	1935	*Proc. Roy. Soc.* A **151,** 370
Little C. G.	1954	*Proc. I.R.E.* **42,** 1700
Massey H. S. W. and Burhop E. H. S.	1952	*Electronic and Ionic Impact Phenomena,* Oxford, 641
Meredith L. H., Gottlieb M. B., and Van Allen J. A.	1955	*Phys. Rev.* **97,** 201
Nicolet M.	1953	*J. Atmosph. Terr. Phys.* **3,** 200
Rocket Panel	1952	*Phys. Rev.* **88,** 1027
Shaw I. J.	1951	*Proc. Phys. Soc.* B **64,** 1
Van Allen J. A.	1955	*Phys. Rev.* **99,** 609, A 12; see also A 9–11
Wilkes M. V.	1954	*Proc. Phys. Soc.* B **67,** 304

VOL.
10
1957

Journal of Atmospheric and Terrestrial Physics, 1957, Vol. 10, pp. 32 to 43. Pergamon Press Ltd., London

Some measurements of ionospheric absorption at Delhi

S. N. Mitra and S. C. Mazumdar
Research Department, All India Radio, New Delhi

(*Received* 18 *June* 1956)

Abstract—The results of some measurements of ionospheric absorption taken at Delhi during June 1954 to December 1955 are described. The measurements were carried out on 5 and 2·5 Mc/s. A brief description of the experimental setup is included in the paper.

The analysis of data shows that the diurnal variation of absorption gives $|\log \rho| \propto (\cos \chi)^{0.43}$. The value of αN has been indicated from the observed value of the "relaxation time." The absorption at night has been observed to be considerable at our latitude. It has been postulated from the low value of the exponent in the diurnal variation factor, the magnitude of the relaxation time, and from direct measurements of absorption on *Es* and *F* echoes, that the main absorption is probably taking place in the *D* region.

1. Introduction

In recent years a number of papers have appeared dealing with the measurement of ionospheric absorption. These measurements were mostly carried out at higher latitudes, and data for lower and tropical latitudes are significantly meagre. To a radio engineer, a knowledge of ionospheric absorption at different geographical latitudes is extremely important for planning long-distance radio communication; to a geophysicist it is equally important for obtaining information on the properties of the ionosphere. The present paper deals with some measurements of ionospheric absorption conducted at Delhi (28° 35′ N, 77° 5′ E).

Measurement of ionospheric absorption has been under active consideration of the Research Department of All India Radio for some time in the past. New circuit techniques were being evolved which would enable measurement of ionospheric absorption continuously and automatically. It was in May 1954 when we were able to finalize our "absorption recorder" and then we commenced regular measurements. To begin with, we confined our measurements to local noon on 5 Mc/s. The scope of the investigation was extended later to include diurnal variation of absorption, its variation during night, and sluggishness of the ionosphere. The analysis of observations has yielded some useful results. The object of the present paper is to describe them, the period of observation being June 1954 to December 1955. In an investigation of this nature, one requires systematic observations spread over a large number of years in order to arrive at any statistically significant result. Our conclusions will, therefore, be somewhat preliminary. The technique of measuring absorption will be briefly outlined, the detailed experimental setup will be published in a separate paper.

2. Experimental Procedure

Our method of measurement is more or less the same as Appleton's (1937), with the difference that instead of measuring the amplitudes of successive echoes, we have employed suitable circuit techniques to obtain directly the reflection coefficient on a logarithm scale. We shall closely follow Appleton in the general nomenclature used in the paper.

The apparent reflection coefficient ρ may be defined as

$$\rho = \frac{\text{Electric field of the polarized wave reflected from the layer}}{\text{Electric field of the corresponding polarized wave incident on the layer}}$$

$-\log \rho$ is defined as the measure of absorption. The measurement of ionospheric absorption could be carried out by comparing the amplitude of successive echoes, taking advantage of the fact that such echoes arrive at distinct time intervals and can easily be separated when pulsed transmission is used.

At vertical incidence,

$$\rho = \frac{\beta R_1}{G} = \frac{2R_2}{\rho' R_1} \tag{1}$$

where β = a constant,
G = ground signal,
R_1 = amplitude of the first echo,
R_2 = amplitude of the second echo,
and ρ' = apparent reflection coefficient of the ground for the wave frequency employed.

VOL. 10 1957

Thus,

$$\log \rho = \log \beta + \log \frac{R_1}{G}$$

$$= \log 2 - \log \rho' + \log \frac{R_2}{R_1} \tag{2}$$

One can evaluate $\log \beta$ from simultaneous measurements of $\log \frac{R_1}{G}$ and $\log \frac{R_2}{R_1}$. Once $\log \beta$ is known, $\log \rho$ could be determined on first reflection alone. This procedure has to be adopted, since in routine observations, often the first-order reflection is alone present. It is, of course, necessary to evaluate $\log \beta$ each time any change in the experimental setup is made.

Our technique of measuring absorption is based on the above principles. We have, however, kept the transmitter and the receiver at the same place. A suitable pulsed signal from a signal generator adjusted to the same frequency is utilized in place of the ground signal for comparison purposes.

3. Experimental Setup

A block schematic of the experimental setup is shown in Fig. 1. A 1-kW pulsed transmitter connected to a vertical delta aerial acts as the signal source. The signal is received by a Hammarlund Super Pro receiver modified for pulsed reception (Mitra and Roy, 1951). The receiver is connected to another vertical delta aerial oriented at right angles to the transmitting antenna. A suitable pulsed signal from a signal generator adjusted to the transmitter frequency is also injected to the input of the receiver. To minimize desensitization of the receiver by the strong ground pulse, the receiver is muted during the time interval occupied by the ground pulse by means of an externally generated disabling timegate. The rectified video output of the receiver is then passed on to the absorption recorder.

The basic operating principles of the absorption recorder are as follows. An electronic gate of variable width and delay (Mazumdar and Mitra, 1954) "selects" the calibrating pulse (or the first echo, as the case may be). The "gated echo" is then passed on to a logarithm

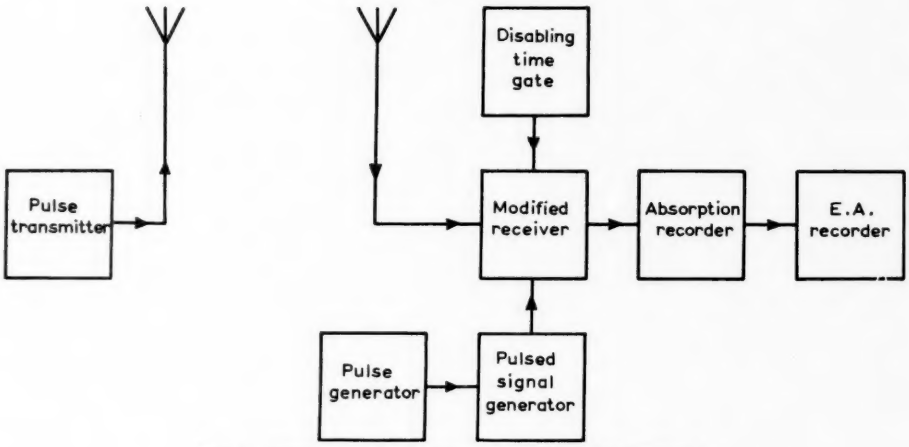

Fig. 1. Experimental set-up—absorption measurement.

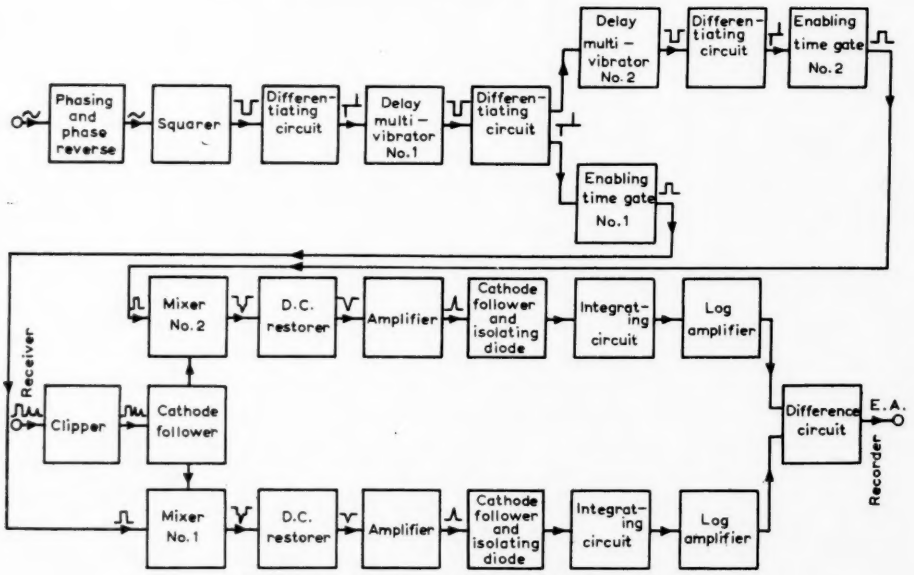

Fig. 2. Block schematic—absorption recorder.

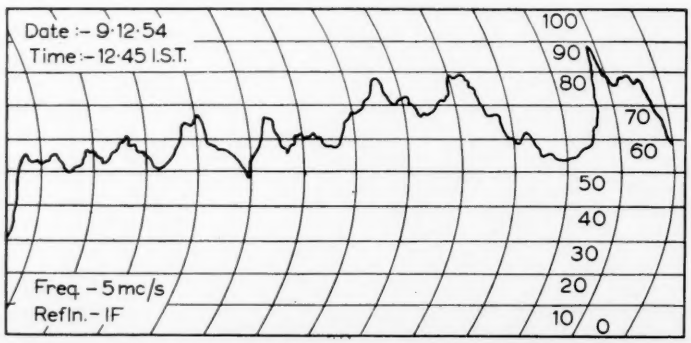

Fig. 3. A typical $|\log \rho|$ curve (speed 3 in./min).

amplifier which gives log G (or log R_1). Another electronic gate of independently variable width and delay selects the first echo (or the second reflection). The gated output is similarly passed on to a second independent logarithm amplifier, which gives log R_1 (or log R_2). The two logarithm outputs are combined in a difference circuit which gives log $\frac{R_1}{G}$ $\left(\text{or log } \frac{R_2}{R_1}\right)$. The d.c. output from the difference circuit is recorded on an Esterline Angus recorder which records the time-variation of $|\log \rho|$. The circuit parameters are so adjusted that each division in the recorder chart represents 1 dB. The block schematic of the absorption recorder is shown in Fig. 2 and a typical absorption record is shown in Fig. 3. The recording speed is kept at 3 in. per minute.

The variation of $|\log \rho|$, as indicated in Fig. 3, is due to the fading of the received signal. An absorption record on any wave frequency is usually taken for 5 min or more continuously, depending upon the nature of the fading, and the average $|\log \rho|$ is then worked out.

The noontime measurements are taken on a wave-frequency of 5 Mc/s, and daily measurements are available since June 1954. Since no polarized aerial system has been used in the experiment, some records of $|\log \rho|$ indicated periodic variations due to the interference between magnetoionic components (Mitra, 1950). Such records are excluded from our analysis. Quite a large number of records are, however, available in which only the ordinary component was gated, either when the two components were distinctly split, or when the extraordinary component was too weak in intensity. We have verified this point from the vertical incidence h'-f records taken simultaneously with the absorption measurements. We selected 5 Mc/s, as this wave frequency was well above the critical frequency of the E layer and well below the critical frequency of the F layer, during the period of observation, so as to avoid any deviative absorption. The measurements during night were carried out on 5 and 2·5 Mc/s.

VOL. 10 1957

4. Diurnal Variation of $|\log \rho|$

Appleton (1937) has shown that for a simple Chapman layer, the nondeviative absorption is given by

$$\int k\, ds = -\log \rho = 4{\cdot}13\left(\frac{4\pi e^2}{mc}\right)\frac{N_0 \nu_0 H \cos^{3/2}\chi}{(p \pm |p_L|)^2} \qquad (3)$$

provided $\nu \ll p$;

where k = spatial absorption coefficient,

e, m = charge and mass of the electron,

N_0 = electron density at the level of maximum electron production when χ, the solar zenith angle, is zero,

ν_0 = electron-collision frequency at the same level,

H = scale height,

p = angular wave frequency,

p_L = angular gyrofrequency component in the direction of propagation,

ν = electron-collision frequency,

$\pm$ signs refer to the ordinary and the extraordinary components respectively.

According to this theory, therefore,

$$|\log \rho| \propto (\cos \chi)^{3/2} \tag{4}$$

It has been observed by several observers that the simple relation[4] is not strictly obeyed. It is, therefore, preferable to start with the following relationship between $|\log \rho|$ and solar zenith angle χ;

$$|\log \rho| \propto (\cos \chi)^n . \tag{5}$$

Observations so far carried out by different workers have given different values of n, but mostly lower than 3/2. BEST and RATCLIFFE (1938) found, however, that $|\log \rho|$ varied as $(\cos \chi)^{3/2}$. But, as pointed out by APPLETON and PIGGOTT (1954), this result might have been influenced by deviative absorption. TAYLOR (1948), from observations on continuous waves at practically vertical incidence, has deduced the value of n as 0·8. APPLETON and PIGGOTT have shown from an analysis of several hundred observations of diurnal variation of $|\log \rho|$ that the most frequent value of n is 0·75. MITRA and SHAIN (1953) have indicated from an investigation of ionospheric absorption on 18·3-Mc/s cosmic radio noise that the mean value of n for D-layer absorption is 0·83. DAVIES and HAGG (1955) have shown that n is about 0·5 in the auroral zone.

Our values of $|\log \rho|$ have been evaluated from the half-hourly absorption records taken on various occasions. Such values were plotted on a logarithmic scale to indicate the variation of $|\log \rho|$ against $\cos \chi$. The slope of the straight line that best fits the observed points gives n. Strictly speaking, one should denote the variation of $|\log \rho|$ against $1/Ch(R, \chi)$, where $Ch(R, \chi)$ is the appropriate Chapman function for the layer. We have calculated the values of $1/Ch(R, \chi)$ assuming the scale-height as 5·8 km. It has been found that $\cos \chi$ does not vary appreciably from $1/Ch(R, \chi)$ for $\chi \leqslant 85°$. We shall, therefore, indicate the diurnal variation of $|\log \rho|$ against $\cos \chi$.

On one or two occasions we have grouped together the half-hourly values for a few days and calculated the average. This was done only when the day-to-day variations were small. Such average values of $|\log \rho|$ were then plotted against $\cos \chi$ to determine n. Fig. 4 shows the logarithmic plot of $|\log \rho|$ and $\cos \chi$ for one such occasion. The value of the exponent n as given by the slope of the straight line in the figure comes out to be 0·54 for this particular record.

It would be seen from Fig. 4 that the curve showing diurnal variation of $|\log \rho|$ is a fairly straight line. We have taken a large number of such observations of diurnal variation on 5 Mc/s. But many of the records could not be utilized because of partial reflection, magneto-ionic fading, and high level of noise. Twelve sets of reasonably good observations are available and have been analysed. Table 1 below gives the values of n on these occasions.

The above table indicates that n lies between 0·33 and 1·13. But in the case of eight observations, the value of n has been found to be within the range 0·53 to 0·8. The average of all the values comes out to be 0·62. We therefore conclude from our measurements conducted so far that the variation of $|\log \rho|$ with solar zenith distance obeys the following law for our latitude (Delhi, 28° 35′ N, 77° 5′ E):

$$|\log \rho| \propto (\cos \chi)^{0.62} . \tag{6}$$

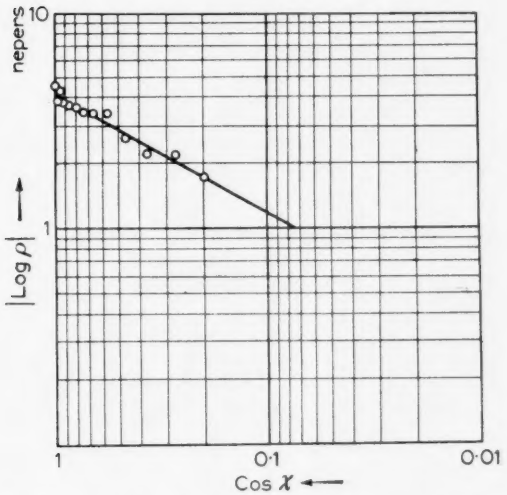

Fig. 4. Diurnal variation of $|\log \rho|$ on 5·0 Mc/s (averaged over 10 days' readings, 25.6.54 to 5.7.54).

VOL. 10 1957

Table 1

	Date	n
1.	25.6.54 to 5.7.54	0·54
2.	9.5.55	0·66
3.	10.5.55	1·13
4.	21.10.55	0·80
5.	16.11.55	0·41
6.	24.11.55	0·58
7.	30.11.55	0·33
8.	12.12.55	0·79
9.	14.12.55	0·71
10.	15.12.55	0·38
11.	21.12.55	0·62
12.	28.12.55	0·53

During our measurements we observed that, on 5 Mc/s, reflections from *F* layer alone were not always present. Sometimes *Es* and *F* could be simultaneously seen. At some other time a "blanketing *Es*" or single returns from *F* could be noticed. The values of $|\log \rho|$ on blanketing *Es* are found to be of the same order as those taken on *F*-layer returns (taking into account the difference in spatial attenuation in the two cases). But when *Es* and *F* returns are simultaneously seen, the values of $|\log \rho|$ on echo from the *F* layer are found to be appreciably different from those taken on *F* return when no *Es* was present. This was presumably due to

extra loss of energy caused by *Es*. In our analysis, we have omitted those measurements when both *Es* and *F* were present.

A change in the value of the exponent n from unity (as assumed by CRPL, 1948) or 0·75 will produce a significant variation in the overall absorption. Some calculations of the nondeviative absorption have been made assuming the CRPL approximation and the variation as would be produced with n as 0·62. The results are discussed below.

In the CRPL formula, the absorption factor K is given by:

$$K = 0{\cdot}142 + 0{\cdot}858 \cos \chi \,. \tag{7}$$

K has also been calculated assuming

$$K = (\cos \chi)^{0{\cdot}62} \tag{8}$$

as experimentally obtained by us. The relative increase of absorption on equation (8) over that on (7) has been calculated for various values of χ and is shown in Table 2.

Table 2. Relative increase of absorption for $(\cos \chi)^{0{\cdot}62}$

$\cos \chi$	Increase in absorption (%)
0·9	2·5
0·8	5·1
0·7	7·9
0·6	10·9
0·5	14·0
0·4	16·8
0·3	18·6
0·2	17·6
0·1	5·3

The maximum relative increase is 18·6% for $\cos \chi = 0{\cdot}3$. The CRPL formula will, therefore, require suitable revision if applied for calculating the sky-wave field intensity at our latitude.

5. Other Daytime Measurements

(*a*) *Relaxation time*

Appleton (1953) has indicated that due to finite time of recombination in the ionosphere the diurnal maximum of the absorption is reached not at local noon but a certain time after midday. This time is called the "relaxation time" of the ionosphere and is given by:

$$t \text{ (in secs)} = \frac{1}{2\alpha N} \tag{9}$$

where α is the effective recombination coefficient and N is the density of ionization of the absorption region.

We have recorded the variation of $|\log \rho|$ continuously from 1000 to 1400 IST (LMT −22 min) on several occasions during each month. A typical variation of $|\log \rho|$ with local time is shown in Fig. 5 which indicates the value of t as 53 min. αN comes out to be $1{\cdot}6 \times 10^{-4}\,\mathrm{sec}^{-1}$. We have also averaged on a

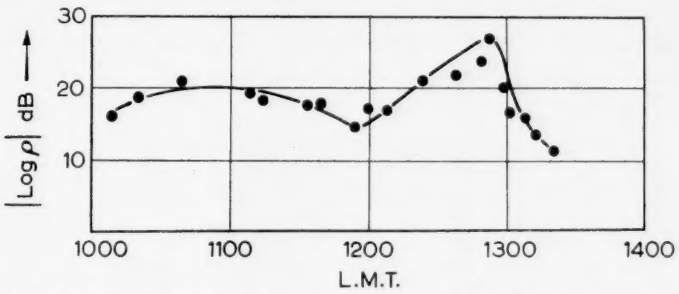

Fig. 5. Showing the relaxation time of the ionosphere. Date 1 April 1955. Frequency 5 Mc/s.

monthly basis the values of $|\log \rho|$ at fixed times and plotted the average variation with local time (local time is derived from LMT corrected for equation of time). The relaxation time for such several instances lies between 30 and 60 min. with a mean near about 45 min.

VOL. 10 1957

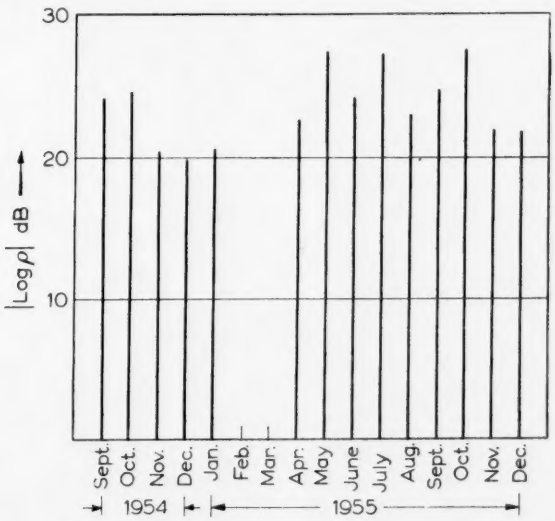

Fig. 6. Seasonal variation of $|\log \rho|$, frequency 5 Mc/s.

(*b*) *Seasonal variation of* $|\log \rho|$ (*midday*)

The measurements of the midday values of $|\log \rho|$ on 5 Mc/s are available for a period of about eighteen months. These data have been averaged over various months, to indicate seasonal variation of absorption. Fig. 6 represents the monthly midday values of $|\log \rho|$ from September 1954 to December 1955. The

highest average value of 27·4 dB has been obtained in summer and the lowest in winter of 19·5 dB. However, the data collected so far is considered insufficient for going into the question of "seasonal variation factor."

(*c*) *Direct-current conductivity*

We may also calculate the direct-current conductivity from the value of absorption, assuming the absorption region as a simple Chapman layer. The method of calculation has been given by APPLETON (1937). The relation is:

$$\int \sigma \, dh = \frac{4\pi}{c} \left[\frac{f + |f_L|}{f_H} \right]^2 |\log \rho| \, . \tag{10}$$

Our wave frequency f was 5 Mc/s, $f_H = 1{\cdot}02$ Mc/s (MITRA, 1955), $f_L = 0{\cdot}7$ Mc/s, and $|\log \rho|$ at midday was about 3. Thus the total electron conductivity comes out to about $2{\cdot}25 \times 10^{11}$ e.s.u.

6. NIGHT-TIME ABSORPTION

We have carried out measurements of $|\log \rho|$ at night on 5 and 2·5 Mc/s. The half-hourly values of $|\log \rho|$ on returns from F layer on each day have been

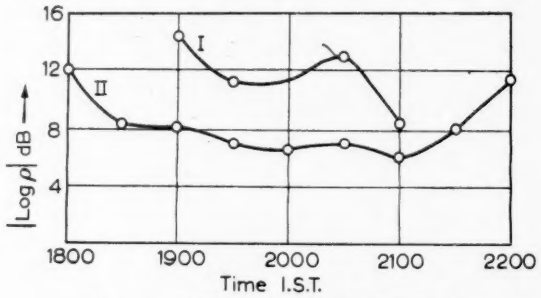

Fig. 7. Variation of $|\log \rho|$ after sunset.
I. Summer (June–July 1954)—5 Mc/s.
II. Winter (Nov.–Dec. 1955)—2·5 Mc/s.

averaged for a few days, and Fig. 7 shows the variation of $|\log \rho|$ with time after sunset. Curve I in Fig. 7 pertains to measurements on 5 Mc/s for a few consecutive days during June–July 1954 and curve II gives the variation of $|\log \rho|$ on 2·5 Mc/s during Nov.–Dec. 1955. It will be seen from this figure that the absorption during night on vertical incidence is quite appreciable in our latitude. The average critical frequencies of the F layer during June–July 1954 was varying between 6·2 and 5·8 Mc/s from 1900 to 2100 IST. It is possible that there might have been some amount of deviative absorption present late in the evening. But during Nov.–Dec. 1955 the critical frequency was much above 2·5 Mc/s during the period of measurement, and the possibility of any deviative absorption was, therefore, less.

Fig. 7 reveals the following interesting results. Our measurements on 5 Mc/s during summer indicate that the absorption was remaining practically constant,

varying between 11 and 8 dB from 1930 to 2100 IST. The measurements during winter on 2·5 Mc/s follow more or less the same pattern; the absorption came down from about 8 dB at 1830 to about 6 dB at 2100 IST. After 2100 IST, there was a rise in the value of $|\log \rho|$, possibly due to deviative absorption.

The residual absorption at night has not hitherto received serious consideration. This has been considered to be negligible for all practical purposes. An analysis of eleven years' measurements of field strength of internal short-wave transmitters of AIR taken during night over various distances has revealed (Mitra and Srivastava, 1953) that night-time field strength is correlated with sunspot number, indicating a solar control of absorption at night. The mechanism responsible for producing and maintaining ionization in the absorbing layer at night is, however, not clearly understood. Davies and Hagg (1955) have found quite appreciable nondeviative absorption at night on 2 Mc/s, and have concluded from a correlation between absorption and magnetic index that the residual ionization during night may be caused by corpuscular radiation. We have also found some confirmation of this view from our analysis of solar-eclipse observations of June 1954. We have observed from a comparison between the values of $|\log \rho|$ on the control days and those on the eclipse day that there were two corpuscular eclipses of $|\log \rho|$ corresponding to two different speeds of the corpuscular radiation. (The results are described in a paper in course of publication.) This indicates that at least a part of the ionization of the absorbing region is caused by corpuscular emission from the sun, and this may explain the high value of residual absorption in the night observed by us. But a difficulty arises in explaining the correlation between nighttime absorption and sunspot number as also observed by us.

VOL. 10 1957

7. Discussion of Results

Summarizing the main features of our observations, we arrive at the following conclusions:

(i) The average diurnal variation factor is 0·62.
(ii) The relaxation time of the absorbing region varies between 30 and 60 min with a mean around 45 min.
(iii) The midday absorption varied between 27·4 dB in summer and 19·5 dB in the winter during the period September 1954 to December 1955.
(iv) The residual absorption at night is appreciable.

The assumption of a simple Chapman layer for the absorbing region would require n to be 1·5. There is now enough evidence to indicate that n is always less than 1·5. One of the reasons may be that the main absorption is taking place at the D layer, which does not strictly behave as a simple Chapman region. If one assumes that for the D region the recombination coefficient varies directly with pressure, the value of n becomes of the order of unity (Appleton and Piggott, 1954). There is also other experimental evidence to indicate that when n is of the order of 0·6, the main absorption takes place in the D layer. Benner (1951) has shown from daytime measurement of ionospheric absorption by means of pulsed transmissions on 150 Kc/s (at which frequency most of the absorption will be

from the D layer) that n is 0·62 in the morning and 0·42 in the afternoon. It appears, therefore, that higher values of n can be attributed to contribution from the E layer, whereas the lower values indicate that most of the absorption is from the D region. Our average value of n was 0·62, which would indicate, from the arguments advanced, that the main absorption was taking place below E region. The same order of magnitude for the values of $|\log \rho|$ as obtained from measurements on blanketing Es and on F (in the absence of Es) would also support this hypothesis.

The absorbing region may also be identified from the observation of the relaxation time. The probable value of the relaxation time for the E layer (t_E) can be worked out from the recombination coefficient α_E obtained otherwise and from the electron density in the E region. Since α_E is of the order of $1{\cdot}0 \times 10^{-8}$ cm^3/sec (PIGGOTT, 1953) and $N_E \simeq 10^5$/cc, the value of t_E comes to about 8 min. t_E can also be obtained from solar eclipse observations where the time taken by the E layer to show a minimum in the ionization density reckoned from the maximum of the eclipse gives the value of the relaxation time. Thus BARAL and MITRA (1944) found t_E as 8 min. But the relaxation time for the D layer (t_D), as determined from direct experiments, gives a much higher value. BENNER'S measurements of D-layer absorption on 150 kc/s give t_D as 60 min. A theoretical estimate of t_D from observed value of α_D has been shown by MITRA (1954) to be about 70 min at a height of 80 km. From these observations it is reasonable to take 60 min as the relaxation time for the D region. In our experiments, we have found the value of the relaxation time as 45 min, which shows that the main absorption was taking place in the D region.

APPLETON and PIGGOTT'S (1954) values of n and relaxation time (0·75 and 20 min respectively) appear, therefore, to be consistent with the hypothesis that an appreciable contribution to absorption at their latitudes was presumably coming from the E layer. Our values, however, indicate that the main absorption was taking place probably in the D region.

In a recent paper, MITRA (1955) has worked out relationships between n,t and absorption for the D and E regions. His formula can be utilized to ascertain the relative proportion of D and E layers' absorption from a knowledge of n or relaxation time. He has shown that under some plausible assumptions the following relationships can be established:

$$K = \frac{n\bar{A}_D + p\bar{A}_E}{\bar{A}_D + \bar{A}_E} \tag{11}$$

and

$$\frac{p}{n}\frac{\bar{A}_E}{\bar{A}_D} = \frac{t_D - \bar{t}}{\bar{t} - t_E} \tag{12}$$

where n, p = diurnal variation factors for D and E layers respectively (assumed).

$\bar{A}_D, \bar{A}_E$ = values of D and E layer absorption, respectively at the time of maximum resultant absorption.

K = observed diurnal variation factor.

and $\bar{t}$ = resultant relaxation time for both D and E layers.

Taking $K = 0{\cdot}62$, $n = 0{\cdot}5$, $p = 1{\cdot}5$, we find that $\bar{A}_D \simeq 7\bar{A}_E$. Thus, our measurements indicate that the absorption suffered in the D layer by a 5-Mc/s wave must have been at least seven times that of the E region. Similarly, taking $t_D \simeq 60$, equation (12) shows that for a relaxation time of 45 min for a 5-Mc/s wave, the absorption in the D layer must have also been seven times that in the E region. We may, therefore, conclude that the daytime absorption at our latitudes on high frequencies is mostly contributed by the D layer.

Another feature of our observation is the fact that there is appreciable absorption at night, and which does not vary much with time. This cannot be explained in terms of solar ultra-violet radiation as the only ionizing agency. The possibility of the corpuscular radiation maintaining the residual ionization of the absorbing region at night cannot be overlooked. The evidence of "corpuscular eclipse" on $|\log \rho|$ measurement as observed by us during our investigations of the solar eclipse of 30 June 1954 indicates that a part of the ionization in the absorbing layer may be caused by the incidence of corpuscular emission. But our analysis of field-strength measurements over a complete solar cycle indicates a correlation between nighttime absorption and sunspot numbers. Further measurements of $|\log \rho|$ at vertical incidence may clarify the situation.

VOL. 10 1957

Acknowledgements—The work described in this paper forms a part of the programme of ionospheric research of All India Radio and is published by permission of Mr. B. V. Baliga, Chief Engineer, All India Radio. The authors wish to thank Mr. S. Thiruvenkatachari, Research Engineer, for helpful discussions, and Mr. B. V. T. Rao, Assistant Engineer, All India Radio, for helping us in taking some of the observations.

References

Appleton, E. V.	1937	*Proc. Roy. Soc.* **A162,** 451.
	1953	*J. Atmosph. Terr. Phys.* **3,** 282.
Appleton E. V. and Piggott W. R.	1954	*J. Atmosph. Terr. Phys.* **5,** 141.
Baral S. S. and Mitra S. N.	1944	*Science & Culture* **10,** 175.
Benner A. H.	1951	*Proc. Inst. Rad. Engrs.* **39,** 186.
Best J. E. and Ratcliffe J. A.	1938	*Proc. Phys. Soc.* **50,** 233.
CRPL	1948	Circular No. 462, National Bureau of Standards.
Davies K. and Hagg E. L.	1955	*J. Atmosph. Terr. Phys.* **6,** 18.
Mazumdar S. C. and Mitra S. N.	1954	*Ind. J. Phys.* **28,** 251
Mitra A. P.	1954	*Trans. I.R.E.* AP-2, 99.
Mitra S. N.	1950	*Ind. J. Phys.* **24,** 197
	1955	*Ind. J. Phys.* **29,** 518.
Mitra A. P. and Shain C. A.	1953	*J. Atmosph. Terr. Phys.* **4,** 204.
	1955	*Physics of the Ionosphere* The Physical Society. 71.
Mitra S. N. and Roy J. M.	1951	*Electrotechnics*, No. 23, 56.
Mitra S. N. and Srivastava R. B. L.	1955	*Ind. J. Phys.* **29,** 167.
Piggott W. R.	1953	*Report of the Proceedings of the Third Meeting of the Mixed Commission on the Ionosphere, Brussels*, p. 42.
Taylor E. W.	1948	*Res. Bur. of Stand.* **41,** 575.

RESEARCH NOTES

Drift measurement of the *E* layer during the solar eclipse 30 June 1954

(*Received* 26 *June* 1956)

At Kjeller the drift of the *E* layer using the Mitra method has been recorded during a two-years period 1953–55 on a fixed frequency of 2 Mc/s. In the following the results from the records on the day of eclipse and the two subsequent days will be discussed. At Kjeller the eclipse was 99·5%. The *P'f* curves were recorded at short intervals on the days before, during and after the eclipse and the changes in maximum electron densities have been

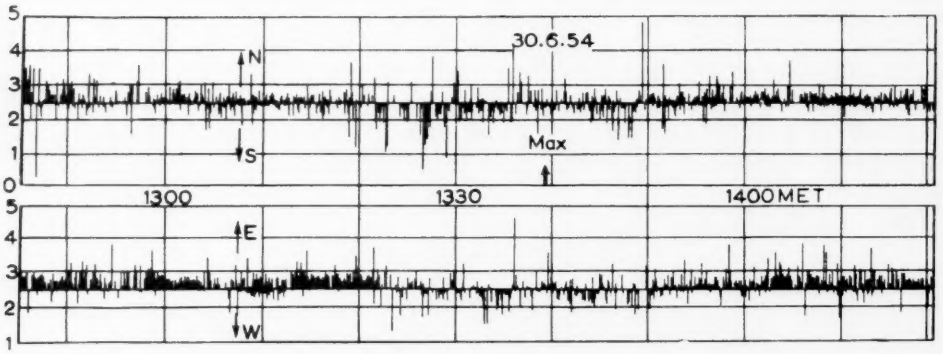

Fig. 1. Phillips record of *E*-layer drift.

discussed by Landmark, Lied, Orhaug, and Skribeland (1956). On Fig. 1 a Phillips record of the "spikes" indicating the drift directions is shown and on Fig. 2 the components of the wind directions have been marked off for each ten minutes. The record shows a steady component towards E and N during the day of the eclipse, which are the normal mean drift directions during summer day. During the *maximum* period of the eclipse the wind directions were reversed for both components. A closer study of the simultaneous *P'f* curves indicates the following explanation of this effect.

During the day of eclipse the *E* layer consisted of a normal *E* imbedded in a stratum of *Es*. From the *P'f* records it was, however, possible to follow the gradial changes in the critical frequency of the normal *E*. From Fig. 2 it is evident that at the moment when the critical frequency of the normal *E* decreased below 2 Mc/s (which was the test frequency for the drift measurements) the drift directions were reversed. During the maximum period of the eclipse we were apparently recording the drift of the *Es* layer. Similarly, when at the end of the eclipse the critical frequency of the normal *E* increased, the drift directions were again reversed when the critical frequency of normal *E* passed the test frequency 2 Mc/s. The drift of the normal *E* was again recorded.

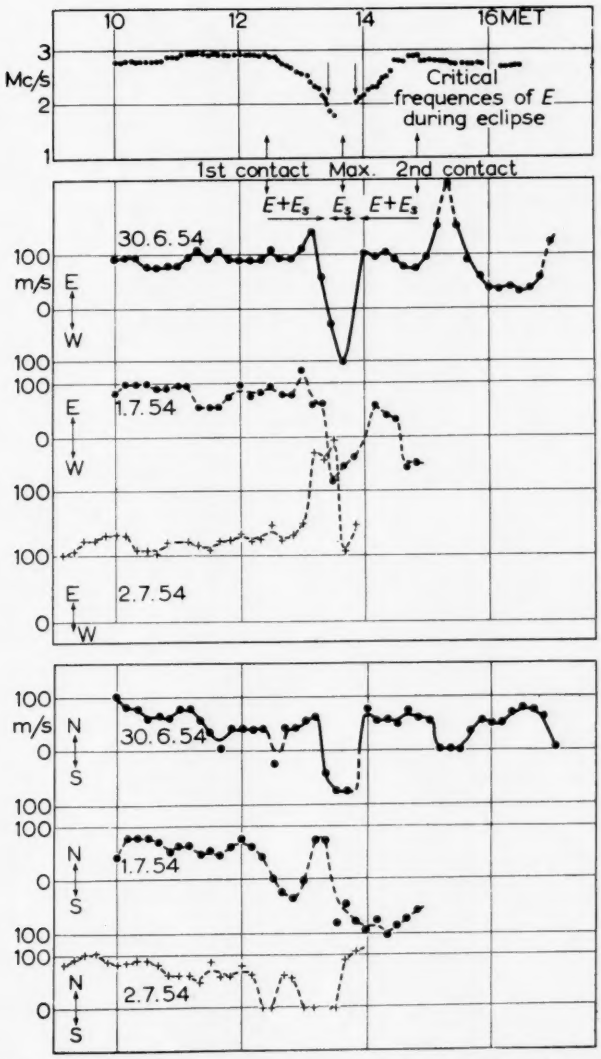

Fig. 2. Components of *E*-layer drift. On the upper part of the figure the critical frequencies of the normal *E* during the eclipse day are indicated.

The effect stated is an example of variation in drift directions when going from normal *E* to an *Es* layer lying at a somewhat greater height.

L. Harang
K. Pedersen

Norwegian Defence Research Establishment
Kjeller, Norway

Reference

Landmark, B., Lied F., Orhaug, T., and Skribeland S. 1956 *Geofys. Publ. (Oslo)* **19**, No. 8

VOL. 10 1957

On the intersection of two slender cones

(*Received* 25 *June* 1956)

THIS note determines an approximate volume of the intersection of the cone of a searchlight and the cone of vision of a telescope, under the restrictions that the axes of the cones intersect. An error curve is shown in Fig. 2 for the limits considered. The "true" volume was computed by numerical integration on an International Business Machines Corporation Type-701 digital computer.

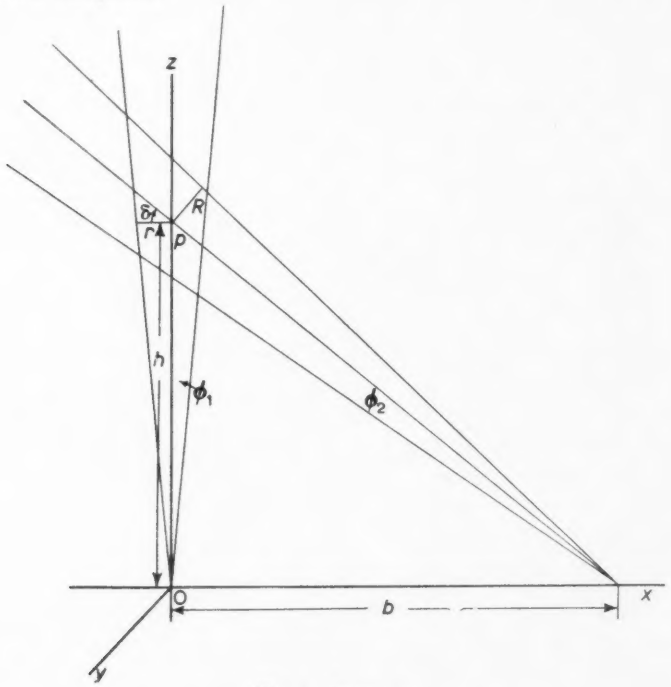

Fig. 1. Geometry.

In Fig. 1 R is the larger radius at the intersection P, and r is the smaller. The angle δ is the angle between r and the axis of the larger cone.

The volume of the intersection of two right circular cylinders having radii r and R whose axes intersect at P with an angle δ is $V = 4\int_0^r \frac{(R^2 - y^2)^{1/2} 2(r^2 - y^2)^{1/2}}{\cos\delta}\, dy$. Thus, if

$$y = r\sin\theta \text{ and } r/R \leq 1, \quad V = \frac{8}{\cos\delta}\int_0^{\pi/2} (R^2 - r^2\sin^2\theta)^{1/2}\, r^2\cos^2\theta\, d\theta$$

$$= \frac{8R^3}{3\cos\delta}\,[(1 + r^2/R^2)E(r/R) - (1 - r^2/R^2)K(r/R)],$$

where $K(r/R)$ and $E(r/R)$ are the complete elliptic integrals of the first and second kinds.

The computation of the "true" volume is made by using the definition of the Riemann integral and summing. Thus the truncation error of computation can be indicated by

computation with two different mesh sizes. This has been done, and the truncation error, which is proportional to the square of the mesh size, is indicated in Table 1. The computation is simple enough to make the round-off error small compared with the truncation

Table 1

h	Mesh size 1	Volume 1	Mesh size 2	Volume 2	Indicated truncation error	Approximate volume
1/3	5×10^{-5}	$1{\cdot}71805\times10^{-6}$	$4{\cdot}5\times10^{-5}$	$1{\cdot}71811\times10^{-6}$	$2{\cdot}4\times10^{-10}$	$1{\cdot}7178\times10^{-6}$
1·0	2×10^{-4}	$2{\cdot}630516\times10^{-5}$	10^{-4}	$2{\cdot}631457\times10^{-5}$	$3{\cdot}3\times10^{-9}$	$2{\cdot}629\times10^{-5}$
3·0	8×10^{-4}	$1{\cdot}109315\times10^{-3}$	4×10^{-4}	$1{\cdot}110152\times10^{-3}$	$3{\cdot}3\times10^{-7}$	$1{\cdot}1013\times10^{-3}$

In all cases b is assumed to be 1 and $\phi_1 = \phi_2 = 0{\cdot}0065449880$ radians.

error. In Fig. 2 there are plots of the differences between the "true" volumes for the geometric representation of Fig. 1 for different ratios h/b.

VOL. 10 1957

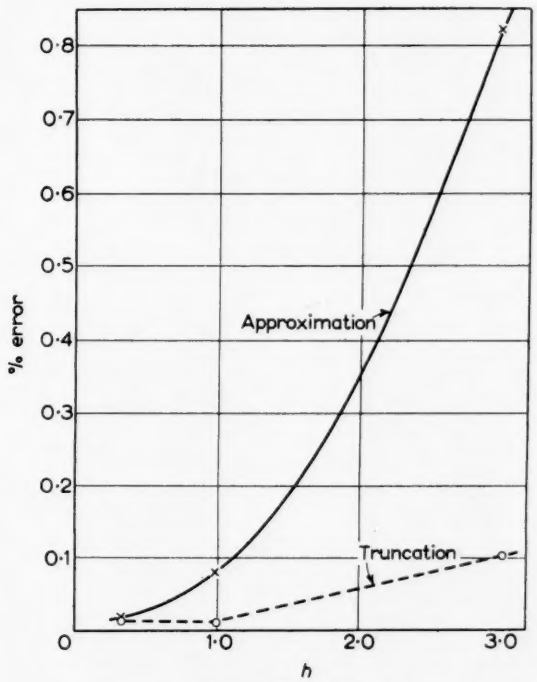

Fig. 2. Error curves.

The approximation error is primarily a function of the angle δ, and as long as the ϕ_i are small is almost independent of the specific values of the ϕ_i.

Naval Ordnance Test Station
China Lake, California

JOHN E. MAXFIELD
R. G. SELFRIDGE

Ionospheric absorption observed on the 23rd February 1956 at Kjeller and Tromsö

(*Received* 27 *August* 1956)

RESULTS of absorption measurements carried out at Kjeller (60° N, 11° E) and at Tromsö (70° N, 19° E) during the intense solar eruption of 23 February 1956 may be of some assistance when discussing the magnitude of the ionization built up in the nighttime ionosphere during the event.

Both at Kjeller and at Tromsö, ionospheric absorption measurements were carried out at vertical incidence with the usual multiple reflection technique. In Fig. 1 the detailed observations of absorption index at Kjeller are plotted together with apparent height of the reflecting layer at the frequency in use.

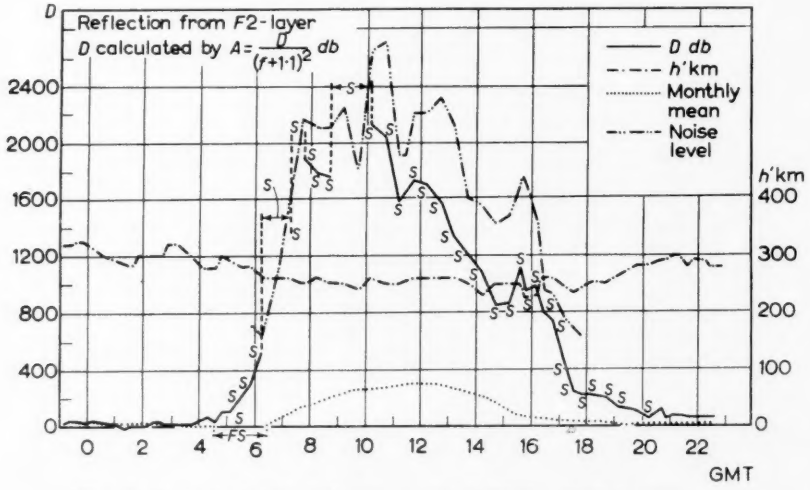

Fig. 1. Ionospheric absorption measured at Kjeller, 23 February 1956

The atmospheric noise level is indicated by the value of D that would make the reflected signal equal to the noise, i.e. when the noise-level index is above the observed absorption index, the measurements are reliable.

The echoes were not lost at any time at Kjeller, though between 0600 and 1000 GMT the echoes were most of the time of the same magnitude as the noise.

Our measurements at Tromsö gave similar results, the echoes were, however, lost at approx. 0500 GMT and the "no echo" condition lasted for forty-eight hours.

It is apparent from Fig. 1 that at Kjeller nothing very extraordinary happened to the total nondeviative absorption in the D and E layers during the solar flare at approximately 0335 GMT and the following cosmic-ray disturbance.

But absorption increased gradually from 0400 GMT and throughout the day showing a diurnal trend very different from the normal one also indicated in the figure.

Norwegian Defence Research Establishment
Kjeller, Norway

F. LIED

On the remarks of D. R. Bates and B. L. Moiseiwitsch (1956) regarding the O_3 and O_1* hypotheses of the excitation of the OH airglow†

(*Received* 15 *September*, 1956)

THE rocket investigations of KOOMEN, SCOLNIK, and TOUSAY (1956) have shown that the nocturnal emission in the region of 5300 Å appears at an altitude of from 80 to 115 km, attaining maximum intensity at about 100 km. As HUNAERTS and NICOLET (1950) had supposed earlier, this emission consists of two rotational-vibrational bands, namely 6-0 and 9-2 hydroxyl in the ground state. The O_2* hypothesis of hydroxyl excitation put forward by KRASSOVSKY (1952, 1954, 1956) is thus completely confirmed in view of the fact that the O_3 hypothesis does not explain the appearance of hydroxyl emission at an altitude of about 100 km. The considerations put forward by BATES and MOISEIWITSCH (1956) on the O_3 and O_1* hypotheses before the results of the investigations of KOOMEN, SCOLNIC, and TOUSAY were made known, are inexact and in the light of the new facts have to a great extent lost their original value.

Here we shall briefly outline these considerations, a fuller treatment of which will be published in *The Progress of Physical Sciences* (*USSR*).

GAYDON's (1947) data on the dissociation energy of molecules leave no room for doubt that the excitation of tenth OH vibrational level in the ground state is inevitable. The new data supplied by BRIX and HERZBERG (1954) are not so favourable as to enable us to exclude completely the possibility of such excitation. Even if the sum total of the reaction energy of the process and its activation energy were to be 1–2 kcal/mole below the excitation energy of the tenth level (80·6 kcal/mole), this level would be inevitably excited, as at a temperature of about 260°K, a considerable part of the molecule would have a degree of energy exceeding the activation energy which equals 3 kcal/mole. Moreover, experimental data have only shown that the activation energy of the (O_3 + H) process is less than 5 kcal/mole (cf. JOST, 1946). The figure of 3 kcal/mole is therefore a rather arbitrary quantity and cannot serve to prove the limit of excitation exactly.

We are happy to note that BATES and MOISEIWITSCH agree with the process of the suppression of OH* bands, beginning with the tenth level and higher as a result of the reaction of so great a degree of excitation of the OH molecule with O_2 and N_2 molecules as suggested by us. Thus, the fact that high OH vibrational levels were not observed in mixtures of ozone and atomic hydrogen in the experiments made by MCKINLEY, GARVIN, and BONDART (1955) may be explained by the presence of the O_2 molecule.

Though extremely popular, the argument put forward regarding the ninth level was by no means decisive.

When evaluating the reaction $O + O_2 + M \rightarrow O_3 + M$ we made use of the new value of the rate coefficient of the reaction $= 10^{-33} T^{1/2}$ cm^6 sec^{-1} from the research of ENIKOLOPJAN and NALBANDJAN (1950), and not the old value of $5 \cdot 10^{-36} T^{1/2}$ cm^6 sec^{-1} used by BATES and NICOLET (1950). The result was thus different and not in favour of the O_3-hypothesis.

As SHKLOVSKY (1951) took the OH oscillator strength as equal to 1, his evaluation of the maximum OH content of the earth's atmosphere was in reality lowered.

The ozone-forming radiation absorbed at altitudes of about 75 km would be insufficient to support the hydroxyl emission at the level observed, as there are a number of obstacles that prevent the complete transformation of the migrating energy into the hydroxyl emission. The newly formed ozone molecules are used up not only in reactions with atomic

† An asterisk (*) is affixed to the chemical symbol for a molecule when it is desired to draw attention to the presence of vibrational excitation in the ground state.

4—(8 pp.)

VOL. 10 1957

hydrogen, but also in reactions with atomic oxygen. According to HEAPS and HERZBERG (1952), the mean radiative life of OH* is in the magnitude of 10^{-2} sec. At an altitude of 75 km the number of collisions reaches $5 \cdot 10^5$ sec^{-1}. The OH* collisional deactivation will thus be exceptionally high and should not be ignored, as was done by BATES and MOISEIWITSCH. Further, when the O_3 and O_2* hypotheses are compared, the same effective temperature of the sun should be used. The data of JOHNSON, PARCELL, TONSEY, and WATANABE (1952), which were used to support the O_3 hypothesis, correspond to a temperature exceeding 4500°K, whereas the O_2* hypothesis was criticized precisely for using a temperature of 4500°K. The foregoing is completely borne out by the fact that the hydroxyl emission does not arise at altitudes lower than 80 km, as was supposed in the O_3 hypothesis.

Criticizing the O_1* hypothesis, BATES and MOISEIWITSCH exaggerated the role of the deactivation of O_2 vibrational excitation in the ground state. According to KONDRATJEV (1936), the vibrationally excited molecules in the ground state during collisions decrease the vibrational quantum number v per unit, the probability of this process, calculated per collision, ranging within the limits of 10^{-2} for large v and 10^{-4} for small v. Further, the interchange processes O_2* with O need not necessarily be accompanied by a change of v. But processes that take place without any change in v may escape notice, as they are not accompanied by any change in the O_2* concentration.

The O_2* molecule at $v > 27$ will react to O_2 at practically every collision, but for the deactivation of O_2* at $v \leqslant 27$ no less than one hundred collisions are necessary. Should O_2* at $v > 27$ and O_2* at $v \leqslant 27$ arise in similar quantities, the concentration of O_2* at $v > 27$ will be not less than one hundredth part of the O_2* concentration at $v \leqslant 27$.

The density of the medium is unimportant, as O_2* is deactivated only by collisions and not by radiation. OH* at $v \leqslant 9$ may appear in O_2* at $v \leqslant 27$ reactions.

All our suppositions have been completely borne out by the fact that the hydroxyl emission arises in the zone of effective association of oxygen at an altitude of approximately 100 km, where no OH* bands are observed in transition from the initial level above the ninth level.

There are obviously still a number of questions that need further investigation. Among them we might point, for example, to the necessity of obtaining further data on the effective cross-sections of elementary chemical reactions and deactivation processes. The question of the transitional probabilities of OH* is still unclear (SHKLOVSKY, 1951, and HEAPS and HERZBERG, 1952). We still have no exact information on the H content in the upper atmosphere. Nevertheless, the foregoing gaps in our knowledge will, we believe, not materially change our basic conceptions of the nature of the OH airglow.[1]

V. I. KRASSOVSKY

Institute of Physics of the Atmosphere,
Academy of Sciences USSR, Moscow

REFERENCES

BATES D. R. and MOISEIWITSCH B. L.	1956	*J. Atmosph. Terr. Phys.* **8,** 305.
BATES D. R. and NICOLET M.	1950	*J. Geophys. Res.* **55,** 301.
BRIX P. and HERZBERG G.	1954	*Canad. J. Phys.* **32,** 110.
ENIKOLOPJAN N. S. and NALBANDJAN	1950	*The Kinetics of Chain Reaction of Oxidation* (ed. A. B. NALBANDJAN and N. M. AMANOUEL) Publishing House of the Acad. of Sci. of USSR.

[1] In the paper by BATES and MOISEIWITSCH (1956), two errors are to be observed, in that part that deals with KRASSOVSKY's article; firstly, in the phrase "the process $O + O_2 + M \rightarrow O_3 + M$ causes $n(O)$ to fall to half the day-equilibrium value within 5 sec of sunset at an altitude of 70 km", "50 sec". And, again, where for O_2* V is shown to equal 25 and 26, the figures should read 27 and 28 respectively.

GAYDON A. G.	1947	*Dissociation Energies and spectra of diatomic Molecules.* London.
HEAPS H. S. and HERZBERG G.	1952	*Z. Phys.* **133,** 48.
HUNAERTS J. et NICOLET M.	1950	*Ciel et Terre* **66,** 213.
JOHNSON F. S., PARCELL J. D., TONSEY R., and WATANABE R.	1952	*J. Geophys. Res.* **57,** 157.
JOST W.	1946	*Explosion and Combustion Processes in gases,* New York and London, McGraw-Hill Book Co., Inc.
KONDRATJEV V. N.	1936	*Elementary Chemical Processes,* Leningrad.
KOOMEN M. J., SEOLNIK R., and TONSAY R.	1956	*Astron. J.* **61,** 182.
KRASSOVSKY V. I.	1952	*Prog. Phys. Sci.* **47,** 493.
	1954	*ibid.* **54,** 469.
	1956	*The Aurorae and the Airglow* (ed. E. B. ARMSTRONG and A. DALGARNO), Pergamon Press, London.
MCKINLEY J. D., GARVIN D., and BONDART M. J.	1955	*J. Chem. Phys.* **23,** 284.
SHKLOVSKY I. S.	1951	*Publ. Crim. Obs.* **7,** 34.

VOL. 10 1957

On the energy distribution of secondary auroral electrons

(*Received* 24 *September* 1956)

FOR the interpretation of the auroral spectrum it is necessary to know the energy distribution of the electrons ejected by the primary particles. Quantal calculations relating to ejection from atomic hydrogen have been carried out by BATES and GRIFFING (1953, 1955). However, atomic hydrogen is unrepresentative of the atmospheric constituents as is evident from the fact that the distribution of the absorption cross-section through its photoionization continuum (which is closely related to the energy distribution of electrons removed in fast collisions) is very different from the corresponding distributions through the photoionization continua of atomic oxygen and nitrogen: thus the absorption cross-section of hydrogen falls off rapidly above the spectral head, whereas the absorption cross-sections of oxygen and nitrogen first increase and then fall off quite slowly (cf. BATES and SEATON, 1949).

Neon is sufficiently similar to oxygen and nitrogen for an investigation on it to be of relevance in connection with aurorae. In the present note we briefly report some results obtained for the case of proton impact.

The mathematical analysis involved is rather lengthy but not difficult, and need not be described. It is enough to state that BORN's approximation (cf. MOTT and MASSEY, 1949) was used; that the active electron when bound was represented by a Hartree-Fock wave function* (the radial part being fitted to a pair of exponentials), and when free by a unit-charge Coulomb wave-function of which only the d component was taken into account.† The final formulae are given in the appendix.

* We wish to thank Miss B. H. WORSLEY, who computed this wave function, for making it available to us in advance of publication.

† Though the p component gives an appreciable contribution to the ionization cross-section, it has little influence on the energy distribution of the ejected electrons (LEDSHAM, 1951). The other components are unimportant.

A convenient means of presenting the main results is provided by the function $F(\varepsilon|\mathscr{E})$, which gives the fraction of the electrons ejected from the outer shell by protons of energy $\mathscr{E}$ keV which have an energy in excess of ε times the ionization potential of atomic hydrogen (13·6 eV). Plots of $F(\varepsilon|\mathscr{E})$ versus log $\mathscr{E}$ for some selected values of ε are shown in Fig. 1.

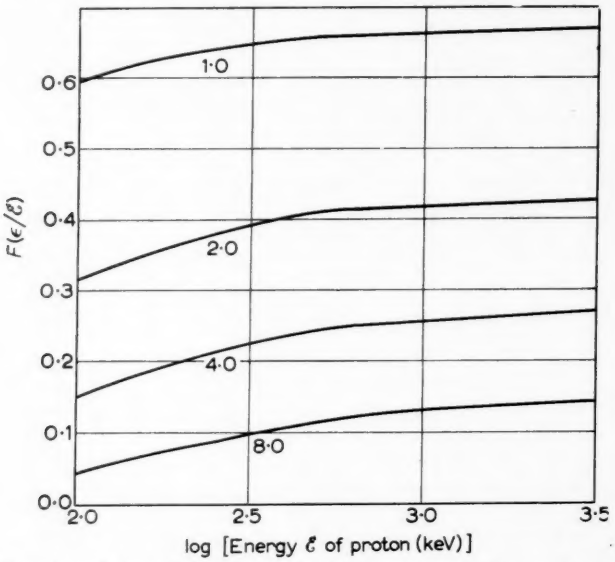

Fig. 1. Fraction of ejected electrons which have an energy of more than ε times the ionization potential of atomic hydrogen. The value of ε is given on each curve.

It is seen that a considerable proportion of the secondary electrons of very energetic protons are able to excite spectral lines originating from high levels, and to liberate tertiary electrons. As would be expected from a comparison of the photoionization continua $F(\varepsilon|\mathscr{E})$ for neon is a much more slowly decreasing function of ε at fixed $\mathscr{E}$ than is $F(\varepsilon|\mathscr{E})$ for hydrogen (cf. Bates and Griffing, 1953).

D. R. Bates
M. R. C. McDowell
A. Omholt*

Department of Applied Mathematics,
The Queen's University of Belfast

References

Bates D. R. and Griffing G. W.	1953	*Proc. Phys. Soc.* **A66,** 961.
	1955	*ibid.* **A68,** 90.
Bates D. R. and Seaton M. J.	1949	*Monthly Not. Roy. Astron. Soc.* **109,** 698.
Ledsham F. C.	1951	Thesis, London University.
Mott N. F. and Massey H. S. W.	1949	*Theory of Atomic Collisions* (2nd Ed.) Clarendon Press, Oxford.

Appendix

Let $(Q_m\ d\epsilon)\pi a_0^2$ be the cross-section per p-shell electron describing ejection into the d component of the continuum with energy between εI_H and $(\varepsilon + d\varepsilon)I_H$, m being the magnetic quantum number, πa_0^2 the area of the first Bohr orbit, and I_H the ionization potential of atomic

* On leave from The Auroral Observatory, Tromso, Norway.

hydrogen. If $(s^2)I_H$ is the energy the incident proton would have if its mass were that of the electron, then

$$Q_m = s^{-2}\int_{t_m}^{\infty} J_m(\varepsilon, t)\, dt,$$

where

$$t_{min} = (\Delta E + \varepsilon)/2s,$$

$(\Delta E)I_H$ is the ionization potential of neon and J_m is a certain function. Taking the normalized radial part of bound-wave function to be of the form

$$r\,[N_1 \exp(-\alpha_1 r) + N_2 \exp(-\alpha_2 r)]$$

and taking (for the sake of generality) the nuclear charge controlling the free-wave function to be β, we find

$$J_m = \beta\sigma\rho|W_m|^2/t^{11}\,[1 - \exp(-2\pi\beta/\kappa)],$$

where

$$\kappa = \varepsilon^{\frac{1}{2}}, \qquad \sigma = 1/(\kappa^2 + \beta^2), \qquad \rho = 1/(4\kappa^2 + \beta^2),$$

$$W_{\pm 1} = 2\sqrt{15}\{N_1 \exp(-\theta_1)X_1 + N_2 \exp(-\theta_2)X_2\},$$

$$W_0 = 2\sqrt{5}\{N_1 \exp(-\theta_1)Y_1 + N_2 \exp(-\theta_2)Y_2\};$$

in which, omitting for brevity the identifying subscripts corresponding to the parameters α_1 and α_2,

$$\theta = (\beta/\kappa)\,\tan^{-1}(2\alpha\kappa/\alpha^2 + t^2 - \kappa^2),$$

$$X = P\{U\cos\phi + V\sin\phi\}, \qquad Y = P\{(3U - 2u)\cos\phi + (3V - 2v)\sin\phi\},$$

with

$$P = 1/(S^2 - 4t^2\kappa^2), \qquad \phi = (\beta/2\kappa)\log\{(S - 2t\kappa)/(S + 2t\kappa)\},$$

$$U = (2t/\rho)\{3\rho S(2\alpha S + \beta D) - 4\alpha t^2\},$$

$$V = (1/\beta P)\{3(2\alpha S + \beta D) - 4\beta P t^2(\beta^2 D + 3\alpha\beta S - 2\kappa^2 D)\},$$

$$u = (2t^3/\sigma\rho\kappa^2)\{\sigma[S(2\alpha - \beta) - 2\kappa^2(\alpha - \beta) + 4\alpha^2\beta] - \rho PS[2\alpha S^2 - \beta D^2 + 4\alpha(\alpha^2 + \kappa^2)(\alpha\beta - 2\kappa^2)]\},$$

$$v = (t^2/2\beta\sigma\rho P\kappa^4)\{3\alpha - 2\beta\sigma SP[2\alpha\beta S - \kappa^2 D - 2\alpha\kappa^2(\alpha + \beta)] + \beta\rho P^2(S^2 + 4t^2\kappa^2)[\alpha\beta S^2 + 2\kappa^2 D^2 - 4\kappa^2\alpha(\alpha^2 + \kappa^2)(2\alpha + \beta)]\},$$

$$S = \alpha^2 + \kappa^2 + t^2, \qquad D = \alpha^2 + \kappa^2 - t^2.$$

When t is small, considerable simplification may be effected by expanding in powers of this variable in the original matrix element.

VOL. 10 1957

Journal of Atmospheric and Terrestrial Physics, 1957, Vol. 10, pp. 54 to 56. Pergamon Press Ltd., London

Indices of geomagnetic activity

of the Observatories ABINGER (*Ab*), ESKDALEMUIR (*Es*) and LERWICK (*Le*)

July 1956

The figures given on pages 54 to 56 represent the K-indices for three-hour intervals, beginning with 00–03 hrs for the first and ending with 21–24 hrs for the eighth figure.

July 1956

Day	*Ab* *Range for* $K = 9 : 500\gamma$		*Sum*	*Es* *Range for* $K = 9 : 750\gamma$		*Sum*	*Le* *Range for* $K = 9 : 1000\gamma$		*Sum*	*Day*
	K-Indices			*K-Indices*			*K-Indices*			
1	2233	3433	23	2233	3332	21	1122	3333	18	1
2	3143	3442	24	3232	3432	22	3132	3332	20	2
3	3333	3311	20	3233	4311	20	3333	4311	21	3
4	1223	2322	17	1222	2221	14	1322	1121	13	4
5	1223	3323	19	1123	3322	17	1123	3222	16	5
6	2223	3320	17	2213	2321	16	2112	2320	13	6
7	0222	2321	14	0111	2321	11	1111	2211	10	7
8	4232	3234	23	3332	2224	21	2321	1224	17	8
9	3332	3312	20	3322	2212	17	3222	2212	16	9
10	1133	2453	22	1122	1353	18	1122	1343	17	10
11	3332	4433	25	3232	4332	22	3322	3322	20	11
12	2332	3232	20	2232	2331	18	2331	2231	17	12
13	3212	4554	26	3212	3554	25	4311	3455	26	13
14	4212	3334	22	4212	3333	21	6222	2233	22	14
15	2112	2232	15	2211	2331	15	1111	2232	13	15
16	2322	3322	19	2222	3322	18	3222	3322	19	16
17	1223	2222	16	1222	1222	14	1222	1212	13	17
18	1111	2322	13	1112	2232	14	1111	2232	13	18
19	3232	4334	24	3222	3334	22	3222	3323	20	19
20	4232	4422	23	4222	3332	21	3221	3322	18	20
21	1012	2122	11	1011	2121	9	1011	2111	8	21
22	1112	3322	15	1111	2312	12	1111	2212	11	22
23	2222	4444	24	2212	4333	20	2112	3336	21	23
24	4245	4422	27	3244	4422	25	3245	3321	23	24
25	3334	3434	27	2334	3334	25	3233	4326	26	25
26	4344	4544	32	5354	4545	35	7444	4445	36	26
27	3333	4333	25	3332	4233	23	4433	3234	26	27
28	3334	4444	29	3233	3444	26	3333	3344	26	28
29	3243	4532	26	3142	3532	23	3142	3532	23	29
30	3233	3232	21	3232	2232	19	3322	2222	18	30
31	1223	4322	19	1122	4231	16	1122	4321	16	31

August 1956

Day	*Ab* Range for $K = 9 : 500\gamma$		Sum	*Es* Range for $K = 9 : 750\gamma$		Sum	*Le* Range for $K = 9 : 1000\gamma$		Sum	Day
	K-Indices			*K-Indices*			*K-Indices*			
1	4222	3322	20	3212	3321	17	4312	3321	19	1
2	3213	3232	19	2112	2222	14	2112	2222	14	2
3	2232	3312	18	1122	3311	14	1122	3311	14	3
4	2222	3332	19	1111	1222	11	1111	1212	10	4
5	1322	1321	15	1211	1221	11	1211	1221	11	5
6	2223	2332	19	1112	3321	14	1112	3321	14	6
7	1222	2222	15	1101	1121	8	1111	1121	9	7
8	2223	3443	23	2122	2443	20	2123	3343	21	8
9	2234	4454	28	2223	4553	26	2223	4545	27	9
10	3333	3323	23	3323	3223	21	3322	3212	18	10
11	5444	4443	32	5344	4443	31	3334	4553	30	11
12	3333	4344	27	3333	3334	25	3333	4333	25	12
13	1123	3333	19	1112	3222	14	1122	2222	14	13
14	3222	2222	17	2211	2112	12	2212	1112	12	14
15	2222	3222	17	1112	3222	14	1111	3221	12	15
16	1122	2433	18	1101	2322	12	1011	2322	12	16
17	4444	4422	28	3433	4321	23	3433	4311	22	17
18	2122	2222	15	1111	2211	10	1233	2111	14	18
19	0112	3222	13	0001	2212	8	0022	3211	11	19
20	1122	2321	14	1011	1211	8	1133	2210	13	20
21	1224	6533	26	1123	5533	23	0233	5433	23	21
22	3223	4333	23	2112	4333	19	3112	3333	19	22
23	3243	5345	29	3233	5335	27	3233	5447	31	23
24	6435	4645	37	7434	5654	38	9434	7764	44	24
25	4334	4544	31	4333	5544	31	5333	5545	33	25
26	5343	3442	28	5343	3442	28	8543	3342	32	26
27	3333	4322	23	2322	3322	19	3232	4322	21	27
28	4323	3432	24	3323	3322	21	4312	3422	21	28
29	2233	4423	23	2122	4322	18	1222	4323	19	29
30	3233	3331	21	2123	2221	15	2222	2221	15	30
31	1234	4543	26	1014	4433	20	1023	4543	22	31

September 1956

1	3323	3333	23	3123	3332	20	3113	3331	18	1
2	5665	4443	37	4665	4343	35	4776	4443	39	2
3	4554	4333	31	6644	5322	32	7754	5443	39	3
4	2333	3232	21	2222	3121	15	3122	3221	16	4
5	3323	3223	21	3322	2212	17	3222	2211	15	5
6	3334	4333	26	3334	4333	26	3334	5533	29	6
7	3233	3322	21	3133	2311	17	3322	2211	16	7
8	2135	8853	35	1134	9953	35	1134	8953	34	8
9	3244	4344	28	3242	3232	21	2234	4243	24	9
10	3322	3332	21	2112	3331	16	3212	3332	19	10
11	2323	3322	20	1222	2222	15	1112	2212	12	11
12	2223	3234	21	1112	2234	16	1111	2126	15	12
13	4423	2332	23	4422	2322	21	5533	2322	25	13
14	1222	2212	14	1111	1211	9	1111	1111	8	14

VOL. 10 1957

September 1956 (*contd.*)

Day	*Ab* Range for $K = 9 : 500\gamma$		Sum	*Es* Range for $K = 9 : 750\gamma$		Sum	*Le* Range for $K = 9 : 1000\gamma$		Sum	Day
	K-Indices			*K-Indices*			*K-Indices*			
15	2213	2213	16	3211	2113	14	2112	1113	12	15
16	3122	3323	19	2111	3323	16	2122	3433	20	16
17	1222	2221	14	1121	2221	12	1112	3221	13	17
18	2123	2211	14	1011	1000	4	2011	1101	7	18
19	1122	1212	12	1011	1011	6	1011	1101	6	19
20	2444	4644	32	1334	5643	29	1333	4545	28	20
21	5543	4433	31	5544	3333	30	5543	3333	29	21
22	3343	3443	27	2443	4443	28	4444	3443	30	22
23	3233	3312	20	3232	2212	17	3322	2212	17	23
24	1122	3133	16	1122	2123	14	1122	2133	15	24
25	3222	3334	22	3121	2223	16	3311	2224	18	25
26	3333	2321	20	2332	1211	15	3322	1211	15	26
27	0133	3333	19	0022	2232	13	0122	2232	14	27
28	3332	2322	20	2322	2322	18	3331	2312	18	28
29	2222	2223	17	1111	2122	11	1011	2211	9	29
30	3323	3213	20	2221	1113	13	3222	1113	15	30

ERRATUM

J. Atmosph. Terr. Phys. 1956, **9**, 347.

"The Measurement of Cosmic Radio Emission for Ionospheric Studies" was in error credited to the co-authorship of M. LAFFINEUR and J. D. WHITEHEAD. M. LAFFINEUR is the sole author of this Research Note.

Journal of Atmospheric and Terrestrial Physics, 1957, Vol. 10, pp. 57 to 72. Pergamon Press Ltd., London

The theoretical length distribution of ionized meteor trails*

VON R. ESHLEMAN
Radio Propagation Laboratory, Stanford University, Stanford, California

(*Received* 31 *March* 1956)

Abstract—The lengths of the columns of ionization formed by meteors are determined theoretically from the available theoretical and experimental information on (1) the production and radio detection of meteoric ionization, (2) the mass distribution of shower and sporadic meteors, and (3) the distribution of sporadic meteor radiants. The primary factors controlling the length of an individual meteor trail are the mass of the meteoric particle and its angle of approach (radiant) into the upper atmosphere. The most likely (modal) value of trail length for meteors from the same radiant is found to be 12 sec ζ km for sporadic meteors, and approximately 17 sec ζ km for shower meteors, where ζ is the zenith angle of the radiant. The distribution of sporadic trail lengths is found to be relatively insensitive to the exact radiant distribution. For a representative radiant distribution, the most likely trail length for sporadic meteors is 15 km. When these trails are detected by a radar system, there is a selection process which favours the longer trails, so that the most likely length of the trails detected by a radar system employing a broad-beam antenna is about 25 km. This value compares well with a previous experimental determination of trail lengths. The theory indicates that the length distribution of detected trails is essentially independent of the sensitivity of the radar receiver and the power output of the radar transmitter.

VOL.
10
1957

1. INTRODUCTION

WELL over one hundred articles have been published in the past ten years on the subject of the production and radio detection of meteor ionization trails (MANNING, 1955). While most of the physical and radio-reflecting characteristics of meteor trails have been treated in some detail, relatively little has been written about the most distinctive dimension of these columns of ionization; namely, their lengths.

The seeming lack of attention given ionized trail lengths may result from the fact that the length of the column is not one of the factors controlling the amplitude, duration, and polarization of most radio echoes from meteors. That is, the characteristics of almost all meteor echoes are determined by that portion of the trail in the immediate vicinity of the point where rays from the radio transmitter and receiver make supplementary angles with the trail axis. The remaining portions of the trail make no appreciable contribution to the radio echo.

However, it should not be inferred from the above statements that information on trail lengths is not important in the study of meteors and meteoric ionization by radio techniques. Knowledge of trail length—and variation of ionization density with length—is important in studies of (1) the scattering polar diagram of the trails; (2) the total contribution of meteors to the ionization of the E region; (3) the characteristics of the long-enduring echoes from the high-density trails which are contorted by ionospheric turbulence; (4) the characteristics of the echo obtained from the "head" of the column while it is being formed;

* This work has been sponsored by the U.S. Air Force Cambridge Research Center, Air Research and Development Command. This paper is a condensed version of Scientific Report No. 4, Contract AF 19 (604)-1031, Stanford University, December, 1955.

and (5) the relationship between the number of echoes obtained and the space density of meteoric particles.

While the lengths of meteor ionization trails are mentioned briefly in quite a few articles, only one paper has appeared which is devoted specifically to this subject. MANNING, VILLARD, and PETERSON (1953) analysed the times of occurrences of meteor echoes on two separated radar systems, from which they deduced the distribution of the lengths of the ionized columns. (The term radar, as used here, implies that the radio transmitter and receiver are at the same location.) To determine the number of true coincidences recorded by the two radars, the number of random coincidences—computed on the basis of statistical independence—was subtracted from the number of apparent coincidences. In relating the measured time separations of the true coincidences to the trail lengths, it was assumed that the average particle velocity is 50 km/sec. The resultant plot of number vs. length shows a broad peak between 25 and 30 km. That is, the analysis of the experimental measurements indicates that the most likely (modal) length of the meteor ionization trails detected during this test was approximately 25 to 30 km.

The treatment in the present paper is divided into two categories. The theory of the production of ionized meteor trails is applied to illustrate those factors which control individual trail lengths. Then the statistical properties of sporadic and shower meteors are used to determine theoretical trail length distributions.

2. INDIVIDUAL TRAIL LENGTHS

The present treatment of trail lengths is based upon the theory of meteoric ionization which appears in papers by WHIPPLE (1943), HERLOFSON (1948), and KAISER (1953). Following the formulas and discussion presented by KAISER, the ratio of the line density of electrons q (the number of free electrons produced per unit trail length) at atmospheric height h to the maximum line density q_{max} at height h_{max}, is given to a good approximation by

$$\frac{q}{q_{max}} = \frac{9}{4}\exp\left(\frac{h_{max}-h}{H}\right)\left[1-\frac{1}{3}\exp\left(\frac{h_{max}-h}{H}\right)\right]^2 \qquad (1)$$

where H is the atmospheric scale height. In the limited height differential of the upper atmosphere in which meteor ionization trails are formed, H is nearly constant and equal to about 7 km. The height h_{max} of maximum ionization is determined by the mass, velocity, size, shape, and material of the meteoric particle, and by the zenith angle of its path into the upper atmosphere. In particular, h_{max} is greater for high velocities, large zenith angles, and small masses. However, the percentage change in h_{max} is relatively small, since h_{max} is between 85 and 100 km for most of the meteors detected by radio. It will be assumed in the following treatment that H and h_{max} are constants, so that the main factors controlling trail length can be considered in detail.

In Fig. 1, $(h - h_{max})/H$ is plotted as a function of q/q_{max} from (1). Note that the high-altitude "tail" of the column is theoretically infinite in length, since (1) indicates that the ionization line density falls off exponentially with increasing

height. The term "trail length" is therefore not uniquely defined until some criterion is given for determining an effective end of the exponential tail. Several definitions of trail length will be discussed in terms of their usefulness in different applications.

The length of the trail L is related to the height differential Δh over which it exists by $L = \Delta h \sec \zeta$, where ζ is the zenith angle of the meteor's track. In solving (1) for h, only two of the three roots are significant, and these two values

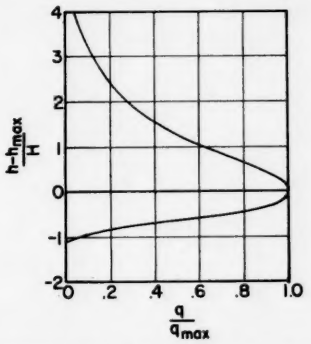

Fig. 1. The relationship between height h and line density of electrons q along a meteor trail. The height h_{max} of maximum ionization q_{max} is near 100 km, and the scale height H is approximately 7 km in this height region.

VOL. 10 1957

of h determine the height differential. From (1) the length of the trail L between the two positions where the line density is q_{min}, $(q_{min} < q_{max})$, is

$$L = H \sec \zeta \ln \left(\frac{1 + \cos \alpha_1}{1 + \cos \alpha_2} \right) \tag{2}$$

where

$$\alpha_1 = \frac{1}{3} \cos^{-1} \left(\frac{2q_{min}}{q_{max}} - 1 \right) + \frac{4\pi}{3}$$

$$\alpha_2 = \frac{1}{3} \cos^{-1} \left(\frac{2q_{min}}{q_{max}} - 1 \right) + \frac{2\pi}{3}$$

In Fig. 2, the relationship between Δh $(= L \cos \zeta)$ and $(q_{min}/q_{max})^2$ is plotted (solid line) from (2), assuming $H = 7$ km. Solving (2) for the line-density ratio in terms of L and ζ would produce an expression ill-suited for algebraic manipulation. In searching for a more tractable approximate expression, it was found that

$$\left(\frac{q_{min}}{q_{max}} \right)^2 \cong \exp \left[- \left(\frac{7L}{12H} \cos \zeta \right)^2 \right] \tag{3}$$

as can be seen in Fig. 2, where (3) is plotted as a dotted line which closely follows the solid line plotted from (2). Thus, the approximate length between two positions of line density q_{min} is

$$L \cong \frac{12}{7} (H \sec \zeta) \left[2 \ln \left(\frac{q_{max}}{q_{min}} \right) \right]^{1/2} \tag{4}$$

A simple definition of trail length is the length of the column along which the electron line density is greater than some fraction of the maximum line density. In particular, the half-density length $L_{0.5}$ is found from (2) or (4), or Fig. 2, by setting $q_{\min} = 0.5\ q_{\max}$, so that

$$L_{0.5} \cong 2H \sec \zeta \tag{5}$$

(For example, the electron line density along the trail exceeds half the maximum value over a distance of $2H$, or about 14 km, for a vertically descending meteor, and over a distance of nearly 20 km for a trail inclined 45° from the vertical.)

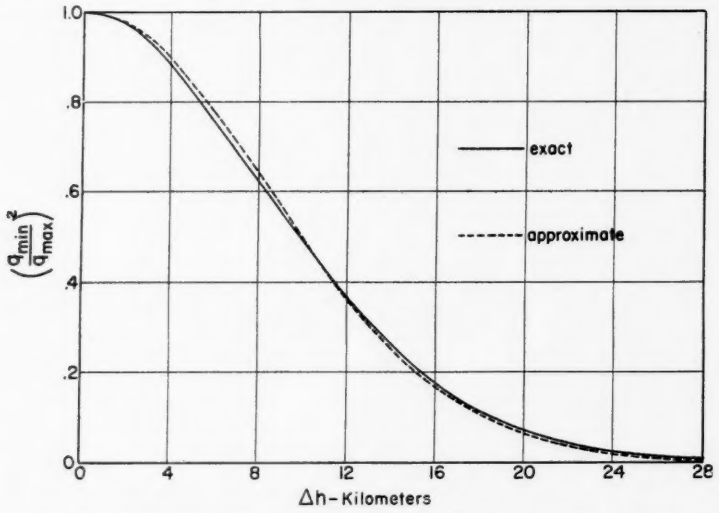

Fig. 2. Exact and approximate curves for the relationship between the square of the line-density ratio which exists at various height differentials along a meteor trail. The exact curve is plotted from (2), while the approximate curve is from (3).

A similar definition of equivalent trail length is the length L_Q of a trail of constant line density, equal to $q_{\max}$, which has the same total ionization content Q as the actual trail. By integrating (1) along the column axis, the total number of electrons in the trail is $Q = \frac{9}{4} H q_{\max} \sec \zeta$, so that

$$L_Q \cong \frac{9}{4} H \sec \zeta \tag{6}$$

While (5) and (6) provide a useful interpretation of meteor trail length, careful attention should be given the manner in which they are defined. In each case the defined length is related to the maximum line density, $q_{\max}$. But the value of $q_{\max}$ is controlled by the value of ζ which also occurs in the expression for the length. The total number of electrons Q produced by the particle is equal to the number of meteoric atoms times the probability β that a single atom will produce a free electron. Thus, $Q = \beta m/\mu$, where m is the initial mass of the meteoric

particle and μ is the average mass of one meteor atom. Relating this formula to the value of Q found by integrating along the meteor's path, it is seen that (KAISER, 1953)

$$q_{max} = \frac{4}{9}\frac{\beta m}{\mu H}\cos\zeta \tag{7}$$

Each of the lengths defined above is proportional to sec ζ, while q_{max} is proportional to cos ζ. Thus, while the length along which the line density exceeds a certain fraction of q_{max} becomes very great for large zenith angles, the value of q_{max} becomes very small. With this effect in mind, the simple definitions of trail length are useful for relating length to the linear distribution of line

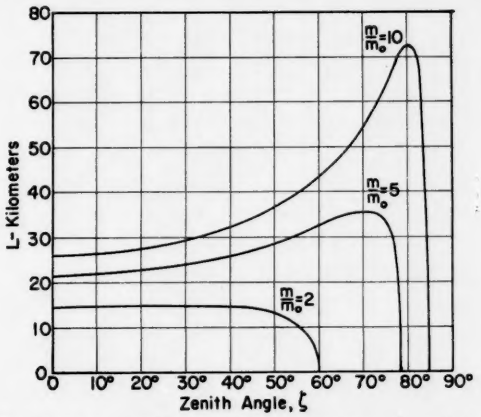

Fig. 3. The length of meteor trails plotted as a function of particle mass m and zenith angle of approach ζ into the upper atmosphere. Meteor trail length is defined here as the distance along the ionized trail between two positions where the line density is q_{min}, where $q_{min} = q_{max}$ when $m = m_0$ and $\zeta = 0$.

density, and for considerations involving the total amount of ionization produced in the E region by meteoric bombardment. However, a definition of length based on an absolute instead of relative value of line density is needed for problems related to the radio-detectability of meteors.

For a trail to be detected by a given radio transmitting and receiving system, two conditions must be satisfied. First, the trail axis must, at some position along its length, make supplementary angles with rays from the transmitter and receiver, and second, the value of q at this point on the axis must be equal to or greater than the minimum value which can be detected by the system. In the remainder of this section, the lengths between a threshold value of line density q_{min} will be determined for individual trails created by particles of various masses and directions of approach. In the next section, these results will be used in conjunction with the positional and mass distributions of meteors to deduce the length distribution of the trails

Let $q_{min} = q_{max}$ when $\zeta = 0$ and $m = m_0$. With β, μ, and H assumed constant, (4) and (7) may be used to determine L as a function of m/m_0 and ζ. That is, in (4), $q_{max}/q_{min} = (m/m_0)\cos\zeta$. In Fig. 3 the length L between constant q_{min} points is plotted as a function of m/m_0 and ζ for an assumed scale height H of

7 km. These curves illustrate the principal characteristics of individual meteor trail lengths. Second-order refinements to this picture of trail lengths could be made by including the effects of meteor velocity, mass, and zenith angle on the height of maximum ionization and hence the scale height. However, the uncertainties in the theories of the production and detection of meteoric ionization are such as to preclude the desirability of a more detailed treatment of theoretical trail lengths at this time.

For a particle of given mass, the maximum trail length occurs when $\cos \zeta = (m_0/m) \exp (0{\cdot}5)$ if $m > m_0 \exp (0{\cdot}5)$, or when $\zeta = 0$ if $m < m_0 \exp (0{\cdot}5)$. The value of trail length at this zenith angle is approximately Hm/m_0 in the former case, and $2{\cdot}4\ H[\ln (m/m_0)]^{1/2}$ in the latter case.

3. Trail Length Distributions

Individual meteor trail lengths were determined above as a function of particle mass and zenith angle of approach into the upper atmosphere. In order to determine the distribution of meteor trail lengths, then, the mass and radiant distributions of meteors must be known. (The radiant of a meteor is the point on the celestial sphere from which it appears to emanate.) The mass distribution of sporadic meteors is fairly well known over a large mass range. It appears that most meteor showers (streams of meteoric particles following the same orbits) contain a larger percentage of large meteors than the sporadics. All of the meteors of a given shower have the same radiant. The exact distribution of sporadic radiants is not well known, but it is known that these radiants are concentrated toward the apex of the earth's way, and are also concentrated to some extent toward the ecliptic plane. (Lovell, 1954; Whipple, 1954). (The apex concentration results from the motion of the earth through the interplanetary distribution of meteoric dust, while the ecliptic concentration implies that the individual meteor orbits tend to lie in the same plane as the planetary orbits.)

While complete and exact information on the distribution of sporadic radiants is not now available, it will be shown that the distribution of trail lengths is relatively unaffected by changes in the radiant distribution. Thus, reasonable estimates of radiants may be used to derive fairly reliable values for the trail-length distribution. Similarly, the range of uncertainty of the exact mass distribution is small enough to have little effect upon the theoretical trail lengths. Thus, the reliability of the following theory of meteor trail-length distribution is primarily set by the applicability of the present theory of trail production and the theory of the mechanism of radio reflections from meteoric ionization.

If all the meteors have the same radiant point, they move in parallel paths into the upper atmosphere, where they produce parallel ionization trails. Such is the case for shower meteors. Sporadic radiants may be considered as a distribution of point radiants over the area of the celestial hemisphere. In this treatment of the effects of meteor radiants on trail length, point and area radiants will be considered in turn. For the determination of the length distributions of the trails which are detected, the geometry of detection will be assumed to be that of the radar case, where the radio transmitter and receiver are at the same location on the ground.

A. *Point Radiants*

It has been determined from visual-photographic and radar investigations that, over a wide mass range, the mass distribution of meteors follows an inverse power law (WATSON, 1941; MCKINLEY, 1951; ESHLEMAN, 1953; KAISER, 1953). Thus, the number-density of particles of mass between m and $m + dm$ may be written as $dn/dm \sim m^{-k}$. Since $q_{\max}$ is proportional to $m \cos \zeta$, $dn/dq_{\max} \sim q_{\max}^{-k} \cos^{k-1} \zeta$ for meteors from a point radiant. Using the relationship between the reference line density and $q_{\max}$ given in (3),

$$\frac{dn}{dL} \sim q_{\min}^{1-k} L \cos^{k+1} \zeta \exp\left[\left(\frac{1-k}{2}\right)\left(\frac{L}{12}\cos\zeta\right)^2\right] \tag{8}$$

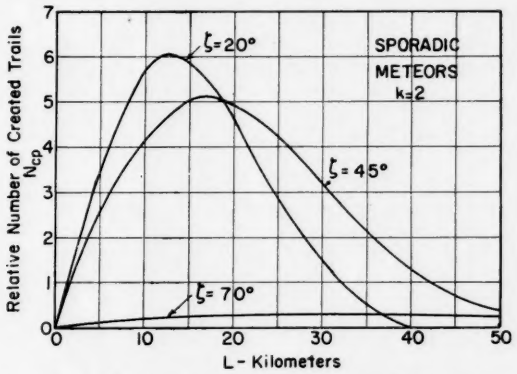

Fig. 4. Relative number density of sporadic meteor trails created per unit time per unit $h_{\max}$-plane area, plotted as a function of their length and zenith angle.

where dn/dL is the number density (in a plane normal to the radiant direction) of trails which are created per unit time in the upper atmosphere having lengths (measured between $q_{\min}$ points) of between L and $L + dL$ km.

The number of point-radiant trails N_{cp} created per unit time in the upper atmosphere which cross a unit area in a horizontal plane at height $h_{\max}$($h_{\max}$ plane), and which have lengths between L and $L + dL$ km, is $\cos \zeta$ times the density of trails in a plane perpendicular to the radiant direction. Thus, neglecting the $q_{\min}$ factor in (8) which was carried along for later application to detected trails,

$$N_{cp} \sim L \cos^{k+2} \zeta \exp\left[\left(\frac{1-k}{2}\right)\left(\frac{L}{12}\cos\zeta\right)^2\right] \tag{9}$$

where the subscripts on the number-density function N indicate created trails, and point-radiant meteors, respectively. Equation (9) is maximum when $L = 12(k-1)^{-1/2}$ sec ζ km. The value of N_{cp} at this most likely (modal) length is proportional to $\cos^{k+1} \zeta$. In Figs. 4 and 5, N_{cp} is plotted as a function of L for $\zeta = 20°$, 45°, and 70°. In Fig. 4, k is set equal to 2, which corresponds to the measured mass distribution of sporadic meteors. In Fig. 5, $k = 1{\cdot}5$, a value chosen to be roughly representative of the meteors of most showers (KAISER, 1953). Note that the shower meteors are longer than sporadic meteors having

VOL. 10 1957

the same radiant point. That is, the mass distribution (k value) of shower meteors differs from that of the sporadics in that there is a higher percentage of larger meteors (and hence longer trails) in the showers.

By integrating (9) from $L = 0$ to infinity, it can be shown that the total number of trails created per unit area and time in the h_{max} plane by a point radiant of zenith angle ζ, is proportional to $\cos^k \zeta$.

While (8) shows a relationship between number and length of the trails which are *created* in the upper atmosphere, several additional factors must be considered in determining the number of trails *detected* by a radar system. These factors

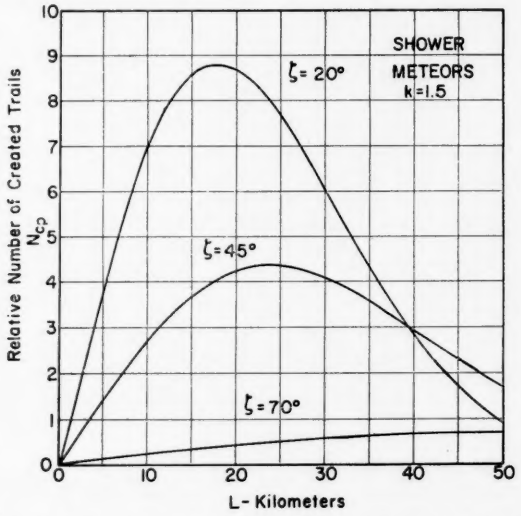

Fig. 5. Relative number density of shower meteor trails created per unit time per unit h_{max}-plane area, plotted as a function of their length and zenith angle.

include the control of radar range and antenna gain on the echo strength, and the orientation of the trails with respect to the radar site.

From the simple electron-scatter theory of radio reflection from meteoric ionization (BLACKETT and LOVELL, 1941; FEINSTEIN, 1951; KAISER and CLOSS, 1952; ESHLEMAN, 1955), the square of the minimum electron line density which can be detected by a given radar system is proportional to R^3G^{-2}, where R is the range to the meteor trail, and G is the antenna power gain over an isotropic radiator in the direction of the trail. Thus, q_{min}^{1-k} in (8) is proportional to $(R^{-3}G^2)^{(k-1)/2}$. (For very low sensitivity radars, where q_{min} is greater than 10^{14} electrons per metre, q_{min}^2 is proportional to $(R^3G^{-2})^4$. However, this case will not be considered here, since q_{min} for a practical meteor-detection radar is considerably less than 10^{14} electrons per metre. For example, if the minimum detectable input signal of a radar operating at 15-m wavelength is 10^{-15} W, and if $G = 1$ and $R = 150$ km, the transmitted power would have to be less than about 3 W for q_{min} to be greater than 10^{14} electrons per metre.)

In addition to the range and antenna gain factors, trail orientation plays a large role in the detectability of meteor trails. In Figs. 6 and 7, the geometry

of radar detection of meteors is illustrated. (The criterion for detection is that a ray from the radar site meets the trail axis at right angles.) Consider meteors from a point radiant of zenith angle ζ and azimuthal angle θ. Consider a ray from the transmitter of elevation angle ε and azimuthal angle ϕ. These angles

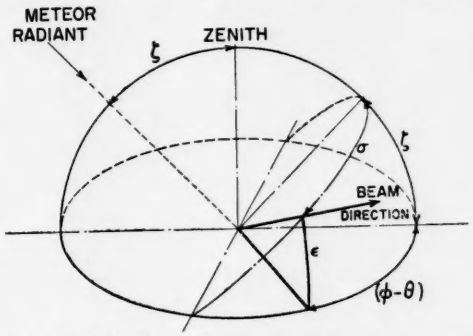

Fig. 6. Geometry of meteor detection. The meteor radiant is at zenith angle ζ and azimuthal angle θ, and a ray from the radar is at elevation angle ε and azimuthal angle ϕ. In order for the ray to be perpendicular to a meteor trail, $\cos(\phi - \theta)$ must equal $\tan \varepsilon / \tan \zeta$.

VOL.
10
1957

are illustrated in Fig. 6, where it can be seen that the geometry of detection is satisfied only if $\cos(\phi - \theta) = \tan \varepsilon / \tan \zeta$. (Plane-earth geometry is assumed. This assumption simplifies the interpretation without invalidating the results, since the range and antenna gain factors usually control the detectability of

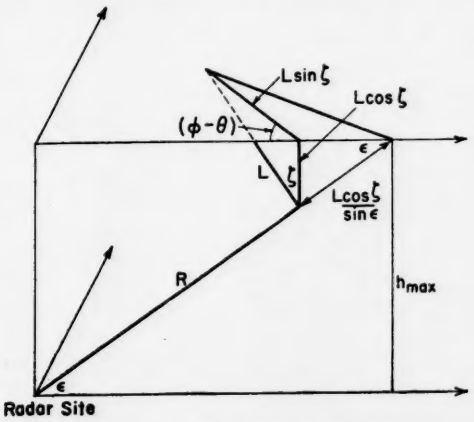

Fig. 7. Geometry of meteor detection, illustrating that the range depth along a ray at elevation angle ε where meteors of length L and zenith angle ζ can be detected is $L \cos \zeta / \sin \varepsilon$.

nearly vertical meteors more than does the curvature of the earth.) With the above angular relationship satisfied, Fig. 7 illustrates that the range depth on the ray along which the perpendicularity criterion holds for trails of constant height h_{max} and length L is $L \cos \zeta / \sin \varepsilon$. As the width of this ray is proportional to R $(= h_{max} / \sin \varepsilon)$, the number of echoes detected is proportional to $(L \cos \zeta / \sin^2 \varepsilon)\ (dn/dL)$.

The above results are directly applicable to the pencil-beam radar case, where all of the radiation is in one differential bundle of rays. Here, the number of trails detected per unit time of length between L and $L + dL$ km is

$$N_{dp}\ (\text{pencil beam}) \sim G^{k-1} L^2 \cos^{k+2} \zeta \sin^{(3k-7)/2} \varepsilon \exp\left[\left(\frac{1-k}{2}\right)\left(\frac{L}{12}\cos\zeta\right)^2\right] \quad (10)$$

if $\cos(\phi - \theta) = \tan\varepsilon/\tan\zeta$. (The subscripts on N denote detected trails, and point-radiant meteors, respectively.) If this angular relationship is not satisfied, no trails are detected. Equation (10) is maximum when $L = 17(k-1)^{-1/2} \sec\zeta$ km. with the number detected of this most likely length being proportional to $\cos^k \zeta \sin^{(3k-7)/2} \varepsilon$. The total number of point-radiant trails of all lengths detected per unit time by the pencil-beam radar is proportional to $\cos^{k-1} \zeta \sin^{(3k-7)/2} \varepsilon$. (Because the above factors are derived using plane-earth geometry, they are applicable only when $\zeta \geqslant \varepsilon \geqslant 10°$.)

The results for the pencil-beam radar may be integrated to find the number of point-radiant trails detected per unit time by a radar having an antenna gain given by $G(\varepsilon,\phi)$. Since only those rays satisfying $\cos(\phi - \theta) = \tan\varepsilon/\tan\zeta$ yield echoes, G may be written as a function of position on the great-circle line on the celestial hemisphere along which this condition holds. Thus the integration is performed along σ from $-\pi/2$ to $\pi/2$, where $\cos\sigma = \sin\varepsilon/\sin\zeta$, so that

$$N_{dp} \sim L^2 \cos^{k+2}\zeta \sin^{(3k-7)/2}\zeta \exp\left[\left(\frac{1-k}{2}\right)\left(\frac{L}{12}\cos\zeta\right)^2\right] \int_{-\pi/2}^{\pi/2} G^{k-1}(\sigma) \cos^{(3k-7)/2}\sigma\, d\sigma \quad (11)$$

Curves could be plotted from (11) for many different antenna gain functions. However, in order to illustrate the principal factors controlling the numbers and lengths of detected trails, without confusing the issue with too many examples, only a few gain functions will be considered. The pencil-beam antenna, considered above for point radiants, will be used to illustrate the effect of having very high antenna directivity. The gain function $G \sim \sin\varepsilon = \cos\sigma \sin\zeta$ will be the primary function considered in the following, since it is a reasonable representation for the antenna used in the trail-length experiment (MANNING, VILLARD, and PETERSON, 1953); namely, a half-wave dipole placed one-quarter wave over ground.

With $G(\sigma) \sim \sin\zeta \cos\sigma$, (11) becomes

$$N_{dp}\ (G \sim \sin\varepsilon) \sim L^2 \cos^{k+2}\zeta \sin^{(5k-9)/2}\zeta \exp\left[\left(\frac{1-k}{2}\right)\left(\frac{L}{12}\cos\zeta\right)^2\right] \quad (12)$$

In Figs. 8 and 9, (12) is plotted as a function of L for $\zeta = 20°$, $45°$, and $70°$. In Fig. 8, the curves are for sporadic meteors ($k = 2$), while Fig. 9 shows the expected length distribution for shower meteors ($k = 1{\cdot}5$). Comparing Figs. 4 and 5 with 8 and 9, it can be seen that the length distributions of the detected trails peak up at greater lengths than the length distributions of the trails created in the meteor region. The principal factor involved in this difference is the probability

of detecting a meteor trail, this probability being proportional to—among other things—the length of the trail (ESHLEMAN and MANNING, 1954). Thus, the most important distinction between the length distributions of created and detected

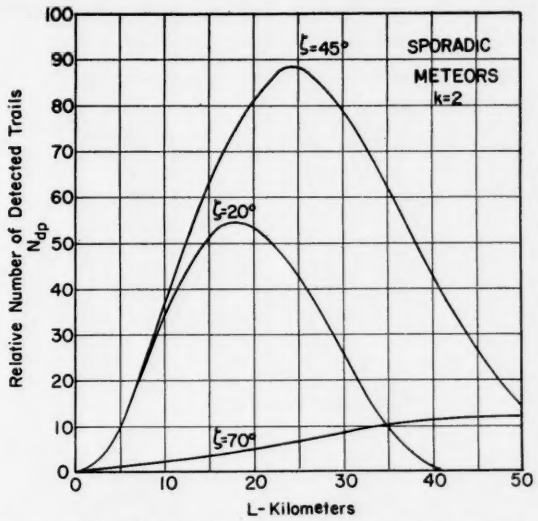

Fig. 8. Relative number density of sporadic meteor trails detected per unit time, plotted as a function of their length and zenith angle. The radar antenna is assumed to have a gain function proportional to the sine of the elevation angle.

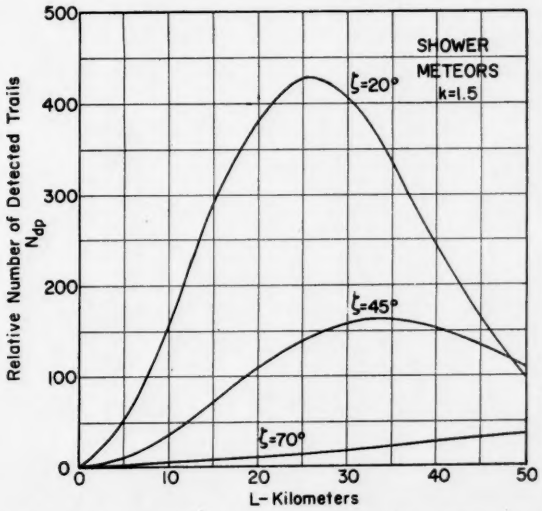

Fig. 9. Relative number density of shower meteor trails detected per unit time, plotted as a function of their length and zenith angle. The radar antenna is assumed to have a gain function proportional to the sine of the elevation angle.

trails is that the latter is fundamentally a modified form of the first moment of the former.

As with the pencil beam, the number of detected trails for conditions of (12)

VOL. 10 1957

is maximum when $L = 17(k-1)^{-1/2} \sec \zeta$ km. The number detected of this length is proportional to $\cos^k \zeta \sin^{(5k-9)/2} \zeta$. The total number of point-radiant meteors of all lengths detected per unit time by a radar with $G \sim \sin \varepsilon$ is proportional to $\cos^{k-1} \zeta \sin^{(5k-9)/2} \zeta$. This last factor is plotted in Fig. 10 for $k = 2$ and 1·5. Note that for $k = 1{\cdot}5$, the integrated number of trails detected per unit time becomes very large for small values of ζ. In practice, earth's curvature limits the minimum value of ζ to about 10°.

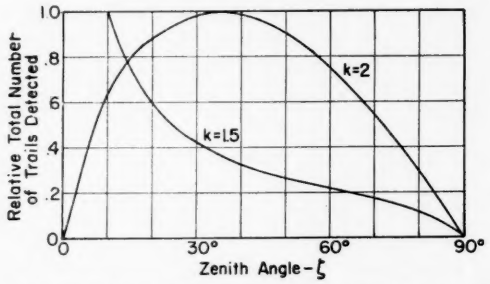

Fig. 10. Total number of trails of all lengths detected, plotted as a function of the zenith angle of the meteor radiant. The radar antenna is assumed to have a gain function proportional to the sine of the elevation angle. The two curves are for shower ($k = 1{\cdot}5$) and sporadic ($k = 2$) meteors, and their absolute magnitudes are not related.

B. *Area Radiants*

Sporadic meteors can best be considered as an area distribution of point radiants upon the celestial hemisphere. The distribution of intensities of these point radiants will be represented by $f(\zeta,\theta)$. That is, $f(\zeta,\theta)$ is the relative number of meteors emanating from each differential radiant position per unit time. Since shower meteors have point radiants, only sporadic ($k = 2$) meteors will be considered in this section. The relative number of sporadic trails created per unit area and time in the $h_{\max}$ plane, having lengths between L and $L + dL$ km, becomes

$$N_{ca} \sim \int_{\zeta=0}^{\pi/2} \int_{\theta=0}^{2\pi} f(\zeta,\theta) N_{cp} \sin \zeta \, d\zeta \, d\theta \tag{13}$$

where the subscript (a) indicates area radiants. Similarly, the number of sporadic trails detected per unit time having lengths between L and $L + dL$ km is

$$N_{da} \sim \int_{\zeta=0}^{\pi/2} \int_{\theta=0}^{2\pi} f(\zeta,\theta) N_{dp} \sin \zeta \, d\zeta \, d\theta \tag{14}$$

The distribution of sporadic radiants is not well known. However, consideration of several simple assumed functions $f(\zeta,\theta)$ shows that the length distribution is affected relatively little by the exact form of the radiant distribution. With $f(\zeta,\theta) = f(\zeta)$ only, and with $k = 2$,

$$N_{ca} \sim \int_0^{\pi/2} f(\zeta) L \cos^4 \zeta \sin \zeta \exp\left[-\frac{1}{2}\left(\frac{L}{12}\cos\zeta\right)^2\right] d\zeta \tag{15}$$

For all but a few very specialized, and unrealistic, classes of functions $f(\zeta)$, (15)

must be integrated numerically for various values of L to find the number of trails created as a function of their length.

Of particular interest is the value of L which corresponds to the maximum value of N_{ca}; i.e. the most likely length. It has been found that this most likely length is very closely approximated by finding the value of L (and ζ) which maximize the integrand of (15). For example, the integrand is maximum when $L = 13{\cdot}9$ km and $\zeta = 30°$ for $f(\zeta) = 1$, when $L = 15{\cdot}5$ km and $\zeta = 39{\cdot}3°$ for $f(\zeta) = \sin \zeta$, and when $L = 17{\cdot}0$ km and $\zeta = 45°$ for $f(\zeta) = \sin^2 \zeta$. That is, the deviation in most likely trail length is only about 10% for such drastic changes in radiant distribution as are represented by the change of $f(\zeta)$ from 1

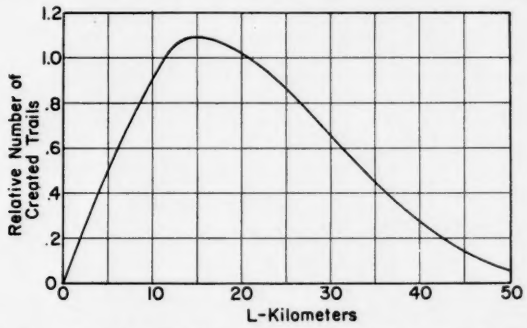

Fig. 11. Relative number density of sporadic meteor trails created per unit time per unit h_{max}-plane area, plotted as a function of their length. It is assumed that the area distribution of sporadic radiants over the celestial hemisphere is proportional to the sine of the zenith angle.

VOL. 10 1957

to $\sin^2 \zeta$. In view of the small effect of radiant distribution on trail-length distribution, a fairly rough approximation to the radiant distribution should yield reliable trail lengths. The rough approximation to $f(\zeta,\theta)$ which will be used here is $\sin \zeta$, indicating that there are, on the average, somewhat more sporadic radiants per unit solid angle near the horizon than near the zenith. This choice of $f(\zeta,\theta)$ is believed to be representative of the middle latitudes, where neither the apex nor ecliptic approach the zenith.

In Fig. 11 the complete N_{ca} curve is plotted as a function of L, with $f(\zeta) = \sin \zeta$. Fig. 11 thus shows the number of trails created in the meteor region plotted as a function of their length, for a reasonable estimate of the sporadic radiant distribution at middle latitudes. Note that the most likely created trail length is about 15 km, as predicted above.

For the sporadic trails detected by a pencil-beam radar, assuming $f(\zeta,\theta) = f(\zeta)$ only,

$$N_{da} \text{ (pencil beam)} \sim \int_{\omega=0}^{\pi/2} f(\zeta) L^2 \cos^4 \zeta \sin^{-1/2} \varepsilon \exp\left[-\frac{1}{2}\left(\frac{L}{12}\cos \zeta\right)^2\right] d\omega \quad (16)$$

where $\cos \varepsilon \cos \omega = \cos \zeta$. While this equation will not be treated in detail, it is evident that when high-gain antennas are used, the number and lengths of the detected trails are critically dependent upon the direction of the antenna beam. For example, when the beam is directed nearly vertically ($\varepsilon \cong 90°$), very

few trails are detected, and these trails are quite long. Decreasing the elevation angle of the beam increases the number of trails detected, and decreases their most likely length. The assumption that f is a function of ζ only is probably not justified for the general pencil-beam radar, since the sharp antenna beam is very selective in determining the radiants from which meteors can be detected.

For the sporadic trails detected per unit time by a radar with $G \sim \sin \varepsilon$, assuming again $f(\zeta,\theta) = f(\zeta)$ only,

$$N_{da}\,(G \sim \sin\ \varepsilon)\ \sim \int_0^{\pi/2} f(\zeta) L^2 \cos^4 \zeta \sin^{3/2} \zeta \exp\left[-\frac{1}{2}\left(\frac{L}{12}\cos\zeta\right)^2\right] d\zeta \qquad (17)$$

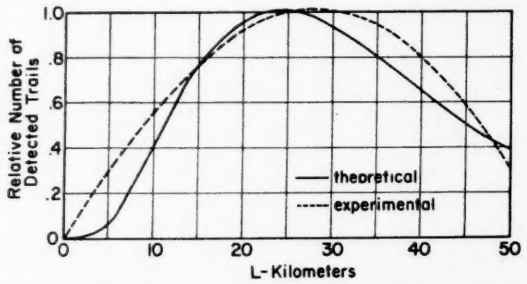

Fig. 12. Relative number density of sporadic meteor trails detected per unit time, plotted as a function of their length. For the theoretical curve, it is assumed that the area distribution of sporadic radiants over the celestial hemisphere is proportional to the sine of the zenith angle, and that the gain function of the radar antenna is proportional to the sine of the elevation angle. The experimental curve is from MANNING, VILLARD, and PETERSON (1953).

The integrand of (17) is maximum when $L = 22{\cdot}4$ km and $\zeta = 40{\cdot}9°$ for $f(\zeta) = 1$, when $L = 25{\cdot}4$ km and $\zeta = 48{\cdot}2°$ for $f(\zeta) = \sin \zeta$, and when $L = 28{\cdot}1$ km and $\zeta = 52{\cdot}9°$ for $f(\zeta) = \sin^2 \zeta$. As before, large changes in $f(\zeta)$ cause relatively small changes in the most likely trail length.

The approximate treatment and discussion above indicates that the most likely trail length detected by a radar located at a middle (30°–60°) latitude, and having an antenna gain function $G \sim \sin \varepsilon$, is about 25 km. Actually integrating (17) numerically with $f(\zeta) = \sin \zeta$ yields the solid curve of Fig. 12 for number of detected trails as a function of their length.

Also plotted in Fig. 12 (dashed line) is the meteor trail-length distribution measured at Stanford University by MANNING, VILLARD, and PETERSON.

The comparison of theory and experiment pictured in Fig. 12 is remarkably good, in view of the various uncertainties in both methods. The fact that they both show a most likely detected trail length near 25 km indicates that both approaches to the problem are probably sound and yield valid results. The agreement between trail-length theory—based on the simple ballistic theory of meteors—and radio measurements of trail length, appears to provide evidence against the fragmentation theory of JACCHIA (1955), for the fainter meteors, since the lengths would be considerably shorter for fragmenting meteors.

An interesting conclusion which can be drawn from the theoretical treatment of sporadic trail-length distributions is the fact that the shape of the distribution

curve—and the value of the most likely trail length—for the trails detected by a radar system, is independent of the transmitter power or receiver sensitivity of the radar system, as long as k is constant. (It is assumed here that the system is at least sensitive enough so that $q_{\min} < 10^{14}$ electrons per metre. If the system-sensitivity to meteor trails is very low, and the rate of detection is only a few echoes per hour, the most likely trail length will be greater than indicated above.) For example, when the radar transmitter power is increased, the lengths of all of the trails which could be detected before the power was increased will be greater. However, many new, short-length trails will be detected which could not produce a measurable response before the power was raised. The net effect of the increased power is to increase the total number of trails detected, with their length distribution remaining the same.

Appendix

Field Strength Contours

In the body of this paper, meteor trail lengths are treated directly so that the length information will be available for later application to such problems as the detectability of meteor trails, their scattering polar diagrams, the fading of long enduring echoes, and meteor head-echoes. In this appendix, the detectability and polar-diagram problems are considered very briefly from a different point of view.

Consider a flat ground plane under a meteor trail whose projected axis lies along the x axis in the plane. Let the $q_{\max}$ point in the trail be at height $h_{\max}$ directly over the origin of the ground plane. For a radar (transmitter and receiver at the same location) on the ground plane at (x,y), the range R to the specular reflection point on the trail is found from

$$R^2 = y^2 + (x + z \sin \zeta)^2 + (h_{\max} - z \cos \zeta)^2 \tag{18}$$

where z is the distance along the trail measured from the $q_{\max}$ point, and ζ is the meteor's zenith angle. For the variation of electron-line density given by (1), the value of q as a function of $q_{\max}$, z, and ζ is

$$q = \frac{q_{\max}}{2}\left\langle 1 + \cos\left\{3\cos^{-1}\left[\frac{1}{2}\exp\left(\frac{z\cos\zeta}{H}\right) - 1\right]\right\}\right\rangle \tag{19}$$

Since the echo voltage strength is proportional to $qR^{-3/2}$ for the low-density trails, the positions on the ground where radars would obtain equal amplitude echoes from the trail are given by

$$qR^{-3/2} = \text{constant} \tag{20}$$

or from (7), (18), and (19),

$$\frac{m\cos\zeta\left\langle 1 + \cos\left\{3\cos^{-1}\left[\frac{1}{2}\exp\left(\frac{z\cos\zeta}{H}\right) - 1\right]\right\}\right\rangle}{[y^2 + (x + z\sin\zeta)^2 + (h_{\max} - z\cos\zeta)^2]^{3/4}} = \text{constant} \tag{21}$$

In Fig. 13, contours of constant radio-echo signal strength are plotted on the ground plane for meteor trails formed by particles of equal mass and velocity approaching at zenith angles of 75°, 45°, and 15°. (It is assumed here that $h_{\max}/H = 14$; e.g. $H = 7$ km and $h_{\max} = 98$ km.) The signal-strength values are in arbitrary units. The maximum signal strength is always on the x axis, and its relative value is 4·9 for $\zeta = 75°$, 8·45 for $\zeta = 45°$, and 2·55 for $\zeta = 15°$. Since $q_{\max}$ is proportional to $\cos\zeta$, and $R_{\min}$ is proportional to $\sin^{-1}\zeta$, the strongest radar echo which can be obtained from a trail formed by a given particle at a given geocentric speed will occur for the ζ which satisfies $\cos\zeta \sin^{3/2}\zeta$ = maximum. This occurs for $\zeta = 50{\cdot}75°$, and the maximum signal strength is then 8·62 in the above arbitrary units.

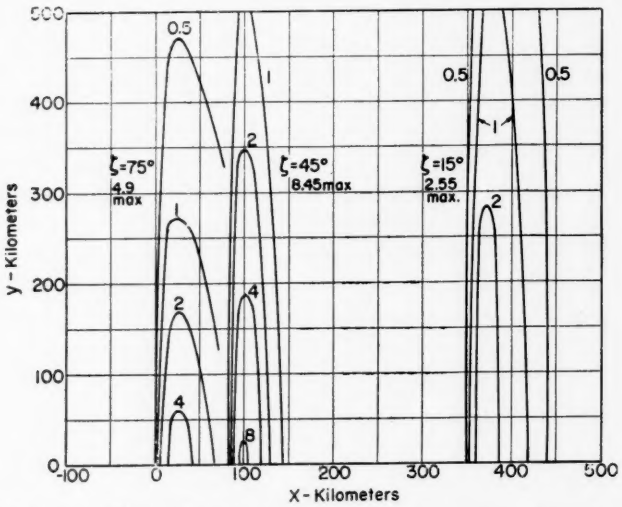

Fig. 13. Relative amplitude of echoes from trails located over $x = 0$, $y = 0$, and detected by radars at general positions on the x,y-plane. The trails considered are those formed by particles of the same size and velocity with zenith angles of 75°, 45°, and 15°. The projections of the axes of the trails lie along the x axis.

Acknowledgements—The author wishes to acknowledge the assistance of Messrs. WU CHEN, ROBERT MLODNOSKY, and DONALD HELLBAUM in the computational work reported here. The helpful discussions and suggestions of Professors L. A. MANNING, O. G. VILLARD, JR., and A. M. PETERSON are also gratefully acknowledged.

REFERENCES

BLACKETT P. M. S. and LOVELL A. C. B.	1941	*Proc. Roy. Soc.* **A177,** 183.
ESHLEMAN V. R.	1953	*Trans. I.R.E., P.G.A.P.* **AP-1,** 37.
	1955	*Trans. I.R.E., P.G.A.P.* **AP-3,** 32.
ESHLEMAN V. R. and MANNING L.A.	1954	*Proc. I.R.E.* **42,** 530.
FEINSTEIN J.	1951	*J. Geophys. Res.* **56,** 37.
HERLOFSON N.	1948	*Phys. Soc. Rep. Prog. Phys.* **11,** 444.
JACCHIA L. G.	1955	*Meteors,* Special Supplement to *J. Atmosph. Terr. Phys.* **2,** 36.
KAISER T. R.	1953	*Adv. Phys.* **2,** 495.
KAISER T. R. and CLOSS R. L.	1952	*Phil. Mag.* **43,** 1.
LOVELL A. C. B.	1954	*Meteor Astronomy,* Clarendon, Oxford, Ch. 6.
MANNING L. A.	1955	A survey of the literature of the ionosphere, Final Report, Contract AF19 (604)-686, Stanford University, Calif.
MANNING L. A., VILLARD O. G. JR., and PETERSON A. M.	1953	*Trans. Amer. Geophys. Un.* **34,** 16.
MCKINLEY D. W. R.	1951	*Canad. J. Phys.* **29,** 403.
WATSON F. G.	1941	*Between the Planets,* Blackiston Co., Philadelphia.
WHIPPLE F. L.	1943	*Rev. Mod. Phys.* **15,** 246.
	1954	*Astron. J.* **59,** 201.

Journal of Atmospheric and Terrestrial Physics, 1957, Vol. 10, pp. 73 to 83. Pergamon Press Ltd., London

Velocity of a body falling through the atmosphere and the propagation of its shock wave to earth

G. V. GROVES
Department of Physics, University College, London

(*Received* 23 *February* 1956)

Abstract—A solution is obtained for the velocity of a body falling to earth from a point outside the appreciable atmosphere on the assumption that (i) the flight path is a straight line inclined at an angle θ to the horizontal, (ii) the drag coefficient C_D is constant, (iii) gravitational acceleration g is constant within the atmosphere, and (iv) the scale height H of the atmosphere is constant. The motion is characterized by the single parameter $p^* = mg \sin\theta/SC_D$, where m is the mass and S the frontal cross-sectional area of the body. Graphs are presented showing velocity and deceleration against height for falls from 100, 200, and 300 km and for various values of p^*. It is shown that the deceleration is greatest at heights where the atmospheric pressure is approximately p^*, and that the rate of loss of energy is greatest at heights where the pressure is approximately $\frac{2}{3}p^*$ (provided the maximum deceleration is somewhat larger than the gravity component along the trajectory). The maximum deceleration is shown to be approximately $[e^{-1}(E/gH + \log_e p^*) - 0{\cdot}5152] \sin\theta$ (provided the body falls at least two to three scale heights before reaching maximum deceleration), where E is the initial energy of the body and p^* is measured in atmospheres.

The effect is considered of refraction arising from the temperature structure of the atmosphere on the shock wave generated by a vertically-falling body. It is shown that only a part of the shock wave originating in the lower atmosphere will reach earth in the case of falls from above 120 km; but for falls from below this height, an additional part of the shock wave originating in the region of the temperature maximum at 50 km may also reach earth. Curves are plotted showing the horizontal range from the impact point at which shock waves originating in the lower atmosphere reach earth for bodies falling vertically from 100, 200, and 300 km with various values of p^*.

VOL. 10 1957

1. INTRODUCTION

A MATERIAL body falling to earth from outside the atmosphere would be expected to generate a shock wave on reaching denser air, provided its velocity was in excess of that of sound. This happens in the case of so-called detonating meteors, which are heard with a crack and thunder-like noise several minutes after being visible. It was once proposed that observations on this interval of time might lead to information on the speed of sound in the upper atmosphere (WHIPPLE, 1923); but the method has never produced reliable results, on account of several practical difficulties. As the velocity of a meteor is several tens of times that of sound, the shock wave that it produces is a very sharp cone, and is therefore propagated almost radially outwards from the flight path. When the shock wave reaches an observer, the meteor is heard, the noise having been produced by the meteor's passage through the air and not by an explosive process, as might be imagined.

Another occasion on which a shock wave would be propagated in the atmosphere is when a high-altitude research vehicle falls back to earth. (A free fall of only 5 km is required in order to attain sonic velocity.) The present paper is concerned with this occurrence and the conditions under which the shock wave from such a body would reach ground. In an isothermal atmosphere at rest, the shock wave would be propagated without refraction in a downward direction, reaching ground over a wide area. In practice, vertical gradients in the wind and temperature structure of the atmosphere will cause refraction, and possibly total reflection, according to the initial direction in which the shock wave is propagated. As this

direction depends on the velocity of the body, consideration must first be given to its motion through the atmosphere.

2. Motion of a Body Falling into the Atmosphere

At heights where air resistance is negligibly small, the velocity v of a moving body is related to the height z by the energy equation

$$\tfrac{1}{2}(v^2 - V^2) = g_0 a^2[(a + z)^{-1} - (a + Z)^{-1}], \tag{1}$$

where V is the velocity at the vertex of the trajectory at height Z, a the earth's radius, and g_0 the gravitational acceleration at ground-level. On its downward path into the atmosphere, the body continues to accelerate until the drag force equals its weight component along the trajectory. This occurs at height z', satisfying

$$\tfrac{1}{2}\rho(z')\, v'^2\, SC_D = mg \sin\theta, \tag{2}$$

where m is the mass, S the cross-sectional area, C_D the drag coefficient, θ the trajectory inclination to the horizontal, $\rho(z)$ the air density at height z, and v' the velocity at z'.

If the work done against drag above height z' is negligibly small compared with the total energy of the body, (1) holds for $z \geqslant z'$, and z' can then be evaluated from (1) and (2).

As an example, a high-altitude vehicle will be considered having (case C.1) $C_D = 0{\cdot}25$, $m/S = 200$ gm/cm^2 (410 lb/ft^2). These values are appropriate to the Aerobee-Hi, for which a plot of C_D has been given by the Rocket Panel (1955). From (1) and (2), z' is found to be 19, 24, and 27 km, when $Z = 100$, 200, and 300 km respectively (taking $V = 0$). To recover the Aerobee instrumentation, the nose section is separated from the remainder of the vehicle. This procedure increases C_D and decreases m/S for the nose section, and appropriate values may be taken to be (case C.2) $C_D = 1{\cdot}0$, $m/S = 100$ gm/cm^2 (205 lb/ft^2). z' is then 32, 37, and 41 km for $Z = 100$, 200, and 300 km. Atmospheric data used in these calculations have been taken from the Rocket Panel (1952) summary.

Below z', the body decelerates with increasing deceleration until a height z'' is reached at which the deceleration is greatest. From the equation of motion

$$\dot{v} = g \sin\theta - \tfrac{1}{2}\rho(z) v^2\, SC_D/m, \tag{3}$$

it is seen, on taking g, θ, and C_D to be constant, that the deceleration is maximum, i.e. $\ddot{v} = 0$, when

$$\dot{\rho} v^2 + 2\rho(z)\, v\dot{v} = 0. \tag{4}$$

If the maximum deceleration is large compared with the gravity component along the trajectory, $g \sin\theta$ can be neglected in (3); and in view of the relation

$$dz/dt = -v \sin\theta,$$

(4) becomes,

$$\sin\theta\, d\rho(z'')/dz + \rho^2(z'')\, SC_D/m = 0. \tag{5}$$

In terms of the scale height $H(z) = p(z)/\rho(z)\, g(z)$, where $p(z)$ is the pressure at height z, this can be written

$$p(z'') = p^*[1 + dH(z'')/dz], \tag{6}$$

where

$$p^* = mg \sin\theta / SC_D. \tag{7}$$

For a high-altitude vehicle falling vertically, z'' is found from (6) to be 4 km and 17 km in the two cases C.1, C.2 above. The rate of energy dissipation is $\frac{1}{2}\rho v^3 SC_D$, and this can be shown by similar reasoning to be maximum at height z''' satisfying

$$p(z''') = \tfrac{2}{3}p^*[1 + dH(z''')/dz]. \tag{8}$$

This gives $z''' = 7$ and 19 km for the cases C.1, C.2 respectively.

To determine other properties of the flight path, it is necessary to integrate the equation of motion, equation (3). This can be written, using the hydrostatic equation $dp/dz = -\rho g$, as

$$\frac{dv^2}{dz} + \frac{1}{p^*}\frac{dp}{dz}v^2 = -2g. \tag{9}$$

As initial conditions, the body is taken to enter the atmosphere at a chosen height z_1, above which drag can be considered negligible; the velocity v_1 at this height being given by (1). Below z_1, a solution for the motion is obtained by integrating (9) on the assumption that p^* and g are constant. It is found that

$$v^2 = \exp\{-[p(z) - p(z_1)]/p^*\}v_1^2 + 2g \exp[-p(z)/p^*]\int_z^{z_1} \exp[p(\zeta)/p^*]\, d\zeta. \tag{10}$$

To evaluate the integral in this equation, the atmosphere is taken to be isothermal in $(0, z_1)$ with scale height H. Then

$$dp/d\zeta = -p/H,$$

and (10) becomes

$$v^2 = \exp\{-[p(z) - p(z_1)]/p^*\}v_1^2 + 2gH \exp[-p(z)/p^*]\{\overline{Ei}[p(z)/p^*] - \overline{Ei}[p(z_1)/p^*]\}, \tag{11}$$

where (JAHNKE and EMDE, 1945)

$$\overline{Ei}(x) = \int_{-\infty}^{x} e^t\, dt/t. \tag{12}$$

Equation (11) is plotted in Fig. 1 for $p^* = e^{-3}$, e^{-2}, e^{-1}, 1, ∞ atmospheres, taking $H = 7{\cdot}25$ km, $z_1 = 50$ km, $g = 9{\cdot}7$ m/sec^2 (corresponding to 25-km altitude), and three values of v_1 corresponding to vertex heights Z of 100, 200, 300 km. It is seen that if log p^* is less than about -2, the impact velocity is independent of the vertex height Z up to at least 300 km. This is true in case C.2 of the falling nose-section, for which log $p^* = -2{\cdot}3$, and the velocity of impact is 134 m/sec. In case C.1, log $p^* = -0{\cdot}25$ and the velocity at impact is 760, 1027, and 1235 m/sec for falls from 100, 200, and 300 km respectively. Separation of the nose section is therefore a very effective means of reducing impact velocity.

From (3) and (7), the deceleration can be written

$$-\dot{v}/g \sin\theta = (v^2/2gHp^*)e^{-z/H} - 1, \tag{13}$$

VOL. 10 1957

where p^* is in atmospheres. Curves of $-\dot{v}/g \sin\theta$ against z are shown in Fig. 2, corresponding to those in Fig. 1. From (6), the maximum deceleration occurs at height $z'' = -H \log p^*$, when the scale height is constant. This gives $z'' = 0$, 7·25, 14·5, and 21·75 km (approximately) for the curves in Fig. 2. Substituting for v^2 from (11) into (13) and putting $p(z) = p^*$, the maximum deceleration is obtained as

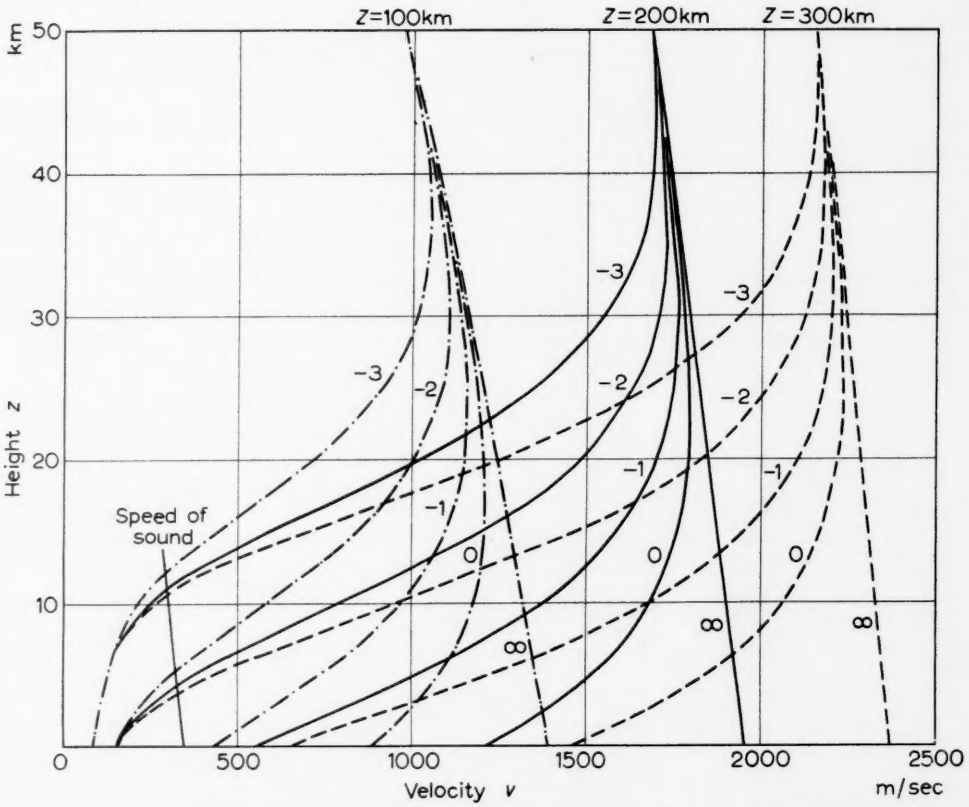

Fig. 1. Curves of velocity for bodies falling into the atmosphere from 100-, 200-, 300-km altitude. Numbers on curves denote values of $\log_e p^*$, where $p^* = mg \sin\theta/SC_D$ (atmos).

$$(-\dot{v}/g \sin\theta)_{\max} = \exp[-1 + p(z_1)/p^*]\,(v_1^2/2gH) + e^{-1}\{\overline{Ei}(1) - \overline{Ei}[p(z_1)/p^*]\} - 1 \qquad (p^* \leqslant 1).$$

If z_1 can be chosen sufficiently large for $p(z_1)/p^*$ to be small, this equation becomes, on giving $\overline{Ei}(x)$ its asymptotic form $\overline{Ei}(x) \sim \gamma + \log x$ for small x (where γ is Euler's constant, 0·5772),

$$(-\dot{v}/g \sin\theta)_{\max} = e^{-1}[E/gH + \log p^*] + \kappa \qquad (p^* \leqslant 1), \qquad (14)$$

where

$$E = \tfrac{1}{2}v_1^2 + gz_1$$

$$\kappa = e^{-1}[\overline{Ei}(1) - \gamma] - 1 = -0{\cdot}5152.$$

VOL. 10 1957

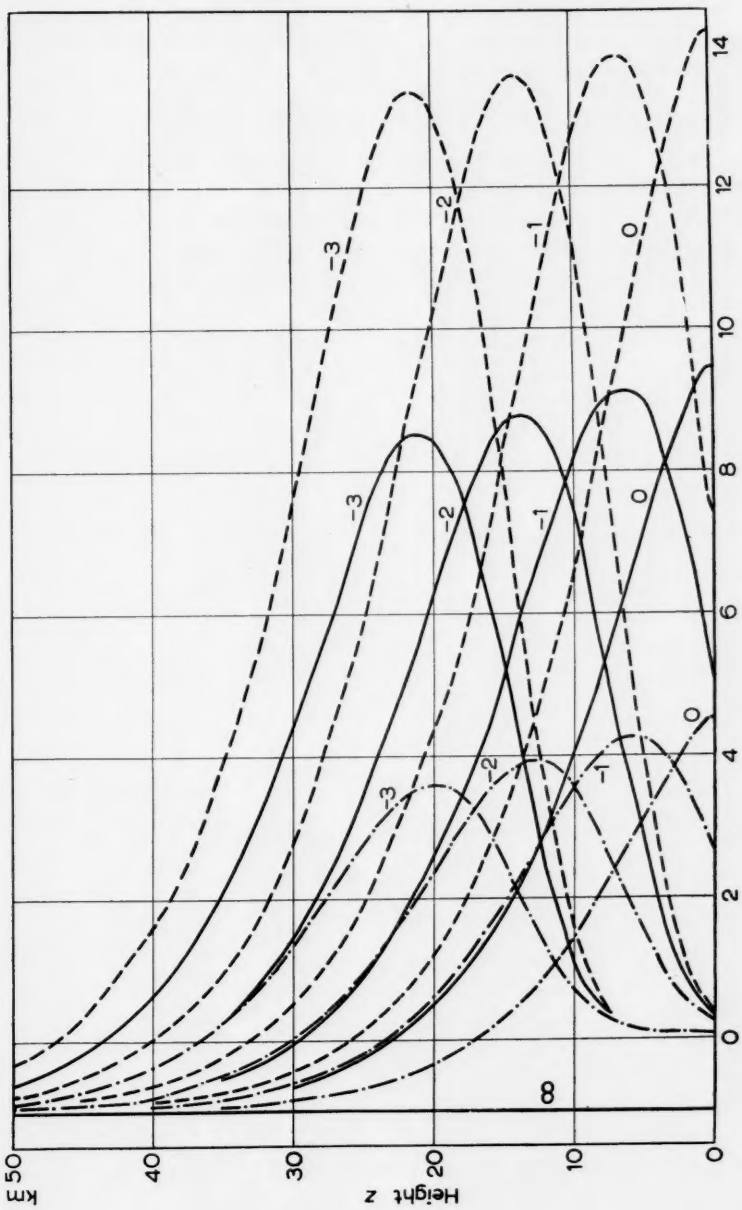

Fig. 2. Curves of deceleration for bodies falling into the atmosphere from 100-, 200-, 300-km altitude.
—·—·— $Z = 100$ km.
———— $Z = 200$ km.
— — — $Z = 300$ km.
Numbers on curves denote values of $\log_e p^*$, where $p^* = mg \sin\theta / SC_D$ (atmos).

If the vertex height Z of the trajectory is small compared with the radius of the earth, $E = \frac{1}{2}V^2 + gZ$, and (14) can be written

$$(-\dot{v}/g \sin\theta)_{\max} = e^{-1}[(V^2/2gH) + (Z - z'')/H] + \kappa. \qquad (15)$$

(14) and (15) are valid so long as $p(z_1)/p^*$ can be made small, i.e. so long as $Z - z''$ is greater than two to three times H.

3. Propagation of a Shock Wave from a Falling Body

On falling into the atmosphere, the nature of the air-flow round a body changes on account of the decreasing mean free path-length l of the air molecules. When l is large in comparison with the characteristic dimension d of the body, molecules hitting it rebound and move away from its vicinity before encountering other molecules. As l decreases, rebounding molecules make collisions nearer and nearer to the body, and a small pressure disturbance is produced along its flight path. The initial pressure disturbance at any point of the flight path is propagated radially outwards at the speed of sound; and the total disturbance can be taken as arising from a line of such disturbances generated at the speed of the body. If this speed is supersonic, the boundary to the pressure field set up in the atmosphere will be the envelope of these individual disturbances (Fig. 3). When l

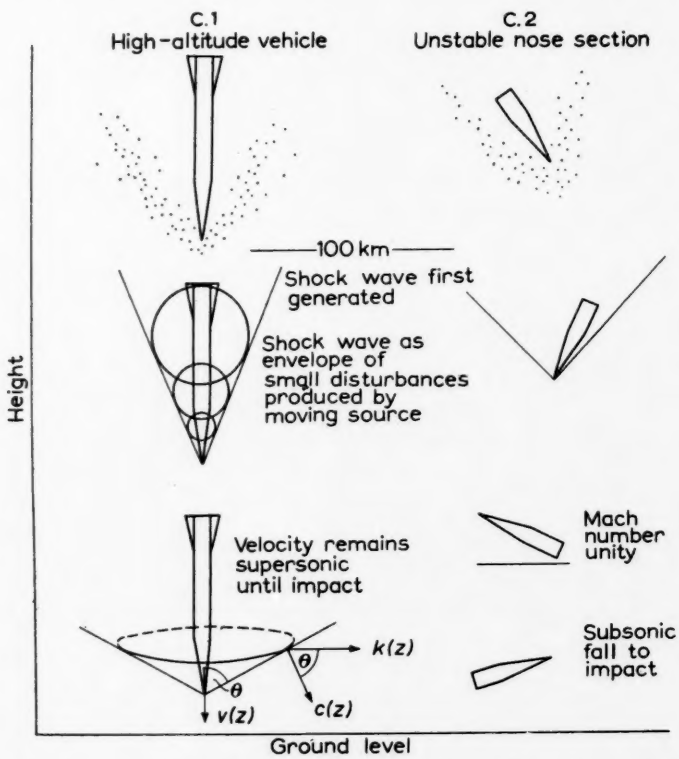

Fig. 3. Diagram showing shock-wave production by a vertically-falling body.

becomes small compared with d, the pressure gradient at the boundary becomes large compared with other pressure gradients in the flow, and a shock wave arises, which is no longer diffuse. In the case of a high-altitude vehicle, a typical value of d is 1 m, and such a shock-wave would first be produced at altitudes where l is of the order of 5 cm, i.e. in the region of 90 to 100 km.

In travelling through the atmosphere, the shock-wave front will become distorted due to atmospheric refraction. In the vicinity of the falling body, though, its shape is approximately conical with semi-vertex angle θ (the Mach angle) given by

$$\sin \theta = 1/M, \tag{16}$$

where M is the Mach number (Fig. 3). For M greater than say 3, θ is less than 20°; and so, for a body falling vertically, an element of the shock front will be propagated in a direction at less than 20° with the horizontal. For inclinations as small as this, refraction by vertical gradients in the wind- and temperature-structure of the atmosphere may result in total reflection of the front before it reaches ground. To investigate this possibility, it is convenient to introduce the *characteristic velocity* k of a shock-front element. This is defined as the velocity with which the line of intersection of the tangent plane to this element and the horizontal plane moves parallel to itself as the tangent plane moves instantaneously parallel to itself at the speed of sound. It can be shown that, for a particular element, k remains constant during propagation, provided horizontal variations in the wind-field and speed of sound are negligibly small (GROVES, 1955). In the case of a body falling vertically in the absence of wind, all shock-front elements produced at height z have the same characteristic velocity (Fig. 3)

$$k(z) = c(z) \sec \theta.$$

Hence, by (16),

$$1/k^2(z) = 1/c^2(z) - 1/v^2(z). \tag{17}$$

In Fig. 4, values of $k(z)$ are shown corresponding to those of $v(z)$ in Fig. 1 for $0 \leqslant z \leqslant 50$ km, and those to given by (1) for $50 \leqslant z \leqslant 100$ km. The values used for $c(z)$ are based on the Rocket Panel (1952) summary of temperatures, and are also shown in Fig. 4.

If a particular shock-front element originating at height z has inclination $\theta(\zeta)$ to the vertical at height ζ $(0 \leqslant \zeta \leqslant z)$, the constancy of its characteristic velocity is expressed by

$$c(\zeta) \sec \theta(\zeta) = k(z). \tag{18}$$

Total reflection of the element occurs when $\theta(\zeta) = 0$, i.e. at heights ζ satisfying

$$c(\zeta) = k(z).$$

The element therefore reaches ground if

$$k(z) > \max c(\zeta) \qquad (0 \leqslant \zeta \leqslant z);$$

i.e. if

$$k(z) > c(0),$$

since for the data shown in Fig. 4 the greatest value of $c(\zeta)$ occurs at $\zeta = 0$. Hence,

VOL. 10 1957

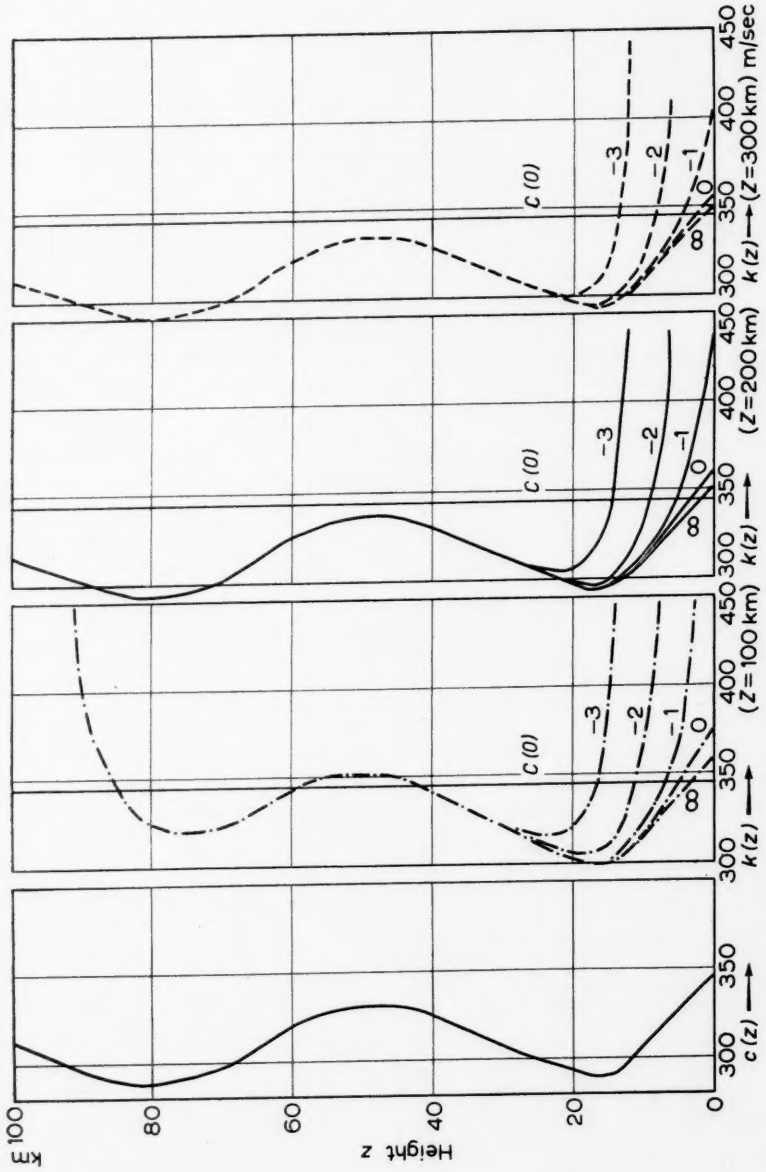

Fig. 4. Curves of characteristic velocity $k(z)$ for bodies falling vertically into the atmosphere from 100-, 200-, 300-km altitude. The speed-of-sound curve is also shown. Numbers on curves denote values of $\log_e p^*$, where $p^* = mg \sin\theta / SC_D$ (atmos).

to the right of the ordinates erected at $k = c(0) = 345$ m/sec in Fig. 4, lie those parts of the trajectory from which the shock wave is received at ground. For a body falling vertically from 100 km, it is seen that the shock wave reaches the ground from the region of 85 to 90 km, where the velocity first becomes supersonic; from the region at about 50 km, where atmospheric temperature has a maximum; and from heights in the lower atmosphere depending on p^*. For falls from 200 and 300 km, no shock wave reaches the ground from the 50-km region on account of the higher velocity there in these cases. The critical value of Z for which the shock wave from the 50-km region no longer reaches ground is 120 km (calculated from (1) and (17) with $k(z) = c(0)$).

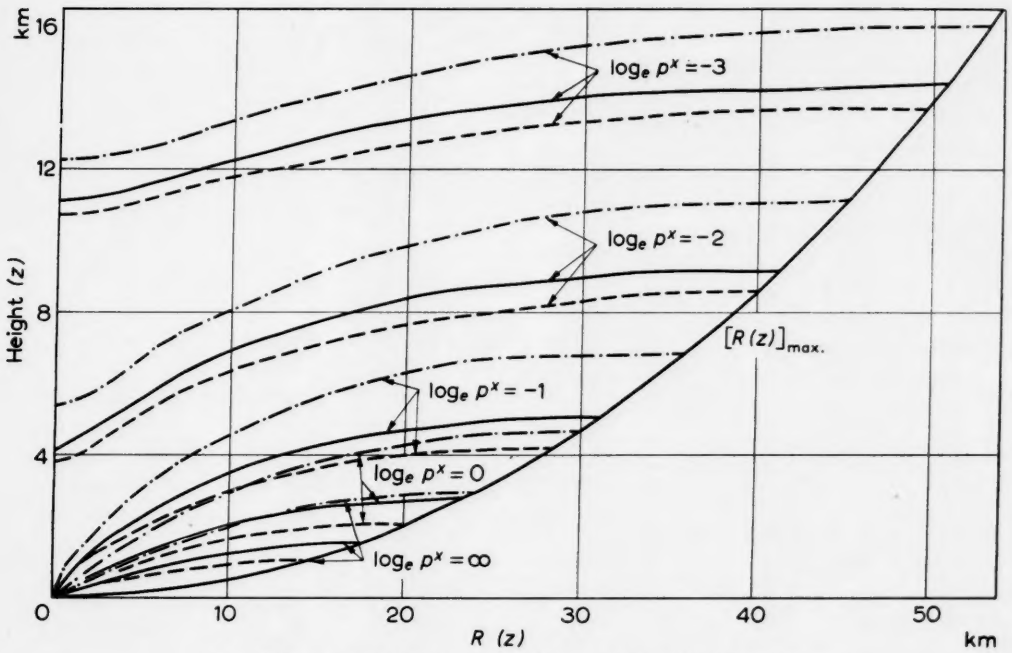

Fig. 5. Distance $R(z)$ from impact point at which a shock-wave element originating at height z reaches ground.
—·—·— $Z = 100$ km.
——— $Z = 200$ km.
— — — $Z = 300$ km.
$p^* = mg \sin\theta / SC_D$ (atmos).

The distance from the impact point to the point at which the shock wave originating at height z reaches ground is

$$R(z) = \int_0^z \cot\theta(\zeta)\, d\zeta = \int_0^z [k^2(\zeta) - c^2(\zeta)]^{-\frac{1}{2}}\, c(\zeta)\, d\zeta \qquad (19)$$

by (18). If the temperature lapse-rate is constant, $dc^2(\zeta)/d\zeta$ has a constant value $-\alpha$, and (19) can be evaluated as

$$R(z) = (-2/\alpha) \int_{c(0)}^{c(z)} [k^2(z) - c^2]^{-\frac{1}{2}}\, c^2\, dc = \{F[c(z)/k(z)] - F[c(0)/k(z)]\}\, k^2(z)/\alpha, \quad (20)$$

VOL. 10 1957

where

$$F(x) = \cos^{-1} x + x(1 - x^2)^{\frac{1}{2}}$$

$$c^2(z) = c^2(0) - \alpha z.$$

This solution has been applied to the velocity curves in Fig. 1, and the results are shown in Fig. 5. The height interval concerned is 0 to 16 km, and for this region the assumption of a constant temperature gradient is justified. α has been given the value 2·4 m/sec², corresponding to a temperature lapse-rate of 6°/km. Putting $k(z) = c(0)$, the shock wave generated at height z is found to reach ground at the maximum range.

$$[R(z)]_{\max} = F[c(z)/c(0)]\, c^2(0)/\alpha.$$

From Fig. 5 it is seen that $[R(z)]_{\max}$ increases as p^* decreases for a body falling from a given height. For a falling nose-section (C.2), $[R(z)]_{\max}$ is about 45 km, while for a complete vehicle (C.1) it is about 25 km.

4. Discussion of Results

A solution of the equation of motion for a body falling through the atmosphere has been obtained on the assumption that p^* $(= mg \sin\theta/SC_D)$ is constant. C_D varies with Mach number in practice, particularly near Mach number unity, and therefore needs to be given a mean value for this solution to be applied. A suitable choice for C_D would be the value where the drag is greatest. This occurs at Mach numbers greater than about 3 in the cases considered. Usually, C_D is nearly constant at these higher Mach numbers, and the solution can justifiably be applied.

Since part of the energy lost from a moving body appears in its shock wave, it is of interest to consider the height at which the maximum rate of loss of energy occurs. This has been found to be the height z''', at which atmospheric pressure is approximately $\frac{2}{3}p^*$ (or, more generally, $\frac{2}{3}p^*\,[1 + dH(z''')/dz]$ when the scale height is not constant). z''' is therefore independent of the energy with which the body enters the atmosphere. This result has also been found to be true for the height z'', at which the deceleration is greatest. The maximum deceleration itself, though, has been found to depend on the initial energy of the body and to vary only slowly with p^*: a decrease in p^*, i.e. a higher drag coefficient surprisingly produces a slight *decrease* in the maximum deceleration. These results are apparent in Fig. 2. As a rough and ready rule, the maximum deceleration is 4·5 g per 100 km of vertex height for vertical falls.

The greatest height at which a supersonic body generates a shock wave depends on its dimensions, and for a high-altitude vehicle is about 90 to 100 km. For a fairly large-sized meteor of diameter 0·6 cm (mass 10 g), the corresponding height is 60 km, where the mean free path-length is 0·03 cm. Very few meteors would be sufficiently large to be audible above this height. This result is in agreement with observation. The rarity of audible meteors above 60 km has previously been associated with the temperature maximum at these heights in no very certain way. Whipple (1929) suggested that the air may be unstable and turbulent in the region of decreasing temperature above 60 km, so causing the energy of

air-waves to be damped out. The foregoing explanation appears to be the more satisfactory, though, particularly in view of the fact that sound-waves from grenade explosions at 80 km have been received at ground in the rocket-grenade experiment (WEISNER, 1954).

For a vertically falling body, the effect of refraction on the shock wave becomes appreciable at Mach numbers greater than about 2. The Mach cone is then more slender, and the direction of propagation is closer to the horizontal. The effect of the temperature structure of the atmosphere is to trap segments of the shock wave by successive total reflections between two height levels at the same temperature. At lower Mach numbers the direction of propagation is in a more downward direction, and the shock wave reaches ground. This state of affairs arises only in the lower atmosphere for falls from above 120 km. For falls from below this height, it may also arise in the region of 50 km; and, for falls below 100 km, in the region where the velocity first becomes supersonic. These last two regions would be expected to merge for falls from about 75 km.

In order to recover the instrumentation in a high-altitude experiment, it is first necessary to locate the point of fall. A possible method of doing this would be to detect the arrival of the shock wave of the falling vehicle at various points on the ground. (This problem will be dealt with in a later paper.) It is therefore of interest to consider the distances from the impact point at which the shock wave can be expected to be received. For shock waves produced in the lower atmosphere, these results are shown in Fig. 5. With a falling nose-section, the maximum distance at which the shock wave would be received is about 45 km, depending on its drag coefficient and the height from which it has fallen. If the vehicle falls intact, a likely maximum distance would be 25 km. If the vertex height is below 100 km, the part of the shock wave generated on supersonic speed first being reached would give a second reception in the vicinity of the impact point. If wind-velocity gradients are at all significant compared with those in the speed of sound, the shock wave would no longer be propagated symmetrically about the vertical flight path, and the above results would need to be modified.

Acknowledgements—The author would like to thank Prof. H. S. W. MASSEY, F.R.S., for his interest in this work, and Dr. R. L. F. BOYD for giving helpful criticisms on this paper. The assistance provided by the computing section of this department is gratefully acknowledged.

VOL. 10 1957

REFERENCES

GROVES G. V.	1955	*J. Atmosph. Terr. Phys.* **7,** 113.
JAHNKE E. and EMDE F.	1945	*Tables of Functions,* Dover Publications.
ROCKET PANEL	1952	*Phys. Rev.* **88,** 1027.
	1955	Minutes of meeting, Report 40, Part I, 3.
WEISNER A. G.	1954	*Rocket exploration of the upper atmosphere,* Pergamon Press, 133.
WHIPPLE F. J. W.	1923	*Nature* **112,** 759.
	1929	*Beitr. Geophys.* **24,** 72.

Journal of Atmospheric and Terrestrial Physics, 1957, Vol. 10, pp. 84 to 95. Pergamon Press Ltd., London

Temperatures in the earth's interior

J. J. GILVARRY*
The Rand Corporation, Santa Monica, California

(*Received* 11 *September* 1956)

Abstract—Fusion temperatures are evaluated for the earth's mantle from LINDEMANN's law by use of elastic parameters determined for a given depth from seismic data. The results are substantially consistent with prediction from the Simon equation, on the basis of a theoretical evaluation of the Simon exponent. The same formulation of the Simon equation is used to obtain fusion temperatures for the core. No inconsistency with these values is shown by deductions from LINDEMANN's law for the outer core. The melting temperatures found for the core are considerably higher than those predicted by SIMON or BULLARD, and show no substantial conflict with JACOBS's hypothesis on the origin of a solid inner core. By using data on the temperature in the earth at small depth, and limits imposed on the possible values by melting temperatures at large depth, the actual temperature in the earth is represented approximately by a quartic polynomial in the depth; the limit of error at large depth if the inner core is solid is estimated as $\pm 25\%$.

1. INTRODUCTION

TEMPERATURES in the earth's mantle have been estimated by ADAMS (1924) and JEFFREYS (1932) on the assumption that the material is everywhere close to the point of fusion, in which case an estimate can be made from CLAPEYRON's equation. The melting-point gradient for the mantle has been determined by UFFEN (1952) from LINDEMANN's law, and by BULLARD (1954) from SIMON's semiempirical fusion equation; the results yield an upper limit on the actual temperature. SIMON (1953) and BULLARD (1954) have estimated melting temperatures in the core from the Simon equation, and VALLE (1955) has done so by use of the Lindemann law; the values provide a lower limit to the corresponding temperature if the outer core is presumed liquid. DALY (1943) has made estimates of actual temperature in the earth by use of Clapeyron's equation as a guide, and SHIMAZU (1954a, b) has used the calculated adiabatic gradient in the mantle for the same purpose.

In a recent paper, GILVARRY (1956a) has derived the Lindemann law, under certain assumptions, from the theory of DEBYE and WALLER for the thermal dependence of the intensity of reflection of X rays by a crystal. The theory yields an experimentally verified relation for the Grüneisen constant of a solid at melting in terms of fusion parameters, which shows that the reformulated Lindemann law yields not only approximately correct magnitudes of melting temperatures, but also correct slopes of fusion curves. The development yields the Simon melting equation very directly (GILVARRY, 1956c). The purpose of this paper is to improve the estimates of the melting-point made by UFFEN, SIMON, BULLARD, and VALLE, and to use the results to estimate actual temperatures in the earth's interior.

2. THEORY

For a monatomic solid, the Lindemann frequency ν_L is given by

$$\nu_L = cm^{-1/2}v_m^{-1/3}(kT_m)^{1/2}\,, \tag{1}$$

* Now at Research Laboratories, Allis-Chalmers Manufacturing Company, Milwaukee, Wisconsin.

where m is the mass of an atom, v_m is the volume per atom of the solid at fusion, T_m is the absolute melting temperature, k is BOLTZMANN'S constant, and the Lindemann constant c is a function of lattice type and the critical ratio of root-mean-square amplitude of thermal vibration to nearest-neighbour distance of the atoms in the solid at fusion. The Debye frequency $\nu_{D,m}$ of the solid at fusion is given by

$$\nu_{D,m} = s_m m^{-1/2} K_m^{1/2} v_m^{1/6}, \tag{2}$$

where K_m is the bulk modulus of the solid at melting, and s_m is defined by

$$s_m = \left[\frac{3}{2(1+\sigma_m)}\right]^{1/2} \left[\frac{9/4\pi}{[2(1-\sigma_m)]^{-3/2} + 2[1-2\sigma_m]^{-3/2}}\right]^{1/3}, \tag{3}$$

as a function of the fusion value σ_m of POISSON'S ratio for the solid. The Debye-Waller theory yields the relation

$$\nu_L = \nu_{D,m} \tag{4}$$

for classical excitation of the lattice waves. Equation (4) represents the Lindemann law on the further assumption that c in equation (1) is a constant along the fusion curve of a solid; the validity of this assumption, in general, has been verified by GILVARRY (1956f) by means of a theoretical evaluation of the variation along the fusion curve of the Lindemann constant. Note that all thermodynamic quantities appearing in equation (4) must be evaluated for the solid at fusion.

VOL. 10 1957

To extend the preceding results to a solid which is not monatomic, it will be assumed that each atom in a molecule can be replaced by an atom with the average mass. If M is the molecular weight and V_m the molecular volume at fusion, one has

$$m = M/nN, \qquad v_m = V_m/nN, \tag{5}$$

under this assumption, where n is the number of atoms in a molecule and N is AVOGADRO'S number. One obtains

$$\nu_L = n^{5/6} N^{1/3} c M^{-1/2} V_m^{-1/3} (RT_m)^{1/2}, \tag{6a}$$

$$\nu_{D,m} = n^{1/3} N^{1/3} s_m M^{-1/2} K_m^{1/2} V_m^{1/6}, \tag{6b}$$

from equations (1) and (2), respectively, where R is the gas constant. Equation (4) yields

$$nRT_m = (s_m/c)^2 K_m V_m \tag{7}$$

as a particularly useful form of the Lindemann relation. Equation (4) is based on the Debye model, and thus this extension to polyatomic crystals can be valid only as an approximation, since it neglects the optical modes of an ionic crystal in general (SLATER, 1939).

The formulation (4) of the Lindemann law yields the Simon equation under the assumption that the Poisson ratio σ_m is constant or slowly varying along a fusion curve. This equation appears as

$$P_m - P_{m,0} = (a/B)[(T_m/T_{m,0})^B - 1], \tag{8}$$

where P_m is the fusion pressure, and $P_{m,0}$ and $T_{m,0}$ represent values of P_m and

T_m, respectively, at the point selected as the arbitrary origin of the fusion curve. The parameter a is given by CLAPEYRON'S equation from the initial slope as

$$a = L_0/\Delta_0 V, \tag{9}$$

where L_0 is the latent heat and $\Delta_0 V$ is the volume change of fusion, at the origin.* The Simon exponent B is determined by quantities associated with the Grüneisen parameter (or constant) γ_m of the solid at fusion, by

$$B = (\eta + \mu)/(\eta - 1), \tag{10}$$

where μ is defined, in terms of a derivative evaluated at the origin, by

$$\mu = d \ln (\gamma_m - 1/3)/d \ln V_m, \tag{11}$$

and η is given in terms of an average Grüneisen parameter $\gamma_{m,\mathrm{av}}$ of the solid, over the range of interest on the fusion curve, by

$$\eta = 2\gamma_{m,\mathrm{av}} + 1/3. \tag{12}$$

Consistently, equations (11) and (12) imply that the Grüneisen parameter of the solid along the fusion curve is a variable. The value $\gamma_{m,0}$ at the origin is fixed by

$$\gamma_{m,0} = 1/3 + (1/2)q_0 K_{m,0}\Delta_0 V/L_0, \tag{13}$$

where

$$q_0 = (1 - K_{m,0}\alpha_{m,0}T_{m,0}\Delta_0 V/L_0)^{-1}, \tag{14}$$

in which $K_{m,0}$ is the value of K_m, and $\alpha_{m,0}$ is the volumetric coefficient of thermal expansion of the solid, at the origin of the fusion curve. When the curve is known experimentally over a sufficient range, the value of B can be obtained from the initial curvature.

3. FUSION TEMPERATURES

To obtain the melting-point gradient, it will be assumed that chemical inhomogeneity in mantle or core does not result in significant variation of the Lindemann constant. The mantle will be presumed to consist of olivine, and the core (both outer core and central body) to consist of pure iron. The effect on the Lindemann constant of inhomogeneity of lattice structure in a solid phase will be neglected.

A. *The mantle*

The Lindemann law (7) can be written in ratio form as

$$T_m/T_{m,0} = (s_m/s_{m,0})^2(K_m/K_{m,0})(\rho_{m,0}/\rho_m), \tag{15}$$

if ρ_m is the fusion value of the density of the solid, $\rho_{m,0}$ is the corresponding value at the origin of the fusion curve, and $s_{m,0}$ is given by equation (3) in terms of the value $\sigma_{m,0}$ of the Poisson ratio of the solid at the origin. Following UFFEN, one can take the origin at a depth in the mantle of 100 km, for which GUTENBERG (1939) has estimated the melting temperature† of ultra-basic rock (or olivine) as 1800°K at the prevailing pressure. The corresponding values of $\sigma_{m,0}$, $K_{m,0}$, and $\rho_{m,0}$, and of σ_m, K_m, and ρ_m as a function of the depth were obtained from values determined from seismic data (BULLARD, 1954). Such determinations are

* Equation (8) is usually written with a/B replaced by a constant A, in which case $AB = a = L_0/\Delta_0 V$.

† As noted by UFFEN, the melting-point of olivine varies with the relative content of iron and magnesium; it is necessary to ignore this fact.

used as approximations to the fusion values for the solid, since all quantities appearing in the Lindemann law must be evaluated for the solid at fusion, as has been emphasized. Melting temperatures thus calculated from equation (15) are shown in Fig. 1 as a function of depth in the mantle.

UFFEN determined the melting-point gradient in two ways: by equating the Lindemann frequency to the Debye frequency, as done here, and by equating

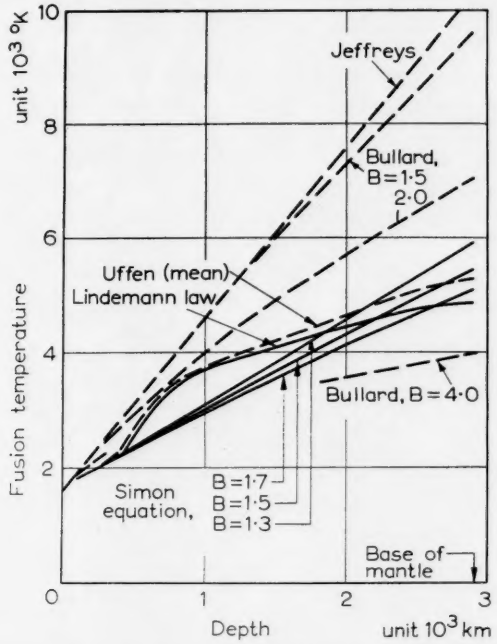

Fig. 1. Fusion temperatures for the mantle as obtained from the Lindemann law and the Simon equation (solid), with values from UFFEN, BULLARD, and JEFFREYS (dashed) for comparison.

it to EINSTEIN'S expression for the characteristic frequency of a solid in terms of elastic parameters. His results by the former method agree with those presented here, inasmuch as his equation (8), in terms of seismic velocities, is equivalent to equation (15) above. The results obtained by use of the Einstein frequency should be less reliable on theoretical grounds, however, since this characteristic frequency for a solid corresponds to a model in which coupling of the atoms and variation of the Poisson ratio are neglected (GILVARRY, 1956d). UFFEN presents a mean as the favoured value, and his mean values for the melting temperature are shown in Fig. 1 for comparison purposes. Likewise shown are JEFFREYS'S values obtained by extrapolation from laboratory data with use of CLAPEYRON'S equation; not that the gradient is considerably higher than implied by the Lindemann law for layer *B*.

It is desirable to check the prediction from the Lindemann law by means of the Simon equation. The parameter a of equation (9) for the mantle is shown in the first column of Table 1, as determined by CLAPEYRON'S equation from the

VOL. 10 1957

initial slope of the fusion curve given by the Lindemann law, for $T_{m,0} = 1800°K$ at a depth of 100 km. Values of B will be obtained by three different methods. Estimates of the Grüneisen parameter γ for compressions corresponding to the mantle have been made from the Birch equation of state (BIRCH, 1952), and these estimates can be used to approximate the fusion value γ_m. BIRCH's data for $\gamma - 1/3$ are shown in Fig. 2 (logarithmic scales) as a function of the ratio ρ/ρ_0 of density ρ at depth d relative to the initial density ρ_0. The first line of Table 1 shows the corresponding values of $\gamma_{m,0}$, μ as evaluated at the origin, $\gamma_{m,av}$ as

Table 1. Parameters of the Simon equation for the mantle (origin at a depth of 100 km)

$10^{-6}a$ (bar)	$\gamma_{m,0}$	μ	$\gamma_{m,av}$	B
0·47	1·8	1·2	1·5	1·7
0·47	1·85	0·6	1·7	1·5
0·47	1·9	0	1·9	1·3

estimated for the mean value of ρ/ρ_0 in the mantle, and B from equation (10). The third line of Table 1 shows a value of $\gamma_{m,0}$ obtained by applying equation (13) for the value $L_0/\Delta_0 V = a$ in the table, with a bulk modulus corresponding to a depth of 100 km, and a mean value for olivine (BIRCH, SCHAIRER, and SPICER, 1942) of $\alpha_{m,0}$ entering q_0 of equation (14). The value $\mu = 0$ was taken to obtain the value of B in the third line, mainly to obtain an upper limit on the temperature

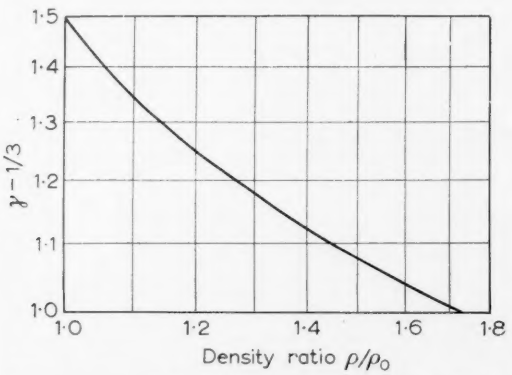

Fig. 2. Estimated values of $\gamma - 1/3$ as a function of density ratio for the mantle, from data of BIRCH; scales are logarithmic.

implied by the Simon equation, and partly on the basis of considerations discussed later which dictate this choice for iron. The second line of Table 1 shows averages of quantities in the first and third lines. Fusion temperatures computed for these three sets of values of a and B from equation (8), as a function of pressure, are shown in Fig. 1 as a function of depth in the earth. It can be pointed out that all values of $\gamma_{m,0}$ shown in Table 1 are consistent among themselves and with independent estimates by SHIMAZU (1954a, b).

One notes that the fusion temperature from the Lindemann law agrees reasonably well at the base of the mantle with the mean value from the Simon equation. The disparity over layer C, arising when the 20° discontinuity is crossed, reflects inhomogeneity. Since the Simon equation represents an interpolation formula (GILVARRY, 1956c), it should be applied in each layer of the mantle separately; in view of this fact, the agreement indicated in Fig. 1 is satisfactory. Also shown in Fig. 1 are BULLARD'S values of the fusion temperature for the mantle, corresponding to selection of values of B in the Simon equation; he gives $B = 2$ as a favoured value, and includes $B = 3$ (curve not shown). BULLARD evaluated a by CLAPEYRON'S equation from the data for the crust which yield JEFFREYS'S curve of Fig. 1 when extrapolated, whereas the initial slope of the fusion curve for layer B, as determined from the Lindemann law, has been used here to fix a.

B. *The core*

In contrast to the case of the mantle, direct application of the Lindemann law (15) cannot be made to the core, since the seismic data for the liquid core yield no information on the fusion value of POISSON'S ratio for solid iron at the pressure prevailing, and no reliable data exist for elastic constants of the central body. Thus, primary recourse must be made to the Simon equation, which, on the derivation (GILVARRY, 1956c) from the Lindemann law, requires (essentially) only the assumptions that the Lindemann constant be fixed and the Poisson ratio be slowly varying. As regards the first assumption, results of GILVARRY (1956f) imply that c changes for iron by no more than 1% for a pressure change of 100 kilobars on the fusion curve.

VOL. 10 1957

The initial curvature of the fusion curve of iron is unknown, and, in their estimates of fusion temperatures in the core by means of the Simon equation, SIMON and BULLARD selected the values of B by arguments based on the known values for the alkali metals. Values of the parameter μ of equation (11), which enters the Simon exponent B, have been obtained by GILVARRY (1956c) for the alkali metals from BRIDGMAN'S fusion data. The values fall in the range 2·6–4·7. These relatively high values, implying a fair variation of γ_m along the fusion curve, are a consequence of the high compressibility of the alkali metals, by virtue of which a number of terms up to nine must be taken in a Taylor expansion to fit the volume-pressure data up to the moderate pressure of 40 kilobars under isothermal conditions (GILVARRY, 1955). One should expect considerably lower values for the relatively incompressible metals, where a two-term Taylor expansion is sufficient to fit the equation of state. For iron, the volume-pressure relationship under isothermal conditions can be represented up to about $\frac{1}{3}$ megabar (roughly the limit of measurement) by the Bridgman equation of state (GORANSON *et al.*, 1955).

It will be assumed that the dependence of V_m (initial value $V_{m,0}$) on P_m is of the Bridgman form

$$-(V_m - V_{m,0})/V_{m,0} = a_m P_m - b_m P_m^2, \tag{16}$$

with constants a_m and b_m, up to the highest pressures considered. When one notes that $K_m = -(V_m/q)\, dP_m/dV_m$ (GILVARRY, 1956c), and assumes that q along the

fusion curve has the constant value q_0 of equation (14), one obtains

$$K_m = K_{m,0}[1 - (2b_m/a_m^2 - 1)(V_m - V_{m,0})/V_{m,0}], \tag{17}$$

from equation (16). Direct use of the expression (GILVARRY, 1956d) of SLATER (1939),

$$\gamma_m = -1/6 - (1/2)d \ln K_m/d \ln V_m, \tag{18}$$

for the Grüneisen parameter from the equation of state, yields

$$\gamma_m = b_m/a_m^2 - 2/3 = \gamma_{m,0}, \tag{19}$$

to the order of approximation corresponding to equation (17), for which $(V_m - V_{m,0})/V_{m,0} = \ln (V_m/V_{m,0})$. Since γ_m is constant to this order, the parameter μ of equation (11) vanishes. Thus, one has $\eta = 2\gamma_{m,0} + 1/3$ from equation (12), and

$$B = (6\gamma_{m,0} + 1)/2(3\gamma_{m,0} - 1), \tag{20}$$

from equation (10). This equation for B can be established directly by noting that iron is sufficiently incompressible for osculating approximations at the origin of the fusion curve to be satisfactory (GILVARRY, 1956c).

Table 2. Parameters of the Simon equation for iron

$\Delta_0 V$ cm³ mole	L_0 cal mole	$10^{-6}a$ bar	$10^{-6}K_{m,0}$ bar	$10^6\alpha_{m,0}$ $(°C)^{-1}$	q_0	$\gamma_{m,0}$	B
0·27	3600	0·56	0·81	64	1·20	1·2	1·6
0·23	**3600**	**0·66**	**0·68**	**64**	**1·14**	**0·92**	**1·9**
0·19	3600	0·79	0·54	64	1·09	0·71	2·3

In the first column of Table 2, a value of $\Delta_0 V$ for iron at the normal fusion temperature 1532°C appears in the second line, which corresponds to the density 7·273 for the solid at fusion given by STOTT and RENDALL (1953), and an increase in volume of 3%; the first and third lines show values corresponding to an uncertainty* of $\pm 0{\cdot}5$ in the percentage volume increase (SIMON, 1953). The value† of J. H. AWBERRY for L_0 (uncertainty less than 2%) appears in the second column. The corresponding values from equation (9) of the parameter a which enters the Simon equation are tabulated in the third column. From equation (13), the value of $\gamma_{m,0}$ necessary to evaluate B depends with equal weight on $\Delta_0 V$ and the bulk modulus $K_{m,0}$ of the solid at the normal fusion point. In Table 2, the first entry in the fourth column shows a value of $K_{m,0}$ for iron obtained by extrapolation to the melting-point of static compression data of BRIDGMAN for the range 0–100°C (GILVARRY, 1956a). Subsequent work has shown that bulk moduli extrapolated from ultrasonic data at temperatures extending relatively close to

* The figure $3 \pm 0{\cdot}5\%$ quoted by SIMON (1953) corresponds to limits set by the results of STOTT and RENDALL (1953) and values from prior work discussed by these authors.

† Quoted by SIMON (1953).

the fusion point are generally lower than corresponding values extrapolated from static measurements (GILVARRY, 1956e). The average difference found (for Pb and Al) was about one-sixth of the statically determined value. Correspondingly, the second entry for $K_{m,0}$ in Table 2 represents five-sixths of the first, as a mean, and the third entry is two-thirds of the first, as a possible extreme. The value shown for $\alpha_{m,0}$ is from KUBASCHEWSKI (1949); the next column gives

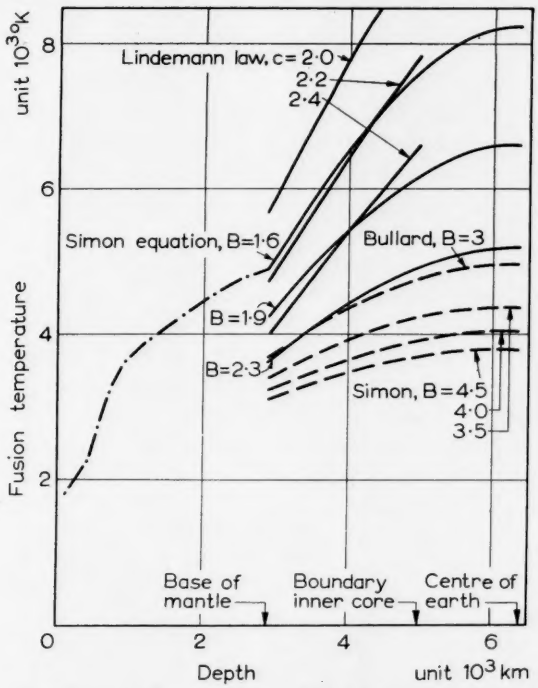

Fig. 3. Fusion temperatures for the core as obtained from the Simon equation and the Lindemann law (solid), with values from SIMON and BULLARD (dashed) from comparison. Values from LINDEMANN'S law for the mantle shown dot-dashed.

values of q_0 from equation (14). The penultimate and last columns show the corresponding values of $\gamma_{m,0}$ and B from equations (13) and (20), respectively. The procedure adopted correlates high extremes and low extremes of $\Delta_0 V$ and $K_{m,0}$ together, so that the corresponding temperatures represent possible limits; mean values of parameters appear in Table 2 in bold face.

The fusion temperatures T_m computed as a function of pressure from equation (8), with use of the three sets of values of a and B in Table 2, are exhibited in Fig. 3 as a function of depth in the earth. It is necessary to show that these curves are not inconsistent with direct prediction from the Lindemann law, from which equation (9) was derived. GILVARRY (1956e) has estimated the Lindemann constant of iron as $c = 2{\cdot}2 \pm 0{\cdot}2$.* A method suggested by ELSASSER

* This estimate of c presupposes a somewhat different definition of s_m than corresponds to equation (3); since a range of values is taken for c the difference has been ignored in applying equation (7).

VOL. 10 1957

(1950) of inferring the Poisson ratio in the central body (presumed solid iron) yields a value of 0·45, as corrected numerically by BIRCH (1952). No inconsistency appears with an estimate by GILVARRY (1956e) of the fusion value of POISSON's ratio for iron at normal pressure as 0·40, since the increase of Poisson ratio throughout the mantle is 0·03, and an increase of about twice this amount is reasonable for the higher pressure of the core. By using bulk moduli and densities from seismic data (BULLARD, 1954) with this value of σ_m and the three possible values of c in question, one can obtain fusion temperatures for the outer core from equation (7). One notes from Fig. 3 that the two lower curves from LINDEMANN'S law bracket fairly well the two upper curves from the Simon equation. Further, the lowest curve from Lindemann's law is reasonably consistent with values obtained by VALLE (1955) on essentially the same method, but with use of some analytic approximations and neglect of the variation of POISSON'S ratio.

In their estimates of fusion temperatures, SIMON and BULLARD used the values of a in the second and first lines respectively, in Table 2. The results of SIMON and BULLARD are shown in Fig. 2 for comparison purposes (BULLARD also chose the value $B = 4$). One notes that melting temperatures obtained by the method of this paper exceed those given by SIMON or BULLARD, in general. If the positive sign of μ shown by the values for the alkali metals is generally valid, the curve of T_m vs. P_m is concave to the pressure axis for $\gamma_m > 1/3$, and in this respect the fusion curve is normal in the sense of BRIDGMAN (GILVARRY, 1956a). All the melting-point gradients in Fig. 3 are consistent with this demand.* Since the value $\mu = 0$ is taken to evaluate the Simon exponent for iron in this paper, this procedure assigns the minimum magnitude of initial curvature consistent with a nonnegative value of μ to the corresponding fusion equation (GILVARRY, 1956a). On the other hand, the use made by SIMON and BULLARD of values for the alkali metals as a guide led them to assign to the fusion curve for iron the high curvature one expects for a compressible element; their values for the melting temperature are necessarily below those obtained here, in view of the sign of the curvature.

The bulk modulus of olivine at fusion under normal pressure can be evaluated (GILVARRY, 1956a) from available data (BIRCH, SCHAIRER, and SPICER, 1942; BIRCH, 1952) as 0·8 megabar for $T_{m,0} = 1800°\text{K}$, which can be compared with the values of Table 2 for iron. Thus, olivine at low pressure is about as incompressible as iron, although its equation of state has not been determined experimentally for very high pressures. These considerations tend to favour the lower values of μ, and the corresponding values of B, shown in Table 1.

4. ACTUAL TEMPERATURES

An explanation of the possibility of a solid inner core has been given by JACOBS (1953) on the basis of an earth once completely molten (by virtue of radioactive heating if formed by cold accretion). A solid inner core and solid mantle would form if successive adiabatic curves of temperature vs. depth, on cooling, intersected the curve of fusion temperature vs. depth first for the inner core and then for the mantle. This explanation requires that the fusion temperature for the inner

* Except for the fusion curve given by the Lindemann law for layer B, which shows a slightly positive value of d^2T_m/dP_m^2.

core be higher than that for the mantle at its base; UFFEN and MISENER (1954), and JACOBS (1954), called attention to the difficulty in this connection raised by SIMON's lower estimates of melting temperature for the core. One notes from Fig. 3 that the lowest melting temperature estimated for the inner core by the methods of this paper is about 5200°K, as compared to a high estimate for the mantle at its base of 5500°K as a mean from the Simon equation. These limits are

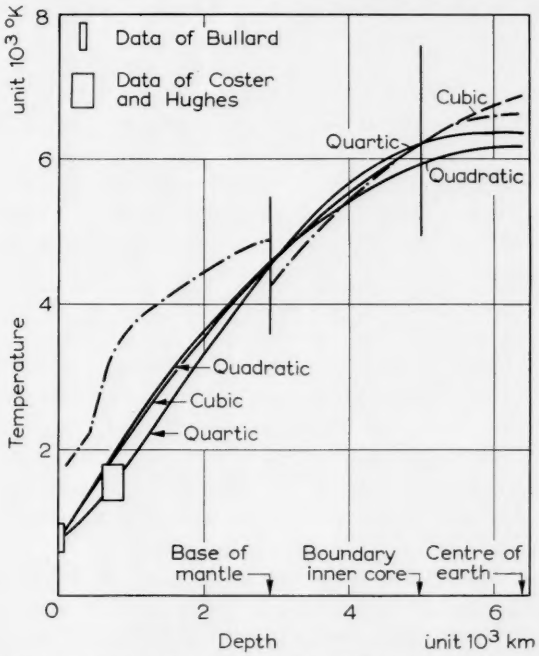

Fig. 4. Actual temperatures in the earth as estimated from quadratic, cubic, and quartic interpolation polynomials. Fusion temperatures, from LINDEMANN's law for the mantle and the mean curve from the Simon equation for the core, shown dot-dashed.

sufficiently close so that, substantially, no conflict appears with JACOBS's hypothesis, without which the origin of a solid inner core is difficult to understand, in view of the low thermal conductivity of the mantle.

BULLARD (1954) has estimated the temperature in the earth at the base of the crust for three different assumptions on the source of the measured heat arriving at the surface. These estimates yield a temperature of 800 $\pm$ 200°K at a depth of 35 km. Computed fusion temperatures yield immediate limits to the temperature at the base of the mantle, which must lie between the fusion temperatures of the liquid core and the solid mantle at this point. The actual temperature at this point will be taken as an average corresponding to the fusion temperature in the mantle from LINDEMANN's law, and the mean fusion curve in the core from the Simon equation; the limits of error fixed by the mean for other fusion curves at this point are shown by a vertical line in Fig. 4. The two temperatures in question can be used to construct a quadratic polynomial for the temperature as a function of depth, when one imposes the constraint that the temperature gradient

VOL. 10 1957

vanishes at the centre of the earth (this conclusion follows by applying GAUSS's theorem to the thermal flux through the surface of a small sphere at the earth's centre). The curve given by the quadratic interpolant is shown in Fig. 4. Furthermore, if the inner core is solid, the fusion temperature at its boundary is the actual temperature (for inner and outer core of the same composition). For this case, one obtains the curve shown in Fig. 4 for a cubic interpolation formula. It is shown dashed inside the inner core, where, inconsistently, it rises above the fusion temperature.

The only experimental evidence on the temperature at depth is the determination by COSTER (1948) and HUGHES (unpublished) of 1300–1800°K as the temperature at which silicates show the low resistivity for a depth of 600–900 km, required by geomagnetic results. The average point from these data is represented in Fig. 4 by a rectangle of area indicating limits of error; the rectangle is intersected by the quadratic and cubic interpolation curves, but both lie above the average point. By including this point for the case of a solid inner core, one can construct the quartic polynomial*

$$T = 0{\cdot}773 + 0{\cdot}750d + 0{\cdot}463d^2 - 0{\cdot}1148d^3 + 0{\cdot}00708d^4, \qquad (21)$$

for the temperature T in 10^3°K, in terms of the depth d in 10^3 km. The corresponding curve shown in Fig. 4 correctly lies below the fusion temperature for the inner core. The limits of error of equation (21) are given as about $\pm 25\%$ by the limits indicated in Fig. 4. The temperatures implied are quite close to those given by DALY (1943) for the greater depths in the mantle. In this region, JEFFREYS's hypothesis that the material of the mantle is close to the point of fusion is satisfied fairly well.

The mean temperature gradient shown by Fig. 4 for the mantle is 1·3°C/km when taken as the value for the chord, which is closely the value given by equation (21) for the base of the mantle. Inasmuch as this figure exceeds substantially the adiabatic gradient of 0·17°C/km estimated by VERHOOGEN (1951) for the (solid) mantle, the results are consistent with solidification of the mantle from the base up. The mean temperature gradient for the outer core is 0·78°C/km (value for the chord). Since the region is a liquid in convective equilibrium, this gradient should equal the adiabatic gradient. For the latter quantity, results of VALLE (1952) corresponding to the temperatures of Fig. 4 yield 0·8°C/km as a mean, in excellent agreement with the value above; values from BIRCH (1952) are somewhat lower, 0·7°C/km at the top and 0·5°C/km at the base of the liquid core. Since the adiabatic gradient for the mantle is considerably below the actual temperature gradient found, the use by SHIMAZU (1954a, b) of the former quantity to estimate the temperature at the base of the mantle necessarily yields values below those obtained here.

The derivation by GILVARRY (1956c) of the Simon equation presupposes a dependence of K_m on V_m along the fusion curve, of a form corresponding to an equation of state which has been verified for isothermal conditions only up to 100 kilobars. Since pressures toward the centre of the earth approach those at which the equation of state from the Thomas-Fermi atom model becomes valid

* Coefficients given to figures shown, merely for proper round-off.

(GILVARRY, 1956b), predicted melting temperatures in this region are correspondingly less reliable than values toward the boundary of the core, where the pressure is about a megabar. Aside from this uncertainty, and that in values of the necessary parameters, it is felt that the interpolation procedure used here yields a practical method of estimating temperatures in the earth's interior.

The author wishes to thank Dr. F. R. GILMORE of the Rand Corporation for a critical discussion of the manuscript, and Miss E. FORCE for the computational work. Thanks are also due Dr. N. H. MARCH of the University, Sheffield.

REFERENCES

ADAMS L. H.	1924	*J. Washington Acad. Sci.* **14,** 459.
BIRCH F.	1952	*J. Geophys. Res.* **57,** 227.
BIRCH F., SCHAIRER J. F., and SPICER H. C.	1942	*Handbook of Geological Constants*, Geological Society of America, New York, pp. 33, 56.
BULLARD E.	1954	*The Earth as a Planet* edited by G. P. KUIPER, University of Chicago Press, Chicago, pp. 96–115.
COSTER H. P.	1948	*Monthly Notices, Roy. Astron. Soc., Geophys. Suppl.* **5,** 193.
DALY R. A.	1943	*Bull. Geol. Soc. Amer.* **54,** 401.
ELSASSER W. M.	1950	*Rev. Modern Phys.* **22,** 1.
GILVARRY J. J.	1955	*J. Chem. Phys.* **23,** 1925.
	1956a	*Phys. Rev.* **102,** 308.
	1956b	*ibid.* **102,** 317.
	1956c	*ibid.* **102,** 325.
	1956d	*ibid.* **102,** 331.
	1956e	*ibid.* in press.
	1956f	*ibid.* submitted.
GORANSON R. W., BANCROFT D., BURTON B. L., BLECHAR T., HOUSTON E. E., GITTINGS E. F., and LANDEEN S. A.	1955	*J. Appl. Phys.* **26,** 1472.
GUTENBERG B.	1939	*Internal Constitution of the Earth*, McGraw-Hill Book Co., New York, p. 160, first edition.
JACOBS J. A.	1953	*Nature* **172,** 297.
	1954	*ibid.* **173,** 258.
JEFFREYS H.	1932	*Monthly Notices, Roy. Astron. Soc., Geophys. Suppl.* **3,** 6.
KUBASCHEWSKI O.	1949	*Trans. Faraday Soc.* **45,** 931.
SHIMAZU Y.	1954a	*J. Earth Sci.* Nagoya Univ. **2,** 95.
	1954b	*J. Phys. Earth* **2,** 55.
SIMON F. E.	1953	*Nature* **172,** 746.
SLATER J. C.	1939	*Introduction to Chemical Physics*, McGraw-Hill Book Co., New York, pp. 238, 252, 393.
STOTT V. H. and RENDALL J. H.	1953	*J. Iron & Steel Inst.* **175,** 374.
UFFEN R. J.	1952	*Trans. Amer. Geophys. Union* **33,** 893.
UFFEN R. J. and MISENER A. D.	1954	*Nature* **173,** 259.
VALLE P. E.	1952	*Ann. Geofis.* **5,** 41.
	1955	*ibid.* **8,** 189.
VERHOOGEN J.	1951	*Trans. Amer. Geophys. Union* **22,** 41.

VOL. 10 1957

Journal of Atmospheric and Terrestrial Physics, 1957, Vol. 10, pp. 96 to 102. Pergamon Press Ltd., London

Recombination in the ionosphere during an eclipse

D. R. Bates and M. R. C. McDowell
Department of Applied Mathematics, The Queen's University of Belfast

(*Received* 31 *October* 1956)

Abstract—Calculations are carried out to determine how the electron concentration in a layer in which there are two species of ion, with different recombination coefficients, varies during an eclipse. The variation exhibits several features of interest. In particular, the minimum electron concentration is reached sooner after totality than it is in the case of a layer which decays to the same extent but which contains only one species of ion.

1. Introduction

Appleton (1937) and others have derived much information on recombination in the ionosphere from studies of the diurnal variation of the electron concentration. The value of such studies is, however, limited, in that the variation may be completely controlled by a slowly recombining species of ion and give no indication of the presence of a rapidly recombining species (Bates, 1951). In consequence, naive use of the measured effective recombination coefficient may lead to a serious underestimate of the total ionization rate, which rate, as well as being of interest in itself, is of great importance in connection with investigations on the thermal balance in the upper atmosphere.

During an eclipse, the intensity of the incident solar radiation changes comparatively quickly, and it has been suggested (Bates, 1956*a*) that it might therefore be possible to find evidence in the radio records for the occurrence of ionization which is normally undetectable. Some encouragement for this is provided by the fact that the records often exhibit apparent inconsistencies (cf. Ratcliffe, 1956), when analysed on the assumption that a single species of ion is involved; but a definite conclusion is difficult to reach because of uncertainties concerning the emission from the sun. The main aim of this paper is merely to discuss the type of effect that arises when there are two species of ion. It should be noted that the existence of several species must be regarded as beyond dispute, since solar ultraviolet and X-radiation ionize all atmospheric constituents.*

A survey of the recombination mechanisms thought to be operative in the E and F layers need not be given here, but it is perhaps worth recalling that it is thought likely (cf. Bates and Massey, 1947; Bates, 1956*a*) that atomic ions are converted into molecular ions by charge transfer

$$O^+ + O_2 \rightarrow O + O_2^+, \tag{1}$$

or by ion-atom interchange

$$O^+ + O_2 \rightarrow O_2^+ + O \tag{2}$$

$$O^+ + N_2 \rightarrow NO^+ + N, \tag{3}$$

and that free charges are removed by dissociative recombination

$$O_2^+ + e \rightarrow O' + O'' \tag{4}$$

$$NO^+ + e \rightarrow N' + O' \tag{5}$$

$$N_2^+ + e \rightarrow N' + N''. \tag{6}$$

* See any review (e.g. Bates, 1956b) of the theory of the origin of the ionospheric layers.

Unfortunately, neither the rates of formation (direct and indirect) of O_2^+, NO^+, and N_2^+ nor the rate coefficients of (4), (5), and (6) are known reliably. Hence, a proper treatment of the eclipse problem cannot yet be given. It is, however, of interest to consider some illustrative cases.

2. Mathematical Treatment

For simplicity we shall assume that the sun emits uniformly (and only from the visible disc) and shall ignore the variation in its angle of elevation. Suppose that there are two species of ion, A^+ and B^+, in a particular layer. Let $x(t)$ and $y(t)$ be their respective concentrations (number per cm^3) at time t; let $af(t)$ and $bf(t)$ be their rates of production (per cm^3 per sec), where $f(t)$ is the fraction of the solar disc unobscured by the moon; and let α and β be their recombination coefficients. We then have that

$$dx/dt = af - \alpha x(x + y) \tag{7}$$

$$dy/dt = bf - \beta y(x + y). \tag{8}$$

The eclipse function, $f(t)$, has been discussed by Rydbeck and Wilhelmsson (1954). We shall confine our attention to a total eclipse, and take the angular diameters of the sun and moon to be equal. In this case

$$f = 1 - \frac{2}{\pi}\left[\sin^{-1}r - |1 - s|\, r\right] \tag{9}$$

where

$$\left.\begin{aligned} r &= \{s(2 - s)\}^{\frac{1}{2}} && (0 < s < 2) \\ &= 0 && (s < 0 \text{ or } > 2) \end{aligned}\right\} \tag{10}$$

with

$$s = 2t/T \tag{11}$$

t being measured from first contact and T being the total duration of the eclipse. Some computed values are presented in Table 1, as they may be of service to other workers.

Equations (7) and (8) may now be cast into forms better suited to numerical integration. Writing

$$u = x/x_0, \qquad v = y/y_0, \tag{12}$$

where x_0 and y_0 are the equilibrium values of x and y outside the eclipse, so that

$$x_0 = a\beta/\{\alpha\beta(a\beta + b\alpha)\}^{\frac{1}{2}} \tag{13}$$

$$y_0 = b\alpha/\{\alpha\beta(a\beta + b\alpha)\}^{\frac{1}{2}} \tag{14}$$

it is seen that

$$du/ds = \theta_1(f - u^2) + \theta_2(f - uv) \tag{15}$$

$$dv/ds = \phi_1(f - v^2) + \phi_2(f - uv), \tag{16}$$

in which

$$\left.\begin{aligned} \theta_1 &= \tfrac{1}{2}\alpha x_0 T, & \theta_2 &= \tfrac{1}{2}\alpha y_0 T, \\ \phi_1 &= \tfrac{1}{2}\beta y_0 T, & \phi_2 &= \tfrac{1}{2}\beta x_0 T. \end{aligned}\right\} \tag{17}$$

A brief account of the procedure followed in solving the equations is given in the appendix.

VOL. 10 1957

Table 1. The eclipse function

s	$f(s) = f(2-s)$	s	$f(s) = f(2-s)$	s	$f(s) = f(2-s)$	s	$f(s) = f(2-s)$
0·00	1·00000	0·26	0·84721	0·51	0·59794	0·76	0·30262
0·01	0·99880	0·27	0·83858	0·52	0·58680	0·77	0·29024
0·02	0·99661	0·28	0·82981	0·53	0·57559	0·78	0·27784
0·03	0·99379	0·29	0·82091	0·54	0·56432	0·79	0·26540
0·04	0·99045	0·30	0·81188	0·55	0·55298	0·80	0·25294
0·05	0·98668	0·31	0·80272	0·56	0·54158	0·81	0·24045
0·06	0·98252	0·32	0·79345	0·57	0·53012	0·82	0·22794
0·07	0·97800	0·33	0·78406	0·58	0·51859	0·83	0·21540
0·08	0·97317	0·34	0·77455	0·59	0·50701	0·84	0·20284
0·09	0·96803	0·35	0·76492	0·60	0·49537	0·85	0·19027
0·10	0·96261	0·36	0·75519	0·61	0·48367	0·86	0·17767
0·11	0·95693	0·37	0·74536	0·62	0·47192	0·87	0·16505
0·12	0·95101	0·38	0·73542	0·63	0·46012	0·88	0·15242
0·13	0·94484	0·39	0·72538	0·64	0·44826	0·89	0·13977
0·14	0·93845	0·40	0·71524	0·65	0·43636	0·90	0·12711
0·15	0·93185	0·41	0·70501	0·66	0·42441	0·91	0·11443
0·16	0·92504	0·42	0·69468	0·67	0·41241	0·92	0·10175
0·17	0·91804	0·43	0·68427	0·68	0·40037	0·93	0·08905
0·18	0·91084	0·44	0·67376	0·69	0·38828	0·94	0·07635
0·19	0·90346	0·45	0·66317	0·70	0·37616	0·95	0·06364
0·20	0·89591	0·46	0·65249	0·71	0·36400	0·96	0·05092
0·21	0·88819	0·47	0·64174	0·72	0·35179	0·97	0·03819
0·22	0·88030	0·48	0·63090	0·73	0·33955	0·98	0·02546
0·23	0·87225	0·49	0·61999	0·74	0·32727	0·99	0·01273
0·24	0·86405	0·50	0·60900	0·75	0·31496	1·00	0·00000
0·25	0·85571						

3. Results and Discussion

3.1

The number of parameters in the equations is such that it is scarcely practicable to provide solutions to cover all eventualities. We judged it best to fix T the duration of the eclipse, α the smaller recombination coefficient, and $(x_0 + y_0)$ the equilibrium electron concentration outside the eclipse; and we took

$$T = 8 \times 10^3 \text{ sec}, \quad \alpha = 1 \times 10^{-8} \text{ cm}^3/\text{sec}, \quad x_0 + y_0 = 1{\cdot}5 \times 10^5/\text{cm}^3. \qquad (18)$$

To show the essential pattern of the behaviour, we obtained solutions for a selection of values of β, the larger recombination coefficient, and of x_0/y_0, the ratio of the equilibrium concentration of the more slowly recombining species to that of the more rapidly recombining species. The selected values are as follows:—

$$\beta = 1 \times 10^{-8}\text{cm}^3/\text{sec}, 4 \times 10^{-8}\text{cm}^3/\text{sec}, 16 \times 10^{-8}\text{cm}^3/\text{sec}, \text{ and } \infty; \qquad (19)$$

$$x_0/y_0 = 1 \text{ and } 4. \qquad (20)$$

The corresponding values of the various ionospheric parameters are collected in Table 2. Figs. 1 and 2 give the calculated electron concentration curve for each

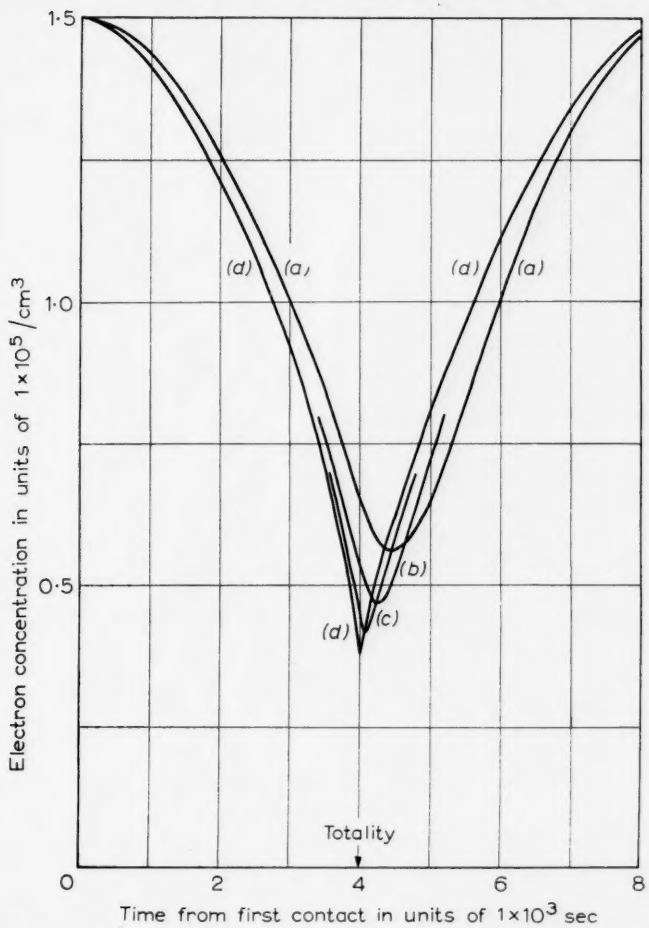

Fig. 1. Electron concentration during eclipse: $x_0/y_0 = 1$; $\alpha = 1 \times 10^{-8}$ cm³/sec; curve (a) $\beta = 1 \times 10^{-8}$ cm³/sec, curve (b) $\beta = 4 \times 10^{-8}$ cm³/sec, curve (c) $\beta = 16 \times 10^{-8}$ cm³/sec, curve (d) $\beta = \infty$.

Table 2. Ionospheric parameters

x_0	y_0	α	β	a	b
(10^5/cm³)		(10^{-8} cm³/sec)		(cm^{-3} sec^{-1})	
0·75	0·75	1	1	112·5	112·5
0·75	0·75	1	4	112·5	450
0·75	0·75	1	16	112·5	1800
0·75	0·75	1	∞	112·5	∞
1·2	0·3	1	1	180	45
1·2	0·3	1	4	180	180
1·2	0·3	1	16	180	720
1·2	0·3	1	∞	180	∞

VOL. 10 1957

of the cases investigated. As would be expected, both the decay and the recovery are more rapid when β/α is large than when this ratio is unity (which case is of course equivalent to a single species layer).

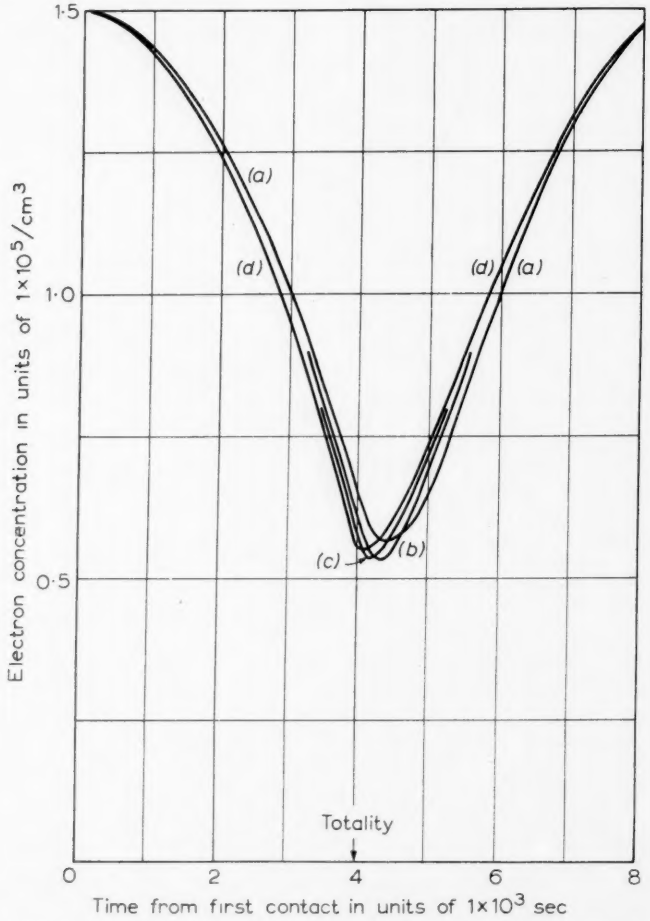

Fig. 2. Electron concentration during eclipse: $x_0/y_0 = 4$; $\alpha = 1 \times 10^{-8}$ cm³/sec; curve (a) $\beta = 1 \times 10^{-8}$ cm³/sec, curve (b) $\beta = 4 \times 10^{-8}$ cm³/sec, curve (c) $\beta = 16 \times 10^{-8}$ cm³/sec, curve (d) $\beta = \infty$.

When there is only one species, the recombination coefficient γ can be found at once from the variation of the electron concentration through the eclipse: thus Rydbeck and Wilhelmsson (1954) have proven that for the type of eclipse we are considering we may take

$$\gamma n_0 T \simeq 2(0{\cdot}68 n_0/n_m)^3 \qquad (21)^*$$

$$\simeq 2(0{\cdot}18 T/\delta t)^{3/2} \qquad (22)^*$$

where n_0 is the equilibrium electron concentration outside the eclipse, n_m is the

* It is assumed here that $\gamma n_0 T > 6$.

minimum electron concentration reached, δt is the time-lag between totality and this minimum, and T, as usual, is the duration of the eclipse.

Formulae (21) and (22) are, of course, not valid for a layer containing two species of ion, but nevertheless it is instructive to apply them to the electron concentration curves of Figs. 1 and 2. Table 3 gives the effective recombination coefficient, γ_n and γ_t, obtained from (21) and (22) respectively. When the true recombination coefficients differ, so do γ_n and γ_t, the former being smaller than the

Table 3. Layer with two species of ion

					Effective recombination coefficients	
	α	β	n_m	δt	γ_n	γ_t
	(10^{-8} cm^3/sec)		(10^4/cm^3)	(10 sec)	(10^{-8} cm^3/sec)	
$x_0/y_0 = 1$	1	1	5·7	44	1·0	1·0
	1	4	4·7	23	1·7	2·6
	1	16	4·2	8	2·4	12
	1	∞	3·8	0	3·1	∞
$x_0/y_0 = 4$	1	1	5·7	44	1·0	1·0
	1	4	5·3	31	1·2	1·7
	1	16	5·4	18	1·2	3·8
	1	∞	5·5	7	1·0	15

VOL. 10 1957

latter and lying closer to α, which is clearly the coefficient which exerts the main control. If β is increased, γ_n, unlike γ_t, does not necessarily also increase, since the faster decay of the electron concentration may be off-set by the shorter time-lag.

3.2

To account for the lack of accord between the eclipse radio records and the predictions of simple theory (cf. RATCLIFFE, 1956), it is usually supposed that the intensity of the ionizing radiation falling on the upper atmosphere is not strictly proportional to the area of the unobscured part of the solar disc, because of the existence of active areas and perhaps also because of the corona. Attempts have been made to use the records to chart the relevant emissitivity of the sun, and in some instances fair correlation is found with the distribution of the intensity of the line at 5303 Å (MINNIS, 1955); but as RATCLIFFE (1956) has emphasized, the evidence for the reality of the active areas postulated is not always convincing.

A striking feature of the data is that the minimum electron concentration is invariably greater than would be predicted from the time-lag by the application of (21) and (22) combined.* This feature indicates that active areas cannot be the sole cause of the failure of simple theory, for if the n_m-δt anomaly were due to them, its sense would not be expected to be the same on all occasions (RATCLIFFE,

* The main results published prior to 1955 have been tabulated by RATCLIFFE (1956). Some more recent results of special interest in the present connection are to be found in the papers of HENNESSEY and TORRES (1956) and STOFFREGEN (1956).

1956). An effect of the required type would, however, occur if some of the ionizing radiation originates in the corona (Piddington, 1951). It can thus be argued that active areas and the corona may together provide a complete explanation of the observations. Without seeking to deny the importance of these solar influences, we wish to draw attention to the fact that the n_m-δt anomaly must be partially due to the presence of several species of ion. It is not yet possible to judge whether or not the contribution to the anomaly from this cause is considerable. Analysis of the layers by rocket-borne instruments and laboratory measurements on the recombination coefficients of the ions detected would clarify the situation.

Appendix

The solutions of (15) and (16) corresponding to any chosen set of values of the basic parameters may be obtained by, for example, the method described by Hartree (1952). However, the labour required is considerable, especially when the recombination coefficients are large: thus, in Hartree's terminology, the first *predicted* solutions, ${u_1}^i$ and ${v_1}^i$ and the first *corrected* solutions, ${u_1}^j$ and ${v_1}^j$, are generally in poor agreement unless the interval, δs, is inconveniently small, and the convergence of successive solutions is slow so that many predictions and corrections must be made before self-consistency is attained. Instead of using the nth corrected solutions as the $(n+1)$th predicted solutions, it was found that it is advantageous to take

$$ {u_{n+1}}^i = {u_n}^j + p \qquad {v_{n+1}}^i = {v_n}^j + q \tag{A1} $$

where

$$ p = \{(2X - Z)\Delta u - 2\theta_2 {u_n}^j \delta s \Delta v\}/Z \tag{A2} $$

$$ q = \{(2Y - Z)\Delta v - 2\phi_2 {v_n}^j \delta s \Delta u\}/Z \tag{A3} $$

with

$$ \left.\begin{aligned} X &= 2 + (\phi_2 {u_n}^j + 2\phi_1 {v_n}^j)\,\delta s \\ Y &= 2 + (\theta_2 {v_n}^j + 2\theta_1 {u_n}^j)\,\delta s \\ Z &= XY - \theta_2\phi_2 {u_n}^j {v_n}^j \delta s^2 \\ \Delta u &= {u_n}^j - {u_n}^i, \qquad \Delta v = {v_n}^j - {v_n}^i \end{aligned}\right\} \tag{A4} $$

The derivation of those formulae is elementary.

References

Appleton E. V.	1937	*Proc. Roy. Soc.* **A162,** 451.
Bates D. R.	1951	*Proc. Phys. Soc.* **B64,** 805.
	1956a	*Solar Eclipses and the Ionosphere* p. 191 Eds. W. G. Beynon and G. M. Brown, Pergamon Press, London.
	1956b	*Solar Eclipses and the Ionosphere* p. 184.
Bates D. R. and Massey H. S. W.	1947	*Proc. Roy. Soc.* **A192,** 1.
Hartree D. R.	1952	*Numerical Analysis* Clarendon Press: Oxford.
Hennessey J. J. and Torres J. S.	1956	*Solar Eclipses and the Ionosphere* p. 65.
Minnis C. M.	1955	*J. Atmosph. Terr. Phys.* **6,** 91.
Piddington J. H.	1951	*J. Geophys. Res.* **56,** 403.
Ratcliffe J. A.	1956	*Solar Eclipses and the Ionosphere* p. 1.
Rydbeck O. and Wilhelmsson H.	1954	*Acta Polytechnica, Electrical Engineering Series* **5,** No. 12.
Stoffregen W.	1956	*Solar Eclipses and the Ionosphere* p. 57.

Journal of Atmospheric and Terrestrial Physics, 1957, Vol. 10, pp. 103 to 109. Pergamon Press Ltd., London

The calculation of ionospheric electron density distributions

JOHN M. KELSO
Communications Division, The Ramo-Wooldridge Corporation, Los Angeles 45, Calif.

(*Received* 9 *October* 1956)

Abstract—A method is given for calculating the vertical distribution of electrons in an ionosphere in the presence of the earth's magnetic field. The data required are obtained from experimental records of group height as a function of frequency. The usual restriction to monotonic layers applies.

The general procedure is an iteration method which makes it possible to correct a first approximation to yield improved results. Two methods of applying the general procedure are given. The first, an integral equation method, obtains the first approximation by solving the integral equation for true height in the absence of the earth's magnetic field. The second, or parabolic layer method, is the more efficient of the two, and makes use of a generalized form of the Appleton-Beynon method to get a parabolic layer as a first approximation.

VOL.
10
1957

APPLETON (1930) and DE GROOT (1930) showed that the electron-density distribution of a monotonically varying ionosphere layer can be determined from experimental h'-f data (vertical incidence group height of reflection versus operating frequency) using an integral-equation method. Their method did not require that assumptions be made in advance concerning the shape of the layer, but, unfortunately, did neglect the effects of the earth's magnetic field. For an extensive bibliography of work on this and related topics, the reader is referred to the summary paper by BECKER (1955).

During the past few years, several attempts have been made to include the effects of the earth's magnetic field. In particular, we mention the methods suggested by KELSO (1954a) and BUDDEN (1955). In such methods, the computing labour is divided between the effort of preliminary computations and the effort required for each individual record studied subsequently. The two methods cited above differ considerably in the distribution of the labour between the two phases of computation. The method proposed by KELSO requires a relatively modest amount of preliminary calculation, but the analysis of each experimental record is very laborious. In contrast, BUDDEN's highly accurate method greatly simplifies the treatment of any single experimental record, but necessitates extensive preliminary calculations which require access to electronic digital computing facilities if the analysis is to be performed for conditions other than those for which BUDDEN has supplied the numerical data.

This paper discusses a general technique lying somewhere between these two extremes. Thus, the technique discussed requires less preliminary work than does BUDDEN'S method, and also less effort per record studied than the other method. The present technique is suggested for use only when the numerical coefficients for BUDDEN'S method are not available, and when high-speed digital computing assistance is either not to be had or is uneconomic because of the number of records to be studied.

We begin by noting that the group height as a function of frequency, $h'(f)$ or h'-f, can be written as,

$$h'(f) = \int_0^{z_r} \mu' dz = \int_0^1 \frac{dz}{df_0^2} \mu'(x)\, dx \tag{1}$$

where

$$x = \frac{f_0^2}{f^2} = \frac{Ne^2}{\pi m f^2}$$

f = operating frequency,

N = electron density,

e = electronic charge,

m = electronic mass,

μ' = group index of refraction,

z = height measured from the bottom of the layer,

z_r = actual height of reflection of a ray.

(The group index of refraction μ' depends upon the properties of the magnetic field as well as upon x. However, for any fixed operating frequency, μ' can be considered as a function of x alone, as long as the magnetic field properties do not change significantly over the range of interest.)

Let us arbitrarily assume that the actual layer is formed of the sum of two (or more) layers. Then we can write the height z as the sum of the two heights z_1 and z_2,

$$z = z_1 + z_2 \tag{2}$$

and we have also,

$$\frac{dz}{df_0^2} = \frac{dz_1}{df_0^2} + \frac{dz_2}{df_0^2} \tag{3}$$

and

$$h' = h_1' + h_2' \,. \tag{4}$$

We now find some approximate height distribution $z_1(f)$ which leads to a group height $h_1'(f)$; then we must find a second distribution $z_2(f)$ leading to a group height $h_2'(f)$, so that equation (4) is satisfied approximately. As the sum of the separate values of h' approaches the measured value, the sum of the height distributions must approach the correct distribution. (It is not essential, of course, to use only two steps; a sequence of distributions z_1, z_2, z_3, . . . , can be used if this proves desirable.)

The remainder of this paper discusses two methods of applying this general technique, whereby the first approximation z_1 and the correction z_2 can be found. These two methods do not exhaust the possibilities, since other procedures could be developed to fit different computational aids. Although no great amount of effort has been expended in an attempt to simplify the application of these methods, there is a likelihood that the use of charts, nomograms, and curves could increase the ease of computation.

The parabolic-layer method is the more rapid of the two procedures discussed,

and is preferred where applicable. However, the zero magnetic-field method is discussed first because it clearly exhibits all of the steps of the general technique presented above.

A. Zero Magnetic-field Method

One way to obtain a first approximation to the correct electron density distribution is to neglect the effects of the earth's magnetic field, and to follow the procedure suggested by Appleton and De Groot. The numerical evaluation of the resulting integral has been simplified by Kelso (1952), so that a first approximation can be obtained from an experimental record in a few minutes.

Using this method, we find a distribution of electron density which, in the absence of the earth's magnetic field, would yield the observed h'-f curve. However, in the presence of the earth's field, this layer would lead to a different h'-f curve, which must now be found. A procedure for calculating the h'-f curve for a given distribution of electron density in the presence of the earth's magnetic field was given by Kelso (1954b), and this method was used here.

Thus, we find the h'-f curve which results from the approximate distribution in the presence of the earth's field. The difference $h_2'(f)$ between this curve and the observed h'-f curve, we attribute to a superimposed distribution, $z_2(f)$, which must be found.

VOL. 10 1957

The difference curve $h_2'(f)$ can be treated as if it were an observed h'-f curve, and the above procedure can be reapplied. These steps may be repeated until some nth stage is found where the difference curve $h_n'(f)$ is negligibly small. However, the no-field approximation is sufficiently close to make the results converge very rapidly. Therefore, the no-field approximation for z_2 is likely to lead to results which are about as accurate as the experimental errors permit. However, if doubt exists, an additional iteration of the procedure can be made to determine whether or not the next difference curve $h_3'(f)$ is of the order of the experimental errors.

This method, using only two distributions z_1 and z_2, has been applied to an exact h'-f curve calculated by Shinn and Whale (1952) for a parabolic layer in the presence of the earth's field. The solid curve of Fig. 1 is the exact parabolic layer, the triangles show the first approximation obtained by neglecting the earth's field, and the circles show the results obtained by the method just described. The determination of the circled points took approximately 1 hour, starting from the original h'-f curve. At the lower frequencies there is some error which can be attributed to the necessity for extrapolation of the original h'-f curve to obtain low-frequency data

This method has been used for a layer whose h'-f curve (Kelso, 1954b) is given by Fig. 2 and illustrates the applicability of the method to more complicated cases. The results are shown in in Fig. 3. In this case, the errors at the lower frequencies are caused by the process of numerical differentation used in finding $h_1'(f)$.

B. Parabolic Layer Method

Since the ionosphere is frequently of roughly parabolic form, the first approximate distribution could be taken as a parabola, found in the well-known manner

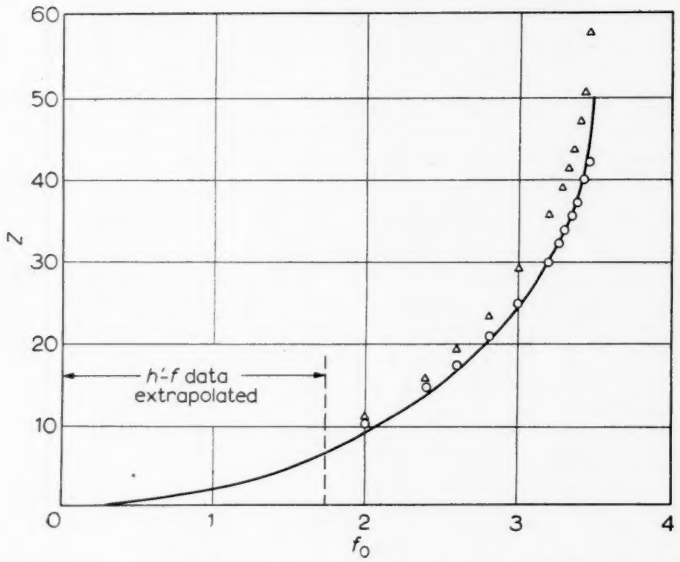

Fig. 1. True heights of a parabolic layer versus f_0. Based on group height curve calculated by SHINN and WHALE by method including the earth's magnetic field.
— Exact. ○ Calculated with magnetic field. △ Calculated without magnetic field.

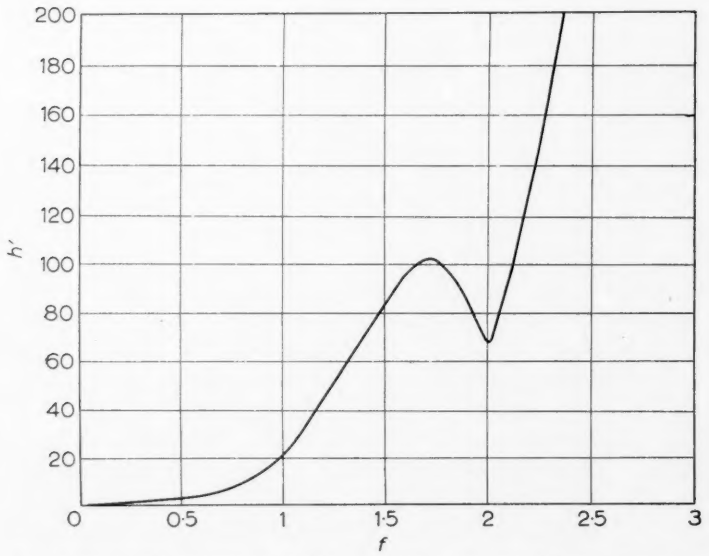

Fig. 2. Calculated values of $h'(f)$ for a double arc-cosine layer. Effects of earth's magnetic field are included.

proposed by APPLETON and BEYNON (1940) and modified to include the earth's magnetic field as suggested by SHINN and WHALE (1952). Thus, we write,

$$h' = h_0 + y_m\phi(f/f_c) \tag{4}$$

where h_0 is the "bottom" of the layer ($N = 0$), y_m is the semi-thickness of the layer, f_c is the critical frequency of the layer, and ϕ is a function which must be

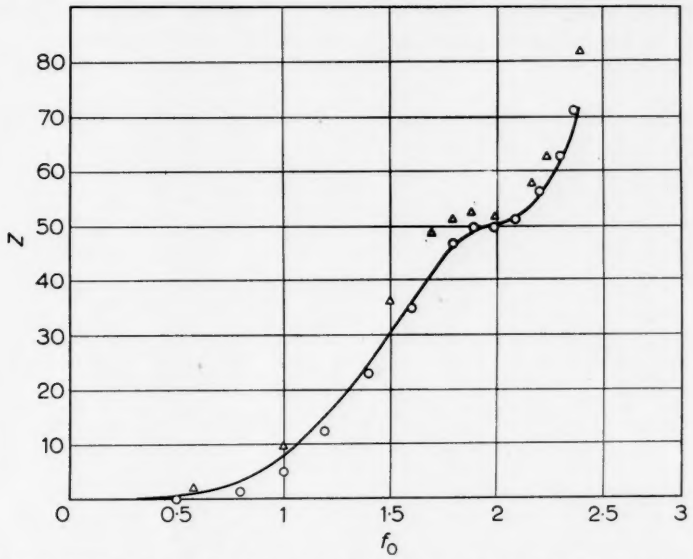

Fig. 3. True height as a function of f_0. Calculations were based on $h'(f)$ curve given in Fig. 2. — Exact. ○ Calculated with magnetic field. △ Calculated without magnetic field.

calculated for particular magnetic-field conditions. Any single calculation of the function ϕ is valid for only a single critical frequency f_c, but this calculation can be used approximately over some range of critical frequencies. SHINN and WHALE have tabulated a certain amount of such data, and if more are needed, they can be obtained by various procedures including the procedure used above to obtain $h_1'(f)$, and the procedures developed by ARGENCE and MAYOT (1953) and by MARIANI (1953).

The parabolic layer method is illustrated by applying it to the h'-f curve shown in Fig. 4. This curve was drawn arbitrarily to simulate those frequent cases in which the observed layer is roughly parabolic, but contains regions of irregularity.

For the function ϕ, we use the same data of SHINN and WHALE which were used to give the h'-f curve studied in the first example. We plot representative values of h' from Fig. 4 against the corresponding values of ϕ for the same f/f_c ratio. The result is shown in Fig. 5. If the original layer had been parabolic, the points would all lie on some straight line. Since this is not true, the original layer is not parabolic. We attempt to fit a straight line which gives the smallest deviation of the points from the line. The result is shown in Fig. 5, as a dashed line. The slope of this line gives the semi-thickness of the parabolic layer, and the intercept at $\phi = 0$ gives the height of the bottom of the layer. In addition to

VOL. 10 1957

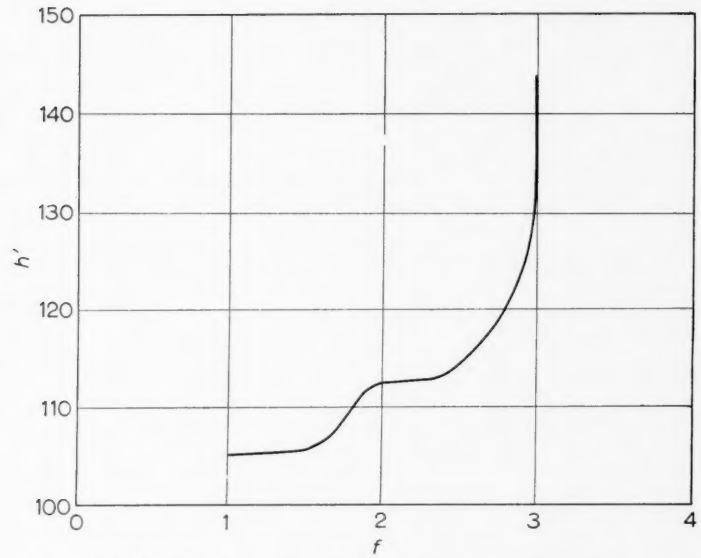

Fig. 4. Curve showing $h'(f)$ for "typical layer." This curve was drawn arbitrarily to simulate a distorted parabolic layer.

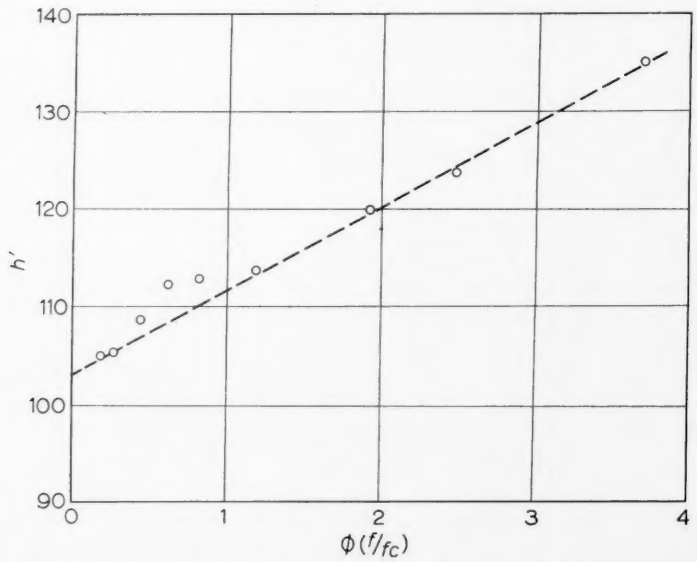

Fig. 5. Application of generalized APPLETON-BEYNON method to the $h'(f)$ curve shown in Fig. 4. $h' = h_0 + y_m\phi(f/f_c)$

defining a particular parabola (characterized completely by f_c, y_m, and h_0), the act of plotting the dashed line also defines the group height curve h_1' corresponding to the parabolic layer. Hence, the difference curve, $h_2'(f)$, can be obtained from Fig. 5 merely by plotting the vertical difference between the experimental points and the straight line as functions of frequency. Then, we neglect the earth's field and use the integral-equation method to find the distribution z_2, corresponding to $h_2'(f)$. The distribution z_2 is added algebraically to the parabolic layer (defined by h_0, y_m, and f_c) to obtain the final result.

This procedure is much more rapid than the zero magnetic-field method, since it obtains the first approximation and the corresponding group height curve in a single step which is itself more rapid than a single application of the integral-equation procedure. (The procedure involved can be carried out in about thirty minutes.) Thus, it is better to use the parabolic method whenever the layer is not too distorted.

The criterion to use in determining the best fit of a straight line to the experimental data is likely to be somewhat different from that which is applied in the normal use of the APPLETON-BEYNON method. In the direct use of this method, it is generally desirable to have the straight line fit the points near the critical frequency. In the present application, a limited amount of experience indicates the importance of keeping the deviations of the points at low frequencies to reasonably small values. This need arises from the application of the integral-equation method, in which the values of h_2' at low frequencies have an effect on the calculations for higher frequencies.

VOL. 10 1957

It should be remembered that both of the methods described, like most other methods, are restricted to monotonic layers and cannot properly be applied to regions above the lowest maximum of the layer. MANNING (1949) and PIGGOTT (1954) have given detailed discussions of the difficulties arising when the layer is not monotonic. Some interesting results on multi-layers have been obtained recently by JACKSON (1956), who used rocket data to supplement radio soundings, and by SHMOYS and KARP (1956), who require data measured at some fixed point in or above the layer.

REFERENCES

APPLETON E. V.	1930	*Proc. Phys. Soc.* **42,** 321.
APPLETON E. V. and BEYNON W. J. G.	1940	*Proc. Phys. Soc.* **52,** 518.
ARGENCE E. and MAYOT M.	1953	*J. Geophys. Res.* **58,** 147.
BECKER W.	1955	*A.E.Ü.* **9,** 277.
BUDDEN K. G.	1955	*Phys. Soc. Report of Cambridge Conf. on the Physics of the Ionosphere* p. 332.
DE GROOT W.	1930	*Phil. Mag.* **10,** 521.
JACKSON J. E.	1956	*J. Geophys. Res.* **61,** 107.
KELSO J. M.	1952	*J. Geophys. Res.* **57,** 357.
	1954a	*J. Atmosph. Terr. Phys.* **5,** 11.
	1954b	*J. Atmosph. Terr. Phys.* **5,** 117.
MANNING L. A.	1949	*Proc. I.R.E.* **37,** 599.
MARIANI F.	1953	*An. Geofis.* **6,** 21.
PIGGOTT W. R.	1954	*J. Atmosph. Terr. Phys.* **5,** 201.
SHINN D. H. and WHALE H. A.	1952	*J. Atmosph. Terr. Phys.* **2,** 85.
SHMOYS J. and KARP S. N.	1956	*J. Geophys. Res.* **61,** 183.

Journal of Atmospheric and Terrestrial Physics, 1957, Vol. 10, pp. 110 to 113. Pergamon Press Ltd., London

Long-path V.L.F.—Frequency variations associated with the solar flare of 23 February 1956

A. H. Allan, D. D. Crombie, and W. A. Penton
Dominion Physical Laboratory, Department of Scientific and Industrial Research
Lower Hutt, New Zealand

(*Received* 2 *October* 1956)

Abstract—The frequency and phase variations of GBR on 16 kc/s as received in New Zealand during the solar flare of 23 February 1956 are described and compared with the effects during a normal flare. The difference is attributed to the cosmic-ray increase accompanying the 23 February flare.

Introduction

The solar flare which commenced at approximately 0331 UT on 23 February 1956 was unusual in that it was accompanied by an increase in cosmic ray activity commencing 20 min later. During the period of the flare and the later cosmic-ray increase, observations were made at Lower Hutt, New Zealand, of the received frequency of transmitting station GBR Rugby of 16 kc/s, using a method which has been reported briefly (Allan, Crombie, and Penton, 1956). The shortest path from Rugby to Lower Hutt is approximately 19,000 km, and at the time of the flare about three-quarters of this path was illuminated by the sun and the rest in darkness.

Frequency Variations of GBR 23 February 1956

Fig. 1 reproduces the original beat-frequency record between GBR and a locally-generated signal of nominal frequency 16 kc/s, the stability of which is estimated to be not worse than ± 2 parts in 10^9 over the period. Fig. 2 shows the apparent frequency change in the incoming GBR signal as deduced by measurement from Fig. 1. It will be seen that at approximately 0330 UT the frequency of GBR increased rapidly, reaching a maximum at 0333½ UT, at which time it had increased by 285 parts in 10^9. It then decreased less rapidly until 0340, at which time it was within 15 parts in 10^9 of its original value, and then increased slowly until 0347, at which time the increase was 40 parts in 10^9. The frequency then decreased slowly to approximately normal at 0405 UT.

The apparent decrease in signal strength during the rapid increase in frequency, suggested by Fig. 1, is largely due to the narrow bandwidth (0·02 c/s) of the receiver. The resultant time delay of 1 min has been taken into account in Fig. 2 and in the text. However, later at 0340 the signal strength did decrease, but recovered by 0800 UT. This period of low-signal strength covers the usual sunset "minimum," which on the previous two days occurred between 0630 and 0730 UT.

As well as the major effects noted above, there were changes in received frequency of GBR before the flare occurred, the greatest being an increase of 14 parts in 10^9 at 0240 UT. There is also evidence of an increase at 0550 superimposed

on the general decrease in frequency following the main disturbance. Fig. 3, derived from Fig. 1, shows the approximate phase change of the GBR signal, during the disturbance.

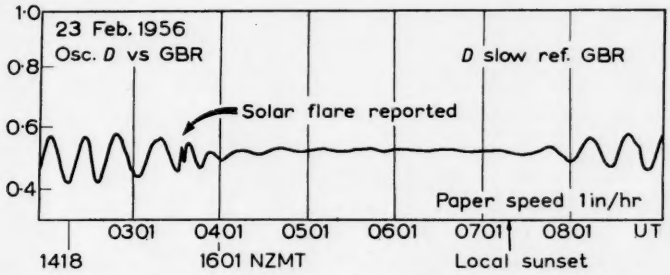

Fig. 1. Beat frequency record of GBR against local reference oscillator during the disturbance.

Comparison with Frequency Variations During the Solar Flare of 10 February 1956

The foregoing results may be contrasted with the variations of GBR measured during the sudden phase anomaly (SPA) on 10 February at 2125 UT, which

VOL. 10 1957

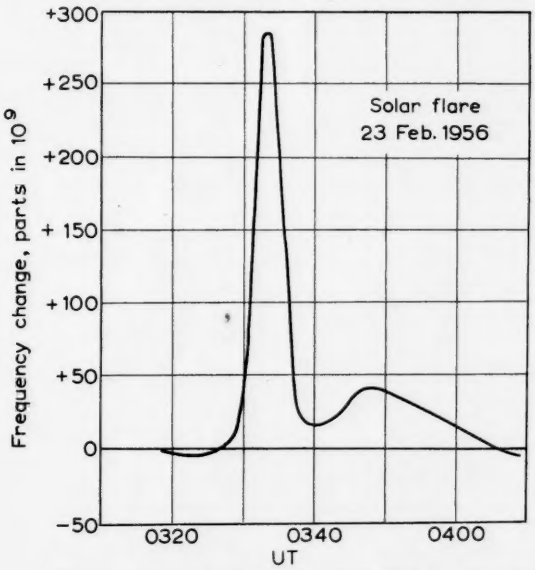

Fig. 2. Frequency changes of GBR deduced from Fig. 1.

represents the behaviour during more usual solar flares. On 10 February the signal amplitude increased to twice the value prior to the disturbance and slowly returned to normal in 45 min. The frequency variations are shown in Fig. 4.

There are some important differences between Fig. 2 and Fig. 4. In Fig. 4 the maximum increase in frequency is 130 parts in 10^9 followed by a decrease in frequency below normal to a maximum value of 22 parts in 10^9, the areas under

the positive and negative excursions being approximately equal. This is what one might expect (Bracewell and Straker, 1949) if an equivalent reflecting region were suddenly moved downward and then slowly reverted to its former height, remembering that instantaneous frequency is equivalent to rate of change

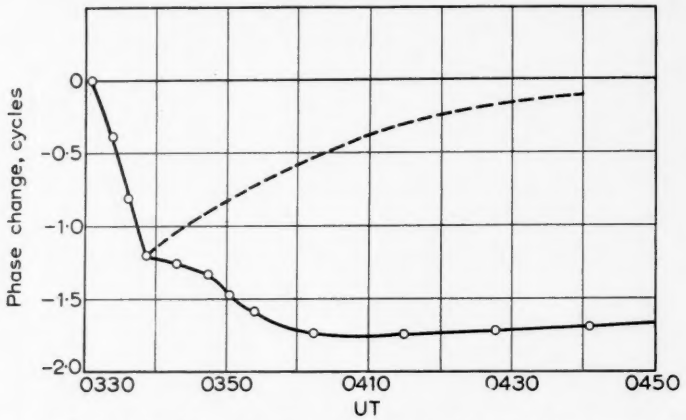

Fig. 3. Phase change of GBR deduced from Fig. 1. The dashed line shows approximately what might be expected during a more usual flare.

of phase. However, in Fig. 2 there is no appreciable reduction in frequency below that prevailing before the flare, but in fact the frequency increases again. After 0410 UT the frequency remains about 10 parts in 10^9 low, except near 0600 UT, and does not recover to its initial value until about 0900 UT. The same behaviour is shown in the phase curve of Fig. 3 on which is superimposed the

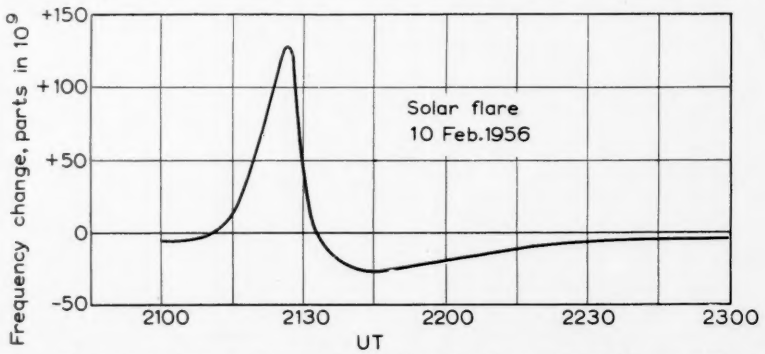

Fig. 4. Frequency changes of GBR during the solar flare of 10 February 1956 at 2125 UT.

phase change that might be expected during a more normal type of flare. J. A. Pierce has pointed out to us in a private communication that the second increase in frequency at 0347 UT coincides closely with the increase in frequency of GBR which he observed at the same time over a transatlantic path. We have also seen a copy of a paper by Belrose, Davenport, and Weekes (1956), dealing *inter alia* with the sudden phase anomaly of GBR observed on this occasion at Cambridge (England). This also occurred at 0345 UT.

Discussion

Pierce (1956) suggests that our record shows both the primary effect of the solar-flare photons and the delayed effect 10 min later observed by him and also by Belrose, Davenport, and Weekes, and also suggests that the delayed effects on the dark side of the earth is associated with the cosmic-ray burst. With this view we agree.

The phase change observed by Pierce is slightly greater than the total phase change after 0345 observed by us, in spite of the much greater length of our path. This suggests that the *D*-region changes responsible were largely confined to the dark portion of the earth rather than spread uniformly over the whole surface.

It has been pointed out by Elliot (1952) that there have been four previous occasions recorded when widespread cosmic-ray increases have been associated with solar flares, together with some other less-marked increases. It would be of great interest if V.L.F. ionospheric data obtained on such occasions were examined for changes.

Acknowledgements—We wish to acknowledge the encouragement given us in the work of which this forms part by J. A. Pierce of the Cruft Laboratory, who pointed out the possible special significance of our original data. Our thanks are also due to Dr. K. Weekes of the Cavendish Laboratory for access to the results obtained by his group, prior to publication.

VOL.
10
1957

References

Allan A. H., Crombie D. D., and Penton W. A. 1956 *Nature* **177**, 178–179.

Belrose J. S., Devenport M. H., and Weekes K. 1956 Some unusual radio observations made on 23 February, 1956. *J. Atmosph. Terr. Phys.* **8**, 281.

Bracewell R. N. and Straker T. W. 1949 *Mon. Not. Roy. Ast. Soc.* **109**, No. 1, 28.

Elliot H. 1952 *Progress in Cosmic Ray Physics* North-Holland Publishing Co., Amsterdam, p. 492.

Pierce J. A. 1956 V.L.F. phase shifts associated with the disturbances of February 23, 1956. *J. Geo. Res.* **61**, No. 3.

RESEARCH NOTES

Note on a "QL-QT" transition level in the ionosphere

(*Received* 27 *September* 1956)

Introduction

In a recent paper, Lepechinsky (1956) discusses the existence of a QL-QT transition level in the ionosphere. He argues that at the height where the collision frequency $\nu = \nu_c$, where

$$\nu_c = \pi f_H \frac{\sin^2\theta}{\cos\theta},$$

there must be an abrupt fall of the refractive index for the ordinary component, associated with a reflection condition, if this level occurs at values of X between 1 and $1 + Y$.

Lepechinsky also shows that, if one assumes a certain curve for the variation of the collision frequency with height, the reflection level for the ordinary wave from the E layer should be as follows:

$$\text{At } X = 1 \qquad \text{for dip angles } <60°$$

$$\text{At } X = 1 + Y \text{ for dip angles } >70°,$$

and that there probably should be a change over from the one to the other near midday at latitudes with dip angles between 60 and 70°.

The purpose of this note is, firstly, to throw further light on Lepechinsky's two main points from observations made at high latitudes, and secondly, to suggest a method by which information may be obtained about the electron density in the dip between the E and F layers of the ionosphere.

The Transition Level

In his paper, Lepechinsky points out the marked difference in the dispersion curves drawn for constant values of ν greater or smaller than ν_c. In the QT case ($\nu < \nu_c$), the refractive index for the "ordinary" wave will fall abruptly near $X = 1$ to a very small value and will remain small in the range of X from 1 to $1 + Y$. In the QL case ($\nu > \nu_c$), on the other hand, there will be no such abrupt fall at this level, and the refractive index will fall more slowly towards a small value at $X = 1 + Y$. If now the collision frequency decreases through the value ν_c at a height where X is between 1 and $1 + Y$, Lepechinsky argues that the refractive index must suffer an abrupt fall at this level.

A closer study of the dispersion curves shows that this is not so. In Fig. 1 we have drawn the curves for the "ordinary" component (here defined as the component which would leave the ionosphere after reflection with a left-handed sense of polarization) for two models of the ionosphere. To the left we have chosen an E- and F-layer model with no marked dip between the two layers, and a frequency such that the maximum electron

density in the E layer corresponds to a value of X between 1 and $1 + Y$. The level where $\nu = \nu_c$ also occurs at a height where X is between 1 and $1 + Y$. The curves are for the geomagnetic conditions at Tromsö. It is obvious from Fig. 1(a) that there will be no transition level associated with an abrupt change in the refractive index at the level $\nu = \nu_c$, but that the wave will continue to be propagated as a 'longitudinal' type until it eventually is reflected from the height where $X = 1 + Y$ in the F layer.

Observations at Tromsö

In Fig. 2, examples of typical $h'f$ records obtained at Tromsö during quiet conditions are shown. In (a) a record is shown, where it is possible to determine two critical frequencies

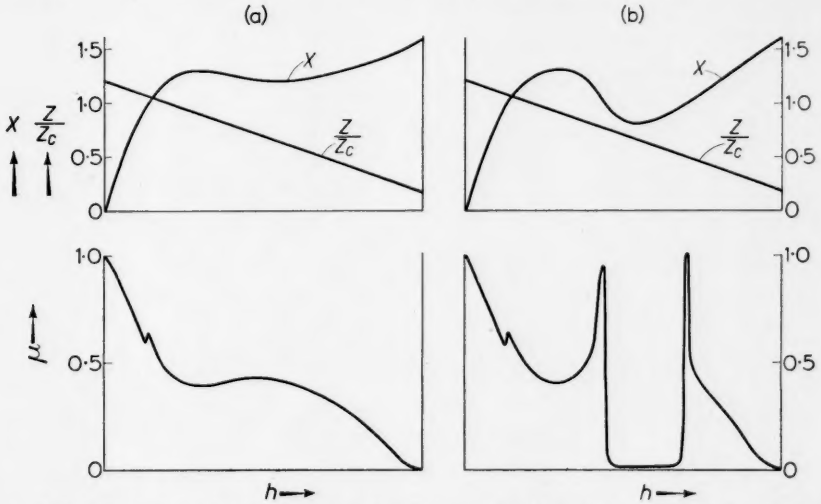

Fig. 1. Refractive index μ for the "ordinary" component as a function of height h for two-layer models.

of the "ordinary" type for the E layer. These are usually referred to as the o and z components. The z component corresponds to the longitudinal type of propagation, and the simultaneous occurrence of the o and z waves has been explained in terms of coupling effects (see, for example, Rydbeck, 1951.) In (b) in Fig. 2 a record is shown where only one critical frequency for the E layer can be determined. It is clear from the observed traces from the F layer that this must correspond to the o mode, and that consequently the propagation must be quasi transverse at the height $X = 1$ for waves near the critical frequency of and reflected from the E layer. In fact, for two years of observations, it was impossible to find a single record when a critical frequency could be determined in which there was doubt as to whether this was an o or a z component, and it was nearly always found when both were present that the ordinary component was stronger than the corresponding z component.

A Method by which Information may be Obtained of the Electron Density between the E and F Layers

In Fig. 1(a) we saw that a z wave for a frequency between fz and fo for the E layer, for an E- and F-layer model with no marked dip in the electron density between the layers, would penetrate the E layer and eventually be reflected from the F layer above. This wave has been referred to in the literature as the penetration triple split or penetration z wave, and a typical example of the phenomenon is shown in Fig. 2(a).

VOL. 10 1957

In Fig. 1(b) the dispersion curve is shown for the "ordinary" component for a different layer model, in which there is a marked decrease in the electron density between the layers. In this case we see that the longitudinal type of the ordinary curve does in fact belong to the curve which in the zero-collision case is referred to as the extraordinary mode. For this model there will be no possibility for the z component to penetrate the E layer.

It now appears that, according to a ray theory, for a frequency between fz and fo for the E layer, a penetration z component is only possible if the electron density between

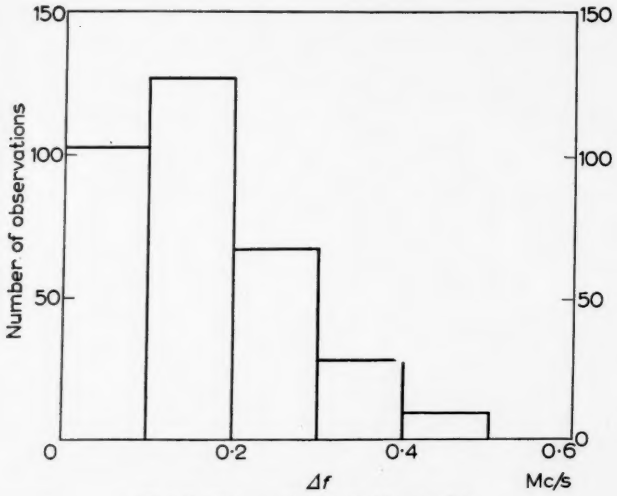

Fig. 3. Observed distribution of Δf.

the layers is not reduced to a value making X smaller than 1, when QT propagation is assumed at this height. In other words, there must be a maximum value of the frequency at which the penetration triple split can be observed, determined by the value of the electron density between the layers. Although these results are strictly correct only for a ray theory, a full wave theory would also result in a marked decrease of the strength of the penetration triple split at this frequency. In Fig. 3 we have shown in a histogram the observed distribution of the parameter $\Delta f = fo - fm$, where fm is the highest frequency at which the penetration triple split was observed, for all the penetration triple splits which were observed at Tromsö in 1950. We see that most often the penetration triple split was observed up to a frequency fairly close to fo, a result which indicates that there was no marked decrease in the electron density between the E and F layers.

Norwegian Defence Research Establishment
Kjeller, Norway

B. Landmark
F. Lied

References

Lepechinsky D. 1956 *J. Atmosph. Terr. Phys.* **8,** 297–304.
Rydbeck O. E. H. 1951 *Trans. Chalm. Univ. of Technology* **101,** Rep. No. 14.

VOL.
10
1957

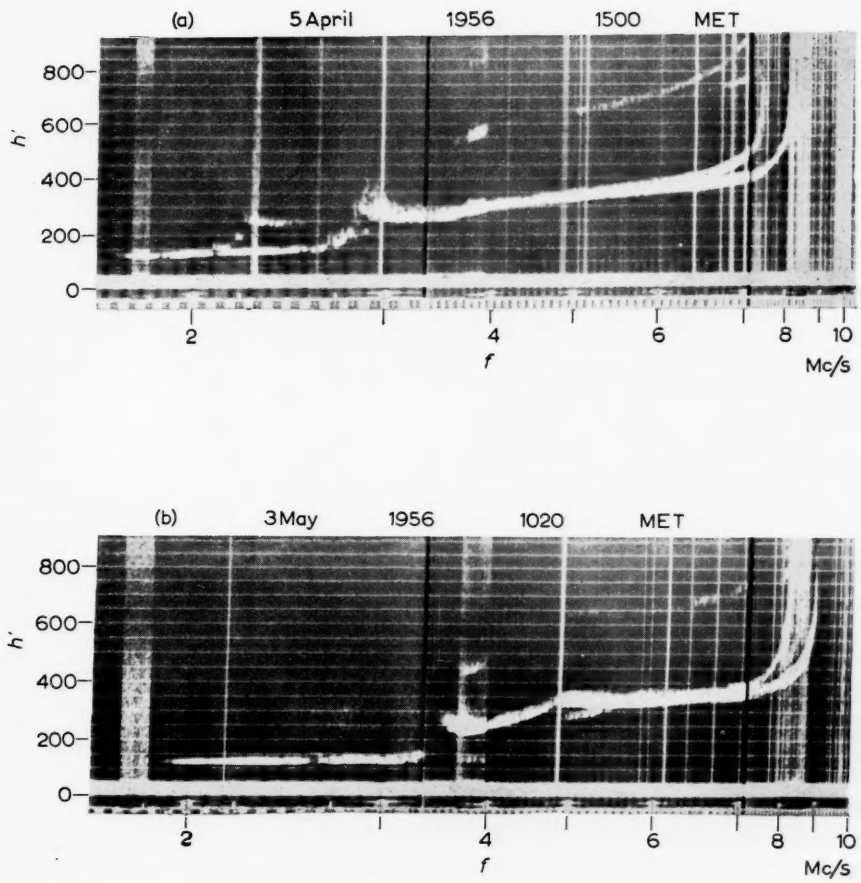

Fig. 2. Typical records obtained at Tromsö.

Geomagnetic variations in the cosmic-ray disturbance of 23 February 1956

(*Received* 11 *October* 1956)

An investigation into the variation with geomagnetic latitude of the sea-level intensity of the nucleonic component of cosmic rays by Simpson, Fenton, Katzman, and Rose (1956) shows that the effective geomagnetic equator for the deflection of cosmic-ray primaries does not coincide with that determined from field measurements at the surface of the earth. The results indicate that for this particular feature the effective deflection field may be represented as that of an inclined eccentric dipole which is rotated some 40° to the west of the dipole determined from surface measurements, but with approximately the same inclination. This shift of axis does not give a complete explanation of the behaviour of all geomagnetic-effect measurements, particularly in regard to the longitude effect near the knees (Rose and Katzman, 1956; Rose, Fenton, Katzman, and Simpson, 1956) but Simpson *et al.* (1956) show that there is considerable supporting evidence from comparisons between measurements taken in Europe and U.S.A. The shift of axis leads only to a small change of "geomagnetic latitude" over the eastern United States, but produces a southerly shift of 6°–7° over Europe.

VOL. 10 1957

In the generally quoted Centre Dipole Field (CDF) co-ordinates, the laboratories at Ottawa and Leeds lie in almost the same latitude, and it is of interest to compare the responses of neutron monitors at these stations, together with data published elsewhere, during the exceptional solar disturbance of 23 February 1956. The CDF latitudes calculated, using the data of Vestine, Laporte, Lange, and Scott (1947), are: Ottawa 56·8° N, Leeds 56·7° N.

The response of neutron monitors to particles associated with the disturbance may be divided into two parts:

(i) A part sensitive to local time, during which particles are incident upon earth preferentially from the direction of the sun. This part is associated with an enhanced response to the products of slow primaries in specific "impact zones" (Frior, 1954), and perhaps with an increased flux of more energetic primaries, which may have been present during this disturbance on the sunward side of the earth;

(ii) A part which lasted for many hours and which is probably insensitive to local time. This part is attributed to the incidence upon the earth of particles arising from the initial disturbance, but which have been constrained to a region, within the solar system, which has been shown (Meyer, Parker, and Simpson, 1956) to extend to no great distance beyond the orbit of the earth.

The second part of the recorded response is strongly latitude-sensitive and is the subject of this note.

In Fig. 1 the ratio of the percentage increases of the responses above normal of the monitors at Ottawa and Leeds is shown as a function of UT for a period of thirteen hours after the onset of the disturbance. Similar ratios using data published by other observers for stations near sea-level are shown for Durham (N. H.)/Leeds (Lockwood, Yingst, Colawa, and Saramaniote, 1956) and for Chicago/Leeds (Meyer *et al.*, 1956). The CDF geomagnetic latitudes of Durham and Chicago are 54·7° N and 52·6° N respectively. All three of these ratios show a rapid initial increase, which has not been shown in the diagrams, arising because Leeds lay in a primary impact zone; thereafter they all show no significant variation. Thus the comparison of the response of the monitor at Leeds with that at the North American stations during this later phase of the disturbance reveals no detectable

variation sensitive to local time. In particular, there is no change of the ratio as the several stations enter solar impact zones. This constancy of ratio is shown in Fig. 1 to be maintained for at least ten hours and it must be regarded as direct evidence of the isotropic distribution

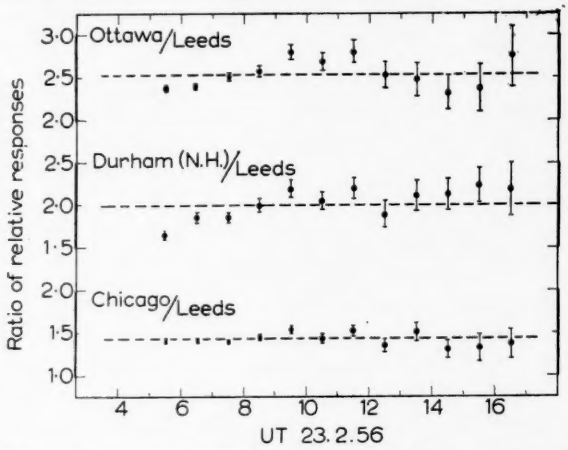

Fig. 1. Time variation of the ratio of the relative response at Leeds to that at North American stations.

of the radiation, or at least of the uniform distribution in longitude of the effective source of the particles which leads to the response of the monitors in this later phase of the disturbance.

Among the North American stations, the percentage increase of response during this period is very strongly latitude-sensitive, and we draw attention to the fact that the

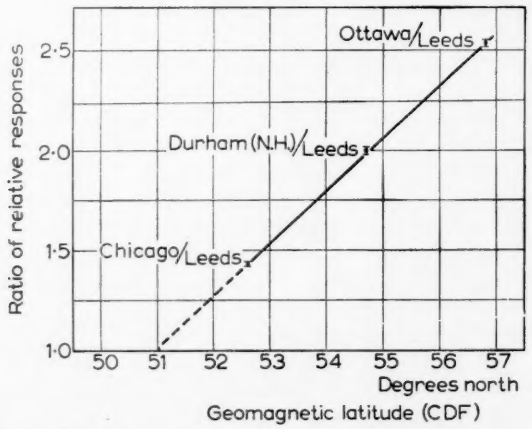

Fig. 2. Ratio of the relative response at Leeds to that at North American stations as a function of CDF geomagnetic latitude of these stations.

increase at Leeds does not correspond to that at Ottawa (which is at the same CDF geomagnetic latitude), but to a markedly lower latitude. This effect is in qualitative agreement with recent evidence from several sources and from different phenomena (see, in particular Fay, 1955; Waddington, 1956; Danielson, Freier, Naugle, and Ney, 1956).

The broken lines in Fig. 1 correspond to the mean values of the ratios of the relative responses evaluated over the interval 0600–1700 UT (both Durham and Ottawa records do

not appear to have reached a constant value relative to that of Leeds before 0600 UT). In Fig. 2 the mean values are plotted against the CDF geomagnetic latitudes of the North American stations, and it is apparent that a monitor in eastern North America at CDF latitude 51° N would be expected to give the same response during the later phase of the disturbance as that at Leeds.

It is premature to specify the function of the external field of the earth which is effective for the particle distribution responsible for the later phases of neutron monitor records discussed here, but we draw attention to the fact that in the middle latitudes this effect allows very precise equivalents to be established in different longitudes. Only a few neutron monitors were in operation during the recent disturbance, but many more will be operating in the near future, and information of the character of that outlined here is likely to be much more extensive for solar disturbances in the future. Because of our limited understanding of the particle distribution which leads to the later phase of these events, it will be of particular interest to determine whether the equivalence of response at stations in differing longitudes is maintained from one event to another.

The University,
Leeds

P. L. MARSDEN
J. G. WILSON

National Research Council, Ottawa

D. C. ROSE

REFERENCES

DANIELSON R. E., FREIER P. S., NAUGLE J. E., and NEY E. P.	1956	*Phys. Rev.* **103,** 1075.
FAY H.	1955	*Z. Naturforsch.* **10a,** 572.
FRIOR J.	1954	*Phys. Rev.* **94,** 1017.
LOCKWOOD J. A., YINGST H. E., CALAWA A. R., and SARMANIOTE G.	1956	*Phys. Rev.* **103,** 247.
MEYER P., PARKER E. N., and SIMPSON J. A.	1956	*Phys. Rev.* (to be published).
ROSE D. C., FENTON K. B., KATZMAN J., and SIMPSON J. A.	1956	*Canad. J. Physics* **34,** 968.
ROSE D. C. and KATZMAN J.	1956	*Canad. J. Physics* **34,** 884.
SIMPSON J. A., FENTON K. B., KATZMAN J., and ROSE D. C.	1956	*Phys. Rev.* **102,** 1648.
WADDINGTON C. J.	1956	*Nuovo Cim.* **3,** 930.
VESTINE E. H., LAPORTE L., LANGE I., and SCOTT W. E.	1947	*Carnegie Institution of Washington, Publication* 580.

VOL. 10 1957

Erratum

ELLIS, G. R. 1956 *J. Atmosph. Terr. Phys.* **8,** 338.

Equation (11), p. 344, should read

$$\left(1 + \frac{X}{Y-1}\right)^{\frac{1}{2}} + \frac{X}{2}\frac{2-Y}{(Y-1)^2\left(1 + \frac{X}{Y-1}\right)^{\frac{1}{2}}}$$

and equation (12) should read

$$t = \int \frac{\mu'}{c}\, ds$$

Books received

PEARCEY, T. (compiled by). *Table of the Fresnel Integral to Six Decimal Places.* (Cambridge: Cambridge University Press, 1956) 12s. 6d.

BEYNON W. J. G. and BROWN G. M. (edited by). *Solar Eclipses and the Ionosphere.* pp. 330 (London: Pergamon Press, 1956.) £7 ($21.00).

ARMSTRONG E. B. and DALGARNO A. (edited by). *The Airglow and the Aurorae.* pp. 420 (London: Pergamon Press, 1956) £7 10s. ($22.50).

VASSY, ETIENNE. *Physique de l'Atmosphére.* pp. 338. (Paris: Gauthier-Villars, 1956.)

Journal of Atmospheric and Terrestrial Physics, 1957, Vol. 10, pp. 121 to 135. Pergamon Press Ltd., London

Wave-guide interpretation of atmospheric waveforms

F. HEPBURN
Physics Department, University of Nottingham

(*Received* 10 *October* 1956)

Abstract—The precise current variation in the lightning discharge channel and the propagation characteristics of the transmission path for the low-frequency radio waves generated, provide possible explanations of the finer details of recorded electric-field change waveforms and some of the observed anomalies in the application of the pulse-reflection theory to "atmospherics." A graphical construction for the prediction of waveforms, given the source conditions, indicates how the change in shape with reflection order of the ionosphere-reflected pulses can be explained in terms of source effects and the mode responses of an imperfectly conducting infinite parallel-plane wave-guide, whose known propagation characteristics give a qualitative explanation of the diversity of waveforms recorded. The dependence upon range and time of day provides experimental confirmation of BUDDEN's wave-guide approach. One type of waveform, observed during day and night, indicates a directional variation of the propagation factor transcending the diurnal variation over a certain region.

VOL.
10
1957

1. INTRODUCTION

IN recent years there have been several isolated attempts to explain atmospheric waveforms, in terms of wave-guide responses. It is the purpose of the present discussion to show the comprehensive application of such a treatment, by indicating how the various waveforms, observed in practice, can be predicted theoretically and so provide an understanding of the source and propagation effects resulting in such diversity of detail.

As early as 1945, HAUBERT applied wave-guide considerations to the very smooth type of atmospherics, and deduced an effective height for the reflecting layer of the ionosphere of 50 km. Later (1948), HALES estimated a height of 75 km, based upon a wave-guide analysis and a source distance obtained from a "Sferics" network—since the analysis alone was insufficient to distinguish between pairs of values of distance and height. In a theoretical paper, BUDDEN (1951) calculated the response of the earth-ionosphere system, to a step function impulse, for various ionospheric conductivities, and was able to show that in the case of infinite conductivity the successive mode responses could combine to give a waveform showing a series of peaks, such as would be expected by simple specular pulse-reflection. The wave-guide interpretation was thus extended to reflection-type waveforms, though the actual form obtained was deduced for a step-function discharge, rather than for physically possible cases. A recent paper on reflection-type atmospheric waveforms (HEPBURN and PIERCE, 1954) has shown the significance of source phenomena, so that it is desirable to discuss this aspect in detail, when considering the modifications produced by propagation.

2. OBSERVED TYPES OF ATMOSPHERICS

Observations at Cambridge (HEPBURN, 1952) showed the possibility of classifying waveforms in two main groups, namely reflection and smooth types. Return-stroke discharges, producing less confused waveforms than precursor or cloud discharges, show the distinction most clearly and they only are considered in the

Fig. 1. Typical waveforms.
Waveforms 1–5 were obtained with a 10-ms sweep: 6–10 have a duration slightly greater than 1 ms.
Tracings are given, as the large range in writing speed on some of the waveform traces made satisfactory reproduction of the originals impossible.
Notes on individual examples include recording date and time and the Sferics fix for the individual discharge or storm centre in terms of geographical location, range, and azimuth, and the variety and type of the waveform.

present paper, which discusses principally the more complicated, but inherently more interesting, reflection type. Fig. 1 illustrates typical waveforms of the two types.

Reflection-type waveforms are obtained from discharges in a region including the British Isles, Europe, and the Mediterranean bounded to the south-west at a distance of 1500–1700 km, and derive their name from the nighttime long-train variety exhibiting a series of peaks interpreted as successive reflections of an original pulse between the earth and an ionospheric layer. The peaky form becomes more rounded and eventually smooth as the propagation distance increases from 2000 to 4000 km, and also at the shorter range under twilight conditions. The daytime peaked variety is included within this type, because of the observed transition at dawn from long-train waveforms to the daytime variety having only a few oscillations of rapidly decaying amplitude but almost identical time separation, and the observation, although rare, of reflection trains in daytime having up to fifteen peaks. The great disparity in amplitude of the initial and subsequent peaks is a possible cause of their previous rejection as a variety of reflection type waveform.

Smooth-type waveforms originate beyond the transition region at distances greater than 1700 km to the south-west and are observed with only minor variation throughout the 24 hours. The amplitude of the quasi-sinusoidal oscillation increases rapidly and then diminishes as the gradually increasing period approaches the maximum value of 250 μs, irrespective of distance of origin, unlike the reflection type, for which the limiting period is about twice this value. Subdivision into regular and irregular varieties according to the presence of an obvious discontinuity in the waveform is possible, but the proportion in each group varies with the criterion of the irregularity.

VOL. 10 1957

3. Source Phenomena

3.1. *Discharge-current variation*

Discussion will be restricted to consideration of the simple current surge of the return stroke. The simplest mathematical form to consider is perhaps the

Figure 1—*continued.*

1. 14.11.50, 2100. Storm centre N. Italy, 1000 km, 127°. Nighttime peaky long-train reflection type, with sharp peaks and considerable harmonic content.
2. 12.12.50, 1900. Trieste, 1200 km, 124°. Earlier nighttime long-train reflection type, showing rounded peaks and little harmonic content.
3. 28.5.51, 0220. N. Germany, 900 km, 85°. Degenerate long-train waveforms, when half the propagation path is illuminated giving smoother and less numerous peaks.
4. 28.5.51, 0520. N. Germany, 900 km, 85°. Daytime peaked variety of reflection type, showing very rapid decay of peak amplitude, but the same time intervals as 3.
5. 14.11.50, 1200. Possibly N. Italy, 1000 km, 127°. Daytime peaked variety, analysed by pulse-reflection theory giving fair fit with $h = 85$ km, $d = 1000$ km.
6. 29.3.55, 1630. Pyrenees, 1150 km, 179°. Daytime peaked variety, showing characteristic lack of sinusoidal nature and rapid decay of pulses.
7. 11.5.55, 1130. Atlantic, 2200 km, 268°. Daytime regular smooth type, with no obvious irregularity.
8. 12.1.55, 2040. Atlantic, 3200 km, 258°. Nighttime regular smooth type, with detectable harmonic.
9. 11.5.55, 1130. Atlantic, 2300 km, 250°. Daytime smooth type, showing irregularity at third peak.
10. 12.1.55, 1830. Atlantic, 3800 km, 259° Nighttime smooth type, showing irregularity as protracted fourth peak.

"idealized flash" taken by BUDDEN, in which the electric moment of the cloud and image charges is destroyed instantaneously, giving a radiation field consisting of a double impulse. Although useful in the first approximation, such a simplified form must be refined to give some indication of the modifications observed in specific instances. Experimental evidence of actual discharge-current variations reveals the general tendency for the current to rise to a peak value, of the order of 20 kA, in 4–7 μs, decaying to half-value in 10–30 μs (BRUCE and GOLDE, 1941). Frequently a continuing current of a few kiloamps takes several milliseconds to die away, as has been directly observed (MCEACHRON, 1939) and deduced from net change records (APPLETON and CHAPMAN, 1937).

From considerations of the distributed capacity of the leader channel, the velocity of return-stroke propagation and the time for charge neutralization, BRUCE and GOLDE (1941) have been able to derive an expression for the discharge current

$$I = I_0(e^{-\alpha t} - e^{-\beta t}) \tag{1}$$

which is in close agreement with average observations for the first few microseconds. Allowing for the increasing length of channel as the return-stroke tip advances, and assuming that the current flows into this tip, the expression for the rate of change of electric moment (M) becomes:

$$dM/dt = 2I_0v_0(e^{-\alpha t} - e^{-\beta t})(1 - e^{-\delta t})/\delta,$$

where I_0 is a current parameter, put equal to 20 kA; v_0 is the average initial rate of advance of the return stroke $8 \cdot 10^4$ km/s, and α, β, and δ are the decay-time constants of the discharge current and return-stroke velocity respectively, $\doteq 5 \cdot 10^4$, $\doteq 5 \cdot 10^5$, and $3 \cdot 10^4$ s^{-1} (after BRUCE and GOLDE). The order of magnitude of the magnetic field radiated by the channel calculated from this moment variation is largely governed by the higher frequencies radiated and the agreement with observation using loop aerials is good in consequence, since the initial current variation is then the governing factor. However, the electrostatic field changes are most inadequately described and the finer details of pulse shape and duration may be misrepresented.

In an attempt to overcome these criticisms, the simple expression for current variation was modified by the writer to include a third term, which decays much more slowly than the other two and is dominant after 40–50 μs (Fig. 2). The current form then becomes:

$$I = Ae^{-\alpha t} - Be^{-\beta t} + Ce^{-\gamma t} \tag{2}$$

where A, B, C = 20, 25, 5 kA, and α, β, $\gamma = 5 \cdot 10^4$, $5 \cdot 10^5$, $7 \cdot 10^2$ s^{-1} (HEPBURN, 1952). This current form gives a truer approximation to the average observations without significantly altering the magnitudes which it was the aim of the earlier expression to predict. Thus a peak current of 18·6 kA after 6·1 μs is little different from the original 14·0 kA at 5·1 μs, and in better agreement with average observed values of 20 kA and 6 μs (Fig. 2). The charge neutralized in the first 100 μs is 0·84C (instead of 0·36) effectively at 1·5 km when the total channel length is 2·67 km, corresponding largely to the capacitatively-bound charge on the channel.

A total of 7·5 C eventually flows, giving a net change of 38 C km, in much better agreement with accepted data. This latter neutralizes remanent charges and perhaps produces leaders to other centres within the cloud in the subsequent readjustments after the discharge. Some is probably sprayed into the region about the channel and its branches by corona discharge, comparable with occurrences in the leader stroke (BRUCE, 1941) and re-establishing a positive space-charge removed by the leader.

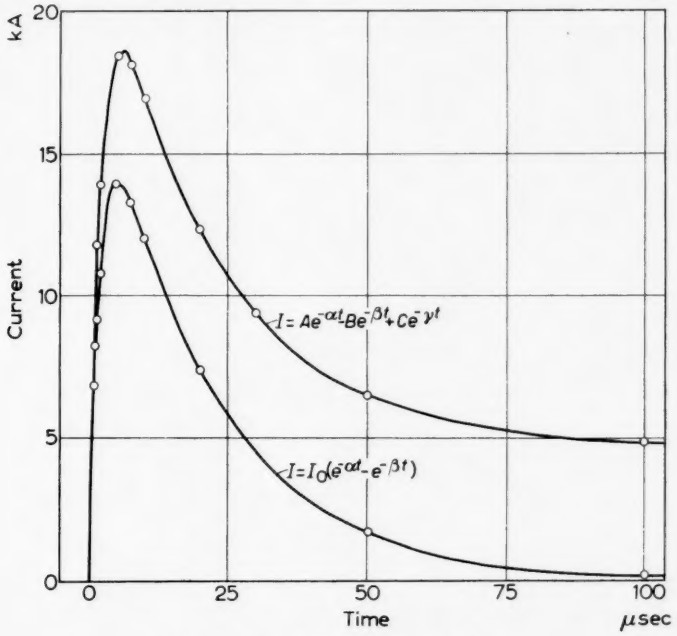

Fig. 2.—Discharge current variations.

$\alpha = 5 \cdot 10^4\ s^{-1}$	$I_0 = 20$ kA
$\beta = 5 \cdot 10^5\ s^{-1}$	$A = 20$ kA
$\gamma = 7 \cdot 10^2\ s^{-1}$	$B = 25$ kA
	$C = 5$ kA

It is to be noted that the magnitude of the moment change is largely governed by the product of the amplitude and decay time-constant of the continuing current, and that pairs of values such as 20 kA × 355 μs or 0·5 kA × 14·3 ms would give the same net field change as the 5 kA × 1·43 ms used in the expression, without causing significant alteration to the initial portion of the current waveform, which is governed by the first two terms, or producing field-change forms outside the observed range.

3.2. *Radiated pulses*

The Bruce and Golde current variation (eq. 1) produces a free-space electric radiation field pulse, lasting 12 μs, followed by one of the opposite sign of about one-fifth the amplitude, rising to crest value in 14 μs; whereas the new form (eq. 2) gives an initial pulse of 22-μs duration followed by a very minor excursion of only a

VOL. 10 1957

twentieth the size, reaching its crest in 15 μs (Fig. 3). These are to be compared with the "equal amplitude" (infinite) double pulses from the "idealized" flash; and it is clear that the longer and smaller the continuing current the more nearly does the new radiated waveform approach that obtained from BRUCE and GOLDE'S expression.

For the subsequent interpretation, the Fourier components and the phase relations of these component frequencies of the radiation field are desired explicitly, and they have been obtained as Fourier transforms from the simple analytical expressions deduced for moment change. In the spectrum of the "idealized"

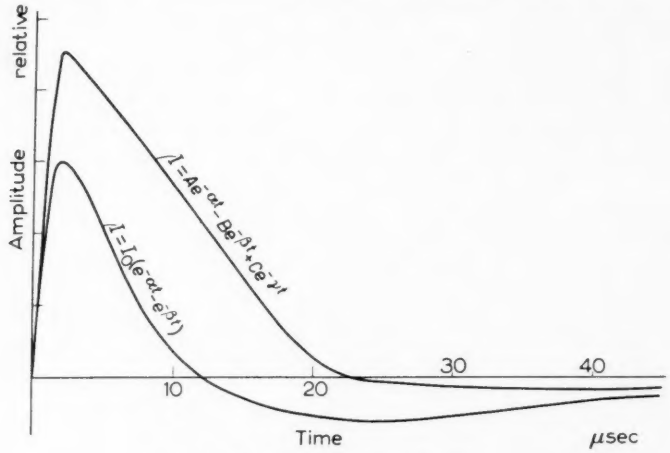

Fig. 3. Radiation-pulse shapes.

discharge the amplitudes are proportional to frequency and the components all have the same phase, giving *k.f.* exp $(i\pi/2)$ as the Fourier transform. The amplitudes have also been evaluated for a discharge producing an electrostatic-field change comparable with that deduced from the Bruce and Golde form of moment change given above. The relative spectra amplitudes for the Bruce and Golde and the new discharge-current forms are given in Fig. 4 (plotted on a logarithmic frequency scale) and Fig. 7b, which show their comparability above 10 kc/s, and the greatly enhanced amplitudes in the range 100–1000 c/s produced by the continuing current. This range of frequencies is responsible for the production of the slow-tail phenomena, which are to be discussed in detail in a subsequent paper. The phase angles of the component frequencies in the radiation fields are given in Fig. 5 for the two realistic discharges, showing the considerable divergence in the range of appreciable amplitude.

4. PROPAGATION EFFECTS

4.1. *Wave-guide and pulse-reflection interpretations of long-train waveforms*

The wave-guide and pulse-reflection interpretations of an observed atmospheric waveform propagated from a distant source approach the subject along essentially different lines. The pulse-reflection theory considers the individual

peaks separately, estimating amplitude, temporal occurrence, and distortion from the geometrical factors and Fresnel reflection coefficients. In contrast, the mode responses of the wave-guide treatment are components of the whole waveform, the fundamental mode response defining the principal temporal occurrences and the later "harmonics" constituting successive corrections, to

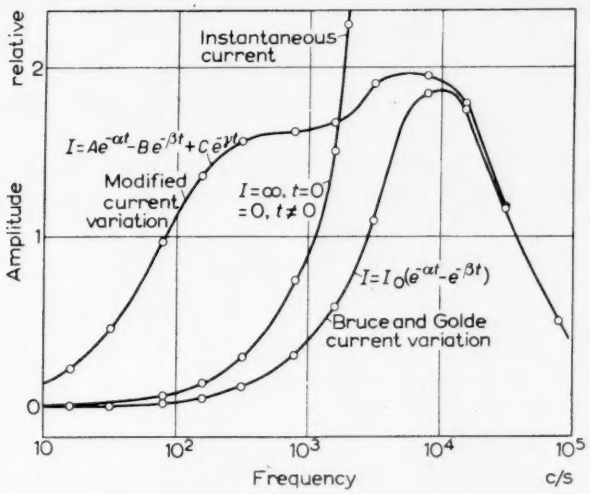

Fig. 4. Radiation-field amplitude spectra.

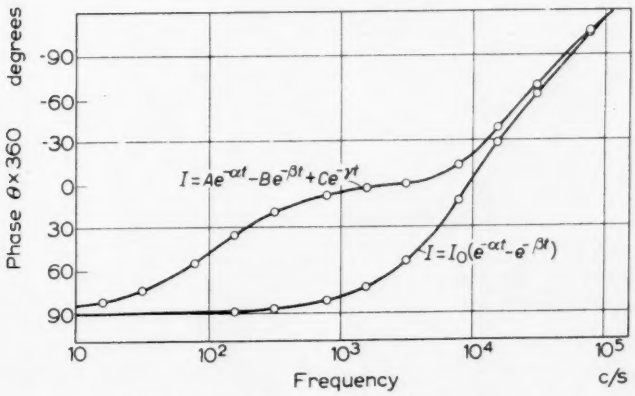

Fig. 5. Phase angles of the Fourier components.

describe more and more adequately the shape of the individual peaks. The diagrammatic analysis of part of a long-train waveform into fundamental and next two harmonics is illustrated in Fig. 6, together with representations of propagation-theory nomenclature to be used. Since the two theories are merely different approaches to a single phenomenon, their results must be mutually equivalent.

In his wave-guide interpretation of what appear to be smooth-type waveforms, HALES (1948) has hinted at the formal equivalence of the mathematical

VOL. 10 1957

equations deduced from the two approaches. However, it is felt that a more general and explicit restatement is to be desired, especially in view of the detailed use to be made of the concepts in the following section.

When the Fourier transform of the source signal is $A(f) \cdot \exp 2\pi \cdot \theta(f) \cdot i$, $\theta(f)$ being measured in cycles for later convenience, and radiation into free space is of the form e^{-ir}/r with velocity c, the field at a large distance d and time t after the start of the signal is proportional to:

$$E(t, d) = \int_{-\infty}^{\infty} A(f) \cdot \exp 2\pi i \{f \cdot t + \theta(f) - f \cdot d/c - \tfrac{1}{8}\} \cdot df,$$

the phase term, $-\frac{1}{8}$ arising from the approximation to the Bessel function for large d. For any mode of propagation m having a phase velocity v in the infinite

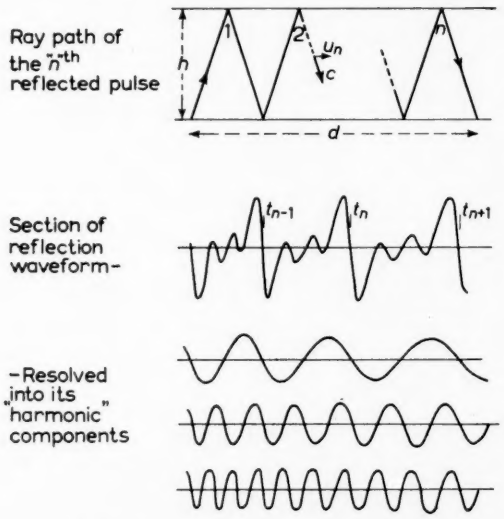

Fig. 6. Propagation theory nomenclature.

wave-guide formed by the earth and ionosphere, initially considered as perfectly conducting parallel planes of separation h, the mode response is of the form

$$E(t, d) = \int_{-\infty}^{\infty} A(f) \cdot \exp 2\pi i \{f \cdot t + \theta(f) - f \cdot d/v - \tfrac{1}{8}\} \cdot df,$$

where wave-guide theory gives the relation

$$(c/v)^2 = (1 - m^2c^2/4h^2f^2).$$

Now

$$\phi(f) = f(d/c - d/v)$$

gives the phase lead in cycles of a given frequency propagated in the wave-guide with respect to the same frequency propagated in free space. The latter expression has been evaluated in a given case for various frequencies and different modes and is plotted in Fig. 7a. The phase leads increase very rapidly to a limiting

value as the cut-off frequency, $f_c = mc/2h$, of the mode is approached and tend to zero asymptotically at high frequencies. The single-mode response may thus be written

$$E(t, d, m) = \int_{-\infty}^{\infty} A(f) \,.\, \exp 2\pi i\{f \,.\, t + \theta(f) + \phi(f) - f \,.\, d/c - \tfrac{1}{8}\} \,.\, df.$$

An asymptotic approximation can be obtained by the method of stationary phase to determine the time variation at a given time, t_n. If $t = t_n + \tau$, we are interested in a small range of τ near zero. The total phase angle, ψ, is given by

$$\psi(f) = \{f \,.\, t + \theta(f) + \phi(f) - f \,.\, d/c - \tfrac{1}{8}\}.$$

The saddle point of ψ in the complex plane of f defining the condition of stationary phase is given by $\dot{\psi} = d\psi/df = 0$. This is satisfied by $f = f_n$ at $t = t_n$,

i.e. $$t_n + \dot{\theta}(f_n) + \dot{\phi}(f_n) - d/c = 0 \qquad (3)$$

Hence ψ may be expanded in the Taylor series

$$\psi(f) = \psi(f_n) + \tfrac{1}{2}(f - f_n)^2 \,\ddot{\psi}(f_n) + \ldots.$$

$$\therefore \quad E(t, d, m) = \int_{-\infty}^{\infty} \exp 2\pi i\{f_n \,.\, t + \theta(f_n) + \phi(f_n) - f_n \,.\, d/c - \tfrac{1}{8}\} \times A(f) \,.\, \exp[\pi i(f - f_n)^2 \,.\, \{\ddot{\theta}(f_n) + \ddot{\phi}(f_n)\}] \,.\, df.$$

This complex Fresnel integral gives

$$E(t, d, m) = 2 \,.\, A(f_n) \,.\, \cos 2\pi\{f_n \,.\, t + \theta(f_n) + \phi(f_n) - f_n \,.\, d/c\}/\{\ddot{\theta}(f_n) + \ddot{\phi}(f_n)\}^{\frac{1}{2}},$$

which varies as $\cos 2\pi\{f_n \,.\, t + \theta(f_n) + \phi(f_n) - f_n \,.\, d/c\}$.

4.2. *Graphical representation by the phase-frequency diagrams*

The tangent to the source phase-frequency diagram (Fig. 7b) at $f = f_n$ makes an intercept θ_n on the phase axis given by

$$\theta_n = \theta(f_n) - f_n \,.\, \dot{\theta}(f_n).$$

Similarly, ϕ_n, the corresponding intercept on the propagation characteristic diagram (Fig. 7a), is given by

$$\phi_n = \phi(f_n) - f_n \,.\, \dot{\phi}(f_n)$$

Using these relations and (3), the mode response becomes

$$E(t, d, m) = 2 \,.\, A(f_n) \cos 2\pi\{f_n \,.\, \tau + \theta_n + \phi_n\} \,.\, \{\ddot{\theta}(f_n) + \ddot{\phi}(f_n)\}^{-\frac{1}{2}}.$$

Thus the slopes of the tangents at corresponding points of the two phase-frequency characteristics give the time of occurrence of a feature in the mode response according to the relation

$$t_n = d/c - \dot{\theta}(f_n) - \dot{\phi}(f_n)$$

and the intercepts on the phase axes give the form of the feature as $\cos 2\pi\{f_n \,.\, \tau + \theta_n + \phi_n\}$ for small values of τ.

VOL. 10 1957

Thus when $\psi_n = (\theta_n + \phi_n)$ has an integral value N, the mode response varies as cos $2\pi f_n \tau$ in the region $\tau \doteqdot 0$, $(t \doteqdot t_n)$, i.e. the feature is a maximum value or crest; $\psi_n = N + \frac{1}{2}$ gives a minimum; $\psi_n = N + \frac{1}{4}$ gives negative slope through zero; $\psi_n = N + 1$ another crest; etc. The time of occurrence of a feature in the mode response may be obtained as a function of ϕ_n rather than $\dot{\phi}(f_n)$ from the relations given previously. Thus

$$t_n = (4h^2 \,.\, \phi_n{}^2/m^2c^2 - d^2/c^2)^{\frac{1}{2}} - \dot{\theta}(f_n) \qquad (4)$$

When ϕ_n/m is integral and $\dot{\theta}(f)$ is constant, this formula gives the usual reflection-theory relation for the time interval between successive ionosphere-reflected

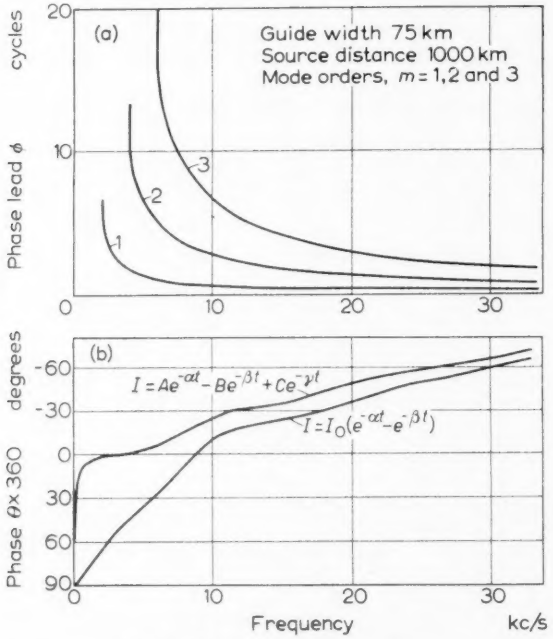

Fig. 7. Phase-frequency diagrams.
(a) Propagation characteristic.
(b) Source characteristic.

pulses, showing that for some feature every mth recurrence in the mth-mode response coincides with the same feature in the first-order mode response reinforcing to give a pulse of appropriate shape. The form of the features which reinforce is obtained by putting ϕ_n integral in the expression for ψ_n and investigating the variation of cos $2\pi\{f_n \,.\, \tau + \psi_n\}$ for small values of τ. Hence, from a knowledge of the phase-frequency characteristics of the source and propagation path the form of the mode responses and the resultant atmospheric waveform may be predicted within the limits of the foregoing theory.

Because of the constancy of $\dot{\theta}(f)$ assumed, implying constant θ_n, the successive features reinforcing to give the resultant waveform are of the same form throughout the mode response.

For the idealized discharge, $\theta(f) = 1/4$ and $\dot{\theta}(f) = 0$ and the mode-response features which reinforce are of the form $\cos 2\pi(f \,.\, \tau + \frac{1}{4})$, i.e. with negative slope through zero, giving a resultant pulse shape centred at $\tau = 0$ consisting of a positive pulse followed by a negative pulse.

4.3. *Modification for long-duration discharge*

When the forms of practical discharge current are considered, the phases of the components are not all the same (Figs. 5 and 7b). The new form of discharge current gives a phase characteristic roughly proportional to frequency in the range 1–50 kc/s; $\dot{\theta}(f)$ constant corresponds to a constant delay of the waveform produced (eq. 4). When θ_n is zero, there is a change of the waveform from a double pulse to a single peak, since the mode responses reinforce when they vary as $\cos 2\pi f_n\tau$, rather than $\cos 2\pi \{f_n\tau + \frac{1}{4}\}$. The positive crests of the mode responses are now the places of reinforcement, and the waveform consists of a series of positive peaks. Such a prediction is in agreement with the fact that the initial radiation pulse is almost entirely positive. The delay of approximately 6 μs from the slope of the phase characteristics is in expected rough agreement with the pulse-rise time, showing that the positive peaks fit the reflection theory to a high degree of approximation, indicated by the closeness to true linearity of the phase characteristic.

VOL. 10 1957

4.4. *Modification for short-duration discharge*

Two current forms have been considered, and an interesting intermediate case is readily obtained by considering the Bruce and Golde discharge, which introduces new phenomena. The source characteristic is more complicated, and may initially be treated in two parts, each of which is almost linear. Above 10 kc/s the characteristic is very similar to that just considered, and below 10 kc/s it is linear, the slope indicating a delay of 30 μs, but for this region the intercept on the phase axis gives $\theta_n = 1/4$ as for the case of the idealized discharge. This leads to interesting conclusions regarding the positions on the mode responses of points which comply with the reflection-theory formulae. For tangents to the source characteristic, which touch at frequencies above 10 kc/s ($f_n > 10$ kc/s), the preceding section has shown that positive maxima would be applicable. For lower frequencies, agreement is obtained when the traces cross the axis, going negative, and have a delay of about 30 μs. Hitherto it has been the practice to measure the peaks throughout the waveforms, when wishing to ascribe such peaks to reflections. In the present instance the limitations of the method are revealed, and for waveforms in which the first-order modes are dominant, it is seen that errors in the high-reflection orders introduced by measuring peaks throughout a waveform can amount to a quarter-cycle, less the delay given by the low-frequency phase-characteristic slope. In the present case, correcting for the delay of positive peaks, this is 101 μs (i.e. 125 — 30 + 6 μs). If the transition frequency of the phase characteristic is above 2 kc/s (as in the case considered), the final frequency of the first-mode response will be unmodified and reflection-theory analysis, based on early- and late-order crests, would give an incorrect range estimate. If the positions of the peaks of high order could be determined sufficiently

accurately, or if the linearity of the phase characteristic were upheld to sufficiently high frequency, i.e. twice the cut-off value, so that the medium-order peaks were formed by frequency components within the range of the low-frequency linearity, then the later orders would be enough to give both distance and reflection height accurately. Calculation of the positions of the early-order crests, neglecting source effects, would place them before the actually observed positions with discrepancies of the order of 100 μs. It is to be noted that the observed (HEPBURN and PIERCE, 1952) and predicted early-order discrepancies are not of the same sign and are of considerably different magnitude. It was assumed that no mistake was made in assessing the numbers of confused orders when analysing the distorted waveforms, but the evidence suggests that an error of one peak may be common, as this would resolve both difficulties of error in sign and magnitude and provide a reason for the earliest orders having greater separation than expected.

In the cases where the source characteristic could adequately be represented by a linear relation over the whole effective spectrum, it was simple to deduce the final waveform, since the variation could be expressed as a constant delay for all frequencies. In the intermediate case, a frequency may be present with a given delay in one mode response, whilst its harmonics in other modes must be attributed different delays, since they are beyond the transition frequency. When the transition occurs well within the excited spectrum, the higher frequencies reinforce to give positive peaks, and the lower frequencies give double pulses. The result of combining the lowest-order mode responses then yields a waveform which starts as a series of fairly sharp positive peaks, gradually giving way to a more saw-tooth symmetrical trace. The high-order modes give positive peaks throughout the response, reinforcing the early peaks and the positive halves of the later double pulses. In this manner the transition from peaks of one sign to a more symmetrical trace can be appreciated.

4.5. *Extension to cases of imperfect boundaries*

Although the linearity of source characteristic is only approximate, a more serious defect is revealed when one considers variations of phase velocity, such as are produced by the presence of imperfectly conducting boundaries to the propagation region. The degeneracy of the modes is removed, modes of order $\pm m$ having slightly different phase velocities. Frequencies in these modes can be propagated with velocities which are not the same as in the degenerate cases, but approximate to these at high mode orders. Oscillations in the lower-order mode responses occur increasingly later than their counterparts in the higher modes, and the responses are not now in harmonic relationship to each other, which produces a progressive modification of peak feature with increasing reflection order.

Smooth-form reflection-type waveforms are particularly interesting, since they appear to be composed of only first-order mode responses (± 1), which, in the absence of complete degeneracy, would be expected to show beat phenomena. BUDDEN (1951) has shown that mode orders 0 and -1 give comparable responses, which are greater than for higher-order modes, for reasonable ionospheric

conductivities, and it is conceivable that these are the two mode responses which interfere.

The peak amplitudes have been observed to show analogous variations, though the subsidiary maxima do not occur at constant peak order, as would at first be expected. However, the problem is complicated by responses varying in direct and relative amplitudes in the two modes due to source and propagation phenomena—one mode response being attenuated more rapidly than the other.

When the boundaries of the wave-guide are not perfectly conducting, the cut-off frequency is not sharply defined and considerable attenuation of near cut-off frequencies occurs as BUDDEN (1951) has shown, the effect being greater for the higher order modes.

5. Applications and Interpretation of Observed Waveforms

The overall picture of the propagation of the higher frequencies (above 2 kc/s) in the atmospheric waveform can now be presented, together with an indication of those factors which are understood and those for which even a general insight is awaited.

VOL. 10 1957

At short range and whatever the conductivity, many mode responses are effective and give sharp discrete peaks, either single or double depending on the discharge. In the case of poor daytime conductivity, the responses are heavily attenuated near their respective cut-off frequencies, and since the waveforms tend to these limiting frequencies very rapidly for short-range observation, only the earliest peaks have noticeable amplitude. Under night conditions greater proportions of these near cut-off frequencies propagate, which results in larger later-order peaks and persistence to nearer the limiting repetition period. The higher-order mode responses are attenuated more rapidly than the lower ones as the observing range increases, and this attenuation is much greater during the day than at night. Absence of high-order mode responses causes the waveforms to be more rounded, so that at medium range (1000 km) during the day the waveforms are smooth (devoid of harmonic content) and short (because of high attenuation near cut-off). At night much greater propagation paths (4000 km) are necessary for the removal of all but the fundamental, and this response persists until the limiting period is approached and the near cut-off period is maintained for many oscillations. At shorter range more harmonic components become effective, depending on range and the approximation to full night conditions. Source and propagation phenomena have been shown to be effective in producing modifications of peak shape.

5.1. *Orientation factor in propagation*

All that has been described so far may be explained by theoretical treatments already known, but considering the waveforms of distant origin to the south-west illustrates the inadequacy in these circumstances. HALES has stated that a similar, smooth type of waveform can be explained as a first-order mode response of a wave-guide having perfectly conducting boundaries. (BUDDEN's work suggests that it is possibly the result of the two nearly degenerate modes in the imperfectly conducting case.) However, the waveforms are quite different from those at

corresponding distances to the south-east in daytime, and, unless it is assumed that discharges to the south-west are deficient in the highest frequencies at the source, it appears very difficult to avoid the conclusion that these frequencies become attenuated during propagation, whilst the lower frequencies are less attenuated. The harmonic responses of the nighttime storms to the South-West are almost completely absent, and comparison with the smooth long-train forms shows that even this fundamental response is quite different, the persistance to a final period close to 500 μs being replaced by a sudden attenuation when the period approaches 250 μs.

The discrimination between regular and irregular smooth-type waveforms can be explained as a source effect, although the full propagation factors are not available. The waveforms are obviously single effective mode responses, even though the attenuation factors may be different from the case of propagation to the south-east. If the source phase-characteristic is linear, there is no cause for irregularities in the mode response, but if it is similar to that obtained for the Bruce and Golde current form it is possible that the first oscillations are governed by the high-frequency part of the source characteristic and subsequent oscillations by the lower-frequency part, the irregularity being produced by the readjustment between the two sequences. This is not noticeable in the presence of higher-order responses, and for the very distant smooth-reflection-type waveforms it takes place gradually over several peak intervals, so that systematic errors are introduced when the waveform is analysed for source distance and reflection height.

Plausible suggestions for the cause of this disparity of propagation factors at large range (beyond 1500 km) would appear to be the modifications and anisotropy of ionospheric conductivity produced by the presence of the earth's magnetic field and differences in the conductivity of land and sea lower boundaries, giving effects which are of different form and magnitude from those produced by simple increase of distance alone, since the transition region has not been observed to show significant diurnal variation—the effects completely transcending the differences in ionospheric layer conductivity.

6. Conclusion

The implications of different forms of discharge current in the lightning channel and the mode responses of an imperfectly conducting wave-guide have indicated anomalous time relations and variation of pulse shape in reflection-type waveforms, whilst known propagation factors can explain the modifying influences of increasing distance and the diurnal variation. A pronounced directional effect is unexplained by the simple considerations, and the variation of the propagation characteristic appears to be associated with the presence of the earth's magnetic field or propagation over land or sea areas.

The amplitudes of successive peaks of the long-train waveforms have not been discussed, though it is obvious that the nonharmonic forms of the mode responses, as in the cases of certain source effects and appreciably finite ionosphere conductivity, produce mode reinforcement which is of a variable form rather

than the fixed feature for perfect conductivity. This variation will yield a peak-amplitude–peak-order relation which is considerably different from the simple form deduced geometrically, apart from the pulse-distortion correction which is the point of difficulty in the reflection-theory treatment. If a complete analysis, including the relative amplitudes of the mode responses, were able to illustrate an increase in peak amplitude with peak order over part of the waveform, the postulation of horizontal discharges would be unnecessary, since it has been indicated how the temporal deviations could be produced by different forms of discharge current in a vertical channel.

Acknowledgements—This research commenced as part of a programme of atmospherics investigation supported by the Department of Scientific and Industrial Research at the Cavendish Laboratory. I should like to thank Dr. T. W. WORMELL for the opportunities of engaging in the work and for his assistance throughout the investigations, Dr. K. G. BUDDEN for very helpful comment and advice, and Professor L. F. BATES for providing facilities for their continuation at Nottingham.

REFERENCES

APPLETON E. V. and CHAPMAN F. W.	1937	*Proc. Roy. Soc.* **A158,** 1.
BRUCE C. E. R.	1941	*Nature, Lond.* **147,** 805.
BRUCE C. E. R. and GOLDE R. H.	1941	*J. Inst. Elec. Eng.* **88**(2), 487.
BUDDEN K. G.	1951	*Phil. Mag.* **42,** 1.
CATON P. G. F. and PIERCE E. T.	1952	*Phil. Mag.* **43,** 393.
HALES A. L.	1948	*Proc. Roy. Soc.* **A193,** 60.
HAUBERT A.	1945	*C.R. Acad. Sci. Paris* **221,** 543.
HEPBURN F.	1952	Thesis, University of Cambridge.
HEPBURN F. and PIERCE E. T.	1954	*Phil. Mag.* **45,** 917.
MCEACHRON K. B.	1939	*J. Franklin Inst.* **227,** 149.

VOL. 10 1957

Journal of Atmospheric and Terrestrial Physics, 1957, Vol. 10, pp. 136 to 139. Pergamon Press Ltd., London

Some effects of intense solar activity on radio propagation*

R. E. Houston jr., W. J. Ross, and E. R. Schmerling
Ionosphere Research Laboratory, The Pennsylvania State University
University Park, Pennsylvania

(*Received* 19 *March* 1956)

1. Introduction

The severe solar flare which occurred about 0300 UT on 23 February 1956 was accompanied by ionospheric disturbances which could be detected even in the nighttime hemisphere. The purpose of this note is to report some observations made at the Ionosphere Research Laboratory, University Park, Pennsylvania (40° 49′ N; 77° 52′ W), on 75 kc/s pulsed transmissions at vertical incidence.

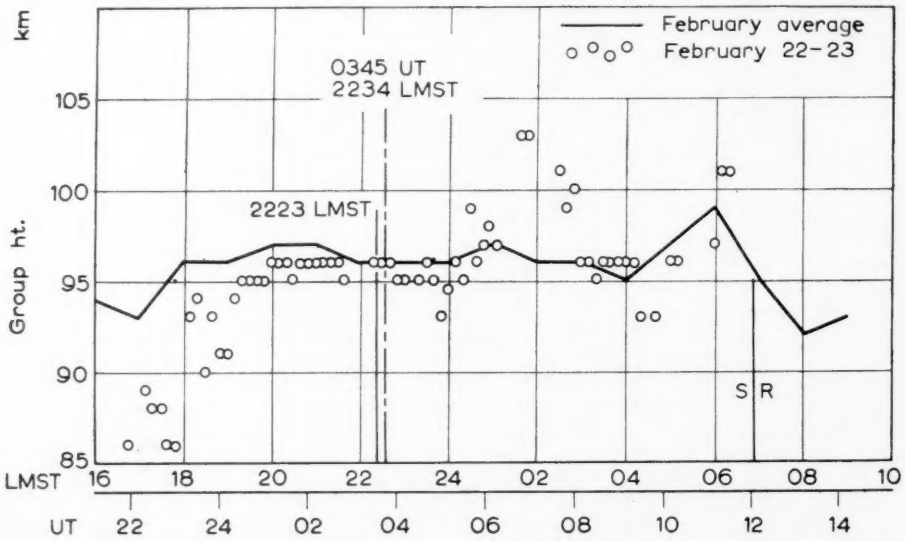

Fig. 1. Group heights at 75 kc/s, vertical incidence.

The start of the visual flare was seen at 0334 UT at Tokyo (McKerrow, 1956). This corresponds to 2223 local mean solar time on 22 February at University Park.

2. Observed Effects

A. *Group height*

Group heights were determined by standard photographic techniques to an accuracy of about ± 1 km.

Our observations are shown in Fig. 1, from which it is apparent that no significant change in group height was noted within an hour before or after the onset of the

* The research reported in this paper has been sponsored by the Geophysics Research Directorate of the Air Force Cambridge Research Center, Air Research and Development Command, under Contract No. AF19(604)-1304.

VOL.
10
1957

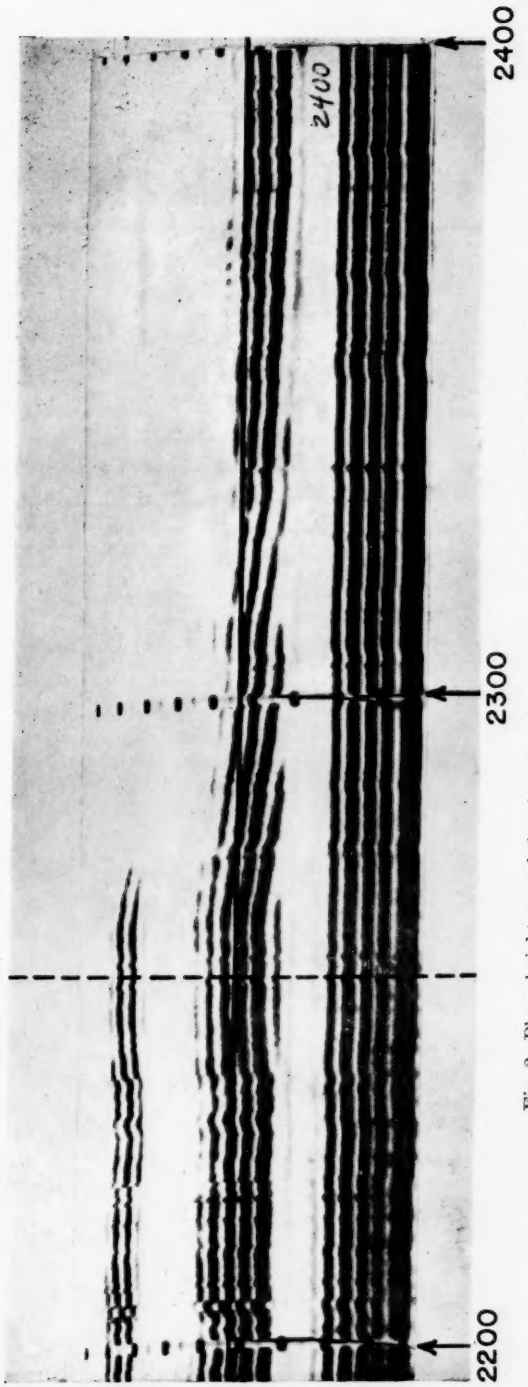

Fig. 2. Phase height record showing the 8-km decrease. The vertical line is 0345 UT.

disturbance. The values recorded during the night did not show unusual scatter, and the large retardation around 0130 LMST has been observed on other occasions. The echo could not be observed after sunrise, as the echo amplitude then decreased to a value too low to be recorded by the group height equipment.

B. *Phase height*

The instrumentation utilized in obtaining phase height records is essentially that described by JONES (1953). The radio frequencies under the ground-wave envelope initiate a phase-coherent oscillation which is used as the reference phase. By beating the sky-wave against this reference oscillator, an interference pattern is obtained, whose movements record changes of phase height.

A portion of the actual record obtained during the night of 22–23 February is shown in Fig. 2. The lower set of parallel lines represents the interference fringes

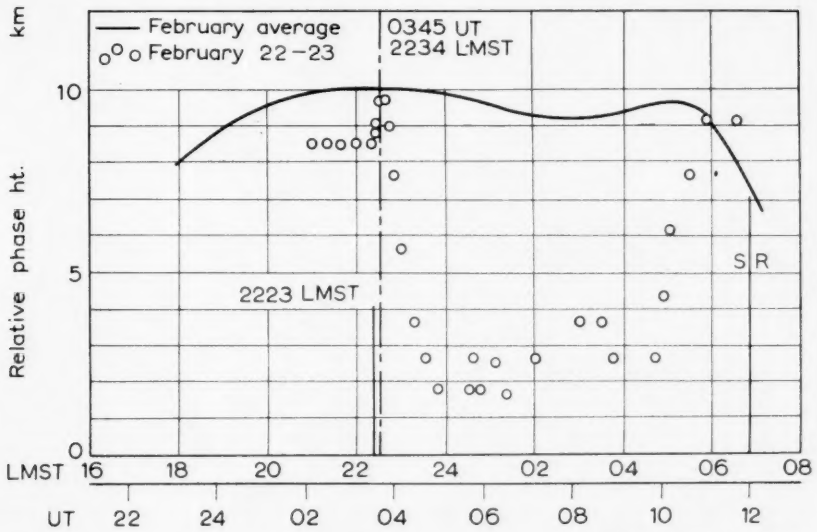

Fig. 3. Phase of sky wave compared to ground wave, converted to change in height.

from the ground-wave, the middle set represents those from the first hop sky-wave, and the upper set represents the fringes from the second hop sky-wave. The horizontal line in the sky-wave is drawn parallel to the lines of the ground-wave pattern. If the effective phase height is decreasing, the "fringe" pattern of the sky-wave will appear as in this figure. Shortly after the onset of the disturbance the absorption had increased sufficiently to cause the disappearance of the second hop.

Fig. 3 shows the phase height record on the same night in its scaled form. It indicates a rather rapid decrease of about 8 km beginning at 2238 (± 3) LMST and lasting approximately an hour. The fall was not abrupt and consequently the precise time of commencement is uncertain to within three minutes. The phase height recovered gradually until just before 0500 LMST, when a more rapid rate of recovery was indicated. It reached the February average a few minutes before 0600 LMST and remained essentially at the same height until 0634 LMST, when the

VOL. 10 1957

record faded out completely. It is interesting to note here that ground sunrise occurred at 0650 LMST. Between 0500 and 0600 LMST the sky-wave was subject to some splitting, which may have reduced the accuracy of the scaling. Because the equipment measures only changes in phase height, it is impossible to compare with a fixed reference level. Thus, the record of 22–23 February is located so as to place the maximum relative phase height just below the monthly average. The unusual drop in phase height is then clearly evident.

C. *Absorption*

The absorption of radio waves can be calculated from the amplitude of the sky-wave, with suitable calibration of the equipment. Using a crossed loop antenna system in conjunction with a mode-selecting device, the amplitude of the circularly

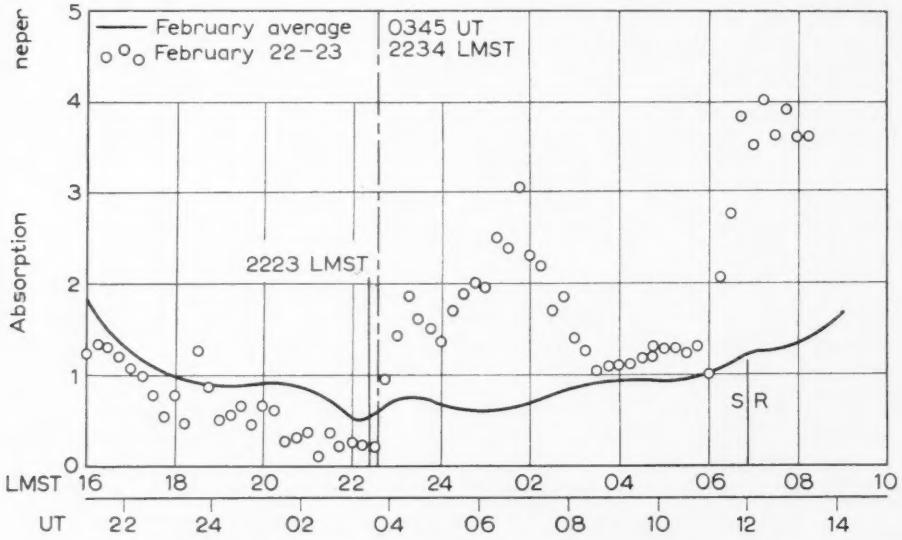

Fig. 4. Absorption of the ordinary mode of the sky wave.

polarized "ordinary" component of the downcoming sky-wave is measured. "Ordinary" here signifies the circularly polarized component whose electric vector rotates from east into north. The observations are shown in Fig. 4. During the early part of the night, the absorption index was about $\frac{1}{2}$ neper lower than the average value for February. Shortly after 2230 LMST, however, a rapid increase of about $1\frac{1}{2}$ nepers occurred, and the absorption remained about 2 nepers above the monthly average for several hours, not returning to normal until about 0400 LMST. Near sunrise an unusually rapid rise in the absorption of the sky-wave was observed. The absorption throughout the rest of the day was beyond the instrumental range of 4 nepers, but returned approximately to normal the following night and day.

3. Outstanding Features of the Above Observations

1. The large increase in absorption which occurred approximately 15 min after visual observation of the solar event. That such an increase should occur at all is

most remarkable when one considers that the reflection region was far removed from the solar radiation field.

2. The concurrent drop in phase height while the group height apparently remained unchanged. Both group and phase height equipment were recording the signal from the same loop antenna during the flare. Hence, neither polarization nor space separation effects can affect the interpretation. One possible explanation of these seemingly divergent facts is a lowering of the reflection height with a simultaneous increase in ionization below this point. However, neither of these possibilities could, by itself, serve to explain these observations.

3. The unusually rapid increase in absorption preceding ground sunrise. This caused the disappearance of the sky-wave in the group and phase height records at a time when the amplitude of this wave is almost always quite large.

4. The rapid increase in phase height beginning about 0500 LMST.

References

McKerrow C. A.	1956	*Nature* **177,** 1223.
Jones R. E.	1953	*Rev. Sci. Instrum.* **24,** 433.

VOL.
10
1957

Journal of Atmospheric and Terrestrial Physics, 1957, Vol. 10, pp. 140 to 152. Pergamon Press Ltd., London

Night-time ionization in the lower ionosphere—I*

Recombination processes

A. P. MITRA†
Ionosphere Research Laboratory, The Pennsylvania State University
University Park, Pennsylvania

(*Received* 6 *December* 1956)

Abstract—Both height and time variations of the effective recombination coefficient at night for the lower ionosphere are obtained from ionospheric data involving the use of radio waves over a wide range of frequencies. The experimental data used include measurements on ionospheric absorption at 18·3 Mc/s and 150 kc/s; hourly values of the night-time E-region critical frequencies for Watheroo, phase height observation at 16 kc/s, and virtual height measurements at 50 kc/s and 150 kc/s. It is found that although at levels near 80 km the effective recombination coefficient increases appreciably immediately after sunset, at higher levels the coefficient decreases. There are both height and time variations of the coefficient.

Theoretical interpretation of these results is based on the idea, recently put forward by NICOLET, that an appreciable number of atomic ions of low ionization potential exist in the lower ionosphere. While the positive molecular ions disappear rapidly through dissociative recombination with electrons, the positive atomic ions disappear very slowly.

1. INTRODUCTION

IN an earlier work by the author and JONES (1954), results of a detailed investigation on the effective recombination coefficient in the lower ionosphere for daytime conditions have been reported. It has been shown in this work that the experimentally deduced values of the recombination coefficient are consistent with the hypothesis of dissociative recombination predominating above 90 km, and recombination proceeding mainly through negative ions below 80 km. Values of the effective recombination coefficient during sudden ionospheric disturbances were also discussed. For night-time conditions, certain values at 80- and 90-km heights were indicated, but no detailed attempt was made to understand the nocturnal recombination processes.

The problem of recombination at night must be fundamentally different from that during the day. While there are indications that the effective recombination coefficients at night for levels around 80 km are increased, the coefficients near the E peak decrease considerably. For the latter, night-time values of the order of 10^{-9} cm^3/s have been quoted by various authors.

In this work we report the results of a detailed examination of the night-time variation of a wide variety of experimental parameters, all involving the lower ionospheric ionization. It is shown that the night-time effective recombination coefficient not only varies with height, but also with time, and that, excepting at levels near 80 km, the nocturnal coefficient is consistently smaller than the corresponding daytime coefficient.

* The research reported in this paper has been sponsored by the Geophysics Research Directorate of the Air Force Cambridge Research Center, Air Research and Development Command, under Contract AF19(604)-1304.

† Present address: Radio Research Committee, National Physical Laboratory of India, New Delhi 12, India.

2. Experimental Analysis

Experimental analyses covered in this work refer to the following:

(I) Hourly values of the night-time E-region critical frequency, f_0E, for a complete year (August 1938–July 1939) for the station at Watheroo. These values were obtained by Dr. Nicolet through the courtesy of the Carnegie Institution of Washington.

(II) Ionospheric absorption using 18·3 Mc/s cosmic radio noise as reported by Mitra and Shain (1953).

(III) Ionospheric absorption at 150 kc/s as measured at The Pennsylvania State University and reported earlier by Benner (1951).

(IV) Phase-height observations at Cambridge as obtained by Bracewell *et al.* (1951).

(V) Virtual height measurements at 50 kc/s obtained by Watts and Brown, using vertical incidence pulse transmissions at Sterling, Virginia, for the period January 1950 till April 1950. These data have been kindly supplied to the author by Mr. Watts of the Central Radio Propagation Laboratory of the National Bureau of Standards, Boulder, Colorado.

(VI) Virtual height measurements at 150 kc/s obtained at The Pennsylvania State University and reported earlier by Lindquist (1953).

VOL. 10 1957

These measurements, made at different frequencies, refer to different levels of the ionosphere, and it was thought that by analysing these observations at different times of the night, it might be possible to follow the variation of the effective recombination coefficient with height as well as with the time of night. The equation to be used is:

$$\frac{\partial n_e(h,t)}{\partial t} = -\alpha(h,t)n_e^2(h,t) \qquad (1)$$

where n_e is the electron density and α the effective recombination coefficient.

Of these, only analysis of (I) is straightforward. The others require previous knowledge of the D-region ionization densities, and, as in the case of height parameters, also the shape of the electron density distribution in the lower ionosphere.

Even before analysing the data, certain significant features, strikingly similar in all these observations, were apparent in the annual average curves (Fig. 1). These may be summarized as follows:

(i) There is a very rapid variation immediately after sunset.

(ii) After the initial rapid variation, the parameter changes very slowly and stabilizes to a more or less constant value around midnight.

(iii) After about 0200, long before layer sunrise, there is a reversal in the direction of the variation, showing an increase in electron density and absorption, and a decrease in certain height parameters.

The later effect cannot be explained by recombination alone and shows that an equation of the type (1) is not always valid. It has been shown by Peiffer and Mitra (1955) that this effect may be caused by a vertical electron drift,

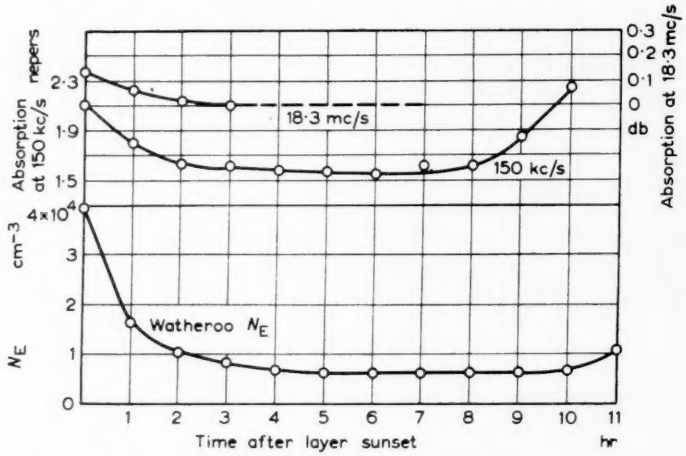

Fig. 1(a). Annual averages of E-region maximum electron density (from data supplied by Carnegie Institution of Washington) and of absorption at 150 kc/s (BENNER) and 18·3 Mc/s (MITRA and SHAIN).

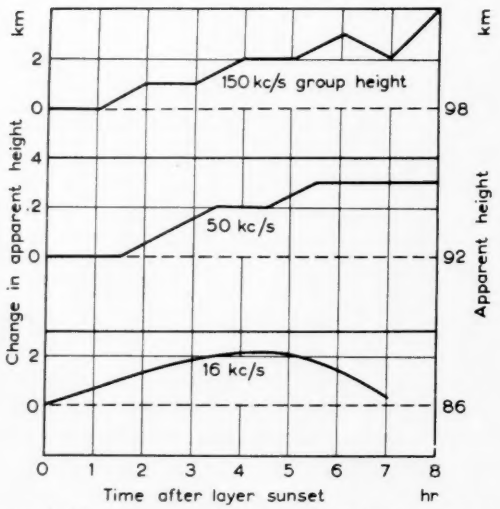

Fig. 1(b). Average variations of phase heights at 16 kc/s (BRACEWELL *et al.*) and 150 kc/s (JONES, 1955), and group heights at 50 kc/s (WATTS and BROWN) and 150 kc/s (LINDQUIST).

reversing in direction a little after midnight. For hours before midnight, the apparent recombination coefficient, determined by equation (1), will decrease for a downward drift and increase for an upward drift. It is necessary to see how large these effects are likely to be.

Consider the equation:

$$\frac{\partial n_e}{\partial t} = -\alpha n_e^2 + \frac{\partial}{\partial z}(n_e v), \tag{2}$$

where the second term on the right-hand side describes the effect of the vertical transport velocity, v, on the decay of the electron density at any level.

Let us concentrate, for simplicity, on the level of maximum ionization. Then

$$\frac{dn_m}{dt} = -\alpha n_m^2 + n_m \frac{\partial v}{\partial z} \tag{3}$$

If the transport velocity, v, has a vertical gradient given by

$$v = v_0 f(z),$$

then

$$\frac{dn_m}{dt} = -\left[\alpha - \frac{v_0}{n_m}\frac{df}{dz}\right] n_m^2 \tag{4}$$

so that the "apparent" recombination coefficient is given by

$$\alpha_{\text{app}} = \alpha - \frac{v_0}{n_m}\frac{df}{dz}. \tag{5}$$

Thus the "apparent" recombination coefficient, under the circumstances where both recombination and transport phenomena are operative, is the algebraic sum of the effective recombination coefficient α and a term due to vertical transport, namely $\frac{v_0}{n_m}\frac{df}{dz}$. For a drift velocity of 1 km/hr, an electron density of $5 \times 10^3/\text{cm}^3$ and

$$\frac{df}{dz} \approx 10^{-2}\ \text{km}^{-1},$$

$$\frac{v_0}{n_m}\frac{df}{dz} \approx 6 \times 10^{-10}\ \text{cm}^3/\text{s}.$$

This is a very small quantity, and becomes comparable to α only after midnight when α falls to very low values. Hence, for determinations before midnight, use of equation (1) will not introduce appreciable errors.

It is also possible to determine the values of v_0 and α for hours after midnight (PEIFFER and MITRA, 1955) for any of the observed parameters. This can be done by comparing the values of the parameter on both sides of the time reversal. For the f_0E observations at Watheroo such a procedure yields a vertical drift of amplitude 1 km/hr and an effective recombination coefficient in the range 10^{-9}–10^{-11} cm^3/s.

VOL. 10 1957

2.1. *Recombination coefficient at night from f_0E values observed at Watheroo*

Determination of the effective recombination coefficient from f_0E is straightforward and involves the direct application of equation (1). From the annual average of f_0E values at Watheroo, the effective recombination coefficient is found to have the daytime, large, value of 10^{-8} cm^3/s for the first hours after sunset, and then to fall rapidly to low values around 10^{-9} cm^3/s. If we add to this the information obtained by PEIFFER and MITRA for hours at and after 0200, it would appear that low values of α persist till the time of layer sunrise. In Fig. 2, the effective recombination coefficient thus obtained is plotted against time measured from the time of layer sunset.

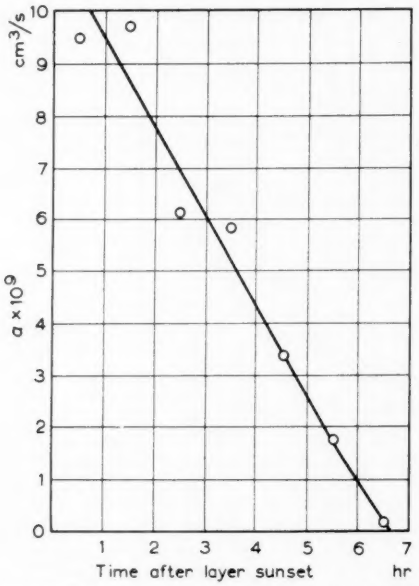

Fig. 2. Recombination coefficient at night obtain from f_0E observations at Watheroo.

2.2. *Recombination coefficient at night from ionospheric absorption measurements*

Our analysis will cover effective recombination coefficients deduced from the measurement of ionospheric absorption by means of cosmic radio noise at 18·3 Mc/s, reported by MITRA and SHAIN (1953), and those at 150 kc/s obtained by conventional pulse techniques as reported by BENNER (1951). In the latter case, the sunset and the post-sunset values include contributions from both the D and E regions which decay according to the coefficients α_D and α_E, respectively, and since α_D is much larger than α_E, the D-region contribution becomes negligible a few hours after layer sunset.

This fortunate circumstance enables us to separate the night-time variations of the two sources of the total absorption. In the case of the 18·3 Mc/s absorption, the referenced authors found that the measured absorption was partly due to region *F2* and partly to region *D*. A method was developed to separate the

* Later work (A. P. MITRA, 1955) appears to indicate that about one-third of the total absorption may be attributed to region *E*.

individual contributions of the two regions. It was observed that absorption attributed to region D, which is of interest in the present work, persisted until sometime after sunset. Although it is by no means certain that this absorption contains no contribution from region E,* the effective recombination coefficient appropriate to this variation has been determined.

Neither the absorption by region D nor that by region E is a single-level effect. However, particularly for region D, maximum absorption is concentrated in a narrow strip of height $\bar{h}$, for which our analysis applies. We can, therefore, write for this level

$$A(t) = Gn_e(\bar{h},t) \tag{6}$$

where $A(t)$ is the measured absorption for any region at any time t, G is a constant of proportionality, and $n_e(\bar{h},t)$ is the value of the electron density at the level $\bar{h}$ at any time t. Hence, the recombination coefficient α may be obtained from the relation

$$\frac{1}{A(t)} = \frac{1}{A_s} + \frac{\alpha t}{G} \tag{7}$$

where A_s is the value of the absorption at sunset. The constant G may be obtained from the noontime relation:

$$A_{\text{noon}} = G(n_e)_{\text{noon}}$$

Using the above expressions, and assuming that $(n_e)_{\text{noon}}$ in the D region is about $700/\text{cm}^3$ on the average, the results given in Table 1 have been obtained.

Table 1. Values of α deduced from absorption measurements

Type of observation	D region		E region	
	Values of α (cm^3/s)	Appr. height (km)	Values of α (cm^3/s)	Appr. height (km)
18·3 Mc/s cosmic-noise experiments	1×10^{-6}	80	—	—
150 kc/s absorption	6×10^{-6}	80	7×10^{-9}	100

The smaller value obtained from the cosmic-noise measurement is presumably due to some E-region contamination remaining in the relevant component in the absorption.

2.3. *Recombination coefficient at night from ionospheric height parameters*

There have been several measurements in recent years of the equivalent heights of reflection of various low-frequency radio waves using both pulse transmissions and continuous waves. Neither the group height nor the phase height is the same as the "true" height of reflection, but in the present work we shall consider their variations to be the same as those in true height.

The determination of the effective recombination coefficient from height parameters is, in principle, indirect. Each variation in a height measurement represents the change in height of a level of constant electron density. The variations in the height of reflection, therefore, depends not only on the effective

VOL. 10 1957

recombination coefficient appropriate to these heights, but also on the height gradient of the electron density at and near these heights. Determination of α from the variation in reflection height, therefore, requires an advance knowledge of the sunset distribution of electron density in the region.

An approximate electron density distribution for the lower ionosphere for sunset conditions may be obtained from experimental data available in the literature. At sunset, the height of reflection of 16 kc/s radio waves is about 86 km (BRACEWELL *et al.*, 1951); and the electron density required for reflection at this frequency must be about 280/cm³. At 50 kc/s, group height measurements by WATTS and BROWN (private communication) yield, for sunset conditions, an average height of 92 km where the electron density must be about 960/cm³. With a correction of 1 km for group delay, the appropriate height becomes 91 km. The average group height corresponding to the "main" reflection level at 150 kc/s is 98 km. For a group delay of 1 km, the true height becomes 97 km and the corresponding electron density is 3×10^3/cm³. Finally, the sunset observations of N_e at Watheroo yield an average sunset value of 4×10^4/cm³ at about 110 km. By using these values it is possible to have a working model of the electron density distribution for the lower ionosphere for sunset conditions. This model is shown by the solid curve in Fig. 3.

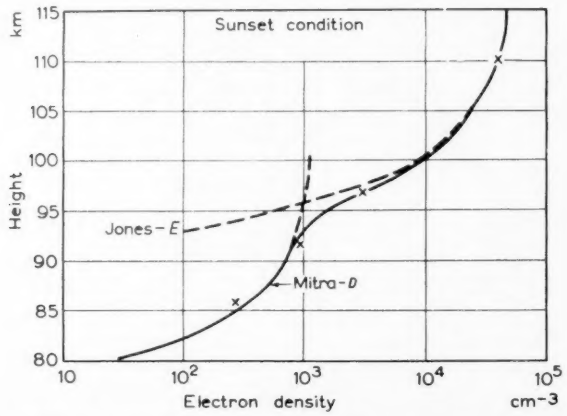

Fig. 3. Sunset model for the distribution of electron density in the lower ionosphere.

Additional information on the sunset electron density distribution in the lower ionosphere is also available in the literature. Thus, JONES has given a model for the electron density distribution for region E, based primarily on his measurements of the phase height at 150 kc/s, appropriate to different values of the solar zenith angle χ. The model for $\chi = 90°$ (with revised height scale) is shown in Fig. 3. The model, it should be noted, has been lowered somewhat from the levels originally assigned by JONES, in order to obtain a fit near the 3000/cm³ level. For the D region, MITRA (1954) has given a distribution from theoretical considerations involving the photo-ionization of NO. However, this distribution is given not in actual electron densities, but as a ratio of $[n_e(h)/(n_e)_{max}]$. The

value of $(n_e)_{max}$ must be chosen from other considerations. In Fig. 3 we have shown a D model of the type given by MITRA, in which the *actual* values of n_e have been computed on the basis of

$$(n_e)_{max} = 2 \times 10^3/cm^3$$

MITRA, 1955). The combined Mitra-Jones model, shown in full lines of Fig. 3, fits the experimental data quite satisfactorily.

Once the sunset electron distribution is known, it is possible to determine the values of the effective recombination coefficient from the variation in the various

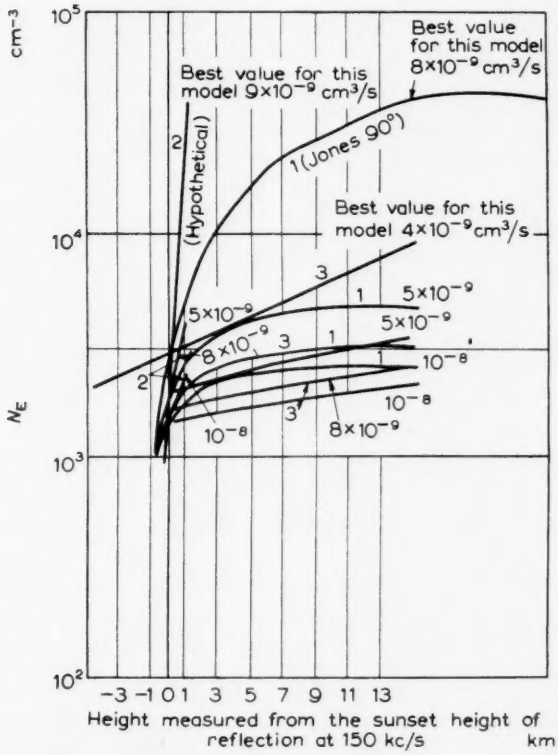

Fig. 4. Effect of sunset electron density models on the determination of α (heights in km).

experimental height parameters. However, since these factors cannot be considered to be as reliably known as might be desired at present, it is necessary to investigate the effect of a change in the sunset electron density model on the values of α so determined. It will be shown below that this effect is, in general, not serious.

Fig. 4 gives an example, in which the variation of the "main" reflection height for 150 kc/s radio waves has been considered. Three widely different models for the sunset electron distribution in the E region have been used. No. 1 is the Jones

VOL. 10 1957

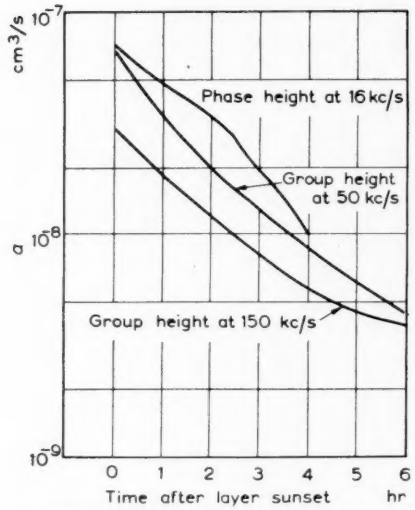

Fig. 5. Night-time variation of α obtained from various ionospheric height data.

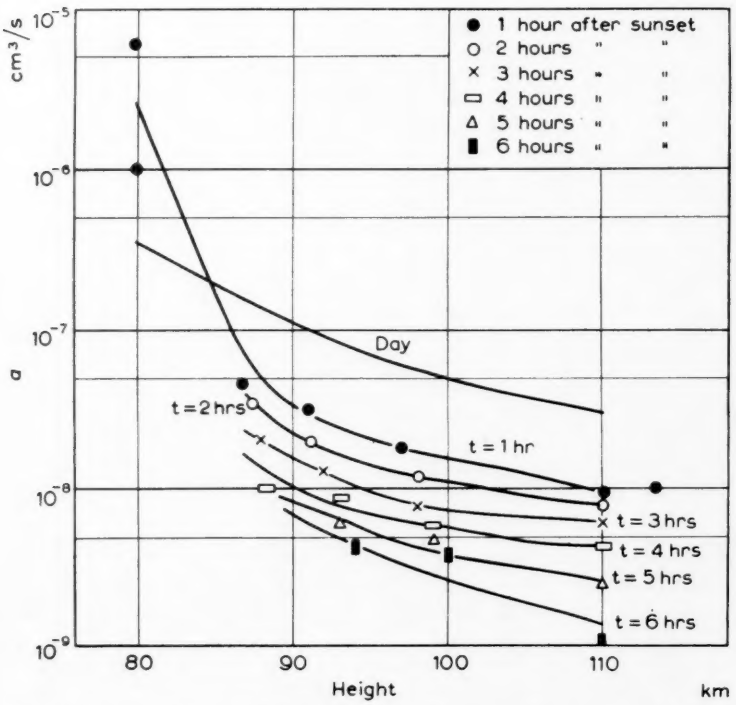

Fig. 6. Observational values of the effective recombination coefficient as a function of height at various hours after sunset.

model. No. 2 is a hypothetical model with a very steep gradient of ionization. No. 3 is a very "flat" ionization distribution. The distributions 2 and 3 are obviously unrealistic and are only used to obtain extreme departures of the values.

Consider a total change of 7 km in reflection height over the entire night for 150 kc/s radio waves; this is the order of height variation observed at this frequency. For a height variation of this order, the three widely different models give, for the effective recombination coefficient, the values 8×10^{-9}, 9×10^{-9}, and 4×10^{-9} cm^3/s, corresponding to the models 1, 2, and 3, respectively. It will be noted that the values of the coefficient are not much different even though the models used are so unlike. It has also been found that, for a parabolic layer with an electron concentration of 3×10^3/cm^3 at 97 km, a maximum electron concentration of 4×10^4/cm^3 and a scale height of 10 km, the height of reflection at 150 kc/s varies by 7 km over the entire night for a recombination coefficient of 8×10^{-9} cm^3/s; again a similar value. We thus conclude that the determination of α from the various ionospheric height variations using any of the distributions given in Fig. 3 will be reliable.

The averaged height parameters for which analyses are made are shown in Fig. 1(b), and the values of α determined from these height variations are given in Fig. 5. In all these measurements, the effective recombination coefficient is large at sunset. The coefficients decrease thereafter, reaching a value of the order of 10^{-9} cm^3/s after midnight.

VOL. 10 1957

It is instructive to plot the various values of α obtained in this work as a function of height for different times of the night. This is done in Fig. 6. Heights are assigned to the different parameters in accordance with the values given in Fig. 5, with appropriate corrections. For E_{max} a constant height of 110 km has been assumed throughout the night. For comparison, the distribution of the effective recombination coefficient for daytime conditions is also shown. It will be noted that, at any time, the value of the coefficient decreases with increasing height.

3. Discussion

In the lower ionosphere during daytime the most potent sources of electron removal are: (i) dissociative recombination of molecular ions and (ii) recombination processes involving negative ions (Bates and Massey, 1951), the former being the predominant process above 90 km and the latter below 80 km (Mitra and Jones, 1954). In the first, given by

$$YZ^+ + e - Y' + Z'$$

the coefficient α_d is large and may range between 10^{-6} and 10^{-8} cm^3/s, depending on the nature of YZ^+. The negative ion processes involve the attachment of electrons to neutral particles which then disappear through a process of collisional detachment and ionic recombination.

At night, α changes due to a change in the value of λ, the negative ion to electron ratio, in the equation

$$\alpha = \frac{1}{1+\lambda} \frac{n(YZ^+)}{n_e} (\alpha_d + \lambda \alpha_i) \qquad (9)$$

the change in λ being of the amount

$$\frac{\lambda(\text{night})}{\lambda(\text{day})} = \frac{\sum_i K_i n_i + \rho + \alpha_i(1+\lambda)}{\sum_r K_r n_r + \alpha_i(1+\lambda)},$$

where K_r is the coefficient of collisional detachment involving particles on the concentrations n_r

ρ is the coefficient of photodetachment,

α_i is the coefficient of mutual neutralization.

For the simple case, where $\sum_r K_r n_r \gg \alpha_i(1+\lambda)$, MITRA and JONES (1954) have predicted the nature of the increase of λ at night for various heights

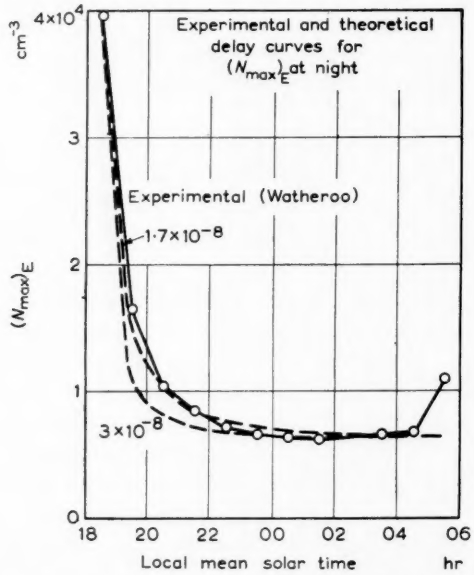

Fig. 7. Experimental and theoretical variations of $(n_{max})E$ at night.

in the lower ionosphere. For a height of 80 km they give a theoretical increase of α from $2{\cdot}4 \times 10^{-7}$ cm^3/s during the day to $6{\cdot}5 \times 10^{-7}$ cm^3/s at night.

Comparison with the experimental results given in Section 2 shows that, while an increase in the effective recombination coefficient is, in fact, observed around 80 km in going from day to night, there is a *decrease* in the effective recombination coefficient near 90 km and above. The latter result is inconsistent with the above hypothesis.

NICOLET has recently indicated the possible existence of an appreciable number of meteoric ions in the E region and has discussed the effect of such ions on the night-time variation of the E region ionization (NICOLET, 1954). The presence of such ions, or any other ions of sufficiently low ionization potential which will not transfer charges to the molecules YZ, will inhibit recombination, since these

positive atomic ions (say, X^+) will either proceed through direct radiative recombination (the coefficient of which cannot be much larger than 10^{-12} cm^3/s) or through negative ions. At levels where λ is small, the concentration of ions will remain appreciably constant throughout the night, while $n(YZ^+)$ will decrease rapidly with a coefficient equal to the dissociative recombination coefficient, which is of the order of 10^{-8} cm^3/s.

An example is shown in Fig. 7. This figure shows that $(n_{\max})E$ attains a constant value around midnight of about $6{\cdot}4 \times 10^3$/cm^3 at a height of about

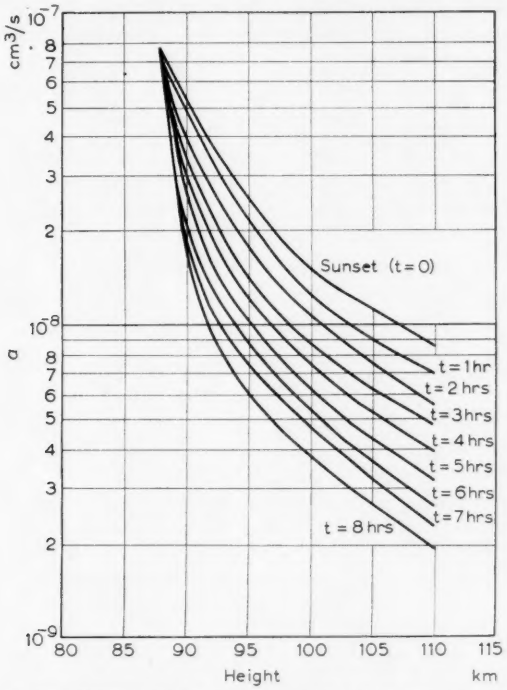

Fig. 8. Equilibrium time for negative ions in the lower ionosphere.
Final model of night time α in the lower ionosphere, obtained from both theoretical and experimental considerations.

110–115 km. This then must be the value of $n(X^+)$ (or, if negative ions are present, of $\dfrac{n(X^+)}{1+\lambda}$). With this value of $n(X^+)$ and with $\alpha_d = 3 \times 10^{-8}$ cm^3/s and $1{\cdot}7 \times 10^{-8}$ cm^3/s, theoretical variations of $(n_{\max})E$ at night have been computed. These are shown in Fig. 7 by the dotted curves. The close relationship is satisfactory.

In general, there will be negative ions in addition to electrons and positive ions. In a companion paper (Part II) it is shown how the concentrations of these various ions may be determined from observational results. With these values, one may obtain a physically consistent model of the nocturnal recombination coefficient in the lower ionosphere, with the help of the equation (9).

The results of such calculations are given in Fig. 8.

VOL. 10 1957

Acknowledgements—The work reported here was carried out in great part at The Pennsylvania State University, while the paper has been prepared at the Radio Research Committee Secretariat of India. It is a pleasure to acknowledge the assistance received from various individuals and organizations during the course of this work. Mr. WATTS of the Central Radio Propagation Laboratory very kindly supplied to the author the observations made by WATTS and BROWN on vertical incidence pulse transmission at 50 kc/s. The f_0E observations at Watheroo for the period 1938 and 1939 were obtained by Dr. NICOLET from the Carnegie Institution of Washington. Our grateful thanks are due to these organizations. Thanks are due to Dr. M. NICOLET for various discussions, and, in particular, for pointing out to the author the importance of meteoric ions at night; to Dr. R. W. PARKINSON for drawing the author's attention to some unexplained features of the night-time variation in height to what is known as the "coupling" echo at 150 kc/s; and to Dr. A. H. WAYNICK for stimulating discussions and for taking trouble to edit this paper. Finally, it is a pleasure to acknowledge the assistance in computations received from Mrs. LOU BARCH.

REFERENCES

BATES D. R. and MASSEY H. S. W.	1951	*J. Atmosph. Terr. Phys.* **2,** 1.
BENNER A. H.	1951	*Proc. I.R.E.* **39,** 186.
BRACEWELL, BUDDEN, RATCLIFFE, STRAKER, and WEEKES	1951	*Proc. Inst. Elec. Eng.* (London) Part III **98,** 15.
JONES R. E.	1955	*J. Atmosph. Terr. Phys.* **6,** 1.
LINDQUIST R.	1953	*J. Atmosph. Terr. Phys.* **4,** 10.
MITRA A. P. and SHAIN C. A.	1953	*J. Atmosph. Terr. Phys.* **4,** 204.
MITRA A. P.	1954	*J. Atmosph. Terr. Phys.* **5,** 28.
MITRA A. P. and JONES R. E.	1954	*J. Geophys. Res.* **59,** 391.
MITRA A. P.	1955a	Scientific Report No. 1, Radio Research Committee, India.
MITRA A. P.	1955b	Progress Report, Radio Research Committee, March–Sept. 1955.
NICOLET M.	1954	Scientific Report No. 72, Ionosphere Research Lab., Pennsylvania State University, November 30.
PEIFFER H. and MITRA A. P.	1955	*J. Atmosph. Terr. Phys.* **6,** 291.
WATTS J. M. and BROWN J. N.	1950	*J. Geophys. Res.* **55,** 179.

Journal of Atmospheric and Terrestrial Physics, 1957, Vol. 10, pp. 153 to 162. Pergamon Press Ltd., London

Night-time ionization in the lower ionosphere—II*

Distribution of electrons and positive and negative ions

A. P. MITRA†
Ionosphere Research Laboratory, The Pennsylvania State University
University Park, Pennsylvania

(*Received* 6 *December* 1956)

Abstract—In Part I of this paper we have discussed the nature of the night-time variation of certain ionospheric parameters, such as height, electron density, and absorption at frequencies in the range 16 kc/s–18·3 Mc/s, and have deduced the time and height variations of the (effective) coefficient of recombination in the ionosphere at night for heights in the range 80–110 km. In this paper, we deduce from the observational results presented in Part I, the distributions of various positive and negative ions and of electrons in the lower ionosphere at night. The positive ions are the atomic ions X^+, which are only predominant at night, and the molecular ions YZ^+ that control the daytime ionization. It is found that the concentration of X^+ increases from a negligible value at about 87 km to about 7×10^3/cm³ at 110 km. Since such ions recombine with a very small coefficient, their concentrations do not appreciably alter during the entire night. While the concentration of negative ions decreases with the progress of the night, the ratio of the concentration of negative ions and electrons remains constant. There is, however, a rapid fall of this ratio from 80 to 110 km by a factor of about 7×10^{-4}.

VOL. 10 1957

1. INTRODUCTION

IN the preceding paper (Part I) we have reported the results of a detailed examination of the night-time variation of a wide variety of experimental parameters, covering a frequency range of 16 kc/s to 18·3 Mc/s. It has been found that the *total* ionization at all levels in the lower ionosphere assumes an approximately constant value, after decreasing rapidly for a few hours following sunset. The resultant effect is a great decrease in the value of the effective recombination coefficient from that at daytime for heights above 90 km, except at and around 80 km, where there is an increase in the coefficient. The latter result indicates the presence of an appreciable number of negative ions at and around 80 km (MITRA and JONES, 1954), the concentration of which may be derived if a suitable assumption is made regarding the value of the coefficient of mutual neutralization. The former has been attributed in Part I to the presence of an appreciable number of atomic ions of low ionization potential so that no charge transfer to the molecular ions occurs.

The night-time ionization in the height range 80–100 km must then consist of: (i) positive molecular ions YZ^+, the coefficient of recombination of which is of the order of 10^{-8} cm³/s, (ii) atomic ions of low ionization potential, X^+, (iii) electrons, and (iv) negative ions, O^- and O_2^-. It is the purpose of this paper to deduce the distributions of these different ions and their variations with the progress of the night.

It is necessary to assume, in these deductions, a reference model for the electron concentration at sunset. The one assumed here is partly empirical and partly theoretical. No other major assumptions are made. So far as the electron concentration is concerned, its distribution at any time at night may be determined directly from the observations. Concentrations of the other ions cannot, however,

* The research reported in this paper has been sponsored by the Geophysics Research Directorate of the Air Force Cambridge Research Center, Air Research and Development Command, under Contract AF19(604)–1304.

† Present address: Radio Research Committee, National Physical Laboratory of India, New Delhi 12, India.

be determined directly. In such cases, the final determination has involved several component steps. In doing so, a certain amount of error must have crept in. It is, however, believed that the general trends of the distributions are not appreciably affected by these errors.

The observations used for the present analysis have been made at different times by different workers at different places. Most of these, however, refer to stations at middle latitudes and, excepting those at 16 kc/s on "apparent" height, are annual averages. The ionization distributions may, therefore, be considered as representing annual averages for stations in middle latitudes

Of particular significance among our deductions are those regarding atomic ions and the negative ions. The possibility of metallic ions being infused into the atmosphere has sometimes been suggested, and NICOLET (1954), in particular, has indicated how the presence of such ions may alter the whole nature of the night-time ionization. From a more limited analysis of ionospheric data than that covered here he has concluded that the rate of production of these ions at E peak is about 1 electron per cm^3 per sec. We shall determine the concentrations of these ions at all heights in the range 80–110 km. Since the recombination coefficient of these ions is only about 10^{-12} cm^3/s, their distribution will not appreciably alter during the night.

We shall also show that while the concentration of negative ions at night decreases with time, the ratio, λ, of negative ions to electrons remains constant. The height distribution of negative ions shows a maximum around 100 km, with low values at 110 km. At the peak, the night-time concentration on the average is about $1{\cdot}5 \times 10^3$/cm^3.

2. THEORETICAL CONSIDERATIONS

Let n_e, n^-, $n(X^+)$ and $n(YZ^+)$ denote, respectively, the concentrations of electrons, negative ions, and of the positive ions of X and YZ. Further, let β_r be the coefficient of attachment of an electron with a neutral constituent whose concentration is n_r, K_i the coefficient controlling detachment of electrons from negative ions by collision with neutral particles of concentration n_i, and let α_i and α_d be the coefficients of mutual neutralization and dissociative recombination, respectively. Then we may write:

$$\frac{dn^-}{dt} = n_e \sum_r \beta_r n_r - \sum_i K_i n^- n_i - \alpha_i n^- (YZ^+) \tag{1}$$

$$\frac{dn_e}{dt} = -\alpha_e n_e^2 (1 + \lambda) - \sum_r \beta_r n_r n_e + \sum_i K_i n_i n^- \tag{2}$$

$$\frac{dn(X^+)}{dt} \approx 0 \tag{3}$$

$$\frac{dn(YZ^+)}{dt} = -\alpha_d n(YZ^+) n_e - \alpha_i n^- n(YZ^+) \tag{4}$$

$$n^+ = n(X^+) + n(YZ^+) = n_e + n^- = n_e(1 + \lambda) \tag{5}$$

From these equations, we obtain the following useful relationships:

$$\alpha = \frac{1}{1 + \lambda} \frac{n(YZ^+)}{n_e} \left[\alpha_d + \lambda \alpha_i\right] \tag{6}$$

and $$\frac{d\lambda}{dt} + \lambda^2 (\sum_i K_i n_i - \alpha_e n_e) + \lambda \Big[\sum_i K_i n_i - \sum_r \beta_r n_r - \alpha_e n_e + \alpha_i n(YZ^+) \Big] - \sum_r \beta_r n_r = 0 \qquad (7)$$

These equations completely specify the nature of the variation at night of the various positive and negative ions and of electrons.

Now, the attachment coefficient β for oxygen molecules is $1{\cdot}5 \times 10^{-15}$ cm^3/sec (Biondi, 1951) and for oxygen atoms probably ranges between 10^{-15} and 10^{-16} cm^3/s. Values of $\sum_i K_i n_i$ and $\sum_r \beta_r n_r$ are, therefore, comparable.

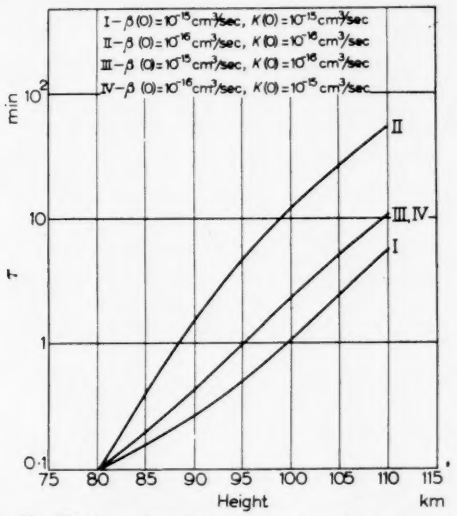

Fig. 1. Equilibrium time for negative ions in the lower ionosphere.

One may, however, ignore $\alpha_i n(YZ^+)$ in comparison to β_n and K_n, since, for values of α_i ranging between 10^{-7} and 10^{-8} cm^3/s, $\alpha_i n(YZ^+)$ does not exceed 4×10^{-3}/s at any level in the height range 80–120 km at any hour of the night (excepting perhaps for a few hours after sunset for the highest levels) and is generally much less. The term $(\alpha_e n_e)$ may likewise be ignored.

We then have $$\frac{d\lambda}{dt} + (\sum_i K_i n_i)\lambda^2 + (\sum_i K_i n_i - \sum_r \beta_r n_r)\lambda - \sum_r \beta_r n_r = 0$$

the solution of which is

$$\lambda = \frac{\sum_r \beta_r n_r}{\sum_i K_i n_i} \left[\frac{1 - \exp\{-(\sum_i K_i n_i + \sum_r \beta_r n_r)t\}}{1 - \frac{\sum_r \beta_r n_r}{\sum_i K_i n_i} \exp\{-(\sum_i K_i n_i + \sum_r \beta_r n_r)t\}} \right] \qquad (8)$$

The equilibrium time for λ may consequently be defined by

$$\tau = (\sum_i K_i n_i + \sum_r \beta_r n_r)^{-1} \qquad (9)$$

The values of τ for different heights are plotted in Fig. 1 for $\sum_i K_i n_i = K(O)n(O)$

and $\sum_r \beta_r n_r = \beta(O)n(O) + \beta(O_2)n(O_2)$. For both $K(O)$ and $\beta(O)$ two values have been assumed, namely 10^{-15} cm^3/s and 10^{-16} cm^3/s. It will be noted that below about 90 km the equilibrium time for negative ions is less than a minute; between 90 and 100 km it is of the order of a few minutes. Above 100 km, the equilibrium time may have appreciably larger values for low values of $K(O)$ and $\beta(O)$, but, at these heights, the negative ion concentration is small, and is of little significance. We are, therefore, permitted to consider the equilibrium equation for λ in measurements of the recombination coefficient with records of one hour duration or more. Hence, the night-time variations of λ will be given by

$$\lambda = \sum_r \beta_r n_r / \sum_i K_i n_i \tag{10}$$

Equation (10) indicates that, at any height, λ must be constant (with time) at night.

3. Electron Removal Rates at Night in the Lower Ionosphere

In Part I of this work we have shown how certain approximate estimates of the electron removal rates at various levels of the lower ionosphere may be determined for various times of the night. Now, these results are based on estimates made at only a few heights, and interpolation was necessary to obtain the distributions. It is, however, possible to improve the distributions by using equation (6), in which α_d, $\lambda\alpha_i$, and $\frac{n(YZ^+)}{n_e}$ are estimated from observational data. This we now proceed to do.

Consider the decay of the positive molecular ions during the night (equation 4). If we consider a short interval of time over which n^- is sensibly constant, and describe $\frac{n(YZ^+)}{n_e}$ by the symbol λ', then the solution of equation (4), subject to the sunset conditions, is given by

$$\frac{\lambda'}{\lambda_s'} = \left(\frac{1+\lambda}{1+\lambda\alpha_i/\alpha_d}\right)\left[1 + \left(\frac{\alpha_i}{\alpha_d} - 1\right)^* \frac{n_s^-}{n(X^+)} \frac{e^{-Bt}}{\xi(t)}\right] \tag{11}$$

where the subscript, s, refers to the values at sunset, and

$$B = \alpha_d n(X^+) + (\alpha_i - \alpha_d)n^- \tag{12}$$

$$\xi(t) = 1 + \lambda_s' \frac{n^-(\alpha_i - \alpha_d)B_s}{n(X^+)(\alpha_d + \lambda\alpha_i)B} e^{-Bt} \tag{13}$$

Now, it will be shown later (Sections 4.2 and 4.3) how one may estimate values of α_d, $\lambda\alpha_i$, $n(X^+)$, and n^- from the observational data considered in this work. With these data it is possible to compute values for λ' and hence for α through equation (6). However, it should be noted that equation (11) is only valid for constant n^-, while, in the actual case, n^- must decrease with time at night. A process of successive approximation has, therefore, been used. The approximation procedure is continued, hour by hour, for eight hours after ionospheric sunset. This has been done separately for the heights 88, 90, 95, 100, 105, 110, and 115 km. From these the final models giving the variations of the night-time α have been derived. These

are shown in Fig. 8 of Part I. They compare very well with values deduced directly from experimental data. In what follows we shall use these semi-empirical curves in preference to those obtained more directly.

4. Distributions of Electrons and of Various Positive and Negative Ions

The various ionic components whose distributions it is our object to deduce in this work are:

1. Electrons,
2. Positive atomic ions, X^+,
3. Positive molecular ions, YZ^+, and
4. Negative ions.

In estimating the densities of these various ions in the lower ionosphere, we shall use the experimental data reported in Part I of this work, which include

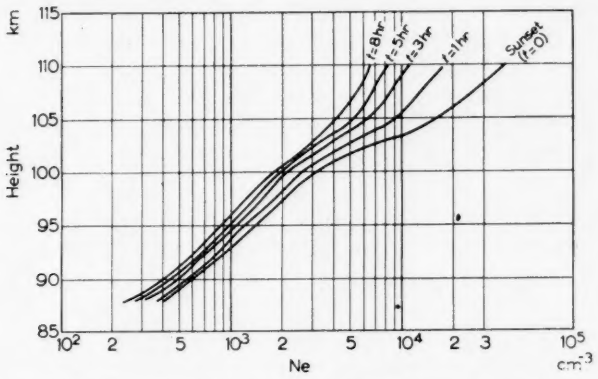

Fig. 2. Variation of the night-time electron density in the lower ionosphere.

measurements on ionospheric absorption at 18·3 Mc/s and 150 kc/s, hourly values of the night-time E region critical frequencies for Watheroo, phase height observations at 16 kc/s, and virtual height measurements at 50 kc/s and 150 kc/s. Detailed information on the night-time variations of these parameters is given in Part I, in which is also given a model of the sunset electron density distribution consistent with these data and with the known physical characteristics of this region. This distribution is our starting-point. From this we will first derive the sunset distributions of $n(X^+)$, $n(YZ^+)$, and n^-; and then the subsequent variations of these quantities as night progresses.

4.1. *Distribution of electrons*

The distribution of electrons in the lower ionosphere at sunset is our starting-point. At any subsequent time t, the electron density at a height h is given by the relationship

$$n_e^{-1}(h,t) = n_s^{-1}(h) + \alpha(h,t)t; \tag{14}$$

values of $\alpha(h,t)$ appearing in this expression have been taken from Section 3. The resultant distributions of the electron density are shown in Fig. 2.

4.2 *Distribution of negative ions*

Since the nocturnal value of λ at any height does not appreciably change over the night, it is sufficient to estimate the distribution of λ at any one time. We estimate the sunset values in the following. At this time the various positive and negative ions are related by the equation

$$\frac{n_s(YZ^+)}{n_{se}} = 1 + \lambda_s - \frac{n_s(X^+)}{n_{se}}.$$

Substituting this equation in equation (6), and rearranging, we obtain

$$\lambda_s \alpha_i = \left[\alpha_s \Big/ \left(1 - \frac{n_s(X^+)}{(1+\lambda_s) n_{se}}\right)\right] - \alpha_d \tag{15}$$

Values of $\lambda_s \alpha_i$ may be estimated from the values of α_s deduced with the help of this equation if values of $\dfrac{n_s(X^+)}{1+\lambda_s}$ and α_d are known.

Values for the former may be obtained from the minimum (and approximately constant) values to which the observed height and ionization parameters asymptomatically approach at late night hours (see Figs. 1(a), 1(b) in Part I). These constant values have been interpreted in Part I as being due to the solitary presence at these times of the ion X^+, YZ^+ having rapidly decreased with its large recombination coefficient. Under this hypothesis, the electron densities corresponding to these constant values, $\{n_e\}_c$, are given by

$$\{n_e\}_c = \frac{n(X^+)}{1+\lambda} \tag{16}$$

We may, therefore, derive the values of $\dfrac{n(X^+)}{1+\lambda}$ from those of the electron density appropriate to the time of constancy of the experimental parameter involved. The height variation of this quantity is obtained by using experimental data at different frequencies. The results of such analyses are given in the Table 1.

Table 1. Values of $\dfrac{n(X^+)}{1+\lambda}$ at different heights

Experimental parameter	Frequency (kc/s)	$[n_e]_c = \dfrac{n(X^+)}{1+\lambda}$ per cm^3	Height (km)
Phase height	16	280	90
Group height	50	950	94
Group height (main reflection)	150	3×10^3	103
f_0E	750	7×10^3	110

To obtain values of α_d we remember that, at 100 km and above, the value of $\lambda_s\alpha_i$ must be close to zero, so that at these heights

$$\alpha_s \Big/ \left[1 - \frac{n_s(\mathrm{X})}{(1+\lambda_s)n_{se}}\right] \approx \alpha_d \tag{17}$$

Computations show that, at these levels, the values of the left-hand side level off to the minimum value of about 1×10^{-8} cm^3/s. This, then, must be the value of α_d. One may also note here that the daytime recombination coefficient is of this order and is consistent with the microwave values of the dissociative recombination coefficient of several molecules. With these values of $\dfrac{n(\mathrm{X}^+)}{1+\lambda}$ and α_d, we may now obtain values of $\lambda_s\alpha_i$ through equation (15). These values are shown in Fig. 3.

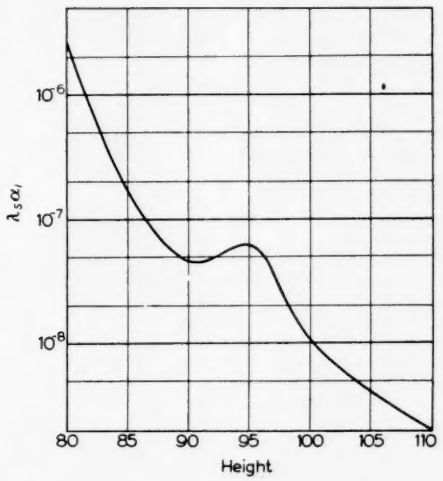

Fig. 3. Height distribution of $\lambda_s\alpha_i$ estimated from experimental data.

It is now necessary to make a few remarks about the accuracies of these estimated values. Below about 87 km, $\dfrac{n(\mathrm{X}^+)}{1+\lambda} \sim 0$, and determination of $\lambda_s\alpha_i$ is independent of the assumed sunset electron density model. For these levels, therefore, the uncertainties in the values of $\lambda_s\alpha_i$ are small. Values above 100 km are also reliable, because here $\dfrac{n(\mathrm{X}^+)}{(1+\lambda)n_{se}}$ rapidly decreases to a small value (less than 0·2 at 105–110 km). However, values of $\lambda_s\alpha_i$ between the heights 85 and 100 km depend, to a very large extent, on the assumed electron density model and should, therefore, be considered with some reserve.

So far we have determined the values of the parameter $\lambda_s\alpha_i$, which does not directly give the densities of the negative ions. One has to assume a value for the mutual neutralization coefficient α_i. In recent years experimental results have been obtained confirming the earlier theoretical estimates of Bates and Massey (1951) for the coefficient of two-body recombination between positive and negative ions;

VOL. 10 1957

which is the important neutralization process for pressures of the order 1 mm or less. The experimental value has been reported by YOUNG and SAYERS (1954) from observations of the decay of ion density in an airglow using ionic probe methods. It was found that over a pressure range of 0·01 to 1·0 mm of Hg the ion-ion recombination coefficient is 8×10^{-8} cm^3/s for an ion temperature of about 300°K. These results refer to iodine.

For oxygen ($O^+ + O^-$) no experimental result is as yet available, but the results on iodine indicate that the theoretical estimates for oxygen are not likely to be seriously in error. In this work we have used a value of 5×10^{-8} cm^3/s for this coefficient. If, subsequently, a different value is obtained for this coefficient, one need only multiply the values of λ given here by $\dfrac{5 \times 10^{-8}}{(\alpha_i)_{obs}}$ to obtain the necessary revision.

With this value of α_i and using the electron density curves given in Fig. 2,

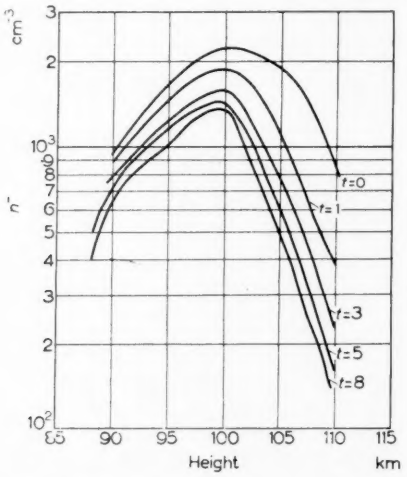

Fig. 4. Variation of the night-time concentration of negative ions in the lower ionosphere.

the height distribution of the negative ion density has been calculated for various times of the night and for heights in the range 80–110 km. These are shown in Fig. 4.

4.3 *Distribution of the atomic ion* X^+

The atomic ion X^+ is, by our hypothesis, the residual ionization existing at E and lower E heights, when the daytime molecular ionization YZ^+ completely vanishes. In the previous section it has been shown how, from the approximately constant values of the ionospheric parameters obtaining at late night hours at these heights, one may deduce the values of the quantity $\dfrac{n(X^+)}{1+\lambda}$ (see also Table 1). To obtain values of $n(X^+)$ we need values of λ. The latter have been determined in Section 4.2. The resultant values of $n(X^+)$ are given in Fig. 5.

VOL. 10 1957

4.4 *Distribution of the positive molecular ions*

The positive molecular ion $n(YZ^+)$ is connected with the other ionizations by the relationship

$$n(X^+) + n(YZ^+) = n_e + n^- = n_e(1 + \lambda)$$

It is easy, therefore, to obtain values for $n(YZ^+)$ when those of $n(X^+)$, n_e, and n^- are known. Values deduced in this way are shown in Fig. 6.

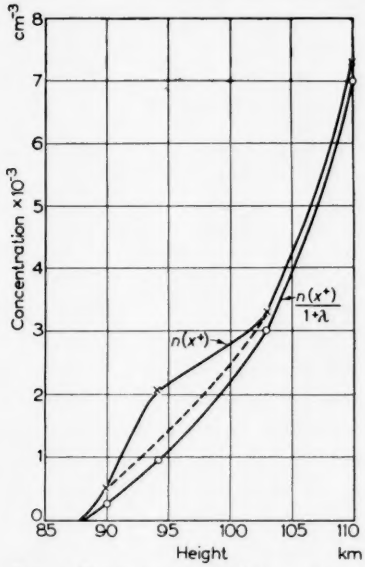

Fig. 5. Variation of $n(X^+)/(1 + \lambda)$ and of $n(X^+)$ with height in the lower ionosphere.

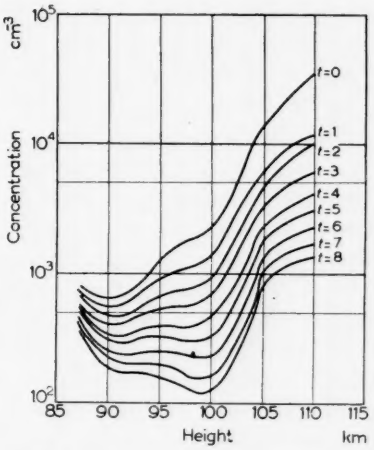

Fig. 6. Variation of the concentration of the positive molecular ions, YZ^+.

5. Conclusions and Discussion

We have presented in this work the results of some tentative deductions concerning the variations of the concentrations of the different positive and negative ions that exist in the lower ionosphere at night from observational data in f_0E and in height and absorption at various frequencies in the range 16 kc/s to 18·3 Mc/s. One satisfactory aspect of these deductions is that, although four different types of ionization are involved in the calculation, *only the sunset model for n_e has been assumed.* All other parameters (excepting α_i) have been deduced from experimental data. The resultant distributions of $n(X^+)$, n^-, and $n(YZ^+)$ at the time of sunset and at the succeeding hours do, of course, depend to some extent on the initial assumption regarding the sunset distribution of n_e*, but may otherwise be considered as representative.

Among the various ionizations deduced, of particular significance is the distribution of the atomic positive ion, X^+, which Nicolet identifies with meteoric ions, and the concentrations of which have been shown in this work to increase from negligible values at 85 km to about $7 \times 10^3/cm^3$ at 110 km.

* One may, for example, compare the values given in Fig. 2 with those recently computed by Parkinson (1955) for a model of n_{se} somewhat different from the one assumed in this work.

The case of negative ions is likewise interesting. While present theory predicts an approximately constant value of λ with height, the experimental values show large variation. It seems possible that this variation is associated with the dissociation of molecular oxygen at these heights. Electrons will be attached to both oxygen molecules and atoms and will vary with $\frac{n(O_2)}{n(O)}$. The equation for λ will, in fact, be given by

$$\lambda = C + D\frac{n(O_2)}{n(O)}$$

where C and D are constants, given by

$$C = \beta(O)/K(O)$$

$$D = \beta(O_2)/K(O)$$

However we may choose to interpret the points of detail, it seems clear that the slower decay of the night-time ionization in the lower ionosphere (principally region E) is due to a mixture of the normal E-region ionization decaying with a coefficient of about 10^{-8} cm^3/s and an additional ionization (which one may term "abnormal" ionization) decaying more slowly. This "abnormal" ionization may well be the same as that of sporadic E normally observed at night with P'-f equipments. In a recent work, PIGGOT (1955) has shown, from observations of the variation of absorption with frequency and time during the night, that, while the normal E region decays at night with a coefficient of 10^{-8} cm^3/s, weaker forms of sporadic E reflection often varied remarkably smoothly with time after sunset with a much lower recombination coefficient. These findings would seem to confirm generally the basis of this work, and it would appear that this variety of sporadic E is the result of ionized atomic ions, presumably of meteoric origin.

Acknowledgements—The work reported here was carried out in great part at The Pennsylvania State University. It was completed and the paper prepared at the Radio Research Committee Secretariat of India. During the progress of the work considerable assistance was received from Dr. NICOLET, who pointed out to the author the serious effects of meteoric ions on the electron removal rates of the night-time lower ionosphere.

My grateful thanks are due to Professor A. H. WAYNICK for stimulating discussions and for taking the trouble to edit this paper, and to Mrs. LOU BARCH for assistance in computation.

REFERENCES

BIONDI M.	1951	*Phys. Rev.* **83,** 1078.
BATES D. R. and MASSEY H. S. W.	1951	*J. Atmosph. Terr. Phys.* **2,** 1.
MITRA A. P. and JONES R. E.	1954	*J. Geophys. Res.* **59,** 391.
NICOLET M.	1954	Scientific Report No. 72, Ionosphere Research Laboratory, Pennsylvania State University, Nov. 30.
PARKINSON R. W.	1955	*J. Atmosph. Terr. Phys.* **1,** 203.
PIGGOT W. R.	1955	*W. Eng.* **32,** 164.
YOUNG and SAYERS.	1954	Proc. Conf. Ion. Physics, Birmingham.

RESEARCH NOTES

Lunar effects on the equatorial *Es*

(*Received* 3 *November* 1956)

In the equatorial region, *Es* reflection is abnormally intense in the daytime (Matsushita, 1951 and 1953; Smith, 1955). This equatorial *Es* occasionally disappears suddenly around noon or the early afternoon, although it usually continues till evening (Matsushita, 1955). Fig. 1 is an example of the effect in ionograms obtained with a vertical incidence ionosonde (N.B.S., Model C–3) made at Huancayo every 15 min. In Fig. 1a, the equatorial *Es* disappeared suddenly at 1345 75° WMT, although it had the usual appearance at 1315 and 1330. The time at which the *Es* disappeared, in this example, was taken to be 1345 for the present study. In Fig. 1b, the *Es* almost disappeared at 1430, and completely disappeared at 1445. As the time at which the *Es* disappeared in this example, 1430 was used, instead of 1445.

VOL. 10 1957

After once disappearing, the equatorial *Es* sometimes reappears a half-hour to a few hours after the time of disappearance, and also occasionally disappears again. For the following study, the time at which the *Es* first disappeared during the period from 1000 to 2000 on each day at Huancayo was obtained from ionograms. The equatorial *Es*, however, usually disappeared between 1700 and 2000. Sometimes it lasted even after 2000, when it changed its type of reflection. In my study, this effect was ignored, because it only occurred on a few days during the month. The geomagnetic storm effect and the power change of the ionosonde were also ignored in finding the *Es* disappearance-time.

The approximate lunar age of each day was calculated, and the local time at which the *Es* disappeared was plotted as a function of the lunar age. The variation of the averaged values is shown in Fig. 2. As can be seen in Fig. 2a, the equatorial *Es* often disappeared earlier than usual in the vicinity of the full and the new moons. This relation is more conspicuous during the December-solstice months than during the June-solstice months. Fig. 2b is the variation during the December-solstice months from 1952 to 1955.

The solar time of the disappearance plotted as a function of corresponding lunar hour shows a much clearer relation, as shown in Fig. 3. The total number of disappearances occurring before 1700 solar time was computed for each lunar hour. (The *Es* usually disappears after 1700 solar time.) This is shown in the upper part of the figure. I conclude from this result that the equatorial *Es* often disappears around noon or the early afternoon (solar local time) if these times lie between 0000 and 0300 or between 1200 and 1500 lunar time. In other words, the equatorial *Es* often disappears during the first half of the periods of the westward lunar electric current flow in the equatorial region. This current is responsible for the lunar daily magnetic variation (Chapman and Bartels, 1940). The lunar tidal variation of f_0Es at Huancayo has minima at 0000–0300 and 1200–1500 lunar time (Matsushita, 1953), which also agrees with the present result.

The equatorial *Es* may be caused by the vertical upward drift force due to the eastward electric current jet, as the author has already suggested. Accordingly, the disappearance of the equatorial *Es* may be explained by the assumption that the vertical upward drift force due to the eastward electric current of the *solar* magnetic variation is weakened by the

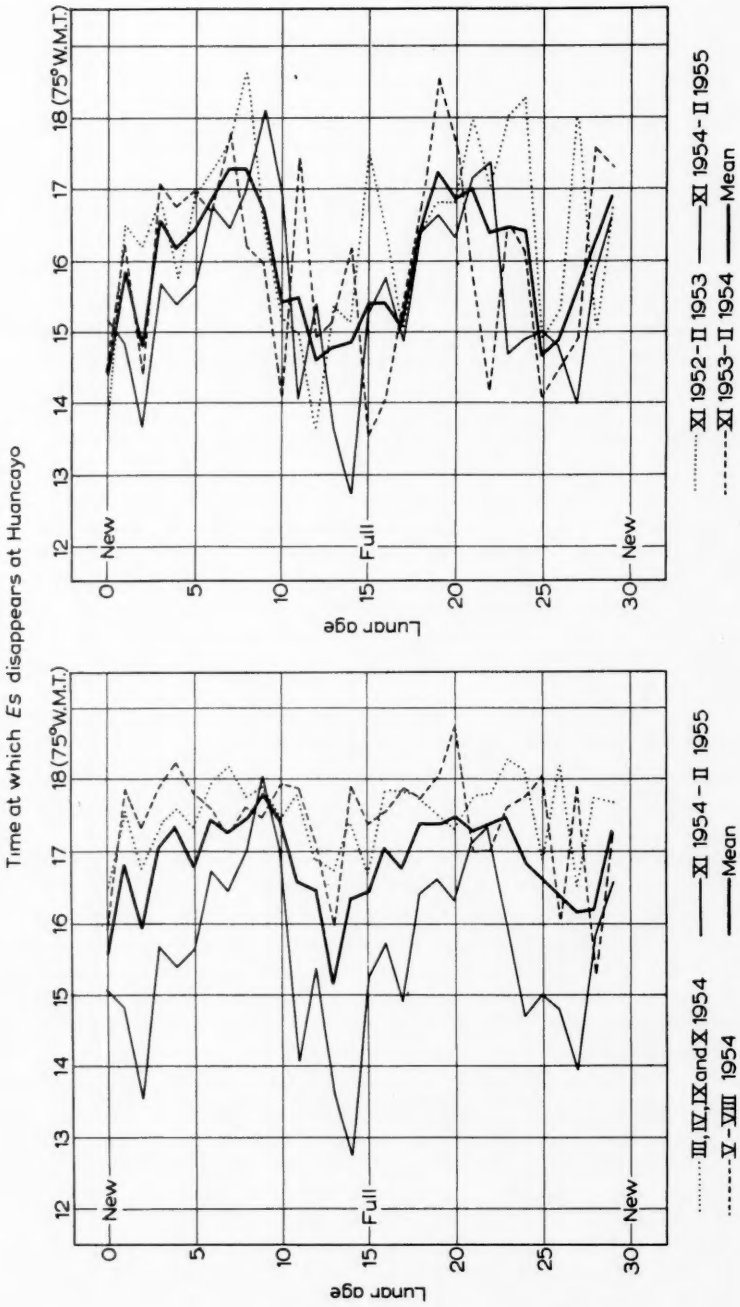

Fig. 2. Variation with lunar phase of the time of sudden disappearance of equatorial *Es*.

VOL.
10
1957

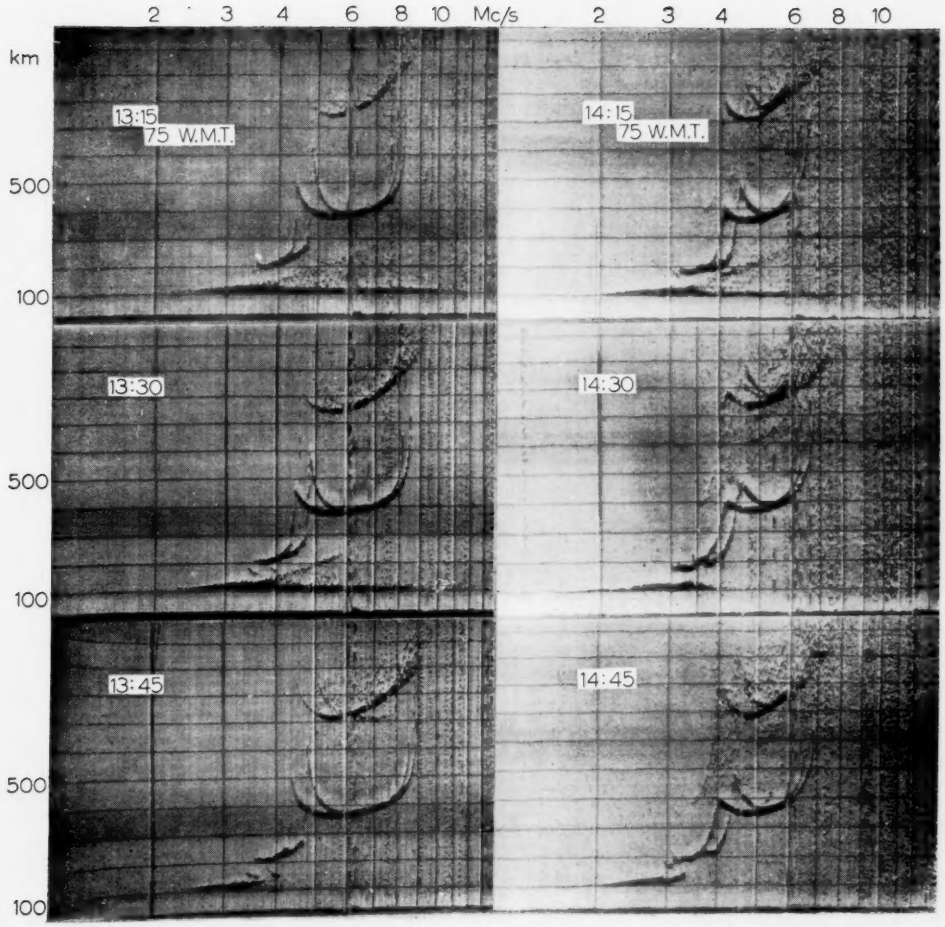

Fig. 1. Ionograms from Huancayo showing sudden disappearance of equatorial *Es*.

downward drift force due to the westward electric current of the *lunar* magnetic variation.

The lunar stratification of the *F2* at Huancayo, reported by GAUTIER, KNECHT, and MCNISH (1951), occurs during the period of 0600–0900 and 1800–2100 lunar time. It is interesting that there is a 6-hours time-lag between the lunar effect on the *Es* and the lunar stratification of the *F*2. This suggests that the lunar stratification is caused by the eastward lunar current effect, in contrast with the disappearance of the *Es*, caused by the westward lunar current.

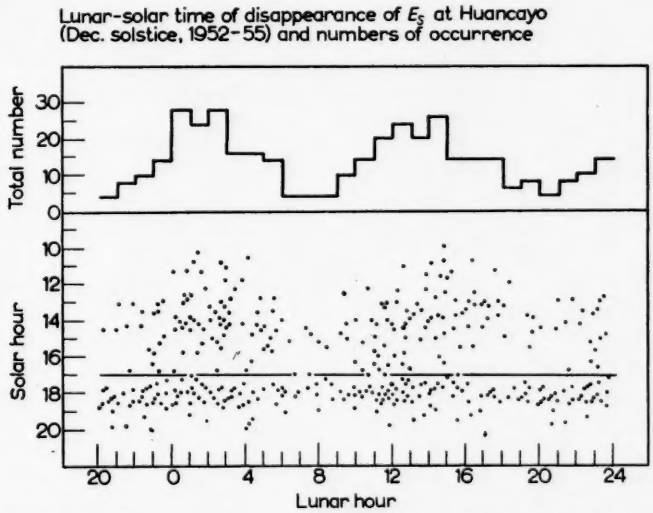

Fig. 3. Sudden disappearances of equatorial *Es* that take place before 1700 solar time occur more frequently between 0000 and 0300 or between 1200 and 1500 lunar time. Dots of lower graph indicate solar and lunar times of sudden disappearances of *Es*; upper histogram indicates total number of such disappearance by lunar hours. Data: December-solstice months, 1952–55.

Acknowledgements—The author wishes to express his thanks for support of the present study by the Geophysical Research Directorate, Air Force Cambridge Research Center, under contract AF19(604)–969. He wishes also to express his sincere gratitude to Dr. L. V. BERKNER, Dr. W. O. ROBERTS, Mr. A. H. SHAPLEY, Mr. T. N. GAUTIER, Mr. A. G. MCNISH, Dr. E. H. VESTINE, and Mr. S. FORBUSH for their kind help and advice, and to the Central Radio Propagation Laboratories, National Bureau of Standards, for use of ionograms involved in this study and for extending to him the facilities of the Boulder Laboratories.

S. MATSUSHITA*

High Altitude Observatory, Boulder, Colorado

REFERENCES

CHAPMAN S. and BARTELS J.	1940	*Geomagnetism* Oxford Press.
GAUTIER T. N., KNECHT R. W., and MCNISH A. G.	1951	Mixed Commission on Ionosphere, Proc. of Second Meeting, page 100.
MATSUSHITA S.	1951	*J. Geomag. Geoelect.* **3**, 44.
	1953	*J. Geomag. Geoelect.* **5**, 109.
	1953	*Rep. Ionos. Res. Japan.* **7**, 45.
	1955	*J. Geomag. Geoelect.* **7**, 91.
SMITH E. K.	1955	NBS Report No. 3575.

* On leave from Kyoto University, Japan.

VOL. 10 1957

Ionospheric self-demodulation of radio waves

(*Received* 7 *November* 1956)

It is well known that, if an unmodulated radio wave and a modulated one traverse the ionosphere simultaneously, then, under some conditions, modulation can be transferred to the originally unmodulated one by a process called "ionospheric cross-modulation." The mechanism of this effect was discussed in a survey paper by Huxley and Ratcliffe (1949), who introduced a parameter T to measure the magnitude of the transferred modulation. In the above description there is no need for the modulated and the unmodulated waves to be different; the modulated wave could produce cross-modulation onto itself, and it can be shown that the result would be to reduce the depth of the original modulation by a "self-demodulation factor" F. F can be calculated in terms of the coefficient T_0 of transferred modulation which would occur at very low modulation frequencies if two separate waves of nearly the same radio frequency were employed. Appleton (1938) appears to have been the first to suggest that ionospheric self-demodulation might occur.

Measurements of ionospheric self-demodulation were made at Cambridge in the summer of 1955, but unfortunately the assumption of new duties by the author in South Africa has delayed the writing of a paper containing the detailed results. The purpose of the present note is to make known the more important of the results obtained. Details will be presented elsewhere.

The Droitwich sender of the BBC (200 kc/s, distant 150 km) was used, modulated at various frequencies in the range 31–750 c/s. Powers ranging from 75 to 400 kW, and different coefficients of modulation, were used in different series of experiments. The received sky-wave was isolated from the ground-wave by means of a loop aerial and the modulation coefficient was compared with that in the received ground-wave. On the higher-modulation frequencies selective fading was troublesome and a large number of observations were taken in order to obtain a statistically reliable result. On the lower-modulation frequencies the selective fading was of little importance. On all modulation frequencies many observations were made from which average values and standard deviations were deduced. The results for a typical series of three nights in June and July 1955 are shown in Fig. 1, in which the mean value of F, together with its standard deviation, is plotted as a function of the modulation frequency. The curve represents the result to be expected according to an extension of the theory of cross-modulation. It is to be noticed that, in agreement with the theory, the demodulation is more marked at the lower frequencies, and is hardly appreciable at frequencies greater than 500 c/s. The mean value of T_0 obtained from all the experiments was of the same order as that deduced from experiments on cross-modulation. The demodulation coefficient was found to be proportional to the transmitted power, in accord with theory.

When experiments were continued through dawn, from night into day, it was found that the demodulation coefficient F increased smoothly to unity, so that there was no demodulation by day. It is deduced that during the day most of the absorption occurs at or below the level where the electron-collision frequency is equal to the angular wave frequency.

These results are quite different from those of Cutolo (1955), who used a wave of frequency 863 kc/sec, transmitted with a modulation coefficient of 0·6. He states that as the modulation frequency increased up to 1000 c/s, the received modulation coefficient fell from 0·5 to 0·1, and as the frequency increased still further from 1000 to 4000 c/s, it remained at 0·1. It is difficult to explain these results theoretically. Cutolo did not state what

precautions were taken to avoid the selective fading which is usually so troublesome at the higher-modulation frequencies. The results are also quite different from those of AITCHISON and GOODWIN (1955) who worked near the gyro-frequency and found demodulation to be most marked when the modulation frequency was between 800 and 1500 c/s.

Since the experiments were made, and the theory extended to deal with self-demodulation, HIBBERD (1955 and 1956) has published two theoretical papers on the subject. In one he deduced the amount of self-demodulation to be expected, and in the other he drew

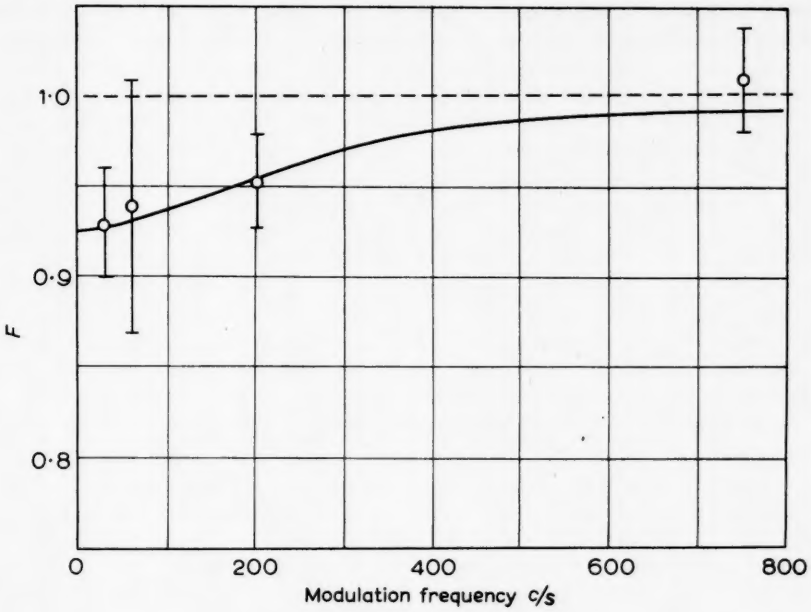

Fig. 1. 22/6/55, 24/6/55, 5/7/55 } Droitwich 200 kW, $M = 0{\cdot}3$
——— theoretical curve.

attention to some of the precautions which would have to be taken in an experimental search for the effect.

This work was done while the author was at the Cavendish Laboratory, Cambridge. He is grateful to the BBC for providing the special transmissions and to Rhodes University for a grant which enabled him to work in Cambridge.

Department of Physics J. W. KING
Rhodes University
Grahamstown, South Africa

REFERENCES

AITCHISON G. J. and GOODWIN G. L.	1955	*Nuovo Cimento* **1**, 722.
APPLETON E. V.	1938	*Proc. Gen. Ass.* U.R.S.I.
CUTOLO M.	1955	*Nuovo Cimento* **1**, 726.
HIBBERD F. H.	1955	*J. Atmosph. Terr. Phys.* **6**, 268.
HIBBERD F. H.	1956	*J. Atmosph. Terr. Phys.* **8**, 120.
HUXLEY L. G. H. and RATCLIFFE J. A.	1949	*Proc. I.E.E.* **96**, Pt. 3, 433.

VOL. 10 1957

Relation between noon *F2*-layer ionization and magnetic dip

(*Received* 19 *November* 1956)

It is now well-known that the geomagnetic field has a dominating influence on the distribution of *F2*-layer ionization. This was first strikingly demonstrated by Appleton (1946), who showed that, under equinox noon conditions, "there is a belt of low values of f_0F2 circling the earth and centred roughly on the magnetic equator." Appleton (1946, 1950, 1954) and all other subsequent workers (Liang, 1947; Bailey, 1948; Maeda, 1955) have demonstrated this equatorial dip effect by plotting the values of $fF2$ at a given local time (say noon) at a particular epoch of the annual solar cycle (say equinox) against one or other of the geomagnetic co-ordinates (say magnetic dip). Such a plot obviously includes the possible variation of fF_2 due to the varying zenith distance of the sun at stations situated at different geographical latitudes. For example, the solar zenith distance at Singapore (geog. lat. 1·3° N) at noon on the equinox day is about 1°, while on the same day the noon-value of χ at Slough (geog. lat. 51·5° N) is about 52°. According to Chapman's theory, the wide difference in the χ value must by itself produce substantial variation of $fF2$ at the two stations. In order to have a correct picture of the dependence of *F2*-layer ionization on the geomagnetic field, this contamination due to variation of solar zenith distance must be eliminated. So far as is known to the present writer, this has not been done by any worker till now.

The object of this note is to depict the true relation between noon $fF2$ and magnetic dip by eliminating the effect of solar zenith distance variation. This has been done by plotting the noon values of $fF2$ against the magnetic dip of the stations keeping solar zenith distance χ as a fixed parameter instead of the equinox or any other epoch of the year. In other words, for stations in different geographical latitudes, noon $fF2$ values of different days in the year have been utilized such that the value of χ at noon is the same for all the stations. For convenience, a table is first prepared showing the dates on which χ_{noon} assumes certain selected values at the different stations. Table 1 given below is compiled to indicate the dates on which χ_{noon} at the different stations assumes the values 0°, 10°, 20°, and 30°. For a particular value of χ_{noon} and for a given station, noon $fF2$ data for five days centred round the date shown in the Table is averaged. In cases where a particular χ_{noon} is attained on more than one date, five days centred round each of these dates are taken and noon $fF2$ for all these days are averaged. This average value (shown within brackets in columns 3–6 in Table 1) is taken as the representative value of noon $fF2$ for the chosen zenith distance. The data thus obtained are then plotted against the magnetic dip of the stations (Fig. 1).

It will be seen in Fig. 1(a) that for $\chi_{\text{noon}} = 0°$, $fF2$ attains a minimum value at the magnetic equator and two maximum values roughly at $\pm 30°$ magnetic dip. The variation of $fF2$ with magnetic dip follows very nearly the same trend for $\chi_{\text{noon}} = 10°$ as shown in Fig. 1(b). In Figs. 1(c) and 1(d), for $\chi_{\text{noon}} = 20°$ and 30° respectively, the peak at 30° N and the minimum at the magnetic equator are clearly maintained. But, the peak to the south of the magnetic equator loses prominence. Closer examination of the figures shows that the southern peak gets flattened out as χ_{noon} increases from 0° to 30°. But this remark is made with some reservation as data for southern magnetic dips between 5° and 35° are insufficient.

For the sake of comparison, one may correspondingly plot $fF1$ and fE values against magnetic dip and check if *F1*- and *E*-layers are subject to any terrestrial magnetic control.

Table 1. Dates on which solar zenith distance χ assumes certain specified values at noon at different stations. The figures within brackets in column 1 indicate respectively the geographical latitude and longitude of the station. The figures within brackets in columns 3–6 represent the average noon fF_2 as explained in the text

Station 1	Magnetic dip 2	Dates for which $\chi_{noon} = 0°$ 3	Dates for which $\chi_{noon} = 10°$ 4	Dates for which $\chi_{noon} = 20°$ 5	Dates for which $\chi_{noon} = 30°$ 6
Bagneux (48·8° N, 2·3° E)	64° N	—	—	—	May 15 (5·4) July 29
Bombay (19° N, 73° E)	24° N	May 16 (9·4) July 28	Apr. 13 (9·7) Aug. 30	Mar. 18 (10·5) Sep. 26	Feb. 21 (10·2) Oct. 22
Brisbane (27·5° S, 153° E)	56° S	—	Feb. 1 (7·2) Nov. 12	Mar. 1 (6·9) Oct. 13	Mar. 27 (6·9) Sep. 17
Calcutta (22·6° N, 88·4° E)	31° N	June 6 (9·6) July 7	Apr. 23 (10·6) Aug. 20	Mar. 27 (11·4) Sep. 17	Mar. 2 (11·5) Oct. 12
Canberra (35·3° S, 149° E)	64·5° S	—	—	Feb. 8 (6·5) Nov. 4	Mar. 7 (6·1) Oct. 7
Capetown (34·2° S, 18·3° E)	60·5° S	—	—	Feb. 12 (7·2) Nov. 1	Mar. 10 (6·7) Oct. 4
Casablanca (33·6° N, 7·6° W)	50·5° N	—	—	Apr. 27 (6·4) Aug. 17	Mar. 30 (6·7) Sep. 14
Dakar (14·6° N, 17·4° W)	26° N	Apr. 30 (10·4) Aug. 13	Apr. 1 (10·7) Sep. 11	Mar. 7 (12·1) Oct. 7	Feb. 8 (11·1) Nov. 4
Delhi (28·6° N, 77·1° E)	41° N	—	May 14 (8·4) July 30	Apr. 12 (11·1) Sep. 1	Mar. 17 (7·8) Sep. 27
Djibouti (11·5° N, 43·1° E)	5° N	Apr. 20 (10) Aug. 23	Mar. 24 May 28 (8) July 15 Sep. 19	Feb. 28 (8·8) Oct. 15	Jan. 28 (9·1) Nov. 15
Falkland Is. (51·7° S, 57·8° W)	46° S	—	—	—	Jan. 13 (6·9) Dec. 1
Freiburg (48·1° N, 7·8° E)	63·5° N	—	—	—	May 12 (4·9) Aug. 1
Hobart (42·8° S, 147·4° E)	71·5° S	—	—	Jan. 4 (5·9) Dec. 9	Feb. 16 (6) Oct. 27
Huancayo (12° S, 75·3° W)	0	Feb. 18 (7·3) Oct. 25	Jan. 11 Mar. 16 (7·8) Sep. 28 Dec. 3	Apr. 10 (7·2) Sep. 2	May 12 (6) Aug. 1
Ibadan (7·4° N, 4° E)	2·5° S	Apr. 9 (8·3) Sep. 4	Mar. 14 May 9 (7·7) Aug. 4 Sep. 30	Feb. 16 ( ) Aug. 27	Jan. 6 (7·5) Dec. 7
Johannesburg (26·2° S, 28° E)	59° S	—	Feb. 5 (8) Nov. 7	Mar. 5 (7·3) Oct. 9	Mar. 30 (7·3) Sep. 13
Khartoum (15·6° N, 32·6° E)	13° N	May 3 (7·8) Aug. 10	Apr. 4 (8·9) Sep. 9	Mar. 9 (10) Oct. 4	Feb. 11 (9·8) Nov. 1

VOL. 10 1957

Table 1—(*continued*)

Station	Magnetic dip	Dates for which $\chi_{noon} = 0°$	Dates for which $\chi_{noon} = 10°$	Dates for which $\chi_{noon} = 20°$	Dates for which $\chi_{noon} = 30°$
1	2	3	4	5	6
Madras (13° N, 80·2° E)	11° N	Apr. 25 Aug. 19 (8)	Mar. 28 (7·3) June 10 July 3 Sep. 15	Mar. 3 Oct. 11 (7·8)	Feb. 3 Nov. 10 (7·5)
Nairobi (1° S, 37° E)	25° S	Mar. 18 Sep. 26 (11·9)	Feb. 21 Apr. 13 Aug. 30 (10·3) Oct. 22	Jan. 17 May 16 July 28 (8·7) Nov. 27	—
Okinawa (26·3° N, 127·8° E)	36° N	—	May 5 Aug. 8 (7·9)	Apr. 6 Sep. 7 (9·8)	Mar. 11 Oct. 3 (9·1)
Panama (9·4° N, 79·9° W)	35·5° N	Apr. 14 Aug. 29 (9·7)	Mar. 19 May 18 July 26 (9·5) Sep. 25	Feb. 22 Oct. 21 (9)	Jan. 19 Nov. 24 (8·8)
Puerto Rico (18·5° N, 67·2° W)	51° N	May 14 July 30 (6·8)	Apr. 12 Sep. 1 (7·6)	Mar. 17 Sep. 27 (8·1)	Feb. 20 Oct. 23 (7·1)
Poitiers (46·6° N, 0·3° E)	62·5° N	—	—	—	May 6 Aug. 7 (5·5)
Raratonga (21·3° S, 159·8° W)	38·5° S	Jan. 15 Nov. 28 (10·8)	Feb. 20 Oct. 23 (9·5)	Mar. 17 Sep. 26 (8·8)	Apr. 12 Aug. 31 (7·4)
Singapore (1·3° N, 103·8° E)	16° S	Mar. 24 Sep. 20 (10·2)	Feb. 27 Apr. 20 Aug. 24 (9·3) Oct. 16	May 27 July 17 (8·6)	—
Slough (51·5° N, 0·6° W)	66° N	—	—	—	May 28 July 15 (5·5)
Tananarive (18·8° S, 47·8° E)	52·5° S	Jan. 27 Nov. 17 (7·4)	Feb. 27 Oct. 16 (8·5)	Mar. 24 Sep. 20 (8·3)	Apr. 19 Aug. 24 (7·3)
Tiruchy (10·8° N, 78·8° E)	5° N	Apr. 18 Aug. 25 (7·2)	Mar. 23 May 24 July 20 (7·1) Sep. 21	Feb. 26 Oct. 17 (8·7)	Jan. 25 Nov. 18 (7·3)
Tokyo (35·7° N, 139·5° E)	49° N	—	—	May 3 Aug. 10 (7)	Apr. 4 Sep. 8 (7·8)
Townsville (19·3° S, 146·8° E)	46° S	Jan. 25 Nov. 19 (7·7)	Feb. 26 Oct. 17 (6·9)	Mar. 22 Sep. 21 (7·8)	Apr. 18 Aug. 25 (7·7)
Wakkanai (45·4° N, 141·7° E)	59° N	—	—	—	May 2 Aug. 11 (6·1)
Washington (38·7° N, 77·1° W)	70° N	—	—	May 15 July 29 (4·6)	Apr. 12 Aug. 31 (5)
Yamagawa (31.2° N, 130·6° E)	43·5° N	—	May 27 July 17 (6·1)	Apr. 19 Aug. 24 (7·5)	Mar. 24 Sep. 20 (8·7)

This has been done and the plots are also depicted in Fig. 1. It will be seen that neither the *F1*-layer nor the *E*-layer ionization exhibits any variation with magnetic dip.

It is to be mentioned that the above plots have been drawn using critical frequency data for the year 1953 which is about the minimum of the sunspot cycle. This ensures that the critical frequencies for the different months of the year were not significantly

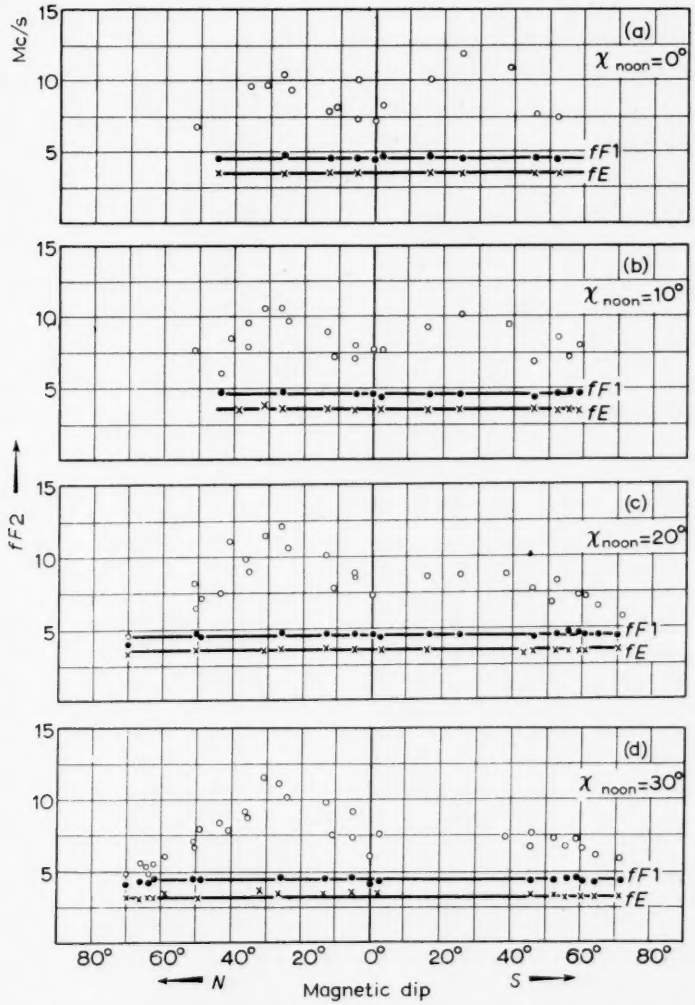

FIG. 1.—Plots showing the relation between noon fF_2 and magnetic dip for the year 1953; for comparison, corresponding plots of fF_1 (dots) and fE (crosses) are also depicted.

affected by the sunspot cycle effect. A more detailed study of *fF2* data in relation to magnetic dip, covering a longer period is in progress. The results will be published in a later paper.

Acknowledgements—I am thankful to Mr. P. DHAR BHOWMICK, Kanodia Research Scholar, for assistance in collecting the data and preparing the plots presented here. Thanks

VOL. 10 1957

are also due to the various institutions which promptly supplied on request certain *fF2* data which were wanting. I am also indebted to Professor S. K. MITRA for helpful discussions.

J. N. BHAR

Institute of Radio Physics and Electronics
University of Calcutta

REFERENCES

APPLETON E. V.	1946	*Nature* **157,** 691.
	1950	*J. Atmosph. Terr. Phys.* **1,** 106.
	1954	*Ibid.* **5,** 349.
BAILEY D. K.	1948	*Terr. Mag. and Atmosph. Elec.* **53,** 35.
LIANG P. H.	1947	*Nature* **169,** 642.
MAEDA H.	1955	*Rep. Ion. Res. Jap.* **9,** 60.

Photoelectric observations of anomalously polarized twilight emission at 5893 Å

(*Received* 20 *November* 1956)

THE extensive investigations of BRICARD and KASTLER (1943), DUFAY (1947), and BARBIER and ROACH (1950) all support the conclusion that the most probable mode of production of the twilight sodium airglow is resonance excitation of neutral sodium atoms by residual solar radiation at 5893 Å. Moreover, the predicted width (~0·03 Å), and weak polarization ($\leqslant 10\%$) of the *D* lines in resonance emission are both confirmed by the twilight observations of BRICARD and KASTLER (1948, 1949, 1950).

With the above facts in mind, it is of more than usual interest to report the presence of strongly polarized twilight emission in a narrow waveband (half-intensity width, 260 Å), centred on the sodium *D* lines, on several occasions following enhanced solar activity during the last sunspot cycle.

The observations were made with a photoelectric polarization photometer employing a selenium photovoltaic cell as receiver, and a rotating type-*H* "Polaroid" filter, driven at 1 r.p.m., as analyser. The modulated photocurrent was fed via a universal shunt to a moving-coil galvanometer of period 2 sec, and sensitivity 970 mm/μA. The required spectral band was isolated by differentiating the measurements made sequentially through two Chance filters, OY1 and OR2, each 3 mm thick. A third filter of didymium glass (ON16) could be combined with the first-named filters in turn to exclude the *D* lines: and so provide a control measurement on the sky-background within the same narrow waveband. The photometer was pointed always to the zenith sky, which subtended a field of 17 degrees radius.

Routine observations commenced early in May 1949: and during the ensuing three months the *D* band was observed repeatedly in emission as an addition to the unpolarized component of the zenithal twilight, first appearing at a solar zenith distance of ~93 degrees. The polarized component remained in absorption throughout the twilight run; and, taking account of the probable experimental error, the degree of polarization could not have exceeded 10%, i.e. of similar magnitude to that found elsewhere (BRICARD and KASTLER 1949, 1950).

However, on the evenings of 9, 11, and 13 August in the same year, the unpolarized component of the sodium band remained in absorption throughout; and, quite unexpectedly, emission was now observed to appear in the *polarized* component. This striking anomaly was again found on a number of occasions during the next three years, its reality being thereby confirmed.

Additional evidence that the anomalous effect just described was actually confined to the narrow D band is found from a comparison of the observed amounts of percentage polarization for sodium band, and sky-background respectively at 95 degrees solar zenith distance. Mean values of these two quantities, for "normal" and "anomalous" groups, are summarized in Table 1. The number of observations in each group appears in parentheses.

Table 1. Percentage polarization observed

	Na band	Sky-background
Normal emission (23)	35	66
Anomalous emission (10)	77	51

VOL. 10 1957

It will be seen that the very large increase of percentage polarization—by a factor of more than 2—shown by the anomalous group is not paralleled in the corresponding values for the sky-background, which show a reversed trend of much smaller magnitude. And since, also, similar trends are found on examining individual observations in the respective emission groups, the marked differences between the results for band and sky appear to be significant.

Although unknown at the time, the abnormal twilight runs of 9, 11, and 13 August followed the intense (3^+) solar flare of 5.3 August. Moreover, on 6 August, normal emission was observed at dusk, thus suggesting either a delayed atmospheric effect of the ultraviolet flare radiation, or possibly an effect of particle radiation from the disturbed region of the sun. This deduction is strengthened when it is mentioned that, of a total of ten observations of polarized emission, nine were preceded by flares of intensity either 3^+, 3, or 2 within an interval of from 2 to 8 days; and the tenth by a moderate geomagnetic storm of M-region type. On no occasion did anomalous emission appear *concurrently* with a major flare disturbance.

By contrast, in a group of sixteen observations of normal D-band emission within the same period, four of these were preceded by a flare within 24 hours, and none fell in the time-interval 2 to 8 days following a major flare. Also, on five occasions when both geomagnetic-storm and auroral activity was present at the time of the twilight observation, sodium-band emission appeared in both components, the unpolarized emission being always of more-than-average intensity.*

To illustrate what is believed to be a characteristic sequence of changes in the character of the twilight emission at 5893 Å, under disturbed conditions of the upper

* This must be attributed to auroral-line and band radiations of atomic and molecular nitrogen, and possibly auroral D-line emission also. Vegard (1949) reports D lines present in auroral spectrograms taken in the middle of the night from the upper parts of auroral treamers. This suggests the presence of sodium atoms, supposedly of solar origin, at heights around 200 km.

Table 2

Date of twilight observation	Date of antecedent flare	Flare intensity	Associated effects[2,3]	Post-flare time (hr)
1950 April 13	1950 April 12.6	3	*A, F, G*	28
1949 August 6	1949 August 5.3	3+	*A, F, G, P*	35
1950 June 10	1950 June 8.6	2	*F, S*	53
1950 June 11[1]	1950 June 8.6	2	*F, S*	60
1949 August 9	1949 August 5.3	3+	*A, F, G, P*	107
1949 August 11	1949 August 5.3	3+	*A, F, G, P*	155
1949 August 13	1949 August 5.3	3+	*A, F, G, P*	203

[1] Morning twilight.
[2] None of the flares cited was followed by a geomagnetic storm.
[3] *A* = sudden enhancement of atmospherics; *F* = short-wave fadeout; *G* = geomagnetic crochet; *P* = sudden phase anomaly; *S* = burst of solar noise.

atmosphere, the seven nonauroral observations listed in Table 2 have been grouped so as to cover a range of post-flare times from 1 to 8 days.

Using the results of the twilight observations tabulated above, smoothed values of the (Na band/sky-background) intensity ratio were computed to cover the needed range of post-flare time and optical sounding height.* The values for heights above 55 km were obtained by extrapolation of the experimental data. One set of intensity ratios included only the values for polarized light; the second those for total (polarized + unpolarized) light.

The march of the intensity ratio with post-flare time at the different sounding levels is best shown by a three-dimensional model, of which two examples are represented in the accompanying figure.

The upper diagram (a) is based on the first set, and the lower (b) on the second set of intensity ratios mentioned above. In both diagrams the contour representing an intensity ratio of unity is shown by the broken line separating emission (unshaded) from absorption (stippled) zones.

Normal *D*-line emission at the 55–65 levels accounts for the additional feature of (b) that is seen to persist up to ~30 hours after the incipient flare. Apart from this, the two models exhibit similar outlines, although the main peak around 100 hours is less evident in total light on account of strong absorption in the unpolarized component for times >40 hours. The surprisingly high intensity-ratio (>3 : 1) found in the polarized component at 65 km is noteworthy, corresponding as it does to a band polarization of over 90%. It will be noted also that the duration of the anomalous emission is sensitive to changes in the level at which it is observed. For example, the duration is only ~50 hours, at the 35-km level; whereas at 65 km the anomaly may persist for periods up to 10 days.

So far as is known, the sequence of changes just described has not previously been reported. But because of the extremely complex nature of the twilight spectrum in the vicinity of the sodium *D* lines it is not possible to state implicitly that the anomalous emission originates either directly or indirectly from excited sodium atoms. All that can

* Following LJUNGHALL (1949), the "optical sounding height" is defined as the effective limit of the earth's shadow for which the light scattered by the atmosphere below this limit just equals the reduction of scattered light by extinction of the atmospheric light above the limit. Between solar Z.D. 91 and 97 degrees, the optical sounding height increases from 14·5 to 65 km.

be said is that the effect appears to be confined to the narrow filter-band including the *D* lines, since it is not present in the adjacent sky continuum.

This central band contains, in addition to the *D* lines, a diffuse and broad emission of unknown origin, observed by BRICARD and KASTLER (1948) to be intense in early twilight;

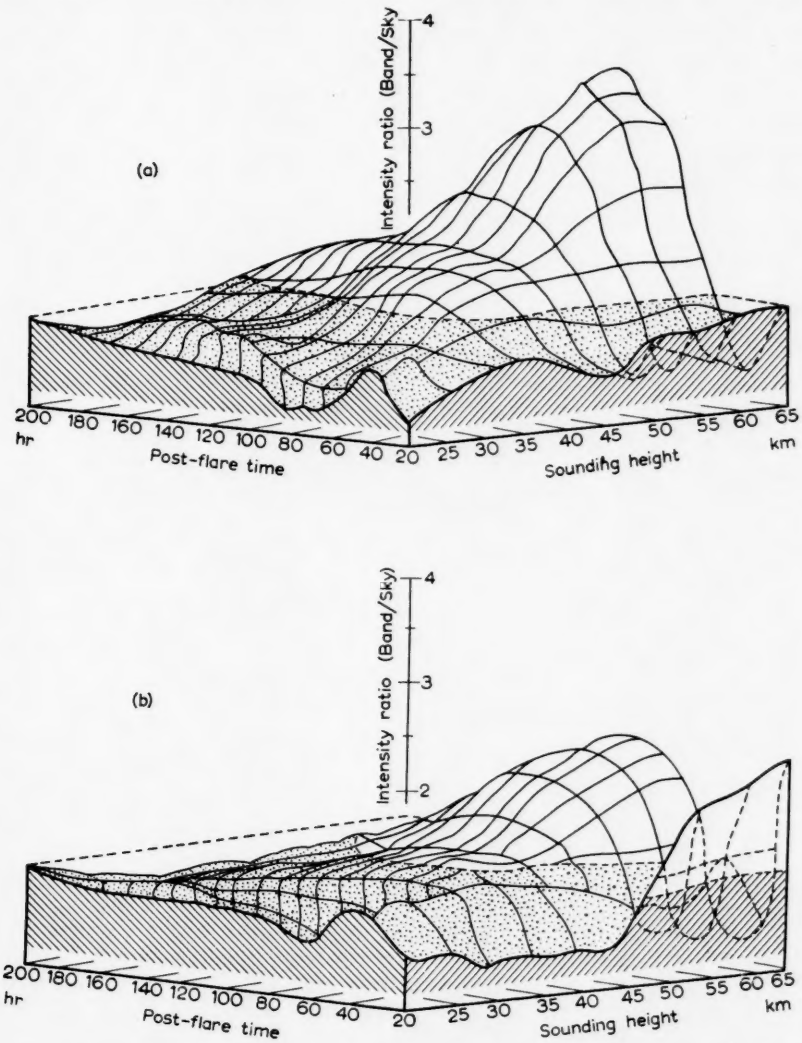

Fig. 1. Three-dimensional plots illustrating anomalous changes in twilight radiation at 5893 Å, following solar activity: (a) polarized component only, (b) total light (both components) from zenith sky.

a part of the Chappuis band of ozone; several Fraunhofer absorption lines; the α(3-0) band of O_2 at 5815 Å, detected by SOMMER (1936) in the night airglow; and numerous water-vapour lines. It is also possible that BRICARD and KASTLER's twilight feature may correspond with the low-level 8-2 ($v' - v''$) band of OH at 5889 Å, first detected in the nightglow by MEINEL (1950); and this same feature may perhaps be responsible for the

VOL. 10 1957

present anomaly. Even if this is so, the cause of the high degree of polarization observed in twilight under disturbed conditions still remains unexplained.

I am greatly indebted to Prof. D. R. Bates, F.R.S., and Mr. H. W. Newton, former superintendent of the Solar Department, Royal Greenwich Observatory, for their interest and advice.

My thanks are due also to the Observatory's mechanic, A. J. Denner, for assistance in the construction of the photometer.

D. R. Barber

Norman Lockyer Observatory
University of Exeter
Sidmouth, Devon

References

Barbier D. and Roach F. E.	1950	*Trans. Amer. Geophys. Union* **31**, 13.
Bricard J. and Kastler A.	1943	*C. R. Acad. Sci.* [Paris] **216**, 878.
Bricard J. and Kastler A.	1944	*Ann. Géophys.* **1**, 53.
Bricard J. and Kastler A.	1948	6th Report, Commission for the study of the relations between Solar and Terrestrial Phenomena, 164.
Bricard J. and Kastler A.	1949	*C. R. Acad. Sci.* [Paris] **228**, 1601.
Bricard J. and Kastler A.	1950	*Ann. Géophys.* **6**, 216.
Dufay J.	1947	*C. R. Acad. Sci.* [Paris] **225**, 690.
Ljunghall A.	1949	*Medd. Lunds Astron. Obs.*, Ser. II, No. 125, 110.
Meinel A. B.	1950	*Astrophys. J.* **121**, 120.
Sommer L. A.	1936	Quatrième Rapport de la Commission pour l'étude des Relations entre les Phénomènes solaires et terrestres, 119.
Vegard L.	1949	Relations entre les phénomènes solaires et géophysiques: Editions de la Revue d'Optique, Paris, 199.

The colour of the zenith twilight sky: absorption due to ozone

(*Received* 6 *December* 1956)

Hulburt (1953) has shown that measures of the luminance of the zenith twilight sky made at Sacramento Peak at different times after sunset cannot be explained by assuming an atmosphere scattering and absorbing light according to the Rayleigh scattering function for the molecules present in the atmosphere. Not only does the computed luminance have a value significantly above that observed during the earlier stages of twilight, but the computed colour of the zenith sky is very close to the colour of an equal energy spectral distribution—the reference white colour of the C.I.E. system of colorimetry. He ascribes the difference between computed and observed luminance and colour to the absorption due to the ozone layer, and has shown that this accounts satisfactorily for the luminance of the zenith sky.

Ashburn (1953) has drawn attention to the work of Grandmontagne and others, who have observed the variation of intensity of the twilight sky in limited spectral ranges. Bullrich (1948) quotes the work of Siedentopf (1941), who has determined the colour

temperature of the twilight sky at the zenith, as a function of the solar depression, θ, below the horizon. SIEDENTOPF found that the colour temperature reaches a maximum at about $\theta = 10°$, thereafter decreasing rapidly. GAUZIT and GRANDMONTAGNE (1942) report on the variation of intensity in the red and infra-red. GRANDMONTAGNE (1938) has measured the intensity of the zenith sky in the blue and red and infra-red, for values of θ greater than 6°. GRUNER (1936) has made most of his twilight observations on the "purple light." He did not use any effective wavelengths between 5300 and 6500 Å. ASHBURN (1952) has made measurements at effective wavelengths through the visible region, at 4400, 5200, 5900, and 7500 Å for values of θ from 0° to 14°. His results indicate quite large changes in the colour of the twilight sky, and also that there is a minimum in intensity of the radiation at about 5400 Å. According to HULBURT'S theory, there should be a minimum corresponding to the Chappuis band of ozone, at about 5900 or 6000 Å.

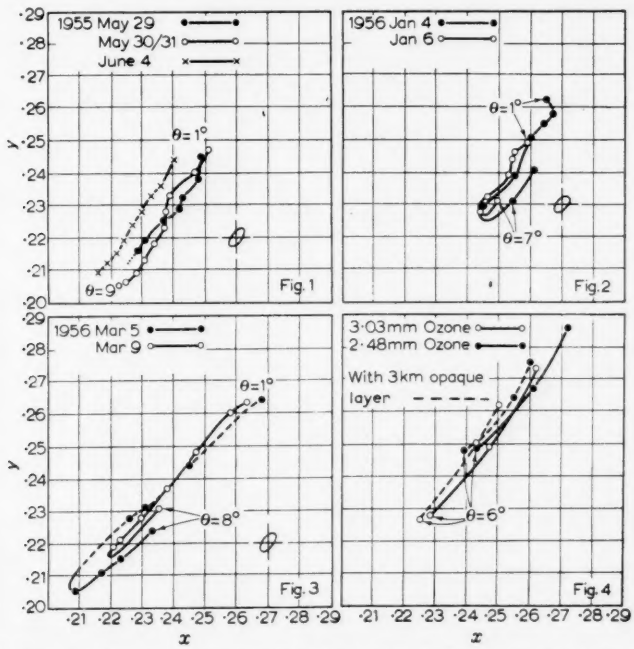

Figs. 1, 2, and 3. Observed chromaticity of the zenith twilight sky as a function of θ, for one degree intervals of θ.
Fig. 4. Computed chromaticity of the zenith twilight sky for $\theta = 1°$, 3°, and 6°.

Observations were made with a small, portable colorimeter, constructed with a system similar to that described by BURNHAM (1952) and designed for auroral colour measurements by Professor W. D. WRIGHT, with the aid of a grant from the Royal Society. Measures of the colour of the zenith sky during twilight have been made on eight evenings—six from an observing site on the South Downs behind Brighton, and two from South Kensington, in London. Once the sun has set, there is not a significant difference between the colours observed at these two sites on different evenings, leading to the conclusion that the industrial haze over London has effectively a neutral transmission.

Figs. 1, 2, and 3 show the observed variations in chromaticity as a function of θ, for the different evenings. (In computing the values of θ, the effect of refraction has been ignored.) It will be seen that the variation on different evenings follows the same direction

VOL. 10 1957

for each evening, and that the curves are displaced diagonally for the different times of the year. A small ellipse shown on each figure gives the standard deviation of the measurements.

On most of the evenings on which observations were made, there were no clouds visible from the observer's position, and generally the whole of the South of England was clear of cloud. The exception is the evening of 5 March 1956, when there were thin patches of high cirrus visible. The effect of this cloud was to increase the luminence and to desaturate the colour of the sky until about $\theta = 4°$. After this time had been reached, the clouds were no longer visible to the naked eye, and there was a drop in luminence and increase in saturation of the colour observed. The change in luminence amounted to 0·26 logarithmic units, and the chromaticity changed from (0·227, 0·228) to (0·216, 0·209). These changes occurred in only five minutes.

The chromaticity of the zenith sky has been computed for $\theta = 1°$, 3°, and 6°, using the following assumptions:

(1) That the molecular density in the atmosphere falls off exponentially with height. The White Sands rocket data (WHIPPLE, 1954) suggest that a suitable relation would be

$$\log_{10} n_h = 19{\cdot}400 - 0{\cdot}0596h$$

where n_h is the number of molecules per cubic centimetre at height h (km).

(2) That the ozone in the atmosphere is distributed in the following concentrations:

(a) 5–19 km: 0·004 cm of ozone (S.T.P.) per km path
(b) 19–30 km: 0·017 cm of ozone (S.T.P.) per km path
(c) 30–45 km: 0·004 cm of ozone (S.T.P.) per km path

The total vertical amount of ozone is thus assumed to be 0·303 atmo. cm.

(3) That the solar radiation is unrefracted in the atmosphere, and originates from a point source at the centre of the solar disc.

(4) That the effective, screening surface of the earth is spherical.

(5) That the spectral distribution of the solar radiation incident on the atmosphere is that determined by ABBOTT *et al.* (1923).

Straightforward geometrical considerations give the length of the ray path through the atmosphere for light scattered down from a particular height above the observer. The correction for the curvature of the earth tabulated by HULBURT (1939) has been applied. Thus the total number of molecules in unit cross-section of a beam of light may be found, using assumption (1), giving the absorption along this light path due to Rayleigh scattering. Assumption (1) also gives the amount of light scattered down from the particular height due to the assumed concentration of molecules at this height. Thus the intensity for varying heights of scattering may be calculated and numerical integration (in this case, at intervals of 5 km) gives the total observed intensity as a function both of wavelength and solar depression, θ.

The calculated chromaticities found in this way, neglecting the absorption occurring in the ozone layer, are almost constant with varying θ (see Table 1), and correspond to a colour very close to white.

Table 1

θ	Chromaticity co-ordinates	
	x	y
1°	0·325	0·343
3°	0·326	0·340
6°	0·329	0·342

Having found, geometrically, the ray path lengths through the ozone layer—assumption (2)—the equivalent amount of ozone in cm at S.T.P. is computed for a particular ray. This then leads to the absorption, as a function of wavelength, due to the Chappuis band of ozone. The values of the optical density per cm for ozone have been interpolated for a temperature of 220°K from the values determined by VASSY and VASSY (1941, 1948), and are given in Table 2.

Calculating the absorption due to the ozone layer, and thus determining modified spectral distributions for the zenith sky, one finds that the chromaticities of the zenith sky for $\theta = 1°, 3°, 6°$ are as given in Table 3. Also in Table 3 are the chromaticities calculated when the assumption is made that the bottom three km of the atmosphere are completely opaque to radiation (v. d. HULST, 1951), and the chromaticities corresponding to a total vertical ozone path equal to 0·248 cm—the concentration from 19–30 km being assumed to be 0·012 cm ozone at S.T.P. per km.

Table 2

Wavelength Å	Optical density per cm	Wavelength Å	Optical density per cm
4000	0·0000	6000	0·0791
4200	0·0000	6200	0·0603
4400	0·0006	6400	0·0441
4600	0·0047	6600	0·0328
4800	0·0110	6800	0·0208
5000	0·0180	7000	0·0131
5200	0·0281		
5400	0·0443		
5600	0·0606		
5800	0·0709		

Table 3

θ	0·303 cm ozone		0·248 cm ozone		0·303 cm (with 3 km opaque layer)		0·248 cm (with 3 km opaque layer)	
	x	y	x	y	x	y	x	y
1°	0·262	0·273	0·272	0·286	0·250	0·262	0·260	0·275
3°	0·247	0·249	0·261	0·267	0·243	0·250	0·255	0·264
6°	0·228	0·228	0·243	0·249	0·225	0·227	0·239	0·248

The chromaticities in Table 3 are plotted in Fig. 4 for comparison with Fig. 1, 2, and 3. It will be seen that HULBURT's explanation of the general decrease of the luminence of the sky as being due to the ozone layer highly absorbing rays passing obliquely through it (giving path lengths up to 1200 km or more) applies with a satisfactory level of agreement with observation to the colour of the zenith twilight sky. His suggestion that for θ greater than 6·5° or so, the majority of the light reaching the observer from the zenith sky is due to secondary and higher orders of scattering, appears to be supported on four evenings

by the observed maximum of "blueness" (chromaticity furthest towards the bottom left-hand corner of Figs. 1, 2, and 3) occurring at about $\theta = 7°$. For values of θ greater than this, the colour of the zenith sky tends to become less saturated. The observations at the low level of luminance at these values of θ are a little uncertain, but the reversal of direction of the colour change is supported by photographic measurements made on colour film exposed on two evenings. The conclusion is that the secondary scattered light coming from the zenith when twilight is half gone has a chromaticity approximately equal to that of the zenith sky at $\theta = 4°$ or $5°$. It should be mentioned, finally, that on all evenings the luminance of the sky was observed to vary in the same manner as that reported by HULBURT (1953), departing from the computed variation at 5°–7° solar depression in the same way.

Technical Optics Section M. GADSDEN
Imperial College of Science and Technology
London, S.W.7.

REFERENCES

ABBOTT C. G., FOWLE F. E., and ALDRICH L. B.	1923	*The Distribution of Energy in the Spectra of Sun and Stars* Smithsonian Misc. Collection, **74,** No. 2714.
ASHBURN E. V.	1952	*J. Geophys. Res.* **57,** 85.
	1953	*J. Opt. Soc. Amer.* **43,** 805.
BULLRICH K.	1948	*Ber. Deut. Wetterd.* Nr. 4.
BURNHAM R. W.	1952	*Amer. J. Psychol.* **65,** 603.
GAUZIT J. and GRANDMONTAGNE R.	1942	*Publ. Obs. Lyon* **3,** fasc. 10.
GRANDMONTAGNE R.	1938	*C.R.* **207,** 1436.
GRUNER P.	1936	*Gerl. Beit, z. Geophys.* **46,** 202.
HULBURT E. O.	1939	*Phys. Rev.* **55,** 639.
	1953	*J. Opt. Soc. Amer.* **43,** 113.
v. d. HULST H. C.	1952	*The Atmospheres of the Earth and Planets* Univ. of Chicago Press p. 84.
SIEDENTOPF H.	1941	*Astron. Nacht.* **271,** 193.
VASSY A.	1941	*Ann. Chim. Phys.* **16,** 145.
VASSY A. and VASSY E.	1948	*J. Chem. Phys.* **16,** 1163.
WHIPPLE F. L.	1954	*The Earth as a Planet* Univ. of Chicago Press p. 498.

ANNOUNCEMENT

Committee on extension to the standard atmosphere*

U.S. Weather Bureau and Geophysics Research Directorate (AFCRC), Co-sponsors

A NEW extension to the 20-km ICAO Standard Atmosphere (the accepted U.S. standard) is being adopted by about twenty-three United States scientific and engineering organizations; this extension provides tables of atmospheric parameters up to 300 km. Because of their great need for such tables and because many have active high-altitude research programs, these organizations met in November 1953 to seek agreement upon a single representation of the atmosphere compatible with the best available data. The *United States Weather Bureau* of the Department of Commerce and the *Geophysics Research Directorate*, Air Force Cambridge Research Center of the Air Research and Development Command, co-sponsored this movement, which included the following participants:

VOL.
10
1957

Air Research and Development Command
Air Technical Intelligence Center†
Air Weather Service
Applied Physics Laboratory
Ballistics Research Laboratory
Boston University (member transferred to Sylvania)
Bureau of Aeronautics, USN
Civil Aeronautics Authority
CONVAIR, San Diego
CONVAIR, Fort Worth
Geophysics Research Directorate (AFCRC)
Harvard College Observatory
International Civil Aviation Organization†
Jet Propulsion Laboratory
National Bureau of Standards
Naval Proving Grounds
Naval Research Laboratory
Office of the Chief Signal Officer
The Rand Corporation
Redstone Arsenal (ABMA)
Signal Corps Engineering Laboratory
United States Weather Bureau
White Sands Proving Grounds
Wright Air Development Center

A working group was appointed to study the problem. This group met several times since 1953 and recommended the basic values and parameters shown in Table 1. These values have now been approved by nearly all the participants listed above. A curve of T_M vs. H is shown in Fig. 1.

Extensive tables expanding the basic framework of Table 1 are currently under preparation at the Geophysics Research Directorate and will follow closely the format of the ICAO Standard Atmosphere which appears as ICAO Document 7488, NACA TN 3182, and NACA Report 1235; moreover, additional information

* Address: Geophysics Research Directorate, 415 Summer Street, Boston 10, Mass.
† Observer.

important at higher altitudes, such as gravity ratio and molecular weight, will be included. Supplemental information to describe the variability of the atmosphere and other parameters will be issued later as appendices. Preliminary copies of these tables, in a form analogous to the NACA TN 3182, should be available in limited quantities during 1957. It is planned to have the final edition printed by the Government Printing Office and made available to the public through the Superintendent of Documents.

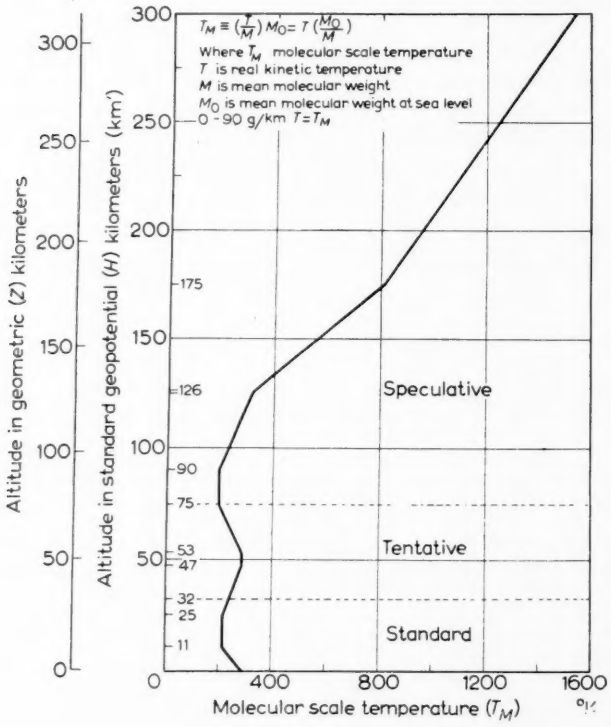

Fig. 1.

By virtue of the wide participation in this effort, these twenty-three organizations established a U.S. standard and are planning action through the Air Coordinating Committee and ICAO to obtain international acceptance for the lowest portion (20 to 32 km) of the tables. In this regard, it should be noted that the 75- to 300-km interval of the extension is termed "Speculative Atmosphere," since it is felt that new experimental data obtained over the next five or ten years may lead to a better representation. The interval, 32–75 km, has been termed "Tentative Atmosphere," since more data may also lead to modification and also because any drastic change in the Speculative Atmosphere may require some change in the adjacent lower levels. The 20–30-km level is termed Standard, since it is a good compromise between the voluminous radiosonde data of the meteorological services

Table 1. United States extension to the standard atmosphere

H (m′)	Z (m)	L (°/m′)	T_M (°K)	T (°K)	M (g/mole)	P (mb)
0·00	0·00		288·16	288·16	28·966	$1{\cdot}01325 \times 10^{3}$
		−0·0065				
11,000·0	11,019		216·66	216·66	28·966	$2{\cdot}2632 \times 10^{2}$
		0·0000				
*20,000·0	20,063		216·66	216·66	28·966	$5{\cdot}4748 \times 10^{1}$
		0·0000				
25,000·0	25,099		216·66	216·66	28·966	$2{\cdot}4886 \times 10^{1}$
		0·0030				
*32,000·0	32,162		237·66	237·66	28·966	$8{\cdot}6776 \times 10^{0}$
		0·0030				
47,000·0	47,350		282·66	282·66	28·966	$1{\cdot}2044 \times 10^{0}$
		0·0000				
53,000·0	53,446		282·66	282·66	28·966	$5{\cdot}8320 \times 10^{-1}$
		0·0039				
75,000·0	75,895		196·86	196·86	28·966	$2{\cdot}4521 \times 10^{-2}$
		0·0000				
90,000·0	91,294		196·86	196·86	28·966	$1{\cdot}8154 \times 10^{-3}$
		0·0035				
126,000·0	128,548		812·86	278·88†	25·02†	$1{\cdot}4510 \times 10^{-5}$
		0·0100				
175,000·0	179,954		322·86	686·13†	24·45†	$6{\cdot}1895 \times 10^{-7}$
		0·0058				
300,000·0	314,859		1537·86	1024·67†	19·30†	$1{\cdot}4473 \times 10^{-8}$

* Top of current ICAO Standard and top of recommended extension for standardization—no discontinuity in temperature-height curve.

† Approximate values subject to minor revision depending upon recomputation of M above 90 km.

Z Altitude in geometric metres,
H Altitude in geopotential metres.
L Temperature lapse rate in Kelvin degrees per geopotential metre.
T_M Molecular-scale temperature in degrees Kelvin.
T Real kinetic temperature in degrees Kelvin.
M Molecular weight in grams per mole.
P Pressure in millibars.

and tables already firmly entrenched in the development of engineering equipment. No changes are foreseen for this level.

Geophysics Research Directorate scientists, R. A. Minzner and W. S. Ripley, are now preparing the completed report.

Harry Wexler
USWB

Co-Chairmen
Committee on Extension to the Standard Atmosphere
Geophysics Research Directorate, Boston, Mass., U.S.A.

Norman Sissenwine
GRD, AFCRC

Note: Groups within the U.S. Air Force's Air Research and Development Command or under contract to ARDC who have had occasion to use "The ARDC MODEL ATMOSPHERE, 1956," will be pleased to note that ARDC tables are based upon and are consistent with the new U.S. extension to the ICAO Standard Atmosphere.

VOL. 10 1957

Book review

L. H. ALLER: **Gaseous Nebulae.** The International Astrophysics Series, vol. 3; London: Chapman and Hall, 1956. 322 + xvi pp. with 28 plates, 38 figures, and 29 tables. 63/- net

DR ALLER has been working on gaseous nebulae for some twenty years. Some years ago he began to prepare a comprehensive book about such nebulae, the observing methods and results, and the physical theory needed to interpret the results. His first version, completed in 1945, has since been completely revised to take account of recent developments, particularly on the observational side. The book under review, which is the first book in English on gaseous nebulae, is the outcome. It is a timely book; both planetary nebulae and diffuse galactic nebulae are of interest to students of stellar evolution, while the diffuse galactic nebulae have recently come to interest workers on cosmic rays and radioastronomy.

After a preliminary chapter on the types of gaseous nebulae, the various methods of observation are described in Chapter 2, and the results as regards distances, dimensions, and spectra of planetary and diffuse galactic nebulae are set out in Chapter 3. Then follow two chapters of astrophysical theory: Chapter 4 explains how the densities, temperatures, and compositions of the nebulae, and the temperatures and luminosities of the exciting stars, can be determined; Chapter 5 gives a good and full account of the formation of forbidden lines. Both these chapters, while applicable also to diffuse nebulae, are in fact mainly applied to planetary nebulae. Chapter 6, on the stars illuminating the nebulae, also considers mainly the planetaries. Finally, Chapter 7 discusses the structure and internal motion of the planetaries, and Chapter 8 does the same for the diffuse galactic nebulae. Throughout, results for the planetaries are given in far greater detail than for diffuse galactic nebulae. The latter are often merely condensed parts of the interstellar medium, which is to be the subject of another monograph in the same series.

The book contains a vast amount of useful information, but it is not always well arranged, and two or three readings are necessary in order to extract the full benefit from it. Sometimes the references to the same subject in different chapters appear uncorrelated; sometimes the observational methods and results and their interpretation are mixed together unsystematically; sometimes the author interrupts the course of his argument to introduce an excursus on a different subject of which he seems to have just thought. Again, the book would have been easier to many readers if the ions responsible for given absorption lines were more regularly quoted; the author's practice is very variable (cf. the references to $\lambda\lambda$3727, 4686 on pp. 66 and 67). These defects detract from the immediate usefulness of the book. Nevertheless, it remains a valuable addition to astronomical literature.

Apart from a few rather obvious misprints, the book is well produced. Its value is enhanced by a large number of diagrams and several beautiful plates. Each chapter is followed by an extensive bibliography.

T. G. COWLING

Journal of Atmospheric and Terrestrial Physics, 1957, Vol. 10, pp. 185 to 188. Pergamon Press Ltd., London

Discrete sources of cosmic radio noise at 18·3 and 10·5 Mc/s

G. R. Ellis* and Gordon Newstead†

(*Received* 20 *December* 1956)

Abstract—Observations of discrete sources of cosmic radio noise at frequencies of 18·3 and 10·5 Mc/s are described. Similar interferometers with a base line of 7 λ were used for detecting the radiation at each frequency. Six sources were observed at both frequencies. Four of the sources were weaker at 10·05 Mc/s than at 18·3 Mc/s and two were stronger. There is an indication that the shape of the low-frequency spectrum of a source is related to its direction.

Introduction

The study of the low-frequency end of the spectra of discrete sources of cosmic radio noise is of some interest, since it can provide new data for theories of the generation and absorption of the radiation. Recent observations of the sources Cassiopeia *A* and Cygnus *A* quoted by Roman and Haddock (1956) have indicated that a low-frequency cut-off in their spectra occurs between 10 and 20 Mc/s. These authors have suggested that this is due to the absorption of the radiation by interstellar-ionized hydrogen in our own galaxy between the solar system and the source. It is conceivable, however, that a change with frequency in the efficiency of the generating mechanism could also produce the observed rapid decline in the intensity of the radiation below 20 Mc/s. A possible way of deciding this question would be to observe the spectra of a sufficient number of sources. Any correlation between the galactic co-ordinates of the source and the shape of the low-frequency end of its spectrum might then be interpreted in terms of absorption.

It is the purpose of this paper to describe observations of six sources at 18·3 Mc/s and 10·5 Mc/s at Hobart, Tasmania. Although the number of sources observable with the low-resolution equipment used was too small to warrant definite conclusions, there is an indication that the spectra of sources well away from the galactic centre extend to lower frequencies.

Equipment

Similar tunable phase-switching interferometers were used at 18·3 and 10·5 Mc/s. The receivers were modified Admiralty-type FHB twin-channel C.R.D.F. receivers with a phase-switching stage inserted in one I.F. channel of each. The bandwidth was 9 Kc/s. Similar aerial systems were used at both frequencies. They were in the form of arrays of six full-wave dipoles, with a width of primary pattern of 30° to zeros in an east–west direction and they were arranged at each end of a base line seven wavelengths long. Preamplifiers were used at each aerial. The preamplifiers and receivers were calibrated with noise generators using noise diodes, the output impedances of the noise generators being adjusted to equal the impedances presented to the preamplifiers by the aerial feeders. The total noise output of each receiver and the component varying at the switching frequency were recorded separately with recording milliammeters.

* Commonwealth Ionospheric Prediction Service, Hobart.
† University of Tasmania.

VOL. 10 1957

Observations

The observations were made at intervals between March and August 1956 at 10·05 Mc/s and during July and August 1956 at 18·3 Mc/s. The sensitivity of the equipment to interference from transmitting stations proved to be the main limiting factor in obtaining good records of discrete sources and no single record showed all of the sources which were observed during the course of the

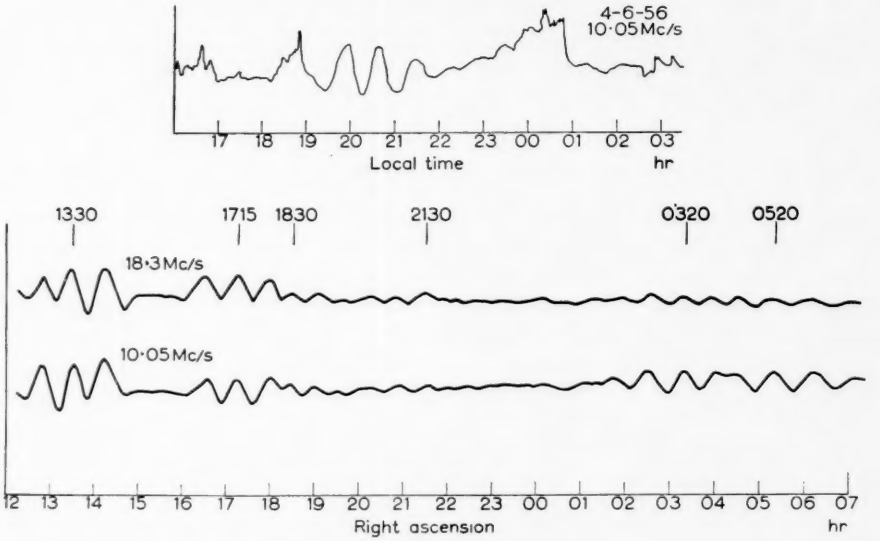

Fig. 1. Records of discrete sources.

experiment. However, most records showed at least two sources, and sufficient good records were accumulated at each frequency to produce the composite picture shown in Fig. 1. Also shown in this figure is a sample record of the Centaurus source RA 1330 Dec. −43°. This record is typical in that the following source at 1715 RA is suppressed by interference from a transmitter.

Table 1 shows the final results of the observations at both frequencies, together with the positions and intensities of nearby extended sources observed by Bolton *et al.* (1954) at frequencies in the vicinity of 100 Mc/s and using interferometers with similar base lines. Using these 100 Mc/s observations, we obtain the spectra shown in Fig. 2. Also shown is the spectrum of Cassiopeia *A* (Roman and Haddock, 1956) and for comparison the spectrum of the background radiation (Ellis, 1957.)

Discussion

The most striking feature of the composite records shown in Fig. 1 is the similarity in the amplitudes at the two frequencies of the records of the four sources *C*, *D*, *E*, *F*, and the relative increase in the amplitudes of the records of the sources *A* and *B* at 10·05 Mc/s. It may be significant that the two sources *A* and *B* are roughly in the same part of the sky (Table 1). The source *C* includes the well-known Centaurus source which other investigators have identified as

Table 1. Observed positions and intensities of discrete sources at 18·3 and 10·5 Mc/s

Source	R.A. (hr)	DEC. (°)	Long. (°)	Lat. (°)	Flux density 10^{-25} WM^{-2}(c/s)$^{-1}$		Nearest large source observed by Bolton 100 Mc/s			
					10·05 Mc/s	18·3 Mc/s	R.A.	Dec.	Flux density 10^{-25} WM^{-2} (c/s)$^{-1}$ 100M/s	Size
A	0320	−43	220	−53	1300	950	0317	−37	60	½° − 1°
B	0520	−50	222	−32	1200	850	0510	−43½	150	1° − 2°
C	1330	−43	280	+18	2400	6000	1322	−43	300	2°
D	1715	−46	315	−5	1200	3200	1651	−45	1000	10° × 6°
E	1830	−22	338	−7	1300	3100	1741	−27½	>3000	12° × 2°
F	2130	−38	335	−50	430	550				

NGC5128, surrounded by an extended object. With low-resolution antennas it is not a good source for spectral measurements.

Sources *D* and *E* are both apparently large objects which are derived from the irregular structure known to exist in the vicinity of the galactic centre. Nevertheless, their spectra are quite different from the spectrum of the background radiation observed in the same direction, using dipole antennas (see Fig. 2), but are similar to the spectrum of Cassiopeia *A*, which is also near the plane of the Milky Way.

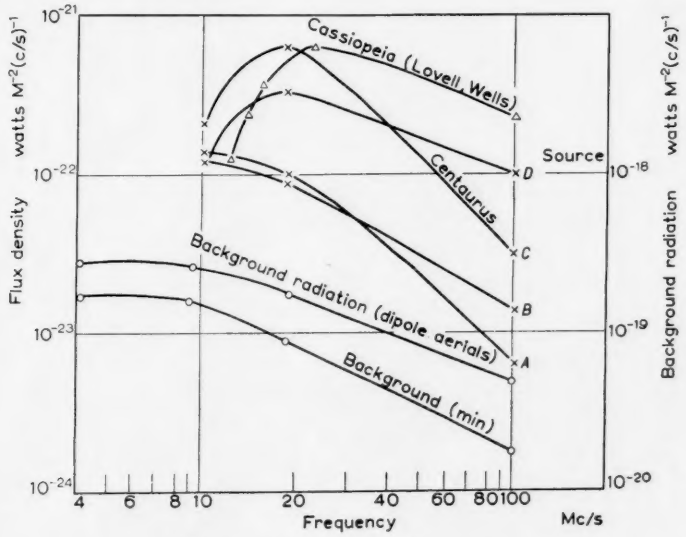

Fig. 2. Spectra of discrete sources.

These differences in the low-frequency parts of the spectra of the sources would seem to point to an explanation based on the absorption of the radiation during its passage through the galaxy. It is not intended here to make any quantitative deductions along these lines, but it is worth noting that Roman and Haddock (1954) have shown that the low-frequency cut-off in the spectrum of Cassiopeia *A* could be produced by a thickness of several kiloparsecs of ionized hydrogen with a gas temperature of 10^4 °K and an electron density of 1 e/cm^3. Slightly less electron densities could explain the results described here with similar values of the other parameters.

Conclusions

The main conculsions which may be derived from this investigation are as follows:

1. Discrete sources may easily be observed at 10 Mc/s. This is lower in frequency than previous recorded observations.

2. The number of sources detected was large in view of the poor resolving power of the equipment. It is possible that many more would be observed with better aerial systems.

3. Considerable differences in the low-frequency end of the spectra of the discrete sources can be detected. The existence of these differences may provide a means of studying the distribution in the galaxy of regions which absorb radio waves.

References

Bolton J. C., Westfold K. C., Stanley G. J., and Slee O. B.	1954	*Austr. J. Phys.* **7**, 1, 97.
Ellis G. R.	1957	(To be published).
Roman N. G. and Haddock F. T.	1956	N.R.L. Report 4712, March.

Journal of Atmospheric and Terrestrial Physics, 1957, Vol. 10, pp. 189 to 193. Pergamon Press Ltd., London

Measurements of the soft component of cosmic radiation by an absorption "well method"

ARMIN W. MANNING
Fordham University, New York, N.Y.

(*Received* 3 *December* 1956)

Abstract—To measure the soft component of cosmic radiation which is defined as that part of the total radiation absorbed in 10 cm of Fe, an absorption "well-method" originally proposed by HESS (1953) was used. This method employs the procedure of taking measurements with the ionization chamber placed so that the top of the chamber was even with the absorbing sides of an iron house and then repeating the same procedure with the chamber "sunk" into the iron house to a depth of one-half of its height. The difference in the solid angle of exposure in the two positions makes it possible to compute the ionization resulting from the soft component plus the gamma rays from the decay products of radon and thoron in the atmosphere. The results of these experiments indicate an ionization ten times greater than the theoretical value of the radiation from the radioactive products in the atmosphere, as computed by HESS (1943).

VOL. 10 1957

EXPERIMENTAL PROCEDURE

AN ionization chamber with a capacity of 4·89 litres (wall thickness 2·5 mm of brass) was used in this experiment. A Lindemann fibre electrometer was mounted directly on the top of the chamber. The guard ring and the case of the electrometer were connected to a 135-volt supply and the centre point of the quadrant battery was kept at the same potential. The fibre system of the electrometer could be connected or disconnected from the battery by means of a contactor needle. When the needle was withdrawn, with the electrometer housing and the guard-ring system being at 135 volts and the wall of the chamber at ground potential, the needle would drift at a rate which was proportional to the ionization current flowing in the chamber.

In order to avoid any possible errors due to insulation leakage, a null-method was used in making these measurements. In this method a compensating potential was gradually added to the guard-ring potential and the housing of the electrometer with a potentiometer circuit. By constantly adjusting this potential, the needle could be kept at the zero point. This compensating voltage divided by the number of seconds during which the measurements were taken and multiplied by a calibration constant gave a measure of the ionization produced in terms of ion pairs per second. The capacitances and induction coefficients of the chamber with the electrometer were measured in the Department of Terrestrial Magnetism by GISH and HESS (1953).

A small iron house providing shielding of 10 cm Fe on the bottom and sides, but not on the top, was erected on the astronomical observatory platform of Concordia Collegiate Institute, Bronxville, N.Y. This location about 60 ft above the ground surface was free of obstructions in all directions and thus there could be no possible gamma radiation from other buildings.

Ionization measurements were taken first of all with the ionization chamber (top) even with the top of the iron house and then with the iron house built up above the top of the chamber to one-half of the height of the chamber. The geometrical conditions for each position and the mathematical analysis determining the ionization by the "soft component" are as follows.

Consider the area of the segment of a sphere:

The ratio of the exposed area between a full half-sphere and a section of the surface as will be governed by the position of the ionization chamber in the snugly-fitting iron house depends on the ratio of h/r equal to $(1 - \cos\varphi)$, where now φ will be the mean solid semi-angle of the cone formed by all points along the vertical axis of the chamber connecting these points to the upper edge of the iron house.

Table 1. Summary of experimental values

Date	Even with well I/c.c. sec	In the well I/c.c. sec	Difference I/c.c. sec	q (absorbed) I
2/6/56	1·96	1·89	0·07	0·54
2/19/56	2·17	1·95	0·22	1·68
2/20/56	2·06	1·97	0·09	0·69
2/22/56	2·15	2·02	0·13	1·00
2/23/56	2·25	1·97	0·28	2·15
2/24/56	2·10	1·95	0·15	1·16
2/26/56	2·11	2·03	0·08	0·62
2/27/56	2·22	2·07	0·15	1·16
2/29/56	2·21	1·97	0·24	1·84
3/1/56	2·22	2·04	0·18	1·38
3/3/56	2·30	2·06	0·24	1·84
3/9/56	2·18	1·93	0·25	1·92
3/10/56	2·02	1·97	0·05	0·39
3/12/56	2·05	1·94	0·11	0·85
3/15/56	1·86	1·81	0·05	0·39
3/17/56	2·26	2·10	0·16	1·23
3/18/56	2·25	2·04	0·21	1·61
3/20/56	2·25	2·12	0·13	1·00
3/21/56	2·15	1·96	0·19	1·45
3/22/56	2·21	1·94	0·27	2·07
3/23/56	2·17	2·07	0·10	0·77
3/25/56	2·26	2·02	0·24	1·84
3/26/56	2·22	2·07	0·15	1·16
3/27/56	2·22	2·08	0·14	1·08
3/28/56	2·20	2·10	0·10	0·77
3/31/56	2·14	2·05	0·09	0·69
4/10/56	2·15	2·08	0·07	0·54
4/11/56	2·25	2·14	0·12	0·92
4/13/56	2·24	1·97	0·27	2·07
4/14/56	2·21	2·15	0·06	0·46
4/15/56	2·10	1·87	0·23	1·76
4/17/56	2·26	2·03	0·23	1·76
4/18/56	2·14	1·87	0·27	2·06
4/19/56	2·25	2·10	0·15	1·15
4/21/56	2·16	1·97	0·19	1·46
4/22/56	2·22	1·97	0·25	1·93
4/24/56	2·21	2·16	0·05	0·39
4/27/56	2·23	1·98	0·25	1·93
5/2/56	2·22	1·99	0·22	1·69
5/5/56	2·21	2·06	0·15	1·15
5/6/56	2·21	1·99	0·22	1·69
5/8/56	2·20	2·10	0·10	0·77
5/9/56	2·10	1·87	0·23	1·76
5/11/56	2·25	2·12	0·13	1·00

The average value for the absorbed "soft component" equals $1{\cdot}26I$; the lowest reading was $0{\cdot}39I$ and the highest reading was $2{\cdot}15I$ (I stands for ion pairs per sec).

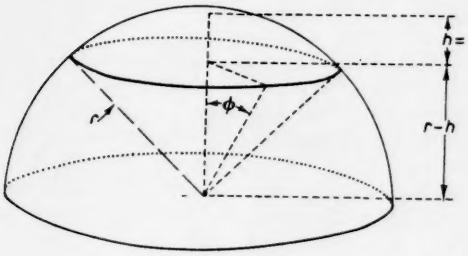

$$\frac{\text{Area of spherical segment}}{\text{Area of hemisphere}} = \frac{2\pi rh}{2\pi r^2} = \frac{h}{r}$$

But the cosine $\phi = \frac{r-h}{r}$

$$\therefore 1-\cos\phi = 1 - \frac{(r-h)}{r} = \frac{r-r+h}{r} = \frac{h}{r}$$

Fig. 1

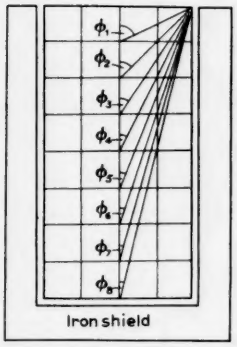

Position	tanϕ	ϕ	cosϕ	1−cosϕ
1	2	63°27′	·44724	·55276
2	1	45°	·70711	·29289
3	·666	33°42′	·83195	·16805
4	·500	26°34′	·89441	·10559
5	·400	21°48′	·92849	·07151
6	·333	18°26′	·94869	·05131
7	·286	15°58′	·96142	·03858
8	·250	14°3′	·97015	·02985
			Average value —	·16381

Fig. 2. Position 1 (the chamber even with the top of the iron house).

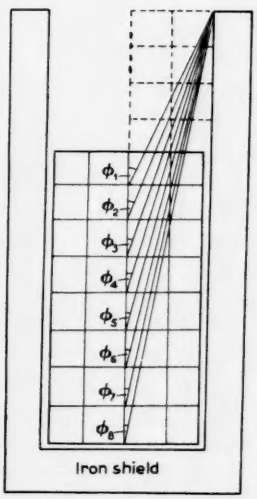

Position	tanϕ	ϕ	cosϕ	1−cosϕ
1	2/5	21°48′	·92849	·07151
2	2/6	18°26′	·94869	·05131
3	2/7	15°58′	·96142	·03858
4	2/8	14°3′	·97015	·02985
5	2/9	12°31′	·97623	·02377
6	2/10	11°19′	·98056	·01944
7	2/11	10°19′	·98383	·01617
8	2/12	9°28′	·98638	·01362
			Average value —	·03303

Fig. 3. Position 2 (with the walls of the iron house built up to one-half the height of the chamber).

VOL. 10 1957

The mean fraction of ionization caused by particles which cannot penetrate the iron walls is 0·163 of the total amount of ionization which would result if the chamber were not in the iron house.

In this second position with the graphical method of integration the mean fraction of ionization caused by particles which cannot penetrate the iron walls is equal to 0·033 of the total amount which would result if the chamber were not in the iron house.

Subtracting 0·033 from 0·163, giving a value of 0·13, the fractional component of this non-penetrating radiation resulting from the difference in the two positions is determined. If the difference in the total radiation for the two positions is divided by this value (0·13), a measure of the total soft component will be obtained. The residual wall-radiation ionization will be eliminated by the subtraction process.

This "soft component," consisting of positive and negative electrons, photons, and also slow mesons, cannot be analysed further by this "well-method." It might be interesting to note, however, that the greatest ionization took place on 23 February 1956, and it was on this day that the astronomical observatories recorded violent eruptions on the surface of the sun. All measurements were taken at approximately the same time each day between 1100 a.m. and 1400 p.m. A complete summary of the experimental values is given in Table 1. There seems to be no connection between the fluctuations and changes in weather conditions.

DISCUSSION

From a theoretical viewpoint it would be difficult to justify the ionization measured in this experiment as produced by the gamma radiation from the natural decay products of the radium and thorium in the atmosphere. HESS (1943) found that the radon content of the air on the campus of Fordham University was about 10^{-16} curie per cm^3. The gamma-ray effect at ground-level would be expressed by $g_c = 2\pi k \int_0^\infty m e^{-\lambda} \, dr$, where $m = 10^{-16}$ curie per cm^3. Assuming a value of K (EVE's constant) as $4{\cdot}8 \times 10^9 I$ per gram Ra per cm^3, and an absorption coefficient γ for the gamma rays of RaC in air to be $4{\cdot}6 \times 10^{-5}$ cm^{-1}, the resulting value of Q would be $0{\cdot}065I$. If one considers that the gamma rays from ThB and ThC in the atmosphere are about equal to that from the radon decay products, then this value of $0{\cdot}065I$ would have to be doubled, resulting in a value of $0{\cdot}13I$.

In 1951, W. F. BURNS carried out a great number of experiments, using an absorption method, and arrived at a value of $0{\cdot}71I$ for the total air radiation (BURNS, 1952). This value is some five times greater than expected. The average value as obtained by the "well-method" previously described in this paper is $1{\cdot}26I$, which is approximately 75% greater than the experimental value of BURNS and approximately ten times greater than the theoretical value of the air radiation computed by HESS (1943).

It has been quite well established that the cosmic-ray intensity for any particular locality remains quite constant (there may be deviations in ionization measurements due to solar bursts or severe magnetic storms), and yet the measurements with the "well-method" experiment indicate great daily fluctuations. It seems reasonable to conclude that this variable amount of "soft radiation" is probably due to the increasing contamination of the air with radio-activity from the many atomic explosions.

In July 1945 (SMYTH, 1946) the first atomic bomb was exploded in the western part of the U.S., and up until 1956 some sixty-seven atomic detonations have been

carried out by the U.S. Government alone, not considering those exploded by the other nations of the world. This could already account for the rise in radiation as measured by BURNS in 1951 and the now greater values observed in 1956.

It is reasonable to assume that this contamination is not evenly distributed in the atmosphere, and this would account for the fluctuations which have been experienced. On four occasions during the five-month period in which these experiments were carried out a single ionization measurement showed a rise to almost three times the well-established average values obtained at that time. It is possible that this was due to a concentration of radioactivity in a cloud above the ionization chamber near enough to cause this very large reading.

If our assumption is correct regarding the cause of the increased gamma-ray ionization produced in the atmosphere, then it is obvious that year after year repeated experiments in atomic explosions may contaminate the atmosphere to the extent where detrimental effects will result.

REFERENCES

BURNS W. F.	1952	Thesis, Fordham University.
HESS V. F.	1953	*Geophys. Res.* **58,** 1.
HESS V. F.	1943	*Terr. Magn. Atmos. Elec.* **48,** 203.
HESS V. F.	1953	*J. Geophys. Res.* **58,** 1.
HESS V. F.	1943	*Terr. Magn. Atmos. Elec.* **48,** 203.
HESS V. F.	1943	*Terr. Magn. Atmos. Elec.* **48,** 203.
SMYTH H. D.	1946	*Atomic Energy for Military Purposes* Princeton University Press.

VOL. 10 1957

Journal of Atmospheric and Terrestrial Physics, 1957, Vol. 10, pp. 194 to 203. Pergamon Press Ltd., London

The correlation of radio-star-scintillation phenomena with geomagnetic disturbances and the mechanism of motion of the ionospheric irregularities in the *F* region

M. DAGG *
Jodrell Bank Experimental Station, University of Manchester

(*Received* 21 *November* 1956)

Abstract—The paper describes an experimental investigation of the relation between the phenomena of scintillations of the radio stars and geomagnetic disturbances. A close correlation is found between the magnitude of the variations in the earth's magnetic field and *F*-region drift velocities as determined by the radio-star scintillation method. There is also occasional correlation between the amplitude of the scintillations and the magnetic variations. These results and those concerned with the reversals in drift directions are shown to be in agreement with the predictions of MARTYN'S theory, which ascribes the *F*-region phenomena to the interaction of the earth's magnetic field with an electric field communicated from the dynamo region.

1. INTRODUCTION

THE first indications of a relation between geomagnetic activity and the drift speeds of the electron concentrations in the *F* region were observed during aurorae when the radio-star scintillation rate increased fourfold, and LITTLE and MAXWELL (1952) found a significant correlation between scintillation rate and the magnetic *K* index. (Radio-star scintillation rate is roughly proportional to drift velocity (MAXWELL and DAGG, 1954)). HEWISH (1952) also found a correlation between *K* index and east–west drift velocity, using radio-star scintillations. BEYNON and THOMAS (1954), using a pulse sounding technique on the *F* region, found a correlation between drift velocities measured on several groups of days and the mean daily summation of *K* indices for those days. They also mentioned that the correlation remained good in more detailed observations.

A more extensive investigation of this relation has been carried out at Jodrell Bank since 1952, and the first year's results have been reported by MAXWELL (1955). These and subsequent work are described in this paper, and the results are discussed in relation to MARTYN'S theory of the mechanism of motion of the *F*-region clouds.

2. APPARATUS

The *F*-region drift velocities were measured with the spaced three-receiver equipment described by MAXWELL and DAGG (1954). The 1955–56 observations of the times of reversals in direction were made using a similar set of equipment at reduced base lines. The long-term observations of radio-star scintillations were made using an equatorially mounted array consisting of six full-wave dipoles and reflector. The axis of the mounting was driven so that the main beam of the aerial was continuously directed at the radio source in Cassiopeia. The receiver was of conventional superheterodyne design, and the output was recorded on a pen-recording milliammeter.

* Now at East African Agricultural and Forestry Research Organization, Kenya.

VOL. 10 1957

3. Results

(a) *K index versus drift velocity.* The *F*-region drift velocities measured in 1952–53 by the three-receiver method have been compared with the corresponding *K* indices (mean of Eskdalemuir and Lerwick *K* indices). The results for the region 400–900 km north of Jodrell Bank (radio source in Cassiopeia near lower culmination) are shown in Fig. 1. The full line is drawn through the mean value of the drift speed at each *K* index and the standard deviations from the mean are shown. It is clear that there is a marked correlation between the drift speed and the *K* index.

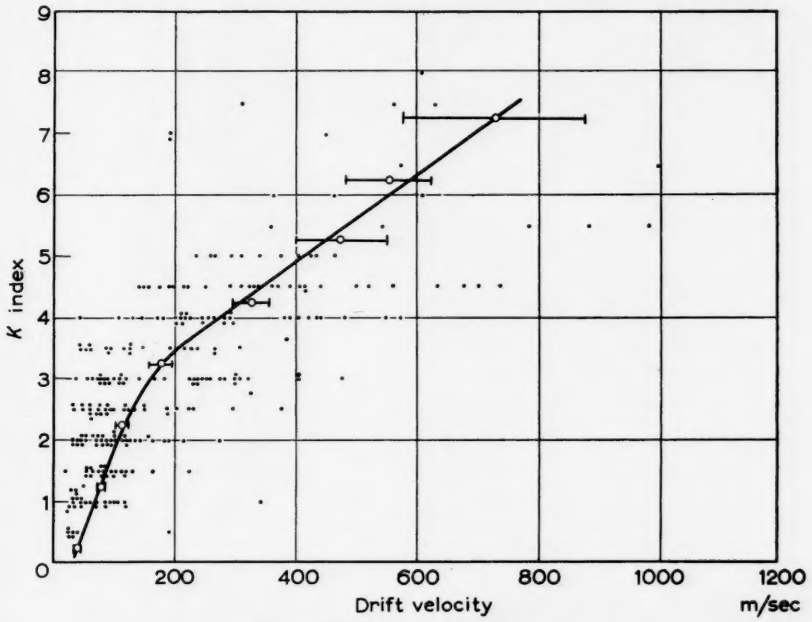

Fig. 1. Drift velocity vs. *K* index.

(b) *Absolute changes in magnetic field intensity versus drift velocity.* The curve shown in Fig. 1 is not a straight line, but this is not unexpected, as the *K* index is not a linear scale. By using the relevant scaling factor for the Lerwick magnetic observatory ($K = 9 \equiv 1000\,\gamma$), the mean drift velocities have been compared with the corresponding magnetic field changes, as shown in Fig. 2.

The drift speed is now seen to vary almost linearly with field changes up to about $200\,\gamma$ ($\equiv K = 5$): for greater changes the magnetic field increases more rapidly than does the drift velocity. It is clear that the drift velocity is sensitive to very small changes in the magnetic field.

(c) *Detailed correlation between magnetic-field changes and fluctuation rate.* The response of the *F*-region drift velocity even to small magnetic changes prompted an investigation beyond the 3-hour *K* index into the detailed correlation between the minute to minute magnetic changes shown on magnetograms and variations in drift velocity. Clearly it would be impracticable for three-receiver measurements to be

made in such detail, but variations in the velocity are reflected in the fluctuation rate, and it was possible to compare rapid changes in fluctuation rate and amplitude over periods of several hours with detailed magnetic disturbances.

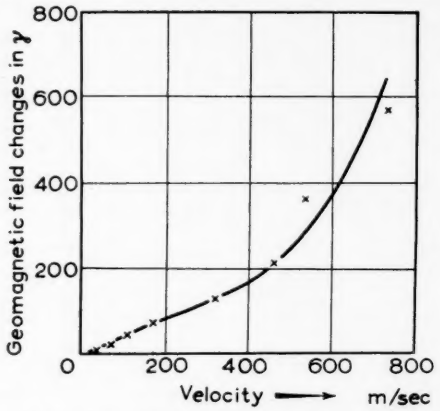

Fig. 2. Geomagnetic field changes vs. Drift velocity.

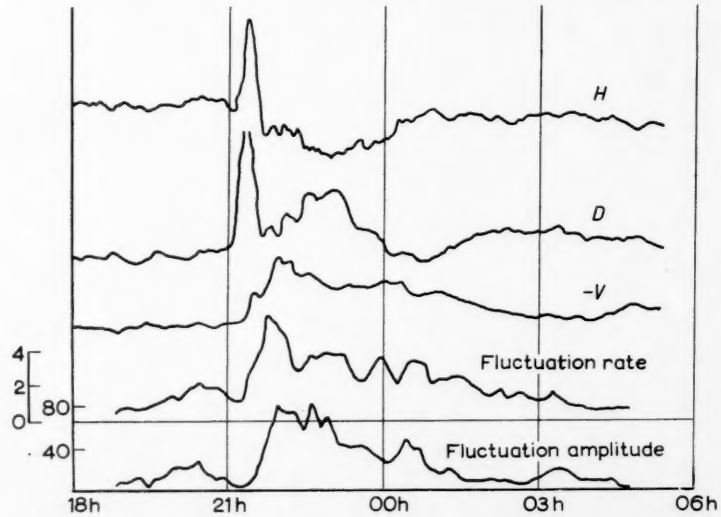

Fig. 3. Lerwick magnetogram 1–2 April 1955. Cassiopeia fluctuations. The fluctuation rate is the number of maxima per minute. The fluctuation amplitude is expressed as a percentage of mean source intensity.

During the period July 1954 to July 1955 comparisons of fluctuations were made in this way with sixty-seven selected magnetograms from Lerwick and Eskdalemuir.* The selection was made on the basis of interesting fluctuation records. From these a few comparisons have been chosen to illustrate the principal results from this investigation (Figs. 3, 4, 5, 6). The curves showing the fluctuation rate and amplitude are based on 10-min mean values.

* The magnetograms were kindly made available by the Superintendent, Meteorological Office, Edinburgh.

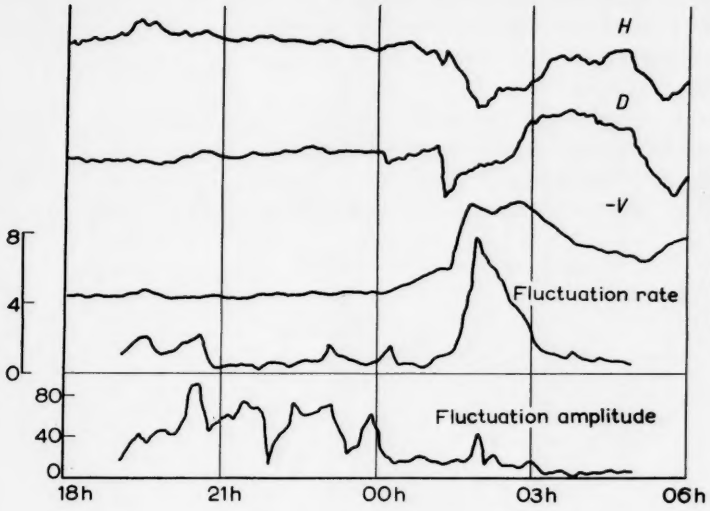

Fig. 4. 21–22 August 1955 Lerwick magnetogram. Cassiopeia fluctuations. The fluctuation rate is the number of maxima per minute. The fluctuation amplitude is expressed as a percentage of mean source intensity.

VOL. 10 1957

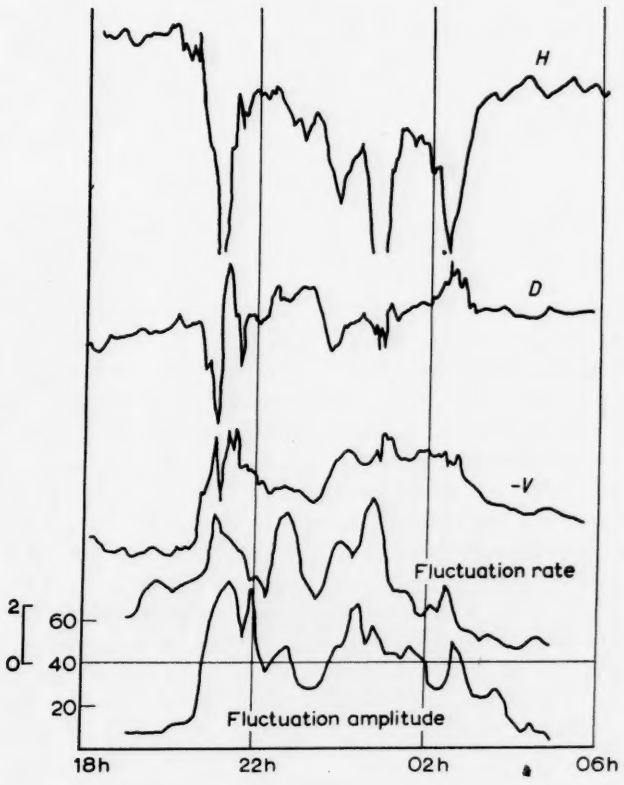

Fig. 5. 28–29 April 1955, Lerwick magnetogram. Cassiopeia fluctuations. The fluctuation rate is the number of maxima per minute. The fluctuation amplitude is expressed as a percentage of mean source intensity.

The results may be summarized as follows:

(i) There was found to be a close correlation between changes in fluctuation rate and changes in the magnetic field, particularly changes in the vertical component of the magnetic field.

(ii) Close correlation was found between fluctuation amplitude and magnetic-field variations on some occasions, but no correlation at all at other times.

(iii) The fluctuation amplitude tended to correlate more closely with changes in the horizontal component than with the vertical component of the magnetic field.

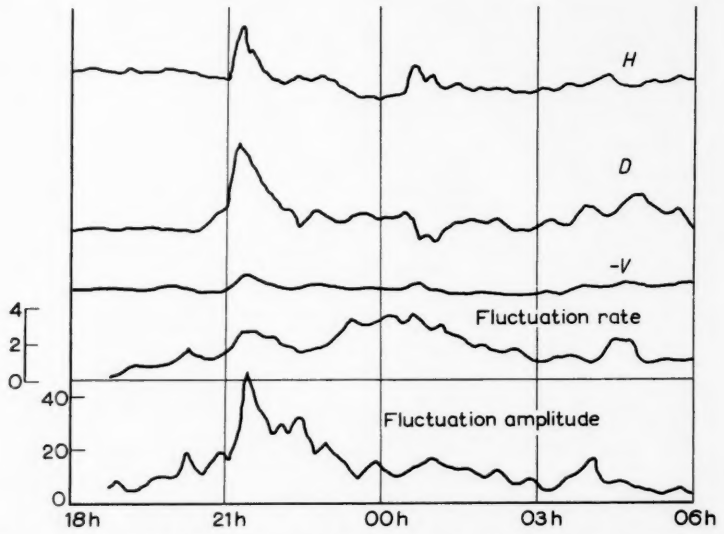

Fig. 6. 5–6 January 1955, Lerwick magnetogram. Cassiopeia fluctuations. The fluctuation rate is the number of maxima per minute. The fluctuation amplitude is expressed as a percentage of mean source intensity.

In more detail, Fig. 3 shows the correlation between both fluctuation rate and amplitude and magnetic variations. On the basis of the number of observations made, the correlation shown is rather better than average for the fluctuation rate and considerably better than average for the fluctuation amplitude.

Fig. 4 demonstrates a typical case where the amplitude showed the normal diurnal variation while the magnetic field was quiet but did not respond markedly to the sudden disturbance at 0130, whereas the fluctuation rate shows fairly good correlation throughout the night. However, if the magnetic changes are large and occur between the hours of 1800 and 0000, then both fluctuation rate and amplitude show close correlation with magnetic changes, as shown in Fig. 5.

On a few occasions, such as that illustrated in Fig. 6, the magnetic changes showed higher correlation with the fluctuation amplitude than with the fluctuation rate. In each case the changes in the magnetic vertical component were small, which is in agreement with the general conclusion that the drift velocity changes correspond most closely to disturbances in the vertical component of the magnetic field.

4. Time Differences between Geomagnetic and Scintillation Changes

On several occasions time differences were clearly discernible between rapid changes in one of the magnetic elements and the associated change in fluctuation rate and/or amplitude. On most occasions some time difference was apparent but not defined clearly by a sharp leading edge, for instance time displacements can be seen in Fig. 3: two examples of clearly defined time differences are shown in Figs. 7a and 7b.

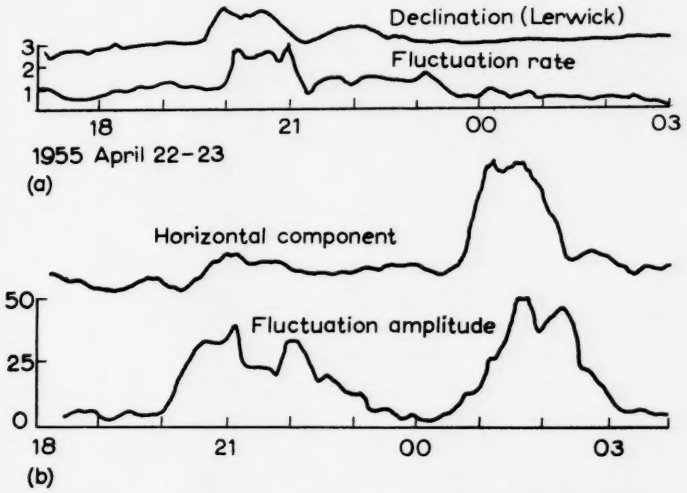

Fig. 7. Time differences between changes in fluctuations and geomagnetic field. (a) April 22–23, 1955. (b) March 6–7, 1955. The fluctuation rate is the number of maxima per minute. The fluctuation amplitude is expressed as a percentage of mean source intensity.

The point in the ionosphere under observation, using the Cassiopeia source, can be as much as 300 km east or west of the magnetic observatory at Lerwick. Thus, it is not surprising that time differences might be observed between associated ionospheric and magnetic changes. No detailed study of these time displacements has yet been attempted, but they could well be caused by a travelling current sheet responsible for a magnetic bay, such as that described and analysed by McNish (1938).

5. The Mechanism of the Movements in the *F* Region

All the movements in the ionosphere detected by radio methods refer to the motion of inhomogeneities in the electron density in the atmosphere and not necessarily to the motion of the neutral air molecules. Measurements of movements in the upper levels of the *F* region have been made from time differences between identical radio-star scintillations recorded at three triangularly spaced receivers (Maxwell and Little, 1952; Hewish, 1952; and Maxwell and Dagg, 1954). Martyn (1953) has shown that it is highly improbable that such movements of the ionized gas can be caused by atmospheric winds in the *F* region, for any movement

VOL. 10 1957

produced mechanically would be subject to powerful electromagnetic damping because the F region is effectively shunted by the highly conducting lower regions of the ionosphere. MARTYN (1955) has therefore suggested that the observed drifts in the F region are due to the interaction of the earth's magnetic field and an electric field communicated to the F region from lower levels. The experimental results given above will now be discussed in relation to this theory.

(a) *Correlation of drift velocity with geomagnetic activity.* MARTYN (1953) has shown that the large east–west motions in the F region that have been observed can only be produced by north–south electric fields interacting with the earth's magnetic field. He has suggested that these electric fields are generated by winds in the "dynamo" region and communicated to the F region along the highly-conducting magnetic lines of force. (The conductivity along the magnetic lines of force is so much greater than in any direction transverse to them that they are essentially equipotentials, and thus the F region is closely coupled to the lower regions of the ionosphere.) The "dynamo" region is that region in which the currents flow which cause the transient variations in the earth's magnetic field according to the well-known atmospheric dynamo theory (CHAPMAN and BARTELS, 1940). According to BAKER and MARTYN (1953) this region is situated at a height between 110 and 150 km in temperate latitudes.

The reversals in drift direction from west to east which are sometimes observed near midnight by the radio-star technique MARTYN (1955) explains in terms of a field (and current) system that reverses in direction near midnight. Such a current system was derived by CHAPMAN (1935) to account for the disturbance daily variation, S_D, of the earth's magnetic field. Thus reversals in drift direction at midnight might be expected on geomagnetically disturbed days but not on quiet days, when the S_q magnetic variation would predominate.

It follows from this theory that the velocities of drifts observed in the F region should be closely correlated with geomagnetic disturbances, as they arise from the same electric-field system in the dynamo region. The experimental observations of this effect have been discussed in Section 3.

It is of interest to note that both Figs. 1 and 2 suggest that the curve does not pass through the origin but denotes a residual drift velocity of about 20 m/s at $K = 0$. It is suggested that this corresponds to the quiet-day magnetic variation S_q, which is excluded from the K index. At the geomagnetic latitude of England, MARTYN (1955) has estimated that the maximum value of the eastward (noon) drift velocity due to the S_q system will be 34 m/s, with a secondary westward maximum at midnight. Thus, experiment and theory are in good agreement on this point.

(b) *Correlation of fluctuation amplitude with geomagnetic activity.* The occasional correlation between fluctuation amplitude and geomagnetic activity is of more significance for any theory of the origin of the ionospheric irregularities responsible for radio star scintillations than for theories of their movement. Therefore a discussion of this effect is left to a subsequent paper concerned with the origin of the ionospheric irregularities. In section 3 it was pointed out that on a few occasions the magnetic changes were more closely correlated with the fluctuation amplitude than with the fluctuation rate. It was also pointed out that in these

cases the changes in the vertical component of the magnetic field were small. It is of interest to enquire whether this is in agreement with MARTYN'S theory.

In their consideration of the conductivity in the ionosphere, BAKER and MARTYN (1953) came to the conclusion that the most important conductivity in middle and high latitudes was the transverse conductivity. Thus a north–south field would produce an east–west current in the dynamo region and an east–west drift in the F region. The most likely cause of a decrease in the vertical component is an east–west current flowing somewhere to the north of Lerwick. Therefore, it would be expected that the fluctuation rate would correlate most closely with changes in the vertical field strength. In the case of the magnetic disturbance of 5–6 January 1955,

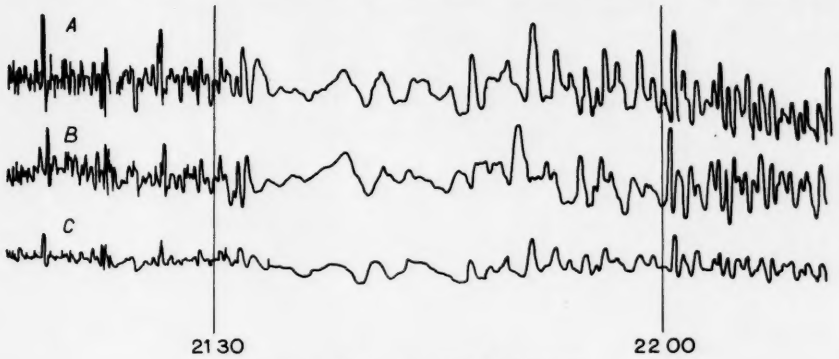

Fig. 8. Reversal, 10 October 1951.
A. Home station
B. 3 km south-east
C. 3·9 km south

VOL. 10 1957

(Fig. 6) the magnetic variations are consistent with a southerly current passing overhead with an overall westerly drift. The field producing this current would be east–west and not likely to cause much change in the east–west F-region velocity. North-south components in velocity would not change the fluctuation rate appreciably (SPENCER, 1955).

(c) *Reversals in drift direction.* If the driving field system was that of the S_q magnetic variation, then reversals in drift direction in the F region would be expected at 1800 and 0600, which is the normal case as observed by pulse sounding techniques. Reversals at these times would not usually be observable by the radio-star-scintillation method. MARTYN suggested that the reversals in drift direction near midnight that are *sometimes* observed by the radio-star method were due to the development of an S_D electric field system in the dynamo region. Fig. 8 shows tracings of scintillations recorded at spaced receivers at the time of a reversal.

It would follow that in times of moderately severe magnetic disturbance a reversal in drift direction should be observed about midnight. However, CHAPMAN (1935) distinguished two stormtime magnetic variations, S_D and D_{St}: the effect of the latter would cause the reversal to take place somewhat earlier, if both systems have a similar origin. At times of great magnetic storms accompanying aurorae, radio-echo observations from Jodrell Bank show a reversal in drift direction, at a

height of 120 km, at 2130. Thus, the time of reversal measured by the radio-star scintillation technique might be expected to vary between 0000 and 2130, depending on the degree of disturbance of the magnetic field and the relative contributions of the S_D and D_{St} systems.

Three-receiver observations of scintillations extending at least from 2230 to 0000 have been made on forty-five occasions in the periods May 1952 to April 1953 and September 1955 to March 1956, and the results are presented in Fig. 9, where the time of reversal is compared with the degree of magnetic disturbance represented by the K_p index.

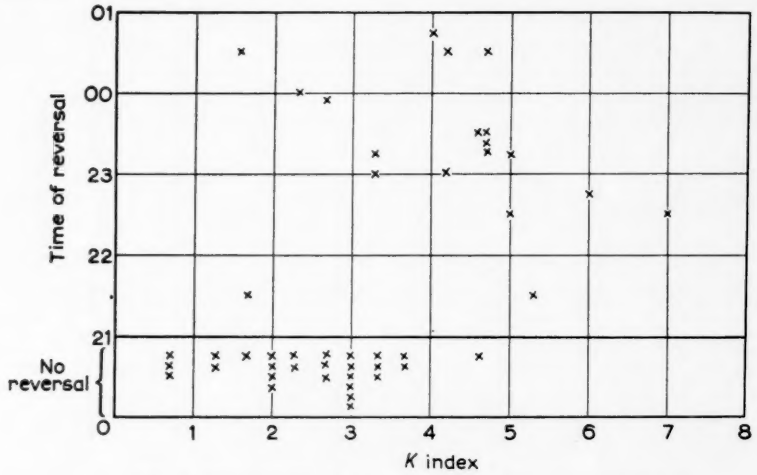

Fig. 9. Comparison of time of reversal with magnetic K index.

The result is far from conclusive, but it may be said that on the twenty-six occasions when no reversal was observed the mean value of K_p was 2·5 and on the nineteen occasions when reversals were observed the mean value of K_p was 4·0. Also, with one exception, on every occasion when the K_p index was greater than 4, a reversal was observed. Furthermore, there was a tendency for the time of reversal to be earlier when the K_p index was high.

6. Conclusions

The detailed correlation between the drift velocity of the ionospheric irregularities responsible for radio-star scintillations and the variations in the earth's magnetic field is strong supporting evidence for the mechanism of motion of ionization in the F region proposed by Martyn. Furthermore, although more observations are required before a final conclusion can be reached, the demonstration of magnetic control over the occurrence of reversals in drift direction is in good agreement with the theoretical prediction. The variation of the time of reversal with K indices greater than 4 suggest that the D_{St} current system also flows in the dynamo region. There is sometimes a close correlation between the scintillation amplitude and the magnetic variations.

Acknowledgements—The experimental work described in this paper was carried out at the Jodrell Bank Experimental Station of the University of Manchester under the direction of Professor A. C. B. LOVELL, as part of a research programme financed by the Department of Scientific and Industrial Research, to which the author is particularly grateful for the award of a maintenance grant from October 1952 to September 1955. The three-receiver experiments in 1952–53 and the analysis of the results were carried out jointly with Dr. A. MAXWELL, to whom the author is greatly indebted for helpful guidance and advice.

REFERENCES

BAKER W. G. and MARTIN D. F.	1953	*Phil. Trans. Roy. Soc.* **A246,** 281.
BEYNON W. J. G. and THOMAS L.	1954	*Rocket Exploration of Upper Atmosphere* (Edit. BOYD and SEATON) p. 131.
CHAPMAN S.	1935	*Terr. Mag.* **40,** 349.
CHAPMAN S. and BARTELS J.	1940	*Geomagnetism* Oxford University Press.
HEWISH A.	1952	*Proc. Roy. Soc.* **A214,** 494.
LITTLE C. G. and MAXWELL A.	1952	*J. Atmosph. Terr. Phys.* **2,** 356.
MCNISH A. G.	1938	*Terr. Mag.* **43,** 67.
MARTYN D. F.	1953	*Phil. Trans. Roy. Soc.* **A246,** 306.
MARTYN D. F.	1955	*Conference on Physics of the Ionosphere* p. 163. Physical Society.
MAXWELL A.	1955	*Conference on Physics of the Ionosphere* p. 166. Physical Society.
MAXWELL A. and DAGG M.	1954	*Phil. Mag.* **45,** 551.
MAXWELL A. and LITTLE C. G.	1952	*Nature,* Lond. **169,** 746.
SPENCER M.	1955	*Proc. Phys. Soc.* **B68,** 493.

VOL. 10 1957

Journal of Atmospheric and Terrestrial Physics, 1957, Vol. 10, pp. 204 to 214. Pergamon Press Ltd., London

Diurnal variations of radio-star scintillations, spread *F*, and geomagnetic activity

M. DAGG*
Jodrell Bank Experimental Station, University of Manchester

(*Received* 3 *December* 1956)

Abstract—An equipment has been constructed to enable a long-term investigation to be made of the temporal variations of radio star-scintillations. A year's observations are presented in terms of the monthly average diurnal variations of scintillations which are compared with monthly average diurnal variations of spread *F* and geomagnetic activity.

1. INTRODUCTION

THE early investigation of radio-star scintillations (LITTLE and MAXWELL, 1951; RYLE and HEWISH, 1950) showed that their most distinctive feature was the marked diurnal variation in occurrence. This was similar to that shown by spread *F* ionospheric echoes, and there was a positive correlation between the occurrence of spread *F* and scintillations. LITTLE (1951) and HEWISH (1951) showed that irregularities in the electron density of the *F* region could be responsible for the scintillation of radio stars, but the origin of the ionospheric irregularities remains uncertain. Alternative suggestions involving accretion (RYLE and HEWISH, 1950), or internal turbulence (MAXWELL, 1954) have been suggested. Such theories of the origin of these irregularities can be tested most satisfactorily against observations accumulated over a long period.

An equipment was designed therefore at Jodrell Bank to facilitate a long-term investigation of radio-star scintillations. This paper describes the equipment used and the analysis of results over a 1-year period. A comparison is made with the corresponding spread *F* and geomagnetic activity. The interpretation of these results will be considered in a later paper.

2. EQUIPMENT

The equipment consisted of an aerial system directed at the radio star in Cassiopeia and a sensitive receiver, the output of which was measured by a pen-recording milliammeter.

(i) *Aerial.* The aerial consisted of a broadside array of six full-wave dipoles with a reflecting screen, which gave a beam width to half-power of $\pm 12°$ in the *E* plane and $\pm 18°$ in the *H* plane. The array was assembled on an equatorial mounting at an angle of 31° to the axis, and was driven by an electric motor through a gear reduction of about 2×10^6, so that it rotated once each sidereal day. Thus, the aerial system, once set at the correct azimuth, followed the radio star in Cassiopeia continuously and an unbroken record of the radio emission was received. The tolerances in the accuracy of following were large, as the beam width was about 3 hours in terms of the motion of the source.

(ii) *Receiver and pen-recorder.* The receiver was of usual superheterodyne design with an overall gain of about 10^8. The operating frequency was 79 Mc/s.

* Now at East African Agriculture and Forestry Research Organisation, Kenya.

The input bandwidth was 0·6 Mc/s and the output time-constant 0·5 sec. A preamplifier consisting of two grounded grid stages gave a noise factor of about 4, which resulted in a noise ripple due to the receiver less than that due to the galactic background radiation in the direction of Cassiopeia. In the analysis, only scintillations with a mean amplitude greater than 5% of the total intensity of the Cassiopeia source were used, and these were clearly distinguishable from the noise ripple.

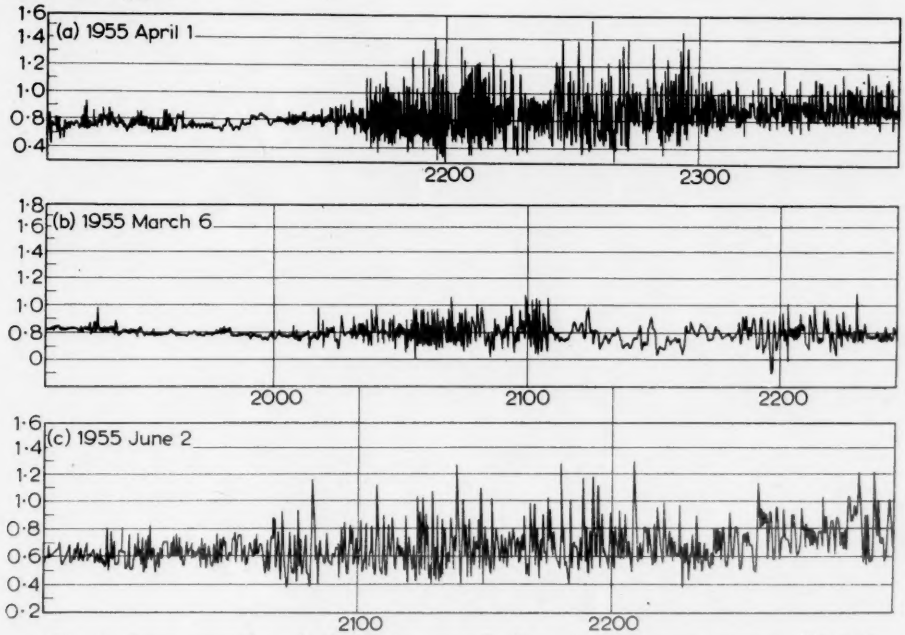

Fig. 1. Some examples of scintillation records from the Cassiopeia source. Time is horizontal and amplitude vertical (arbitrary units).

The output of the receiver was measured on a pen-recording milliammeter, which gave a full-scale deflection of 6 in. for a current of 2 mA. The chart speed was 6 in. per hour, except in cases of very rapid fluctuations, when it was increased to 12 in. per hour.

(iii) *Calibration.* A noise diode was used as a standard noise source to calibrate the input-output characteristics of the receiver. The input power due to the radio source in Cassiopeia was calculated from the published value of its intensity at 81·5 Mc/s (PAWSEY, 1955), and the gain of the aerial which was estimated from its dimensions. The final estimate of the mean intensity of the source in terms of the receiver output was probably accurate to about 20%. The receiver gain was chosen so that the mean intensity of the source was equivalent to a deflection of 0·6 mA on the pen-recorder. Under these conditions the radio noise due to the source and the background radiation gave a deflection of 1·64 mA when the aerial was rotated on its axis. This operation provided a convenient daily calibration mark.

Some examples of scintillation records obtained are shown in Fig. 1.

VOL. 10 1957

3. Method of Analysis

(i) *Fluctuation rate and amplitude.* The analysis of the records was made by assigning a mean value of fluctuation rate and amplitude to each half-hour period.

The fluctuation rate (maxima per minute) was determined by counting the total number of maxima every half-hour. To achieve consistency in estimates of fluctuation rate between large and small fluctuations, only those greater than 10% of the mean amplitude were counted.

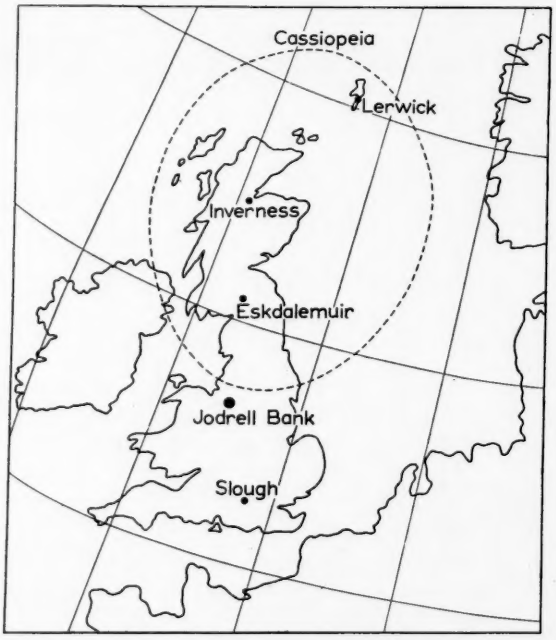

Fig. 2. The intersection of the line of sight from Jodrell Bank to Cassiopeia with the 400-km region (– – – –). The relative location of observatories from which ionospheric and magnetic data were obtained is also shown.

The mean peak to peak fluctuation amplitude was assessed visually in terms of chart divisions and afterwards converted into a percentage of the source intensity by comparison with the nearest calibration mark. The visual estimates were checked periodically by detailed measurements on individual fluctuations: the accuracy remained within 20%, despite large variations in amplitude and rate.

(ii) *Presentation of results.* The results are presented in terms of monthly mean diurnal variations of fluctuation amplitude, fluctuation rate, and occurrence of fluctuations greater than 5% of the mean intensity of the source.

The monthly mean fluctuation rate was determined by summing the observed fluctuation rates for each half-hour period over the month and dividing by *the number of days on which fluctuations were observed.* This procedure meant that when the occurrence of fluctuations was low, the statistics of the average fluctuation rate were very poor. Furthermore, the occasions when fluctuations

were observed outside the usual hours of about 1800 to 0400 often coincided with disturbed magnetic conditions, and the fluctuation rate therefore tended to be higher than the overall average (DAGG, 1957). This helped to make the statistical average even more misleading. Thus the monthly average diurnal variation of the fluctuation rate is only significant in general between the hours of 1800 and 0400 when the statistics are fairly good in most months.

(iii) *Geographical considerations.* The geographical region of the ionosphere under observation varies considerably in the course of one day as the radio source changes in elevation and azimuth. The intersection of the line of sight to the source from Jodrell Bank with the 400-km level of the ionosphere is shown in Fig. 2. In comparing the fluctuations with spread *F*, the ionospheric data were taken from the Inverness station (published in monthly bulletins of ionospheric characteristics by the Radio Research Station, Slough). Magnetic data were taken from whichever of the magnetic observations of Lerwick and Eskdalemuir was the most suitable at the time of day.

Two other factors arise which tend to confuse the interpretation of the results in terms of a diurnal variation and either mask genuine seasonal changes or introduce spurious effects:

(a) The sidereal motion of the radio source results in the observations being made at lower culmination at night in winter and during the day in summer (and vice versa at transit).

(b) The fluctuation amplitude shows a marked dependence on zenith angle (HEWISH, 1952). This may be a genuine zenith angle effect or may be due to the increase in latitude of the region under observation.

VOL. 10 1957

4. DIURNAL VARIATIONS OF FLUCTUATIONS — SPREAD *F* AND MAGNETIC ACTIVITY

Observations for the year August 1954 to July 1955 have been analysed as described in the previous section. The results are based on 6166 hours of observations, i.e. about 70% of the possible time. In every month the results referred to more than 50% of the available days, but the statistics are in general better for the months of 1955 than 1954. The most reliable months were March, April, June, and July 1955, when observations were made on 90% of the available time.

(i) *Monthly average diurnal variations.* The monthly average diurnal variations of occurrence of radio-star scintillations, their amplitude and fluctuation rate, and occurrence of spread *F* echoes at Inverness are shown in Fig. 3, 4, and 5. Also shown is the monthly average diurnal variation of the degree of disturbance of the earth's magnetic field, as represented by the summation of the *K* indices over the month for each 3-hour period. The lightly dashed curve in the scintillation occurrence diagram is the yearly average diurnal variation.

The salient features of the diurnal variations are the general agreement of the occurrence of fluctuations and spread *F* and the correspondence in the decline of fluctuation amplitude, fluctuation rate, and magnetic disturbance after midnight (especially clear in the months of March and April, which have very good statistics). It is also clear that the peak in occurrence of spread *F* is several hours later than that of the scintillations.

(ii) *Yearly average diurnal variation.* The yearly average diurnal variations

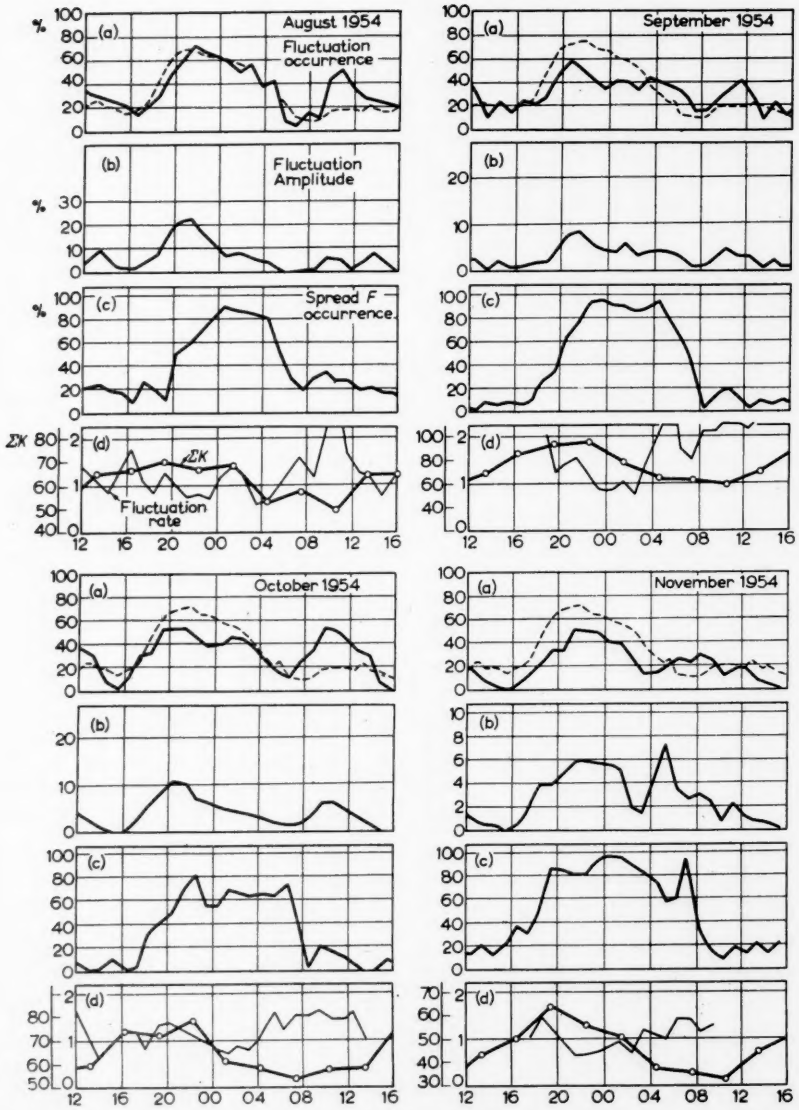

Fig. 3. Monthly average diurnal variations of radio-star scintillations for August 1954 to November 1954

(a) fluctuation occurrence,
(b) fluctuation amplitude,
(c) occurrence of spread F at Inverness,
(d) fluctuation rate compared with summation of magnetic K indices (ΣK).

VOL. 10 1957

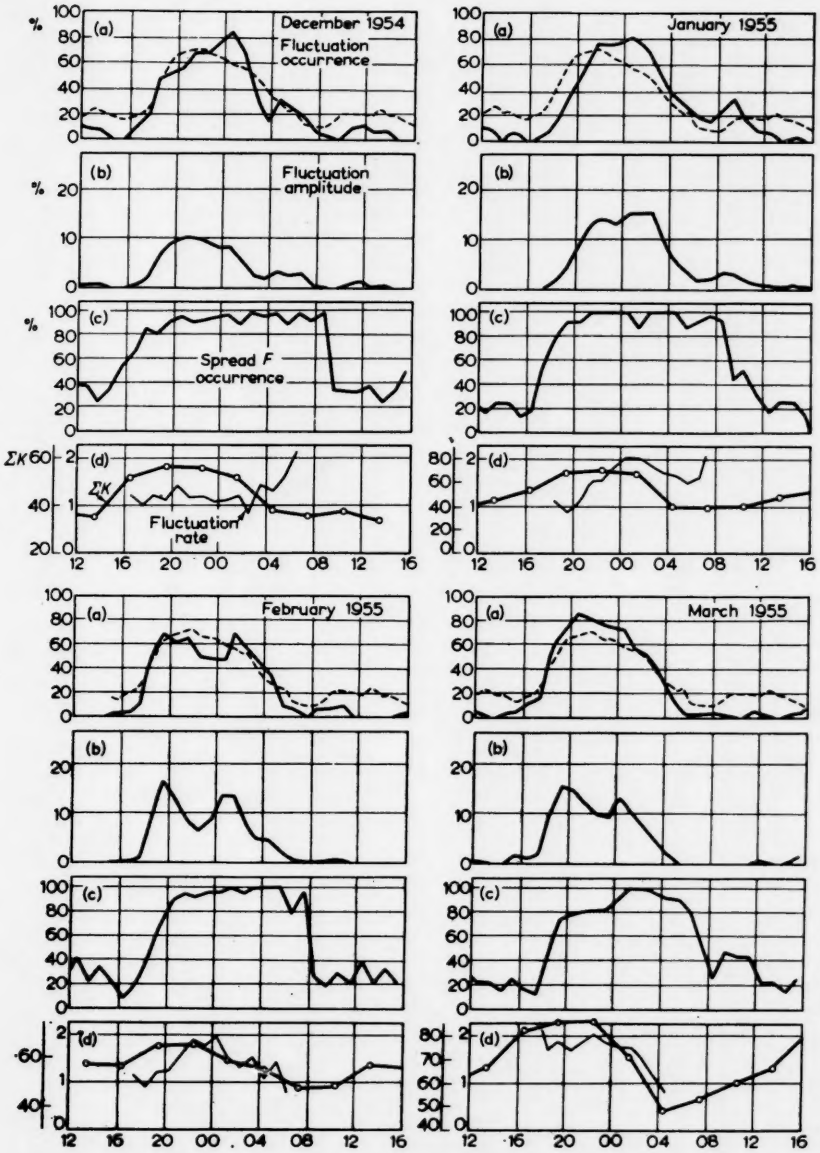

Fig. 4. Monthly average diurnal variations of radio-star scintillations for December 1954 to March 1955

(a) fluctuation occurrence,
(b) fluctuation amplitude,
(c) occurrence of spread *F* at Inverness,
(d) fluctuation rate compared with summation of magnetic *K* indices (ΣK).

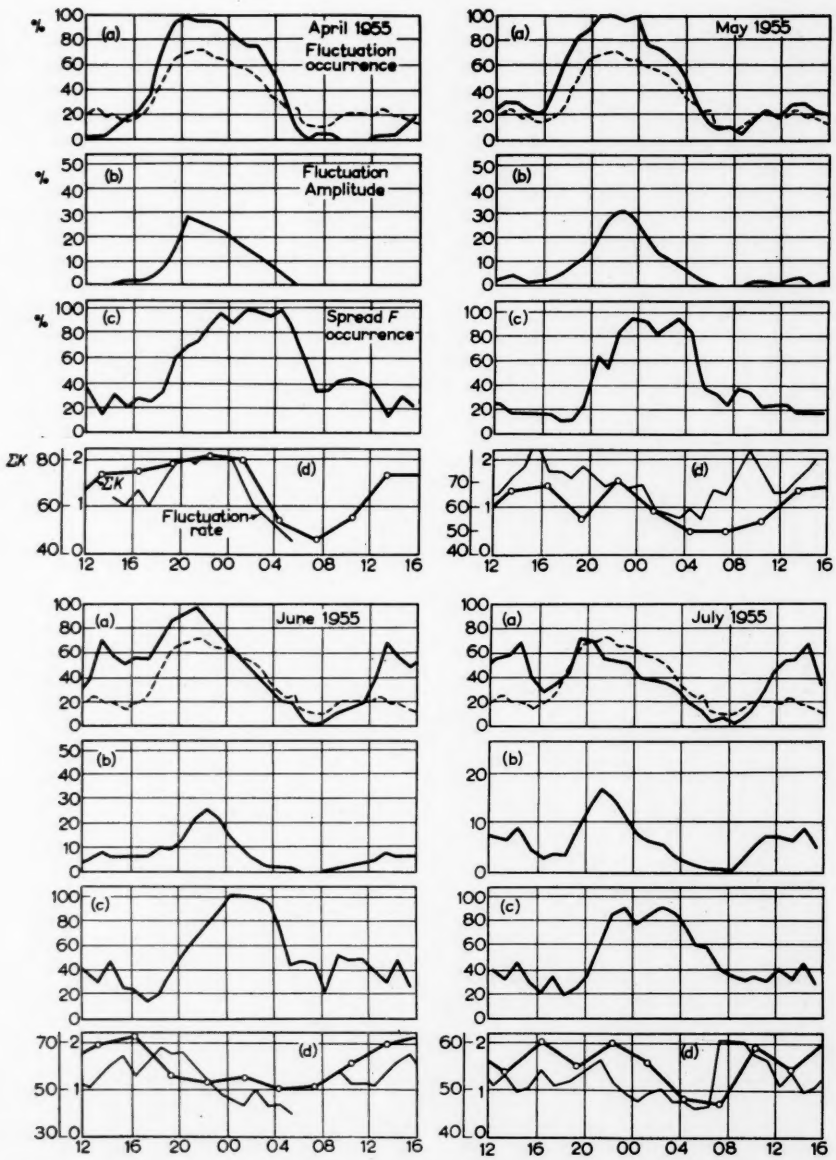

Fig. 5. Monthly average diurnal variations of radio-star scintillations for April 1955 to July 1955

(a) fluctuation occurrence,
(b) fluctuation amplitude,
(c) occurrence of spread F at Inverness,
(d) fluctuation rate compared with summation of magnetic K indices (ΣK).

are shown in Fig. 6. It is clear that the same general characteristics are shown in these diurnal variations as in the monthly averages. A comparison of the yearly and monthly average variations in occurrence of scintillations shows that there is little seasonal variation in the time of occurrence of scintillations; the

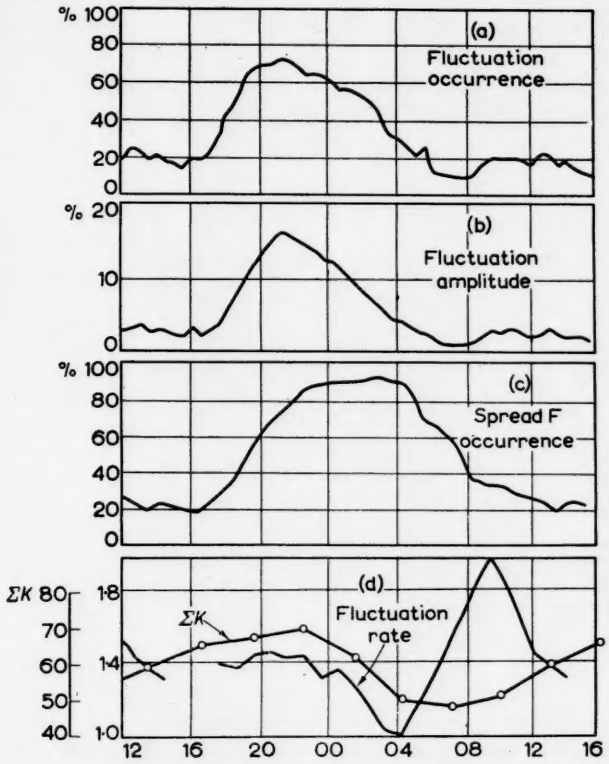

Fig. 6. Yearly average diurnal variations of radio-star scintillations (August 1954 to July 1955)

(a) fluctuation occurrence,
(b) fluctuation amplitude,
(c) occurrence of spread *F* at Inverness,
(d) fluctuation rate compared with summation of magnetic *K* indices (ΣK).

latitude effect is apparent mainly in the greater occurrence of scintillations during the day in summer, when Cassiopeia is at lower culmination, than in winter when the source is in transit during the day.

5. Discussion

The diurnal variation of the occurrence of scintillations shows a fairly rapid rise after 1800 to a peak about 2130, then a gradual fall to a minimum at about 0600 to 0800. The daytime occurrence is slight and shows no regularity. The amplitude variation agrees in general with the variation in occurrence, but the peak is more distinct. No marked seasonal variation is shown in the time of

VOL. 10 1957

occurrence of scintillations. The seasonal variation in the amplitude, which corresponds with that of the magnetic activity, will be considered later.

The diurnal variation of occurrence of spread *F* shows a much slower rise, a broad peak at about 0200 and a fairly rapid fall at about 0500. Spread *F* shows a marked seasonable variation, being more frequent and commencing earlier in the night in winter than summer (this is well known, cf. BOOKER and WELLS, 1938; REBER, 1954).

The diurnal variation of fluctuation rate is unreliable before about 1800 and after about 0400, but starting at 1800 there is a slow rise in fluctuation rate to

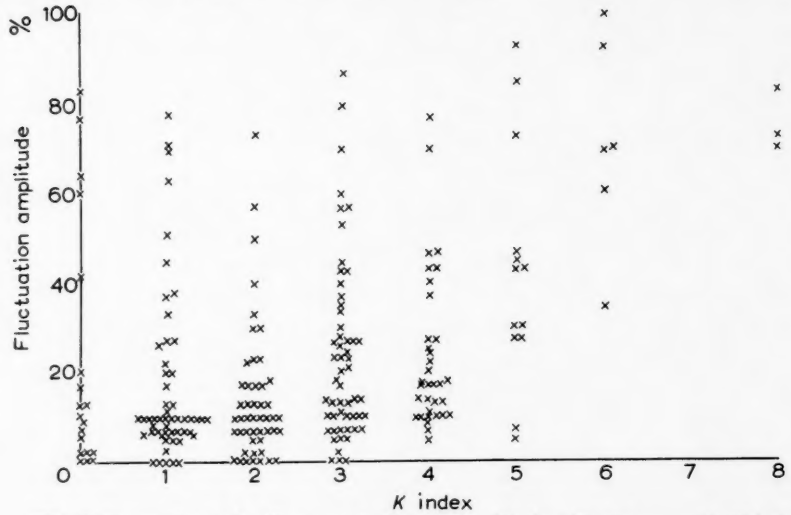

Fig. 7. Comparison of radio-star scintillation amplitude with the magnetic *K* index.

a peak at 2100, then a steady fall to a low value at 0400. The diurnal variation of magnetic disturbance, as would be expected (DAGG, 1957), is similar to that of the fluctuation rate. However, the general similarity between the fluctuation rate, magnetic activity, and the fluctuation *amplitude*, especially the steady decrease after midnight, is a result which would not have been expected from earlier work published by HEWISH (1952). HEWISH found that there was no one-to-one correlation between fluctuation amplitude and magnetic activity (or fluctuation rate). In view of the general correlation found in the diurnal variations, HEWISH'S work was checked by comparing individual values of amplitude over 3 hours with the corresponding *K* index.

(i) *Fluctuation amplitude versus K index.* The comparison of fluctuation amplitude with magnetic disturbance is shown in Fig. 7. The results refer only to the hours 1800 to 0300 of three months, February, March, and April 1955. It is clear that this investigation was in agreement with HEWISH'S result and that the general correlation over a long period was not due to different circumstances in different years of observation.

It follows that there is no one-to-one correlation between magnetic activity and fluctuation amplitude, but over an extended period a correlation is found.

(This might have been deduced from previous results (DAGG, 1957) which showed that there was *sometimes* very close correlation between magnetic activity and fluctuation amplitude.)

(ii) *Correlation between occurrence of scintillations and spread F.* The results of LITTLE and MAXWELL (1951) and RYLE and HEWISH (1950) showed that scintillations and spread *F* tended to occur on the same nights. However, Figs. 3 to 6 show clearly that the peak of occurrence of scintillations is about 4 hours earlier than that of spread *F* and that there is a seasonal variation in the occurrence of spread *F* which is not apparent in the observations of radio-star scintillations. The present results and the earlier observations could be reconciled if the ionospheric irregularities responsible for the two phenomena were produced by the same mechanism, but that some other factor was affecting one but not the other.

It is suggested that the blanketing by the *F* region is a factor that will influence the observation of spread *F* but will not affect radio-star scintillations observed at 79 Mc/s. When spread *F* at Huancayo was investigated by BOOKER and WELLS (1938), they suggested that the diurnal variation in occurrence of spread-*F* echoes was due to the blanketing of the backscatter from the irregularities responsible for spread *F*, and that these irregularities were present throughout the day. When the correlation between the occurrence of spread *F* and radio-star scintillations was discovered, it was thought that the scintillations showed the true time variation in occurrence of the ionospheric irregularities and that the blanketing effect was not of primary importance (WELLS, 1954).

VOL. 10 1957

However, BOOKER and WELLS showed clearly that the *F* region could have a marked effect on the observation of spread-*F* echoes, and it is suggested that the slow rise in the spread-*F* diurnal curve from 1800 to 0200 (compared with that for scintillations) is due to blanketing by the *F* region, the critical frequency of which is falling over this period. Thus spread-*F* echoes could be caused by the same ionospheric irregularities as those responsible for radio-star scintillations and yet have a peak in diurnal occurrence several hours later than that for scintillations. The seasonal variation in occurrence of spread *F*, there being less spread *F* in summer than winter, is readily explicable in terms of *F*-region blanketing, as the *F*-region critical frequency is higher in summer than winter.

6. CONCLUSION

The monthly average diurnal variations of radio-star scintillations have been compared with those of spread *F* and geomagnetic activity. A marked correlation is found between the diurnal variations of scintillation-rate amplitude and geomagnetic activity. The correlation between scintillation amplitude and magnetic activity is not found on an hour to hour basis. The diurnal maximum of occurrence of scintillations is found to be several hours earlier than that of spread *F*. It is suggested that this is due to the blanketing of spread-*F* echoes by the main *F* region in the early part of the night.

Acknowledgements—The work described in this paper was carried out at the Jodrell Bank Experimental Station of the University of Manchester, under the direction of Professor A. C. B. LOVELL. It formed part of a programme made

possible by the assistance of the Department of Scientific and Industrial Research, to which the author is personally indebted for a maintenance grant from October 1952 to September 1955. The author is grateful to Dr. A. Maxwell for helpful criticism and advice.

References

Booker H. G. and Wells H. W.	1938	*Terr. Mag.* **43,** 249.
Dagg M.	1957	*J. Atmosph. Terr. Phys.* **10,** 194.
Hewish A.	1951	*Proc. Roy. Soc.* **A209,** 81.
Hewish A.	1952	*Proc. Roy. Soc.* **A214,** 494.
Little C. G.	1951	*Mon. Not. Roy. Ast. Soc.* **111,** 289.
Little C. G. and Maxwell A.	1951	*Phil. Mag.* **42,** 267.
Maxwell A.	1954	*Phil. Mag.* **45,** 1247.
Pawsey J. L.	1955	*Astrophys. J.* **121,** 1.
Reber G.	1954	*J. Geophys. Res.* **59,** 257.
Ryle M. and Hewish A.	1950	*Mon. Not. Roy. Ast. Soc.* **110,** 381.
Wells H. W.	1954	*J. Geophys. Res.* **59,** 273.

Journal of Atmospheric and Terrestrial Physics, 1957, Vol. 10, pp. 215 to 228. Pergamon Press Ltd., London

The frequency dependence of radio reflections from aurora*

P. A. Forsyth and E. L. Vogan

(*Received* 29 *November* 1956)

Abstract—Auroral radio reflections have been observed at a number of frequencies between 30 and 50 Mc/s using continuous-wave transmitters located at a distance of 860 km from the receivers. The relative amplitudes of signals observed simultaneously at the different frequencies are found to vary widely. The experimental results are compared with those which would be expected for each of five different scattering mechanisms which have been proposed to explain auroral reflections. It is concluded that within small regions of the aurora the ionization is often sufficiently intense to cause complete reflection at these frequencies. Some evidence is presented which indicates that absorption may contribute significantly to the observed frequency dependence.

VOL. 10 1957

Introduction

Radio reflections from aurora were observed nearly twenty years ago by Harang and Stoffregan (1938), but it is only in the last nine years that the subject has received intensive study. Starting with the observations of Lovell, Clegg, and Ellyett (1947) and their subsequent interpretation by Herlofson (1947), there have been a number of attempts to explain the mechanism by which radio waves are scattered in an auroral structure. Herlofson suggested that the radio waves were partially reflected at a nearly-plane interface between ionized and non-ionized regions. Later, Aspinall and Hawkins (1950) modified this picture; they assumed that the partially reflecting surface was in the form of a cylinder with its axis lying along the lines of force of the earth's magnetic field. In both cases the amplitude of the reflected signal was explained in terms of relatively small free electron densities within the auroral structure. By assuming that the auroral structures were nearly transparent to the radio waves and also that most of the reflected energy was directed back toward the receiver, it was possible to interpret the observed echo amplitude as indicating free electron densities within the aurora of the order of 10^6 electrons per cm^3. Another type of interpretation which also postulated relatively low electron densities was first advanced by Moore (1952) and later in modified form by Booker, Gartlein, and Nichols (1955). These authors suggested that the auroral structure consisted of many long narrow columns of ionization, each of which scattered the radiation coherently, in a manner which was similar to the scattering of radio waves by individual under-dense meteor trails. Both this approach and the "partial reflection" interpretation required that the auroral structure be oriented in such a way as to permit the reception of the specularly reflected energy (i.e. that the axis of symmetry of the structure be perpendicular to the direction of incidence of the radio waves). Since it is known that auroral structures are oriented along the magnetic field of the earth, it was possible to test the hypothesis by experiment. From observations made by a number of observers in Alaska, Canada, Great Britain, and Sweden,

* Contribution from the Radio Physics Laboratory of the Defence Research Board, Ottawa, Canada. Work carried out under Project No. PCC D48-28-35-05.

it appears that while the auroral structures are quite aspect-sensitive, the incident radiation is spread out, after reflection, over angles of at least $\pm 15°$ measured in a plane containing the magnetic field and over much larger angles in the plane which is perpendicular to the magnetic field. In view of this difficulty, BOOKER (1956) has recently presented a revised theory involving the presence of a great many partially reflecting "blobs" of ionization in the aurora, each blob being elongated along the magnetic field and having dimensions of about 7 m by 16 cm.

In contrast, some authors have favoured the original suggestion of LOVELL, CLEGG and ELLYETT that the electron density within at least small volumes of the aurora was sufficient to totally reflect the radio waves. Reflections which were sometimes observed at a frequency of 100 Mc/s would indicate, according to this picture, ionized regions where the electron density was in excess of 10^8 cm^{-3}.

In an earlier paper, FORSYTH (1953) undertook to test the various competing interpretations which were current at that time, by studying the frequency dependence of the echoes. The experimental evidence consisted of auroral echo amplitudes measured simultaneously at two frequencies. It was found that the ratio of the amplitudes at the two frequencies was quite variable and frequently was too large to be explained by theories involving only low electron densities. The characteristics of the echoes were, however, consistent with the existence of many clouds or "blobs" of ionization, some of which were sufficiently ionized to reflect totally the incident radiation.

As an alternative to the theory recently advanced by BOOKER, it may be noted that, if intensely ionized clouds are in fact responsible for the radio wave-scattering, the required degree of aspect sensitivity could result from a comparatively modest elongation along the magnetic field. If each cloud were a prolate spheroid, then the ratio of length to diameter might be of the order of 3 or 4, and the actual dimensions could be many times those suggested by BOOKER.

It is the purpose of this paper to examine the reflection process in the light of more recent multifrequency data. In particular, these data are used to test for the occurrence of critical reflection from intensely ionized regions. Since the dimensions of the echoing region are not known, it is not possible to decide between the various possible reflection processes by measuring the signal at only one frequency. However, by measuring the echoes at several frequencies simultaneously, it should be possible to differentiate at least between critical reflection and those processes involving only low electron densities. The amplitude of the signal scattered from intensely ionized regions will change rapidly with frequency in the neighbourhood of the critical reflection frequency, and relatively slowly at frequencies far removed from the critical value. It is this characteristic which is used to distinguish between the scattering processes.

EXPERIMENTAL ARRANGEMENT

The earlier work (FORSYTH, 1953) made use of radar equipment operating at 56 and 106 Mc/s. The pulse lengths and antenna beam widths of the two equipments were not identical, so that it was not possible to ensure that identical volumes of the aurora were being examined simultaneously by the two radars. While allowances were made in the analysis for this effect, the precise correction which should be used differs for different assumed reflection mechanisms. It may also be postulated that quite different reflection mechanisms are operative at frequencies which are so

widely separated. Finally, the use of only two frequencies implies that the degree of frequency dependence can be investigated only after the form of the dependence is assumed. The present work overcomes these difficulties by using exactly scaled equipments and three more-closely-spaced frequencies.

The equipment was installed initially for an investigation of forward-scattered signals from meteor trails (FORSYTH and VOGAN, 1955). Four VHF transmitters are located at Greenwood, Nova Scotia, a distance of 860 km from Ottawa, and are operated continuously without modulation at an output power of 100 W. The resulting meteoric signals are received and recorded at

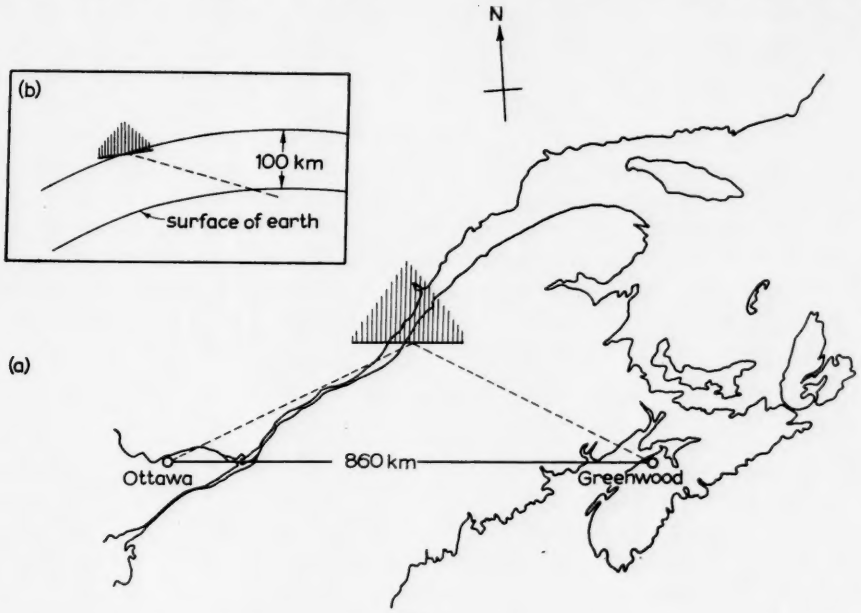

Fig. 1.
(a) Map of Eastern Canada showing the locations of the transmitters (Greenwood) and receivers (Ottawa) and the probable location of the auroral structure which reflected the signals.
(b) Vertical section looking east along the transmission path.

Ottawa. The frequencies used are 32·22, 39·22, 48·82, and 49·98 Mc/s. The transmitting and receiving antennas are scaled exactly in proportion to the wavelength, both with regard to physical dimensions and to height above ground. The amplitudes of the received signals are recorded on moving chart recorders. In order to overcome the inherently slow response of the recording milliammeters, a peak-recording circuit is included in each system. This circuit maintains the peak value of each signal for a sufficient length of time to enable the recorder to respond. For a fading signal this circuit causes all fading components having periods of less than about 3 sec to be suppressed on the record.

The recording equipment has operated continuously for more than a year. In addition to the intermittent meteor signals, many occasions have been noted on which there has been a more or less continuous signal on one or more of the frequencies. A detailed study of these periods of enhanced signals and their correlation with sporadic-*E* and magnetic activity is now in progress. It is hoped to report the results of this work separately. For the present it is sufficient to note that many of them appear to be associated with auroral activity. Characteristically, these signals are not of sufficient amplitude to have been reflected specularly from sporadic-*E* ionization at the midpoint of the path, but they correlate well with the occurrence of auroral activity

VOL. 10 1957

to the north of the path and, when recorded on a high-speed recorder, show at least small amplitude fluctuations at frequencies up to 100 cycles per second.

This paper will deal specifically with two occasions during which the enhancement of the signal was marked at all frequencies and about which there is little doubt concerning the auroral origin of the reflections. It seems most likely that the radio waves were reflected from aurora which was situated to the north of the direct transmitter-receiver path as indicated in Fig. 1.

The Absolute Magnitude of the Received Signal

The appropriate form of the expression relating the transmitted and received powers to the auroral dimensions is dependent upon the mechanism by which the radiation is scattered. For specular reflection from a plane surface there should be only an inverse-square-law dependence on range. For specular reflection from cylindrical surfaces an inverse cube dependence upon range is appropriate. For spherically symmetric reflection or the more general case of multiple scattering there should be an inverse fourth-power dependence upon range. Without in any way attempting to prejudge the issue, the radar equation appropriate to wide-angle scattering is used here. In this way an effective cross-section for the auroral display is obtained. This cross-section may be used for comparison with other measurements, even though it has not yet been shown to have physical significance. The radar equation may be written in the form

$$S = A^2 \frac{P_r}{P_t} \frac{64\pi^3}{G_r G_t \lambda^2} (R_1^2 R_2^2)$$

where

S = cross-section of the auroral display.
A = received amplitude.
P_r = received power corresponding to an amplitude $A = 1$.
P_t = transmitted power.
G = power gain of the antenna systems.
λ = wavelength
R_1 = distance from transmitter to auroral display.
R_2 = distance from receiver to auroral display.

Taking P_r to be the received power corresponding to a signal at the antenna terminals of 10^{-7} V, $G_r = G_t = 10$, and $R_1 = R_2 = 500$ km;

$$S = \frac{A^2}{\lambda^2} (2{\cdot}5)\ 10^6\ \mathrm{m}^2$$

or designating the values of S and A appropriate to each of the wavelengths by a subscript which refers to the approximate value of the wavelength in metres,

$$S_9 = 2{\cdot}9 \times 10^4\, A_9^2\ \mathrm{m}^2$$
$$S_8 = 4{\cdot}3 \times 10^4\, A_8^2\ \mathrm{m}^2$$
$$S_6 = 6{\cdot}6 \times 10^4\, A_6^2\ \mathrm{m}^2.$$

The observed range of A during an auroral display represents cross-sections for the highest frequency ranging from about 2×10^4 m^2 to 10^7 m^2, which may be compared with cross-sections ranging from 4×10^5 m^2 to 4×10^7 m^2 which were

observed at a slightly higher frequency during the earlier backscatter measurements. This comparison is intended only to indicate the relative sensitivities of the equipments and the magnitude of the observed effects. There is no justification for assuming that the auroral displays were comparable for the two sets of measurements.

It is interesting to note that for a specular reflector at the midpoint of the path, the observed signal amplitudes at the highest frequency would correspond to power-reflection coefficients in the range 2×10^{-8} to 10^{-5}.

The Variation of Amplitude with Wavelength

For the case of scattering from a target of constant physical cross-section the received signal amplitude is proportional to the wavelength in use. A similar relation frequently exists even when the reflection process cannot be described in terms of a physical cross-section. For this reason in the following analysis a reduced amplitude A' will be used instead of A, where,

$$A' = A/\lambda.$$

The discussion will be restricted largely to the three lower frequencies: 32·22 Mc/s, 39·22 Mc/s, and 48·82 Mc/s, which are designated respectively by the subscripts 9, 8, and 6. The method to be followed is to examine each of the proposed reflection mechanisms to determine the appropriate value of the ratios X and Y

VOL. 10 1957

where $$X = A'_8/A'_6$$

and $$Y = A'_9/A'_8.$$

These theoretical values can then be compared directly with the experimentally observed values.

(i) *Scattering from nonisotropic irregularities.* It was shown by Booker (1956) that for scattering from nearly-transparent elongated irregularities,

$$A' \propto \exp -K/\lambda^2 \tag{1}$$

where K is a constant which depends both upon the physical dimensions of the irregularities and the angle of incidence of the radiation. Hence

$$X = \exp K(8{\cdot}7)\ 10^{-3} \tag{2}$$

$$Y = \exp K(5{\cdot}5)\ 10^{-3} \tag{3}$$

While K must be a constant for a given set of observations, it may be assumed to vary with time so that equations (2) and (3) will simply define a relation between X and Y with which the observed values should agree.

(ii) *Scattering from isotropic irregularities.* The experimental evidence is thought currently to exclude the possibility that the scattering elements in aurora are spherically symmetric, but for the sake of generality the appropriate expressions are included here. According to Bailey *et al.* (1952), the wavelength dependence is given by

$$A' \propto \frac{1}{1 + K'/\lambda^2} \tag{4}$$

where K' depends upon the physical dimensions of the irregularities and upon an angular parameter. Hence

$$X = \frac{37{\cdot}8 + K'}{58{\cdot}5 + K'}\,(1{\cdot}55) \tag{5}$$

$$Y = \frac{58{\cdot}5 + K'}{86{\cdot}4 + K'}\,(1{\cdot}48). \tag{6}$$

In this case it is seen that the lowest permitted value of X or Y is unity, which occurs when $K' = 0$; the highest values, which occur for K' infinitely large, are

$$X = 1{\cdot}55 \tag{7}$$

and

$$Y = 1{\cdot}48 \tag{8}$$

(iii) *Partial reflection from large surfaces.* The mechanism first proposed by Herlofson (1947) involves a discontinuity reflection at the interface between ionized and nonionized regions. For a sharp boundary,

$$A' \propto \lambda^2$$

and X and Y are given by equations (7) and (8) above. If the boundary of the ionized region is not thin, there is a further dependence upon wavelength which may be expressed by a factor which is similar to the right-hand side of equation (1). In this case, K is related to the thickness of the boundary.

(iv) *Scattering from long, thin columns.* This mechanism, which was proposed by Booker and his associates, is similar to the scattering of radio waves by underdense meteor trails. If the columns are very thin, the frequency dependence is given by

$$A' \propto \lambda^{1/2} \tag{9}$$

hence

$$X \simeq Y = 1{\cdot}11 \tag{10}$$

If the column is not thin, then a factor similar to the right-hand side of equation (1) must be introduced also into equation (9). In this case, the constant in the exponent is related to the diameter of the column.

(v) *Scattering from intensely ionized regions.* For each of the mechanisms discussed above it was possible to write an expression for the frequency dependence of the signal amplitude. In each case it was assumed implicitly that the electron density was everywhere much lower than that required to totally reflect the radio waves. These mechanisms have in common the characteristic that, for all of the frequencies concerned, the radio waves pass freely through the scattering region. On physical grounds, it is apparent that, even for mechanisms other than those mentioned, as long as the radio waves pass freely through the region there should exist a simple law relating the signal amplitude and the wavelength. On the other hand, it is not possible to establish a simple relation for the case of scattering from intensely ionized regions. In the earlier paper, it was suggested that an auroral display contains a number of intensely ionized clouds in which the actual electron density varies from minute to minute and from cloud to cloud. Under these

conditions the observed values of X and Y should vary between wide limits, and all combinations of these values are possible. The critical value of electron density at which the radio wave is totally reflected for each frequency is,

$$N_{09} = 1{\cdot}3 \times 10^7 \text{ electrons per cm}^3$$
$$N_{08} = 1{\cdot}9 \times 10^7 \text{ electrons per cm}^3$$
$$N_{06} = 3{\cdot}0 \times 10^7 \text{ electrons per cm}^3.$$

Whenever the ionization within a cloud reaches one of these values, radiation of the corresponding wavelength (and all longer wavelengths) is strongly reflected. These values apply strictly only for the case of backscatter. There is some reason to believe that more exact values of the critical electron densities would be obtained by multiplying these figures by a constant factor $\cos^2 \varphi$, where φ is one-half the angle between incident and reflected rays. Unfortunately, φ is not known for the present measurements, but it is extremely unlikely that the appropriate value of $\cos^2 \varphi$ is less than 0·5. This factor will be ignored in the following discussion, but it should be remembered that the estimated electron densities may be too large by as much as a factor of 2. If, in fact, the aspect-sensitivity of the scattering centres were significantly greater than that indicated earlier, the uncertainty in the electron density would be reduced correspondingly, that is, the smallest permissible value of the factor $\cos^2 \varphi$ would approach unity.

VOL. 10 1957

(vi) *Absorption.* The presence or absence of absorption is not determined by the mechanism concerned. It is discussed here because it may also affect the wavelength dependence of signal amplitude. Absorption should introduce an additional factor into X or Y of the form,

$$\exp\left(-\alpha(\lambda_a^2 - \lambda_b^2)\right)$$

where α is an absorption coefficient and λ_a and λ_b are the appropriate wavelengths.

The XY Diagram

It is convenient to discuss the behaviour of the ratios of signal amplitudes with the aid of a graph of X against Y. Such a graph is shown in Fig. 2. Considering first the set of curves marked A, the broken line is the curve derived from equations (2) and (3); the solid line is derived from equations (5) and (6) (the end of this line remote from the origin has the co-ordinates given by equations (7) and (8)), and the large solid dot indicates the co-ordinates given by equation (10). No curve has been included specifically to illustrate the case of partial reflection from a boundary of variable thickness (mechanism iii) nor has one been included for scattering from a long column of variable thickness (mechanism iv), since the appropriate curves may be approximated by slight displacements of the broken curve.

The sets of curves marked B and C illustrate the effect of absorption. The set marked B is the same as that marked A, except that an additional factor has been included which represents an attenuation of the lowest frequency by 10 dB (and corresponding attenuations at the other frequencies). Curves C correspond to an attenuation at the lowest frequency of 20 dB.

In the figure, the broken lines have been continued to the right-hand edge of the diagram because no termination is indicated in equations (2) and (3). In fact,

values of X much above 2 are not to be expected for mechanism (i). This is because such values indicate a correlation distance in the aurora which is much larger than the wavelength, and a corresponding decrease in signal amplitude. Similar reasoning applies in the case of mechanisms (iii) and (iv) when an exponential factor is included. In each case, the signal falls off rapidly with increasing X co-ordinate. For example, an increase of X from 1 to 3 corresponds to an attenuation of the signal by 20 dB. It is quite apparent that values of X as great as this

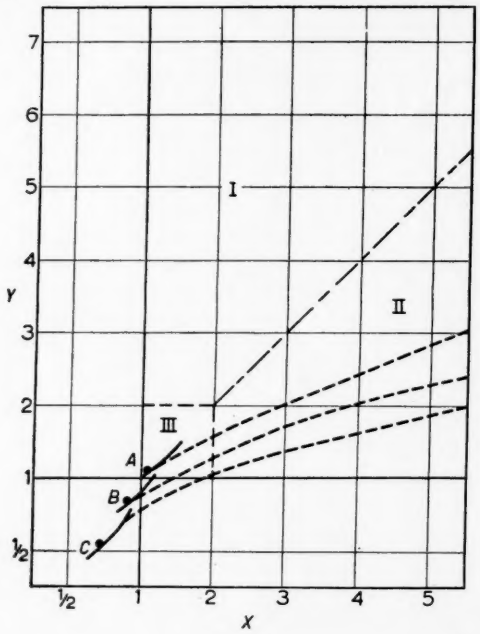

Fig. 2.
The XY diagram showing curves (A) which relate to various reflection mechanisms. Curves (B) and curves (C) show the modification to be expected in the presence of absorption.

can not be considered appropriate to the mechanisms concerned without a drastic revision of the physical models upon which they are based.

In Fig. 2, three areas are marked on the graph. These areas may be characterized by the following conditions:

I:	$Y > 2, \quad Y > X$
II:	$X > 2, \quad X > Y$
III:	$X < 2 > Y.$

From the foregoing discussion it is apparent that if the reflection mechanism is one of those which involve only low electron densities (i.e. mechanisms i to iv above) the observed values of X and Y should be confined largely to area III. If, on the other hand, mechanism (v) is appropriate, then the experimental points should be scattered more widely on the XY diagram. The electron density will certainly vary from cloud to cloud in the scattering region, but it may be assumed

that at any time it is possible to characterize the reflecting properties of an aggregate of the scattering clouds by some suitably weighted mean electron density, $\bar{N}$. Three general conditions can be distinguished for different values of this electron density:

I $$N_{09} \leq \bar{N} < N_{08}$$

hence $$A'_9 > A'_8 \simeq A'_6 \quad \text{and} \quad Y \gg X \simeq 1$$

and the experimental points should lie largely in area I;

II $$N_{08} \leq \bar{N} < N_{06}$$

hence $$A'_9 \simeq A'_8 > A'_6 \quad \text{and} \quad X \gg Y \simeq 1$$

and the experimental points should lie largely in area II;

III $$N_{06} \leq \bar{N}$$

hence $$A'_9 \simeq A'_8 \simeq A'_6 \quad \text{and} \quad X \simeq Y \simeq 1$$

and the experimental points should lie largely in area III.

There is another condition, namely, $\bar{N} < N_{09}$, for which the experimental points should fall in area III, but this case is trivial, since, if the clouds are large, only small signals will be observed. If, on the other hand, the clouds are small, then one of the other mechanisms will become important for small values of electron density.

VOL. 10 1957

Experimental Results

The experimental results are plotted on XY diagrams in Figs. 3 and 4. The observations shown in Fig. 3 were made at intervals of 2·5 min between 0540 and 1100 UT on 25 February 1956. The widespread auroral display which occurred during this period is particularly interesting because it appears to have been associated with the intense solar flare of 23 February. During the night of 24–25 February, aurora was reported over most of the northern and western parts of North America, covering at least the area from the western tip of Alaska to the mid-western states of the U.S.A. The eastern area of North America was cloudy during this interval, but there have been reports of auroral light observed spectroscopically through cloud. In the north-west a red auroral arc was seen between 1015 and 1030 UT.

In the diagram of Fig. 3 the plotted points are scattered widely, but fall most frequently in areas I and III. The experimental points which have a small horizontal bar associated with them indicate points for which the observable ratio was limited by the recording range of the equipment. In each of these cases the true X co-ordinate is greater than the value shown. It appears likely that the true positions of the points should be spread somewhat more uniformly over areas I, II, and III. The presence of a number of points to the left of the $X = 1$ axis suggests that there was some selective absorption of the radio waves. Absorption would tend to move the whole distribution of points diagonally toward the lower left-hand corner.

Fig. 4 shows the observations for two separate periods on 3 March. For the earlier period (0830 to 1130 UT) the points are concentrated in area II, suggesting electron densities between 2 and 3 $\times$ 10^7 electrons per cm^3. There are some points

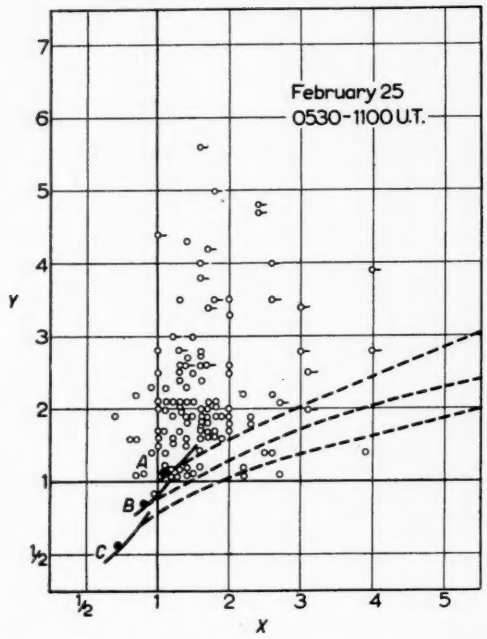

Fig. 3. The XY diagram showing the experimental points derived from observations made during the auroral display of 25 February 1956.

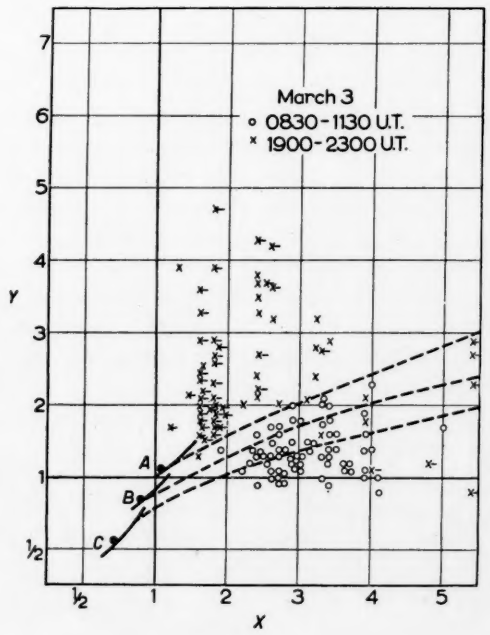

Fig. 4. The XY diagram showing the experimental points derived from observations made during the auroral display of 3 March 1956.

below the $Y = 1$ axis suggesting the existence of absorption. The points for the later period (1900 to 2300 UT) are widely distributed, but appear to fall mostly in area I. The distribution of these points is quite similar to that shown in Fig. 3 and suggests that during the interval in question the electron density was fluctuating through the range of values between 1 and 3×10^7 electrons per cm^3, and possibly beyond this latter value.

A comparison of Figs. 3 and 4 with Fig. 2 suggests that the present results cannot be explained adequately in terms of any of the first four mechanisms discussed in the preceding section. As was indicated earlier, this is quite a general result. Any mechanism which involves only low electron densities implies the relatively free passage of the radio waves through the ionized region, which in turn implies that a simple relation between wavelength and amplitude should exist.

It is interesting also to examine the amplitude of the signal received at the highest frequency (49·98 Mc/s). This frequency was too close to the next lower frequency (48·82 Mc/s) to be useful in the general treatment above, because characteristically the amplitudes observed on the two frequencies were approximately equal. This is to be expected even for mechanism (v), since there is only a very small range of electron densities for which the amplitudes should be significantly different. On several occasions, however, the signal amplitude received at 48·82 Mc/s was more than four times as great as that received at 49·98 Mc/s. So strong a dependence of amplitude upon frequency is further evidence of the operation of mechanism (v). It would seem that on these occasions not only was $\bar{N}$ in the reflecting regions very nearly 3×10^7 electrons per cm^3, but that this electron density must have been remarkably well defined. The critical values of electron density for the two frequencies differ only by about 4%. Most of the received energy must have been reflected by clouds having electron densities within this narrow range.

VOL. 10 1957

Absorption

Some of the evidence presented in the preceding section was interpreted as indicating the presence of selective absorption. There was some similar evidence in the earlier dual frequency results (Forsyth, 1953). Using radar results obtained at Saskatoon, an attempt was made to separate the effect of aspect sensitivity from that due to variation of the altitude angle at which the aurora was observed. This was done by comparing the relative occurrence of echoes at points which were characterized by having the same angle of incidence upon the magnetic field lines, as viewed from the radar station, but different altitude angles. There seemed to be a significant variation of echo occurrence with altitude angle in addition to any effect of aspect sensitivity which was present. It was suggested that this dependence of echo occurrence upon altitude angle might be due to the existence of an absorbing region immediately below each reflecting region (Currie, Forsyth, and Vawter, 1953), although it was pointed out that there was no direct evidence of significant auroral absorption at the frequencies concerned.

During the auroral display which took place in the early morning hours of 27 April 1956, recordings were made which seem to point conclusively to the existence of auroral absorption. In Fig. 5 is shown a recording of the signal received at 39·22 Mc/s during this time. It should be noted that on the record, time increases

from right to left, the times shown being UT, and that the vertical scale is logarithmic in amplitude. This record was made without benefit of the peak-reading circuit mentioned earlier. The large auroral signal is shown on the right-hand (earlier) part of the record and the normal spiky meteoric signal is shown on

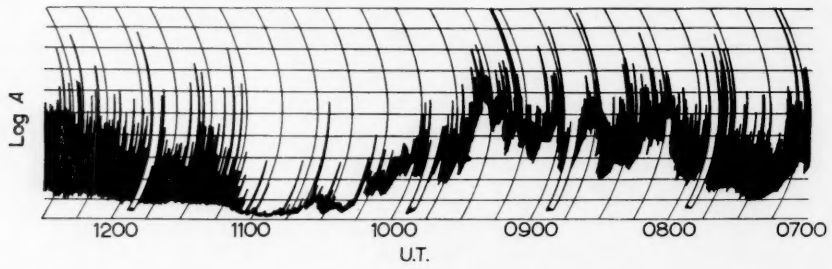

Fig. 5.
Record of the signals received at a frequency of 39·22 Mc/s during an auroral display on 27 April 1956, showing the attenuation suffered by the meteoric signals just before 1100 UT. On this record the vertical amplitude scale is logarithmic; the full-scale deflection range is 35 dB.

the left-hand (later) part of the record. The remarkable drop in the recorded signal for a few minutes before 1100 UT is the significant occurrence. By 1000 UT, the cosmic-noise level, as indicated by the signal received during the short periods of transmitter silence which occur once each hour, had dropped below its normal

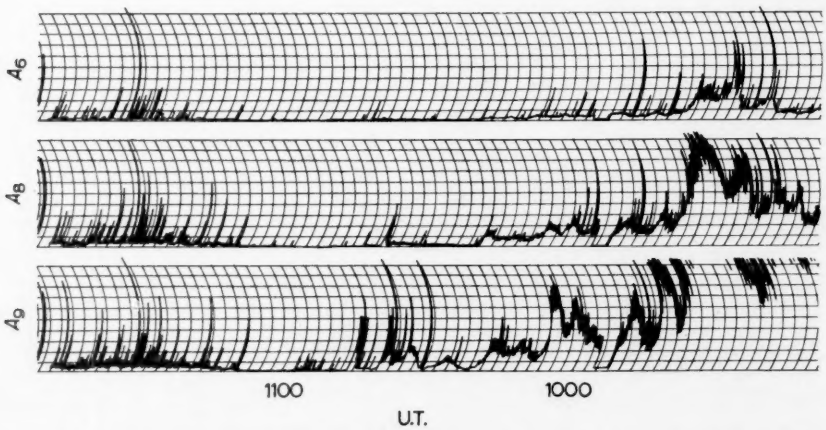

Fig. 6. Three-frequency records, of the type used in the multi-frequency analysis, taken during the period covered by the record of Fig. 5.

value. A decrease in the cosmic-noise level, as recorded by the present equipment, occurs during many but not all auroral displays, nor is the amount of the decrease always consistent. In the present case, just before 1100 UT the auroral signal disappeared and, surprisingly, the meteoric signal disappeared at the same time. Since the meteors occur randomly, it is difficult to assess accurately the amount of attenuation involved, but it must have been of the order of 20 dB.

The three-frequency recordings made with the peak-recording equipments during this same interval are shown in Fig. 6. In this figure the horizontal time axis is much expanded and the vertical scale is approximately linear in signal amplitude. Again, time increases from right to left. The right-hand part of the figure is typical of the records used in the analysis described earlier.

Recordings were made during the same auroral display on equipment operating at 53 Mc/s and looking north at the radiation from Cassiopeia A. For a short period, this signal suffered an attenuation of about 10 dB. Recordings were made also, at a frequency close to 30 Mc/s, of the cosmic noise received on a fairly broad-beamed antenna looking vertically. This signal suffered a large attenuation, but the exact amount is uncertain.

The attenuation of the meteoric signals suggests that the absorbing region was situated below the level at which the meteor trails were being formed. The time in question (0600 local time) is unique, since at this time the most frequently occurring meteors have geocentric velocities in the neighbourhood of 70 km/sec and, in consequence, form trails at a height of about 105 km. At other times of the day the geocentric velocities, and the heights at which the trails are formed, are considerably less. It seems reasonable to assume that the absorbing region was at a height of about 100 km, just below the most frequently occurring height of the lower edge of auroral displays. At other times of the day the meteors would be formed below this height and the meteoric signals would not suffer attenuation even in the presence of intense auroral activity. Since this remarkably clear example of absorption was found on the records several other examples have been noticed. The occurrences found up to the present time have been confined to the early morning hours and none show attenuation as great as the one described above. The records for these occasions are now being studied in relation to the other available evidence, and it is hoped that the results of this study will be published separately. The possible existence of absorption is of interest in the present context only to the extent that it modifies the frequency dependence of auroral echoes. While the absorption of meteor signals is likely to be observable only during the early morning hours, no such limitation should apply to the auroral signals. It seems reasonable to suggest that auroral absorption frequently does exist at these frequencies and that, for example, in the absence of absorption the points plotted in Fig. 4 would all have fallen to the right of the $X = 1$ axis and above the $Y = 1$ axis.

If absorption as intense as that indicated by the present records is a common occurrence, then the auroral-signal amplitudes which should be used for comparison with theory are substantially larger than the observed values. This fact further emphasizes the need for making measurements of the relative signal amplitudes at a number of frequencies rather than making measurements of the absolute amplitude at a single frequency, when the reflection mechanism is being studied.

Concluding Remarks

The present measurements seem to point conclusively to the existence of auroral scattering centres within which the free electron density is of the order of 10^7 electrons per cm^3. It cannot be emphasized too strongly that the operation of

VOL. 10 1957

the critical reflection mechanism does not preclude the simultaneous operation of one or more of the other mechanisms. The present measurements were directed specifically toward a test for the occurrence of critical reflection. The method of analysis which was used would not have indicated the presence of scattering from weakly ionized regions except in the absence of critical reflections. It may be that the weak signals which are often seen during the early stage of an auroral display are due to scattering of a kind similar to that described by Booker (1956). The analysis was restricted to two auroral displays. No claim can be made that these displays were typical.

The evidence concerning auroral absorption refers only to a single occurrence, but it does lend strong support to the suggestion that localized absorbing regions are associated with each auroral display. It is to be hoped that measurements which make use of extra-terrestrial point sources will be able to give positive evidence concerning the existence of such absorbing regions.

The present measurements were confined to relatively low frequencies. Radio reflections from aurora have been observed at much higher frequencies and, in the absence of contrary evidence, it is reasonable to assume that the same reflection mechanism is operative at these higher frequencies. Confirmation of this assumption is badly needed. There appears to be no reason why the multi-frequency technique described in this paper cannot be used at higher frequencies.

Acknowledgements—The authors are indebted to several members of the laboratory staff who are associated with the meteor research programme, notably Mr. J. W. Brown, who supervised the recordings. The transmitters were operated by RCAF personnel at Greenwood, Nova Scotia. The recordings of the signal received from Cassiopeia *A* were made by Mr. T. R. Hartz and those of the integrated cosmic-noise level by Dr. G. C. Reid. During the preparation of the paper valuable discussions were held with Dr. B. W. Currie of the University of Saskatchewan.

References

Aspinall A. P. and Hawkins G. S.	1950	*J. Brit. Astr. Assoc.* **60,** 130
Bailey D. K., Bateman R., Berkner L. V., Booker H. G., Montgomery G. F., Purcell E. M., Salisbury W. W., and Wiesner J. B.	1952	*Phys. Rev.* **86,** 141.
Booker H. G.	1956	*J. Atmosph. Terr. Phys.* **8,** 204
Booker H. G., Gartlein C. W., and Nichols B.	1955	*J. Geophys. Res.* **60,** 1.
Currie B. W., Forsyth P. A., and Vawter F. E.	1953	*J. Geophys. Res.* **58,** 179.
Forsyth P. A.	1953	*J. Geophys. Res.* **58,** 53.
Forsyth P. A. and Vogan E. L.	1955	*Can. J. Phys.* **33,** 176.
Herlofson N.	1947	*Nature* **160,** 867.
Lovell A. C. B., Clegg J. A., and Ellyett C. D.	1947	*Nature* **160,** 372.
Moore R. K.	1952	*Trans. I.R.E. AP-3,* 217.

Journal of Atmospheric and Terrestrial Physics, 1957, Vol. 10, pp. 229 to 236. Pergamon Press Ltd., London

Ionospheric changes at Singapore during the solar eclipse of 20 June 1955

C. M. MINNIS
Official communication from D.S.I.R. Radio Research Station, Slough

(*Received* 7 *January* 1957)

Abstract—Measurements were made, at vertical incidence, of the changes in the ionosphere which accompanied the eclipse. It has been possible to derive the distribution and intensities of the solar sources of ionizing radiation responsible for the *E* layer during the eclipse. Although it would not have been obscured at Singapore, it has been necessary to postulate the existence of a bright source in the sun's Southern hemisphere having an intensity equal to 21% of the total radiation. This figure agrees well with the intensity (23%) derived from measurements made on the control days, of a source of radiation associated with an active group of spots which was in the South-west quadrant on 20 June.

No significant change occurred in the *F2*-layer critical frequency during the eclipse, but the temporary appearance of an *F1½* layer, in addition to the usual permanent ledge in the *F2* layer, indicates that the eclipse was responsible for a rearrangement of the electron distribution in the lower part of the *F2* layer.

1. INTRODUCTION

THE path of the total eclipse of 20 June 1955 passed about 1500 km to the north of Singapore, where the unobscured fraction (A_{min}) of the area of the sun's disk at the maximum phase of the eclipse was about 0·5 (Table 1). On the eclipse day, ionospheric *h'f* records were made at intervals of about 4 min during a period of 5 hours centred on the eclipse; records were also made at quarter-hour intervals during the same period on each of ten control days.

VOL. 10 1957

Table 1. Duration of eclipse at Singapore, 20 June 1955

Noon (LMT)	Height (km)	Beginning (LMT)	Middle (LMT)	End (LMT)	A_{min}
1206	100	0908	1029	1159	0·52
	200	0907	1027	1159	0·53

LMT = UT + 7 hr.

2. *E* LAYER

2.1. *General*

Fig. 1 shows the changes in f_0E on the day of the eclipse and also, for comparison, curves representing 1·04 times the median value for the control days. The figure also shows f_{min} during part of the eclipse period and the corresponding values on the control days. Since f_{min} is an indication of the amount of absorption in the *D* layer, it is clear that just before the eclipse began there was a fairly large, but short-lived, increase in absorption; this began at 0152 UT ± 5 min, went through a maximum at 0203–0216 UT, and returned to normal at about 0300 UT. This increase in absorption made it impossible to read f_0E between 0200 and 0218 UT, but interpolation shows that, just before the eclipse began, f_0E must have attained a value 0·10–0·15 Mc/s above the adjusted median value. Short-term changes of

this kind in f_0E have been studied by BIBL (1951), who has shown that they are frequently associated with solar flares; on this particular occasion the accompanying increase in absorption makes it very likely that a minor flare did, in fact, occur, although no visual evidence of it is available.

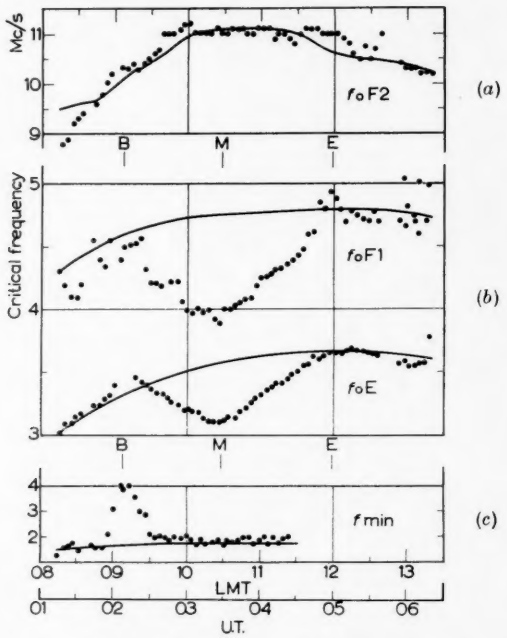

Fig. 1. Critical frequency changes at Singapore during the solar eclipse of 20 June 1955 ●●● 20 June 1955.
——— 1·00 × median (f min)
——— 1·04 × median (E and $F1$ layers)
——— 1·06 × median ($F2$ layer)
The medians refer to ten control days.

After the beginning of the eclipse, the effect of the flare on f_0E was masked by the fall due to the eclipse itself. However, since the absorption remained above normal until 0300 UT, it will be assumed that, for some time, f_0E also remained higher than it would have done had no flare occurred.

The analysis of the observed changes in f_0E during the eclipse has been carried out by evaluating the function

$$\left(N^2 + \frac{1}{\alpha'}\frac{\mathrm{d}N}{\mathrm{d}t}\right)\sec^{4/3}\chi = A'(q_0/\alpha') = J \qquad (1)$$

where

q_0 = rate of generation of electrons per unit volume,
α' = effective recombination coefficient,
N = electron density,
χ = zenith angle of sun,
A' = unobscured fraction of ionizing radiation.

Equation (1) follows directly from the equation for a Chapman layer, except for the exponent of sec χ: this has been changed from unity to allow for the fact that, during the control period, f_0E varied as the cube root of cos χ and not as the fourth root, which is the appropriate relation for a simple Chapman layer. If q_0/α' remains constant, the changes in J during the eclipse can then be assumed to be proportional to the simultaneous changes in the intensity of the ionizing radiation; it will be convenient later to refer to J simply as the intensity of a source of radiation.

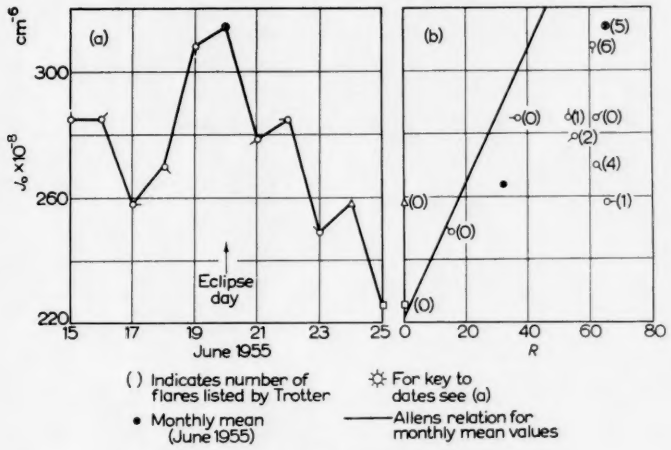

Fig. 2. E layer at Singapore, June 1955.
(a) Day to day changes in J_0 (mean for the period 01–06 U.T.).
(b) Sunspot number (R) plotted aglinst J_0.

VOL. 10 1957

2.2. *Day-to-day changes in* J_0

Before discussing the changes in J which occurred during the eclipse, it is necessary to refer to the day-to-day changes in J_0 ($=q_0/\alpha'$), that is, the intensity of the whole of the sun's disk, during the control period (Fig. 2a). In Fig. 2b the same values of J_0 have been plotted against the daily values of the provisional Zürich sunspot number and there is evidence of a loose correlation between the two quantities. The figure also includes, for comparison, the line representing the relation between monthly mean values of J_0 and sunspot number implied by data given by ALLEN (1948).

There was only one important group of spots on the disk at the time, and this crossed the central meridian on 17 June; judged by the number of flares, as given by TROTTER and ROBERTS (1955), this group was most active on 19 and 20 June, when J_0 also reached its highest level. It seems reasonable to conclude that the value of J_0 ($=314 \times 10^8$ cm^{-6}) on 20 June included a component which represented the emission of ionizing radiation from this spot group and which was superposed on a quasi-permanent background level represented by J_0($=242 \times 10^8$ cm^{-6}) on 24–25 June, when the group was no longer visible. If this interpretation is correct, the difference between these two values of J_0(72×10^8 cm^{-6})

would represent approximately the intensity of the ionizing radiation emitted from the group in question on 20 June.

2.3. *Changes in J during the eclipse*

In computing J from the changes in f_0E during the eclipse, it has been assumed that $\alpha'_E = 1{\cdot}2 \times 10^{-8}$ cm^3 s^{-1}. In Fig. 3 the resulting values of J have been plotted against the unobscured area (A) of the sun's disk. A comparison of the observed J-A relation with the linear relation expected for a uniformly bright disk shows that during the eclipse there must have been considerable nonuniformity in the brightness distribution.

The value of J_0 appropriate to the eclipse period itself has been assumed to be 309×10^8 cm^{-6}, which is the observed value at the end of the eclipse. During the early part of the eclipse, however, it is clear that the appropriate value of J_0 is about 370×10^8 cm^{-6} (Fig. 3), and this high value has been attributed to the

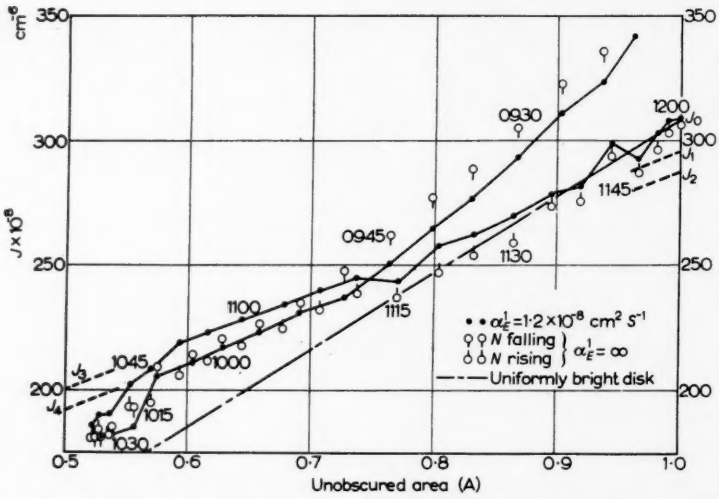

Fig. 3. J-A diagram for the E layer during the eclipse of 20 June 1955 at Singapore.

effects of the solar flare discussed earlier. The influence of this flare on J during the eclipse appears to have become negligible by about 0245 UT, when J had fallen to a level consistent with $J_0 = 309 \times 10^8$ cm^{-6}. This is a reasonable supposition in view of the somewhat slower rate of recovery of the D layer, as indicated by $f_{\min}$ in Fig. 1.

2.4. *The distribution of the radiation sources*

In Fig. 3 the parallel lines indicated by J_1J_3 and J_2J_4 have been drawn through the linear portions of the two branches of the J-A curve for $\alpha'_E = 1{\cdot}2 \times 10^{-8}$ cm^3 s^{-1}. The slope of these lines gives the intensity (J_D) of the component of the radiation which can be represented by a uniformly radiating disk. The difference ($J_0 - J_1$) represents the intensity (J_E) of an additional bright source which was uncovered near the end of the eclipse and which must, consequently, have

been near the east limb; similarly, $(J_0 - J_2)$ represents the intensity (J_W) of a source near the west limb. Finally, the sudden fall in J at $A \simeq 0{\cdot}57$ would be consistent with the existence of a bright area, of intensity J_C, near the centre of the disk. The intensities of all these sources, as derived from Fig. 3, are given in Table 2, but, since the sum of their intensities is less than J_0, it is necessary to postulate the existence of yet another source (J_X) to make up the balance. It is concluded that this source must have been in the southern hemisphere of the sun, since there is no evidence in the Singapore data of its having been occulted during the eclipse; it seems logical, therefore, to identify it with the active spot group in the South-west quadrant which has already been discussed. This conclusion is supported by the good agreement between the magnitude of J_X (65 units) derived from the eclipse results, and the intensity of the spot group (72 units) as deduced from a consideration of the day-to-day changes in J_0 (Section 2.2).

2.5. *The effective recombination coefficient*

It is impossible to determine the value of α'_E from the Singapore results alone, and the intensities given in Table 2 have been computed for an assumed value.

Table 2. Sources of ionizing radiation deduced from eclipse data, 30 June 1955
($\alpha'_E = 1{\cdot}2 \times 10^{-8}$ cm^3 s^{-1})

Source		Intensity (unit 10^8 cm^{-6})
Uniform disk	(J_D)	192
West limb	(J_W)	21
East limb	(J_E)	13
Central area	(J_C)	18
Southern hemisphere	(J_X)	65 (72*)
Whole disk	(J_0)	309

* See Section 2.2.

However, if ionospheric data were available from other observatories in the eclipse path, it seems possible that the method used recently to redetermine α'_E for the 1952 eclipse (Minnis 1956a) might also be applicable in this instance.

3. *F* Layer

3.1. *F1 layer*

During the control days the *F1*-layer cusp was usually not clearly defined, but on the eclipse day, from about 1013 till 1113 LMT, a very sharp cusp was present on the *h'f* records; several examples of these are included in Fig. 4. During the remainder of the eclipse, however, the accuracy with which f_0F1 can be read from the records is not sufficiently high to justify a detailed analysis of the type

VOL. 10 1957

described in Sections 2.3. and 2.4. As can be seen from Fig. 1, the simultaneous changes in f_0E and f_0F1 are very similar. This effect was also observed during the eclipses of 1952 and 1954, and its implications have been discussed elsewhere (MINNIS, 1956b).

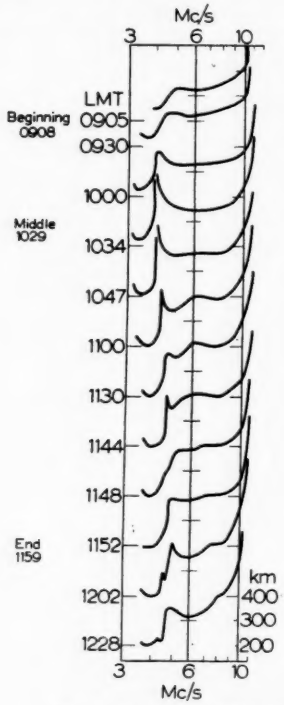

Fig. 4. $h'f$ traces at Singapore during the solar eclipse of 20 June 1955.

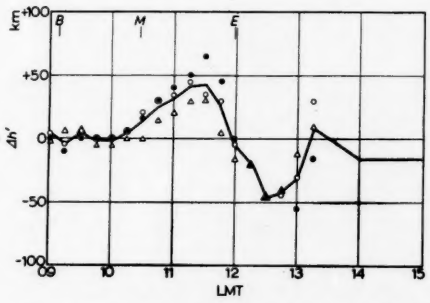

Fig. 5. Changes in the virtual height of the F layer caused by the eclipseof 20 June 1955 at Singapore.
● 6 Mc/s ○ 7 Mc/s △ 8 Mc/s — mean

3.2. *F2 layer*

No significant eclipse effect can be detected in the changes in f_0F2 on 20 June (Fig. 1). A comparison of the $h'f$ curves for the eclipse with those for the control days shows that, even though no change occurred in the critical frequency, the eclipse was accompanied by complex changes in the distribution of electron density with height in the F layer. Soon after the maximum phase of the eclipse, the shape of the $h'f$ curves suggests the formation of an $F1\frac{1}{2}$ ledge, which can be seen developing at 1047 (Fig. 4). At first sight it appears as if the "critical frequency" of this ledge increases gradually from about 6 Mc/s at 1100 to 8 Mc/s at 1228 LMT, but, on further examination, this interpretation proves to be incorrect. Although the ledge which is visible between about 1100 and 1130 is definitely an eclipse phenomenon, the one which is present from 1200 till 1230 is also present on many of the control days. A full investigation of the significance of these changes in layer shape would require the computation of numerous Nh profiles.

A rough quantitative indication of the nature of the changes in the $F2$ layer

which were due to the eclipse can, however, be obtained from a comparison of the changes which occurred in h' at selected frequencies during the eclipse and those for the control days. The values of h' at 6, 7, and 8 Mc/s were read from the $h'f$ records for each control day and also during the eclipse. The median values of h' on the control days were then subtracted from the corresponding values of h' during the eclipse. For each frequency, it was found that the resulting differences ($\Delta' h'$) remained small and constant between 0900 and 1000; these differences are probably due to a small systematic difference between the thickness of the layer on the eclipse day and the median value of the thickness during the control period. For each frequency a small correction ($\delta h'$) was applied to the values of h' on 20 June, so as to reduce to zero, during the interval 0900–1000, the mean value of $\Delta h' = \Delta' h' + \delta h'$; the resulting values of $\Delta h'$ for each frequency are shown in Fig. 5. The variable amount of group retardation due to eclipse effects in the *F1* layer is difficult to assess accurately, but is unimportant at the frequencies in question.

$\Delta h'$ may be assumed to indicate the magnitude of the changes in $h'F2$ due to the eclipse. The rise and fall in $\Delta h'$ between the maximum phase and the end of the eclipse (Fig. 5) is obviously due to the growth and subsequent decay of the $F1\frac{1}{2}$ ledge, which reaches its peak development at about 1130. If the ledge which is visible in Fig. 4 after 1200 had also been an eclipse phenomenon, $\Delta h'$ would have remained positive after 1200; the fact that it becomes negative appears to indicate either that the upper ledge was less well developed than on the control days, or that the newly-formed ionization represented by the temporary lower ledge extended to a lower level than normal and masked the permanent upper ledge. The continuity of the positive and negative phases of the $\Delta h'$ curve suggests that this is probably the correct interpretation. Temporary ledges and layers in the region between the *F1* and *F2* layers have been observed during previous eclipses by Ledig *et al.* (1946), Nakata (1950), Piggott (1953), Estrabaud (1952), Delobeau (1953), and Minnis (1955), but it is not clear whether such ledges differ from those which often occur on normal days in low latitudes. The present Singapore results appear to show that the $F1\frac{1}{2}$ ledge which may appear during an eclipse can exist separately from the ledge normally observed on other days.

VOL. 10 1957

4. Conclusions

The changes in f_0E during the eclipse have been used to deduce the brightness distribution of the ionizing radiation emitted from the sun's disk. 62% has been attributed to a uniformly distributed component and 21% to a bright source in the southern hemisphere which was probably associated with an active spot group in the south-west quadrant. Independent evidence obtained from the control data suggests that this spot group contributed 23% of the ionizing radiation.

The eclipse did not cause any detectable change in f_0F2, but the electron distribution in the region between the *F1*- and *F2*-layer peaks was modified. After the maximum phase of the eclipse, a new $F1\frac{1}{2}$ ledge was formed and remained for a short time in addition to another ledge, at a greater height, which was also present on the control days.

Acknowledgements—The operation of the ionospheric recorder at Singapore was the responsibility of the Officer-in-Charge, Mr. G. H. BAZZARD.

The work described above was carried out as part of the programme of the Radio Research Board. The paper is published by permission of the Director of Radio Research of the Department of Scientific and Industrial Research.

REFERENCES

ALLEN C. W. 1948 Critical Frequencies, Sunspots and the Sun's Ultra-violet Radiation, *Terr. Mag. Atmos. Elect.* **53,** 433–448.

BIBL K. 1951 The Ionization of the *E* layer, its Measurement and its Relation with Solar Eruptions, *Ann. Geophys.* **7,** 208–214.

DELOBEAU F. 1953 The Solar Eclipse of 25th February 1952 at Gao, *Ann. Geophys.* **9,** 317–324.

ESTRABAUD S. 1952 Effects of the Solar Eclipse of 25 February 1952 on the Ionospheric *F2* Region over Equatorial Africa, *C. R. Acad. Sci. Paris* **235,** 1521–1523.

LEDIG P. G., GIESECKE A. A., JONES M. W., and CHERNOSKY E. J. 1946 Effects on the Ionosphere at Huancayo of the Solar Eclipse, January 25, 1944, *Terr. Mag. Atmos. Elect.* **51,** 411–418.

MINNIS C. M. 1955 Ionospheric Behaviour at Khartoum during the Total Solar Eclipse of 25 February 1952, *J. Atmosph. Terr. Phys.* **6,** 91–112.

MINNIS C. M. 1956a The Effective Recombination Coefficients in the *E* and *F1* Layers during the Solar Eclipse of 25th February 1952, *J. Atmosph. Terr. Phys.* **9,** 36–44.

MINNIS C. M. 1956b *Solar Eclipses and the Ionosphere,* Ed. W. J. G. Beynon and G. M. Brown. Pergamon Press, London, pp. 204–211.

NAKATA Y. 1950 Effects on the *F* regions of the Ionosphere of the Solar Eclipse of May 9, 1948, *Rep. Ionos. Res. Japan* **4,** 21–30.

PIGGOTT W. R. 1953 Ionospheric Measurements at Ibadan during the Eclipse of the Sun, February 25, 1952, *Proc. Mixed Commission on the Ionosphere,* August 1952, 42–50.

TROTTER D. E. and ROBERTS W. O. 1955 *Solar Activity Summaries II and III of* 1955 High Altitude Observatory, Colorado; Reports Nos. HAO 30, 31.

RESEARCH NOTES

Scatter-field strengths and large ion concentration

(*Received* 8 *February* 1957)

NUMEROUS studies have shown that the field strength well beyond the horizon at frequencies of 100–4000 mc/s varies only slightly with distance. Several hypotheses have been proposed to account for this phenomenon (CARROL, 1952; CARROL and RING, 1954; FEINSTEIN, 1951; GORDON and BOOKER, 1950).

Although the theories differ, they generally attribute the radio-wave propagation to minute perturbations or discontinuities or to a spatial gradient in the dielectric constant. These views are supported by a considerably body of meteorological measurements which reveal the existence of variations and sharp gradients in the refractive index of the lower atmosphere. The discontinuities presumably arise from turbulence and stratification in the troposphere.

VOL. 10 1957

Recordings of the received signal strength in beyond the horizon propagation display in general two distinct types of fading: fast and slow. The former has been associated with multipath propagation, and the latter with major changes in the meteorological situation. Attempts to correlate specific changes in the refractive index along the propagation path with variations in the depth or character of fading, however, have not been too successful.

The purpose of this note is to suggest that a better correlation might perhaps be found if the large ion concentration is compared with fluctuations in tropospheric "scatter" signal strengths. To explore this possibility further, a very preliminary comparison was made between the concentration of large ions and the atmospheric refractive index, both deduced as a function of altitude from observations taken at the same time.

Measurements of the meteorological variables had been made with an aerograph mounted on an aircraft instrumented for atmospheric conductivity and large-ion concentration measurements. Stepwise ascents were made through a given atmospheric volume, thus allowing the vertical distribution of the meteorological elements to be observed (SAGALYN and FAUCHER, 1954). Using the data obtained, the refractive index was determined as a function of altitude (Fig. 1). Measured values of the large-ion concentration as given by SAGALYN and FAUCHER, is also plotted in Fig. 1.

A similarity is apparent in the gross curves for large-ion concentration and refractive index as a function of altitude. In general, some correspondence between the two would have been expected since the meteorological conditions (pressure, temperature, humidity, degree of turbulence, etc., and their lapse rates with altitude) affecting the index of refraction also influence the concentration of large ions.

In general, the concentration of large ions in the troposphere is 10^2–10^4/cm^3, while their masses are about 10^{-15} g. Consequently, direct contribution to the refractive index is negligible.

Although the refractive index and large-ion concentration are not directly related,

it is conceivable that they both may be indicative of changes in more basic atmospheric parameters which influence signal strengths of the distant fields. In this connection, examination of the limited data available indicated that changes in the large ion concentration (N_+) are, at least on some occasions, much greater than those of the refractive index. In this sense, N_+ may be considered as more sensitive to changes in the basic meteorological elements than is the modified refractive index, N. In the altitude range

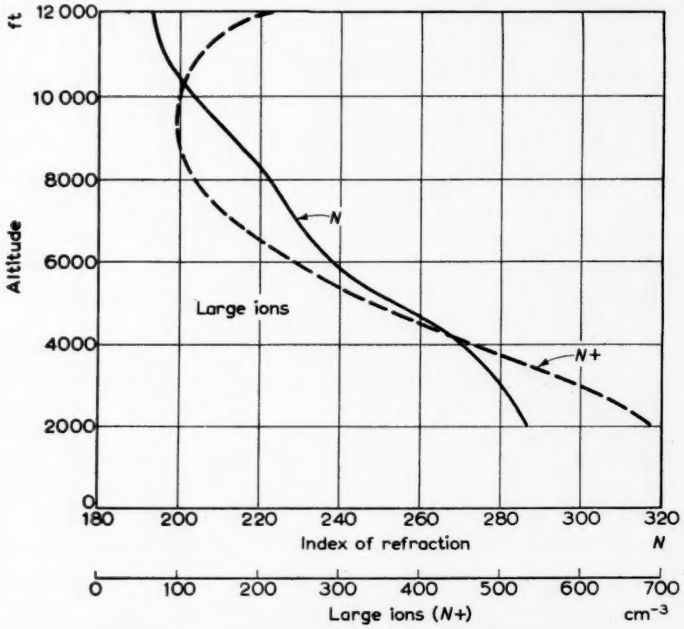

Fig. 1. Variation of large ions and modified index of refraction (N) with altitude.
2325–0125, Nov. 1953

from about 2000–10,000 feet, the relationship found between N and N_+ is

$$N = 210 + 0{\cdot}13N_+$$

for the data examined.

AVCO Research and Advanced Development Division S. C. Coroniti
Boston, Mass.
US National Committee for the IGY N. C. Gerson
National Academy of Sciences
Washington, D.C.

References

Carrol T. J. 1952 Internal reflection in the troposphere and propagation beyond the horizon. *Trans. I.R.E. PGAP*, 2, 9.

Carrol T. J. and Ring R. M. 1954 Normal tropospheric propagation of short radio waves well beyond the horizon. Lincoln Lab., MIT report, No. 38, Cambridge, Mass.

FEINSTEIN J.	1951	Tropospheric propagation beyond the horizon. *J. App. Physics* **22**, 1292.
GORDON W. E. and BOOKER H. G.	1950	A theory of radio scattering in the troposphere. *Proc. IRE* **38**, 401.
SAGALYN R. C. and FAUCHER G.	1954	Aircraft investigation of the large ion content and conductivity of the atmosphere and their relation to meteorological factors. *J. Atmosph. Terr. Phys.* **5**, 253–271.

The electron density in the *F2* layer and its correlation with the solar activity

(*Received* 7 *January* 1957)

A USUAL assumption in the study of the ionospheric electron densities is that of a linear dependence of the running twelve-months mean of the monthly median values of the maximum electron density N (proportional to the square of the critical frequency) upon the running twelve-months mean of WOLF's number R.

VOL. 10 1957

An extensive study of the worldwide distribution of the electron density in the *F2* layer led us to some more definite conclusions: the complete results will appear as soon as possible.

We used the median values of f_0F2 taken from the "ionospheric data" of the National Bureau of Standards for twenty observatories, whose series of data are complete for the decreasing stage of the last solar cycle (at most, two or three not contiguous values are missing); in regard to WOLF's number we used the values of Zurich; moreover, we also considered the series of the areas of hydrogen filaments and flocculi, evaluated at the astrophysical Observatory of Arcetri, respectively indicated A_F and A_ϕ. We obtained the series of values representing the secular behaviour of N, R, A_F, A_ϕ, which we indicate as $\bar{N}$, $\bar{R}$, $\bar{A}_F$, $\bar{A}_\phi$, applying VERCELLI's method of periodical analysis to the series of the monthly values: we successively selected the waves of very high period (i.e. the secular variation) and that of twelve-months period, which we indicate as N_{12}.

Fig. 1 shows the graphs of $\bar{N}(\bar{R})$ for the various observatories, arranged according to the geomagnetic latitudes; the numbers within parentheses indicate the ordinate corresponding to the zero ordinate for every graph; the arrows indicate the date: for example 1-'50 indicates January 1950. Fig. 2 shows the graphs of $\bar{A}_F(\bar{R})$ and $\bar{A}_\phi(\bar{R})$.

The graphs show the following principal features: (1) the points are not distributed on a straight line: (2) a systematic discontinuity of the slope occurs about beginning of 1951 at the same time as the similar discontinuity in the behaviour of $\bar{A}_F$ and $\bar{A}_\phi$; (3) a noticeable correlation between $\bar{N}$ and $\bar{A}_F$, apparently greater in the northern hemisphere and increasing for increasing geomagnetic northern latitudes. On the other hand, we note that the graphs of $\bar{N}(\bar{A}_F)$ and notably that of $\bar{N}(\bar{A}_\phi)$ are not even straight lines, so that one is led to infer a multiple correlation between $\bar{N}$ and both $\bar{R}$ and $\bar{A}_F$.

In effect if one assumes a linear law $\bar{N} = N_0(1 + \beta\bar{R} + \gamma\bar{A}_F)$ and considers also the simpler laws $\bar{N} = N_0(1 + \alpha\bar{R})$ and $\bar{N} = N_0(1 + \delta\bar{A}_F)$, one obtains for N_0, α, β, γ, δ the values indicated in Table 1, which are calculated for the period January 1949–December

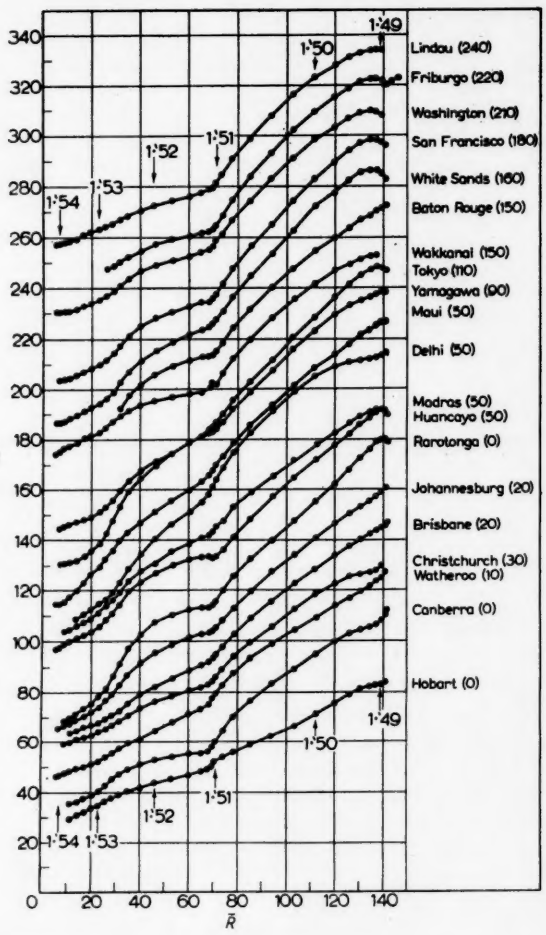

Fig. 1. Graphs of $\overline{N}(\overline{R})$; the points give the calculated values for the odd months.

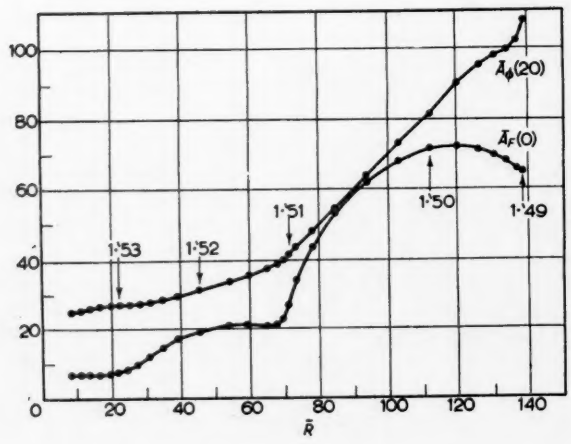

Fig. 2. Graphs of $\overline{A}_\phi$ $(\overline{R})$ and $\overline{A}_F(\overline{R})$; the points give the calculated values for the odd months.

1953; these values show the following principal features: (1) the values of N_0 are, in every case, approximately symmetrical with respect to the geomagnetic equator; (2) the coefficients α and δ are, as a whole, greater in the northern hemisphere and show a systematic tendency to increase with increasing values of the geomagnetic latitude; (3) the coefficients β are approximately similar in the two hemispheres, while the asymmetry between the northern and southern hemispheres appears more distinctly in the coefficients γ.

Table 1

Observatory	$\bar{N} = N_0(1 + \alpha\bar{R})$		$\bar{N} = N_0(1 + \delta\bar{A}_F)$		$\bar{N} = N_0(1 + \beta\bar{R} + \gamma\bar{A}_F)$			Latitude (rounded off)	
	N_0	α	N_0	δ	N_0	β	γ	geogr.	geomagn.
Lindau	16·1	0·039	23·2	0·046	19·0	0·016	0·030	52° N	53° N
Washington	19·1	0·035	26·8	0·041	21·5	0·018	0·022	39° N	50° N
San Francisco	21·5	0·036	31·1	0·041	23·8	0·023	0·016	37° N	44° N
White Sands	26·2	0·031	36·5	0·036	28·3	0·021	0·013	33° N	42° N
Wakkanai	24·6	0·026	33·6	0·032	27·8	0·013	0·018	45° N	35° N
Tokyo	32·7	0·025	43·1	0·032	34·3	0·019	0·009	36° N	26° N
Yamagawa	43·9	0·020	54·9	0·026	45·5	0·015	0·007	31° N	21° N
Maui	69·8	0·012	81·4	0·017	70·6	0·011	0·002	21° N	21° N
Delhi	56·9	0·016	68·4	0·022	58·8	0·012	0·006	29° N	19° N
Madras	53·3	0·013	61·6	0·019	53·1	0·012	0·003	13° N	4° N
Huancayo	40·2	0·018	49·5	0·024	41·2	0·015	0·005	12° S	1° S
Rarotonga	61·3	0·014	72·6	0·019	61·8	0·013	0·002	21° S	21° S
Johannesburg	39·1	0·018	49·0	0·024	39·8	0·016	0·004	26° S	27° S
Brisbane	32·1	0·020	41·0	0·026	34·0	0·015	0·008	27° S	36° S
Christchurch	20·5	0·028	27·5	0·034	22·0	0·017	0·015	33° S	38° S
Watheroo	28·2	0·023	36·0	0·028	29·8	0·016	0·009	30° S	41° S
Canberra	24·2	0·025	31·2	0·032	26·4	0·013	0·016	35° S	44° S
Hobart	24·2	0·017	29·8	0·023	24·5	0·015	0·003	43° S	52° S
		$\bar{\alpha} = 0·020$		$\bar{\delta} = 0·026$		$\bar{\beta} = 0·015$	$\bar{\gamma} = 0·009$		
		$\sigma_\alpha = 0·004$		$\sigma_\beta = 0·004$		$\sigma_\gamma = 0·002$	$\sigma_\beta = 0·003$		

If one assumes the mean values of α, β, γ, δ and the corresponding standard deviations σ_α, σ_β, σ_γ, σ_δ for the observatories of the southern hemisphere as "normal" values, it appears, from the table, that the greater values of α, δ, γ at higher latitudes may have some physical meaning: one could imagine some different dependence or "sensibility" of the two hemispheres to the activity of the hydrogen filaments (or to some other solar phenomenon strictly connected), while the dependence upon the sunspots appears about of the same amount in the two hemispheres.

At first sight, this asymmetry between the two hemispheres may be surprising; however, a further analysis of the component N_{12} shows some other interesting features: at 0000 LT, N_{12} exhibits a "normal" seasonal variation with a maximum at the June solstice and a minimum at the December solstice in the northern hemisphere, with a six-month phase-shift in the southern hemisphere and about the same amplitude at symmetrical geomagnetic latitudes; at 1200, instead, the component N_{12} exhibits very different amplitudes for symmetrical latitudes and a substantial phase-agreement with a maximum at the December solstice and a minimum at the June solstice, for latitudes between about 50° north and 30°–35° south; at higher southern latitudes, always at noon, N_{12} exhibits a tendency to a phase-shift of six months only during high solar activity.

These last features of N_{12}, which do not appear to be explicable either by assuming an extrasolar source of radiation or assuming only seasonal and diurnal effects of ionospheric tidal movements (superposed to the "normal" seasonal variation), suggest some more

VOL. 10 1957

complicated scheme of the geomagnetic control of the *F2* layer electron density; on the other hand, the asymmetric features of N_{12} appear to be correlated with the secular asymmetric effects connected with the activity of the hydrogen filaments. A possible cause of asymmetries might be sought in the unknown general circulation of the high atmosphere; however, at this stage, this possibility needs further observational evidence.

Istituto Nazionale di Geofisica F. MARIANI
Roma

LETTER TO THE EDITORS

The Q.L.–Q.T. transition level

(*Received* 31 *October* 1956)

In a recent paper on "The existence of a Q.L.–Q.T. transition level in the ionosphere and its experimental evidence and effect," published in *J. Atmosph. Terr. Phys.* **8**, 298–304, I stated at the end of paragraph 3, that the transition level "will actually reflect the (ordinary) wave downwards because of the steep gradient of μ_0 occurring there."

Dr. C. O. Hines of the Canadian Defence Research Board, in a letter dated 16 November 1956, has pointed out to me that the polarization of the O-mode immediately below this level is the same as that of the X-mode immediately above it and that consequently the O-mode should propagate across the transition level without hindrance, the changeover occurring, in fact, only in the name assigned to the wave.

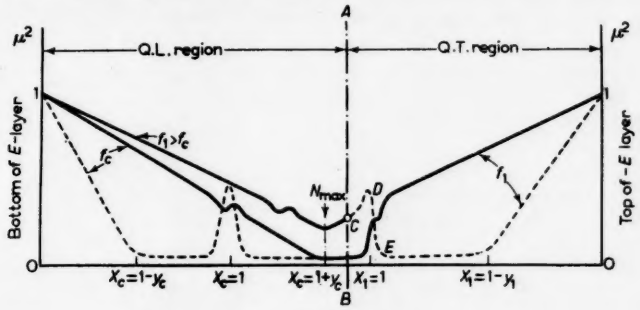

Fig. 1.

I should like to emphasize that this remark is correct as far as the sense of rotation of the field vectors is concerned. It is, however, easy to see (Lepechinsky, 1955) that if the Q.L.–Q.T. level is in the vicinity of $x = 1$ (where $x = 4\pi Ne^2/mp^2$), the axis ratios and tilts of the polarization ellipses of the O-mode immediately below the level and the X-mode immediately above it, are sufficiently different to imply a very rapid variation of the polarization of the wave when crossing the transition level. The absorption characteristics of the wave are similarly subjected to a very rapid variation. The steep gradients of the electron density N and of the collision frequency ν, occurring in the ionospheric region concerned, suggest that this rapid variation of the wave characteristics may take place there within a wavelength, and that consequently the transition level is, in this case at least, quite an efficient partial reflector.

However, if the Q.L.–Q.T. level coincides with a level of N corresponding to $x > 2 - x_T$ (Lepechinsky), the variation of the polarization on both sides of the transition level appears to be less pronounced, and Dr. Hines's statement seems to be justified: the O-mode below the level may become actually "coupled" to the X-mode above it and the Q.L.–Q.T. level may not be appreciably reflecting.

It is nevertheless important to note that even if *this latter assumption is entirely true*, a "crochet" *should* appear on the ionogram beyond the f_0E vertical tangent, when the E layer is plunged into the Q.L. region beyond its maximum ionization level; this "crochet" is then again an *evidence* of the existence of the transition level.

In order to make this point quite clear, let us consider the refractive indexes' μ_0 and μ_e

profiles across the E layer, in this particular case (see Fig. 1) In Fig. 1 the μ_0 profiles are represented by continuous lines and the μ_e profiles by dotted lines. It is assumed here that the distribution of the electron density N of the E layer is symmetrical about its N_{max} level.

Frequency f_c is the critical frequency of the E layer (according to the pure Q.L. type of propagation) and corresponds to a vertical tangent on the ionogram.

The O-mode refractive index profile for a frequency $f_1 > f_c$ extends up to point C of the line AB, representing the Q.L.–Q.T. transition level. If it is assumed that at C the O-mode is "coupled" to the X-mode, the initial O-wave will propagate further in the Q.T. region along the X-mode profile of the f_1 refractive index.

However, this profile falls sharply along DE, which implies a reflection of the wave at this level ($x_1 = 1$). Finally f_1 will be reflected downwards, and it is easy to see that the highest frequency thus reflected downwards will be a frequency f_T for which DE will coincide with AB. The upper frequency of the crochet should thus be f_T. It is clear that for still higher frequencies, the O-mode profiles in the lower and upper part of the E layer join up together and that consequently these frequencies are not reflected by the layer.

If the transition level AB coincides with that of N_{max}, the crochet should, in fact be a U-shaped trace the branches of the U being separated by $f_H/2$, because of the high retardation suffered by the upper frequencies of the crochet when the DE ($x_1 = 1$) reflection level approaches the N_{max} level.

However, if, as I suggested above, the O and X modes "coupling" is not operative near $x = 1$, the reflection should actually happen at the transition level AB, when this level is located in the vicinity of $x = 1$, and the crochet should then be terminated by a "hollow" due to high retardation and absorption near the N_{max} level.

Laboratoire National de Radioélectricité D. LEPECHINSKY
196, *rue de Paris, Bagneux, Seine, France*

REFERENCE

LEPECHINSKY D. 1955 La théorie magnéto-ionique et ses résultats. Note préliminaire, No. 185, du Laboratoire National de Radioélectricité.

Journal of Atmospheric and Terrestrial Physics, 1957, Vol. 10, pp. 245 to 250. Pergamon Press Ltd., London

The radio interference produced by corona discharge

M. I. LARGE
Cavendish Laboratory, Cambridge*

(*Received* 31 *January* 1957)

Abstract—The radio interference produced by corona discharge from a single point is investigated experimentally and theoretically.

1. INTRODUCTION

TRICHEL (1938) showed that corona currents in a point-to-plane gap are not continuous, but pulsed. When the point is negative, the pulses are often regular in form and time-separation. With the point positive, large irregular pulses occur, but only over a narrow range of currents. The subject of corona pulses is reviewed by LOEB (1948). The mechanism is discussed by AMIN (1954), and there are text-book accounts (MEEK and CRAGGS, 1953).

In thundery weather, many conducting "points," such as trees and radio aerials, discharge electricity into the air by the corona mechanism. This discharge is the source of the radio interference known as "rain static".

VOL. 10 1957

Corona from the high-tension lines and insulators of the grid system is a well-known source of radio interference. Previous work (GILL and WHITEHEAD, 1938; SAYERS, FORREST, and LANE, 1952) has been directed to obtaining empirical data on the interference produced by these lines in various weather conditions.

2. APPARATUS

A point-to-plane gap was used. Direct potentials of up to 50 kV could be applied to the plane. The "point" consisted of the clipped end of a piece of 48 s.w.g. copper wire. The radio noise was measured with an Admiralty-type B-28 receiver, run with a dummy load of 37 ohms, and the "point" connected to the aerial input. The corona current from the point was recorded by oscilloscope and galvanometer.

3. OBSERVATIONS

(a) *Band spectra.* At the onset of discharge from a negative point, the radio interference occurs as repeated "clicks" over the entire range of the receiver (60 kc/s to 30 Mc/s). Each click corresponds with one of the Trichel pulses.

As the corona current is increased (by increasing the potential on the plane) the pulse frequency passes from the audio-frequency range to the low radio frequencies, and the interference changes from a "clicking" or "whining" noise detectable on all frequencies to a hiss detectable about the pulse-repetition frequency, f_0, and its harmonics. The noise is concentrated in reasonably sharp bands about the lower harmonics, but the higher harmonics are less well defined. Some ten harmonics can usually be detected before the noise merges into a uniform spectrum.

It proved difficult to plot a typical spectrum directly, as the fundamental pulse frequency, f_0, drifted. A closely related effect is shown in the oscillograph

* Now at Jodrell Bank Experimental Station, University of Manchester.

record of Fig. 1. The receiver was tuned to 5 Mc/s and the detector output was recorded on moving film (upper trace). The corona current (lower trace) was then reduced steadily from 10 μA to zero. Looking from left to right across the record, the peaks in the detector output are produced as the pulse frequency passes through 5, 5/2, 5/3 Mc/s, etc., each of these frequencies having a harmonic at 5 Mc/s. The record shows clearly how the noise spectrum becomes uniform after the first few harmonics. It also confirms TRICHEL's observation that the pulse frequency is roughly proportional to the corona current.

Pulse repetition frequencies up to 10 Mc/s were observed before the gap broke down by sparking.

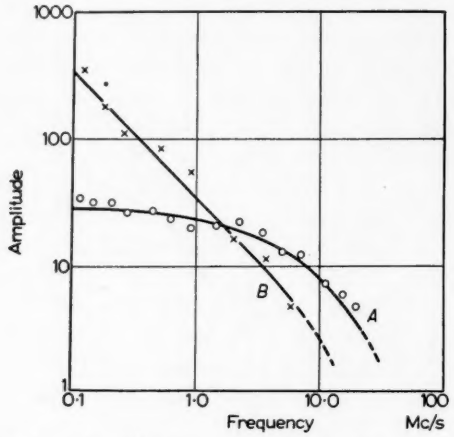

Fig. 2. Experimental graphs of the r.m.s. noise produced by negative corona, as a function of frequency. The amplitude scale is arbitrary.
Curve A—when the discharge is from the receiver aerial.
Curve B—when the discharge is from conductors near to the receiver aerial.

(b) *Continuous spectra.* Beyond about the tenth harmonic of the pulse frequency, f_0, the spectrum of negative-point corona becomes uniform, with harmonics barely distinguishable. Typical amplitude spectra are plotted in Fig. 2. (The pulse repetition frequency was a few kc/s; the receiver was calibrated with a signal generator.) Observations were made both when the point was connected to the receiver input (curve A) and when the noise was detected by an aerial placed near to the discharging point (curve B).

(c) *Positive point.* With a positive point, very little radio noise was produced for currents comparable with those used in the negative-point experiments, except over the narrow range of current where "inductive kicks" occur. These kicks, which occur irregularly a few times a second, produced considerable interference over the entire range of the receiver.

4. INTERPRETATION

(a) *Band spectra.* MACFARLANE (1949) has worked out the mean power spectra for a uniform sequence of pulses which

(i) jitter randomly in position,

(ii) jitter randomly in amplitude.

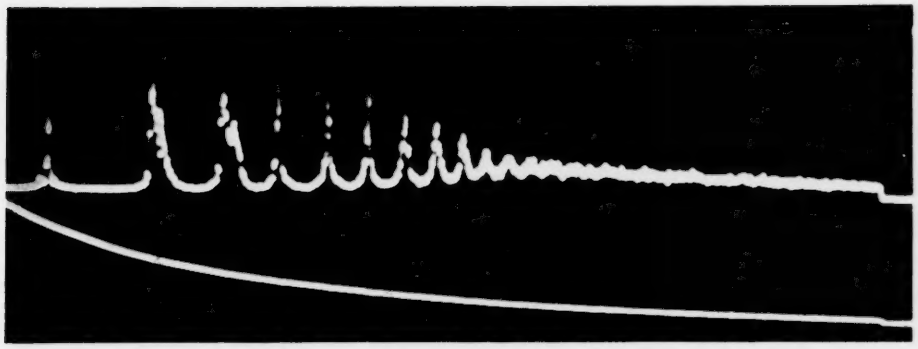

Fig. 1. A simultaneous oscillograph record of the radio interference produced by corona from a negative point (upper trace) and the corona current. The corona current is gradually reduced to zero, and the Trichel pulse-frequency falls roughly in proportion. The first peak in the receiver response is produced as the pulse frequency passes through the receiver-tuned frequency (5 Mc/s). Successive peaks are the receiver response to the nth harmonic of the pulse frequency as it passes through the nth submultiple of 5 Mc/s.

VOL.
10
1957

In each case he finds that the spectrum consists of fine lines at the harmonics of the pulse frequency, with an added continuous or "white" spectrum.

The present observations show clearly that a typical Trichel discharge has a line spectrum in which the higher-order lines are broadened, merging into a continuous spectrum. It is shown in Section 7 that such a spectrum is consistent with the assumption that the time-interval between Trichel pulses is subject to a random variation. This would be expected if the discharge mechanism proposed by AMIN (1954) and others is correct. At first sight it appears that jitter of the pulse interval is trivially different from case (i) above, but the two distributions lead to quite different spectra.

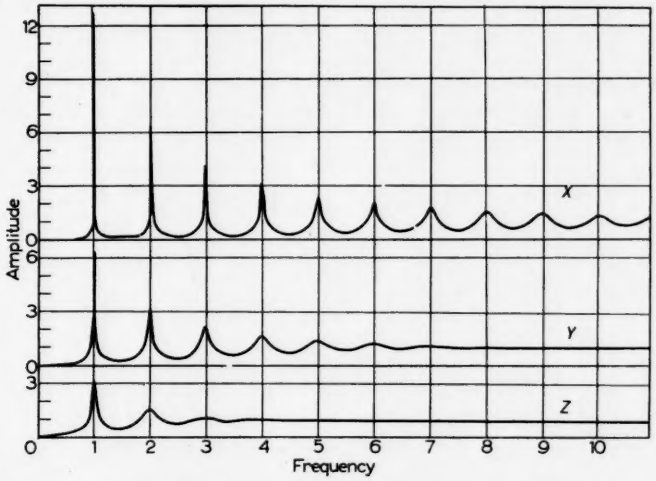

Fig. 3. Theoretical r.m.s. Fourier spectra for a sequence of unit impulses occurring at random intervals, distributed according to a Gauss law, with mean τ and standard deviation Δ. The frequency is plotted in units of $1/\tau$.
Curve X for $\Delta = \tau/40$
Curve Y for $\Delta = \tau/20$
Curve Z for $\Delta = \tau/10$

On the basis of the calculations in Section 7, typical spectra are plotted (Fig. 3). Qualitative comparison of the experimental observations with these curves indicates that for a Trichel discharge of mean pulse interval τ, the standard deviation of the pulse interval lies in the range $\tau/10$ to $\tau/100$. This result is confirmed by direct measurement of pulse intervals, from oscilloscope records.

(b) *Continuous spectra.* The curves in Fig. 2 are noise spectra for negative point corona in a region not complicated by the harmonics of the pulse-repetition frequency. It is shown in Section 7 that this continuous spectrum is determined by the power spectrum of the individual Trichel pulses. When the discharging point is connected to the receiver aerial (curve A), the noise is fairly constant up to some 10 Mc/s, and then falls rapidly with frequency. This is consistent with the observations of ENGLISH (1948) and others that the duration of a Trichel pulse is 10^{-7}–10^{-6} sec.

When the noise is detected by an aerial near the discharging point (curve B),

VOL. 10 1957

the spectrum falls roughly as the reciprocal of the frequency up to about 10 Mc/s, and then more rapidly. This is because the aerial is now responding to the *charge* pulse rather than the *current* pulse. The charge pulse in the present experiments was cleared from the gap in about 1 msec. It therefore appeared as a "step function" as far as radio frequencies were concerned.

With a positive point, only the rare "inductive kicks" produce any appreciable noise. The "self-sustaining burst pulses" (Meek and Craggs, 1953) produce interference several orders of magnitude less than that produced by Trichel pulses. It appears that a large proportion of the current in positive-point corona is a direct current, with the very small burst pulses superimposed.

5. Corona from Power Lines

Corona from power lines is a recognized source of radio interference. The corona occurs from a large number of points on the lines. Any effect due to individual pulse frequencies is obscured, and the interference appears to have a continuous spectrum. Since the receiver is now detecting the *charge* pulses produced by the corona, the general level of interference may be expected to depend on the reciprocal of the frequency (see Section 4). This is in agreement with the observations of Sayers, Forrest, and Lane (1952), who measured the actual interference from a test power line.

6. Rain Static

In stormy weather, radio aerials sometimes discharge into the air, and in principle all the effects described in Section 3 could be observed. In practice, discharge from a receiver aerial rarely passes far beyond the "onset" stage. The clicks have been thought to be rain-drops hitting the aerial. The difference in the effect of corona from a receiver aerial and from nearby conductors is strikingly illustrated by the example of television. Comparatively little corona from a television aerial ruins reception (Large and Pierce, 1955), whereas Sayers, Forrest, and Lane (*loc. cit.*) found that normal reception was possible a few yards from 300 kV power lines with considerable corona loss.

7. Mean Power Spectrum of a Sequence of Pulses of Random Interval

The Fourier transform of a sequence of N pulses of form $f(t)$ occurring at times $t = T_0, T_1, \ldots, T_{N-1}$, is given by

$$F(s) = \sum_{n=0}^{n=N-1} \exp(isT_n) \int_{-\infty}^{\infty} f(t) \exp(ist)\, dt$$

$$= k \sum_{n=0}^{n=N-1} \exp(isT_n) \qquad (1)$$

where k is the Fourier transform of a single pulse.

This equation refers to one sample of N pulses. The mean power spectrum for the distribution is thus given by

$$\overline{F(s)F(s)}^* = k^2 \overline{\left[\sum_0^{N-1} \exp(isT_n)\right]\left[\sum_0^{N-1} \exp(-isT_n)\right]} \tag{2}$$

In the present problem, the T_n are not completely random,* but are such that

$$T_{n+1} - T_n = \tau + \varepsilon_n \tag{3}$$

where τ is the mean pulse interval, and ε_n is the variation in the nth interval.

From (2) and (3) we obtain, by grouping the terms of the product,

$$\begin{aligned}\overline{F(s)F(s)}^* = {} & k^2N + k^2[(N-1)\exp(is\tau)\,\overline{\exp(is\varepsilon_1)} \\ & + (N-2)\exp(2is\tau)\,\overline{\exp[is(\varepsilon_1+\varepsilon_2)]} + \text{further terms}] \\ & + k^2 \text{ (complex conjugate)}\end{aligned} \tag{4}$$

The nth term in (4) may be evaluated by assigning a probability function to the ε_n. Suppose $p(\varepsilon)\,d\varepsilon$ is the probability that ε lies in the range ε to $\varepsilon + d\varepsilon$.

Then we have

$$\begin{aligned}&\overline{\exp(\varepsilon_1 + \varepsilon_2 \ldots \varepsilon_m)} \\ &= \int\int \ldots \int_{-\infty}^{\infty} \exp is(\varepsilon_1 + \varepsilon_2 \ldots + \varepsilon_m) p(\varepsilon_1)p(\varepsilon_2)\ldots p(\varepsilon_m)\,d\varepsilon_1\,d\varepsilon_2\ldots d\varepsilon_m \\ &= \left[\int_{-\infty}^{\infty} p(\varepsilon)\exp(is\varepsilon)\,d\varepsilon\right]^m\end{aligned} \tag{5}$$

since all the ε_n obey the same distribution law, and are all statistically independent.

This result may be substituted into (4) to give

$$\overline{F(s)F(s)}^* = Nk^2 \frac{1-P^2}{1-2P\cos s\tau + P^2} \tag{6}$$

assuming that $N \gg 1$, and that the ε_n are symmetrically distributed about zero. P is given by,

$$P(s) = \int_{-\infty}^{\infty} p(\varepsilon)\exp(is\varepsilon)\,d\varepsilon \tag{7}$$

the Fourier transform of $p(\varepsilon)$.

If the pulse intervals are Gauss distributed, with mean τ and standard deviation Δ, we have

$$p(\varepsilon) = \frac{1}{\sqrt{2\pi}\Delta} \exp -\tfrac{1}{2}\left(\frac{\varepsilon}{\Delta}\right)^2 \tag{8}$$

so that

$$P(s) = \exp(-\tfrac{1}{2}\Delta^2 s^2)$$

* If they were, then the problem reduces to the well-known two-dimensional Drunkard's Walk. This might well be called the "happy walk"; successive steps are not completely independent!

VOL. 10 1957

and (6) becomes

$$\overline{F(s)F(s)^*} = \frac{1 - \exp(-\Delta^2 s^2)}{1 - 2\exp(-\frac{1}{2}s^2\Delta^2)\cos s\tau + \exp(-\Delta^2 s^2)} Nk^2$$

$$= \frac{\sinh \frac{1}{2}\Delta^2 s^2}{\cosh \frac{1}{2}\Delta^2 s^2 - \cos s\tau} Nk^2 \tag{9}$$

The mean amplitude spectrum is thus given by

$$\sqrt{\overline{F(s)F(s)^*}} = k\sqrt{N}\left[\frac{\sinh \frac{1}{2}\Delta^2 s^2}{\cosh \frac{1}{2}\Delta^2 s^2 - \cos s\tau}\right]^{\frac{1}{2}} \tag{10}$$

In Fig. 3 are plotted typical mean amplitude spectra assuming the pulses to be unit impulses ($k = 1$), using the formula

$$G(s) = \left[\frac{\sinh \frac{1}{2}\Delta^2 s^2}{\cosh \frac{1}{2}\Delta^2 s^2 - \cos s\tau}\right]^{\frac{1}{2}}$$

Full spectra may be obtained by multiplying these curves by the spectrum of a single Trichel pulse.

Acknowledgements—The author thanks Dr. T. W. WORMELL and Dr. E. T. PIERCE for their interest and encouragement and Mr. R. BRUNDISH for invaluable assistance. He also thanks the Department of Scientific and Industrial Research for their maintenance grant.

REFERENCES

AMIN M. R.	1954	*J. Appl. Phys.* **25,** 210, 358, 627.
ENGLISH W. N.	1948	*Phys. Rev.* **74,** 170.
GILL A. J. and WHITEHEAD S.	1938	*J. Instn. Elect. Engrs.* **83,** 345.
LARGE M. I. and PIERCE E. T.	1955	*Quart. J. R. Met. Soc.* **81,** 92.
LOEB L. B.	1948	*J. Appl. Phys.* **19,** 882.
MACFARLANE G. G.	1949	*Proc. Inst. Radio Engrs.* **37,** 1139.
MEEK J. M. and CRAGGS J. D.	1953	*Electrical Breakdown of Gases* Clarendon Press, Oxford.
SAYERS D. P., FORREST J. S., and LANE F. J.	1952	*J. Instn. Elect. Engrs.* **99**(ii), 582.
TRICHEL G. W.	1938	*Phys. Rev.* **54,** 1078.

Journal of Atmospheric and Terrestrial Physics, 1957, Vol. 10, pp. 251 to 257. Pergamon Press Ltd., London

The dependence of point-discharge currents on wind as examined by a new experimental approach

M. I. LARGE* and E. T. PIERCE
Cavendish Laboratory, Cambridge

(*Received* 18 *December* 1956)

Abstract—Experiments are described in which a metal point mounted in the open air is artificially raised to a high potential V and the resulting point-discharge current I is measured. The relation

$$I = A(V - V_0)(W^2 + c^2V^2)^{\frac{1}{2}}$$

where A and c are constants, W the wind speed, and V_0 the onset potential, is found to fit the results reasonably well. It is shown that all point-discharge experiments may be interpreted in terms of the rapidity with which the ambient space-charge is removed; this removal may be by the wind or by the ion velocity in the surrounding field, and the relative importance of the two factors will vary from experiment to experiment. Finally, some remarks on the alti-electrograph results are appended.

VOL. 10 1957

1. INTRODUCTION

IT is well known that if a high electric potential gradient exists near a metal point, there is local breakdown, and a current flows from the point. This effect is familiar to electrical engineers under the name of "corona," but meteorologists, who are concerned primarily only with naturally occurring potential gradients, normally use the term "point-discharge." It has been shown (LARGE and PIERCE, 1955) that both point-discharge and corona are essentially the same phenomenon.

WHIPPLE and SCRASE (1936) obtained the relation

$$I = a(F^2 - M^2) \tag{1}$$

for an earth-connected point, where I is the point discharge current and F is the field at the ground. a and M are constants, having slightly different values for positive and negative fields. Relation (1) has the same form as that connecting current and voltage for laboratory experiments on corona (see, for example, PEEK, 1929).

In their experiments, WHIPPLE and SCRASE took no account of the wind, but in the past few years several workers have shown that wind has a pronounced effect on point-discharge, and that the WHIPPLE and SCRASE formula should be modified accordingly. The effect of wind on corona is familiar in other branches of physics; indeed, in wind-tunnel experiments, corona anemometers have long been in use by FUCHS (1954) and others.

Recent experiments on the influence of wind on point-discharge have followed two lines of approach. SEVILLE CHAPMAN (1956), working with a wind tunnel, used artificially produced winds and fields, most of the wind-speeds being far greater than any encountered in nature. Other researchers have carried out their experiments under natural fine-weather conditions, sufficient potential discontinuity to produce discharge being obtained by raising the point to a great

* Now at Jodrell Bank Experimental Station, University of Manchester.

height, either by means of a balloon (Chalmers and Mapleson, 1955), or by using a fixed mast (Kirkman and Chalmers, 1957). With this approach, it is often difficult to measure wind-speeds and fields at closely adjacent localities, and in consequence the intervention of space-charges may lead to widely scattered results.

It occurred to the authors that some of the objections to the above methods could be avoided by experiments in which a high potential is artificially placed on a point in the free atmosphere, so that discharge occurs in fine weather even if the point is close to the ground. The potential on the point, which is equivalent to a large natural field, can then be varied at will, nature providing a range of wind-speeds.

2. Experimental Technique

Direct potential of either sign up to 80 kV could be continuously provided by means of a small H.T. set. The voltage was measured by using a resistance chain and a microammeter, the possibility of error due to discharge from the resistors being eliminated by determining the current at both ends of the chain. The current flowing from the point was measured by means of a mirror galvanometer. The galvanometer casing and one terminal of the galvanometer were connected to the high-voltage output; the lead from the point to the galvanometer was the inner conductor of a length of coaxial cable, of which the outer sheath was connected to the H.T. voltage. The point, which consisted of a short length of platinum wire with a 0·05-cm-diameter spherical tip, was mounted in a special insulator at the top of a pole about 4 m high on the laboratory lawn. These arrangements were to ensure that all the current recorded by the galvanometer was in fact flowing from the point. The method worked well. When the point was removed from the insulator, no current at all could be detected on the galvanometer, even with the set running at its full 80 kV. A rotating cup-type anemometer, giving an integrated wind-speed with a time-constant of a few seconds, was mounted a few metres to the leeward of the point, at the same height.

3. The Observations

Under the conditions used, the onset potential for discharge was about 7kV. It was obvious that with a stable potential on the point, the wind was responsible for considerable variations of current. The point current appeared to respond almost instantly to fluctuations in the wind-speed, whereas the anemometer was more sluggish, effectively giving the wind-speed averaged over a few seconds. Direct readings of the point-discharge current and wind-speed were taken by two observers; the "current" observer selected periods of steady discharge current, and both the wind-speed and current were then recorded. This technique worked well, and in the course of a few hours it was possible to obtain a large amount of data. The experiments were most conveniently done by five people, two to act as observers, one to control the potential on the point, and two keeping watch to ensure that neither person nor animal approached the point and leads, which were at a dangerous voltage.

4. Experimental Results

For a period when the wind was very slight, it was found that the point-discharge current, I, for both positive and negative points was related to the potential, V, of the point by an expression of the form

$$I = B(V - V_0)V \qquad (2)$$

where V_0 is the onset potential, and B is a constant. It will be seen that this equation is very like the WHIPPLE and SCRASE relation (1).

In windy conditions, the main result of the observations was that the current from the point was a linear function of the wind, for wind-speeds above a few m/sec, and was independent of the wind at very low wind-speeds. Very similar results were obtained whether the point was positive or negative. This dependence on the wind-speed is shown in Fig. 1, where the experimental observations for

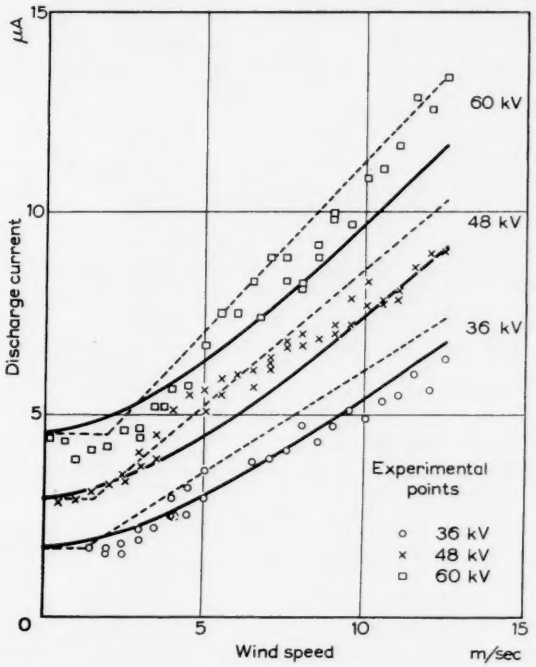

Fig. 1. Dependence of point-discharge current on the potential of the point and on the wind speed.

a positive point at 36, 48, and 60 kV are plotted. Each point on the graph is the mean of a number of observations. In spite of the averaging process there is still some scatter; this is not unexpected, as the observations were necessarily extended over several days, and were therefore subject to alterations in the condition of the point, with consequent "changes of regime" (see LARGE and PIERCE, 1955). On Fig. 1, besides the experimental points, two functions are plotted. These are

$$I = A(V - V_0) \,.\, (W^2 + c^2V^2)^{\frac{1}{2}} \tag{3}$$

which gives the continuous curves, and

$$\left.\begin{aligned} I = A(V - V_0) \,.\, [(W - W_0) + bV], \text{ for } W > W_0 \\ I = A(V - V_0) \,.\, bV, \text{ when } W \leq W_0 \end{aligned}\right\} \tag{4}$$

VOL. 10 1957

which yields the dotted straight lines; W is the wind-speed and W_0 an "onset" wind-speed. The parameters A and c in (3) and A and b in (4) are empirical constants chosen to give the best representation of the points.

In Fig. 2, the record from a field mill some 20 m from the discharging point is shown; the periods during which voltages were applied to the point are also

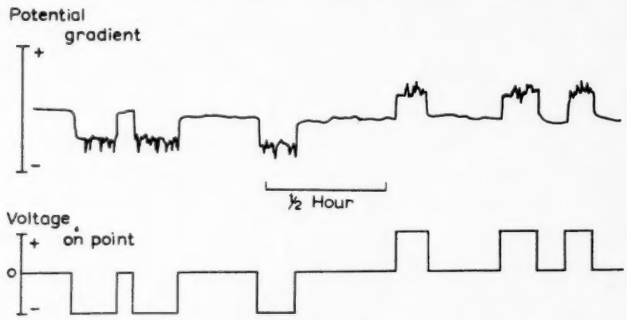

Fig. 2. Simultaneous records of the voltage on the point and the response of a field mill 20 m away.

indicated. Steady field changes due to the potentials on the point, together with superimposed fluctuations caused by the movement of space-charge produced at the point, can be recognized. This suggests an obvious experimental technique, in which air motions and turbulence might be traced by the diffusion of clouds of ions artificially produced at known rates. Such a technique would be somewhat similar to that employed by Cramer, Gill, and Record (1954), in which the movements of aerosols due to pollution are detected by arranging for the aerosols to be artificially charged at their source.

5. Comparison with Previous Experiments

Chapman (1956) suggests that I and V are best related by a formula such as

$$I = A \,.\, (V - V_0) \,.\, v \tag{5}$$

where "v" is the "ion velocity." His idea is that the current depends on (a) the point potential and (b) the clearance time for the ions produced in the discharge. In still air, the ion velocity is due entirely to the ion mobility in the field, so that "v" is proportional to V, giving

$$I = B \,.\, (V - V_0)V \tag{6}$$

where B is a constant; relation (6) is identical with (2) and very like the Whipple and Scrase formula (1). In moving air, however, "v" depends on the "mobility velocity" of the ions, and on the actual wind-speed. Chapman's experimental results, obtained in a wind-tunnel for wind-speeds in the range 18 to 260 m/sec, indicated that the current and the wind were related by an expression of the form

$$I = A \,.\, (V - V_0) \,.\, W \tag{7}$$

At the lower wind-speeds, corresponding to normal meteorological conditions,

the current seems to depend on a square law like (1) or (6), but CHAPMAN's observations are too scanty in the range 0–20 m/sec to show how and where the change over to a square law occurs.

KIRKMAN and CHALMERS (1957), in their experiments using a very high mast to study point-discharge under natural fine-weather conditions, arrived at the formula

$$I = k(W + C)(F - M) \tag{8}$$

where C and k are constants, F is the field at the ground, and M the "onset" field. Relation (8) may be compared with equations (3), (4), and (7) by writing F as V/h, i.e. considering the potential discontinuity at the point to be given by the product of the field at the ground and the point-height, h. (8) then becomes

$$I = A(V - V_0) \,.\, (W + C) \tag{9}$$

6. Application to Discharge in Natural Conditions

In all conditions, the current from a discharging point is determined by the rate of removal of space-charge from the vicinity of the point. This removal may be brought about in two ways; by the wind, with a velocity equal to that of the wind, and by the mobility of the ions in the ambient electrostatic field. Thus we expect a term in our relations combining the two factors. This has indeed been postulated by SEVILLE CHAPMAN (equations 6 and 7) and found by the present authors (equations 3 and 4). We are grateful to Dr. J. A. CHALMERS for pointing out that a vector addition of the wind and the ion "mobility velocity," as in equation (3), is most appropriate to natural conditions where the ion movement and the wind are normally at right angles.

The relative importance of these two factors depends critically on the experimental conditions. For CHAPMAN's experiments, where a high potential point was surrounded by the earthed walls of the wind-tunnel at a few feet distant, the field was large, so that the small ion "mobility velocity" was comparatively high. In consequence, wind-speeds had to be large before their effect was apparent.

In the experiments of KIRKMAN and CHALMERS, the ambient field was the fine-weather electrostatic field, typically 100 V/m, with a corresponding ion "mobility velocity" of about 1 cm/sec. Thus the wind factor became dominant at very low wind-speeds. For this reason, although the general argument would indicate that the "constant" C in equation (8) of KIRKMAN and CHALMERS should be directly proportional to the field F, it is not surprising that such a dependence was not detected.

Our own experiments were of intermediate character. In the fine-weather conditions in which we worked, the natural electrostatic fields were small, and the "clearance field" was effectively that produced between the high potential point and the surrounding earthed surfaces. This field was not as large as in the experiments of CHAPMAN and the wind began to control the current at relatively low wind-speeds. To summarize, we may say that in CHAPMAN's experiments the constant c (equation 3) was large, and in those of KIRKMAN and CHALMERS it was small, by comparison with our value.

VOL. 10 1957

7. Interpretation of Alti-electrograph Results

Seville Chapman (1956) has attempted to re-interpret the alti-electrograph results obtained by himself (1949) in America, and by Simpson and Scrase (1937) at Kew. Chapman assumes that ion "mobility velocities" in thunderclouds are much greater than the wind-speeds; his formula (6) is therefore applicable, and, since V is proportional to E, the natural field, may be approximately rewritten as

$$I = kE^2 \tag{10}$$

where k is a constant. This is similar in form to the Whipple and Scrase formula (1). Chapman, however, considers that k was overestimated in the Kew alti-electrograph work, a dependence on l^2 (l is the length of the trailing wire) being envisaged, whereas the true dependence is on l. Using his revised estimate, Chapman succeeds in finding fields of the order of 2000 V/cm in thunderclouds. He has, however, overlooked the fact that in the original work of Simpson and Scrase (1937) k was directly determined by observations at the instant the alti-electrograph left the ground. Thus it is difficult to see how Chapman's modified interpretation can be applied to the work at Kew.

It is now generally agreed that fields of the order of 2–3 kV/cm exist within thunderclouds; indeed, Simpson and Robinson (1941), in their model thundercloud, give such values, ascribing the small alti-electrograph figures to the particular tracks followed by many of the ascents. The most interesting feature, however, of the alti-electrograph results is not the actual magnitudes of the fields observed, but the absence of any indication of an appreciable increase of the field with height. This implies a constant current in the alti-electrograph as the balloon rises, and therefore any law relating point-discharge current to the field which does not change with height must yield a constant value of the field.

It is interesting to note that even in the work of Ross Gunn (1948), a trenchant critic of the Kew alti-electrograph results, there is strong experimental evidence that comparatively small fields exist, in thundery conditions, at considerable altitudes. Gunn, using a field mill in horizontal flights at a height of 5000 ft, could not detect fields exceeding 200 V/cm. Since an accepted value for the field at the ground is 100 V/cm, this is only an increase by a factor of 2 in 5000 ft. Gunn also states that appreciable increases in field only occur when the cloud is entered, but it is not clear whether this applies only to entry from the sides or to entry from the base as well.

Thus, in spite of many attempts at solution (for information see Chalmers, 1954), the absence of agreement between experimental observations of the field variation with height under a thundercloud, and the theoretical predictions based on point-discharge studies of, for example, Whipple and Scrase (1936), remains one of the major unsolved problems of atmospheric electricity. It would be unfortunate if the criticism, much of it unjustified, of certain aspects of the alti-electrograph results were allowed to obscure this fact.

Acknowledgements—We are grateful to Miss S. M. Cussen and to Messrs. R. V. E. Brundish and R. Pilsworth for assistance with the experimental observations. We also desire to thank Mr. J. A. Ratcliffe and Dr. T. W. Wormell for reading

and commenting on this paper, and Miss S. M. CUSSEN for preparing the diagrams.

One of us (M. I. L.) wishes to acknowledge his tenure of a maintenance award from the Department of Scientific and Industrial Research while the work described in this paper was being carried out.

REFERENCES

CHALMERS J. A.	1954	*Reports on Progress in Physics* Vol. XVII. p. 101. Physical Society, London.
KIRKMAN J. R. and CHALMERS J. A.	1957	*J. Atmosph. Terr. Phys.* **10,** 258.
CHALMERS J. A. and MAPLESON W. W.	1955	*J. Atmosph. Terr. Phys.* **6,** 149.
CHAPMAN SEVILLE	1956	Cornell Aeronautical Laboratory, Report No. C.A.L. 68.
CHAPMAN SEVILLE	1949	*Phys. Rev.* **75** 1333.
CRAMER H. E., GILL G. C. and RECORD F. A.	1954	Mass. Inst. Tech. Report under Contract No. AF-19(604)—145.
FUCHS W.	1954	*Z. Physik* **137,** 49.
GUNN ROSS	1948	*J. Appl. Phys.* **19,** 481.
LARGE M. I. and PIERCE E. T.	1955	*Quart. J. R. Met. Soc.* **81,** 92.
PEEK F. W.	1929	*Dielectric Phenomena in High Voltage Engineering* McGraw-Hill, New York.
SIMPSON G. C. and ROBINSON G. D.	1941	*Proc. Roy. Soc.* **A177,** 281.
SIMPSON G. C. and SCRASE F. J.	1937	*Proc. Roy. Soc.* **A161,** 309.
WHIPPLE F. J. W. and SCRASE F. J.	1936	*Met. Off. Geophys.* Mem. No. 68.

VOL. 10 1957

Journal of Atmospheric and Terrestrial Physics, 1957, Vol. 10, pp. 258 to 265. Pergamon Press Ltd., London

Point discharge from an isolated point

J. R. KIRKMAN and J. ALAN CHALMERS
Physics Department, Durham Colleges in the University of Durham

(*Received* 11 *January* 1957)

Abstract—The point-discharge current I from an isolated point at 27-m and 34-m height was measured and related to the wind-speed W and the potential gradient F at the ground at 47 m to windward, and also to the output of an agrimeter 7 m below the point.

The results were related by $I = K(W + c)(F - M)$, and it is shown that a formula of a similar type also fits earlier results which had previously been thought to obey a square law for I against F.

1. INTRODUCTION

THE phenomenon of point discharge in atmospheric electricity occurs at trees and other exposed points when the atmospheric potential gradient becomes sufficiently great. The lines of force, concentrating on the point, give a field strength in a limited region which is sufficient to produce ionization by collision, so that extra ions of both signs are formed, beyond those which are normally present. The ions of the same sign as the potential gradient flow into the point and give a current considerably greater than the normal conduction current, while the ions of the other sign move upwards and form a space charge. The actual value of the point-discharge current depends upon the nature and situation of the point, the potential gradient, the rate of removal of space charge and perhaps on other factors.

Observations having shown a relation between point-discharge current and potential gradient, SIMPSON and SCRASE (1937), followed by SIMPSON and ROBINSON (1940) and CHAPMAN (1952), attempted to use this to measure potential gradients below, in and above thunder clouds. They sent up balloons with points attached at different heights and made measurements of the current in the wire connecting the points. Some of the conclusions from these measurements were not in agreement with other measurements of potential gradients in and near thunder clouds (GUNN, 1948), and the basic assumptions of the method were questioned; in particular, doubt has been raised as to whether the relation between point-discharge current and potential gradient, as found for a point at the same height as a tree, is applicable to points attached to a balloon.

Suggestions have been made that the true relation between point-discharge current and potential gradient could be obtained by laboratory investigations. However, the conditions are so different that this is not so; the space charge, mentioned above, quickly reaches an electrode in laboratory experiments, whereas in the atmosphere it must travel much farther and produces greater effects; also, wind has an effect in the atmosphere, and this is usually not included in laboratory investigations.

The conditions of a point attached to a balloon are much closer to those of an

isolated point than to those of a point at the same height as neighbouring points. Also, if a point is raised well above other, natural, points it will give point discharge at lower values of potential gradient, which means not only more frequent opportunities of measurement but also that conditions are steadier. CHALMERS and MAPLESON (1955) used a point attached to a captive balloon, but found that observations could be carried out only at low wind-speeds. It therefore seemed desirable to investigate the relation between point-discharge current, potential gradient and wind-speed for a point on a fixed mast at a height well above surrounding trees.

2. PREVIOUS RESULTS

WHIPPLE and SCRASE (1936) measured the current through a point at about the same height as the neighbouring trees and also the potential gradient at the ground nearby, during a few thunderstorms, and found the relation:

$$I = a(F^2 - M^2) \tag{1}$$

where I is the point-discharge current, F the potential gradient, and a and M are constants. CHIPLONKAR (1940) and YRIBERRY (1954) found agreement with this result; HUTCHINSON (1951) also obtained results in general agreement with (1), but found "humps" and also a tendency towards a first-power law for high values of potential gradient.

VOL. 10 1957

CHALMERS (1952) showed that (1) can be deduced theoretically if it is assumed that there is no effect of wind, so that ions are removed from the neighbourhood of the point solely by electric forces. For a system of points close together, it might be expected that the effects of wind would be only to remove ions from above one point to above another point and so to produce little alteration in electrical conditions.

With a single, isolated, point which is the only one to give discharge under the conditions at the time, matters are different and the wind is bound to produce an effect. CHALMERS and MAPLESON (1955) showed theoretically that:

$$I = K V^{q-1} W^{3-q} \tag{2}$$

where V is the potential difference between the point and its surroundings, W the wind-speed and q a number not determined by the theory.

CHALMERS and MAPLESON (1955) measured the current from a point attached to a captive balloon, and found the relation:

$$I = K(Fh)^{7/4} W^{1/4} \tag{3}$$

where h is the height. This agrees with (2), since, in the absence of space charge, $V = Fh$. This gives a value of q of 2·75.

CHAPMAN (1956) suggested that the correct relation should be:

$$I = k(V - V_0)v \tag{4}$$

where V_0 is the threshold potential for discharge to take place, and v is the velocity of the ions, due either to the electric field or to the wind, according to conditions. He verified this formula from measurements on point-to-plane discharge in the

laboratory, discharge in a wind tunnel, and discharge from a point attached to an aeroplane. In the absence of wind, (4) assumes a form similar to (1) and in strong winds a form similar to (2), with $q = 2$.

LARGE and PIERCE (1957) also verified CHAPMAN's formula by measurements on the current through a point maintained at a high potential in the atmosphere; here, v was taken as the vector sum of velocities W, the wind-speed, and a term proportional to V, the potential of the point, the two being assumed to be at right angles.

3. APPARATUS AND MEASUREMENTS

To support the point, a triple-braced pole structure was erected, carrying a 5 m single-pole extension at the top. The original height was 27 m, but this was later extended to 34 m. The point was a stainless-steel rod 0·15 cm in diameter, tapering to a radius of 0·002 cm at the tip, and 1·75 cm long; this was connected to a measuring galvanometer by coaxial cable.

A simple field mill (MAPLESON and WHITLOCK, 1955) was constructed and set up, inverted to avoid effects of rain, at 47 m to the west of the mast, and readings were only taken when the wind was in a westerly direction, so that charge liberated in the point-discharge process would not affect the field mill. Since it was to be expected that the potential gradient recorded by the field mill would be of the same sign as the point-discharge current, no sign discriminating device was used with the field mill, but sign changes could be recognized as the output reached zero. The rectified output from the field mill was recorded by a galvanometer.

A scaled-down agrimeter (CHALMERS, 1953) was set up on the mast 7 m below the point. The output from this also passed through a recording galvanometer.

The wind-speed was measured by the rectified output from a generating anomometer set up 2 m below the point.

The galvanometer deflections were recorded photographically on a drum camera of speed usually 6 cm per min; at 10-sec intervals the background of the record was fogged for 1 sec, and the recordings were usually averaged over the period between two such markings. Fig. 1 gives a portion of a typical record.

4. OBSERVATIONAL RESULTS

Not all of the records were suitable for analysis, and it was necessary to reject portions of records in which there were violent and rapid changes in point-discharge current, potential gradient, wind-speed or wind direction, for example in thunderstorms.

There remained for analysis 1500 10-sec periods at 27 m and 600 at 34 m. In each case, the results were subdivided into wind-speed groups of approximately 1·25 m/sec width, and the variation of current with potential gradient could be investigated for each.

The potential gradient used could be either that measured at the ground at 47 m to windward or that measured by the agrimeter 7 m below the point.

For the potential gradient at the ground, the results show for each range of wind speed that:

$$I = C(F - M) \tag{5}$$

where C and M are constants. Fig. 2 shows an example of this. For the same height of point, M was found to be the same for all wind-speeds.

Fig. 3 shows the variation of C with wind-speed, which was found to be linear up to 33 m/sec, giving the final relation:

$$I = K(W + c)(F - M) \tag{6}$$

VOL.
10
1957

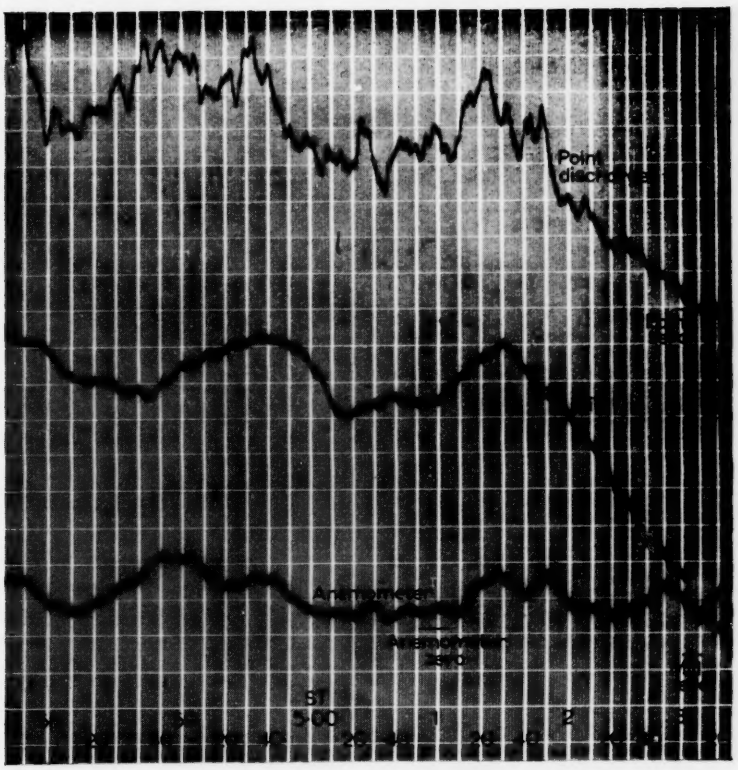

Fig. 1.

VO
1
19

If I is in μA, W in m/sec, and F and M in V/m, the observations give:
at 27 m,

$$I = 1{\cdot}16 \times 10^{-4}(W + 4)(F - 295) \quad (7)$$

and at 34 m,

$$I = 2{\cdot}18 \times 10^{-4}(W + 6{\cdot}8)(F - 220) \quad (8)$$

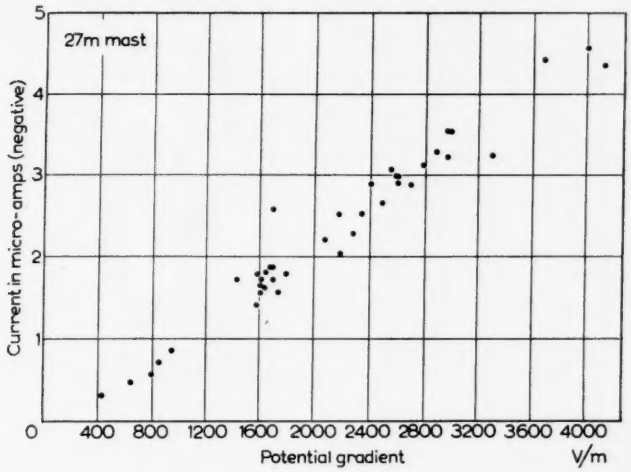

Fig. 2.

VOL. 10 1957

These results were all obtained with negative currents down through the point, as insufficient results were obtained with positive currents. At 34 m there were indications of a lower value of K and a value of M of about 250 V/m for positive currents.

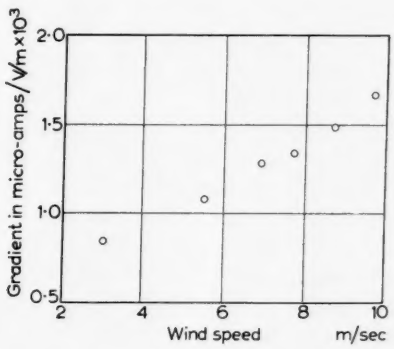

Fig. 3.

Since no absolute calibration could be obtained for the readings of the agrimeter 7 m below the point, the results cannot be expressed in such a definite form as (7) or (8), but they agree with (6) and show, as might be expected, much less scatter.

When the potential gradient and point-discharge current become high, the

variation of I with F ceases to be linear, because of complications produced by point discharge occurring at points lower than the mast and to windward of the field mill. These ions travel with the wind and reduce the measured potential gradient at the mill, sometimes even reversing the sign. Throughout such periods, the agrimeter 7 m below the point showed the usual linear relationship with the point-discharge current. In one particular case shown in Figs. 4 and 5, an interesting comparison was made of the current, mill output and agrimeter output over a period of nearly constant wind-speed. The current altered rapidly from zero to

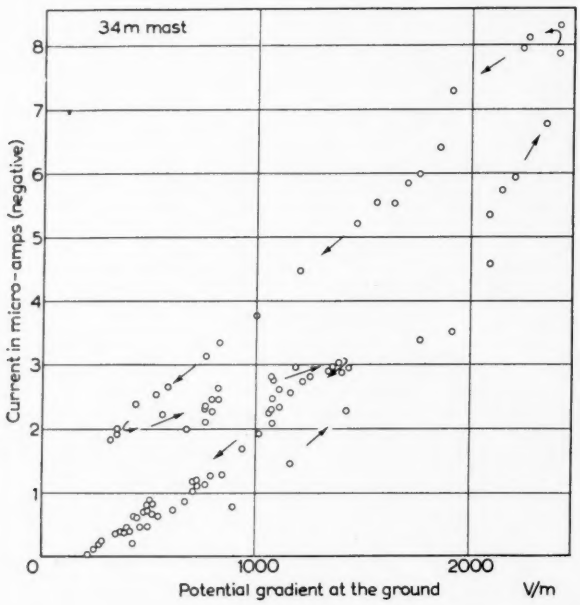

Fig. 4.

-7 μA in under 2 min, during which time the ratio of the mill and agrimeter outputs remained constant. When the potential gradient, as measured by the mill, reached about -2200 V/m, the positive ions liberated at trees, etc. to windward caused a shift of about 750 V/m in the mill-current curve, while the agrimeter-current curve remained unaffected; this shift persisted until the current had fallen to -2 μA, by which time no more ions were being produced to windward and all the charges had moved away.

5. Discussion

The results show good agreement with Chapman's (1956) formula, except that the ratio of the constants K for the two heights is not equal to the ratio of the heights, as would be expected if I depends on V, the potential; no satisfactory explanation of this discrepancy can be suggested.

If the results (7) and (8) are expressed in terms of V, the constants are $4{\cdot}3 \times 10^{-6}$ and $6{\cdot}3 \times 10^{-6}$, to be compared with CHAPMAN's value of 14×10^{-6}; since it is to be expected that the shape of the point must have an influence on the constants, this divergence is not serious. In the present work, V_0 is found to be $8{\cdot}0 \times 10^3$ and $7{\cdot}4 \times 10^3$ V, to be compared with CHAPMAN's value of $6 \pm 4 \times 10^3$ V and LARGE and PIERCE's (1957) value of about 7×10^3 V.

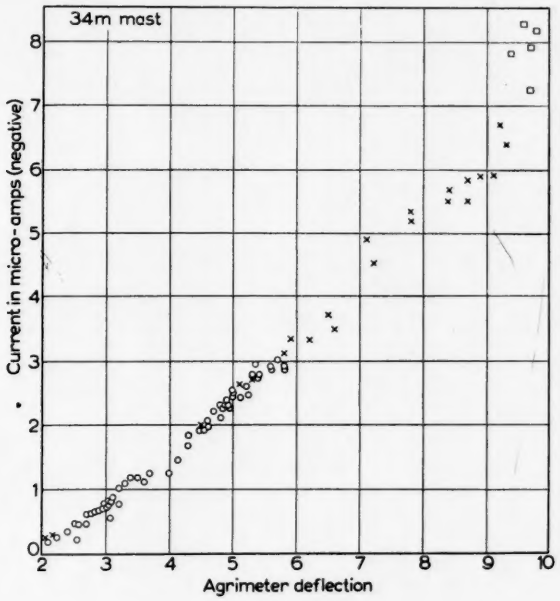

Fig. 5.

LARGE and PIERCE (1957) have discussed the use of results such as the present on the interpretation of the alti-electrograph records and, in view of the complete agreement of the present authors with that discussion, the matter will not be dealt with here, except to emphasize that the original aim of the alti-electrograph was to obtain the sign, rather than the magnitude, of the potential gradient at various points in the cloud, and any discussion or criticism of the interpretation of alti-electrograph records as measuring the magnitudes of the potential gradients cannot in any way detract from the accuracy and importance of the sign measurements, giving the location of the main charges in the cloud.

When WHIPPLE and SCRASE (1936) compared their results with the square-law (1), they were influenced by the fact that laboratory measurements gave such a law. But the present and other results have shown that atmospheric measurements do not agree with (1) in certain cases, so it seemed desirable to re-analyse the earlier results, and the published results of WHIPPLE and SCRASE (1936) and of HUTCHINSON (1951) were analysed statistically to fit a formula:

$$I = B(F - M)^n \tag{9}$$

VOL. 10 1957

using the values of M as found by these authors and finding the best values of n. This gave, for Whipple and Scrase's results, $n = 1{\cdot}07 \pm 0{\cdot}13$, and for Hutchinson's, $n = 1{\cdot}09 \pm 0{\cdot}06$, using negative currents in both cases. In both cases, a test by the method of least-squares showed that (9) with the above values of n gave a better fit than (1). The closeness of these values to 1 suggests that Chapman's (1956) formula (4) is applicable rather than (1); referring to the theory, it would seem that wind must be important even in these cases. If there were no correlation between potential gradient and wind and if Chapman's formula is correct, then (9) would hold with $n = 1$. But if there is a tendency for higher wind-speeds and higher potential gradients to be associated together, then an analysis without using wind-speed would give n greater than 1, and an analysis of the present results in terms of (9) gives $n = 1{\cdot}05 \pm 0{\cdot}10$.

Acknowledgements—The research reported here has been sponsored by the Geophysics Research Directorate of the Air Force Cambridge Research Center, Air Research and Development Command, United States Air Force under Contract No. AF 61(514)-743-C, through the European Office ARDC.

The authors also wish to express their thanks to Mr. J. E. Maund, B.Sc., for much assistance.

References

Chalmers J. A.	1952	The relation between point discharge current and field. *J. Atmosph. Terr. Phys.* **2,** 292–300.
Chalmers J. A.	1953	The agrimeter for continuous recording of the atmospheric electric field. *J. Atmosph. Terr. Phys.* **4,** 124-128.
Chalmers J. A. and Mapleson W. W.	1955	Point-discharge currents from a captive balloon. *J. Atmosph. Terr. Phys.* **6,** 149–159.
Chapman S.	1952	Thundercloud electrification studies—II. Report No. VC-603-P-1 to U.S. Office of Naval Research.
Chapman S.	1956	Electrostatic field measurements, corona discharge and thunderclouds. Report C.A.L. vol. 68 (Buffalo, N.Y.: Cornell Aeronautical Lab.).
Chiplonkar M. W.	1940	Measurement of point-discharge current during disturbed weather at Colaba. *Proc. Indian Acad. Sci.* **A12,** 50.
Gunn R.	1948	Electric field intensity inside of natural clouds. *J. Appl. Phys.* **19,** 481–484.
Hutchinson W. C. A.	1951	Point-discharge currents and the earth's electric field. *Quart. J. R. Met. Soc.* **77,** 627–632.
Large M. I. and Pierce E. T.	1957	The dependence of point-discharge currents on wind as examined by a new experimental approach. *Quart. J. R. Met. Soc.*
Mapleson W. W. and Whitlock W. S.	1955	Apparatus for the accurate and continuous measurement of the earth's electric field. *J. Atmosph. Terr. Phys.* **7,** 61–72.

Simpson G. C. and Robinson G. D.	1940	The distribution of electricity in thunderclouds—II. *Proc. Roy. Soc.* **A177,** 281–329.
Simpson G. C. and Scrase F. J.	1937	The distribution of electricity in thunderclouds. *Proc. Roy. Soc.* **A161,** 307–352.
Whipple F. J. W. and Scrase F. J.	1936	Point discharge in the electric field of the earth. *Geophys. Mem., Lond.* **68,** 1–20.
Yriberry A. J.	1954	Registro del campo electrostatico tormentoso en San Miguel (Argentina) y en Kew (Inglaterra). *Acta Scient. San Miguel Obs. de Fis. Cos.* No. 2.

VOL.
10
1957

Journal of Atmospheric and Terrestrial Physics, 1957, Vol. 10, pp. 266 to 287. Pergamon Press Ltd., London

Atmospheric waveforms with very low-frequency components below 1 kc/s known as slow tails

F. HEPBURN
Physics Department, Nottingham University

(*Received* 7 *March* 1957)

Abstract—Extensive observations are described of the form, magnitude, quasi-period, and delay relative to the high-frequency component of the slow tails of atmospheric waveforms and the variations with time of day and propagation distance. Theoretical considerations of possible source conditions and propagation characteristics fit the observations. They show that the observed linear dependence of the temporal parameters on distance can yield a constant height and conductivity of the equivalent homogeneous ionospheric layer independent of distance, but with different values for day and night.

1. INTRODUCTION

VERY low-frequency components of atmospheric waveforms have been reported by APPLETON, WATT, and HERD (1926) and studied by WATSON-WATT, HERD, and LUTKIN (1937). These initial detailed observations of the slow tail, which was found to consist of "a first quasi half-cycle which may be followed by a second and later half-cycles of sensible or negligible amplitude," are assumed to refer to day-time recording. They were given in terms of two parameters: the delay t as the time between the beginnings of the high-frequency oscillatory and slow-tail portions of the waveform and the half-period $\tau/2$ as the duration of the first half-cycle of the slow tail. Their average quarter period and delay variations with distance are included in Figs. 5 and 6 for comparison. Slow tails were reported on waveforms from discharges as close as 100 km and their quasi periods were considerably larger than those from storms at two or three times this range. In describing the development of atmospheric waveforms with increasing distance, APPLETON and CHAPMAN (1937) also reported the appearance of a slow tail at about 100 km which separated from the high-frequency portion as the propagation distance increased beyond 200 km, indicating considerably different group velocities for the high- and low-frequency components of the waveform. They suggested its possible connection with their c portion of the field change, due to a continuing current in the discharge channel. WATSON-WATT *et al.* (1937) also indicated the fundamental difficulty in explaining the division of some waveforms into discrete high- and low-frequency portions; this requires a gap in the frequency spectrum at the source or selective absorption of frequencies between 1 and 5 kc/s in propagation. BRUCE (1941) attributed the slow tail to the radiation fields of both a and c portions of the field change and so attempted to explain the observations of slow tails commencing before the oscillatory part, and calculated amplitudes in rough agreement with the values of WATSON-WATT. However, neglect of the much greater electrostatic and induction fields at the distance considered vitiates the argument and the agreement appears largely fortuitous. Moreover, the radiation pulses from the a and c portions

of the field change are of opposite sign and would not combine to give a slow tail in the form of a single half-cycle.

HALES (1948) studied the problem in terms of wave-guide mode propagation. Radio propagation in the atmosphere bounded by the conducting earth and ionosphere is an application of wave-guide theory to a wave-guide consisting of only two infinite, parallel, imperfectly conducting boundaries. RYDBECK (1944) showed that for low-order mode propagation the assumed form of ion-density variation with height exercises little influence, so that the approximation of a sharply bounded homogeneous ionosphere is justifiable. HALES obtained group velocities and attenuation coefficients for quasi zero-order mode propagation of the frequencies below 2 kc/s in terms of parameters γ and k, defined by $\gamma = c\tau/2\pi h$ and $k = (c/4\pi h)^{\frac{1}{2}} .(\sigma_e^{-\frac{1}{2}} + \sigma_i^{-\frac{1}{2}})$, where c is the velocity of light, h the height of the ionospheric layer, σ_e and σ_i the earth and ionosphere conductivities, and τ the period of the signal. Assuming the ionospheric layer to begin at 60 km, application of the theory to WATSON-WATT'S observations of slow-tail period and delay gave values of ionospheric conductivity increasing linearly with storm distance beyond 1000 km. This was attributed to the reception of slow tails from distant sources only on occasions when the attenuation was low and the conductivity correspondingly high. More recent and comprehensive theoretical work by BUDDEN (1951) has shown the possible comparable contribution from propagation in the mode of order -1, but doubt exists about the excitation of negative-order modes (private communication). Calculated attenuation curves for propagation in the 0- and -1-order modes both indicate high daytime absorption of frequencies between 1 and 5 kc/s and considerably less absorption over a narrower band at night. CHAPMAN and MACARIO (1956), recording atmospherics with an audio-frequency spectrometer having band-pass filters covering the range 40 c/s to 16 kc/s, have largely confirmed these curves experimentally.

VOL. 10 1957

The present paper gives the results of more comprehensive, recent observations of slow-tail waveforms and their theoretical explanation in terms of source and propagation effects which lead to consistent estimates of conductivity for the equivalent homogeneous ionospheric layer under day and night conditions. It is a detailed account of the results and analysis yielding the preliminary conclusions published earlier (HEPBURN and PIERCE, 1953).

2. EXPERIMENTAL DETAILS

Previous papers have described adequately the low noise-level, open site at Cambridge with the Wilson sphere vertical aerial system (WILSON, 1920) and the associated audio-frequency amplifier and recording system (HEPBURN and PIERCE, 1954). Most of the waveforms discussed were recorded during the winter months of 1949/50 and 1950/51 between 0600 and 2130 hr, when the willing services of the Sferics organization of the Meteorological Office were available for the approximate location of the origin (i.e. fixing) of many individual waveforms. These were supplemented by various night-time recording periods when estimates of source position were available from specially arranged Sferics runs, extrapolation from the results of routine operation, or the direction-finding plus tuned-receiver apparatus operated by Dr. BOWE of the Cavendish Laboratory Radio Group

(BOWE, 1951). The origins of a group of waveforms beyond the 3000 km range of the Sferics organization have been estimated from waveform shape and analysis based upon the pulse-reflection theory (HEPBURN and PIERCE, 1954).

For the present investigation of slow-tail waveforms, defining parameters analogous to, but not identical with, those of WATSON-WATT *et al.* (1937) have been used. WATSON-WATT defined the beginning of the slow tail as the first detectable departure from the mean position. Because of the indeterminate beginnings of many of the slow tails, especially in daytime, an arbitrary criterion was chosen for defining their commencement. This was the beginning of the sinusoidal half-cycle whose form best fitted the first half-cycle of the slow tail. The interval from the triggering of the apparatus by the start of the high-frequency oscillatory portion of the waveform up to this defined point is taken as measuring the delay t of the slow tail, and the quarter period of this sine wave is taken as the quarter period $\tau/4$ of the slow tail. The separation $s = t + \tau/4$ refers to the initial high-frequency oscillation and low-frequency peaks, assuming no oscillatory portion of the waveform occurs before the triggering of the apparatus. Thus the separation is the only temporal measurement directly comparable with the earlier observations. Delays and quarter periods were estimated to the nearest 50 μs for intervals less than 1 ms, and proportional accuracy was maintained for the longer times. The lower limit of measurement of about 20 mV/m is set by the risk of confusion with harmonics in the mains supply pick-up, which are not annulled by the 50-c/s compensating circuit. Full-scale deflection corresponds to ± 350 mV/m.

3. APPEARANCE AND OCCURRENCE OF SLOW TAILS

The appearance of the low-frequency field variation, which follows the initial high-frequency oscillations originating in the return stroke of lightning discharges to earth, varies with observing conditions. During daytime it consists of a single aperiodic excursion of either sign, intermediate in shape between a sinusoidal half-cycle and a Gaussian error curve (Fig. 1b). The time-separation of the high-frequency oscillations and the slow tail is often large enough for the start of the tail to show a gradual increase in slope. With the approach of night-time conditions the separation becomes smaller and, for the nearer discharges especially, the tail lacks the gradual variation and shows a more abrupt change from the zero level (Fig. 1a, e) and occasionally has the oscillations superimposed on it particularly in the case of reflection-type waveforms. Simultaneously, a second half-cycle of opposite sign usually develops, following the first smoothly and having up to twice its duration (Fig. 1a). The beginning of this second half-cycle is of considerably greater slope than its end, which tends to the mean level very gradually. For the nearest storms considered (at about 1000 km) the first quarter-cycle is of shorter duration than the second, the latter being quite sharply defined when the trace crosses the mean position to give the degenerate second half-cycle. Triggering of the apparatus on short-duration precursors, which are irregular high-frequency waveforms due to the stepped nature of the leader, just before the return stroke occurs, suggests that the tail does not start before the oscillatory portion in such cases (Fig. 1a, d). Under night-time conditions at much greater distances to the south and south-east, as indicated by the smooth form of long-train reflection-type

waveforms (HEPBURN and PIERCE, 1954), the slow tail starts abruptly near the beginning of the waveform but gives a roughly symmetrical half-cycle, frequently ending abruptly also but often being followed by a second half-cycle of very similar

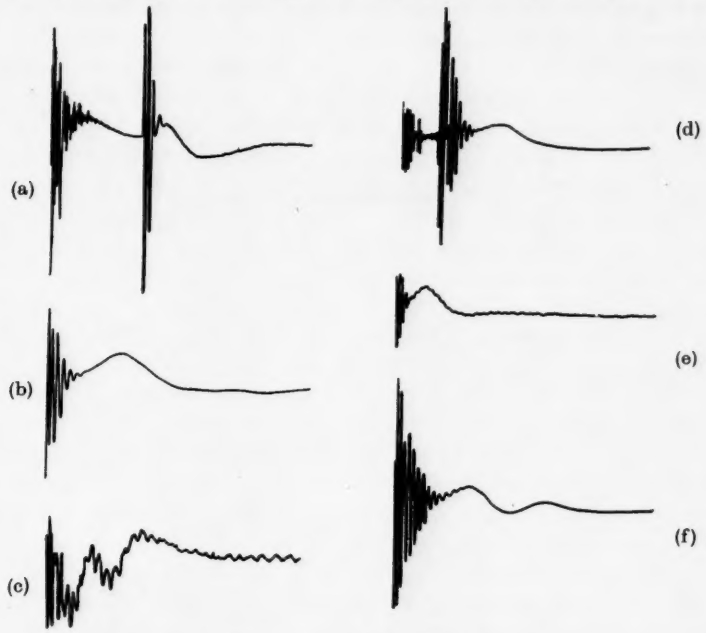

Fig. 1. Slow-tail waveforms.

The time-sweep is 10-ms duration in each case. Tracings are given, as the large range in writing speed on some of the waveform traces made satisfactory reproduction of the originals impossible. Notes on particular examples include recording date and time, the Sferics fix for the individual discharge or storm centre in terms of geographical location, range, and azimuth, and the characteristics of the waveform.

(a) 28.5.51, 0500. N. Germany, 1300 km, 78°. Precursor and return-stroke waveforms both with associated slow tails.
(b) 27.5.51, 1920. N. Atlantic, storm at 2200 km, 270°. Quasi-sinusoidal waveform with slow tail of one half-cycle.
(c) 27.5.51, 2300. Storm at ≃4000 km, 194°. Long-train reflection waveform superposed on slow tail having several half-cycles.
(d) 27.11.50, 1900. N. Atlantic, 2600 km, 284°. Irregular quasi-sinusoidal waveform with precursor and slow tail.
(e) 12.12.50, 1900. Storm beyond 3000 km to the south. Smooth long-train reflection waveform and slow tail of one half-cycle.
(f) 22.2.51, 0520. N. Atlantic, storm at 3200 km, 250°. Quasi-sinusoidal waveform with delayed slow tail of three half-cycles.

amplitude and period (Fig. 1e). To the west and south-west also, shown by the presence of a quasi-sinusoidal-type waveform (CATON and PIERCE, 1952),* very similar phenomena occur, but it is more common for the tail to consist of two nearly equal almost symmetrical half-cycles which do not commence until the high-frequency oscillations have decayed (Fig. 1f). Later in the night, particularly towards the early hours of the morning, more half-cycles up to five have been

* The author maintains (HEPBURN, 1952) that quasi-sinusoidal waveforms are characteristic of all storms to the west and south-west beyond about 1700 km, irrespective of time of day, and that differences —from Caton's Smooth Day-time type—of oscillation-amplitude decay and increase of period are functions of distance rather than time of day.

VOL. 10 1957

recorded (Fig. 1c). The half-cycles gradually decrease in amplitude and the durations increase very slowly. Slow tails occasionally accompany waveforms of leader-stroke origin (Fig. 1a).

On the basis of the present results there is no evidence for a clear division between waveforms showing slow tails and those possessing none. A continuous range of amplitude is noted from the limit of measurement to full-scale deflection—a range of 15 to 1 (Fig. 4). The frequency of occurrence of positive slow tails (those having a positive first half-cycle) increases rapidly as the amplitude considered decreases. Large amplitudes are relatively much more common for the negative slow tails (Table 1); i.e. the variation of occurrence with amplitude is much less. A decrease of occurrence with decreasing amplitude is not noted until the limit of measurement is reached for positive or negative slow tails. The proportion of waveforms having measurable slow tails varies considerably from time to time, averaging about 10 per cent for day-time records and 20 per cent in the evening, although individual storm centres show appreciable variations. Under full night conditions it has been observed that almost all of the quasi-sinusoidal waveforms have a measurable low-frequency component and the proportion of large slow tails greater than one-fifth of the oscillatory portion is comparatively great, often amounting to 40 or 50 per cent. Smooth long-train reflection-type waveforms almost always have slow tails also. Large amplitude pulses of the nearer night-time, peaked variety of long-train waveform confuse the start of the trace and often make assessment of the slowly varying component impossible; however, the great majority show slow tails. During the sunrise period, when the reflection peaks of the long-train waveforms are becoming attenuated, most waveforms possess a slow tail, but the majority are of small amplitude, although the later day-time records from the same centre show no unduly great proportion (Fig. 1a).

The relative proportion of positive to negative slow tails is variable from storm to storm. The average for night-time storms within 5000 km is 2·8 (138 slow tails). The day-time ratio decreases as the more distant storms are included and falls from 2·5 for storms within about 3000 km to 2·2 when storms up to 5000 km are included, suggesting that the more numerous small positive slow tails become increasingly too small to be measured. The slow tails associated with the smooth long-train waveforms are more predominantly positive—4 or 5 to 1. The mean proportion for the 620 waveforms measured in detail and for which estimates of the source are available is 3·5 to 1.

4. Diurnal Variation of Slow-tail Quarter Period

4.1. *Characteristic slow-tail quarter period*

The quarter period is the most characteristic parameter of the slow tails originating in a given storm centre, and the probable error of the mean can be found to an accuracy of a few per cent for day or night. For day, significantly different mean values are frequently obtained for the various active storm centres. Thus, on one occasion the mean values for three centres were 1080, 1550, and 1970 μs for 4, 9, and 20 waveforms respectively, each with a statistically probable error

of 65 μs, deduced from the spread of the results assumed normally distributed. In the evening, significantly different mean values are only obtained for two storms when they both occur in the south-west quadrant at different distances, or one is to the south-east and the other to the south-west. When slow tails originate to the east or south-east at night, the mean quarter period is close to 600 μs and any differences are not generally significant. For 80 slow tails recorded and fixed

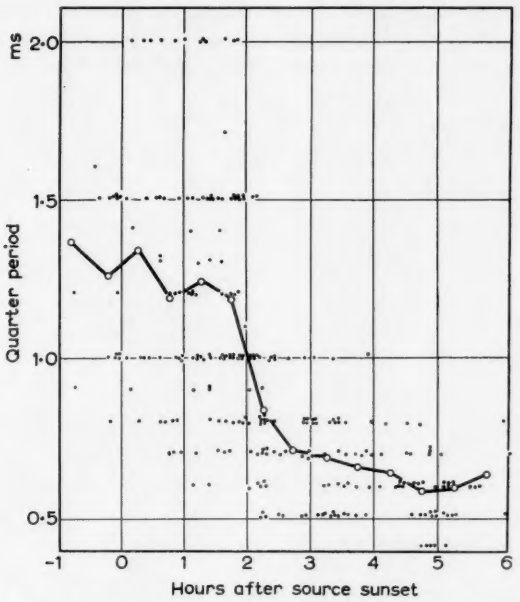

Fig. 2. Slow-tail quarter period against time after sunset at source.
—○— Mean value for each half-hour interval.

during the evenings of one fortnight in November 1950, those from the south-east had a much shorter quarter period of 580 μs and showed a smaller probable variation of ± 160 μs than those from a comparable range of distances to the south-west, for which the value was 900 ± 300 μs. The mean quarter period may be characteristic of a chosen source during the day and early evening, but when full night-time conditions occur, the mean values are so similar that they are not sufficiently accurately determined by the few observations available to be significantly different.

4.2. *Sunrise and sunset phenomena*

The 271 evening observations have been arranged so that any effects of the day-to-night transition would be more obvious by plotting observed quarter period against time of occurrence measured in hours after sunset at the source as a convenient parameter (Fig. 2). Periods recorded just before sunset are typical of full day-time conditions. The limitations of the graph must be remembered in attempting its interpretation. No account has been taken of source distance or direction, and because of the absence of afternoon observations all the points

VOL. 10 1957

referring to discharges occurring within an hour of source sunset are from discharges at considerable distances over the Atlantic Ocean, whereas flashes over the Mediterranean are the only ones contributing to the "4 and 5 hours after sunset" averages. For slow tails of westerly origin, source sunset occurs considerably later than sunset at the observing station, so that such waveforms produced at source sunset are propagated in a region after local sunset, whereas from Mediterranean storms in winter-time propagation is almost along rather than perpendicular to

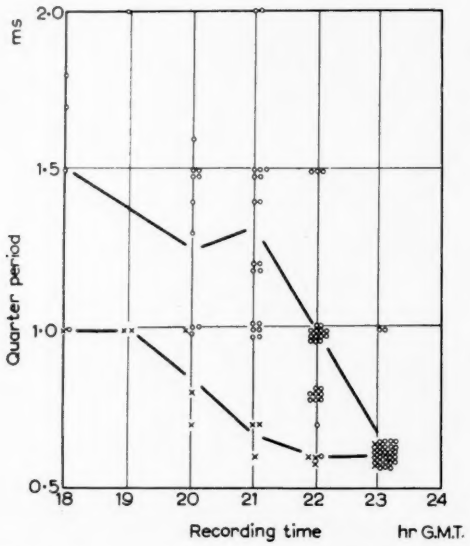

Fig. 3. Slow-tail quarter period against recording time for two Atlantic storms.
○ Distant origin, × near origin, — mean variation.

the sunset isochrones. The graph suggests that the transition from day to night conditions begins after local ground sunset at the midpoint of the propagation path and is completed less than $2\frac{3}{4}$ hr after sunset. In the present investigation "night-time" signifies that all the direct propagation path lies in regions at least $2\frac{3}{4}$ hr after local sunset.

The Sferics organization was not available for locating night-time storms over the Atlantic Ocean, but slow tails from such storms were shown to exhibit the same transition (Fig. 3) by recording waveforms from two centres to the south-west each hour of a 6-hour series, distinguishing the centres on the basis of the relative responses of tuned amplifiers (BOWE, 1951). For the nearer centre off the Portuguese coast the final quarter period was reached about 2 hours after source sunset, which was 3 hours after sunset at the observing station.

Early morning recording of waveforms from 3200 km over the Atlantic Ocean showed an appreciably greater rate of change of quarter period with time during sunrise than occurs at sunset. Mean values of 660 and 1060 μs were found for 11

and 18 slow tails recorded at 0620 and 0720 hr respectively. Sunrise was at 0700 hr at Cambridge and 0845 hr at the estimated storm centre.

5. Variation of Parameters with Distance

By considering only typically day-time or night-time waveforms, the complications of the transition are avoided and the effects of distance can be studied, as there is apparently no major variation during the day or night. Day-time results are from waveforms recorded within 3 hours of noon and have no restrictions on source position other than storm occurrence. Night-time results are largely from storms to the south and south-east, with a few from the nearest storms to the south-west and west. Distance estimates are from Sferics information unless otherwise stated. Mean curves have been plotted from scatter diagrams of the various parameters for day and night conditions (Figs. 4–7) and the values obtained by Watson-Watt *et al.* added for comparison. Averaging is generally over 500 km intervals centred every 500 km.

5.1. *Amplitude*

The mean amplitude of negative slow tails is consistently 50 to 70 per cent greater than for positive slow tails, although they are found only 40 per cent as frequently (Table 1, Fig. 4). By day, the mean amplitude decreases with increasing distance, but at night this is not observed. However the running means of the three largest amplitudes within 1000 km intervals decrease steadily, conforming remarkably well to an inverse distance law by day and an inverse square-root law at night.

For a small group of 55 waveforms the mean ratio of slow-tail to high-frequency oscillatory amplitude decreased with increasing distance during the early evening, but increased at night. A mean value of 0·2 at 1500 km for either time falls to 0·1 at 2000 to 3000 km in the evening but rises to 0·4 at 4000 km at night.

5.2. *Quarter period*

For both day and night the mean slow-tail quarter periods show a systematic almost linear increase with storm distance (Fig. 5): by day at a distance of d km $\tau/4 = 0{\cdot}24d + 520$ μs and at night $\tau/4 = 0{\cdot}08d + 510$ μs. These best straight lines through the scattered points for the two conditions give almost the same intercept of 515 μs at zero distance, but this is by extrapolation from minimum distances of 500 to 1000 km.

By day for a given distance the slow-tail quarter periods show large scatter which increases with the observing distance from 20 to 30 per cent at 1000 km to 40 or 50 per cent at 4500 km. At night this scatter is less at comparable distances. No difference has been found between the temporal parameters for the positive and negative slow tails.

An exception to the generally applicable conclusions reported above has been discovered on only one day (21.11.50), when a storm-centre south of Italy gave waveforms almost all of which showed slow tails of small amplitude and abnormally short mean quarter period which increased significantly from 550 to 610 μs between

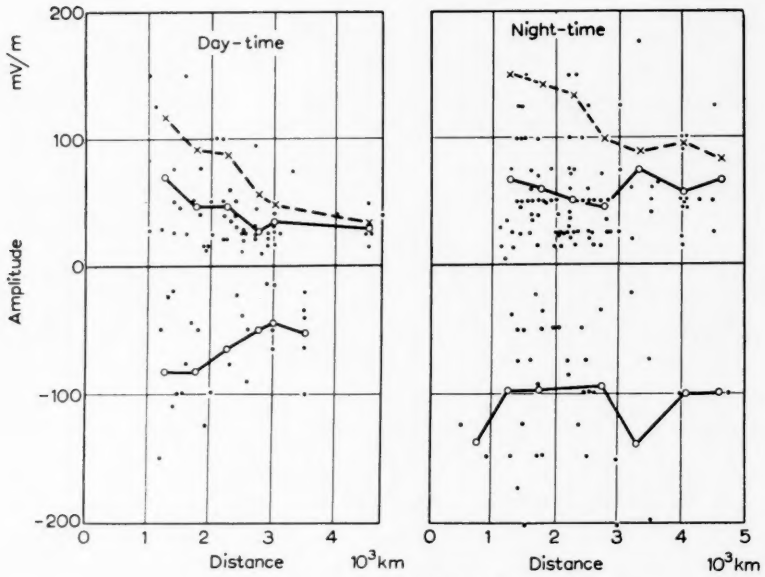

Fig. 4. Slow-tail amplitudes against distance.
— Running means, - - × — × — means of three largest.

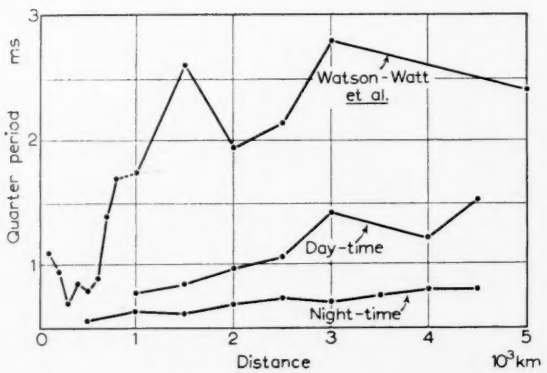

Fig. 5. Mean slow-tail quarter-period against distance.

Table 1. Slow-tail occurrence and amplitude

	Day							
D (km)	750	1250	1750	2250	2750	3250	3750	>4000
N^+	—	7	9	13	14	6	—	5
N^-	—	4	6	3	4	3	5	—
A^+ (mV/m)	—	70	47	48	28	35	—	32
A^-	—	83	82	67	49	44	52	—
P^+	—	117	92	87	57	49	—	34
P^-	—	104	109	67	60	—	69	—
	Night							
N^+	1	17	18	25	16	10	10	5
N^-	2	5	10	6	6	5	1	1
A^+ (mV/m)	50	68	60	51	47	77	57	64
A^-	138	98	98	73	94	140	10	10
P^+	150	142	134	99	89	97	—	84
P^-	134	175	95	99	—	—	—	—

Overall totals and averages

Time	Distance	N^+	N^-	N^+/N^+	A^+	A^-	A^+/A^-
Day	1–3000 km	43	17	2·5	45	72	0·63
Night	..	76	27	2·8	56	92	0·61
Day	0–5000 km	55	25	2·2	42	64	0·66
Night	..	102	36	2·8	59	102	0·58
All	..	157	61	2·5	56	87	0·64

The numbers (N), mean amplitudes (A), and mean amplitudes of the three largest (P) for positive and negative slow tails in 500-km source distance intervals (D) by day and night.

VOL. 10 1957

1100 and 1300 hr GMT. No reports of ionospheric or magnetic disturbance for that day have been discovered.

5.3. *Delay*

The mean values of slow-tail delay increase with distance more rapidly than the corresponding quarter periods. A linear law is a reasonable approximation in each case (Fig. 6), giving $t = 0{\cdot}33d - 370$ μs by day and $t = 0{\cdot}13d - 140$ μs by night.

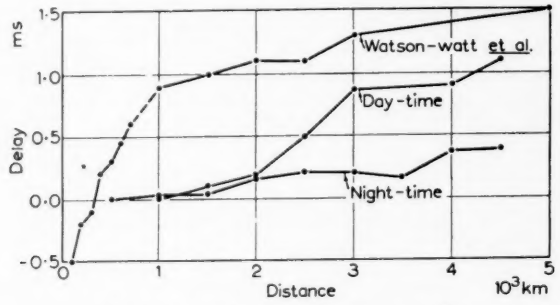

Fig. 6. Mean slow-tail delay against distance.

At the shorter distances of 1000 to 1500 km by day and 1000 to 2500 km at night there is considerable aggregation of points along the zero delay axis, but beyond 1700 km in each case the individual values show even greater scatter than the corresponding quarter periods.

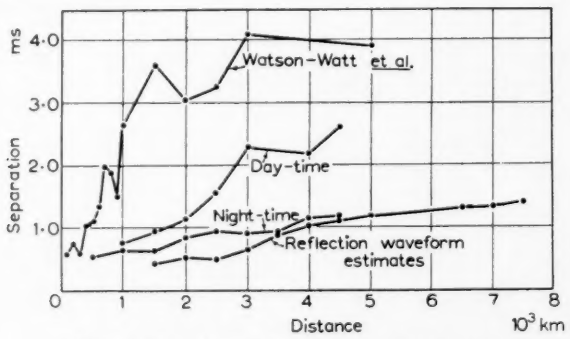

Fig. 7. Mean slow-tail separation against distance.

5.4. *Separation*

Mean values of separation are given in Fig. 7 for comparison with earlier results and with estimates from long-train reflection-type atmospherics. For the latter, direct estimates of delay and quarter period are impossible when a smooth waveform triggers on the slow tail (Hepburn and Pierce, 1954), the beginning of which cannot be estimated reliably. The interval between the calculated beginning of the train of oscillations and the observed maximum of the slow tail is taken as the separation for these slow tails. The night-time and long-train waveform estimates appear to be in good agreement between 3500 and 4500 km but at shorter range the

calculated values are noticeably shorter. The slopes of the best straight-line averages for these night-time cases agree within 8 per cent, but the intercepts at zero distance are 370 and 80 μs, suggesting that direct measurement may include extra time not accounted for by straightforward calculation (HEPBURN and PIERCE, 1954; HEPBURN, 1957).

5.5. *Directional and random effects*

Possible effects of propagation path orientation upon the slow-tail parameters were investigated because the direction of the source exercises so large an effect upon the high-frequency part of the waveform (CATON and PIERCE, 1952; HEPBURN, 1952). Also, time of occurrence and source distance gave an incomplete specification for the average quantities for a given storm centre, apart from outstandingly abnormal conditions as described in 5.2. Divergences of the mean quarter-period for individual storm centres from the value indicated by the average distance relationship suggest systematic directional, or perhaps random, effects. Thus, on one day previously cited, when several slow tails were received from three storm centres, waveforms from the south-west, ascribed to a centre at 2000 km on the evidence of the Sferics information half an hour earlier, gave a mean quarter period of 1970 μs, which is more characteristic of a storm at 6000 km (Fig. 5). At the same time slow tails from a centre to the south-east had a mean quarter period of 1100 μs typical of 2400 km, but the Sferics organization fixed a storm at 1400 km. Similar discrepancies were found at night. The mean limiting quarter period of 640 μs for the distant storm to the south-west referred to in 4.2 is less than the 800 to 850 μs expected, if the distance is estimated roughly from the time at which the limiting period was attained.

VOL. 10 1957

The day-time records referring to numerous occasions and a wide range of storm distance and direction, which tend to average out any random phenomena, have been investigated for a directional effect by grouping the results corresponding to the sources occurring in four overlapping 50° sectors from south-east to west. In each group the quarter period-distance relation was investigated and the differences were shown to be statistically insignificant for the small number of records (84) available.

Agreement of the results for individual storm centres with average behaviour is not as good as might reasonably have been expected and the difference does not appear to be a directional effect. More accurate range determination would be of great help in checking the significance and magnitude of the discrepancies and may resolve the problem without invoking other variables. In the latter event the consistency of slow-tail quarter period from a given centre and the average variation with distance suggest an extremely simple method of source-distance estimation from a single observing station capable of a day-time accuracy of a few hundred kilometres in several thousands (HEPBURN, 1952).

6. THEORETICAL CONSIDERATIONS

6.1. *Possible origin in leader strokes*

For the correct application of theoretical considerations to the experimental results, in an attempt to derive ionosphere properties, due regard must be paid to

the origin of the slow tail. BRUCE (1941) has suggested a possible partial origin in the radiation field of the *a* portion of the net field change of the discharge which is due to the leader stroke. An approximate average field change due to an α-type leader stroke (PIERCE, 1955) corresponds to the lowering of 10 coulombs half-way to earth from a height of 3 km, giving electrostatic field changes of 270 and 10 mV/m at distances of 100 and 300 km, respectively. The radiation and induction fields depend upon the time-variation of the electrostatic field. This increases as a low-order power function of time (SCHONLAND, HODGES, and COLLENS, 1938) and gives a radiation to electrostatic field change ratio of $(br/ct)^2$, where b is the low-order power, r is the storm distance, c the velocity of light, and t the duration of the leader stroke. Values of t are in the range 3 to 30 ms or greater, giving a maximum value of 1 : 9 for the ratio at a distance of 100 km, taking b as large as 3; and unity at a distance of 300 km. Thus any field change at short range is largely due to the electrostatic term. The rapidly occurring electrostatic field changes of β-type leader strokes occur several milliseconds before the return stroke (SCHONLAND *et al.*, 1938), so that any slow tail produced would be quite distinct from a low-frequency component generated by the return stroke. Even the more rapid leaders to subsequent strokes in a discharge, of similar form and of about 1-ms duration, are comparatively ineffective, since the net field changes occurring are much less than for α-type leaders (SCHONLAND *et al.*, 1938). Thus the origin of the slow tail must generally be sought entirely in the field radiated by the much heavier current of the return stroke of the lightning discharge.

6.2. *Origin in the radiation field of the return stroke*

The precise variation of current in the lightning-discharge channel governs the amplitude of the low-frequency component produced (HEPBURN, 1957). BRUCE and GOLDE (1941) have given an analytical expression for a typical initial current variation which explains adequately the form and magnitude of the response recorded with loop aerials due to the higher frequencies. More recently, NORINDER (1951) has suggested a much slower but similar variation of discharge current, which MORRISON (1953) has shown may be expressed for the first 300 μs in the analytical form given by BRUCE and GOLDE with appropriate reduction of parameter values by factors of the order of 10. A modified form of the BRUCE and GOLDE expression has been suggested (HEPBURN, 1952 and 1957) which is very much more adequate for describing the net changes and corresponding low-frequency components without modifying the higher frequencies. From such a typical modified expression of the form $I = Ae^{-\alpha t} - Be^{-\beta t} + Ce^{-\gamma t}$, where A, B, $C = 20, 25, 5$ kA and $\alpha, \beta, \gamma = 5 \times 10^4, 5 \times 10^5, 7 \times 10^2\ s^{-1}$, respectively, the relative Fourier components in the free-space radiation, induction, and static electric fields are given in Fig. 8. The component fields contribute comparably at frequencies of 200 and 50 c/s for distances of 250 and 1000 km respectively, and only at several times these frequencies are the induction and static fields negligible. The curves show that if slow tails contain appreciable component frequencies around 100 c/s, as the graph suggests, the slow-tail form is only predominantly of radiation-field origin at distances greater than 1000 km.

6.3. *Field equation and amplitude decay*

Expression of the resultant electric field in terms of the familiar radiation, induction, and static components is only justified in the case of an infinite homogeneous medium or a semi-infinite medium bounded by a perfectly conducting

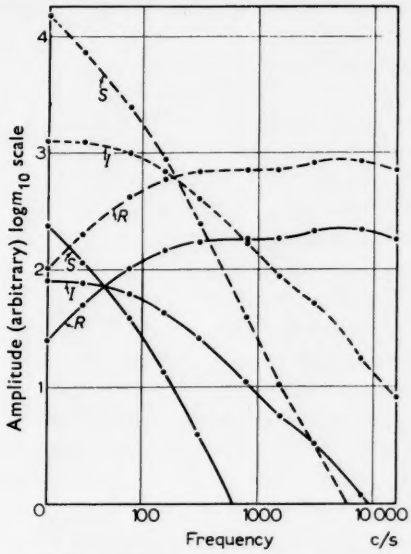

Fig. 8. Radiation, induction, and static field components.
– – – – – Fields at 250 km, ——— fields at 1000 km.

sheet. Numerical values in the preceding section have been used to give clarity rather than strict precision to the discussion of the effect of increasing distance. In the presence of a second parallel conducting layer (e.g. ionosphere) it has been suggested that the radiation field should be governed by the $1/d$ spatial attenuation given by the field equation up to distances of the order of 300 km and thereafter vary as $1/\sqrt{d}$, because of the two-dimensional divergence of the energy (THOMAS and BURGESS, 1947). These considerations are applicable to single-frequency field strengths and not waveform measurements in all cases. The observed $1/d$ attenuation of the high-frequency portion of the waveform does not conform to this suggestion, as the effect of the ionosphere is to reflect the incident pulse which is received later than the direct pulse and so cannot modify its amplitude. However, the duration of the slow tail is such that overlap of the reflected low-frequency component may be visualized when recording at large distances from the source, and $1/\sqrt{d}$ attenuation can be expected at such range in the absence of strong attenuation by imperfectly conducting boundaries (cf. night-time amplitudes described in 5.1). Alternatively, consideration of the propagation of cylindrical waves from a source between parallel conducting surfaces (BUDDEN, 1951) leads to a solution in the form of a series of Bessel functions which approximate to the radiation-field spectrum with $1/\sqrt{d}$ attenuation at large distances and of which generally only the first term contributes at such low frequencies.

VOL. 10 1957

The three-term field equation is thus applicable up to a few hundred kilometres where ionospheric effects become significant, beyond which the strict analysis including a second conducting boundary is required; however, the latter gives the same results as the former at large distances, provided the simple correction is made for the two-dimensional energy divergence.

6.4. *Frequency components and form of the slow tail*

For the current variation considered, frequency components of the radiation field in the range 100 to 1000 c/s are excited with amplitudes closely approximating to the empirical form $A = A_0\{1 - \exp(-f/f_1)\}$, where $f_1 = 200$ c/s. From the work of BUDDEN, the relative amplitudes of corresponding frequencies remaining after attenuation by a propagation of 1000 km under day-time conditions for the modes of order 0 and -1 can be expressed empirically by the factor $\exp(-f/f_2)$, where $f_2 = 700$ c/s. The resultant low-frequency component spectrum $A_0 . \exp(-f/f_2)\{1 - \exp(-f/f_1)\}$ shows a maximum at 300 c/s and half-power points at 100 and 700 c/s. Fourier synthesis of this type of spectrum gives a form having "duration" at greater than half-amplitude equal to the reciprocal of the bandwidth modulated by a frequency of the order of the predominant frequency of the spectrum. For the current variation considered, the phase angles of the low-frequency components are all close to zero (HEPBURN, 1957) and the synthesis yields a distorted half-cycle of about the predominant frequency of the spectrum with a very degenerate subsequent excursion. The BRUCE and GOLDE current variation gives amplitudes less by a factor of about 10 and phase angles $\theta(f) = -\pi/2$, resulting in a much smaller waveform having two half-cycles of the order of the predominant frequency in the spectrum.

Slow-tail frequency components are largely determined by the individual values of the amplitude and time-constant of the continuing current—the quantities C and γ of the expression for the discharge current—and the magnitude of the net change by their product. Pairs of values such as 20 kA, 358 μs or 0·5 kA, 14·3 ms would give the same net change without significantly altering the initial part of the current waveform. Variation of the amplitude of the continuing current, C, has an almost directly proportional effect on the slow-tail amplitude. Reducing the time-constant γ modifies the spectrum, which is of significance in producing variation of observed slow-tail quarter periods. It is estimated that the greatest variations in the increase of amplitude with frequency can only be by a factor of 2 either way if the amplitudes are to stay of significant magnitude; i.e. f_1 lies in the range 100 to 400 c/s, corresponding to short- and long-duration slow tails. The time-constant also controls the slope of the phase-frequency characteristic in the region of the slow-tail frequencies, causing scatter in the delay of the slow tail with respect to the higher frequencies (see 6.5). Calculated frequency spectra for short, average, and long slow tails observed at 1000 km by day are shown in Fig. 9, and the deduced slow-tail durations and approximate quasi-periods given in Table 2.

Propagation paths greater than 1000 km give increased attenuation, and the appropriate value of f_2 is correspondingly reduced to values of 700/2 and 700/3 c/s for distances of 2000 and 3000 km respectively. This reduces the upper half-power

frequency limit of the spectrum (Fig. 9), giving correspondingly narrower bandwidth and longer tail duration and quasi-period (Table 2). As the predominant frequencies decrease with the bandwidths, the general forms of the slow tails are substantially unaltered. Approximately linear increases of duration and quasi-period with distance are an interesting feature of the analysis.

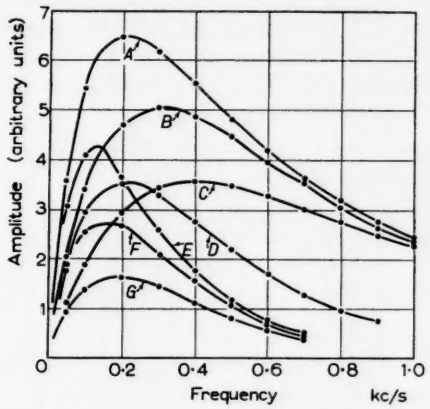

Fig. 9. Calculated slow-tail frequency components.

A Short tail at 1000 km
B Average ,, ,, ,,
C Long ,, ,, ,,
D Average ,, 2000 ,,
E Short tail at 3000 km
F Average tail at 3000 km
G Long ,, ,, ,, ,,

At night the ionosphere lower boundary is higher and more well defined, so presenting a higher conductivity. The effects in these circumstances are more difficult to assess; however, the attenuation of frequencies near 2 kc/s is much less complete (BUDDEN, 1951; CHAPMAN and MACARIO, 1956), indicating an appropriate

Table 2. Estimated slow-tail duration and quasi-period

Spectrum (Fig. 9)	Source effect	Distance (km)	Bandwidth (c/s)	Duration of tail (ms)	Freq. of max. ampl. (c/s)	Tail period (ms)
A	Short	1000	715	1·40	220	4·55
B	Average	1000	870	1·15	320	3·13
C	Long	1000	1150	0·87	400	2·50
D	Average	2000	540	1·85	220	4·55
E	Short	3000	320	3·12	130	7·70
F	Average	3000	400	2·50	160	6·25
G	Long	3000	460	2·17	190	5·26

value of f_2 much above the 700 c/s for 1000 km path in daytime which gives a wider spectrum and correspondingly reduced slow-tail duration and quasi-period. For long, slow tails in these circumstances, i.e. $f_1 \simeq 400$ c/s, the bandwidth may be

as short as for day-time, but the predominant frequency considerably larger, giving correspondingly more half-cycles to the slow tail.

6.5. *Slow-tail delay at zero distance*

The transmission path causes a delay of the slow tail and also attenuates the higher frequencies of its spectrum. The presence of induction and static electric fields at short range makes it impossible to observe the undelayed position of the slow tail, and even without this complication the absence of attenuation beyond the slow-tail spectrum because of negligible propagation path would result in a discrete slow tail not appearing. However, it is necessary to know the undelayed positions of the appropriate frequencies to determine the absolute dispersion. This can be assessed by extrapolation of the delay-distance graph to zero distance, assuming its linearity, or by estimation from theoretical considerations. However, in the former case the negative values of delay at zero distance could possibly be all attributed to the loss of the initial portion of the waveform occurring before triggering of the apparatus. The magnitudes are large, but the suggestion is supported by the greater value of the intercept by day, for which a proportion of the waveforms are of the quasi-sinusoidal type where the oscillation amplitude increases to a maximum over several cycles.

Theoretical considerations in 6.4 show the earliest slow tails to occur when the low frequencies all have phase $\theta(f) = -\pi/2$ at the source, giving two comparable half-cycles. They are of small amplitude, as these are the conditions for little or no continuing current in the discharge (HEPBURN, 1957). The high frequencies then result in a pulse situated between the half-cycles of the slow tail before dispersion and give a delay at source t_s equal to $-\tau/2$. In addition, when the slope of the phase characteristic $\dot{\theta}(f)$ is not equal for the low frequency f_L and high frequency f_H regions of the spectrum, a phase delay $t_p = \dot{\theta}(f_H) - \dot{\theta}(f_L)$ of the slow tail with respect to the high frequencies occurs as another source phenomenon quite distinct from propagation effects. The observed delay t is the sum of the total source delay t_s and the true propagation delay T less any time t_t due to late triggering: $t = t_s + T - t_t$. For the particular current variation considered in detail, the appropriate frequencies are of greater amplitude and give a slow tail in the form of a half-cycle starting $\tau/4$ before the high-frequency pulse less 125 μs due to the differences in slope of the high- and low-frequency ends of the phase characteristic: i.e. $t_s = t_p - \tau/4$. A continuing current of longer duration would give a similar delay and be unlikely to have much more than the correspondingly decreased amplitude. The form of current variation used above is not far from that which gives the largest slow tails consistent with acceptable averages of net field change and radiation pulse amplitudes. Hence the most common source delay giving recorded slow tails is expected to be close to $t_p - \tau/4$.

An associated problem in the evaluation of the true retardation of the slow-tail frequencies is the point on the slow tail to which the time is measured. This could reasonably be measured from the first high-frequency peak to the first slow-tail peak, or from the beginning of the high-frequency oscillations to the start of the slow tail, as done by WATSON-WATT *et al.* It is seen that in the case of slow tails having a single predominant half-cycle, corresponding to appreciable energy in the

very low frequencies and hence to the most frequently observed day-time slow tails, the separation $s = t + \tau/4$, rather than the delay, is desired. For discharges not having long-duration currents and giving slow tails of two half-cycles, the retardation should be measured to the point between the two half-cycles, i.e. $t + \tau/2$.

7. Ionosphere Parameters

7.1. *Parameter magnitude and consistency from delay measurements*

Following the method of Hales (1948), values of slow-tail quarter-period and delay, obtained at 1000 km intervals from the best linear relations of these measurements with distance, have been used to determine corresponding values of his parameters $(c/u - 1)$ and γ (Hepburn and Pierce, 1953). Whereas Hales chooses

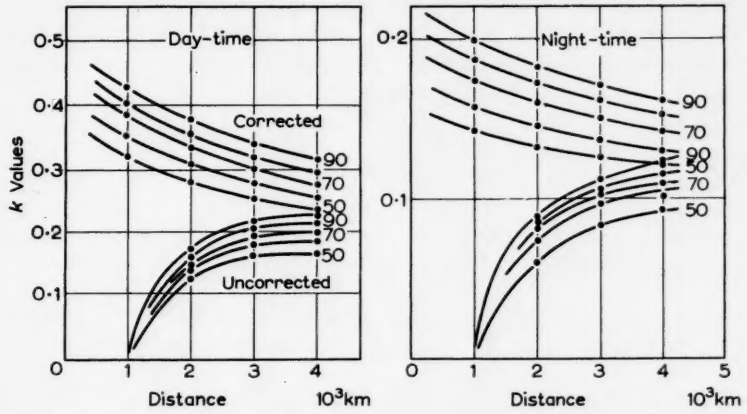

Fig. 10. Consistency of derived ionosphere parameter k for assumed layer height.

a definite ionosphere height of 60 km to which to refer his estimates, in the present instance they are evaluated for the 50- to 90-km range at 10 km intervals. By means of the graphs given by Hales (*loc. cit.*, p. 70) these pairs of parameter values have given estimates of the parameter k for various distances and ionosphere heights for day and night (Fig. 10). The procedure has been repeated for "corrected" delay values, increased by their respective intercepts along the delay axis, on the assumption that the linear delay-distance relation should pass through the origin. In each case variation of ionosphere height has comparatively little effect upon the values of k obtained. The method fails completely for distances less than 1000 km in the uncorrected case, as the delays become negative. As the range increases, the method is less sensitive to errors in the evaluation of delay and the k values tend to the same steady value in either case.

The uncorrected delay values give an untenable result, the corrected values give a fairly constant result, but departures from constancy are primarily due to the magnitude of the correction. Hales has accepted the correction as fixed at the value of the intercept and explains the variation of k with distance (which is three times larger than the present estimate) as a natural selection of observations. Because the scatter of observed quarter-period and delay from a given distance

VOL. 10 1957

can be explained in terms of source phenomena and perhaps inaccurate distance estimates rather than day to day fluctuations of the ionosphere, it is felt desirable to adhere to a constant ionosphere specification in the first instance. For a value of k independent of distance and equal to the limiting value at large range obtained from the curves of Fig. 10, the true values of propagation delay T may be calculated. They differ from the observed mean delays by an amount independent of the assumed ionosphere height and storm distance. With $k = 0{\cdot}22$ and $0{\cdot}29$ for heights of 50 and 90 km respectively as day-time estimates, and $0{\cdot}12$ and $0{\cdot}157$ at night, the delay corrections $(t_t - t_s)$ become 240 ± 15 μs by day and 105 ± 4 μs at night. Conversely, if constant correction is assumed, the k values are constant to 4 per cent.

The above situation, being the most consistent interpretation of the results as applied by HALES, indicates that the slow tail must be ascribed a negative delay at zero distance $t_t - t_s$ by extrapolation for both day and night conditions. The difference between the day and night corrections gives an estimate of the difference of the average triggering delays, if the average source delay remains constant. The triggering delay is thus 135 μs greater by day than at night, substantiating the expectation expressed earlier (6.5). If the triggering delay on night-time waveforms is negligible, the source delay $t_s = 105$ μs is considerably less than the 510-μs value of $\tau/4$ at zero distance, indicating an average phase delay of about 405 μs. However, the difference in triggering delays estimated from the intercepts gives 230 μs, possibly indicating that the average source delay is not constant.

7.2. *Parameter values from separation measurements*

From theoretical considerations in 6.5 the retardation of the slow component is generally more accurately measured by the separation. Using separation in place of delay values and assuming an ionosphere height of 60 km, as the distance increases from 1000 to 4000 km, values of k fall from $\simeq 0{\cdot}8$ to $0{\cdot}455$ by day and $\simeq 0{\cdot}7$ to $0{\cdot}31$ at night. The asymptotic value cannot be estimated accurately because of the rapid variation of k. However, with fixed values of $0{\cdot}39$ by day and $0{\cdot}20$ at night the calculated separations are consistently less than the observed values at each 1000-km interval by 420 ± 20 and 445 ± 10 μs respectively. For an ionosphere height of 90 km by night, $k = 0{\cdot}25$ gives the most uniform values of -430 ± 10 μs for the separation correction over the distances considered. Once more if the night-time triggering delay is negligible and the source delay remains constant, these results indicate negligible triggering delay by day and a phase delay of about 425 μs. The consistent values of the parameter k deduced from the separation measurements are both 60 per cent greater than those obtained using delays.

7.3. *Ionosphere height and conductivity*

Having estimated the k values which give consistency for the various assumed ionosphere heights, it is desirable to compare the corresponding conductivities of the equivalent homogeneous ionosphere for these heights with values actually observed or independently estimated. RYDBECK (1944) has calculated that the

form of the electron density variation with height in the ionosphere has little effect upon the propagation of the lowest-order modes, but has given no indication of the relations between height and conductivity of the equivalent homogeneous ionosphere and the height, maximum conductivity, and scale height of the equivalent parabolically varying electron density (i.e. Chapman layer) which are necessary for equal propagation factors. It will be taken that equivalence occurs when the conductivity at the base of the homogeneous layer is comparable with

Table 3. Ionosphere conductivity

Day-time

Height h (km)	Collision frequency ν (s^{-1})	Electron density N (cm^{-3})	Conductivity $=Ne^2/m\nu$ (e.s.u.)	from delays		from separations	
				k	$\sigma\times10^{-3}$ (e.s.u.)	k	$\sigma\times10^{-3}$ (e.s.u.)
50	2×10^8	—	—	0·22	9·9	0·36	3·7
60	5×10^7	<2	<10	0·24	7·0	0·39	2·6
70	10^7	30–200	10^3–5×10^3	0·26	5·2	0·42	1·9
80	2×10^6	5×10^2–2×10^3	5×10^4–3×10^5	0·28	4·0	0·45	1·5
90	5×10^5	2×10^3–2×10^4	5×10^6–10^8	0·29	3·1	0·48	1·2
100	10^5	10^4–3×10^5	3×10^7–10^9	0·31	2·4	0·51	0·9

Night-time

h	ν	N	$Ne^2/m\nu$	k	$\sigma\times10^{-3}$	k	$\sigma\times10^{-3}$
50	2×10^8	—	—	0·12	33	0·18	14
60	5×10^7	—	—	0·13	24	0·20	10
70	10^7	—	—	0·14	18	0·22	7·3
80	2×10^6	<10	$<10^3$	0·15	14	0·23	5·5
90	5×10^5	50–200	2×10^4–10^5	0·16	11	0·25	4·2
100	10^5	$>10^3$	$>3\times10^6$	0·17	9	0·27	3·4

that at the same height for the electron density actually occurring, in order that separate estimates may be made of height and conductivity.

Agreed values of electron density N and collisional frequency ν for day and night are difficult to obtain, but as the former varies so rapidly with height, little is lost by lack of precision.

Depending upon the use of separation or delay measurements, corresponding values of conductivity of 1·9 or 5·2 . 10^3 e.s.u. occur at about 70 km by day, and 4·2 or 11 . 10^3 e.s.u. near 90 km at night. At night the actual conductivity increases very rapidly in the region of 90 km, and there can be little ambiguity about the actual position of the layer. By day the change in conductivity is not as obvious, but below 70 km the conductivity varies more rapidly with height than above this level. The difference in conductivity values depending upon the use of delay or

separation measurements is not large enough to indicate appreciably different heights of the equivalent layer, but use of the latter gives layer conductivities only 40 per cent of those previously obtained from the delays for both day and night conditions.

8. CONCLUSION

Theoretical discussion has shown that the properties of slow tails and their variations with recording time and storm distance may be explained in terms of acceptable source and propagation factors. Analysis of these more recent results by a critical application of HALES' method indicates that they are most satisfactorily explained in terms of constant ionosphere properties and an average source for which the slow-tail frequencies have a relative delay of about 425 μs with respect to the high frequencies of the spectrum. Equivalent homogeneous ionospheric layers at heights of 70 km by day and 90 km at night having conductivities of 1·9 and 4·2 . 10^3 e.s.u. respectively are deduced from comparison with estimates of ionosphere conductivity variation with height and are only 40 per cent of the values obtained by HALES' direct application of the theory.

Acknowledgements—The work reported is part of a programme of atmospherics investigation initially supported by the Department of Scientific and Industrial Research at the Observatories and Cavendish Laboratory, Cambridge, and continued at the Physics Department, Nottingham University. It is a pleasure to thank the directors of these establishments for the provision of suitable facilities, and the Director of the Meteorological Office and staff of the Sferics organization of the Central Forecasting Office, Dunstable, for their unfailing courtesy and co-operation in supplying Sferics information. I am grateful to Dr. T. W. WORMELL and Dr. E. T. PIERCE for their encouragement and advice throughout the research and in the preparation of this paper, and to Dr. P. G. F. CATON for his assistance in the recording.

REFERENCES

APPLETON E. V. and CHAPMAN F. W.	1937	*Proc Roy. Soc.* **A158,** 1.
APPLETON E. V., WATSON-WATT R. A., and HERD J. F.	1926	*Proc. Roy. Soc.* **A111,** 615 and 654.
BOWE P. W. A.	1951	*Phil. Mag.* **42,** 121.
BRUCE C. E. R.	1941	*Nature, London* **148,** 165.
BRUCE C. E. R. and GOLDE R. H.	1941	*J. Instn. Elec. Engrs.* 88(2), 487.
BUDDEN K. G.	1951	*Phil. Mag.* **42,** 1.
CATON P. G. F. and PIERCE E. T.	1952	*Phil. Mag.* **43,** 393.
CHAPMAN F. W. and MACARIO R. C. V.	1956	*Nature, London* **177,** 930.
HALES A. L.	1948	*Proc. Roy. Soc.* **A193,** 60.
HEPBURN F.	1952	Thesis, University of Cambridge.
HEPBURN F. and PIERCE E. T.	1953	*Nature, London* **171,** 837.
HEPBURN F. and PIERCE E. T.	1954	*Phil. Mag.* **45,** 917.
HEPBURN F.	1957	*J. Atmosph. Terr. Phys.* **10,** 121.
MORRISON R. B.	1953	*Phil. Mag.* **44,** 979.
NORINDER H.	1951	*Joint Commission on Radio-Meteorology* International Council of Scientific Radio.

Pierce E. T.	1955	*Quart. J. R. Met. Soc.* **81,** 348, 211.
Rydbeck O.	1944	*Trans. Chalmers University* Gotenburg, 34.
Schonland B. F. J., Hodges D. B., and Collens H.	1938	*Proc. Roy. Soc.* **A166,** 56.
Thomas H. A. and Burgess R. E.	1947	*D.S.I.R. Radio Res. Spec. Rep.* 15.
Watson-Watt R. A., Herd J. F., and Lutkin F. E.	1937	*Proc. Roy. Soc.* **A162,** 267.
Wilson C. T. R.	1920	*Phil. Trans.* **A221,** 73.

VOL.
10
1957

Journal of Atmospheric and Terrestrial Physics, 1957, Vol. 10, pp. 288 to 295. Pergamon Press Ltd., London

The fading of radio waves reflected from the *E* layer

B. LANDMARK
The Auroral Observatory, Tromsö

(*Received* 31 *January* 1957)

Abstract—The amplitude and phase of waves of frequency 2 Mc/s reflected vertically from the *E* layer were studied. It was found that there were regions in the wave pattern, of extent D, at the centre of which the phase-path exceeded that at the edges by ΔP. When $\Delta P/D < 0{\cdot}025$ approximately, the variations of amplitude and phase were associated as they would be if the phase variation was caused by a concavity in the reflecting layer. There resulted a "burst" of amplitude caused by focusing, inside which there was comparatively rapid fading. When $\Delta P/D > 0{\cdot}025$, the conditions became more complicated, but on one occasion could still be analysed in terms of a moving concavity in the layer. Observations made at night on waves of frequency 200 kc/s reflected at an angle of incidence of about 40° were explicable in terms of the same model.

1. INTRODUCTION

WHEN a single downcoming radio wave, reflected vertically from the *F* layer, is examined, it is found that, for most of the time, there is irregular fading about a mean value which is approximately constant for periods of the order of 1 hour, but that sometimes the mean amplitude increases, by a factor which may be 5 or more, for periods of the order of 5 or 10 min. These "bursts" of amplitude in waves reflected from the *F* layer have been investigated by WHITEHEAD (1956). He showed, by comparing the variations of amplitude and phase, that they could be ascribed to a "focusing" caused by an effective concave reflecting mirror passing overhead in the ionosphere.

It is the purpose of this paper to examine similar "bursts" of amplitude observed by day in the wave reflected vertically from the *E* layer and to relate them to focusing effects in that layer. It will be shown that the more rapid fading which is observed during a "burst" could itself be caused by the focusing process which produced the "burst."

Observations made at night on the amplitude and phase of waves of frequency 200 kc/s are used to show that similar focusing phenomena occur.

SCHRAGG (1955) appears to be the only worker who has so far observed the effects of focusing on waves reflected from the *E* layer. He used a frequency of 150 kc/s reflected vertically, at night, and based his conclusions on observations of the strength of higher-order echoes.

2. HIGH FREQUENCIES (2 Mc/s) DAY-TIME RESULTS

2.1. *The observations*

In this section, the following results will be analysed: (a) Observations of amplitude and variations of phase-path of radio waves reflected from the *E* layer, made by Dr. FINDLAY on a frequency of 2·4 Mc/s for most of the years 1948 and 1949; (b) measurements of phase path made by Dr. FINDLAY on a frequency of 2·0 Mc/s from April to December 1949; (c) observations of amplitude and variations of phase-path made by the author on a frequency of 2·05 Mc/s during

VOL. 10 1957

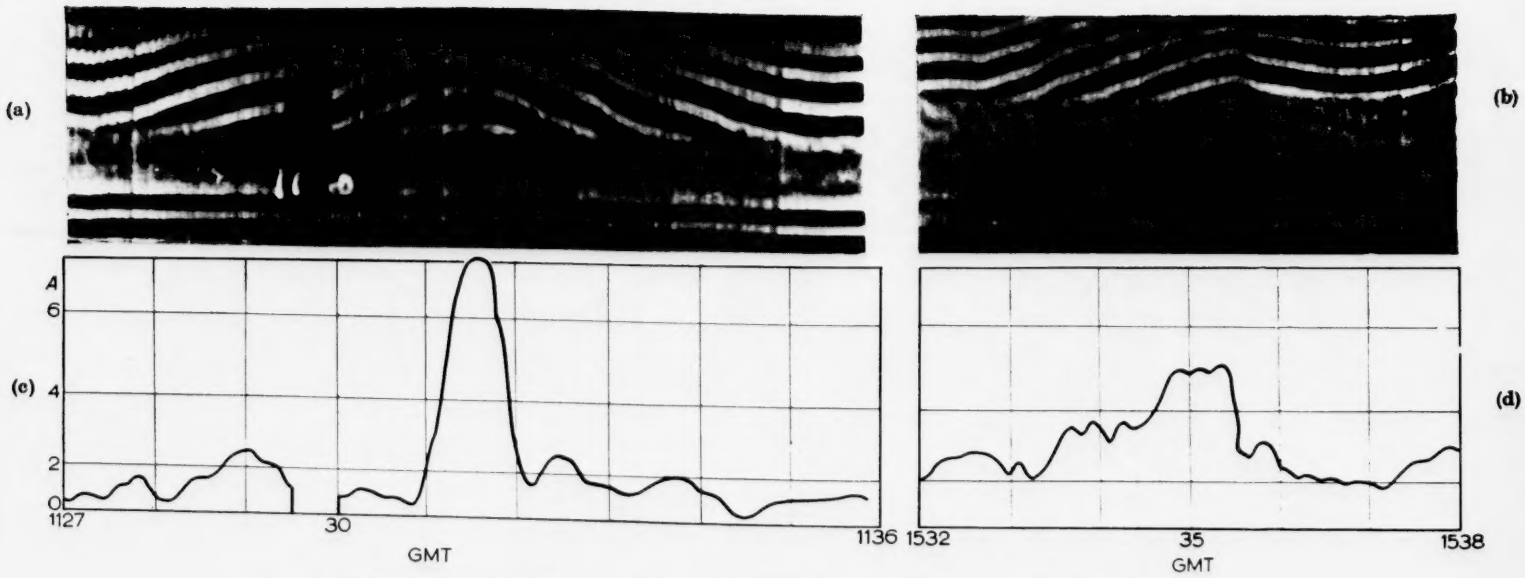

Fig. 1. Typical records of phase-path and amplitude, obtained during quiet ionospheric conditions on a frequency of 2·05 Mc/s.

VOL
10
195

March and April 1956. The method used to observe variations of phase-path has been described by FINDLAY (1951).

In Fig. 1 are shown typical records of phase-path and amplitude, obtained during quiet ionospheric conditions. A positive slope of the interference fringes in the phase-path record corresponds to increasing phase-path, and an increase of one fringe is equal to an increase of phase-path of 1 wavelength. Fig. 1 shows a close association between the observed variations of amplitude and phase-path, which is typical of most of the observations made during quiet conditions.

2.2. *Amplitude and phase during bursts*

WHITEHEAD (1956) considered a "curved mirror" which moved horizontally overhead at a mean phase height h with a velocity V, and derived the following

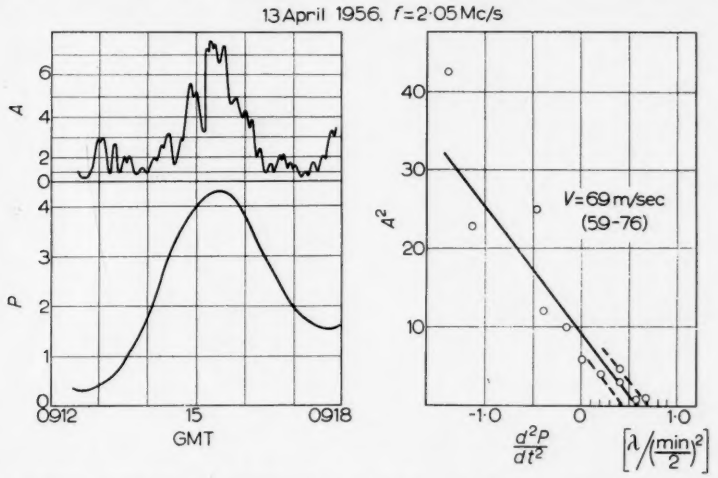

Fig. 2. Observed variations of amplitude A and phase-path P on a frequency of 2·05 Mc/s, together with "straight-line" plot to obtain the drift velocity.

relation between the amplitude A and the phase-path P of the reflected wave

$$A^2 \propto 1 - \frac{h}{2V^2}\frac{d^2P}{dt^2} \qquad (1)$$

according to which a plot of A^2 against d^2P/dt^2 should give a straight line, from which the drift velocity can be determined. Typical results for a wave reflected from the E layer are shown in Fig. 2. If h is put equal to 100 km this gives the magnitude of V equal to 70 ± 10 m/s.

Seventy-one amplitude variations of the burst type have been analysed in this way, and reasonably good straight lines have been obtained for most of them.

In Fig. 3 the distribution of the calculated velocities is shown in a histogram. This is similar to histograms of the velocities measured by the method of closely-spaced receivers. In a companion paper (JONES, LANDMARK, and SETTY, 1957) it is shown that measurements made by the two methods simultaneously often give the same result.

The horizontal extent, D, of a burst of amplitude can be deduced from its

VOL. 10 1957

duration T and its drift velocity V. The observed distribution of D is shown in the histogram of Fig. 4.

2.3. *The changes of group-path during a "burst"*

It has been supposed, in Section 2.2, that the "burst" is caused by a focusing process, and the fact that the results satisfy equation (1) seems to justify the supposition. It is, however, possible that the increase of amplitude, and the accompanying increase of phase-path, could be caused by a decrease in the electron density in the absorbing region. This alternative explanation can be tested by making observations on the changes of group-path during the burst. If the bursts were caused by a focusing process involving parallel curvatures of the contours of

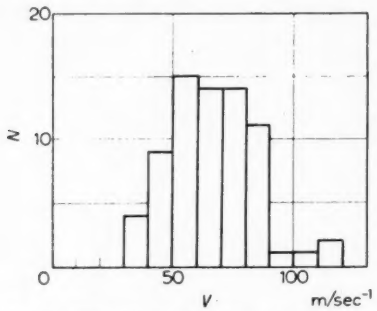

Fig. 3. Histogram showing the distribution of the observed drift velocities.

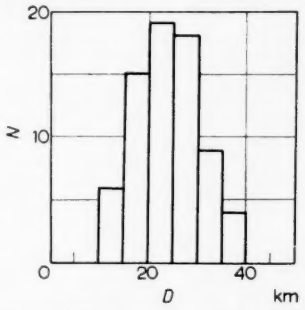

Fig. 4. Histogram showing the distribution of the horizontal extent of the large-scale irregularities.

electron density, the changes of group-path and of phase-path would be the same. If, however, it were caused by a reduction of the electron density in the absorbing region, they would be equal, but opposite in sign.

A direct measurement of the change in group-path is very difficult, since the changes would be of the same order as the changes in phase-path, that is a few wavelengths. This difficulty may be overcome by observing the phase-path on two adjacent frequencies and using the well-known relation between group-path (P') and phase-path (P),

$$P' = P + f\left(\frac{dP}{df}\right) \tag{2}$$

In Fig. 5 the magnitudes ($\Delta P_{2\cdot4}$) of the changes in phase-path obtained during amplitude bursts on 2·4 Mc/s are plotted as functions of the corresponding change ($\Delta P_{2\cdot0}$) in phase-path on 2·0 Mc/s. The theoretical lines for the conditions $\Delta P' = \Delta P$ and $\Delta P' = -\Delta P$ are drawn and the results are seen to agree better with the former. This appears to suggest that the bursts are not caused by varying absorption but are produced by large-scale irregularities near the reflection level.

2.4. *The rapid fading during a burst*

During a burst it is often found that the fading becomes more rapid, and it is interesting to enquire whether this fading could have been caused by the focusing

process itself. The primary result of a focusing process is to impose a phase gradient across a horizontal wave front as it leaves the ionosphere. Suppose that this phase-gradient simulates that which would have been produced by a concave mirror of width L and that the phase-deviation produced at the centre is $\Delta\phi$ radians, then theory (HEWISH, 1951 and BRAMLEY, 1955) summarized by RATCLIFFE (1956) shows that the wave which reaches the ground will have irregularities of amplitude of horizontal extent l, where

$$l = L/\Delta\phi \tag{3}$$

If the phase were examined on the ground, it would be found to have a large-scale structure of extent L, on which were superimposed small-scale amplitude variations

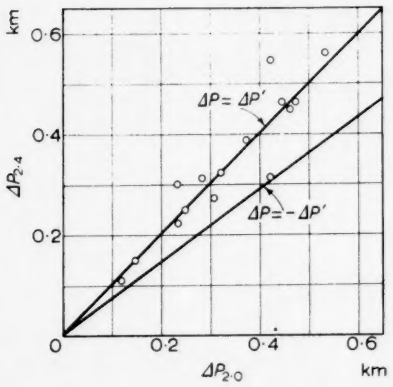

Fig. 5. The magnitudes ΔP of the changes in phase-path on two adjacent frequencies.

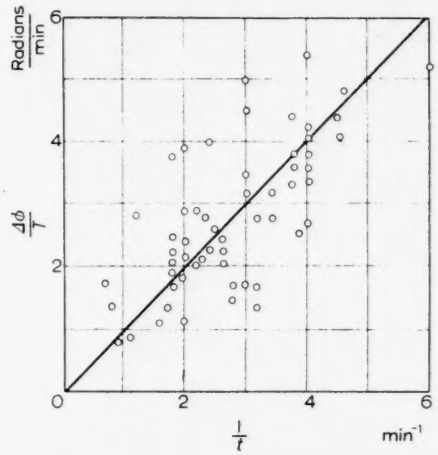

Fig. 6. Relation between observed rapid type of fading and the deep-phase modulation. See equation (4).

of extent l. Suppose now that both the burst and the rapid amplitude fading occur because the above-mentioned wave pattern drifts smoothly past the observer at a constant speed. Then the duration (T) of the large-scale phase variation and the period (t) of the small-scale amplitude variations would, from equation (3), be related by the expression

$$t = T/\Delta\phi \tag{4}$$

To test this relation, the quantities T and $\Delta\phi$ were derived from the phase records and t from the amplitude records, and were plotted against each other, as in Fig. 6. Most of the observations yielded points which fell near the straight line which represents equation (4). In these cases it seems reasonable to suppose that the rapid fading was caused by the large-scale phase irregularities.

2.5. *The transition to complicated fading*

Previous paragraphs have been concerned with phase-path records which were smooth enough to be interpreted simply. Sometimes the slow oscillations of phase increase in amplitude and are finally replaced by an irregular phase-trace which

VOL. 10 1957

is no longer capable of simple interpretation. At the same time, the fading speed increases considerably.

It has been found that, if the change in phase-path caused by a large-scale irregularity is represented by ΔP, and if its horizontal extent, determined as described in Section 2.2, is represented by D, then the quantity $\Delta P/D$ often increases from one cycle of phase oscillation to the next, and that when this quantity reaches a value of about 0·025, the phase record becomes too complicated to interpret. Similarly, when the phase record once again becomes simple enough to interpret, the quantity $\Delta P/D$ is at first near 0·025 and gradually decreases. This

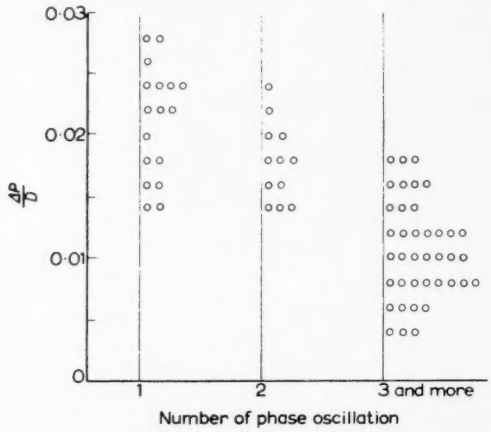

Fig. 7. The effective depth of modulation $\Delta P/D$ for successive phase oscillations which occur before or after the trace becomes irregular.

phenomenon is illustrated in Fig. 7, in which $\Delta P/D$ for successive phase oscillations is plotted against the number of phase oscillations which occur before or after the trace becomes complicated. These observations suggested that conditions of complicated phase are associated with values of $\Delta P/D$ greater than about 0·025.

After the phase record had become complicated, it was sometimes possible to interpret the fluctuations by taking a photograph of the trace on the cathode-ray tube which shows the beats between the downcoming wave and a reference oscillation.* It was then often found that the observed variations of amplitude and phase could be explained in terms of beating between two components. This sometimes occurred when the variation of amplitude appeared to be fairly random, so that observations of the amplitude alone would not have suggested the presence of two components.

An example is shown in Fig. 8, which refers to records obtained a few minutes after the transition from simple to complicated conditions shown in Fig. 1. Over the period indicated, the record was analysed as follows. The amplitude A and the phase ϕ were used to derive a vector which represented the received e.m.f. The mean variation of this vector throughout a fading cycle was deduced by superimposing the variations during a succession of individual cycles, measured from one

* See Fig. 1 of Findlay (1951).

VOL. 10 1957

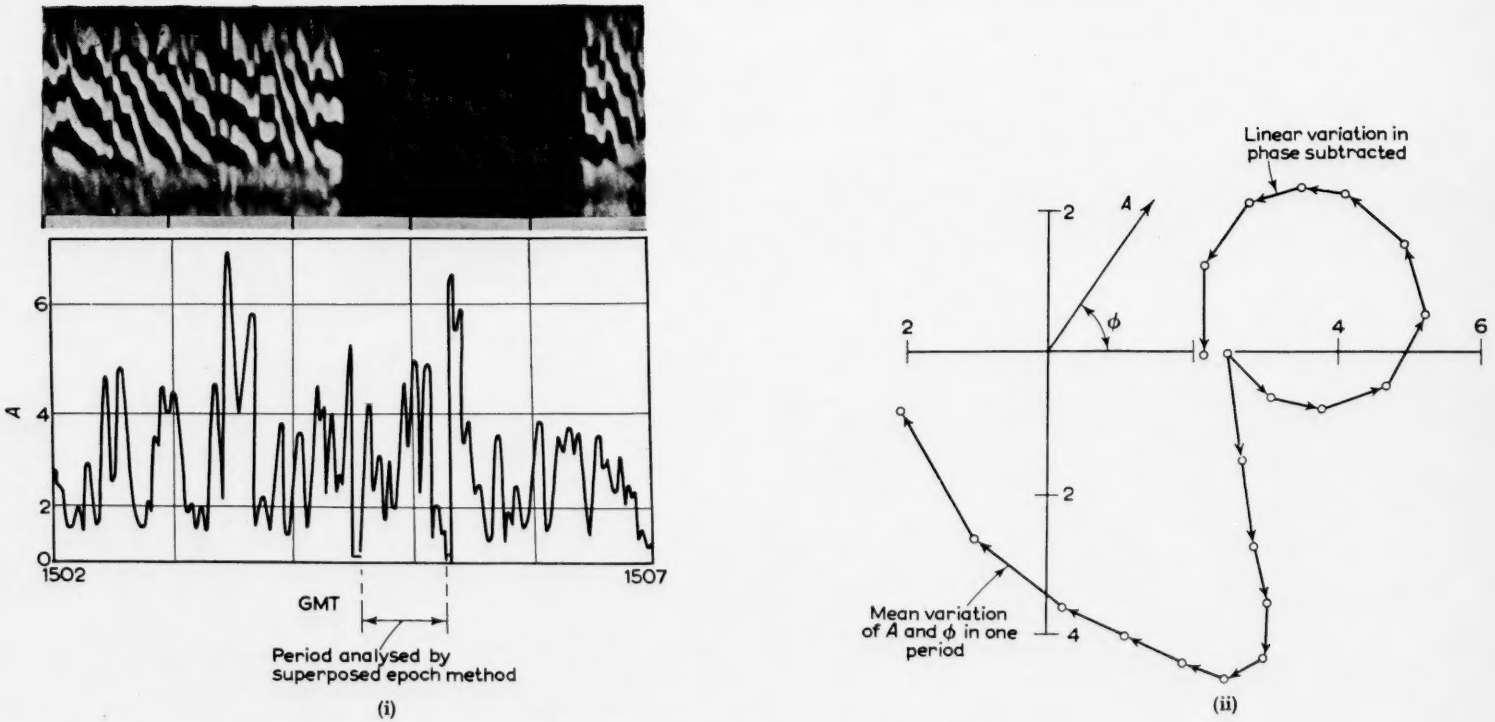

Fig. 8. Observed variations of amplitude A and phase ϕ.

minimum of amplitude to the next. If a phase which varied linearly with time was subtracted,* so that the phase was the same at the beginning and end of a fading cycle, the end of the vector was found to describe a circle. This suggests that the vector was the resultant of two components, which were rotating with different speeds.

If the two component waves arose by reflection from tilted portions of the ionosphere, the observed variations could be explained in terms of two surfaces tilted at 4° and 6° in opposite directions, moving with a horizontal velocity of 75 m/s, as illustrated in Fig. 9. For a sinusoidal surface with $\Delta P/D = 0{\cdot}025$

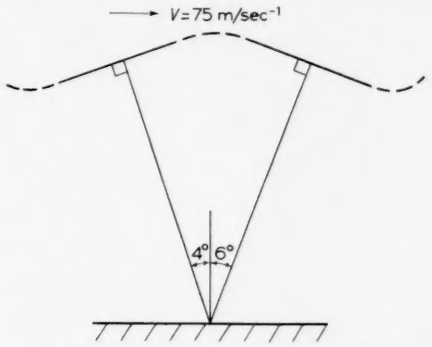

Fig. 9. Model deduced from Fig. 8.

the maximum tilt angle would be about 4°. If this interpretation is correct, the value of $\Delta P/D$ must have continued to increase after the transition to complicated conditions shown in Fig. 1, until the effective reflecting surface was sufficiently curved to provide two points of specular reflection.

3. Low Frequencies (200 kc/s) Night-time Results

Mr J. S. Belrose of the Cavendish Laboratory has been engaged in making records of the phase and amplitude of continuous waves, on a frequency of 200 kc/s, received over a distance of 150 km at night. He has kindly made his records available to the author. The observations discussed here are limited to the two hours preceding ground sunrise and the two hours following ground sunset on ten nights.

Because continuous waves were used, the phase record never become too complicated to measure, even when the phase varied rapidly; this behaviour is different from that observed with Findlay's pulse method used on the higher frequencies. Since it had been found, on the higher frequencies, that changes of phase and of amplitude were closely related, provided the quantity $\Delta P/D$, defined in Section 2, was not too large, an attempt was first made to see whether a similar association occurred on the lower frequency. On that frequency, however, the ground extent (D) of the phase variation was not known, only its duration (T) was recorded. The assumption was therefore made that the wave-pattern moved over the ground with a velocity V so that

$$\Delta P/D = \Delta P/TV \qquad (5)$$

* The superimposed linear variation corresponds to a continuous change of the height of reflection

VOL. 10 1957

Inspection of the records then showed that there was close association between phase and amplitude if $\Delta P/T$ was less than 1·6 m/s, but not if it was greater than this. Fig. 10 shows examples of close association and of little association.

It is of interest to enquire whether the condition $\Delta P/D > 0{\cdot}025$ that makes the FINDLAY phase-trace too complicated to read on 2 Mc/s is the same as that which determines when phase and amplitude are unrelated on 200 kc/s. Insertion of the values for $\Delta P/D$ and $\Delta P/T$ into equation (5) yields a value $V = 65$ m/s.

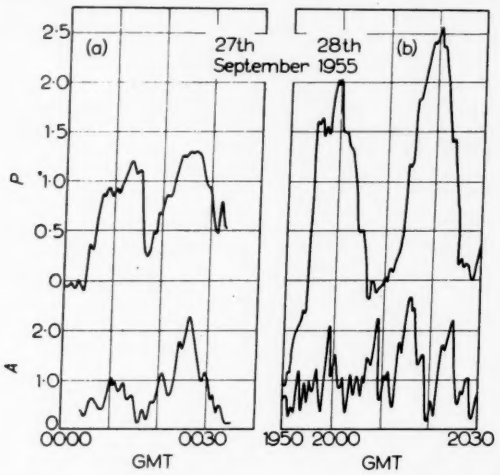

Fig. 10. Observed variations of amplitude A and phase-path P on a frequency of 200 kc/s at steep incidence.

Since this value agrees well with direct measurements of V we conclude in the two that the same factors determine the association of phase and amplitude variations cases.

4. CONCLUSIONS

When the phase of a wave of frequency 2 Mc/s reflected from the E layer is measured, it is found that irregularities of size between 10 and 40 km occur. If the phase-path variation in these irregularities is ΔP, and their extent D, then if $\Delta P/D < 0{\cdot}025$, approximately, the phase variations are associated with corresponding amplitude variations in a simple way; but if $\Delta P/D > 0{\cdot}025$, approximately, this simplicity is no longer apparent.

A large-scale phase irregularity causes a focusing of the wave which is seen as a "burst" of amplitude lasting about 5 min. If $\Delta P/D < 0{\cdot}025$, the rapid fading inside the burst can be shown also to be the result of the focusing effect. If, however, $\Delta P/D > 0{\cdot}025$, conditions become more complicated. On one such occasion the changes of amplitude and phase variations could be interpreted in terms of two separate component waves reflected from different parts of the ionosphere.

Observations made at night on a frequency of 200 kc/s at an angle of incidence of about 40° also showed an association between the amplitude and phase when $\Delta P/D < 0{\cdot}025$, but no simple association when $\Delta P/D > 0{\cdot}025$.

These results are as would be expected if the phase changes were caused by a reflecting process which simulated a concave mirror.

Acknowledgements—I am indebted to the Royal Norwegian Council for Scientific and Industrial Research for a grant which has enabled me to do this work at the Cavendish Laboratory Cambridge. I also wish to express my sincere thanks to Dr. J. W. FINDLAY and Mr. J. S. BELROSE for permission to use their records.

I have benefited much from discussions with Mr. J. A. RATCLIFFE and and Dr. B. H. BRIGGS.

REFERENCES

BRAMLEY E. N.	1955	*Proc. Instn. Elect. Engrs.* **102,** Part III, 533.
FINDLAY J. W.	1951	*J. Atmosph. Terr. Phys.* **1,** 353.
HEWISH A.	1951	*Proc. Roy. Soc.* **A209,** 81.
JONES I. L., LANDMARK B., and SETTY C. S. G. K.	1957	*J. Atmosph. Terr. Phys.* **10,** 296.
RATCLIFFE J. A.	1956	*Reports on Progress in Physics* Vol. XIX. p. 188. Physical Society, London.
SCHRAG R. L.	1955	*The Physics of the Ionosphere* Physical Society, London.
WHITEHEAD J. D.	1956	*J. Atmosph. Terr. Phys.* **9,** 269.

VOL. 10 1957

Journal of Atmospheric and Terrestrial Physics, 1957, Vol. 10, pp. 296 to 301. Pergamon Press Ltd., London

Movements of ionospheric irregularities observed simultaneously by different methods

I. L. Jones, B. Landmark,* and C. S. G. K. Setty
Cavendish Laboratory, Cambridge

(*Received* 31 *January* 1957)

Abstract—It is shown that horizontal movements of large-scale irregularities in the ionosphere can be conveniently investigated by recording "bursts" of the amplitude of a reflected radio wave received at one point from three transmitters separated by about 15 km. Measurements of the movements of large-scale irregularities made by this and other methods were compared with the results of simultaneous observations of ordinary fading made at three closely-spaced receivers. It was concluded that the large-scale irregularities had the same movements as those irregularities which produced the ordinary fading.

1. Introduction

Movements of large-scale distortions in the ionosphere have been studied by various workers: in the F region by Beynon (1948), Munro (1948, 1950), Price (1955), and others, and in the E region by Landmark (1957). All investigations have shown that the large-scale irregularities move with a horizontal drift velocity of about 100 m sec^{-1} in a direction showing seasonal and diurnal variations. The results are in fair agreement with those found by observing small-scale irregularities at closely spaced receivers.

The purpose of this paper is to make a detailed comparison of the results of the two kinds of measurements. The different methods used to observe the velocity of drift of the irregularities will be described in Section 2. The results from the observations will be presented in Section 3, and discussed in Section 4.

2. Methods of Observation

The following four different methods were used to determine the velocity of movement of the irregularities in the ionospheric layers:

(a) Observations with closely spaced receivers (about 1 wavelength apart),
(b) Recording of group height as a function of time for more widely spaced transmitters (about 200 wavelengths apart).
(c) Recording of amplitude as a function of time for more widely spaced transmitters (about 200 wavelengths apart).
(d) Simultaneous observations of changes of amplitude and of phase path.

By method (a) the movements of the irregularities which produce the rapid variations of amplitude could be determined, while the methods (b) to (d) were used to determine the movements of the large-scale irregularities in the layers. The different methods are described below.

(a) *Observations with closely spaced receivers*

In this method a common transmitter was used and the drifts were determined from the time-shifts in the amplitude records obtained at three receivers about 1 wavelength apart. The

* On leave from the Auroral Observatory, Tromsö.

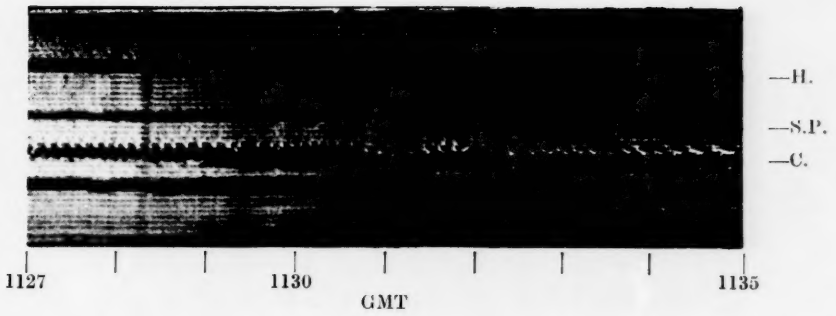

Fig. 2(a)

VOL.
10
1957

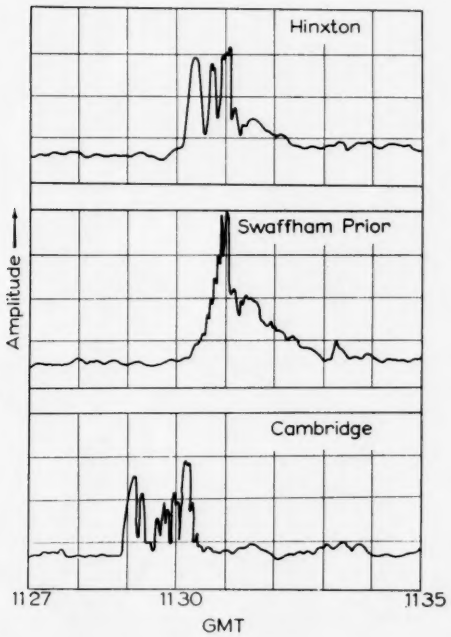

Fig. 2(b).

Fig. 2(a). The *Z* traces of Fig. 2(a) were recorded simultaneously with the amplitude records of Fig. 2(b), from the three transmitters located as shown in Fig. 1.

VO
1
19

frequencies used were 2·05 Mc/s for waves reflected from the *E* layer, and 4·1 Mc/s for waves reflected from the *F* layer. The method has been in use for some years at Cambridge, and has been described by MITRA (1949).

It was found that, when the large-scale irregularities could be recorded in such a way that drift velocities were obtainable by methods (b) to (d), the fading was usually so shallow that the time-delays in method (a) could not be obtained by the automatic technique introduced by PHILLIPS (1955). It was then necessary to record the amplitudes of the signals from the three receivers and to make deductions from these records.

(b) *Recording of group height as a function of time for more widely spaced transmitters*

In this method the waves from three spaced transmitters were received at a single point and the three group heights were recorded together photographically as functions of time.

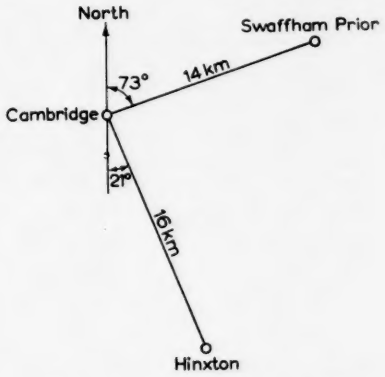

Fig. 1. Location of transmitters.

The transmitters, at Cambridge, Hinxton, and Swaffham Prior, were located as shown in Fig. 1. The common receiver was at Cambridge. A constant frequency of 4·1 Mc/s was used.

A typical example of observed variations of group height during conditions when a large-scale distortion in the *F* layer was passing overhead is shown in Fig. 2(a). In this particular case the group-height traces were disturbed so as to form a *Z* of the type described by MUNRO (1950). From the time-intervals between the occurrence of the *Z* in the three traces the direction and magnitude of the velocity can be determined.*

(c) *Recording of amplitude as a function of time for more widely spaced transmitters*

When records were made by the method described under (b), it was found that whenever a *Z* occurred in the group-height traces, sudden increases of mean amplitude ("bursts") were also recorded. Thus Fig. 2(b) shows the amplitude bursts which were recorded at the same time as the *Z* traces shown in Fig. 2(a). From Fig. 2 it can be seen that the time-delays obtained from observations of group height and of amplitude are the same. This was always found when *Z* traces and bursts were recorded together.

In view of the fact that amplitude bursts occur more often than *Z* traces, the method was extended so that the times of occurrence of bursts were recorded and the velocities were deduced from them.

---

* If the ionospheric disturbance is elongated, the velocity deduced is not necessarily the true velocity, and in extreme cases it is only the velocity normal to the line of elongation.

VOL. 10 1957

(d) *Simultaneous observations of changes of amplitude and of phase path*

Whitehead (1956) has shown that if, during a "burst," the amplitude A and the phase path P of an echo reflected from a height h are measured, then they satisfy the equation:

$$A^2 \propto 1 - \frac{h}{2V^2}\frac{d^2P}{dt^2} \tag{1}$$

Where V is the velocity of drift of the "burst," Whitehead (1956) applied this method to the F layer and Landmark (1957) to the E layer. It was used in the present work on frequencies of 2·05 Mc/s (E layer) and 4·1 Mc/s (F layer).

3. Results

In this section, results obtained in the period 1 March to 15 May 1956 will be described.

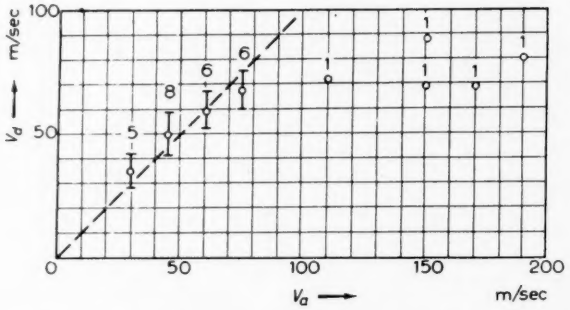

Fig. 3. Comparison of results for waves reflected from the E layer on a frequency of 2·05 Mc/s. V_a and V_d represent the magnitude of the drift values measured by methods (a) and (d) of Section 2. The number of observations in each group is indicated in brackets, and the vertical lines indicate the S.Ds.

(a) *E layer*

A single sender was used, working on a frequency of 2·05 Mc/s, and the waves were received at a nearby point after reflection at vertical incidence. Method (d) of Section 2 was used to determine the drift velocity of the large-scale irregularities. Only the magnitude of the velocity can be determined by this method. We shall denote it by V_d. Method (a) was used simultaneously to determine the velocity, V_a, of the small-scale structure.

In Fig. 3 the observed values of V_d are plotted as functions of the simultaneously observed values of V_a. Each pair of values was deduced from a period of observation of about 5 to 10 min. The results are shown as mean values with standard deviations, except for five single observations. The agreement between the velocities found by the two methods is seen to be quite close except for the five single points, which all correspond to large velocities measured by method (a). More detailed analysis of many results obtained on other occasions by method (a) lead us to think that these large values of V_a are spurious, and are the result of changes in the amplitude pattern as it moves from one receiver to another.*

* These changes have been described by Briggs, Phillips, and Shinn (1950) in terms of a velocity which they called V_c. It should not be confused with the velocity called V_c in this paper.

(b) *F layer*

WHITEHEAD (1956) compared four values which he obtained for the drift velocity in *F* region by his method (see Section 2d), with values obtained on the same four occasions by the MITRA (1949) method (see Section 2a). He found that the magnitudes of the velocities deduced by the two methods were in reasonable agreement, but there was no evidence about the directions.

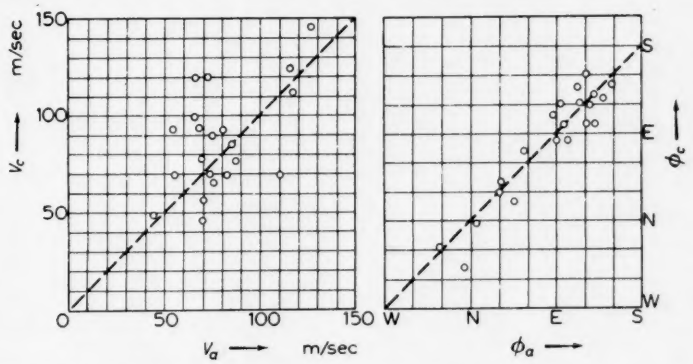

Fig. 4. Comparison of results for waves reflected from the *F* layer on a frequency of 4·1 Mc/s. $V_a(\phi_a)$ and $V_c(\phi_c)$ represent the magnitude and directions of the drift velocities measured by methods (a) and (c) of Section 2. V_c should not be confused with V_c of BRIGGS, PHILLIPS, and SHINN (1950).

VOL. 10 1957

WHITEHEAD's work has been extended by using all the methods of Section 2 to investigate the nature of a wave reflected from the *F* layer on a frequency of 4·1 Mc/s. The magnitudes V_c and directions ϕ_c of the velocities of the large-scale irregularities determined by method (c) are compared in Fig. 4 with the corresponding magnitudes V_a and directions ϕ_a determined simultaneously by method (a) for the small-scale irregularities. Sometimes both "bursts" and "*Z* traces" were present simultaneously, so that results from both methods (b) and (c) could be used; on these occasions the mean values were taken and are plotted as V_c and ϕ_c. We see that the direction found by the two methods agrees well. The observed magnitudes do not show a very good agreement, but the observed correlation is just significant.

Table 1

$\frac{\lvert V_c - V_a \rvert}{\frac{1}{2}(V_c + V_a)}$	$\lvert \phi_c - \phi_a \rvert$	
	$<20°$	$>20°$
$>0{\cdot}2$	3	8
$<0{\cdot}2$	8	2

The table shows the number of occasions on which the magnitude of $\lvert V_c - V_a \rvert / [\frac{1}{2}(V_c + V_a)]$ and $\lvert \phi_c - \phi_a \rvert$ fell, simultaneously, within the ranges listed.

Table 1 shows the relation between the observed differences of magnitudes ($V_e - V_n$) and differences of directions ($\phi_e - \phi_n$) of the velocities. The table shows that when the directions agree, so do the magnitudes, and when the directions are different, so are the magnitudes.

The main conclusion from these results is that the irregularities which produce the rapid fading during the bursts have the same movements as the large-scale distortions which produce the bursts. There is of course still the possibility that the fading in between the bursts is produced by irregularities whose movements are different from those of the large-scale distortions. To find out whether or not this was so, the velocity before and after each burst was determined when possible. The difficulty here was that between the bursts the fading was often so shallow that it was difficult to determine a reliable velocity.

No significant correlation was found between the velocities observed during the bursts, and the mean velocity observed before and after the bursts, nor was there any correlation between the values obtained before and after each burst.

Table 2

$\phi_1 - \phi_3$	$\lvert\phi_2 - \frac{1}{2}(\phi_1 + \phi_3)\rvert$		
	0–30°	30–60°	60°
0–30°	6	0	0
30–60°	3	2	1
60°	1	1	5

The table shows the number of occasions on which the magnitude of $|\phi_1 - \phi_3|$ and $|\phi_2 - \frac{1}{2}(\phi_1 + \phi_3)|$ fell within the ranges listed.

These facts would be explained if values deduced between the bursts were unreliable. If this explanation is correct, it would be expected that, when the values found before and after the bursts agreed, the values observed during the bursts should also give the same result. This is shown to be the case in Table 2, where the observations have been classified into groups according to the differences ($\phi_1 - \phi_3$) between the observed directions before and after the bursts, and the differences $[\phi_2 - \frac{1}{2}(\phi_1 + \phi_3)]$ between the directions during the bursts and the mean of the directions before and after the bursts.

The probability of obtaining the results of Table 2 by pure chance is 0·03, and it is concluded that the large-scale irregularities have the same movements as those irregularities which produce the rapid type of fading.

4. Discussion

Previous workers have deduced the drifts of large-scale disturbances in the F layer from $h'(t)$ records made with widely spaced receivers or transmitters. In the present paper it is shown that observations of the bursts of amplitude

observed under the same conditions can be at least as useful. In particular it has been found that:

(a) The result is the same as that obtained from smaller-scale irregularities observed at closely spaced receivers.
(b) Results are obtainable even when the rapid fading is so shallow that results cannot be determined from records of the PHILLIPS (1955) type made at closely spaced receivers.
(c) The records obtained are easy to analyse.
(d) The method of observing amplitude has the great advantage over the method of observing group height, that amplitude bursts occur more often than distortions in the group-height traces.
(e) Since bursts of amplitude are often observed in echoes reflected from the *E* layer, the method can also be used for determining the drift in that layer.

It has been suggested by BRAMLEY (1955) that the fading of waves reflected from the *F* layer during quiet conditions is produced as the wave traverses the *E* layer. Since it has been shown in this paper that the irregularities which cause the fading have the same motions as the large-scale distortions in the *F* layer, it appears probable that all the fading must be caused by irregularities which occur in the *F* layer.

VOL. 10 1957

Acknowledgements—We are much indebted to Tube Investments Ltd., and Dr. K. WEEKES, who provided facilities for the running of transmitters at Hinxton and Swaffham.

We wish to express our thanks to the Gassiot Committee of the Royal Society (I. L. J.), the Royal Norwegian Council for Scientific and Industrial Research (B. L.), and the Government of India (C. S. G. K. S.) for grants which enabled us to take part in this work.

We have benefited much from discussions with Mr. J. A. RATCLIFFE, Dr. B. H. BRIGGS, and Mr. D. M. SCHLAPP.

REFERENCES

BEYNON W. J. G.	1948	*Nature, Lond.* **162,** 887.
BRAMLEY E. N.	1955	*Proc. Instn. Elect. Engrs.* Pt B **102,** 533.
BRIGGS B. H., PHILLIPS G. J., and SHINN D. H.	1950	*Proc. Phys. Soc.* **B63,** 106.
FINDLAY J. W.	1951	*J. Atmosph. Terr. Phys.* **1,** 353.
LANDMARK B.	1957	*J. Atmosph. Terr. Phys.* **10,** 288.
MITRA S. N.	1949	*Proc. Instn. Elect. Engrs.* Pt III, **96,** 441.
MUNRO G. H.	1948	*Nature, Lond.* **162,** 886.
MUNRO G. H.	1950	*Proc. Roy. Soc.* **A202,** 208.
PHILLIPS G. J.	1955	*J. Atmosph. Terr. Phys.* **6,** 124.
PRICE R. E.	1955	*The Physics of the Ionosphere* Physical Society, London.
WHITEHEAD D.	1956	*J. Atmosph. Terr. Phys.* **9,** 269.

Low-frequency radio emission from aurorae*

G. R. Ellis

(*Received* 3 *March* 1957)

Abstract—This paper discusses the possibility that Cerenkov radio emission by auroral particles approaching the earth may contribute to the level of the continuous component of atmospheric radio noise observed at frequencies of hundreds of kilocycles per second.

It is shown that, providing the Cerenkov process is valid at radio frequencies, the flux density of the radiation may be as high as 10^{-21} W m^{-2}(c/s)$^{-1}$ at these frequencies, well above the minimum observable using current techniques. The frequency range of the emission would extend from a few hundred kc/s to low-audio frequencies.

1. Introduction

Recent observations by Reber and Ellis (1956) of the continuous component of atmospheric radio noise at frequencies below 10 Mc/s have shown that a major proportion is of cosmic origin when the ionospheric critical frequency f_0F2 is less than the observing frequency, even as low as 900 kc/s. Lower in frequency still, at 520 kc/s, well below f_0F2, some continuous noise was observed at night which did not have any significant correlation with f_0F2. More recent measurements by Reber (1956) have confirmed the existence of this low-frequency radiation. Its origin, however, is still not understood, and it is the purpose of this paper to examine a possible mechanism.

It is well established that electromagnetic radiation (Cerenkov radiation), at optical frequencies, may be emitted by fast charged particles traversing an optical medium for which the refractive index is greater than the ratio of the velocity of light to the particle velocity, i.e. $n > c/v$, (Schiff, 1950; Mather, 1953). That Cerenkov radiation may also occur at radio frequencies where the medium is an ionized gas has recently been discussed by Marshall (1956) with reference to the emission of solar radio waves. He pointed out that the refractive index of the solar corona can increase to values sufficiently large to satisfy the Cerenkov condition in the vicinity of the levels where the wave-frequency f is equal to either the plasma frequency $f_0 = \left(\frac{Ne^2}{m\pi}\right)^{\frac{1}{2}}$ or the gyrofrequency $f_H = \frac{eH}{2\pi mc}$, these frequencies being of the order of tens of megacycles per second.

There is an interesting application of this idea to the emission of Cerenkov radiation in the upper ionosphere by auroral particles approaching the earth. It will be shown that, providing the Cerenkov process is valid at radio-frequencies, emission may occur throughout a frequency band extending from hundreds of kilocycles per second to low audio-frequencies and the intensity may be sufficient to make it observable at the ground, using recently described techniques for reducing interference by terrestrial atmospherics (Reber and Ellis, 1956).

2. Emission Regions

The refractive index of an ionized medium for the extraordinary mode of

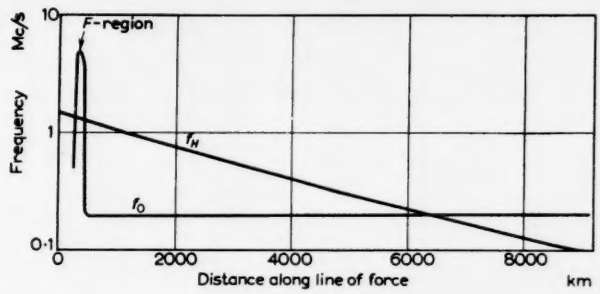

Fig. 1

propagation is given by the expression:

$$n^2 \geqslant 1 + \frac{x}{y-1} \quad \text{if} \quad x = \frac{Ne^2}{m\pi f^2} > 1 \qquad y = \frac{f_H}{f} \geqslant 1 \tag{1}$$

The condition for Cerenkov emission, $n > c/v$, then gives

$$\frac{c^2}{v^2} < 1 + \frac{x}{y-1} \tag{2}$$

For a particle velocity $v \ll c$, equation (2) may be satisfied either when $x \gg 1$ or when $y \sim 1$. There will thus be two regions of emission corresponding to these two extremes: x will be greatest at the electron density maximum of the F region, while y may approach unity at any level, depending on the wave-frequency and the intensity of the geomagnetic field.

That is, $y = 1$

when $$f = f_H = \frac{eH}{2\pi mc} = \frac{e}{2\pi mc}\, 0{\cdot}31\ R_0^{-3} \cos^{-5}\psi (1 + 4\tan^2\psi)^{\frac{1}{2}}$$

ψ = geomagnetic latitude

R_0 = radial of distance of line of force for $\psi = 0$, in units of earth radius.

These considerations may be illustrated by taking an actual model of the ionosphere. For example, Fig. 2 shows the variation in refractive index for different wave-frequencies, along a geomagnetic line of force ending at geomagnetic latitude 60°, assuming a parabolic F layer with $f_0F2 = 5$ Mc/s, semi-thickness 100 km, and a uniform electron density with $f_0 = 200$ kc/s, outside it.

To proceed further, we need some estimate of the velocity of auroral particles. MEINEL (1951) has reported the observation of protons entering the earth's atmosphere from the direction of the magnetic zenith, during an intense aurora, with velocities of about 0·01 c. On the other hand, calculations by VEGARD (1937) have shown that electrons would need a velocity of about 0·3 c in order to penetrate the atmosphere to a height of about 90 km. For particle velocities of 0·01, 0·1, and 0·3 c, Fig. 2 shows those regions in which Cerenkov emission may be expected at different frequencies.

VOL. 10 1957

3. The Intensity of the Emission

The theory of Cerenkov radiation shows that the number of photons emitted per charged particle per unit pathlength per unit frequency interval is given by

$$\frac{dI}{df} = \frac{4\pi^2 e^2}{hc^2}\left(1 - \frac{1}{\beta^2 n^2}\right)$$

h = Planck's constant

$\beta = v/c$

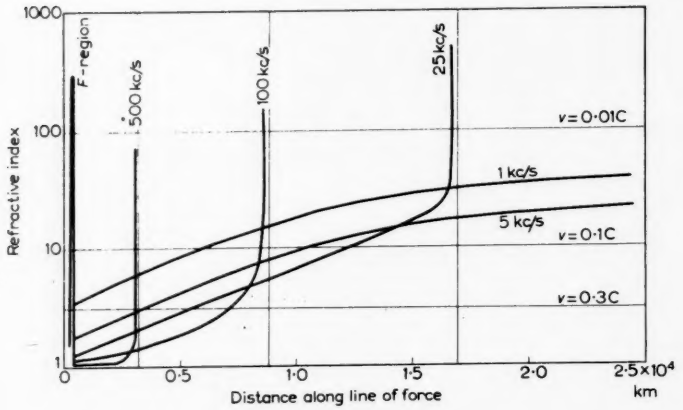

Fig. 2

This may be expressed in units of watts per square metre per cycle per second, per unit pathlength (Marshall, 1956).

$$S = \frac{4\pi^2 e^2}{hc^2}\left(1 - \frac{\beta^2 n^2}{1}\right)\frac{hfvN \times 10^4}{10^7}$$

Assuming $\left(1 - \frac{1}{\beta^2 n^2}\right) \sim 1$, we have for the total emission in a column of length l metres.

$$S = 3 \times 10^{-31}\frac{vNl}{\lambda}\ \mathrm{W\ m^{-2}\,(c/s)^{-1}}$$

v in cm/sec,

N in particles/c.c.,

l in metres,

λ = wavelength in metres.

The length of the column l may be obtained from Fig. 2 for different particle velocities. The final quantity needed, the particle density N, is a matter for conjecture. Bennett (1954) has estimated that about 10^{-3} protons per cubic centimetre, with a speed of 10^{10} cm/sec, might be sufficient to produce the visible light of an average aurora. With these and nearby values of N and v we obtain the Cerenkov radiation intensities shown in Table 1.

Table 1. Calculated flux densities of Cerenkov radiation, in emitting region

	Thickness of emitting region			Flux density W m^{-2} (c/s)$^{-1}$ × 10^{-25}		
Particle speed	0·3 c	0·1 c	0·01 c	0·3 c	0·1 c	0·01 c
Particle density	10^{-3}	3×10^{-2}	3×10^{-1}	10^{-3}	3×10^{-2}	3×10^{-1}
Wave frequency 500 kc/s	km 230	km 8	km 0·08	11000	350	3·5
100 kc/s	1800	240	1·6	17000	2300	150
25 kc/s	12000	4500	50	27000	3100	240
5	23000	14000	—	11000	12500	—
5	26000	2000	40	2500	190	4

VOL. 10 1957

4. Discussion

To be observable, the radiation must reach the ground. If it is generated in a region in which $x > 1$, then it must pass through the coupling level $x = 1$ on the way down.

For extraordinary waves from a region $x > 1$, $y > 1$, $n > 1$, this level is only transparent if the propagation is quasi-longitudinal (Mitra, 1948).

i.e. if $$\theta < \cos^{-1}\left[\left(\frac{\nu^2}{4\pi^2 f_H{}^2} + 1\right)^{\frac{1}{2}} - \frac{\nu}{2\pi f_H}\right], \qquad x = 1$$

θ = propagation angle,

ν = collision frequency.

Fortunately, at wave-frequencies of hundreds of kilocycles per second, $x = 1$ will occur normally below the E region, where the collision frequency is sufficiently high to prevent the restriction in the allowable values of θ from being serious. If we assume $x = 1$ at 80 km, we have $\nu = 5 \times 10^6$/sec (Nicolet, 1953). With $f_H = 1{\cdot}5$ Mc/s, $\theta < 41°$ for QL propagation.

At the lowest frequencies it is well known from whistler observations that X-mode quasi-longitudinal penetration of the lower ionosphere is commonplace.

In the example considered here, Fig. 1 shows that the large refractive indices near $y = 1$ will, for wave-frequencies between 200 kc/s and 1150 kc/s, occur in a region where $x < 1$ above the F region. Since $x > 1$ at $N_{\max}(F2)$, radiation in this frequency range would have to penetrate two $x = 1$ levels, one below and one above the electron density maximum. In the latter case, the collision frequency would be low ($\sim 10^2$/sec) and the allowable range of the propagation angle θ for quasi-longitudinal propagation would be very small: $\theta < 0{\cdot}3°$ if $f_H = 1$ Mc/s. As

a result, the flux density would be greatly reduced below the ionosphere at frequencies greater than 200 kc/s for the model chosen.

A further limitation in the observability of Cerenkov radiation is the increase in D-region ionization and absorption during strong aurora. At frequencies above 1 Mc/s this has the effect of producing an auroral blackout with cessation of ionospheric echoes. However, there is little information about D-region absorption at much lower frequencies, and whistler activity at few kc/s does not appear to show any significant correlation with geomagnetic disturbances (STOREY, 1953).

Although the intensities calculated for the lower frequencies (Table 1) would be less than the minimum observable using conventional inefficient antennae, the focusing effect thought to occur with whistler propagation (STOREY, 1953) might substantially increase the probability of observation. It is worth noting that continuous radio noise at audio-frequencies has been observed by a number of investigators during whistler observations.

At frequencies of hundreds of kc/sec the calculated intensities are well above the minimum observable with known techniques.

During their measurements at 520 kc/s, REBER and ELLIS (1956) observed continuous radio noise with flux densities of up to 10^{-22} W m^{-2} (c/s)$^{-1}$. This was about 100 times greater than the minimum observable at night, using their technique for reducing interference from atmospherics.

If this radiation is of Cerenkov origin, then it would be expected to show a strong correlation with auroral activity.

Further, it would be most intense in the auroral zone, where it would appear to come from an area of the sky surrounding the magnetic zenith.

If along a flux line of the geomagnetic field f_0 became less than f_H, then the spectrum of the radiation could have a sharp cut-off on the high-frequency end at the least frequency for which $f_0 = f_H$.

If the auroral particles arrive in individual bursts, then one might expect that the frequency of emission would increase with time as the particles penetrated to regions of greater geomagnetic field intensity and therefore gyrofrequency.

In the example discussed above, for a particle speed of 0·01 c there would be a delay of slightly less than 1 sec between the time of appearance of a burst of noise at 100 kc/s and at 200 kc/s.

REFERENCES

BENNETT W. H. and HULBERT E. O.	1954	*Phys. Rev.* **995,** No. 2, 315.
MARSHALL L.	1956	*Astrophys. J.* **124,** 2, 469.
MATHER R. L.	1951	*Phys. Rev.* **84,** 181.
MEINEL A. B.	1951	*Astrophys. J.* **113,** 50.
MITRA S. K.	1948	*The Upper Atmosphere* p. 167. Royal Asiatic Society of Bengal Calcutta.
NICOLET M.	1953	*J. Atmosph. Terr. Phys.* **3,** 200.
REBER G.	1956	*Proceedings Radio Astronomy Symposium* September, 1956, C.S.I.R.O., Sydney.
REBER G. and ELLIS G. R.	1956	*J. Geophys. Res.* **61,** 1.
SCHIFF L. I.	1949	*Quantum Mechanics* p. 261. McGraw-Hill.
STOREY L. R. O.	1953	*Phil. Trans. Roy. Soc.* **A246,** 113.
VEGARD L.	1937	*Terrestrial Magnetism and Electricity* (Edited by J. A. FLEMING) p. 609. McGraw-Hill.

Journal of Atmospheric and Terrestrial Physics, 1957, Vol. 10, pp. 307 to 317. Pergamon Press Ltd., London

Analysis of fading records from four spaced receivers for ionospheric wind measurements

M. Srirama Rao and B. Ramachandra Rao
Ionospheric Laboratory, Andhra University, Waltair

(*Received* 3 *December* 1956)

Abstract—This paper deals with the analysis of fading records from four spaced receivers of pulsed radio waves reflected at vertical incidence from the ionosphere, with a view to finding out the shape of lines of maxima and evolve a better method of calculating wind data. The usual three-station method of measurement of ionospheric winds using average displacements is found to give inaccurate results. It is shown that the method of calculating wind data using median values of displacements gives reliable results. A new and improved method of analysing wind records for evaluation of true velocities and direction is also presented.

VOL. 10 1957

1. Introduction

It is well known that the time-delays between any two fading records in the spaced-receiver method for investigating movements in the ionosphere are widely variable. In the usual method of analysis of these fading records, the average effect of the moving diffraction pattern on the ground is considered equivalent to a straight line of maximum amplitudes moving in a direction normal to it. Calculations based on the average of the time-delays thus yield only the normal component of the drift which is at right angles to the line of maxima. In a recent communication, Ratcliffe (1954) has shown that the variation of the time-delays observed in this method need not necessarily be taken as evidence of changing velocity or direction of the wind and that these variations could be produced by the random variation of the orientation of the line of maxima with respect to the direction of motion, even if the wind is constant. For the simple case of a straight line of maxima, expressions have been obtained for the probability distribution of the time-delays, and out of the two records analysed, only one of them is found to agree fairly well with the theoretical curve. Very recently, Barber (1956) has attempted a correlation method of interpretation of fading records, assuming first elliptical contours for the cross-correlograms, and later a drifting pattern without change of form, but it is found that the latter form is satisfied by only one of the two records analysed.

An entirely new approach to this problem is attempted in this investigation by taking fading records from four spaced receivers and analysing the time-delays observed in these records. A new and improved method of obtaining ionospheric wind velocities and directions by this four-station method is also outlined.

2. Experimental Details

For this investigation, the three-station method developed at Cambridge (Mitra, 1949; Phillips, 1952) has been extended into a four-station method by introducing a fourth aerial A_4, as shown in Fig. 1, in a line with A_1,A_2 such that A_1 is at the centre point of A_2 and A_4. The two sets of aerials, A_1,A_2,A_3 and A_1,A_4,A_3, occupy the corners of adjacent and identical right-angled triangles whose sides are of length 108 m each. The usual three-station recording

equipment in use here is modified in this investigation by converting the triple-beam oscillograph so as to give four time-base traces using an electronic switch to split one of the beams into two. A good number of four station fading records were obtained with this equipment by photographing simultaneously the echo due to the single-hop reflection from the E region received at the four spaced receiving aerials. As an example, the detailed analysis of a typical

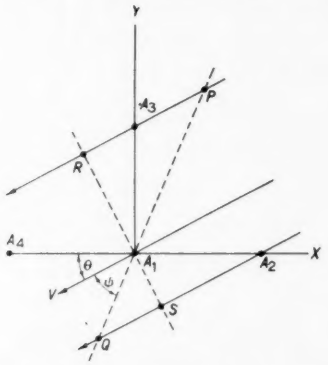

Fig. 1. Diagram showing the location of the four aerials and indicating the wind parameters along with a typical straight line of maxima.

record taken at 1625 IST on 27 November 1955, part of which is reproduced in Fig. 2, is treated in the following sections. The displacements a_{12}, a_{13}, and a_{14}, measured under a microfilm reader, of the corresponding peaks in the fading patterns of A_2 A_3, and A_4 respectively, are measured with respect to the aerial A_1, the time being taken to be positive if it is earlier and negative if it is a later occurrence in these patterns. The corresponding time displacements and wind data by the three-station method are calculated in the usual manner as described in an earlier paper (Rao, Rao, and Murty, 1956).

3. Nature of Lines of Maxima of the Diffraction Pattern

The fourth aerial is introduced in this investigation to test experimentally the validity of the assumption made by almost all the previous investigators that the line of maxima is straight. If this assumption is right, it is to be expected that the displacements a_{12} and a_{14} would be equal and opposite as aerials A_2, A_1, and A_4 are situated at equal distances along a straight line. Analysis of the records taken during the months of July and November 1955 showed that, in general the displacements a_{12} and a_{14} are nearly equal and opposite for about half the readings in each record. For these sets of readings, the lines of maxima may therefore be regarded as being either nearly straight or slightly curved. The remaining half of the readings for which a_{12} and a_{14} are quite different and sometimes of the same sign cannot be explained on this basis unless we assume that the angle between the straight line of maxima and the direction of motion is continuously changing as it moves from one extreme aerial to the other. As there is no experimental evidence to show such rapid changes of the orientation of the line of maxima in such a short distance, we will make the plausible assumption that each particular line of maxima maintains its shape throughout its traverse of the four spaced aerials. It is now easy to show that most of the remaining half of the readings correspond to the movement of curved lines of maxima.

VOL. 10 1957

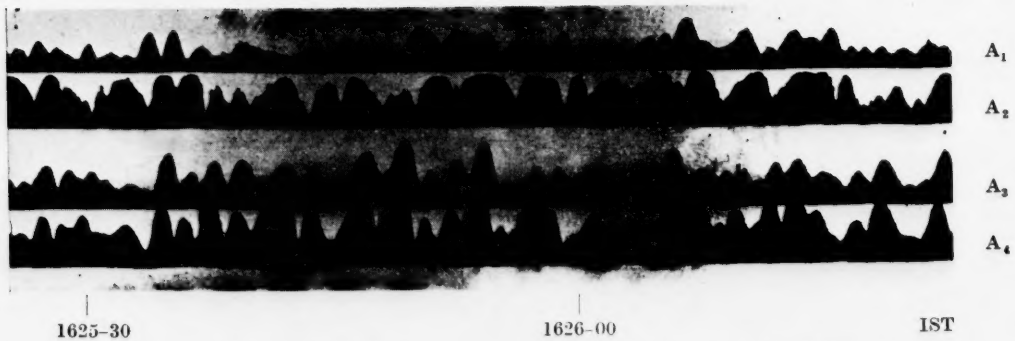

Fig. 2. Part of the four-station fading record taken on 27-11-1955 at 1625 IST.

We shall now take up some specific readings given in Table 1 of the record reproduced in Fig. 2, and illustrate the method of drawing the lines of maxima from the displacements, assuming them to be moving in a fixed direction with a constant velocity.

Table 1

Sl No.	a_{12} (mm)	a_{13} (mm)	a_{14} (mm)	v_2 (m/s)	v_4 (m/s)	ϕ_2 °E of N	ϕ_4 °E of N	Type of line of maxima
1	+5	+5	−5	88	88	225	225	1
2	+4	+7	−7	77	63	210	225	1
3	+7	+5	−8	72	66	234	238	1
4	+2	+17	+5	36	35	187	164	2
5	+4	+1	+3	151	197	256	252	2
6	−10	+5	−6	56	80	117	230	3
7	+5	−5	−12	88	48	315	293	4

VOL. 10 1957

Table 1 shows the values of the velocities v_2 and v_4 and directions ϕ_2 and ϕ_4 calculated individually for each set of displacements for the two adjacent triangles by the usual three-station formulae. We shall take the mean values v_n and ϕ_n to represent very nearly the velocity and direction of ionospheric wind and assume that the diffraction pattern on the ground moves with velocity $2v_n$ in the same direction. Parallel lines drawn through all the spaced points along the wind direction will cut the lines of maxima at specific points whose distances from the three outer aerials at the instant when the line touches A_1 can be calculated from the time-delays and known velocity of drift of line of maxima for each set of readings. By measuring off these distances from A_2, A_3, and A_4 along these lines, taking the sign into account, these points are located, and by joining them by a smooth curve so as to pass through A_1, we get the approximate shape of the line of maxima for each set.

We shall now take specific sets of readings to illustrate the various types of lines of maxima. For the sake of convenience, we shall classify all the different lines of maxima, observed in the normal records taken during winter months, into four types based on the sign of the displacements. Observations in which the line touches A_2 and A_3 earlier and A_4 later than A_1 are classified under Type 1. In fact these types of observations correspond to the principal direction of motion for the winter months, and more than three-fourths of the observations in this record come under this class. The first three observations in Table 1 belong to this category. The continuous straight line in Fig. 3(a) is the line of maxima for the first observation. For the second observation the points A, A_1, B, and C on the line of maxima are obtained by taking the mean direction of 225° E of N, and B do not fit in a smooth curve. Actually, if all these four points are joined there will be a sharp rectangular bend at B, which is quite unlikely. To avoid this difficulty, other angles in the range of 207° to 236° are tried, and it is found that a smooth curve is obtained for an angle of 236° E of N, as shown by the dashed

line in Fig. 3(a). Observations in which the line of maxima touches all the outer aerials earlier than A_1 are classified under Type 2. About one-fourth of the total number of observations in this single record come under this category. It is easy to show that the lines of maxima of this type are invariably curved and concave

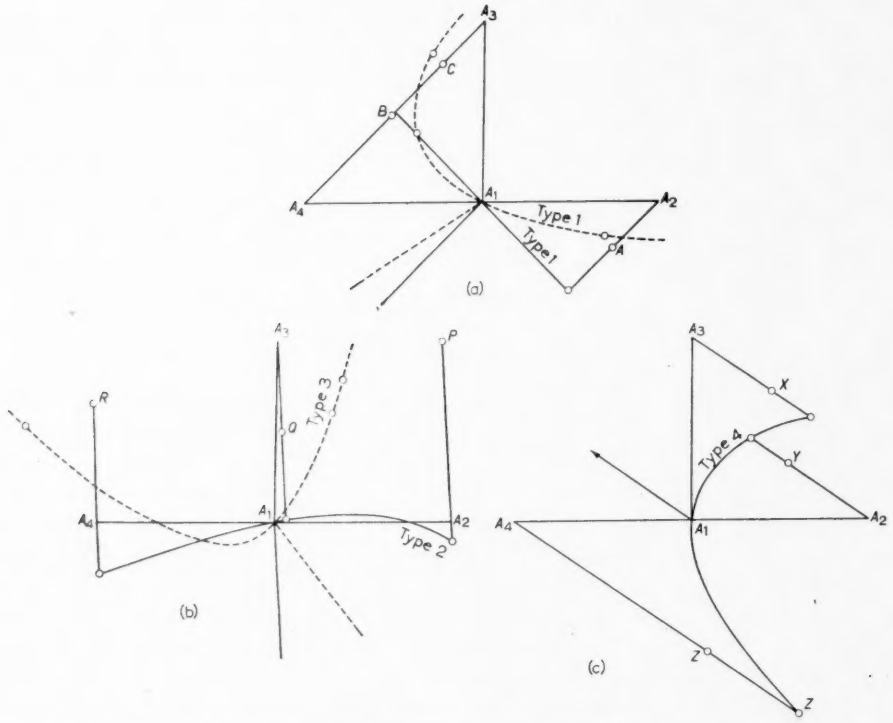

Fig. 3(a), (b), and (c). Diagrams showing typical lines of maxima for all the four types.

towards the direction of motion. One typical line of this type representing the fourth observation in the table is shown by the continuous line of Fig. 3(b). All those observations in which the lines of maxima touch A_3 earlier, and A_2 and A_4 later, are classified under Type 3. This type of observation is very rare, being one in thirty of the total number of observations. A typical line representing the sixth reading in Table 1 is shown by the dotted line in Fig. 3(b). For this case also a smooth curve could be drawn by adjusting the direction of motion to be about 141° E of N, which is far from the mean value. A characteristic of this type is the convex shape of the line in the direction of motion. It is felt in general that whenever there is a large difference between ϕ_2 and ϕ_4, no smooth line of maxima can be drawn around the mean direction of motion. Type 4 observations are those in which the line of maxima touches A_2 earlier and A_3, and A_4 later than A_1, and are as infrequent as Type 3. For the seventh observation in Table 1, points X, Y, A_1, and Z on the line of maxima shown in Fig. 3(c) are obtained using the mean direction 304 and mean velocity of 68 m/s, but these points do

not fall on a single smooth curve. As there is no improvement by changing the direction, different values of velocity are tried and a best-fit curve is obtained for a velocity of 100 m/s. This illustrates a type of line of maxima where the velocity of motion may be higher than the individual values calculated for each triangle.

From a study of the lines of maxima for about fifty observations in this record, it is observed that the lines of least curvature are more numerous, being about 50% of the total. The rest are highly curved lines and correspond to abnormally large deviation of these displacements from the usual median values. An interesting feature observed for all these readings in this record as well as other records which are analysed is the gradual nature of the variation of the curvature of the lines of maxima in consecutive observations. Sometimes a line of high curvature may appear suddenly due to some sudden change in ionospheric irregularities or occurrence of small sporadic E clouds, but it is always followed by lines of gradually decreasing curvature indicating a kind of continuity in the nature of the diffraction pattern.

4. Method of Analysis of Fading Records using Median Values of Time-delays

In the usual three station method, the displacements a_{12} and a_{13} do not enable us to have any idea of the shape of the lines of maxima, and as such for simplicity, Ratcliffe has assumed all these as due to straight lines of maxima whose orientation with respect to the direction of motion is continuously changing in order to account for the variability of these time-delays. Assuming all values of Ψ to be equally probable, he has shown that the average time displacements give the true velocity and direction of motion of the diffraction pattern on the ground. We have already shown in the previous section that the assumption of the lines of maxima which are straight is untenable, as a_{12} and a_{14} are not equal and opposite for all observations. It can now be shown that the method of averages

Table 2

Sl No.	Date	Time in hours (IST)	Number of readings	a_{12} median (mm)	a_{12} average (mm)	a_{14} median (mm)	a_{14} average (mm)
1	23-7-55	1740	11	−9·5	−7·5	+10·5	+8·3
2	24-7-55	0810	8	−20·8	−11·0	+20·3	+16·0
3	25-7-55	1730	53	+7·3	+6·5	−7·4	−6·5
4	26-7-55	1500	8	+6·5	+3·7	−6·4	−5·1
5	26-7-55	1510	25	+7·2	+8·1	−7·1	−7·4
6	24-11-55	1540	21	+10·2	+10·0	−8·8	−9·2
7	24-11-55	1640	24	+9·4	+12·5	−7·0	−7·5
8	27-11-55	1625	48	+5·1	+3·8	−5·1	−2·1
9	27-11-55	1700	34	+4·1	+4·7	−4·1	−4·2
10	28-11-55	0800	39	+4·6	+4·0	−4·6	−3·6
11	28-11-55	0825	25	+6·2	+3·7	−6·0	−3·0

VOL. 10 1957

does not give the true wind velocity or direction, for, if this is true, the wind data obtained from the average time displacements for the two adjacent triangles should be same. Table 2 gives the average values of a_{12} and a_{14}, which are in general unequal and sometimes differ widely. This gives rise to two different values for v and ϕ for the two adjacent aerial sites which are so close, and the general wind movement should be substantially the same at such close distances, and hence it is concluded that the method of averages gives incorrect values of wind data.

This discrepancy is at once removed by following the modified method of calculating wind data from the median values of time displacements employed in this laboratory, as the median values of a_{12} and a_{14} considered separately from the observations for the two sets of aerials are nearly equal. In this method the median values are obtained by eliminating all those observations which are widely deviating from the most probable values and taking the average of the rest.

The relative differences between displacements a_{12} and a_{14} can now be usefully utilized in evolving a more exact method of evaluating the median values of the time displacements and hence the wind velocities and directions. All the observations classified under the last three types and some even among the Type 1 readings, which correspond to highly curved lines of maxima, are first eliminated by judging from the differences between a_{12} and a_{14}. Median values are then obtained by averaging the rest of the observations, and it is found that these median values of a_{12} and a_{14} are in good agreement, as can be easily seen from the values shown in Table 2. This signifies that the average of these readings corresponds to a straight line of maxima, implying thereby that lines of either curvature are equally probable. The values of v and ϕ obtained by this method are found to be more consistent and accurate.

It is interesting to note that the median values give consistent values even when two readings are available, as, for instance, when the length of the useful portion of the record is very small. It can be also said, in a general way, from a study of the data in Table 2, that the more the number of readings, the less the difference between the true averages of a_{12} and a_{14}. In two records taken on 23 July and 24 November 1955, both the median and the average values do not agree. It is likely that, in this record, one type of curvature (concave or convex) of the lines of maxima predominates, giving rise to a curved line of maxima in taking the average. Another interesting feature which can be noticed from Table 2 is the fact that the true averages are in general lower than the median values. In some cases the disparity is very large. Hence the velocities calculated from the median values are in general lower than those calculated from the average values.

5. A New and Improved Method of Evaluating Wind Data

With a view to evolving an accurate method of determining wind movements, using the additional fading record from the fourth aerial, values of v_2,v_4 and ϕ_2,ϕ_4 are calculated for all the fifty readings of the record under consideration, and histograms are drawn showing the variation of the number of observations

versus the differences v_2 and v_4 and ϕ_2 and ϕ_4. It will be seen from these histograms shown in Figs. 4(a) and (b) that the number of observations falls off rapidly as $v_2 \sim v_4$ or $\phi_2 \sim \phi_4$ increases. It will be noticed that for nearly half the observations the wind directions for the two sets of aerials are agreeing within 10°, while

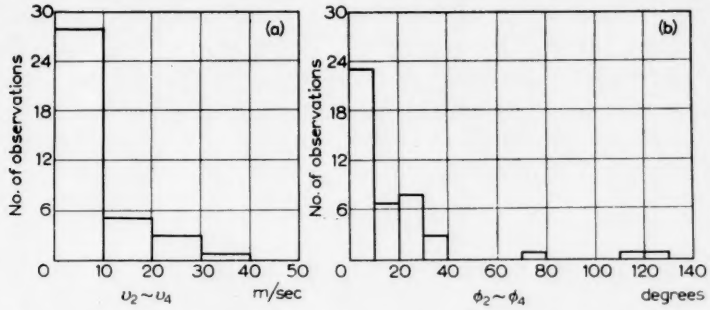

Fig. 4(a) and (b). Histograms showing variation of the number of observations versus $v_2 \sim v_4$ and $\phi_2 \sim \phi_4$ respectively.

for nearly three-fourths of the observations the velocity differences are less than 10 m/s. Among these observations there is a sufficient number of common readings for which both velocity and angle differences are less than 10 m/s and 10° respectively. These observations reproduced in Table 3 correspond to lines of maxima which are either straight or slightly curved, while the remaining ones are due to more curved lines. The mean values v_n and ϕ_n of the wind velocities and directions calculated for the two sets of triangles for each observation are given in Table 3.

The average values of these normal components of the wind velocity and wind

Table 3

Sl No.	a_{12} (mm)	a_{13} (mm)	a_{14} (mm)	v_n (m/s)	ϕ_n (°E of N)	v for $\phi = 225°$ E of N (m/s)	
1	+1	+9	−2	68	190	80	
2	+5	+6	−6	76	223	73	
3	+6	+4	−6	86	236	88	($\Psi = 79°$)
4	+3	+7	−3	82	203	88	($\Psi = -68°$)
5	+5	+5	−5	88	225	88	($\Psi = 90°$)
6	+4	+6	−3	89	211	98	
7	+4	+6	−5	83	217	80	
8	+6	+6	−7	70	227	68	
9	+3	+7	−3	82	203	88	($\Psi = -68°$)
10	+3	+7	−4	79	207	80	
11	+4	+7	−4	77	210	80	
12	+8	+2	−9	71	257	80	
13	+6	+10	−5	55	210	59	
14	+5	+7	−6	70	219	68	
15	+7	+5	−8	69	236	68	

direction are shown in Table 4 along with the values obtained by other methods. Comparison of these values with results obtained by using median and average displacements, reveals the interesting fact that the wind direction agrees better with the values obtained from median displacements.

A more accurate method of determining true wind data is evolved by finding out if some of the observations in Table 3 can be explained on the basis of RATCLIFFE'S assumption of the variation of Ψ, which is the angle between the lines of maxima PQ and the wind direction, as shown in Fig. 1. For instance, observations 3, 4, 5, 9, and 11 correspond to straight lines of maxima which give different normal components of wind data. If these observations are due to wind moving with a constant velocity v in a fixed direction ϕ, it can be easily shown that

$$v_n = v \sin \Psi \tag{1}$$

and

$$\tan \phi_n = \tan \phi \cdot \frac{1 - \cot \phi \cot \Psi}{1 + \tan \phi \cot \Psi} \tag{2}$$

The highest value of v_n among the observed values is therefore likely to be more nearer the true velocity v. Assuming the fifth observation to give the true velocity and direction, the values for the observations 3, 4 and 9 are found to satisfy the relations (1) and (2) for values of Ψ shown against the true wind velocities given in Table 3. Observation number 11 did not satisfy these relations. Assuming that the wind direction for this observation is the same as above, the velocity has been calculated and is found to be different. This may be due to errors in the measurement of displacements or may be due to genuine change of velocity.

An attempt is now made to fit the remaining observations in Table 3 having slight curvature on the same basis by assuming the wind direction to be 225° E of N and adjusting the velocity such that each observation gives rise to a line of maxima of least curvature. The values of velocities v thus obtained are shown in the last column in Table 3. It can be seen that the variation in the individual values of the estimated true velocities in most cases is limited to a narrow range of 80 to 88 m/s, and can be explained as due to inaccuracies in the measurement of displacements. As the maxima in the fading records are sometimes not quite sharp, it is not possible to estimate the displacements to an accuracy of more than a millimetre. An inaccuracy of ± 1 mm in the measurement of displacements leads to a wide variation of nearly ± 8 m/s in the true velocities. As for most of the observations the velocity is 80 or 88 m/s, either of these or preferably the mean value 84 m/s can

Table 4

Description	Velocity (m/s)	Direction (°E of N)
1. Method of average displacements	92	198
2. Average of v_n and ϕ_n values in Table 3	76	218
3. Method of median displacements	82	221
4. New method	84	225

be taken to be the true velocity. The final values of the true velocity and direction are given in Table 4, along with the values obtained by other methods for the purpose of comparison. The remaining few observations having very low velocities may be due to genuine velocity changes.

6. Discussion

The use of four spaced receiver fading records has established the important fact that the lines of maxima are not necessarily straight, as has been hitherto assumed by almost all the investigators. For the case of separation of aerials of the order of one wavelength, as used in this investigation, it has also been shown that nearly half the observations correspond to straight or slightly curved lines of maxima, so that the average of these displacements known as median values corresponds to a straight line of maxima and gives fairly accurate wind data. The remaining highly curved lines are ignored for the purpose of wind calculations. It is possible that for smaller aerial separation the lines are less curved and the number of observations corresponding to lines of maxima of smaller curvature are more numerous. The occurrence of a large number of highly curved lines of maxima for such a small aerial separation may be due to the ionosphere near the low latitudes being more irregular and disturbed. For instance, from systematic study of the dependence of fading period on wind velocity at this place, we arrived at the empirical relation

$$vT = 1{\cdot}86\lambda \tag{3}$$

and, following Pawsey (1935), if we assume D as the maximum distance of aerial separation for which the signal variations are sensibly the same, the period of fading is given by $2D/v$. From these two relations, D is found to be nearly $0{\cdot}9\ \lambda$ for this place as against $2\frac{1}{3}\lambda$ obtained by Pawsey for the high latitudes. Since D is small for this place, it appears that the dissimilarities between the records are more pronounced for this latitude, simulating the appearance of a highly curved line of maxima. These highly curved lines of maxima may be either genuine or might have come about as a consequence of the change in the diffraction pattern as it moves from one end of the aerial system to the other. The assumption of a constant diffraction pattern over such distances is not likely to be valid for all observations. As such, if the line of maxima undergoes a change of shape as it moves across the four spaced receivers it will simulate the action of a highly curved line of maxima moving unchanged.

It can be easily seen from relation (1) that, if Ψ can take all values equally randomly as Ratcliffe assumed, the value of v_n should vary from 0 to v. The limited range of variation of v_n values given in Table 3 shows that this assumption is not valid. Considering those observations for which the line of maxima are either straight or slightly curved, it can be shown that Ψ varies over a limited range equally on either side of the normal position. Using expressions (1) and (2) given by Ratcliffe in his paper, it can be shown that the average of time displacements for these observations leads to equations (3) and (4) in his paper, even though Ψ lies in a limited range, provided the values on either side of $\pi/2$ are equally probable.

VOL. 10 1957

Obviously, this is the main reason why the median value of time displacements gives values which are quite close to the true values.

Some of the observations, particularly those which are due to the straight lines of maxima, fitted well into the expressions given by Ratcliffe, and support the idea that lines of maxima have different orientations with respect to the direction of motion. In fact, it is possible to evaluate wind data which are very near the true values from the very few observations corresponding to straight lines of maxima. Though the analysis of all the observations in Table 3 has shown that the wind has, in general, a constant velocity and direction, there are cases when it takes different values for a short duration. There is actually no need to presume that the wind at the ionospheric levels is constant.

Comparison of wind data obtained by all the four methods shown in Table 4 reveals the interesting fact that the usual method of calculation by using average displacements invariably gives higher values of velocity and a different value of direction as compared to the data obtained by more exact methods. Barber has also noticed that this method overestimates the wind velocities. In view of the large discrepancies at two adjacent sites, this method does not yield reliable wind data. The method of taking the average of the individual calculated values of v_n for observations shown in Table 3, corresponding to straight or slightly curved lines of maxima, gives nearly the normal component of velocity, which is always lower than the true velocity v, as can be seen from the relation (1). The wind velocities obtained by this method are invariably lower than the more exact values determined by the last two methods. The method of using median values for calculating wind data has the decided advantage that it is simple, rapid, and fairly accurate. Though the improved method based on the variation of orientation of the lines of maxima gives more exact data, it is rather laborious. In view of the fact that the results obtained by both these methods are quite in good agreement with each other, as seen in Table 4, the median method is to be preferred for general analysis of wind records.

7. Conclusions

The use of a fourth aerial for obtaining an additional fading pattern in the usual three-station method enabled us to show that the assumption of the lines of maxima which are straight is untenable, as more than half of the readings for any record correspond to lines which are either straight or slightly curved. It has been possible for the first time to delineate roughly the shape of the lines of maxima of a diffraction pattern.

It is shown that the usual method of analysis of wind records by taking average displacements does not yield reliable wind data, as different values are obtained for two adjacent sites. A better method of evaluating winds, by using median-time displacements with the help of the fourth aerial fading record, is evolved. This method is simple, rapid, and fairly accurate. It is shown that the usual method of wind calculations by taking average displacements overestimates the wind velocities by a significant fraction.

Another useful and accurate method of evaluating true wind data is also presented. This method is based on the assumption that the observed variation of

v_n and ϕ_n is due to varying angles of tilt of the line of maxima with respect to the direction of motion, which is assumed to be fixed. The wind data determined by this method are found to be in good agreement with the values obtained by the method of using median displacements. This method also supports RATCLIFFE'S assumption of varying angle of tilt Ψ over a limited range.

REFERENCES

BARBER N. F.	1956	*J. Atmosph. Terr. Phys.* **8,** 318.
MITRA S. N.	1949	*Proc. Instn. Elect. Engrs.* **96,** (Pt. III), 441.
PAWSEY J. L.	1935	*Proc. Camb. Phil. Soc.* **31,** 125.
PHILLIPS G. J.	1952	*J. Atmosph. Terr. Phys.* **2,** 141.
RAMACHANDRA RAO B., SRIRAMA RAO M., and SATYANARAYANAMURTY D.	1956	*J. Sci. Industr. Res.* **15A,** 75.
RATCLIFFE J. A.	1954	*J. Atmosph. Terr. Phys.* **5,** 173.

VOL. 10 1957

Journal of Atmospheric and Terrestrial Physics, 1957, Vol. 10, pp. 318 to 319. Pergamon Press Ltd., London

A spectrophotometric investigation of the air afterglow

D. T. STEWART
Physics Department, Queen's University of Belfast

(*Received* 16 *January* 1957)

Abstract—The spectral energy distributions of the yellow-green afterglow produced by a discharge in air, and of a similar continuum produced by mixing nitric oxide and atomic oxygen, have been measured. They were found to be identical, and have a short wavelength limit at 3700 Å, providing further evidence that the continuum in both cases can be attributed to the nitrogen dioxide molecule.

QUANTITATIVE data appear to be lacking for the intensity distribution in the yellow-green glow emitted when nitric oxide and atomic oxygen combine to form nitrogen dioxide. It is particularly important for the theory of the process involved (GAYDON, 1944) to find how closely the short wavelength limit of its continuum is to 3700 Å, which is the long wavelength limit for the photo-dissociation of NO_2, viz.

$$NO_2 + h\nu\ (<3700\ \text{Å}) = NO + O$$

The present note describes briefly the determination of the energy distribution, when the continuum was produced from two sources. The first was the afterglow of a discharge through commercial oxygen, which contains a trace of nitrogen, and the second the glow produced by mixing NO with O produced from a discharge through pure oxygen.

In both cases the oxygen was activated in a Wood-type discharge tube and streamed through an observation tube, 100 cm long and 5 cm diameter, with a quartz window at the gas-inlet end. A d.c. discharge was used at approximately 1000 V and 200 mA, with pressures in the range 0·2–1·0 mm Hg. Alternating and Tesla discharges were found to give stray discharges in the observation tube, which were absent with d.c. excitation.

When commercial oxygen was used, the whole of the observation tube was filled with a bright afterglow. When it was replaced by oxygen prepared by electrolysis of water, the gas being freed from hydrogen by passing it over platinized asbestos at 300°C and from water by drying with phosphorous pentoxide and traps cooled with liquid oxygen, only a very faint afterglow could be seen. In the latter case the introduction of pure NO, prepared and purified in the usual manner (FARKAS and MELVILLE, 1939), through a capillary jet, care being taken to prevent any back diffusion of NO into the discharge, again produced a bright yellow-green glow.

The spectra of the bright glows were examined with a Hilger $f/5$ monochromator adapted for use as a spectrophotometer by the addition of a photomultiplier and calibrated by a standard tungsten filament lamp. The relative spectral energy distributions of the glows are shown in the figure, with the measurements in each case normalized to a common maximum. It can be seen that the two distributions are identical and that there is no obvious banded structure. The continuum has a short wavelength limit between 3700 Å and 3800 Å and a flat maximum between

5400 and 5600 Å. It was not followed beyond 6200 Å. The identity of the distributions and the value of the short wavelength limit provide additional support for GAYDON's views on the origin of the continuum.

The afterglow from "pure" oxygen was too faint to be investigated by this method. Its spectrum was continuous in the visible region and may be identical with the spectrum of the bright afterglow due to the presence of a small residual trace of nitrogen. Its main feature was, however, the "atmospheric" band of O_2,$[A'\Sigma_g^+ - X^3\Sigma_g^-]$ at 7593 Å. The intensity of this band was approximately

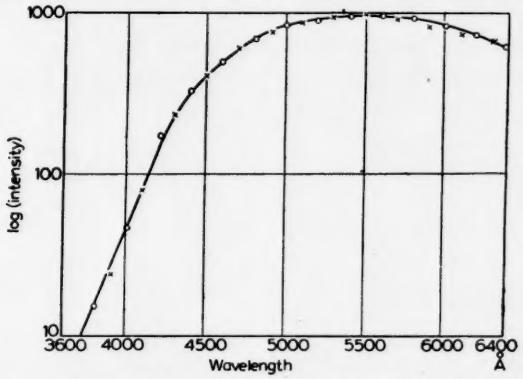

Fig. 1. Relative spectral energy distribution of yellow-green glow.
○ Air afterglow.
× Glow produced by mixing nitric oxide with atomic oxygen.

doubled when NO was added. The appearance of the band in the pure afterglow might be due to a process such as

$$O + O + M \rightarrow O_2(A'\Sigma_g^+) + M^*$$

where M is a third atom or molecule and its enhancement to the process (NICOLET, 1954).

$$NO_2 + O \rightarrow NO + O_2(A'\Sigma_g^+)$$

but more extensive experiments would be required to establish definitely that these actually occur.

It is a pleasure to express my thanks to Professor K. G. EMELEUS for his interest in this investigation and for his helpful advice.

REFERENCES

FARKAS A. and MELVILLE H. W.	1939	*Experimental Methods in Gas Reactions* Macmillan, London.
GAYDON A. G.	1944	*Proc. Roy. Soc.* **A183,** 111.
NICOLET M.	1954	*The Earth as a Planet* (Ed. G. P. Kuiper) University of Chicago Press.

VOL. 10 1957

Journal of Atmospheric and Terrestrial Physics, 1957, Vol. 10, pp. 320 to 331. Pergamon Press Ltd., London

The red and near-infra-red auroral spectrum*

A. OMHOLT†
Yerkes Observatory, University of Chicago, Williams Bay, Wisconsin

(*Received* 12 *March* 1957)

Abstract—Six auroral spectra covering the wavelength range 5400–8800 Å have been subject to thorough intensity measurements. The intensity distributions in the First Positive band system and the Meinel band systems were measured and related to theoretical data. The altitude variations of these band systems and the strongest oxygen lines and bands were studied, the intensity ratio between the red [O I] lines 6300/64 and the First Positive bands being taken as an indication of relative altitude. An auroral feature detected at 7325 Å on spectra from high altitudes is tentatively identified as the [O II] multiplet $^2D - {}^2P$. The intensity distribution and its variation with altitude are briefly discussed.

1. INTRODUCTION

THE red and near-infra-red auroral spectrum has previously been studied by several authors (cf. MEINEL, 1951a, b, 1954; VEGARD and TÖNSBERG, 1952; PETRIE and SMALL, 1953; FAN and SCHULTE, 1954; CHAMBERLAIN, FAN, and MEINEL, 1954), and it appears from the published spectra that there are significant relative intensity variations with altitude. However, no extensive quantitative measurements of relative total (integrated) intensities and intensity variations have so far been made. The purpose of this paper is to present the result of quantitative measurements of six auroral infra-red spectra obtained at Yerkes Observatory (geom. lat. 53°N) during four nights.

2. OBSERVATIONS

The spectra were obtained with a small grating spectrograph with a dispersion of approximately 350 Å/mm in the first order (the same spectrograph as used by FAN and SCHULTE, 1954). The spectrograph pointed north with its slit aligned vertically, and an image of the sky was focused upon the slit so that this covered the range from 5° to 25° above the northern horizon. Only a smaller part near the centre of the slit was covered with a yellow filter, so that a second-order violet and ultra-violet spectrum was overlapping the upper and lower part of the first-order spectrum, which extended from about 5400 Å to near 9000 Å. The purpose with this arrangement was to obtain simultaneous measurements of the N_2^+ First Negative (0-0) band at 3914 Å, which, apart from the (0-1) band of N_2 Second Positive band system, was the only visible feature in the second-order spectrum. However, since a great number of corrections were necessary, the absolute intensity measurements of this N_2^+ band and also its variation with altitude were extremely doubtful, so nothing more could be said than that its intensity was of the same order of magnitude as the oxygen line 5577 Å.

* The research reported in this paper was supported in part by the Geophysics Research Directorate of the Air Force Cambridge Research Center, Air Research and Development Command, under Contract AF 19(122)-480.

† Fulbright Research Fellow, on leave from the Auroral Observatory, Tromsö, Norway.

The analysed spectra are shown in Fig. 1, and exposure details are given in Table 1. On a number of other spectra obtained, the auroral emissions were too weak compared with the underlying OH-bands from the nightglow, so that reliable intensity measurements were impossible or very difficult.

Table 1

Sp. no.	Day	Time (GT)	Auroral forms
1	27 Oct. 1956	03–05	Draperies and diffuse aurorae with rays
2	27 Oct. 1956	05–10	Diffuse glow
3	28 Oct. 1956	0740–1100	Pulsating, diffuse aurora. Some ray-structure
4	10 Nov. 1956	0630–0750	Rays and draperies
5	11 Nov. 1956	0515–0635	Rays and draperies
6	11 Nov. 1956	0635–1000	Rays and draperies, also diffuse glow

Eastman-Kodak I-N film, hypersensitized with ammonia, was used. Calibration spectra from a tungsten standard lamp were secured for each individual sheet of film, on the same day as the auroral spectra were taken; this type of film has a fairly constant sensitivity for 10–14 days after the hypersensitizing (BERTIER, 1956).

VOL. 10 1957

The intensities given in this paper are all integrated, total intensities. The line intensities are perhaps a little uncertain owing to the narrowness of the lines, but this should not give rise to errors larger than about 20 per cent in the intensities of lines relative to bands, and no significant error in the intensity variations. Corrections for the atmospheric transmission as a function of wavelength and elevation angle were made, standard transmission tables (ALLEN, 1955) being adopted. It may be mentioned that the use of these tables gave extremely peculiar results for the λ3914-band at elevation angles of 10° or below, for the spectra dealt with here as well as for photo-electric measurements made during these same auroras. The corrected intensities for λ3914 seem far too large at low-elevation angle, which may be due to the fact that the atmospheric attenuation of the radiation occurs mainly through Rayleigh scattering. The transmission tables used are therefore strictly valid for point sources only. However, this scattering effect is probably not important for the wavelength range within which intensity measurements were made.

3. Relative Intensities of the Nitrogen Bands

Although there are variations in the intensity ratio between the First Positive bands of N_2 and the MEINEL bands of N_2^+, there are apparently no or very small variations in the relative intensity within the individual band systems. The intensities are given in Table 2, together with theoretical values after NICHOLLS (1956). The values given are for the middle sector of spectrum No. 6, which is free of the second-order spectrum, but the relative values are consistent with several measurements on the other spectra. The sum of the intensities of the (2-0) and (4-2) First Positive bands is put equal to 100. The agreement with PETRIE and SMALL's (1953) values is not too bad.

Table 2. Relative intensities (RI) for the red and infra-red nitrogen bands and relative population of upper vibrational levels $N(v')$

First Positive bands of N_2				Meinel bands of N_2^+			
v'-v''	RI aurora	RI_{theor}*	Rel. $N(v')$ aurora	v'-v''	RI aurora	$c \times RI_{theor}$*	Rel. $N(v')$ aurora
8-5	(7)	55	(13)	3-0†	11·0	57	19
7-4	14·0	61	23	4-1	10·3	94	11
6-3	21·7	59	37	5-2	(4)‡		
5-2	24·0	47	51	2-0	78	78	100
4-1	22·3	30	74	3-1	38	80	47
3-0†	11·7	15·5	76	4-2	12	44	27
6-4	(7)‡	17·5	(40)				
5-3	18·9	38	50				
4-2	44	56	79				
3-1	(56)	60	(93)				
2-0	56	44	127				

* For equal population of upper levels. After NICHOLLS (1956). Cf. the text.

† The (3-0) bands of both systems are partly overlapping and may be partly absorbed due to the (1-0) Atmospheric absorption band. The intensities are therefore somewhat uncertain and probably slightly too low.

‡ The total intensity of the overlapping First Positive (6-4) and MEINEL (5-2) bands is 11, the given intensities (7 and 4) being rather uncertain.

As will be seen from the relative populations of the upper vibrational levels, derived from the two sets of intensities, there is excellent agreement between measured and theoretical values for the First Positive system. The relative populations N(v') form a fairly smooth curve when plotted against v'. From MEINEL'S (1951a) intensities, $N(v = 1)$ is estimated to be 175 on the same scale, a value which fits well with those given here.

The discrepancy between theoretical and measured values for the MEINEL band system seems too large to be accepted as an error in the measurements. The theoretical values are, however, not corrected for variations in the electronic transition moment $R_e(r)$ (cf. NICHOLLS, 1956). The variation of $R_e(r)$ is relatively small within one sequence, whereas it may be appreciable from one sequence to another. It is interesting to note that the results may be brought in harmony if we assume that $R_e^2(r)$ varies with a factor 2·5 (or $R_e(r)$ with 1·6) from the sequence $\Delta v = 3$ to $\Delta v = 2$. This is a large, but not undue, variation compared with other band systems*. A slight correction of the theoretical relative intensities within one sequence would also be required, so that the relative populations for the levels $v' = 2$, 3, and 4 will be approximately $1 : 0{\cdot}4_4 : 0{\cdot}2_0$.

BAGARIAZKY and FEDOROVA (1956) have obtained auroral spectra up to 11,800 Å, but failed to find the (0-0) band of the MEINEL system (11,100 Å). They suggested that the vibrational numbering of the MEINEL system as accepted

* The author is indebted to Dr. R. W. NICHOLLS for informative correspondence regarding these matters.

hitherto is wrong with one unit, so that the band now designated as (1-0) is really the (0-0) band. If this were the case, the disagreement between the theoretical and the auroral intensities increases with a factor 5 or more. The intensity distribution thus favours MEINEL'S vibrational numbering (1951a). This numbering is also favoured by a Ryderg series of N_2 found by WORLEY (1953).

4. INTENSITY VARIATIONS

(a) It is readily seen from Fig. 1 that there are pronounced variations in the relative intensities with the angle of elevation. Similar variations in infra-red have also been noted by FAN and SCHULTE (1954) and by CHAMBERLAIN, FAN, and MEINEL (1954), and seem also present in the intensity-altitude curves presented by MEINEL (1954).

The exposure times of the spectra are long, more than 1 hr in each case, and the auroral forms move rapidly, so there will be no clear correspondence between angle of elevation above the horizon and the relative altitude in the aurora. However, the upper part of a spectrum will generally originate from aurora at significant higher altitude than the lower part of the same spectrum. It is well known that the red [O I] lines at 6300/64 Å show a pronounced altitude effect, being stronger at higher altitudes, relative to any other known emissions. The measurements revealed that the intensity ratio between these oxygen lines and the First Positive bands was among the ones which showed the largest and most consistent variation with the elevation angle. This intensity ratio was therefore chosen as an indicator of average altitude, and all lines and bands were measured relative to the First Positive bands. The sum of the intensities of the (2-0) and (4-0) bands was put equal to 100, and the relative intensity obtained this way will be designated *RI*(line or band).

VOL. 10 1957

Intensity measurements were made in the upper, medium, and lower (*U*, *M*, and *L*) part of each spectrum, except in the upper part of spectrum No. 1, which was very weak and also contained fairly strong OH bands from the nightglow. The result of these measurements are given in Table 3, and the correlation between some of the strongest features is illustrated in Fig. 2, where *RI's* are plotted against *RI*(6300/64) on logarithmic scales.

(b) Spectrum 2 is omitted from Fig. 2, because it shows a marked difference from the other spectra. *RI*(6300/64) show little or no variation with the elevation angle, although the other prominent emissions behave approximately normal. This spectrum is of a fairly weak auroral glow on the north sky after a bright display, and shows a strong H_α line. A similar "enhancement" of the red [O I]-lines at the bottom of an aurora with strong H_α line has been observed by MEINEL (1954). VEGARD (1956) also finds a correlation between the intensities of these lines and H_α in Tromsö (geom. lat. 67°N), although in that case it may be an accidental coincidence of altitude effects, since at that latitude the hydrogen lines appear to be strongest in spectra from the upper part of auroras (VEGARD, 1955, 1956). Also, the lower part of spectrum 6 show a similar irregularity in *RI*(6300/64), and is omitted from Fig. 2.

The *RI* for the O I lines at 7990 Å (3^3P–$3s'^3D^0$) is sometimes disturbed by the presence of weak OH bands from the nightglow, notably in spectra 1 and 3.

Table 3. Relative intensities in the upper, middle, and lower (U, M, and L) part of auroral spectra. The sum of the intensities of the (2-0) and (4-2) First Positive bands is put equal to 100. The absolute value of this sum is given at the bottom line

Spectrum No.	1		2			3			4			5			6		
	M	*L*	*U*	*M*	*L*	*U*	*M*	*L*	*U*	*M*	*L*	*U*	*M*	*L*	*U*	*M*	*L*
[O I] 5577	305	275	285	360	285	260	250	220	—	—	—	300	—	165	—	—	—
[O I] 6300 + 6364	275	85	90	78	82	225	110	54	270	115	53	122	55	43	83	40	60
H_α	—	—	25·0	23·5	17·0	—	—	—	—	—	—	—	—	—	—	—	—
O_2 Atmospheric (1-1)	21	20	19·4	18·5	16·9	27	23·4	17·7	28·4	19·9	16·3	19·6	16·5	13·2	22·5	20	16·3
O I 7774	39	25	25·0	17·1	15·5	30·1	20·2	15·9	34	19	14·2	22·5	16·6	13·4	31	20	17·5
N_2^+-MEINEL, (2-0) + (3-1)	96	118	78	85	96	—	126	110	80	93	106	94	115	118	96	124	111
O I 7995	(10)	(6)	3·6	3·5	3·1	—	6·8	5·5	4·1	3·8	3·3	(2·3)	3·3	3·3	3·6	2·8	3·5
O I 8446	85	41	film defect	30·4	26·1	65	43	30	52	33	23	39	35	23	41	27	20
Absolute intensity First Positive bands	13·2	31	18·3	24·4	21·2	2	5·7	12·1	9·2	32·5	32·5	18·5	33·3	24·2	28·2	78	34

VOL.
10
1957

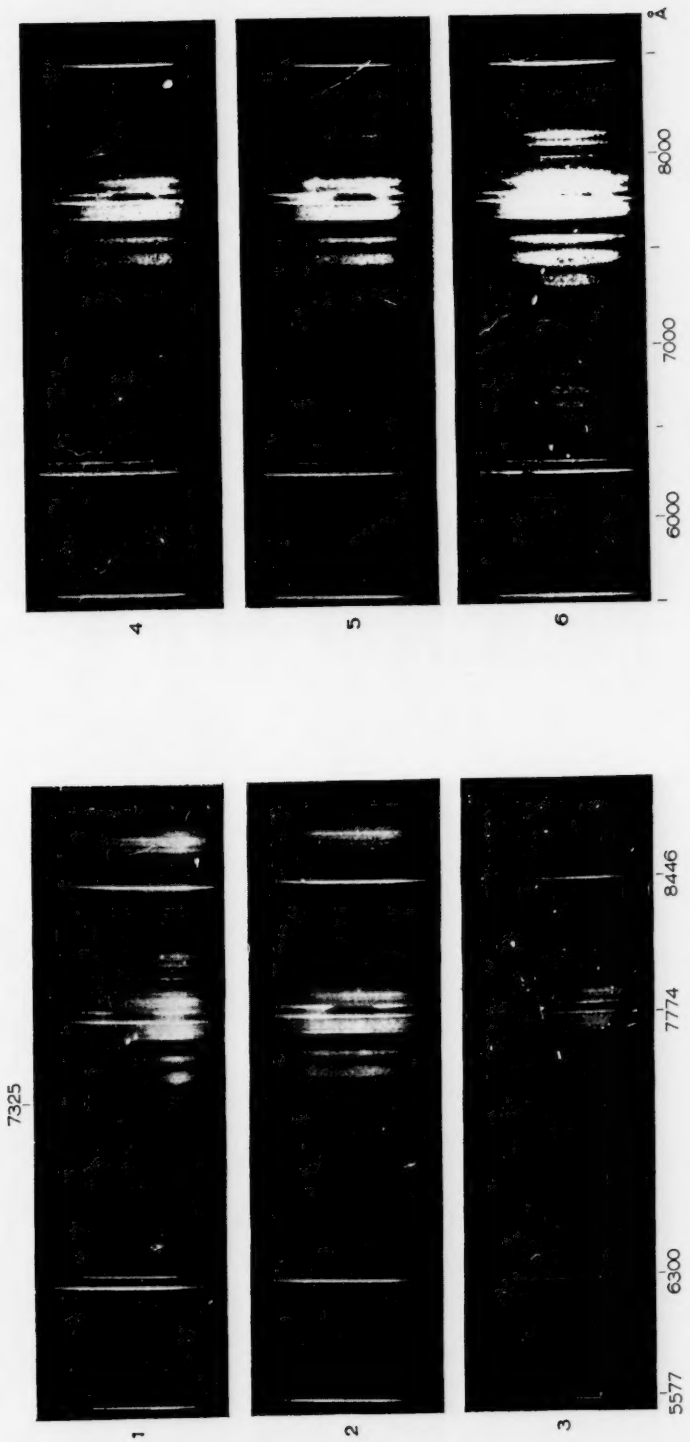

Fig. 1. The auroral spectra. Cf. Table 1.

This blending also makes the measured intensity variations less significant, but it is highly probable that *RI*(7990) varies similarly to *RI*(O_2 Atmospheric).

The *NI* lines at 8186 Å and 8126 Å are very weak, but measurements on spectrum 6 gave *RI*(8186) = 1·5 and *RI*(8216) = 2·5, values which showed little or no variation with altitude.

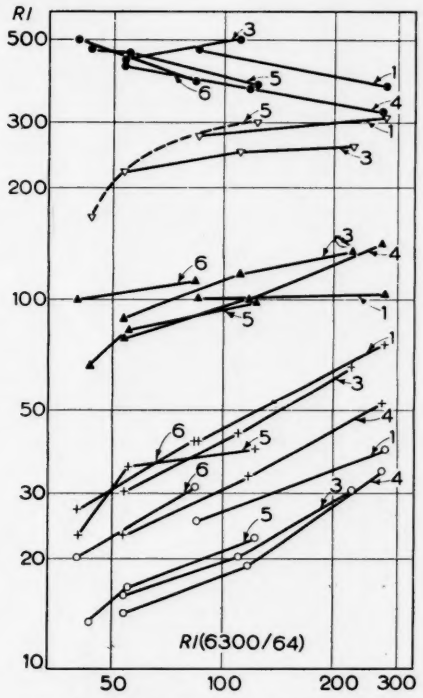

Fig. 2. *RI* for the strongest lines and bands against *RI*(6300/64). Lines are drawn between points from the same spectrum. Spectrum numbers to the right.
● N_2^+ Meinel; (2-0) + (3-1); *RI* × 4
▲ O_2 Atmospheric (1-1); *RI* × 5
▽ [O I] λ5577 ○ O I λ7774 + O I λ8446

The absolute value of the *RI* for the Atmospheric O_2 band (1-1) is somewhat uncertain because it is partly blended by the short wave part of the (0-2) First Positive band. For the same reason also its variation may be slightly attenuated for lower *RI*'s, but it is believed that its behaviour is significantly different from that of the oxygen multiplets at 7774 Å and 8446 Å.

Some spectra (1 to 3) extended as far in the infra-red as the (0-1) band of the O_2 Atmospheric system (8640 Å). This showed an intensity variation somewhat different from that of the (1-1) band; the (0-1) band seems more uniform with altitude. This may be due to absorption and fluorescence of the (0-0) band in the 50-km region (Chamberlain, 1954). The intensity of the (0-1) band is approximately twice that of the (1-1) band, in accordance with the intensities given by Meinel (1951a)* and estimates by Chamberlain *et al.* (1954).

* Meinel (1951a) did not explicitly give the intensity for the (1-1) band, which was then not discovered; however, he measured its intensity, attributing it to the First Positive band (2-0).

VOL. 10 1957

On spectra Nos. 2, 4, and 6 the green auroral line ([O I] λ5577) was too strongly exposed to be reliably measured, but the points plotted in Fig. 2 from spectra Nos. 1, 3, and 5 are probably reliable.* The dip in the left-hand part of the curve may be due to collisional deactivation (OMHOLT, 1956).

As mentioned in Section 2, the results for the N_2^+ First Negative (0-0) band (3914 Å) were very unreliable, but photo-electric measurements of N_2^+(3914) and

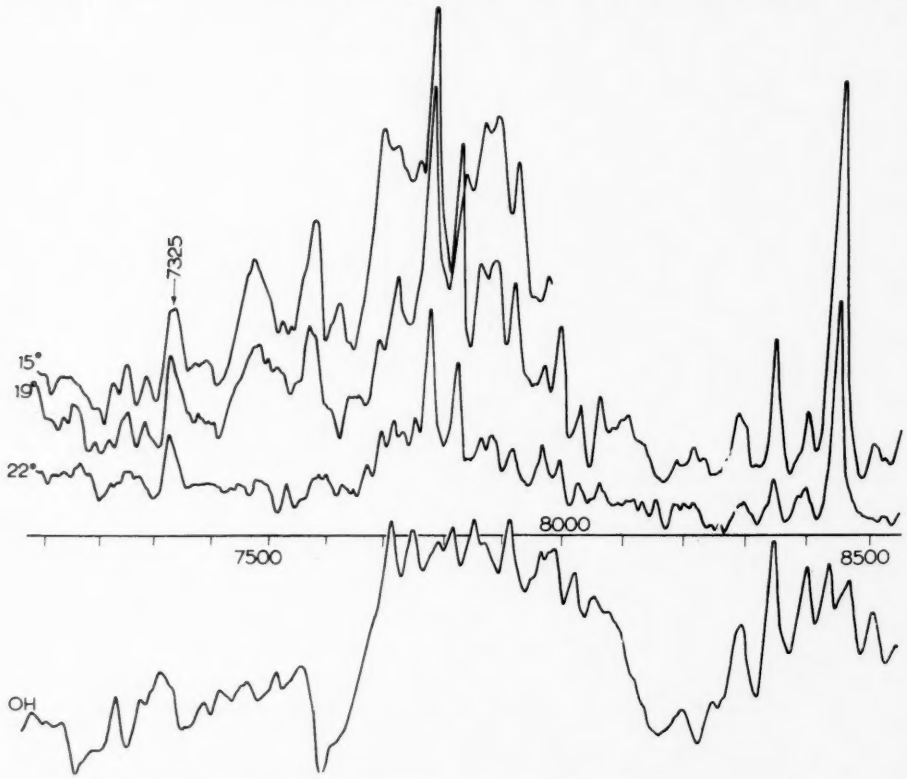

Fig. 3. Microphotometer tracings of spectrum No. 1. Angle of elevation above horizon is given for each curve. Tracing of a nightglow spectrum (OH) is shown for comparison.

[O I] λ5577 were made up to 60° above the horizon on one occasion during the exposure of spectrum 6. In that case auroral rays extended from the horizon nearly up to the zenith. Although individual rays could not be followed, one should expect that one at higher angles observes light from greater altitudes. The variation in the intensity ratio $I(3914)/I(5577)$, when corrected for atmospheric transmission, was small, but a slight, approximately linear, increase with elevation angle was noted, the intensity ratio being about 20 per cent higher at 60° than at 20° (above horizon).

5. An Auroral Emission at 7325 Å

In the upper part of spectra 1 and 4 there is a weak, but clearly visible, feature

* These results are also in reasonable agreement with photoelectric measurements on an auroral arc made by HARANG (1956) in Tromsö.

which was measured on both spectra to have the wavelength 7225 ± 5 Å. It is somewhat diffuse, but in particular at spectrum 1 very persistent with elevation angle. In the lower part of the spectra it appears only as a slight broadening on the short-wave side of the First Positive (5-3) band. Also on the other spectra it was noticed that this band sometimes was slightly broadened, in particular in the upper part of the spectra. Since there are no changes in intensity on the borderline between the upper and middle sections of the spectra (without and with second order superimposed) it is evidently an infra-red feature, and it is tempting to identify it with the [O II] multiplet ^2D–^2P (7318·7, 7319·3, 7330·0, and 7330·7 Å). Microphotometer tracings of spectrum No. 1 are shown in Fig. 3, taken at heights corresponding to elevation angles 15°, 19°, and 22° above the horizon. The feature observed at 7325 Å is broadened compared with other lines, but not unreasonably so compared with the wavelength spacing of the [O II] lines. With slightly higher dispersion the multiplet should appear as two lines at 7319·0 and 7330·3 Å, the first being 1·4 times stronger than the latter if the upper levels are in statistical equilibrium (GARSTANG, 1956). As pointed out by CHAMBERLAIN and ROESLER (1954) the superposed presence of a faint OH spectrum from the nightglow will seriously hamper the identification of the [O II] multiplet, since two of the strongest rotational lines in the OH(8-3) band, $P_1(2)$ and $P_2(3)$, have wavelengths 7316 and 7330 Å respectively. Comparison with the tracing of a night-sky spectrum (exposed 8 hr), also shown in Fig. 3, reveal clearly that although these OH lines may give some contribution to the discussed feature in the auroral spectrum, they are not sufficiently intense to explain it.

VOL. 10 1957

Another argument in favour of this identification is the fact that on spectrum 1 the other oxygen lines are unusually strong. In the middle part of the spectrum RI(6300/64) is 225, and in the upper part these lines are probably much stronger (cf. also Fig. 2). The feature at 7325 Å is therefore probably noticeable only at great heights. In this connection it may be noted that deactivation of the [O II] ^2P term is energetically possible in collisions with atomic as well as molecular oxygen and nitrogen. In the case of collisions with molecules, the $A^2\Pi$ state of N_2^+ and all known states of O_2^+ may be excited by charge transfer processes, the closest energy resonance occurring in

$$O^+(^2P) + O_2(X^3\,\Sigma_g^-) \rightarrow O(^3P) + O_2^+(b^4\Sigma_g^-) \qquad (1)$$

(0·3 eV excess energy for $v' = v'' = 0$; cf. HERZBERG, 1950). The lifetime of the ^2P term is about 5 sec (GARSTANG, 1956).

In the upper part of spectrum 1 the integrated intensity of λ7325 is about 10 per cent of that of the green [O I] line 5577 Å. The variation of RI(7325) with altitude is apparently even larger than that of RI(6300/64). An unambiguous identification of this auroral feature will, however, require spectra of higher resolution, capable of resolving the multiplet into at least two lines on the spectrogram.* For obvious

* The wavelength 7325 Å also coincides with the calcium line $^1P_1$–$^1D_2$ at 7326·1 Å, but this identification would require the $^1S_0$–$^1P_1$ transition at 4226·7 Å to be much stronger than the observed line. With the intensities quoted for the upper part of the auroral spectrum one would expect λ4226 to have nearly the same or even larger intensity than the head of the N_2^+ 4278 band. Despite the fact that this wavelength region has been thoroughly investigated by several workers, no outstanding feature at this wavelength appears to have ever been reported.

reasons it should be sought for at great altitudes; possibly the upper part of auroral rays would be the best source.

6. DISCUSSION AND CONCLUSION

(a) When discussing the results reported here, one must bear in mind that most of the RI's measured may depend on the energy of the primary particles and possible electric fields at the point considered, rather than on the actual altitude. If we consider the aurora to be primarily caused by incident fast electrons and protons, auroras with different lower boundaries may be considered as caused by streams of particles having different maximum energy. It is therefore not at all surprising that there is a considerable scattering in the individual curves for the same emission in Fig. 2, whereas the slope is approximately the same.

(b) The well-known increase with altitude in the intensity of the red [O I] lines λ6300/64 has not yet been convincingly explained. Cross-sections for electron excitation evaluated by SEATON show that if the excitation of the [O I] ^1S and ^1D terms arise only from secondary electrons with low energy, the ratio between the rates of excitation of the ^1D and ^1S terms should be at least 6·5 and probably much greater (cf. SEATON, 1954). To explain the low intensity of the [O I] λ6300/64 lines in the main part of the aurora it is necessary to assume that almost all the oxygen atoms in the ^1D term loose their excitation energy by collisional deactivation. SEATON (1954) suggested that this may be due to electron deactivation, but the electron densities in auroras are probably too small to give the necessary effect (OMHOLT, 1955; CHAMBERLAIN, 1956).

SEATON also pointed out that there is a close energy resonance in the process

$$O(^1D) + O_2(X\ ^3\Sigma_g^-) \rightarrow O(^3P) + O_2\ (b\ ^1\Sigma_g^+, v = 2). \qquad (2)$$

The vibrational energy of the O_2 molecules may be removed in collisions with other atoms and molecules, so that the reverse process may not be important.

If slow electrons excite and O_2 deactivates the red [O I] lines, the rate of excitation of the $O_2(b^1\Sigma)$ state by process (2) alone, in the main part of the aurora, would exceed the rate of excitation of $O(^1S)$ (the upper term for λ5577) by a factor of at least 6, and probably much more. On the other hand, the metastable $b^1\Sigma$ state emits the Atmospheric oxygen bands, whose intensity yields the rate of excitation of this state, if it is de-excited only by radiation of these bands. Utilizing the intensity ratio $I(0\text{-}1)/I(1\text{-}1) = 2$ for the Atmospheric bands, the Franck-Condon factors published by NICHOLLS (1956) and intensities derived from Fig. 2, we arrive at the semi-empirical result that the rate of excitation of the $O_2(b^1\Sigma)$ state is only about five times larger than the rate of excitation of the $O(^1S)$ term, or less than that required by the proposed excitation and deactivation mechanisms. By using SEATONS lower limit for the excitation ratio of the metastable O I terms and a liberal allowance for errors in the intensity ratio, the figures may harmonize, but this seems rather unlikely.

The relative band intensities and the adopted Franck-Condon factors lead to a population of the $v' = 0$ and 1 levels of the $b^1\Sigma$ state corresponding to a temperature of 550° (CHAMBERLAIN *et al.*, 1954). It should be noted that the actual relative transition probabilities are somewhat different from the Franck-Condon factors,

owing to the variation in the electronic transition moment $R_e(r)$, and that the Franck-Condon factor for the (0-1) band is very low ($0{\cdot}06_5$), and may therefore not be very accurate. Although it is not to be expected that the distribution on vibrational levels is in thermal equilibrium with the atmosphere, the use of the correct, but still unknown, transition probabilities and the observed intensities may give relative population corresponding to a slightly lower vibrational temperature as well as higher rate of excitation of the $b^1\Sigma$ state.

It is possible that the O_2 molecules in the metastable $b^1\Sigma_g^+$ state may be transferred to the metastable $a^1\Delta_g$ state by spontaneous, but forbidden, radiation. The observable bands from this transition as well as from the transition $a^1\Delta_g^- - X^3\Sigma_g^-$ lie in the far-infra-red, longward of 12,000 Å, a region which is not well explored, neither in the auroral nor in the night-sky spectrum (cf. CHAMBERLAIN and MEINEL, 1954).

Collisional deactivation of the O_2 molecules might occur through "atom exchange" (BATES, 1955), but in this case one would expect a larger increase with altitude of the RI for the O_2 Atmospheric, bands since the rate of deactivation necessarily must decrease with altitude.

It seems thus at present possible, but far from certain, that process (2) may account for the deactivation of the O^1D term. More detailed computations show that a rate coefficient for process (2) of the order 10^{-11} to 10^{-12} is required to make the process sufficiently effective.

VOL. 10 1957

(c) The relative intensity for the oxygen multiplets $\lambda 7774$ ($3s^5S$–$3p^5P$) and $\lambda 8446$ ($3s^3S$–$3p^3P$), when excited by inelastic collisions with low-energy electrons, has been predicted by PERCIVAL and SEATON (1956), who find $I(7774)/I(8446) \leqslant 0{\cdot}3$. On the other hand, they predict the intensity of the green line $\lambda 5577$ (^1D–^1S) to be much more than ten times stronger than that of the $\lambda 7774$ multiplet. These intensity ratios are obviously not consistent with auroral intensities, neither with those given here nor with those adopted by PERCIVAL and SEATON, and they concluded that these oxygen multiplets are excited mainly by dissociation of O_2:

$$O_2 + X \rightarrow O' + O'' + X \qquad (3)$$

The energy required for this process is at least 16 eV, and possibly more, since the first stage of the process may be excitation of the O_2 molecule to a strongly repulsive state. It is interesting to note that these multiplets increase in relative intensity with altitude at approximately the same or even at a larger rate than do the Negative nitrogen bands (excitation potential 18·7 eV). The Meinel bands, however (excitation potential 16·7 eV), behave quite differently, decreasing in intensity with altitude compared to any other emission.

If the auroral luminosity is mainly due to impact of particles of high energy upon the earth's atmosphere, secondary electrons will play an important role, not only in exciting low-energy levels, but also by secondary ionization and dissociation (cf. BATES, MCDOWELL, and OMHOLT, 1957). The actual energy distribution of the secondary electrons is, however, not well known, and the cross-sections for the different excitation and ionization mechanisms are to a large extent uncertain. A thorough and accurate discussion of the excitation mechanisms in aurorae is therefore not yet feasible.

A detailed treatment by CHAMBERLAIN (1956) favours strongly the suggestion that auroral rays are due to discharge mechanisms. But his computations also show that the electron energies are expected to be very low, and that it would require a large electric field to produce excitation of the higher levels and ionization in agreement with the intensities in the main part of the aurora. Most of the spectra dealt with here are of auroras with ray structure, but apart from the behaviour of [O I] λ6300/64, they show no significant difference from spectrum 2, which is of a weak glow and contains strong H_α. Since the well-defined rays may give only a minor contribution to the total amount of auroral light observed on these occasions, we are not permitted to draw any definite conclusions. But attention should be directed to the fact that the Negative bands and in particular the oxygen multiplets become much stronger with increasing altitude, compared with the [O I] line λ5577 and the First Positive bands, whereas one would expect the light from auroral rays to yield a relatively larger contribution to the total intensity at greater elevation angles. Certainly, from CHAMBERLAIN's theory the intensity of lines and bands with a high excitation potential should increase relative to λ5577 upwards along an auroral ray, but with the high conductivity in the ionosphere it seems rather difficult to maintain the electric field required to give the observed intensities.

(d) The Meinel bands may also be excited through the charge-transfer process

$$O^+(^2D \text{ or } ^2P) + N_2\,(X\ ^3\Sigma) \rightarrow O\ (^3P) + N_2^+\,(A\ ^2\Pi) \qquad (4)$$

With $O^+(^2P)$, there is 1·92 eV excess energy which must be absorbed as vibrational or kinetic energy. With $O^+(^2D)$ there is almost exact resonance for $v' = 1$. The first case, if it is important, would contribute to an altitude distribution of the Meinel bands as observed, the latter to emissions from the $v' = 0$ and 1 levels only, which are not included in the present measurements. The process may be important for the deactivation of the O II(^2D) term.

Acknowledgements—It is a great pleasure to acknowledge valuable discussions and help from Dr. J. W. CHAMBERLAIN and Dr. Y. C. FAN during the preparation of this paper, as well as discussions with Prof. K. G. EMELEUS.

REFERENCES

ALLEN C. W.	1955	*Astrophysical Quantities*. The Athlone Press, London.
BAGARIASKY B. A. and FEDOROVA N. I.	1956	*The Airglow and the Aurorae* p. 174. Ed. E. ARMSTRONG and A. DALGARNO. Pergamon Press, London.
BATES D. R.	1955	*J. Atmosph. Terr. Phys.* **6,** 171.
BATES D. R., MCDOWELL M. R. C., and OMHOLT A.	1957	*J. Atmosph. Terr. Phys.* **10,** 51.
BERTHIER P.	1956	*Ann. Geophys.* **12,** 113.
CHAMBERLAIN J. W.	1954	*Astrophys. J.* **119,** 328.
	1956	*The Airglow and the Aurorae* p. 206. Ed. E. ARMSTRONG and A. DALGARNO. Pergamon Press, London.
CHAMBERLAIN J. W., FAN C. Y., and MEINEL A. B.	1954	*Astrophys. J.* **120,** 560.

CHAMBERLAIN J. W. and MEINEL A. B.	1954	*The Earth as a Planet.* Ed. G. P. KUIPER. University of Chicago Press.
CHAMBERLAIN J. W. and ROESLER F. L.	1954	*Astrophys. J.* **121,** 541
FAN C. Y. and SCHULTE D. H.	1954	*Astrophys. J.* **120,** 563.
GARSTANG R. H.	1956	*The Airglow and the Aurorae,* p. 324. Ed. E. ARMSTRONG and A. DALGARNO. Pergamon Press, London.
HARANG L.	1956	*J. Atmosph. Terr. Phys.* **9,** 157.
HERZBERG G.	1950	*Spectra of Diatomic Molecules.* D. Van Nostrand, New York.
MEINEL A. B.	1951a	*Astrophys. J.* **113,** 583.
	1951b	*Astrophys. J.* **114,** 431.
	1954	*Proc. Conf. Auroral Physics,* Geophys. Res. Papers No. 30.
NICHOLLS R. W.	1956	*The Airglow and the Aurorae,* p. 302. Ed. E. ARMSTRONG and A. DALGARNO. Pergamon Press, London.
OMHOLT A.	1955	*J. Atmosph. Terr. Phys.* **7,** 73.
	1956	*The Airglow and the Aurorae,* p. 178. ed. E. ARMSTRONG and A. DALGARNO. Pergamon Press, London.
PERCIVAL I. C. and SEATON M. J.	1956	*The Airglow and the Aurorae,* p. 244. Ed. E. ARMSTRONG and A. DALGARNO. Pergamon Press, London.
PETRIE W. and SMALL R.	1953	*Canad. J. Phys.* **31,** 911.
SEATON M. J.	1954	*J. Atmosph. Terr. Phys.* **4,** 295.
VEGARD L.	1955	*Geof. Publ.* **19,** No. 4.
	1956	*Geof. Publ.* **19,** No. 9.
VEGARD L. and TÖNSBERG E.	1952	*Geof. Publ.* **18,** No. 8.
WORLEY E. R.	1953	*Phys. Rev.* **89,** 863.

VOL. 10 1957

Journal of Atmospheric and Terrestrial Physics, 1957, Vol. 10, pp. 332 to 337. Pergamon Press Ltd., London

Diffraction microscopy and the ionosphere

G. L. Rogers
Department of Natural Philosophy, Marischal College, University of Aberdeen

(*Received* 12 *March* 1957)

Abstract—The application of diffraction microscopy to Mitra records is considered. It is shown that its application to existing records might result in some slight improvement, probably scarcely justifying the effort. If, however, tests should show that the combination would work with aerial spacings of 3–10 λ, the advantages of the combined method would be substantial.

An important practical limitation on any type of Mitra method is the complexity of the record normally obtained, and it may prove impossible adequately to analyse any but the simplest of them by any technique.

The question of future development is briefly touched on.

1. Introduction

It has been suggested in a preliminary note (Rogers, 1956) that the technique of diffraction microscopy might be applied to the interpretation of Mitra records (Mitra, 1949) of ionospheric movement. The establishment of the method would take some time, and before launching a full-scale investigation, it is desirable to form an estimate of (a) how far diffraction microscopy can help in developing the Mitra technique and (b) how the Mitra technique itself stands in relation to other techniques (e.g. following meteor-trail drifts) which have subsequently been developed. This paper addresses itself to the first of these questions: the second must be left to others more versed in ionospheric matters than the writer.

2. Outline of Diffraction Microscopy

A full theoretical treatment of diffraction microscopy has been given by its originator, Gabor (1948, 1949, 1950, 1955), and simplified treatments designed for non-physical scientists have been given elsewhere by other authors (Rogers, 1952a and b; Baez, 1952). Basically, the process is a two-stage image-forming process, similar to Bragg's "X-ray microscope," now called a diffraction spectrometer. In the Bragg case, a stage of X-ray diffraction is followed by the reciprocal diffraction operation in an optical apparatus using a different wavelength to give an "image" of the atomic pattern of the diffracting crystal. Both processes are Fraunhofer processes. In the Gabor case, the two reciprocal diffraction processes are both of them Fresnel diffractions, and this is more general and introduces a focusing condition as an additional factor. In either case the two-stage nature of the processes allows the first stage to be performed in a non-refractible radiation, the necessary focusing being done when the second stage is completed with light.

The successful application of the Gabor technique pre-supposes:—(a) a highly coherent source, of diameter $d < 0{\cdot}16\ \lambda/\sin\alpha$, where α is the half-angle of the cone of emergent radiation; (b) a small object in an otherwise open space, so that the first diffraction pattern recorded has everywhere a substantially undisturbed or

coherent background, upon which the waves scattered by the object are superimposed as a small ripple. In the radio case, the coherent background may be supplied artificially by a link from the transmitter, and this difficulty is not as acute as in optics.

In the radio case a radio star can be used as a source, in which case no link with the transmitter is possible, and a fairly "open" object is required. Alternatively, a

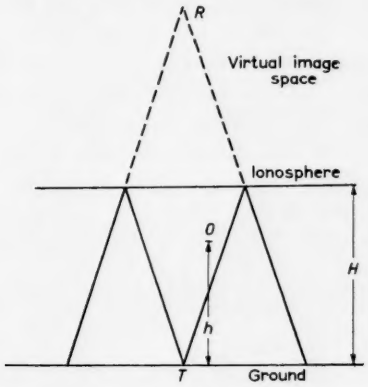

Fig. 1.

VOL. 10 1957

transmitter reflected in the ionosphere may be used as a source, but this case is dependent on good reflecting conditions in the ionosphere. Only fairly long experience will show how far suitable reflecting conditions are likely to be obtained.

3. The Radio Situation

Mitra fading patterns are essentially one-dimensional sections of a Fresnel diffraction pattern projected from a virtual image of the transmitter in the ionosphere, through the ionosphere (which acts as "object") onto the ground, which acts as the "screen," or photographic plate. The fact that the ionosphere is often equivalent to a plane mirror just behind an exceedingly rough diffusing screen, does not alter the fundamental assessment of the situation as a Fresnel diffraction pattern, but simply makes it the diffraction pattern of a rough screen. It is not impossible, in principle, to "image" this rough screen, subject to the usual resolving-power considerations, even though it would require advanced techniques not yet fully developed in practice.

Fig. 1 shows roughly how this Fresnel diffraction operates in terms of a general point, O, not necessarily in the plane of the ionosphere. To give some idea of the scale of the phenomenon, take $\lambda = 125$ m, reflected in an ionosphere at $H = 120$ km, and a pulse length of 200 waves. The diameter of the "cone" of coherently illuminating rays, measured at the ionosphere, is $\sim$80 km, and the diameter of the first Fresnel half-period zone within it is 5·4 km. Diffraction effects are therefore large, and the traditional "ray" approach to ionospheric problems is very approximate.

The diffraction pattern *on the ground* is even larger. If they originate in a point on the ionosphere, the zones will be twice the size of the Fresnel half-period zones

mentioned above (ROGERS, 1952a). Considering interference up to order 12 as reasonably strong in practice, this means the pattern on the ground will be about 54 km across. The patterns which must be recorded are thus fairly large, and at a ground speed of 300 m/sec will take 3 min to cross the aerial. At lower ground speeds the time might easily go up to 20 min. This emphasizes the need for recording fairly long runs if good two-stage diffraction is required, though useful results may be obtained by only recording up to order 4 or 5, which reduces the times to less than half.

There is, however, a more important consequence of these large-scale diffraction patterns: it means that the fading frequencies due to genuine ionospheric diffraction will be relatively slow. Table 1 gives details of periodic times likely to be observed in different parts of the pattern. It will be seen at once that they are all fairly long, and the appearance of frequencies inconsistent with this table was the first sign that Mitra records cannot always be interpreted as genuine ionosphere effects. It also means that A.V.C circuits must be used with caution.

Table 1. Sizes and periods of ground patterns due to ionospheric scatterers

Order of interference		Periodic times of fading (sec)			
		Ground velocity of	300 m/s	100 m/s	50 m/s
Order Nos.	Spacing (km)	"Ionospheric" velocity of	150 m/s	50 m/s	25 m/s
$\frac{1}{2}$–1	4·48		15·0	44·8	89·6
2–2$\frac{1}{2}$	2·30		7·6	23·0	46·0
5–5$\frac{1}{2}$	1·66		5·6	16·6	33·2
12$\frac{1}{2}$–13	1·06		3·6	10·6	21·2
Indefinitely large,	0·125 = λ		0·42	1·25	2·5

4. THE OPTICAL SITUATION

A photographic plate has to be produced which represents, on a small scale, the Fresnel diffraction pattern on the ground as seen from each of the three aerials. The scale of this representation is of some importance in practice, and must be considered in detail.

Diffraction microscopy is subject to the invariant:

$$\frac{f_1\lambda_1}{{L_1}^2} = \frac{f_2\lambda_2}{{L_2}^2}$$

where L_1 and L_2 are corresponding distances in the initial Fresnel diffraction pattern and on the photographic plate—conveniently the distance travelled by the pattern over the ground in 1 sec (V_g) and the corresponding distance, p, on the plate, representing a 1-sec run of the Mitra record. If f_1 is the radio focus, and f_2 the visual or optical focus there follows:

$$f_2 = f_1\left(\frac{\lambda_1}{\lambda_2}\right)\left(\frac{p}{V_g}\right)^2$$

In practice, f_1 is about 240 km; $\lambda_1 \simeq 125$ m; $\lambda_2 = 5461 \times 10^{-10}$ m; and V_g anything

from 50 to 300 m/sec. It is found that if p is made about 12 μ for every second's run of the Mitra record, f_2 will range from about 10 cm to 3 m for the range of ground velocities quoted. As f_2 varies as the square of the scale factor p, the choice of p is necessarily restricted to a range from about 8–20 μ for a 1-sec run if anything like convenient optical foci are to be produced.

It can be shown that, so far as concerns the ultimate resolving power of the process *in time*, i.e. in aerial delay between successive tracks, the scale factor p is irrelevant, but there are two further factors which have to be considered. The first is the grain size of the film, which argues a large p, and the second is the need to illuminate the plate with a small source to obtain coherence. This is more readily done if p is small as α becomes small and the source diameter can be increased. This, too, is to some extent self-compensating in terms of the speed and grain size of the film used to record the final "reconstruction" of the ionosphere, but the advantages for a visual search in using a small p are undeniable. It should be emphasized that the range of p dictated by the optical focus represents a quite possible working region, though scarcely a comfortable one, as it runs so close to the practicable limits of the processes involved.

It seems reasonable to suppose that with a good record aerial, time-delays of $\frac{1}{2}$ sec should be detectable, and under exceptionally favourable conditions, perhaps $\frac{1}{4}$ sec. It will almost certainly not be possible to do better than this without radical changes of technique.

VOL. 10 1957

5. The Radio-record to Optical Plate Transformation

This is essentially based on the cylindrical lens technique (Rogers, 1952b; 1956) and has been described elsewhere. Its application to three tracks, using successive exposures through three or four zones of the cylindrical lens (perpendicular to the cylinder axis), is readily imagined. Direct variable density recording is also conceivable, but as far as is known has not yet been attempted. If the whole method proves satisfactory, some such method of direct variable-density recording must be developed to avoid the considerable labour of the cylindrical lens technique.

6. Interpretation of Height Measurements

As explained elsewhere (Rogers, 1956), the radio focus f_1 may be obtained from the visual focus f_2, and hence the height of a scattering-point object can be determined. It is readily shown that the focal length of the system is unaffected if the point scatterer does not pass directly above the aerial, though the phase of the focused wavefront, relative to the background, will change if the path is off centre.

If, however, the scatterer is a line scatterer, some ambiguity arises because the line may not be moving perpendicular to its length. If the line is inclined at an angle θ to the direction of drift, the recorded focal length will be $\mathrm{cosec}^2\,\theta$ greater than the true focal length. Put another way, the height determination takes account of the component of motion perpendicular to the length of the line, but ignores the rest. As $\mathrm{cosec}^2\,\theta \ll 1$, the heights so obtained are maximum heights, and in some cases, e.g. where they turn out sub-ionospheric, they provide conclusive evidence that the scatterer is itself sub-ionospheric.

7. Tests of The Method

One possible test of the method is published elsewhere (Rogers, 1957), when an aircraft is flown on a known course and detected by the reconstruction methods. This, of course, begs the important question of the size and shape of the scatterers by using an object substantially smaller than a wavelength.

The only other immediately applicable test depends on making some assumptions about the nature of normal Mitra records. If we assume that these records normally represent the superimposed effects of several layers at different heights moving with different speeds in different directions, the observed difficulty of correlating the three tracings if the aerial spacings are much more than λ is readily appreciated. Nevertheless, if the complex patterns can be sorted out into their component height elements, the correlation *at a given height* should be observable over much longer aerial spacings. It would be useful to try and correlate by diffraction microscopy records obtained with aerial spacings of 3 λ or 10 λ, not otherwise easily correlated by normal methods. If it proved possible to do this consistently, the increased time-delays which would result from the greater aerial spacing would contribute greatly to the accuracy of speed determinations, and largely offset the difficulties at present involved in the small values of the scale factor p needed to get reasonable optical foci. This test is regarded as important.

It is recognized that the general complexity of the phenomena usually involved does make any method of analysis liable to fail adequately to resolve the various moving ionospheric and sub-ionospheric elements.

8. Possible Developments

If the method of diffraction microscopy proves successful in developing a one-dimensional picture of the ionosphere, it is interesting to see if it could conceivably give a two-dimensional picture. It is possible that something of this kind could be achieved by the simultaneous recording of traces from 101 aerials spaced at $\frac{1}{2}$-km distances along a line of length 50 km transverse to the currently prevailing ionospheric wind. The techniques for optical reconstruction would involve many complications, of which a variable magnification in two directions at right angles appears to be the most difficult.

It is also possible to get complete amplitude and phase information about scatterers by producing the radio-analogue of the Gabor and Goss interferometer (Gabor, 1955). An instrument of very similar design has been produced to study meteor trail drifts (Greenhow, 1954: seen in abstract only).

Finally, it is in principle possible to obtain some incomplete evidence of the non-linear and three-dimensional motion of a point scatterer by measuring the optical aberrations of the zone-plate resulting from the photographic operations. An aberration-free zone-plate only results from a point or line scatterer moving uniformly and horizontally, and any deviation from uniform motion or from horizontal motion will produce an appropriate type of aberration. While, however, the aberration can be calculated if the supposed type of motion is specified, it is not possible to work back without ambiguity from the aberration to the particular type of motion causing it, as there is some overlap of solutions.

Acknowledgements—I am indebted to Mr. G. J. BURTT and members of the Radio Research group of the Dominion Physical Laboratory, New Zealand, for access to Mitra methods and much useful discussion, also to Professor R. V. JONES, Department of Natural Philosophy, the University of Aberdeen, for a temporary lectureship while writing up the results.

REFERENCES

BAEZ	1952	*J.O.S.A.* **42**, 756 1952.
GABOR	1948	*Nature, Lond.* **161**, 777.
	1949	*Proc. Roy. Soc.* **A197**, 454.
	1950	*Proc. Phys. Soc.* **B64**, 449.
	1955	BP 727,893.
GREENHOW J. S.	1954	*Phil. Mag.* **45**, 471.
MITRA	1949	*J. Instn. Elec. Engrs.* III **96**, 441.
ROGERS	1952a	*Proc. Roy. Soc. Edinb.* **A63**, 193.
	1952b	*Proc. Roy. Soc. Edinb.* **A63**, 313.
	1956	*Nature, Lond.* **177**, 613.
	1957	*J. Atmosph. Terr. Phys.* **10**, 336.

VOL.
10
1957

RESEARCH NOTE

The effect of the recorder time constant on the apparent speed of fading of a radio signal*

(*Received* 21 *March* 1957)

THE purpose of this note is to indicate the importance, when taking continuous records of the fading of a radio signal, of making an appropriate choice of recording time constant.

Most practical recording systems incorporate a post-detector integration circuit of the kind shown in Fig. 1. A sine wave of frequency f, is reduced in amplitude by a factor of

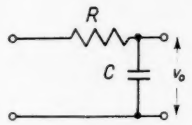

Fig. 1

$\{1 + (2\pi CRf)^2\}^{1/2}$ by this circuit. If the amplitude of the fading signal has a Gaussian autocorrelogram of the form

$$\rho(\tau) = \exp(-\tau^2/2b^2) \tag{1}$$

the power spectrum of this signal is given by

$$W_1(f) = 2\pi b \exp(-2\pi^2 b^2 f^2) \tag{2}$$

The power spectrum of the open-circuit voltage $v_0(t)$ is, therefore,

$$W_2(f) = \frac{2\pi b \exp(-2\pi^2 b^2 f^2)}{\{1 + (2\pi CRf^2\}^{1/2}} \tag{3}$$

It is possible to define two measures T_1 and T_2 of fading time for any signal (BOWHILL, 1956). These are derived respectively from the mean slope and from the number of maxima of the signal amplitude. If the signal has a Gaussian correlogram of the form of equation (1), and is not fading deeply, they are given by $T_1 = b$, $T_2 = 3{\cdot}63b$. RICE (1944) gives formulae for calculating them from the power spectrum:

$$\begin{aligned} T_1 &= \frac{1}{2\pi}\left\{\int_0^\infty W_2(f)\,df\right\}^{1/2} \cdot \left\{\int_0^\infty f^2 W_2(f)\,df\right\}^{-1/2} \\ T_2 &= \left\{\int_0^\infty f^2 W_2(f)\,df\right\}^{1/2} \cdot \left\{\int_0^\infty f^4 W_2(f)\,df\right\}^{-1/2} \end{aligned} \tag{4}$$

These integrals can be evaluated in closed form in terms of the error integral. The ratios T_1/b and $T_2/3{\cdot}63b$ are plotted in Fig. 2.

* The research reported in this paper has been sponsored by the Geophysics Research Directorate of the Air Force Cambridge Research Center, Air Research and Development Command under Contract AF19(604)-1304.

It can be seen that the recorder time constant must be less than one-sixteenth of the mean fading period T_2 of the fading function, if the deduced fading speed is to be within 5 per cent of the correct value.

The experiments of HARWOOD (1953) illustrate the importance of this effect. He recorded the amplitude of a 16 kc/s ionospheric echo, using a recorder time constant of

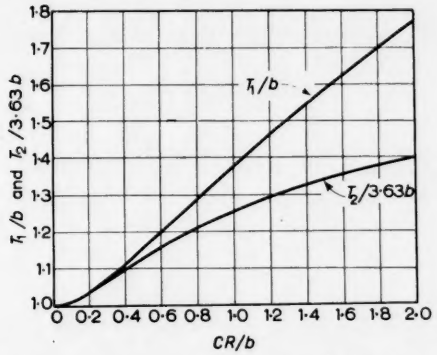

Fig. 2. The effect of recorder time constant on the ratios of observed to actual values of T_1 and T_2 for a fading curve with a Gaussian correlogram.

100 sec. Using a value (BOWHILL, 1956) of 7 min for T_2, the observed value of T_2 at the detector output is found as $7 \times 1{\cdot}32 = 9{\cdot}2$ min, an error of over 30 per cent. Ignoring small turning points in the records, HARWOOD found a mean T_2 of 11 min. The whole of the discrepancy in fading speed is, therefore, thought to be accounted for.

S. A. BOWHILL

Ionosphere Research Laboratory
The Pennsylvania State University
University Park, Pennsylvania

VOL. 10 1957

REFERENCES

BOWHILL S. A. 1956 The fading of radio waves of frequencies between 16 and 2400 kc/s. *J. Atmosph. Terr. Phys.* **8,** 129.

HARWOOD J. 1953 Spaced receiver experiments on radio waves of 19 km wavelength. *Monograph No.* 86. Institution of Electrical Engineers, London.

RICE S. O. 1944 Noise through non-linear devices. *Bell. Syst. Tech. J.* **23,** 109.

Journal of Atmospheric and Terrestrial Physics, 1957, Vol. 10, pp. 340 to 344. Pergamon Press Ltd., London

Indices of geomagnetic activity

of the Observatories ABINGER (*Ab*), ESKDALE (*Es*), and LERWICK (*Le*)

October 1956

The figures given on pages 340 to 344 represent the *K*-indices for three-hour intervals, beginning with 00–03 hr for the first and ending with 21–24 hr for the eighth figur

October 1956

Day	*Ab* Range for $K = 9 : 500\gamma$			*Es* Range for $K = 9 : 750\gamma$			*Le* Range for $K = 9 : 1000\gamma$			*Day*
	K-Indices		*Sum*	*K-Indices*		*Sum*	*K-Indices*		*Sum*	
1	2323	3334	23	2223	3324	21	2212	3325	20	1
2	5343	4344	30	4233	4344	27	5223	4345	28	2
3	3333	3444	27	3333	3443	26	4323	3435	27	3
4	3123	3333	21	3122	2323	18	4222	2343	22	4
5	1243	2333	21	1143	2232	18	1143	2233	19	5
6	3334	4334	27	3233	4333	24	3223	4333	23	6
7	3333	3443	26	2232	2332	19	3222	2333	20	7
8	3233	3343	24	3232	2243	21	3232	1243	20	8
9	3233	3333	23	2222	3323	19	3222	2222	17	9
10	3222	2222	17	2111	2211	11	2111	1111	9	10
11	2223	3222	18	2212	2112	13	1221	2111	11	11
12	1123	3223	17	0012	2123	11	0012	1113	9	12
13	2223	2211	15	2011	1101	7	2011	1011	7	13
14	1122	2111	11	1111	0110	6	1111	0011	6	14
15	0022	2222	12	0000	1111	4	1011	1111	7	15
16	1222	2221	14	1121	1111	9	1021	1101	7	16
17	1122	2112	12	1012	1101	7	1011	1111	7	17
18	1222	1121	12	1111	0101	6	1111	1111	8	18
19	2222	2221	15	1212	1111	10	0112	2111	9	19
20	1343	4545	29	0343	3445	26	0433	3667	32	20
21	4443	3344	29	4433	3333	26	6534	4343	32	21
22	3332	3233	22	3320	3232	18	4421	3332	22	22
23	4332	3343	25	3232	2234	21	4322	3343	24	23
24	2322	2231	17	1321	1121	12	2321	1120	12	24
25	1122	2232	15	0111	0012	6	0011	0012	5	25
26	3343	4466	33	2232	3366	27	2132	3578	31	26
27	6543	3343	31	6532	3333	28	6732	3334	31	27
28	3333	3223	22	3333	3222	21	3344	4323	26	28
29	2123	2242	18	2112	2232	15	2112	2332	16	29
30	1223	3321	17	1122	3311	14	1112	3321	14	30
31	1122	3314	17	1012	2213	12	0012	2113	10	31

November 1956

Day	*Ab* Range for $K = 9 : 500\gamma$		Sum	*Es* Range for $K = 9 : 750\gamma$		Sum	*Le* Range for $K = 9 : 1000\gamma$		Sum	Day
	K-Indices			*K-Indices*			*K-Indices*			
1	4322	3323	22	3311	2322	17	3321	3323	20	1
2	2223	3323	20	1112	2213	13	2123	3323	19	2
3	4334	3333	26	4333	2232	22	4333	3232	23	3
4	3333	3323	23	3222	2222	17	3222	1322	17	4
5	2233	2223	19	2112	1112	11	2111	1112	10	5
6	2333	3333	23	1223	2233	18	1222	2333	18	6
7	3234	3232	22	2112	2111	11	2213	2122	15	7
8	2223	3221	17	1112	1110	8	2112	2211	12	8
9	2223	3354	24	1112	2235	17	1111	1354	17	9
10	4444	4456	35	7733	4667	43	5443	3455	33	10
11	5554	4355	36	6654	3357	39	6553	4356	37	11
12	5344	5555	36	6333	4755	36	5333	5645	34	12
13	4323	3323	23	6412	3213	22	4322	3213	20	13
14	3454	3465	34	5453	3587	40	3343	2466	31	14
15	5566	5443	38	6666	5343	39	5566	5433	37	15
16	5544	3353	32	6753	2253	33	5543	3253	30	16
17	2223	4443	24	2122	3443	21	2122	3332	18	17
18	3433	3232	23	5442	2121	21	4332	2121	18	18
19	0122	2221	12	1012	1111	8	1011	2211	9	19
20	1023	3343	19	0012	2343	15	0023	3332	16	20
21	4333	3335	27	3333	2234	23	4333	2334	25	21
22	4323	4445	29	3222	3567	30	3222	4345	25	22
23	4434	3432	27	6333	5443	31	4334	4332	26	23
24	2222	3443	22	2112	2443	19	1212	3443	20	24
25	2222	6433	24	3112	4333	20	2122	6332	21	25
26	3122	2221	15	3210	1011	19	3110	0011	7	26
27	2222	1155	20	1101	1145	14	1111	0145	14	27
28	4333	2233	23	7222	1121	18	5322	2222	20	28
29	3232	2344	23	1122	1234	16	2122	2234	18	29
30	3323	3223	21	3322	1122	16	3332	2223	20	30

December 1956

1	2123	3233	19	1112	2232	14	1112	2122	12	1
2	4223	3333	23	4222	2333	21	4312	2333	21	2
3	2233	3342	22	2122	2232	16	2122	2232	16	3
4	3323	2333	22	2222	2233	18	3312	2233	19	4
5	3222	3321	18	2221	2311	14	2211	2321	14	5
6	1221	3344	20	0211	2344	17	1111	2245	17	6
7	2322	2423	20	2222	2323	18	2211	1313	14	7
8	3233	2132	19	2122	2131	14	2222	2132	16	8
9	1212	2233	16	1122	2223	15	1021	2123	12	9
10	3434	3334	27	2424	3224	23	3423	3224	23	10
11	2222	2121	14	1101	1121	8	1101	1010	5	11
12	0112	2444	18	0011	2343	14	0011	2444	16	12
13	4333	4333	26	3232	3333	22	4232	3324	23	13
14	3323	2232	20	3222	1232	17	3212	1133	16	14
15	1112	2210	10	1101	1110	6	1111	1101	7	15

VOL. 10 1957

December 1956 (*continued*)

Day	*Ab* Range for $K = 9 : 500\gamma$			*Es* Range for $K = 9 : 750\gamma$			*Le* Range for $K = 9 : 1000\gamma$			*Day*
	K-Indices		*Sum*	*K-Indices*		*Sum*	*K-Indices*		*Sum*	
16	0112	1110	7	1111	1110	7	1111	1110	7	16
17	1112	1110	8	0111	1100	5	0111	1101	6	17
18	1121	3211	12	0112	3110	9	0112	2211	10	18
19	0022	2223	13	0012	1213	10	0011	1113	8	19
20	2112	1111	10	2112	1111	10	2102	1001	7	20
21	1122	2222	14	1112	1101	8	1011	1002	6	21
22	1222	3220	14	1212	3220	13	1112	2121	11	22
23	0023	2123	13	0002	1112	7	0002	1112	7	23
24	3333	2222	20	3322	2121	16	3311	1121	13	24
25	2124	4335	24	2024	3335	22	2113	3345	22	25
26	3333	2210	17	3333	2110	16	4332	1011	15	26
27	0011	1344	14	0012	1343	14	0001	1443	13	27
28	3243	4343	26	3233	3232	21	3232	3232	20	28
29	4322	3232	21	3222	2232	18	4312	2132	8	29
30	2134	3233	21	1134	2233	19	1133	2223	17	30
31	2123	3221	16	1102	2111	9	1002	2011	7	31

January 1957

1	1224	3221	17	1103	2121	11	0002	2111	7	1
2	2134	2255	24	2124	2255	23	2113	2256	22	2
3	3233	3222	20	3223	2112	16	3212	1111	12	3
4	2223	2111	14	1122	1101	9	1011	1001	5	4
5	0121	2121	10	1111	1111	8	1001	1110	5	5
6	1212	3123	15	0222	2112	12	0112	1111	8	6
7	2222	3111	14	2112	2111	11	1111	2111	9	7
8	3323	3343	24	3213	3333	21	3212	2333	19	8
9	2222	3444	23	2112	3334	19	1011	3334	16	9
10	2343	3455	29	2343	3454	28	3343	3455	30	10
11	4232	3222	20	4132	3212	18	4133	3112	18	11
12	2322	1102	13	2321	1102	12	3310	0101	9	12
13	2123	2212	15	2102	1101	8	1002	1101	6	13
14	1012	2220	10	1011	1110	6	0011	1100	4	14
15	1111	3233	15	1112	2233	15	1011	2223	12	15
16	3223	3222	19	3111	2121	12	3112	2221	14	16
17	2223	2222	17	2102	2122	12	2101	1111	8	17
18	1112	2110	9	1011	1100	5	0011	1111	6	18
19	0033	3332	17	0112	2332	14	0012	2332	13	19
20	2113	2100	10	2111	2110	9	2102	2110	9	20
21	2234	5579	37	1233	4689	36	1222	4789	35	21
22	8564	4432	36	9554	4432	36	9664	4432	38	22
23	3334	3343	26	3343	3343	26	2234	3353	25	23
24	4422	4255	28	4422	3254	26	4312	3256	26	24
25	4343	2234	25	4333	2224	23	6333	1124	23	25
26	2233	3323	21	2223	2323	19	2212	2213	15	26
27	1234	3322	20	1223	2222	16	1213	3221	15	27
28	1122	3232	16	1112	2132	13	1111	2122	11	28
29	1223	5444	25	1213	4444	23	1112	5664	26	29
30	4444	3343	29	5443	3333	28	6543	3343	31	30
31	2323	3333	22	2322	2333	20	2212	1333	17	31

February 1957

Day	*Ab* Range for $K = 9 : 500\gamma$		Sum	*Es* Range for $K = 9 : 750\gamma$		Sum	*Le* Range for $K = 9 : 1000\gamma$		Sum	Day
	K-Indices			*K-Indices*			*K-Indices*			
1	2222	3221	16	2112	2221	13	2111	2121	11	1
2	0222	3333	18	1112	3233	16	1111	2232	13	2
3	2212	2355	22	1211	2245	18	1101	1245	15	3
4	4333	4444	29	3223	4445	27	3222	4567	31	4
5	5533	4343	30	5533	4333	29	5543	4433	31	5
6	3133	2221	17	3122	2211	14	3112	1111	11	6
7	1023	2222	14	0122	1212	11	0012	1122	9	7
8	2233	2222	18	1222	2222	15	1121	1112	10	8
9	2322	2322	18	1211	1222	12	1212	1232	14	9
10	2232	1101	12	2013	1111	10	2112	0010	7	10
11	1223	3422	19	1213	2422	17	1211	2322	14	11
12	2433	2243	23	2322	2142	18	2421	1131	15	12
13	3434	5563	33	3433	5563	32	3433	4463	30	13
14	2222	2121	14	2222	1111	12	2121	1111	10	14
15	0134	3323	19	1133	2323	18	0022	2313	13	15
16	1222	2332	17	0122	2222	13	0111	1231	10	16
17	2123	3333	20	2113	3233	18	1112	2233	15	17
18	3233	3344	25	3233	3344	25	3222	2345	23	18
19	3333	3455	29	3233	3354	26	3232	2355	25	19
20	4333	3333	25	4322	3223	21	4322	2213	19	20
21	4343	4444	30	4343	3444	29	4433	3436	30	21
22	4333	4344	28	4333	4444	29	5333	3344	28	22
23	4322	3365	28	3321	3365	26	3221	2367	26	23
24	6544	4322	30	7544	4321	30	7664	4322	34	24
25	3324	3111	18	3223	2210	15	3212	2110	12	25
26	1122	3322	16	1011	1211	8	1001	1111	6	26
27	3322	1222	17	2311	0111	10	2211	0111	9	27
28	1012	2211	10	1011	2211	9	1001	1112	7	28

March 1957

1	1122	3454	22	1111	3444	19	1011	2554	19	1
2	5776	5456	45	4886	7557	50	5995	6667	53	2
3	4343	3433	27	4343	2433	26	5442	2433	27	3
4	3332	2123	19	3322	2113	17	3321	2113	16	4
5	3333	3343	25	3222	3233	20	3322	3343	23	5
6	4223	3332	22	3112	3332	18	4112	3322	18	6
7	2222	3333	20	2112	2322	15	2211	2333	17	7
8	4133	3235	24	3122	2234	19	3122	2234	19	8
9	4423	3344	27	3422	2344	24	4332	2334	24	9
10	3335	6455	34	3335	6455	34	3434	7586	40	10
11	3232	2232	19	3221	2221	15	4221	2111	14	11
12	3333	2211	18	2322	2100	12	1222	1100	9	12
13	0223	2432	18	0122	2422	15	0022	2332	14	13
14	1133	2312	16	1122	1201	10	0012	1101	6	14

VOL. 10 1957

March 1957 (*continued*)

Day	*Ab* Range for $K = 9 : 500\gamma$			*Es* Range for $K = 9 : 750\gamma$			*Le* Range for $K = 9 : 1000\gamma$			*Day*
	K-Indices		*Sum*	*K-Indices*		*Sum*	*K-Indices*		*Sum*	
15	2232	3345	24	2222	1234	18	2222	1223	16	15
16	5443	3354	31	4342	3355	29	5332	2366	30	16
17	3333	3423	24	3232	3323	21	3332	2332	21	17
18	2223	3223	19	1223	3223	18	1212	3213	15	18
19	2132	2344	21	2122	2343	19	2112	1333	16	19
20	3333	2224	22	3332	2124	20	3332	2114	19	20
21	1322	3545	25	1221	3445	22	1211	2666	25	21
22	3243	3434	26	3233	3334	24	4223	3345	26	22
23	4334	3332	25	4323	3333	24	5423	2333	25	23
24	3222	2144	20	2222	1244	19	2321	1244	19	24
25	4533	4322	26	3533	3221	22	5553	3211	25	25
26	2133	4434	24	1123	4334	21	1112	3335	19	26
27	3323	4456	30	3323	4455	29	5323	4357	32	27
28	6554	3422	31	6555	4421	32	8664	3411	33	28
29	2544	7765	40	2443	6865	38	3433	6876	40	29
30	5432	2224	24	5431	2223	22	6532	2223	25	30
31	3333	3444	27	3232	3444	25	2332	3454	26	31

Book Reviews

M. SCHULER and H. GEBELEIN: **Eight and Nine Place Tables of Elliptical Functions.** Springer Verlag, Berlin; 1955. £5. 1. 6, D.M. 58.

ELLIPTIC functions arise frequently in the evaluation of results in applied mathematics, so it is advantageous to have complete sets of tables of them. The chief purpose of these new tables is to provide the means for making interpolations easily and with accuracy equivalent to that of the tabulated values. This presents great difficulties (since the functions in question are functions of two variables) which the authors claim to have overcome by the systematic use of JACOBI'S parameter q rather than that of LEGENDRE'S modulus Θ.

Functions G and H are defined by the equations

$$G = -\frac{\vartheta_1(x) - 2q^{1/4}\sin x,}{2q^{3/4}\sin x} \qquad H = \frac{\vartheta_3(x) - 1}{q}$$

Almost everything needed for ordinary problems involving elliptic and related functions can be derived in an elementary way from the four theta functions which can be expressed in terms of G and H by the equations

$$\vartheta(x) = 2q^{1/4}\sin x[1 - q^2G(+z)]\,; \quad \vartheta_2(x) = 2q^{1/4}\cos x[1 - q^2G(-z)]$$

$$\vartheta_3(x) = 1 + qH(+z)\,; \quad \vartheta_4(x) = 1 + qH(-z)$$

VOL. 10 1957

where $z = \cos 2x$. The range for z is from -1 to $+1$; in theory, q ranges from 0 to 1, but for ordinary needs, tables with q from 0 to 0·55 are sufficient.

The elliptic functions most important for practical use are the Jacobian functions sn u, cn u, dn u, defined by

$$\frac{\operatorname{sn} u}{\sin x} = \frac{1 + qH(+1)}{1 - q^2H(-1)} \cdot \frac{1 - q^2G(+z)}{1 + qH(-z)}$$

$$\frac{\operatorname{cn} u}{\cos x} = \frac{1 + qH(-1)}{1 - q^2G(-1)} \cdot \frac{1 - q^2G(-z)}{1 + qH(-z)}$$

$$\operatorname{dn} u = \frac{1 + qH(-1)}{1 + qH(+1)} \cdot \frac{1 + qH(+z)}{1 + qH(-z)}$$

where $z = \cos 2x = \cos(\pi u/K)$, where K is the complete elliptic integral of the first kind with $q = q(\Theta)$.

The tables contained in the present volume are:

Tables I, II: $G(q^4,z)$ as a function of z from $-1{\cdot}00$ to $+1{\cdot}00$ (by increments of 0·05), and of q^4 from 0·001 to 0·100 (by 0·001), with the corresponding values of q and Θ.

Tables III, IV: $H(q^3,z)$ as a function of z from $-1{\cdot}00$ to 1·00 (by 0·05), and of q^3 from 0·002 to 0·176 (by 0·002), with the corresponding values of q and Θ.

Tables V, VI: log (sn u/sin u), log (cn u/cos u), log (dn u) as functions of z from $-1{\cdot}00$ to $+1{\cdot}00$ (by 0·05), and of q from 0·01 to 0·55 (by 0·01), with the corresponding values of Θ, $-\log\cos\Theta = -\log k'$, K, and K/E.

Table VII: Conversion tables for LEGENDRE'S modulus Θ and JACOBI'S parameter q with values of $(1 - q)^{-1}$, K, K/E as functions of $-\log k'$ from 0·000 to 3·000 (by 0·005).

The use of these tables is explained clearly (in German and English) in a very full introduction in which the necessary interpolation formulae are included. The full solutions to seven typical problems are also given. Tables I–IV are given up to the ninth decimal place, while Tables V–VII are given to eight places. The tables are clearly printed and easily used, and the whole volume is most beautifully produced.

I. N. SNEDDON

G. C. McVittie: **General Relativity and Cosmology.** Chapman and Hall, London, 1956. 198 pp., 42s.

At a time when much British cosmology may at best be described as science fiction, it is refreshing to read a book which sets out soundly based ways of investigating the observable universe.

Professor McVittie has attempted to write an account of general relativity and cosmology which will be instructive to teacher and student alike, and has succeeded admirably in his task. The book begins with a short account of the author's approach to scientific investigation, and then follows a chapter on tensor calculus and Riemannian geometry which requires only an elementary knowledge of partial differential equations for its understanding. An account of Newtonian mechanics and special relativity is succeeded by a derivation of Einstein's equations and consideration of the principles of general relativity. Then comes a chapter on those aspects of general relativity with which astronomers are, perhaps, most familiar—the advance of Mercury's perihelion, the displacements of the apparent positions of stars viewed close to the sun during eclipse, and the gravitational red shift in stellar spectra. The difficulty of the next two chapters dealing with generalizations of Newtonian gas dynamics, and applications to Galactic gas-clouds, is greater than the rest of the book. Finally, there are two chapters on model universes and the system of galaxies. What has been done in these chapters may be described in the author's own words: "To each type of measurement, whether already made or in process of being carried out, it has proved possible to find a formula which is its theoretical counterpart. These formulae contain a number of parameters whose numerical values can, in principle, be determined from the relevant observations as these increase in scope and accuracy."

The conciseness of McVittie's account enables the arguments to be followed easily without the need to keep turning back the pages. There are, however, a few parts that might have benefitted from a little expansion. For instance, a more adequate description of the objects of Chapter 2 would have helped to make it clear why all this chapter is a necessary preliminary to what follows; a remark such as that on page 54, that the principle of special relativity states that the equations of mathematical physics must retain their form under co-ordinate transformations, and this may be secured by expressing all relations by means of tensors, may with advantage have been placed early in Chapter 2. Similarly, the account of the operations of raising and lowering indices, and contracting tensors, would have been better with examples, or even just a reference to later applications such as the one which occurs on page 75, where contraction of a particular nonzero Riemann-Christoffel tensor is shown to result in a null Ricci tensor. From the student's point of view, it is helpful to be able to see, at the time the operations are developed, what effects they have when applied to specific cases.

The statement on page 135 that spaces between galaxies are probably—if not quite certainly—devoid of matter, is too definite. Observational data is still far too meagre to enable a proper estimate of the density of intergalactic matter to be made. The possible effects of absorbing matter between galaxies deserve more prominent mention than the brief remark on page 180.

The absolute magnitudes of galaxies (page 136) are not on a Gaussian distribution curve. In a paper published in 1950, Holmberg found a considerable excess of the fainter galaxies.

On page 155 it is not made clear how the observer is to choose light sources "similar" to distant galaxies as they are now, and as they were when the light reaching us now left them. What is the criterion by which two galaxies shall be judged to be similar?

If the Stebbins-Whitford excess reddening of distant galaxies is due to a secular change in the quality of the radiation emitted, then it is as closely bound up with the evolution of individual stars and galaxies as with the larger scale of things. This point might well be stressed, because many astronomers have in the past regarded cosmology as being far removed from their researches on objects astronomically near at hand, just as many cosmologists have failed to pay sufficient attention to the evolution of galaxies as a function of time alone.

Professor McVittie has provided us with an excellent book, a book which leaves observers of the large-scale structure of the universe with no excuses for failing to understand the theoretical implications of their work. The same remark applies to cosmologists.

V. C. Reddish

Advances in Geophysics. Edited by H. E. LANDSBERG, Academic Press, New York, 1955. Vol. 2., 286 pp., 60s

THIS is the second in a series of review articles covering recent developments in geophysics, widely interpreted. The use of centimetric radar in the study of precipitation patterns in the atmosphere, and its theoretical explanation in terms of Rayleigh scattering is described by MARSHALL, HITSCHFELD, and GUNN. I. I. GRINGORTEN discusses the fascinating problem of objectivity in weather forecasting. W. J. PIERSON presents a mathematical theory of gravity waves generated by wind.

L. J. KULP describes the lead, strontium, potassium, and carbon-14 methods of geological age determination, and H. BENIOFF reviews the various types of earthquake seismographs now in use. The volume is well illustrated and printed. With its companion volumes it should do a great service to geophysics in showing the rapid progress being made in this subject. This branch of physics is, perhaps, not as "fundamental" as nuclear physics, but such books as this reveal what an extraordinary range of physical ideas and experimental techniques are involved in its study.

S. K. RUNCORN

VOL.
10
1957

Books received

T. PEARCEY (compiled for the Commonwealth Scientific and Industrial Research Organization, Australia) *Table of the Fresnel Integral to Six Decimal Places.* 63 pp. (Cambridge University Press, 1956.) 12s. 6d.

W. J. G. BEYNON and G. M. BROWN (edited by) *Solar Eclipses and the Ionosphere.* 330 pp. (Pergamon Press, 1956.) £7 ($21.00).

E. B. ARMSTRONG and A. DALGARNO (edited by) *The Airglow and the Aurorae.* 420 pp. (Pergamon Press, 1956.) £7 10s. ($22.50).

ETIENNE VASSY *Physique de l'atmosphere.* 338 pp. (Gauthier-Villars, 1956).

W. O. SCHUMANN *Uber die zeitucke Form und das Spectrum ausgesendeten Dipolsignale in einen dielektrixhen Hohlkingel mit leitenden Wanden.* 51 pp. (Verlag der Bayerischen Akademie der Wissenschaften, 1956).

H. SPENCER GREGORY and E. ROURKE *Hygrometry.* 254 pp. (Crosby, Lockwood & Sons Ltd., 1957.) 36s.

JERSY NEYMAN (edited by) *Proceedings of the Third Berkeley Symposium on Mathematical Statistics and Probability. Vol. III—Astronomy and Physics.* 252 pp. (University of California Press, 1956.) $6.00.

A. KOSIBA (edited by) Nr. 9. *Obserwacje Dobowe we Wroclawiu.* (*Daily Observations in Wroclaw.*) 52 pp. Reports of the Meteorological Climatological Institute, and Observatory of the Boleslaw University in Wroclaw.

VOL.
10
1957